GENOMICS AND DISEASE RESISTANCE IN WHEAT AND MAIZE

EDITED BY: James A. Birchler, Mingliang Xu, Cheng Liu, Handong Su, Fangpu Han and Shun Sakuma

PUBLISHED IN: Frontiers in Plant Science

frontiers Research Topics

frontiers

ISSN 1664-8714
ISBN 978-2-83250-898-5
DOI 10.3389/978-2-83250-898-5

About Frontiers

Frontiers is more than just an open-access publisher of scholarly articles: it is a pioneering approach to the world of academia, radically improving the way scholarly research is managed. The grand vision of Frontiers is a world where all people have an equal opportunity to seek, share and generate knowledge. Frontiers provides immediate and permanent online open access to all its publications, but this alone is not enough to realize our grand goals.

Frontiers Journal Series

The Frontiers Journal Series is a multi-tier and interdisciplinary set of open-access, online journals, promising a paradigm shift from the current review, selection and dissemination processes in academic publishing. All Frontiers journals are driven by researchers for researchers; therefore, they constitute a service to the scholarly community. At the same time, the Frontiers Journal Series operates on a revolutionary invention, the tiered publishing system, initially addressing specific communities of scholars, and gradually climbing up to broader public understanding, thus serving the interests of the lay society, too.

Dedication to Quality

Each Frontiers article is a landmark of the highest quality, thanks to genuinely collaborative interactions between authors and review editors, who include some of the world's best academicians. Research must be certified by peers before entering a stream of knowledge that may eventually reach the public - and shape society; therefore, Frontiers only applies the most rigorous and unbiased reviews.
Frontiers revolutionizes research publishing by freely delivering the most outstanding research, evaluated with no bias from both the academic and social point of view. By applying the most advanced information technologies, Frontiers is catapulting scholarly publishing into a new generation.

What are Frontiers Research Topics?

Frontiers Research Topics are very popular trademarks of the Frontiers Journals Series: they are collections of at least ten articles, all centered on a particular subject. With their unique mix of varied contributions from Original Research to Review Articles, Frontiers Research Topics unify the most influential researchers, the latest key findings and historical advances in a hot research area! Find out more on how to host your own Frontiers Research Topic or contribute to one as an author by contacting the Frontiers Editorial Office: frontiersin.org/about/contact

GENOMICS AND DISEASE RESISTANCE IN WHEAT AND MAIZE

Topic Editors:
James A. Birchler, University of Missouri, United States
Mingliang Xu, China Agricultural University, China
Cheng Liu, Crop Research Institute, Shandong Academy of Agricultural Sciences, China
Handong Su, Huazhong Agricultural University, China
Fangpu Han, State Key Laboratory of Molecular Developmental Biology, Institute of Genetics and Developmental Biology, Chinese Academy of Sciences (CAS), China
Shun Sakuma, Tottori University, Japan

The authors declare that the research was conducted in the absence of any commercial or financial relationships that could be construed as a potential conflict of interest.

Citation: Birchler, J. A., Xu, M., Liu, C., Su, H., Han, F., Sakuma, S., eds. (2022). Genomics and Disease Resistance in Wheat and Maize. Lausanne: Frontiers Media SA. doi: 10.3389/978-2-83250-898-5

Table of Contents

frontiers | Frontiers in Plant Science

TYPE Editorial
PUBLISHED 15 November 2022
DOI 10.3389/fpls.2022.1064948

OPEN ACCESS

EDITED AND REVIEWED BY
Brigitte Mauch-Mani,
Université de Neuchâtel,
Switzerland

*CORRESPONDENCE
Fangpu Han
fphan@genetics.ac.cn

SPECIALTY SECTION
This article was submitted to Plant Pathogen Interactions, a section of the journal Frontiers in Plant Science

RECEIVED 09 October 2022
ACCEPTED 26 October 2022
PUBLISHED 15 November 2022

CITATION
Liu C, Su H, Sakuma S, Xu M, Birchler JA and Han F (2022) Editorial: Genomics and disease resistance in wheat and maize.
Front. Plant Sci. 13:1064948.
doi: 10.3389/fpls.2022.1064948

Editorial: Genomics and disease resistance in wheat and maize

Cheng Liu[1], Handong Su[2], Shun Sakuma[3], Mingliang Xu[4], James A. Birchler[5] and Fangpu Han[1,6]*

[1]Crop Research Institute, Shandong Academy of Agricultural Sciences, Jinan, China, [2]National Key Laboratory of Crop Genetic Improvement, Hubei Hongshan Laboratory, Shenzhen Institute of Nutrition and Health, Huazhong Agricultural University, Wuhan, China, [3]Tottori University, Tottori, Japan, [4]China Agricultural University, Beijing, China, [5]University of Missouri, Columbia, SC, United States, [6]Institute of Genetics and Developmental Biology, Chinese Academy of Sciences, Beijing, China

KEYWORDS

disease resistance, gene mapping, distant hybridization, gene structure, wheat, maize

Editorial on the Research Topic
Genomics and disease resistance in wheat and maize

Introduction

Due to the extreme climatic events and inappropriate cropping patterns, numerous diseases are becoming more and more serious for wheat and maize in recent years, which causes yield losses and affects food security worldwide (Krupinsky et al., 2002; Parikka et al., 2012). Fusarium head blight, powdery mildew, and rusts are the most serious diseases of wheat (*Triticum aestivum* L.) (Liu et al., 2020). Stalk rot, head smut, southern corn rust, and ear rot are among the most serious diseases that can substantially reduce maize yield and impact global markets (Zhu et al., 2021). New types or variants of phytopathogens overcome past sources of resistance with the ever-shrinking genetic diversity of crop varieties (Li et al., 2009; Liu et al., 2020). With the rapid advance in genomics tools, genetic and genomic resources are now being the key approach for basic research and breeding for the crop disease resistance community (Feng et al., 2018; Liu et al., 2020). Hence, there is an urgency to explore novel disease resistance genes and their mechanisms of action in wheat and maize. In this topic, recent advances in genomics and disease resistance or stress tolerance studies for wheat and maize are presented in 15 publications, contributed by 131 authors.

Genome assembly and gene structure

Genomic assembly of the pathogen is helpful to understand its pathogenesis. Ma et al. sequenced and assembled the whole genome of *Didymella glomerata*, a new fungal pathogen causing Didymella leaf blight (DLB) in maize. They identified three maize germplasms conferring resistance to DLB, and revealed potential mechanism underlying

DLB resistance. By subjecting wheat to ethyl methane sulfonate treatment, He et al. created 113 mutations in the coding region of the *Pm21* gene that encodes a broad-spectrum resistance to powdery mildew, and revealed the key functional sites for resistance and structural distribution characteristics. Sun et al. analyzed the expression pattern of the type-A response regulatory gene family under different stresses in wheat.

Disease resistance gene mapping or mining

It is very important to locate the disease resistance genes and explore their alleles for studying their genetic evolution and evaluating their breeding value in crops (Fu et al., 2012). Sun et al. mapped a new powdery mildew resistance gene $Pm_{SN15218}$ on wheat chromosome 2AL from the breeding line SN15218, which is distinct from the known resistance gene *Pm4b*. Mu et al. identified a recessive powdery mildew resistance gene *pmYN99102* on wheat chromosome 2BL *via* bulked segregant exome capture sequencing. The gene can be traced when it is integrated into those susceptible cultivars. Yu et al. mined the alleles of wheat powdery mildew resistance gene *Pm2*, providing valuable information for the utilization of *Pm2* alleles in wheat breeding. Tong et al. verified the great breeding value of the maize *ZmCCT* haplotype *H5*, which synchronously modulates the yield potential, stalk-rot resistance, and drought tolerance. Lv et al. proposed that different adaptive patterns played important roles under complex drought tolerance based on integrated transcriptome and metabolome profiling.

Mapping quantitative disease resistance loci

Mapping QDR locus is a critical for cloning and utilizing the resistance gene resources in crops. Bai et al. mapped three new QDR loci from wheat cultivar "Pascal" with resistance to stripe rust at the adult plant stage using a recombinant inbred line population. Zhang et al. found four possible new FHB resistance loci in hard winter wheat germplasm using a multi-locus genome-wide association study. Xia et al. fine mapped a Fusarium ear rot resistance gene in maize by QTL mapping and RNA sequencing. Zhu et al. performed a high-resolution mapping of a *Helminthosporium turcium resistance 3*-like locus against north corn leaf blight.

Creation of disease resistant distant hybrid germplasm

Distant hybrid material with disease resistance is an important bridge for crop breeding (Liu et al., 2011; Liu et al., 2020). Tian et al. developed and characterized the *Triticum aestivum-Aegilops longissima* recombinants using the CS *ph1b* mutant as an inducing tool, which harbors a novel powdery mildew resistance gene *Pm6Sl*. Duan et al. narrowed down the candidate region of stripe rust resistance gene *Yr83* using newly developed wheat-rye chromosome translocations. These small-segment translocation materials are promising for the improvement of wheat cultivars. Ren et al. developed new wheat-rye 6R, 6RS, and 6RL addition lines, and identified novel resistance genes to stripe rust and powdery mildew.

Author contributions

CL compiled the contributions from all authors. All authors approved the final version of the manuscript and approved it for publication.

Funding

This work was supported financially supported by Taishan Scholars Project (tsqn201812123) and National Natural Science Foundation of China (31971847).

Acknowledgments

We greatly appreciate the contributions from all the authors and reviewers as well as the support of the editorial office of Frontiers in Plant Science.

Conflict of interest

The authors declare that the research was conducted in the absence of any commercial or financial relationships that could be construed as a potential conflict of interest.

Publisher's note

References

Feng, C., Su, H., Bai, H., Wang, R., Liu, Y., Guo, X., et al. (2018). High-efficiency genome editing using a dmc1 promoter-controlled CRISPR/Cas9 system in maize. *Plant Biotechnol. J.* 16, 1848–1857. doi: 10.1111/pbi.12920

Fu, S., Lv, Z., Qi, B., Guo, X., Li., J., Liu, B., et al. (2012). Molecular cytogenetic characterization of wheat-*Thinopyrum elongatum* addition, substitution and translocation lines with a novel source of resistance to wheat fusarium head blight. *J. Genet. Genomics* 39, 103–110. doi: 10.1016/j.jgg.2011.11.008

Krupinsky, J. M., Bailey, K. L., Mcmullen, M. P., Gossen, B. D., and Turkington, T. K. (2002). Managing plant disease risk in diversified cropping systems. *Agron. J.* 94 (2), 198–209. doi: 10.2134/agronj2002.1980

Li, G. Q., Fang, T. L., Zhang, H. T., Xie, C. Z., Li, H. J., Yang, T., et al. (2009). Molecular identification of a new powdery mildew resistance gene *Pm41* on chromosome 3BL derived from wild emmer (*Triticum turgidum* var. *dicoccoides*). *Theor. Appl. Genet.* 119, 531–539. doi: 10.1007/s00122-009-1061-y

Liu, C., Han, R., Wang, S. L., Gong, W. P., Cheng, D. G., Cao, X. Y., et al. (2020). Research progress of wheat wild hybridization, disease resistance genes transfer and utilization. *Sci. Agri Sin.* 53 (7), 1287–1308. doi: 10.3864/j.issn.0578-1752.2020.07.001

Liu, C., Qi, L., Liu, W., Zhao, W., Wilson, J., Friebe, B., et al. (2011). Development of a set of compensating *Triticum aestivum-dasypyrum villosum* robertsonian translocation lines. *Genome* 54 (10), 836–844. doi: 10.1139/G11-051

Parikka, P., Hakala, K., and Tiilikkala, K. (2012). Expected shifts in fusarium species' composition on cereal grain in northern Europe due to climatic change. *Food Addit Contam Part A Chem. Anal. Control Expo Risk Assess.* 29 (10), 1543–1555. doi: 10.1080/19440049.2012.680613

Zhu, M., Tong, L. X., Xu, M. L., and Zhong, T. (2021). Genetic dissection of maize disease resistance and its applications in molecular breeding. *Mol. Breed.* 41, 32. doi: 10.1007/s11032-021-01219-y

frontiers | Frontiers in Plant Science

ORIGINAL RESEARCH
published: 12 May 2022
doi: 10.3389/fpls.2022.912589

Mining of Wheat *Pm2* Alleles for Goal-Oriented Marker-Assisted Breeding

Ziyang Yu[1†], Luning Xiao[1†], Fuyu Su[1†], Wei Liu[2], Fuyi Luo[3], Ran Han[4], Yanjun Mu[1], Wenjing Zhang[1], Liru Wu[1], Xiao Liang[1], Nina Sun[2], Linzhi Li[2]* and Pengtao Ma[1]**

[1]College of Life Sciences, Yantai University, Yantai, China, [2]Institute of Grain and Oil Crops, Yantai Academy of Agricultural Sciences, Yantai, China, [3]Dezhou Agricultural Technology Extension and Seed Industry Center, Dezhou, China, [4]Crop Research Institute, Shandong Academy of Agricultural Sciences, Jinan, China

OPEN ACCESS

Edited by:
Handong Su,
Huazhong Agricultural University, China

Reviewed by:
Zhu-Qing Shao,
Nanjing University, China
Shunzong Ning,
Sichuan Agricultural University, China

***Correspondence:**
Pengtao Ma
ptma@ytu.edu.cn
Linzhi Li
linzhili2002@163.com
Nina Sun
sun200436@163.com

[†]These authors have contributed equally to this work

Specialty section:
This article was submitted to Plant Pathogen Interactions, a section of the journal Frontiers in Plant Science

Received: 04 April 2022
Accepted: 26 April 2022
Published: 12 May 2022

Citation:
Yu Z, Xiao L, Su F, Liu W, Luo F, Han R, Mu Y, Zhang W, Wu L, Liang X, Sun N, Li L and Ma P (2022) Mining of Wheat Pm2 Alleles for Goal-Oriented Marker-Assisted Breeding. Front. Plant Sci. 13:912589. doi: 10.3389/fpls.2022.912589

Powdery mildew of wheat, caused by *Blumeria graminis* f. sp. *tritici* (*Bgt*), is a devastating disease that seriously reduces yield and quality worldwide. Utilization of plant resistance genes is an attractive and effective strategy for controlling this disease. Among the reported powdery mildew (*Pm*) resistance genes, *Pm2* exhibits a diverse resistance spectrum among its multiple alleles. It has been widely used in China for resistance breeding for powdery mildew. To mine more *Pm2* alleles and clarify their distribution, we screened 33 wheat cultivars/breeding lines carrying *Pm2* alleles from 641 wheat genotypes using diagnostic and *Pm2*-linked markers. To further investigate the relationships within the *Pm2* alleles, we compared their resistance spectra, polymorphism of marker alleles and gene sequences, and found that they have identical marker alleles and gene sequences but diverse resistance spectra. In addition, the diagnostic kompetitive allele-specific PCR (KASP) marker, *YTU-KASP-Pm2*, was developed and was shown to detect all the *Pm2* alleles in the different genetic backgrounds. These findings provide valuable information for the distribution and rational use of *Pm2* alleles, push forward their marker-assisted breeding (MAS), and hence improve the control of wheat powdery mildew.

Keywords: wheat, powdery mildew, *Pm2*, MAS, diagnostic KASP marker

INTRODUCTION

Common wheat (*Triticum aestivum* L.) is an important grain crop that provides 20% of the world's food energy and 20% of its protein. Consequently, it is a major contributor to global food security (Hickey et al., 2019). However, wheat yield and quality are seriously affected by a variety of diseases, including powdery mildew caused by *Blumeria graminis* f. sp. *tritici* (*Bgt*; Costanzo and Bàrberi, 2014; Li et al., 2019). This disease can typically decrease wheat yield by 10%–15%, and up to 50% in serious cases (Morgounov et al., 2012; Xu et al., 2015). Several measures have been taken to control this disease, including the spraying of chemical agents and the use of resistance genes, with the latter being considered to be the most effective and the most environmentally acceptable (Zhang et al., 2019). However, to achieve control using resistance genes, both abundant powdery mildew resistance (*Pm*) genes/alleles and diversified donors are the perquisites for developing elite cultivars with high and/or durable resistance to powdery mildew (Laroche et al., 2019).

To date, more than 100 *Pm* genes/alleles (*Pm1–Pm68*, *Pm8* is allelic to *Pm17*, *Pm18* = *Pm1c*, *Pm22* = *Pm1e*, *Pm23* = *Pm4c*, and *Pm31* = *Pm21*) have been identified at 63 loci from common wheat and its relatives, showing that there are abundant genetic resources for controlling wheat powdery mildew (McIntosh et al., 2020; He et al., 2021). However, most of these documented *Pm* genes/alleles cannot be directly used in wheat breeding due to observable linkage drag, adverse pleiotropism, and competition lag. For example, when the gene *Pm16*, derived from *Triticum dicoccoides* and which exhibits broad spectrum resistance to different *Bgt* isolates, was introgressed into wheat backgrounds, it caused up to 15% yield loss during production (Summers and Brown, 2013). Similar yield reductions have been shown for other *Pm* genes derived from wheat relatives and landraces (Xu et al., 2015).

Even for the genes with no linkage drag, evolving *Bgt* variants are another challenge (An et al., 2019). For example, *Pm8* has been a widely used gene in breeding for resistance to powdery mildew. It is also an example of an extremely successful introgression of an elite alien gene from rye into common wheat (Kaur et al., 2017). Unfortunately, *Pm8* has successively lost its resistance due to the co-evolution of pathogen virulence with host resistance (Chai et al., 2005). Clearly, the breeding value of the *Pm* genes depends not only on their effectiveness at disease control, but also on the agronomic performance of their donor (Ma et al., 2015a,b, 2018). Identification and utilization of *Pm* genes with no linkage drag offer an attractive prospect for the rapid improvement of resistance to powdery mildew in wheat.

Conventional breeding has made enormous contributions to resistance breeding in the past (Li et al., 2019, 2022), but marker-assisted selection (MAS) is currently considered to be the most effective way to accurately transfer targeted genes/loci (Li et al., 2019). To improve powdery mildew resistance, MAS has been used with more than 30 *Pm* genes in wheat breeding (Shah et al., 2018). In MAS, the key point is the development and screening of molecular markers that can efficiently trace the targeted genes. Various kinds of markers have been used in MAS, such as expressed sequence tags (EST), sequence-tagged sites (STS), and simple sequence repeat (SSR) markers based on gel electrophoresis detection (Li et al., 2019). With the development of high throughput detection platforms, kompetitive allele-specific PCR (KASP) markers have begun to be used in MAS (Makhoul et al., 2020). KASP was developed based on SNPs in alleles, and enables high-throughput, gel-free screening of markers.

The *Pm2* gene, derived from *Aegilops tauschii*, has been used in resistance breeding for powdery mildew worldwide (Pugsley and Carter, 1953; Li et al., 2011). In our lab, we have identified a series of *Pm2* alleles from different genotypes, including various wheat cultivars/breeding lines, indicating that *Pm2* is a promising *Pm* gene (Gao et al., 2022). Although several *Pm2* alleles no longer exhibit resistance to some *Bgt* isolates, there are still other *Pm2* alleles that confer high resistance to powdery mildew in specific genotypes (Ma et al., 2015a,b, 2018). To maximize the effectiveness of *Pm2* in resistance breeding, in this study we aimed to: (1) mine more *Pm2* alleles and survey their distribution in wheat cultivars/breeding lines; (2) evaluate the resistance of different *Pm2* alleles for their rational utilization in different genetic backgrounds and wheat production regions; and (3) develop diagnostic KASP markers to accelerate the transfer of *Pm2* alleles into breeding lines.

MATERIALS AND METHODS

Plant Materials

Six hundred and thirty-nine Chinese wheat cultivars/breeding lines and two wheat cultivars from New Zealand (**Supplementary Table S1**) were inoculated with *Bgt* isolate E09 for screening resistant genotypes. Twenty-two wheat cultivars/breeding lines (Shimai 22, Hanmai 13, Shixin 633, Taimai 1918, Tainong 18, Shannong 15,381, Taitianmai 118, Zhongxin 7503, Jimai 52, Jimai 61, Yannong 21, Youxuan 134, GY13029, Xinshiji 156, Shi 6609, Jinhe 13–205, Huixianhong, Mingxian 169, 12CA49, GY16022, GY16011, and 12CA49), which are susceptible to all the *Bgt* isolates tested were used as susceptible parents to cross with the resistant genotypes screened from the 641 wheat genotypes (**Supplementary Table S1**), to conduct F_2 and $F_{2:3}$ segregating populations for genetic analysis and molecular detection of their *Pm* genes. Susceptible cultivar Huixianhong was used as the susceptible control for phenotypic assessment. Ulka/8*Cc, which carries the known *Pm2a* gene (Sun et al., 2015a,b), was used as the resistant control.

Reactions to Different *Bgt* Isolates

At the seedling stage, the *Bgt* isolate E09, a dominant *Bgt* isolate in North China, was used to inoculate the 641 wheat cultivars/breeding line (**Supplementary Table S1**). Additionally, the *Pm2* donors along with Ulka/8*Cc and Huixianhong were tested for their seedling reaction patterns to eight other *Bgt* isolates (A3, A10, A45, E15-1, E18, E20, E21, and E32) with different avirulence/virulence patterns and from different wheat production regions of China. The susceptible seedlings inoculated with an individual isolate were put in independent glass tubes to avoid cross infection. Five seeds of each genotype were sown in a 72-cell rectangular tray and put in an independent growth chamber to be infected with a *Bgt* isolate. When the seedlings had grown to the one-leaf stage, they were inoculated with fresh conidiospores previously cultivated on Huixianhong seedlings. At this time, the growth chambers were set at 100% humidity at 18°C for 24 h, after which the growing condition was set at 14 h light at 22°C and 10 h of darkness at 18°C. Inoculations were repeated twice in the following 2 days to ensure full infection. Infection types (ITs) were recorded when the spores were fully developed on the first leaves of Huixianhong seedlings based on the standard described by An et al. (2019), where ITs 0, 0; 1, 2, 3, and 4 are regarded as immune, hypersensitive, highly resistant, moderately resistant, moderately susceptible, and highly susceptible, respectively.

To determine the inheritance of powdery mildew resistance in the resistant genotypes, *Bgt* isolate E09 was selected to inoculate the resistant and susceptible parents and their F_1,

F_2, and $F_{2:3}$ progenies for genetic analysis. After phenotypic evaluation, the numbers of resistance and susceptible plants were counted, and then a goodness-of-fit assessment was performed to determine the resistant/susceptible ratio using a Chi-squared (χ^2) test. The deviations of the observed phenotypic data from the theoretically expected segregation ratios were then evaluated using the SPSS 16.0 software (SPSS Inc., Chicago, United States) at $p < 0.05$.

Marker Analysis

Total genomic DNAs (gDNAs) of all the $F_{2:3}$ families along with their parents were isolated after phenotypic evaluation using the TE-boiling method (He et al., 2017). For each population, equal amounts of gDNAs from 10 random homozygous resistant and 10 random homozygous susceptible $F_{2:3}$ families were pooled to construct resistant and susceptible DNA bulks, respectively. The *Pm2*-linked marker *Cfd81* (Ma et al., 2016) and the *Pm2*-diagnostic marker *Pm2b-map-3* (Jin et al., 2021) were tested for polymorphisms between the resistant and susceptible parents and bulks. The polymorphic markers were genotyped on the corresponding $F_{2:3}$ families. PCR amplifications and visualizations were as described by Ma et al. (2016).

Homology-Based Cloning of the *Pm2* Alleles

Total RNA from each of the genotypes with *Pm2* alleles was extracted using the Spectrum Plant Total RNA kit (Sigma-Aldrich, Shanghai, China) following the manufacturer's recommendations. Then, they were quantified by measuring absorbance at the wavelengths of 260 and 280 nm using a Nano Drop 1000 spectrophotometer (Thermo Scientific, Shanghai, China). High quality RNA was treated by Promega DNase I and then used for cDNA synthesis using Invitrogen SuperScript-II reverse transcriptase following the manufacturer's guidelines. Based on the report of the cloning of *Pm2a* (Sánchez-Martín et al., 2016), the primer pairs JS320 (Forward: 5′-3′: ACGATGATGTGAATCTTCCGTG) and JS305 (Reverse 5′-3′: AATGATAGCATGCATTTGGAG) were used to amplify the first exon of the *Pm2* alleles identified in this study. Then, a nested PCR using the primer pairs JS314 (Forward: 5′-3′: TTTTCGCGGTATTGCTGGTG) and JS315 (Reverse 5′-3′: ACCTCCTGTCATCGGTTCAC) was performed to obtain the final sequence of the first exon. For amplifying the second and third predicted exons of the *Pm2* alleles, primer pairs JS350 (Forward: 5′-3′: CCCTCCTCCTTGAAGAATCTGA) and JS313 (Reserve: 5′-3′: GCACAAACTCTACCCTGTTCC) were used. Finally, they were sequenced using Sanger sequencing and compared with that of the reported *Pm2a* (GenBank: LN999386.1; Sánchez-Martín et al., 2016).

Development of a Diagnostic KASP Marker for MAS

The sequences of the cloned *Pm2* alleles were used to compare with the reference genome of Chinese Spring (v2.1, http://202.194.139.32/). Distinctive SNPs were identified after comparing the *Pm2* sequences to the A, B, and D genomes of Chinese Spring, which does not carry *Pm2* and is susceptible to powdery mildew. Sequences of 100 bp upstream and downstream of the distinctive SNPs were acquired and used for KASP development using both the Polymarker website[1] and Premier 5 software.[2] The amplification sequences of the primers were aligned once again with the reference genome of Chinese Spring in the *Triticeae* Multi-omics Center (http://202.194.139.32/) to ensure specificity of the sequences. The primers were then used to genotype all the $F_{2:3}$ families carrying *Pm2* alleles to confirm their polymorphisms. The diagnostic KASP marker was then used to genotype the breeding populations of *Pm2* donors and susceptible cultivars. Combined with the phenotype against *Bgt* isolate E09, the diagnostic KASP marker was confirmed once again.

Genotyping using KASP primers was performed on a Bio-Rad CFX real-time PCR system (Bio-Rad Laboratories, Inc., CA, United States) with a final volume of 20 μl containing 6.00 μl of gDNA (~250 ng), 11.20 μl of 2 × KASP Master Mix (provided by LGC), 0.34 μl of primer mix (balanced mix of three pairs of primers for each marker), and 2.46 μl ddH_2O. The amplification procedure was set as follows: 94°C for 15 min, followed by 10 touchdown cycles of 94°C for 20 s, 64°C to 58°C (decreasing 0.6°C per cycle), and 38 cycles of regular amplification (94°C for 20 s and 58°C for 60 s), and the final fluorescence was detected at 20°C using Bio-Rad CFX Manager 3.1 software (Bio-Rad Laboratories, Hercules, CA, United States).

RESULTS

Screening of Resistant Genotypes and Inheritance Analysis

When inoculated with the *Bgt* isolate E09 at the seedling stage, 43 of the 641 accessions were resistant with ITs 0–2 (**Table 1**). The 43 resistant accessions were then crossed with susceptible cultivars to produce F_1 hybrids, F_2 populations, and $F_{2:3}$ families (**Table 1**). The F_1 plants of every hybridized combination all showed resistant phenotypes with ITs 0–2, suggesting dominant inheritance of the powdery mildew resistance in these accessions. Of their F_2 populations, 40 fitted the expected ratios of 3:1 (resistant: susceptible individuals) for monogenic segregation using the same *Bgt* isolate, suggesting that a single dominant gene may be involved in the powdery mildew resistance of these accessions (**Table 1**). The 43 F_2 populations were then transplanted in the field to produce $F_{2:3}$ families to further confirm these results and validate the genotypes of the resistant F_2 plants. The results showed that 37 $F_{2:3}$ families fitted the expected ratios of 1:2:1 (Homozygous resistant: segregating: homozygous susceptible families; **Table 1**), confirming that a single dominant gene is involved in the powdery mildew resistance of these accessions. For three populations (Xinong 198 × Yannong 21, GQ17020 × Yannong 21, and GQ17014 × Yannong 21), although their F_2 segregation

[1]http://www.polymarker.info/

[2]https://primer-premier-5.software.informer.com/

TABLE 1 | Segregation ratios of F_2 and $F_{2:3}$ generations of resistant genotypes and different susceptible cultivars following inoculation with *Blumeria graminis* f. sp. *tritici* (*Bgt*) isolate E09 at the seedling stage.

Resistance parents	Susceptible parents	Segregation ratio/F_2		χ^2	*p* Value	Segregation ratio/$F_{2:3}$			χ^2	*p* Value
		Resistant	Susceptible			Homozygous resistant	Segregating	Homozygous susceptible		
Shannong 05-66	Shimai 22	114	40	0.03	0.85	41	77	42	0.24	0.89
Lande 677	Hanmai 13	121	53	2.84	0.12	45	80	55	3.33	0.19
Zhongxinmai 77	Shimai 22	133	33	2.05	0.15	52	85	35	3.38	0.18
Shimai 24	Taimai 1918	145	44	0.21	0.64	60	89	46	3.49	0.17
FC009	Tainong 18	139	46	0.002	0.97	57	86	48	2.74	0.25
HengH13guan26	Shannong 15,381	66	25	0.30	0.59	23	43	25	0.36	0.83
GQ16002	Taitianmai 118	69	26	0.28	0.59	23	46	26	0.28	0.88
HengHBguan 26	Zhongxin 7,503	77	22	0.41	0.52	28	49	22	0.74	0.69
LS4695	Jimai 61	91	28	0.14	0.71	30	61	28	0.14	0.93
LPM8	Huixianhong	77	26	0.003	0.95	26	51	26	0.01	0.99
Shengmai 127	Huixianhong	94	24	1.37	0.24	31	63	24	1.37	0.50
Jimai 416	Huixianhong	74	22	0.22	0.64	27	47	22	0.56	0.75
Zhongmai 570	Huixianhong	81	26	0.28	0.87	34	47	26	2.78	0.25
Heng 14-K2-3	Huixianhong	116	34	0.44	0.51	36	80	34	0.72	0.70
GQ17023	Huixianhong	97	35	0.16	0.69	31	66	35	0.24	0.89
GQ17018	Huixianhong	95	36	0.43	0.51	35	60	36	0.94	0.63
GQ17006	Yannong 21	85	36	1.45	0.23	30	55	26	0.30	0.86
GQ17015	Yannong 21	94	31	0.01	0.92	33	61	31	0.14	0.93
GQ17053	Yannong 21	41	12	0.16	0.69	12	29	12	0.47	0.79
CH7102	Shixin 633	112	28	1.87	0.17	38	74	28	1.89	0.39
SH3556	Huixianhong	83	25	0.20	0.66	28	55	25	0.20	0.90
HB133-4	Youxuan 134	49	18	0.12	0.72	15	34	18	0.28	0.88
NZ8	Mingxian 169	95	30	0.07	0.80	34	61	30	0.33	0.85
NZ13	Mingxian 169	60	15	1.00	0.32	19	41	15	1.08	0.58
GQ16042	GY13029	84	26	0.11	0.74	29	55	26	0.16	0.92
GQ16010	Xinshiji 156	117	38	0.19	0.89	40	77	38	0.06	0.97
GQ16018	12CA49	69	20	0.30	0.58	24	45	20	0.37	0.83
GQ16031	Huixianhong	93	29	0.10	0.75	33	60	29	0.30	0.86
FC0015	GY16022	94	36	0.50	0.48	31	65	36	0.41	0.82
JieA10Haiping6216	Shi 6609	80	24	0.21	0.65	25	55	24	0.37	0.83
JieA1ShiTa14-7022	Shi 6609	56	15	0.57	0.45	18	38	15	0.61	0.74
Shannong 510659	GY16011	82	25	0.15	0.70	27	55	25	0.16	0.92
JieA13Kemao 60	12CA49	115	33	0.58	0.45	36	67	33	0.16	0.92
Jimai 419	Huixianhong	52	37	13.04	0.0003	10	42	37	25.54	2.84
Xinong198	Yannong 21	70	24	0.01	0.91	9	61	24	13.13	0.001
GQ17025	Huixianhong	72	39	6.08	0.01	10	62	39	16.68	0.0002
GQ17020	Yannong 21	107	47	2.50	0.11	22	85	47	9.78	0.007
GQ17007	Huixianhong	85	52	12.26	0.0005	8	77	52	30.37	2.54
GQ17014	Yannong 21	82	24	0.44	0.50	16	62	24	6.00	0.05
Kenxing 7	Huixianhong	78	23	0.27	0.61	23	55	23	0.80	0.67
Shi CG15-009	Yannong 21	54	15	0.39	0.53	18	36	15	0.39	0.82
Yannong 081531	Jinhe 13–205	84	22	1.01	0.37	28	56	22	1.02	0.60
GY16036	Jimai 52	31	13	0.48	0.49	11	20	13	0.55	0.76

ratio fitted the monogenic segregation of 3:1, their $F_{2:3}$ segregation ratio did not fit the monogenic segregation of 1:2:1, suggesting that the powdery mildew resistance in these three accessions may not be controlled by a single dominant gene.

Screening of Genotypes Carrying *Pm2* Alleles

To identify *Pm2* alleles in the 37 populations that fitted monogenic inheritance, the *Pm2*-linked marker *Cfd81* and the *Pm2*-diagnostic marker *Pm2b-map-3* were used to genotype all 37 segregating populations (**Table 2**). The results showed that these two markers can amplify consistent polymorphism between resistant parents and bulks in 33 populations. After genotyping the segregating populations, they were proved to be closely linked (*Cfd81*) and co-segregated (*Pm2b-map-3*) with the *Pm* genes in these resistant accessions (**Figure 1**), suggesting the existence *Pm2* alleles in these resistant accessions. In four other populations (Kenxing 7×Huixianhong, Shi CG15-009×Yannong 21, Yannong 081531×Jinhe 13–205, and GY16036×Jimai 52), the markers *Cfd81* and *Pm2b-map-3* did not detect *Pm2* alleles, suggesting these populations did not carry *Pm2* alleles.

To compare the *Pm2* alleles, the 33 *Pm2* donors were initially analyzed using the *Pm2*-linked marker *Cfd81* and the *Pm2*-diagnostic marker *Pm2b-map-3*. The results showed that the 33 *Pm2* donors have the same marker alleles, suggesting

TABLE 2 | Markers used in this study.

Marker	Primer sequence (5′–3′)	References
Cfd81-F	AAGATGAACTGCGGCTGAAT	Ma et al., 2016
Cfd81-R	CAGATGGACCTCTTCTTCGG	
Pm2b-map-3-F	ACCACAACGAACACCAACCT	Jin et al., 2021
Pm2b-map-3-R	ACGGGTAACCATCGAGATCA	
YTU-KASP-Pm2-F	gaaggtgaccaagttcatgctTGTTGGACGAGAAAAGGAGAAA	Newly developed in this study
YTU-KASP-Pm2-H	gaaggtcggagtcaacggattTGTTGGACGAGAAAAGGAGAAC	
YTU-KASP-Pm2-C	CAATTCATCTGAGGTGTTGGC	

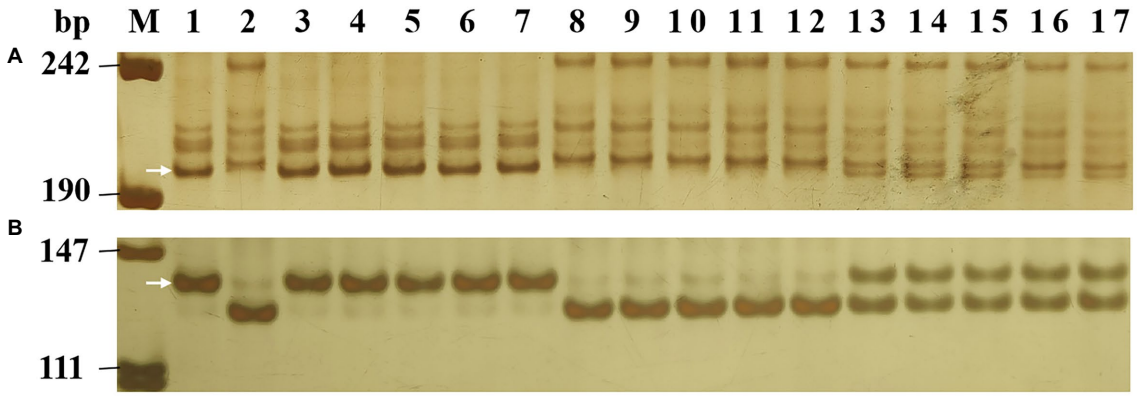

FIGURE 1 | Amplification patterns of the *Pm2*-linked marker *Cfd81* **(A)** and diagnostic marker *Pm2b-map-3* **(B)** in genotyping Lande 677 (*Pm2* donor), Hanmai 13 and random selected $F_{2:3}$ families of Lande 677 × Hanmai 13. Lane M, pUC18 *Msp* I; lane 1, Lande 677; lane 2, Hanmai 13; lanes 3–7, homozygous resistant $F_{2:3}$ families; lanes 8–12, heterozygous $F_{2:3}$ families; and lanes 13–17, homozygous susceptible $F_{2:3}$ families. The white arrows indicate the polymorphic bands in Lande 677.

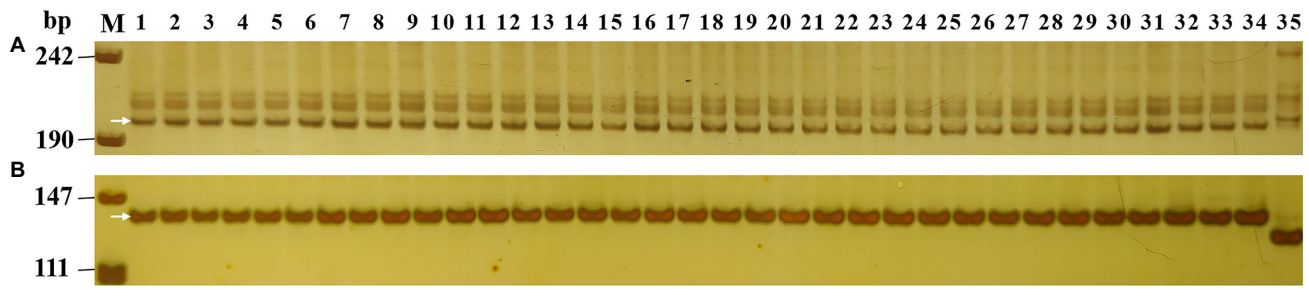

FIGURE 2 | Marker analysis of 33 *Pm2* donors using *Pm2* linked marker *Cfd81* **(A)** and diagnostic marker *Pm2b-map-3* **(B)**. Lane M, pUC18 *Msp* I; lane 1, Huixianhong (control without *Pm2* allele); lane 2, Ulka/8*Cc (control with *Pm2* allele); and lanes 3–35, the *Pm2* donors identified in this study.

consistent genetic diversity in the *Pm2* intervals of these donors (**Figure 2**). To further dissect the relationship of their *Pm2* alleles, the sequences of the *Pm2* alleles were analyzed after homology-based cloning based on the *Pm2a* sequence. The results indicated that all these *Pm2* alleles were the *Pm2a* haplotype, suggesting that this haplotype has been widely used in resistance breeding for powdery mildew.

Resistance Spectra of the *Pm2* Donors

Using nine *Bgt* isolates, including the four highly virulent isolates, E18, E20, E21, and E32, the resistance spectra of the 33 accessions carrying *Pm2* alleles were evaluated. The results showed that the *Pm2* alleles in different genetic backgrounds have different reaction patterns to the nine *Bgt* isolates (**Figure 3**; **Table 3**). Some *Pm2* donors showed resistance to all the nine *Bgt* isolates tested, such as Shannong 05–66, GQ16002, GQ17023, and GQ16042. Some *Pm2* donors have poor resistant spectrum, such as GQ16018 and GQ16031 which were susceptible to seven and six *Bgt* isolates. Other *Pm2* donors were susceptible to *Bgt* isolates that were diversified from 1 to 5 ones. This may be related to diversity of genetic backgrounds and/or the interference of other related genes.

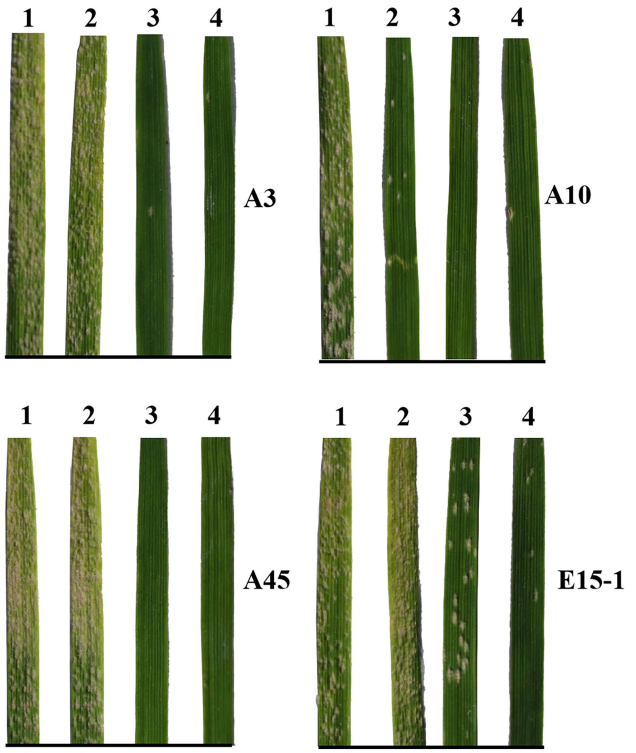

FIGURE 3 | Reaction patterns of several *Pm2* donors to four *Blumeria graminis* f. sp. *tritici* (*Bgt*) isolates, A3, A10, A45, and E15-1, collected from different regions of China using Huixianhong as susceptible control. 1: Huixianhong; 2: Lande 677; 3: Shimai 24; and 4: FC009.

These data provide a useful reference for breeders in different wheat production regions.

Evaluation of Markers for MAS

To transfer these *Pm2* alleles to susceptible cultivars using MAS, the gel-based markers *Cfd81* and *Pm2b-map-3* were initially tested for their usefulness in MAS. The results demonstrated that both markers can detect polymorphic genotypes between the *Pm2* donors and the 15 tested susceptible cultivars, suggesting that they can be used for MAS of *Pm2* alleles when these are transferred into these susceptible cultivars by conventional hybridization (**Figure 4**; **Table 4**).

To transfer *Pm2* alleles using a gel-free and high throughput genotyping platform, the diagnostic KASP marker *YTU-KASP-Pm2* was developed to trace the *Pm2* alleles based on the 609th base of the first exon of *Pm2* (**Figure 5**; **Table 2**). Using this marker, different *Pm2* donors, plants from the segregating populations and susceptible cultivars without *Pm2* alleles all showed the required genotyping, suggesting *YTU-KASP-Pm2* is an efficient diagnostic marker for *Pm2* (**Figure 6**; **Table 4**). *YTU-KASP-Pm2* was then used to genotype the 15 susceptible cultivars to evaluate its suitability for MAS. The result demonstrated that this marker can detect polymorphic genotypes between the *Pm2* donor and each of the tested 15 susceptible cultivars (**Figure 7**). So, once the *Pm2* allele is transferred into these susceptible genetic backgrounds through conventional hybridization, *YTU-KASP-Pm2* can be used to trace it through the gel-free platform, thus providing a valuable supplement for *Pm2* MAS.

DISCUSSION

Many *Pm* genes/alleles have been identified that confer resistance to wheat powdery mildew. Among them, only the *Pm* genes that are free of linkage drag and/or adverse pleiotropism have significant potential in resistance breeding. The gene, *Pm2*, was initially identified in the wheat landrace Ulka from the former Soviet Union in 1953 (Pugsley and Carter, 1953). In the 70 years of breeding history using *Pm2*, this gene has had exceptional performance in conferring resistance to powdery mildew. Many wheat cultivars carrying *Pm2* have been bred and used in production, such as Liangxing 66 with *PmLX66* (Huang et al., 2012), Jimai 22 and Jimai 23 with *PmJM23* (Jia et al., 2020), Yingbo 700 with *PmYB* (Ma et al., 2015c), Zhongmai 155 with *PmZ155* (Sun et al., 2015a), Nongda 399 with *MlND399* (Li et al., 2013), Wennong 14 with *PmW14* (Sun et al., 2015b), and Heng 4568 with *PmH4568* (Gao et al., 2022). Apart from the cultivars in production, many breeding lines and landraces have also been shown to carry *Pm2* alleles, including KM2939 with *Pm2b* (Ma et al., 2015a), Niaomai with *Pm2c* (Xu et al., 2015), Wangfengjian 34 with *PmWFJ* (Ma et al., 2015b), CH1357 with *PmCH1357* (Chen et al., 2019), 10V-2 with *Pm10V-2* (Ma et al., 2018), FG-1 with *PmFG* (Ma et al., 2016), Subtil with *PmSub* (Jin et al., 2018), and X3986-2 with *PmX3986-2* (Ma et al., 2014). After 70 years in production, a number of *Pm2* alleles continue to show high and broad-spectrum resistance in some genetic backgrounds, such as 10V-2, YingBo 700, KM2939, and Niaomai (Ma et al., 2015a,c, 2018; Xu et al., 2015). However, other alleles have reduced their ability to confer resistance (Ma et al., 2014, 2016).

It is necessary to identify more *Pm2* donors from wheat cultivars and breeding lines and to also clarify their distribution in different wheat production regions, so that their use can be promoted in different regions. In this study, after wide screening, we identified a large number of *Pm2* donors from 641 wheat cultivars and breeding lines collected from different wheat production regions. This is the first time that the existence of *Pm2* alleles in current wheat breeding lines has been assessed and summarized, data which will contribute to realizing the synergistic improvement of resistance and other agronomic traits. The results revealed that *Pm2* alleles accounted for a very high proportion of the resistance genes in resistant cultivars and breeding lines. This suggests more careful use of this gene in production is necessary, and the best strategy for its use may be in pyramiding it with other resistance genes to develop durable resistance.

Using mutant chromosome sequencing (MutChromSeq), the *Pm2a* allele was cloned (Sánchez-Martín et al., 2016). Furthermore, Chen et al. (2019) cloned *PmCH1357* using map-based cloning and found that *PmCH1357*, *Pm2c*, *PmLX66*, and *MlND399* all have identical sequences to *Pm2a*. However, Manser et al. (2021) identified seven new allelic variations of

TABLE 3 | Reaction patterns of the wheat genotypes with *Pm2* alleles to nine *Blumeria graminis* f. sp. *tritici* (*Bgt*) isolates.

***Bgt* isolates**	**A3**	**A10**	**A45**	**E15-1**	**E18**	**E20**	**E21**	**E32**	**E09**
Huixianhong	4	4	4	4	4	4	4	4	4
Shannong 05-66	0	0	0	0	0	0	0	0	0
Lande 677	4	2	4	4	0	3	3	0	1
Zhongxinmai 77	4	2	4	4	0	3	3	0	1
Shimai 24	1	0	0	3	0	3	3	0	1
FC009	1	1	0	2	0	3	3	0	0
HengH13guan26	2	0	1	1	2	1	4	0	0
GQ16002	0	0	0	0	0	0	0	0	0
HengHBguan26	0	0	0	0	2	0	4	0	0
LS4695	2	0	1	1	3	4	4	0	0
LPM8	0	0	0	4	0	4	3	0	0
Shengmai 127	0	3	3	4	0	4	0	0	0
Jimai 416	0	0	0	4	3	4	3	3	0
Zhongmai 570	4	0	4	4	0	4	0	3	0
Heng14-K2-3	0	0	3	4	3	4	0	3	0
GQ17023	0	0	0	0	0	0	0	0	0
GQ17018	0	3	4	4	0	4	0	0	0
GQ17006	4	0	0	4	0	3	0	0	0
GQ17015	0	0	0	0	0	3	3	0	0
GQ17053	0	0	0	4	0	3	3	3	0
CH7102	3	0	-	-	0	0	3	0	0
SH3556	0	0	4	0	0	1	3	3	0
HB133-4	0	3	4	4	0	0	3	4	0
NZ8	0	0	4	4	0	3	3	3	1
NZ13	0	0	3	3	0	3	3	3	1
GQ16042	0	0	0	0	0	0	0	0	1
GQ16010	0	3	0	4	0	4	3	3	1
GQ16018	4	0	3	4	4	4	3	3	1
GQ16031	4	0	3	4	4	4	0	3	1
FC0015	0	0	3	0	4	4	0	3	1
JieA10Haiping6216	0	3	-	-	3	4	3	4	1
JieA1Shita14-7022	3	2	-	-	4	4	0	3	1
Shannong 510659	4	2	-	-	4	4	3	3	1
JieA13Kemao60	0	0	4	4	0	1	3	4	1

Wheat cultivar Huixianhong with no powdery mildew (Pm) resistance genes was used as a susceptible control.
Infection types (IT) were scored according to a 0–4 scale, of which 0, 0, 1, and 2 are considered resistant, while those with an IT of 3 or 4 are considered susceptible.

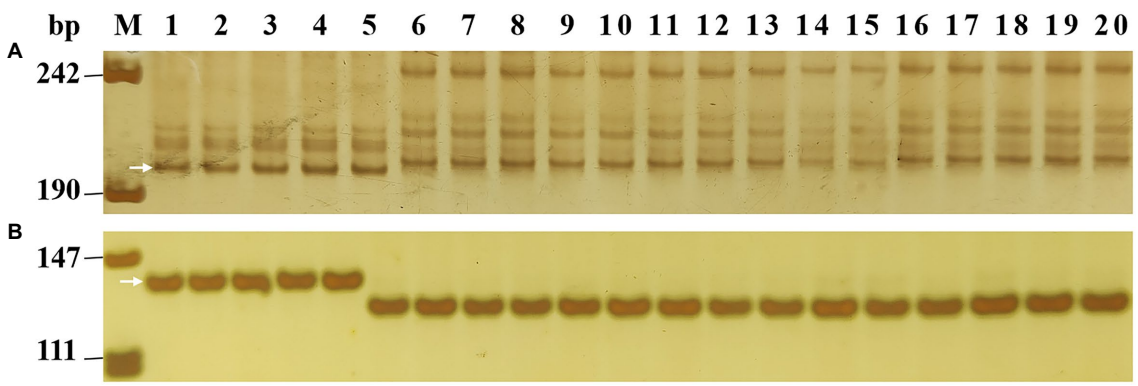

FIGURE 4 | Amplification patterns of *Pm2* linked marker *Cfd81* **(A)** and diagnostic marker *Pm2b-map-3* **(B)** in five *Pm2* donors and 15 susceptible wheat cultivars/breeding lines. M, DNA marker pUC18 *Msp* I; lanes 1–5, five *Pm2* donors with sequential order of Lande 677, LS4695, NZ8, NZ13, and GQ16031; lanes 6–20, wheat cultivars/breeding lines with sequential order of Shimai 22, Taimai 1918, Hanmai 13, Tainong 18, Shannong 15,381, Taitianmai 118, Zhongxin 7503, Jimai 61, Huixianhong, Yannong 21, Shixin 633, Mingxian 169, Xinshiji 156, 12CA49, and Shi 6609. The white arrows indicate the polymorphic bands in *Pm2* donors.

Pm2 from 28 *Aegilops tauschii* accessions. This implies that there may have been only one haplotype of *Pm2* that is *Pm2a*, used in resistance breeding since it was first identified in 1953. To confirm this result, we identified additional *Pm2* alleles in the 641 wheat cultivars and breeding lines and found that all of the *Pm2* alleles were identical to haplotype *Pm2a*, further

TABLE 4 | Evaluation of *Pm2*-diagnostic and linked markers on Ulka/8*Cc (*Pm2a* donor) and 15 susceptible wheat cultivars/breeding lines in marker-assisted selection (MAS) breeding.

Wheat genotypes	*Pm2b-map-3*	*Cdf81*	*YTU-KASP-Pm2*
Ulka/8*Cc	+	+	+
Chinese Spring	–	–	–
SH3566	–	–	–
Youxuan134	–	–	–
Mingxian169	–	–	–
GY13029	–	–	–
Xinshiji156	–	–	–
12CA49	–	–	–
Huixianhong	–	–	–
GY16022	–	–	–
Shi 6,609	–	–	–
GY16011	–	–	–
FC0015	–	–	–
Shixin 633	–	–	–
Yannong 21	–	–	–
Tainong 18	–	–	–

"–" indicates that the markers did not amplify the polymorphic products linked to Pm2 in the relevant cultivar genetic background, and "+" shows that amplification occurred.

FIGURE 5 | Sequence alignment of the first exon of *Pm2a* and its homologous sequences in the A, B, and D genomes of common wheat Chinese Spring to identify distinctive SNPs for development of diagnostic markers.

confirming the conservation of the *Pm2a* haplotype in wheat breeding. From this result, we speculate that the new *Pm2* alleles identified in *Aegilops tauschii* could also become valuable contributors to resistance, just as *Pm2a* has been an elite allele used in breeding for more than 70 years and which still confers considerable resistance.

Nevertheless, there are still unsolved issues associated with the *Pm2* locus. We, and others (Ma et al., 2014, 2018; Sun et al., 2015a,b; Jia et al., 2020), have now shown that different *Pm2* donors have significantly different reaction patterns to different *Bgt* isolates, something that is hard to explain based solely on the different genetic backgrounds. We speculate that there may be other unknown associated genes in the different genetic backgrounds which, together, provide the powdery mildew resistance in specific genotypes. We also note that there is still no transgenic evidence to confirm the functionality of the cloned *Pm2* gene, something that is required to clarify this locus.

Irrespective of the unsolved issues associated with the *Pm2* locus, this has not prevented its use in breeding in view of the advantages of this locus in conferring resistance. In wheat resistance breeding, MAS is a rapid and effective method to trace targeted genes in breeding programs, and development of molecular markers for MAS has been the key factor (William et al., 2007; Gupta et al., 2010; Li et al., 2019). Currently, there are two types of breeding markers (gel-based and gel-free), which can meet the needs of different labs in terms of throughput and which are applicable to different platforms (gel-based or gel-free) for marker analysis. Gel-based markers for *Pm2* have been reported in previous studies (Ma et al., 2015a,b,c, 2016, 2018). We verified their suitability in identifying *Pm2* donors in this study, including both linked and diagnostic markers.

With the development of high throughput genotyping platforms, gel-free KASP markers are now also widely used. Compared with the gel-based markers, KASP markers have the advantages of good stability and high throughput, are free of specific fluorescent probes and are low cost (Rasheed et al., 2016). However, no KASP markers suitable for MAS had been reported for the elite *Pm2* gene. To efficiently and accurately transfer and trace *Pm2* alleles using MAS, we developed the diagnostic KASP maker *YTU-KASP-Pm2* based on the presence of a stable SNP between homologous genes in the susceptible cultivars and the *Pm2* donors. This means that the *Pm2* alleles can be detected through two

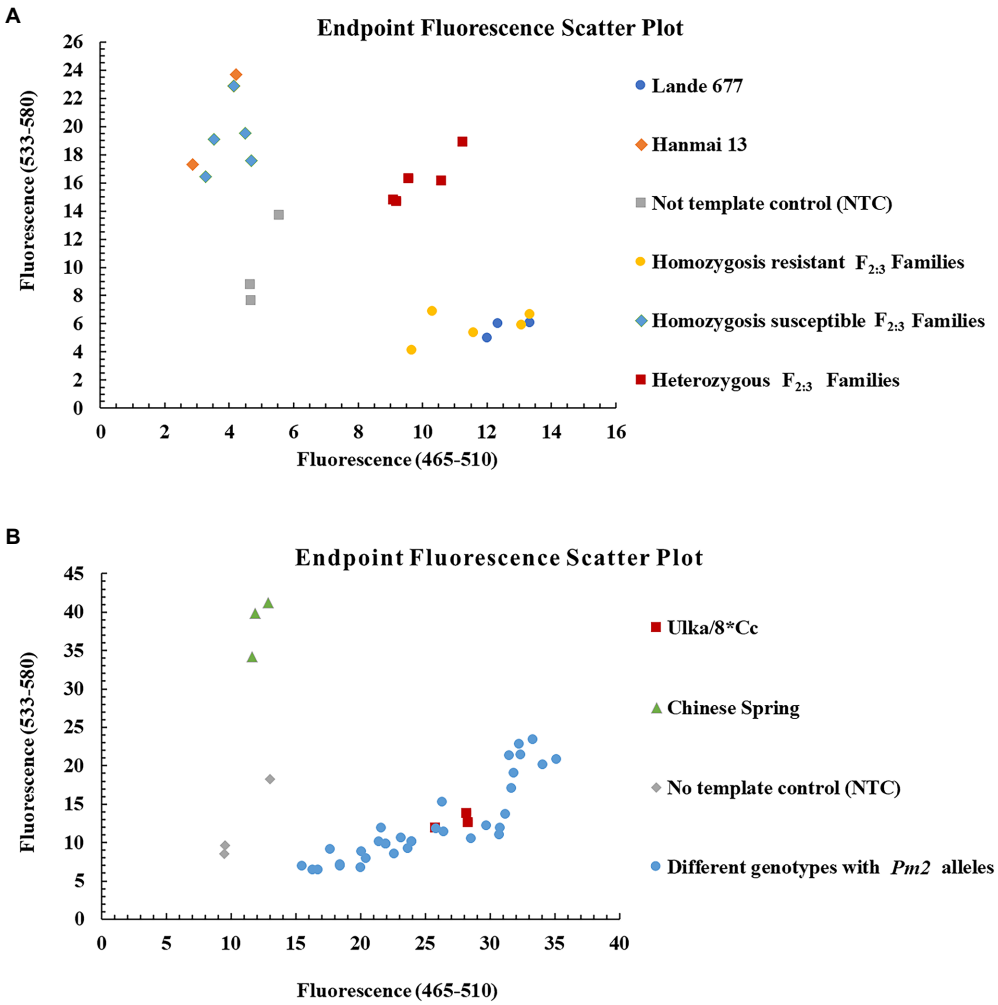

FIGURE 6 | Genotyping results of the *Pm2* diagnostic kompetitive allele-specific PCR (KASP) marker *YTU-KASP-Pm2* for Lande 677 (*Pm2* donor), Hanmai 13 and randomly selected $F_{2:3}$ families of Lande 677 × Hanmai 13 **(A)** and different genotypes with *Pm2* alleles **(B)**.

platforms: the gel-based diagnostic marker *Pm2b-map-3* can be used by breeders with only basic screening facilities, and the gel-free marker *YTU-KASP-Pm2* is available to breeders with high-throughput genotyping platforms.

When an elite resistance gene is identified, its breeding value depends not only on its resistance but also on the agronomic performance of the gene donor. Gene donors with poor agronomic performance will greatly limit their utilization in breeding (Summers and Brown, 2013; Liu et al., 2019, 2020). In this study, all the *Pm2* alleles identified were from wheat cultivars or breeding lines. Their donors all have elite yield and agronomic performance and, more importantly, they came from different wheat production regions, which can meet the requirements of different wheat production regions in corresponding resistance breeding. These *Pm2* alleles can be individually used in corresponding ecoregions, and also can be used in pyramiding breeding with other resistance genes for durable resistance. The abundance of *Pm2* donors provides the possibility of screening the optimum pyramiding model in breeding and realizing the dual improvement in both resistance and agronomic traits.

CONCLUSION

In conclusion, we have identified 37 *Pm2* alleles from wheat cultivars and breeding lines collected from different wheat production regions and confirmed that they all have the *Pm2a* sequence, but have different reaction patterns to different *Bgt* isolates depending on their specific genetic background. Molecular markers available for MAS were screened and confirmed, and a diagnostic KASP marker *YTU-KASP-Pm2* was identified for use in high-throughput genotyping platforms. Our study has provided valuable information on the distribution and rational use of *Pm2* alleles and will contribute to the control of wheat powdery mildew.

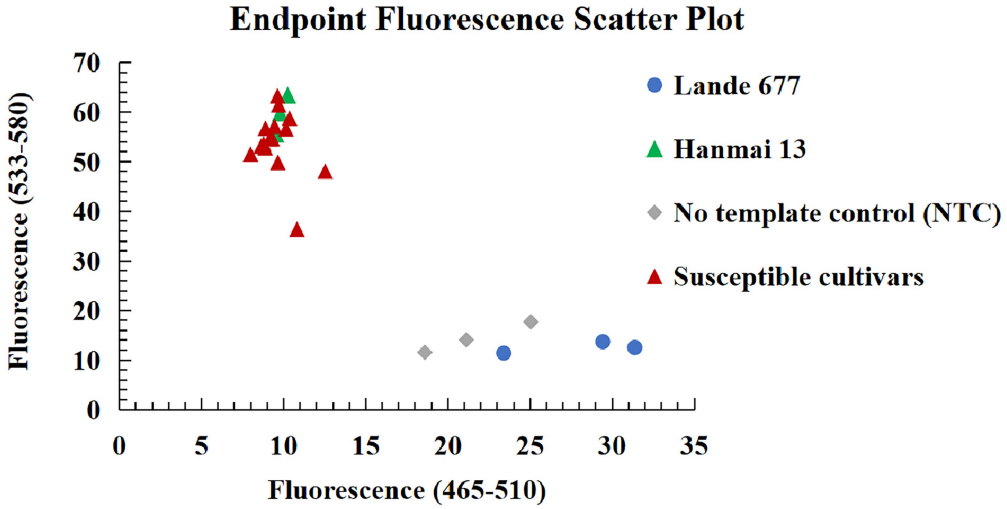

FIGURE 7 | Genotyping results of the *Pm2* KASP marker *YTU-KASP-Pm2* for Lande 677, Hanmai 13 and 15 susceptible wheat cultivars/breeding lines Shimai 22, Taimai 1918, Hanmai 13, Tainong 18, Shannong 15381, Taitianmai 118, Zhongxin 7503, Jimai 61, Huixianhong, Yannong 21, Shixin 633, Mingxian 169, Xinshiji 156, 12CA49, and Shi 6609.

DATA AVAILABILITY STATEMENT

The original contributions presented in the study are included in the article/**Supplementary Material**, further inquiries can be directed to the corresponding authors.

AUTHOR CONTRIBUTIONS

PM, LL, and NS conceived the research. ZY, LX, and FS performed the experiments. WL, YM, WZ, LW, and XL analyzed the data. FL, RH, NS, and LL performed phenotypic assessment. PM wrote the manuscript. All authors contributed to the article and approved the submitted version.

FUNDING

This research was financially supported by the National Natural Science Foundation of China (32072053, 31971874, and 32001544) and Key Technology Research and Development Program of Shandong (2020CXGC010805 and 2021RKY06100).

ACKNOWLEDGMENTS

We are grateful to Emerita Paula E. Jameson, University of Canterbury, financially supported by "Double Hundred" Plan for Foreign Experts in Shandong Province, China, for critically reviewing and editing this manuscript.

SUPPLEMENTARY MATERIAL

The Supplementary Material for this article can be found online at: https://www.frontiersin.org/articles/10.3389/fpls.2022.912589/full#supplementary-material

REFERENCES

An, D. G., Ma, P. T., Zheng, Q., Fu, S. L., Li, L. H., Han, F. P., et al. (2019). Development and molecular cytogenetic identification of a new wheat-rye 4R chromosome disomic addition line with resistances to powdery mildew, stripe rust and sharp eyespot. *Theor. Appl. Genet.* 132, 257–272. doi: 10.1007/s00122-018-3214-3

Chai, J. F., Liu, X., and Jia, J. Z. (2005). Homoeologous cloning of omega-secalin gene family in a wheat 1BL/1RS translocation. *Cell Res.* 15, 658–664. doi: 10.1038/sj.cr.7290335

Chen, F., Jia, H. Y., Zhang, X. J., Qiao, L. Y., Li, X., Zheng, J., et al. (2019). Positional cloning of *PmCH1357* reveals the origin and allelic variation of the *Pm2* gene for powdery mildew resistance in wheat. *Crop J.* 7, 771–783. doi: 10.1016/j.cj.2019.08.004

Costanzo, A., and Bàrberi, P. (2014). Functional agrobiodiversity and agroecosystem services in sustainable wheat production. A review. *Agron. Sustain. Dev.* 34, 327–348. doi: 10.1007/s13593-013-0178-1

Gao, H. M., Xu, X. Z., Ai, P. F., Luo, F. Y., Guo, P., and Ma, P. T. (2022). Identification of the powdery mildew resistance in Chinese wheat cultivar Heng 4568 and its evaluation in marker-assisted selection. *Front. Genet.* 13:819844. doi: 10.3389/fgene.2022.819844

Gupta, P. K., Langridge, P., and Mir, R. R. (2010). Marker-assisted wheat breeding: present status and future possibilities. *Mol. Breed.* 26, 145–161. doi: 10.1007/s11032-009-9359-7

He, H. G., Ji, Y. Y., Zhu, S. Y., Li, B., Zhao, R. H., Jiang, Z. Z., et al. (2017). Genetic, physical and comparative mapping of the powdery mildew resistance gene Pm21 originating from *Dasypyrum villosum*. *Front. Plant Sci.* 8:1914. doi: 10.3389/fpls.2017.01914

He, H. G., Liu, R. K., Ma, P. T., Du, H. N., Zhang, H. H., Wu, Q. H., et al. (2021). Characterization of *Pm68*, a new powdery mildew resistance gene on chromosome 2BS of Greek durum wheat TRI 1796. *Theor. Appl. Genet.* 134, 53–62. doi: 10.1007/s00122-020-03681-2

Hickey, L. T., Hafeez, A. N., Robinson, H., Jackson, S. A., Leal-Bertioli, S. C. M., Tester, M., et al. (2019). Breeding crops to feed 10 billion. *Nat. Biotechnol.* 37, 744–754. doi: 10.1038/s41587-019-0152-9

Huang, J., Zhao, Z., Song, F. J., Wang, X. M., Xu, H. X., Huang, Y., et al. (2012). Molecular detection of a gene effective against powdery mildew in the wheat cultivar liangxing 66. *Mol. Breed.* 30, 1737–1745. doi: 10.1007/s11032-012-9757-0

Jia, M. S., Xu, H. X., Liu, C., Mao, R. X., Li, H. S., Liu, J. J., et al. (2020). Characterization of the powdery mildew resistance gene in the elite wheat cultivar Jimai 23 and its application in marker-assisted selection. *Front. Genet.* 11:241. doi: 10.3389/fgene.2020.00241

Jin, Y. L., Shi, F. Y., Liu, W. H., Fu, X. Y., Gu, T. T., Han, G. H., et al. (2021). Identification of resistant germplasm and detection of genes for resistance to powdery mildew and leaf rust from 2,978 wheat accessions. *Plant Dis.* 105, 3900–3908. doi: 10.1094/PDIS-03-21-0532-RE

Jin, Y. L., Xu, H. X., Ma, P. T., Fu, X. Y., Song, L. P., Xu, Y. F., et al. (2018). Characterization of a new *Pm2* allele associated with broad-spectrum powdery mildew resistance in wheat line Subtil. *Sci. Rep.* 8:475. doi: 10.1038/s41598-017-18827-4

Kaur, R., Vyas, P., Sharma, P., Sheikh, I., Kumar, R., and Dhaliwal, H. S. (2017). "Marker-assisted breeding of recombinant 1RS.1BL chromosome for improvement of bread making quality and yield of wheat (*Triticum aestivum* L)." in *Applications of Biotechnology for Sustainable Development*. eds. K. Mukhopadhyay, A. Sachan and M. Kumar (Singapore: Springer)

Laroche, A., Frick, M., Graf, R. J., Larsen, J., and Laurie, J. D. (2019). Pyramiding disease resistance genes in elite winter wheat germplasm for Western Canada. *Crop J.* 7, 739–749. doi: 10.1016/j.cj.2019.08.005

Li, A. L., Hao, C. Y., Wang, Z. Y., Geng, S. F., Jia, M. L., Wang, F., et al. (2022). Wheat breeding history reveals synergistic selection of pleiotropic genomic sites for plant architecture and grain yield. *Mol. Plant* 15, 504–519. doi: 10.1016/j.molp.2022.01.004

Li, H. J., Wang, X. M., Song, F. J., Wu, C. P., Wu, X. F., Zhang, N., et al. (2011). Response to powdery mildew and detection of resistance genes in wheat cultivars from China. *Acta Agron. Sin.* 37, 943–954. doi: 10.1016/S1875-2780(11)60026-6

Li, D., Yuan, C. G., Wu, H. B., Zhang, D., Liang, Y., Wang, Z. Z., et al. (2013). SSR and AFLP-derived SCAR markers associated with the powdery mildew resistance gene in common wheat cultivar ND399. *J. Plant Genet. Resour.* 14, 104–108. doi: 10.3969/j.issn

Li, H. J., Zhou, Y., Xin, W. L., Wei, Y. Q., Zhang, J. L., and Guo, L. L. (2019). Wheat breeding in northern China: achievements and technical advances. *Crop J.* 7, 718–729. doi: 10.1016/j.cj.2019.09.003

Liu, C., Gong, W. P., Han, R., Guo, J., Li, G. R., Li, H. S., et al. (2019). Characterization, identification and evaluation of a set of wheat-Aegilops comosa chromosome lines. *Sci. Rep.* 9:4773. doi: 10.1038/s41598-019-41219-9

Liu, C., Han, R., Wang, X. L., Gong, W. P., Cheng, D. G., Cao, X. Y., et al. (2020). Research progress of wheat wild hybridization, disease resistance genes transfer and utilization. *Agr. Sci. Sin.* 53, 1287–1308. doi: 10.3864/j.issn.0578-1752.2020.07.001

Ma, P. T., Xu, H. X., Li, L. H., Zhang, H. X., Han, G. H., Xu, Y. F., et al. (2016). Characterization of a new *Pm2* allele conferring powdery mildew resistance in the wheat germplasm line FG-1. *Front. Plant Sci.* 7:546. doi: 10.3389/fpls.2016.00546

Ma, P. T., Xu, H. X., Luo, Q. L., Qie, Y. M., Zhou, Y. L., Xu, Y. F., et al. (2014). Inheritance and genetic mapping of a gene for seedling resistance to powdery mildew in wheat line X3986-2. *Euphytica* 200, 149–157. doi: 10.1007/s10681-014-1178-1

Ma, P. T., Xu, H. X., Xu, Y. F., Li, L. H., Qie, Y. M., Luo, Q. L., et al. (2015a). Molecular mapping of a new powdery mildew resistance gene *Pm2b* in Chinese breeding line KM2939. *Theor. Appl. Genet.* 128, 613–622. doi: 10.1007/s00122-015-2457-5

Ma, P. T., Xu, H. X., Xu, Y. F., Song, L. P., Liang, S. S., Sheng, Y., et al. (2018). Characterization of a powdery mildew resistance gene in wheat breeding line 10V-2 and its application in marker-assisted selection. *Plant Dis.* 102, 925–931. doi: 10.1094/PDIS-02-17-0199-RE

Ma, P. T., Xu, H. X., Zhang, H. X., Li, L. H., Xu, Y. F., Zhang, X. T., et al. (2015b). The gene *PmWFJ* is a new member of the complex *Pm2* locus conferring unique powdery mildew resistance in wheat breeding line Wanfengjian 34. *Mol. Breed.* 35:210. doi: 10.1007/s11032-015-0403-5

Ma, P. T., Zhang, H. X., Xu, H. X., Xu, Y. F., Cao, Y. W., Zhang, X. T., et al. (2015c). The gene *PmYB* confers broad-spectrum powdery mildew resistance in the multi-allelic *Pm2* chromosome region of the Chinese wheat cultivar YingBo 700. *Mol. Breed.* 35:124. doi: 10.1007/s11032-015-0320-7

Makhoul, M., Rambla, C., Voss-Fels, K. P., Hickey, L. T., Snowdon, R. J., and Obermeier, C. (2020). Overcoming polyploidy pitfalls: a user guide for effective SNP conversion into KASP markers in wheat. *Theor. Appl. Genet.* 133, 2413–2430. doi: 10.1007/s00122-020-03608-x

Manser, B., Koller, T., Praz, C. R., Roulin, A. C., Zbinden, H., Arora, S., et al. (2021). Identification of specificity-defining amino acids of the wheat immune receptor *Pm2* and powdery mildew effector *AvrPm2*. *Plant J.* 106, 993–1007. doi: 10.1111/tpj.15214

McIntosh, R. A., Dubcovsky, J., Rogers, W. J., Xia, X. C., and Raupp, W. J. (2020). "Catalogue of gene symbols for wheat: 2020 supplement," in *Annual Wheat Newsletter*. ed. W. J. Raupp (Manhattan, USA), 98–113.

Morgounov, A., Tufan, H. A., Sharma, R., Akin, B., Bagci, A., Braun, H. J., et al. (2012). Global incidence of wheat rusts and powdery mildew during 1969–2010 and durability of resistance of winter wheat variety Bezostaya 1. *Eur. J. Plant Pathol.* 132, 323–340. doi: 10.1007/s10658-011-9879-y

Pugsley, A. T., and Carter, M. V. (1953). The resistance of twelve varieties of *Triticum vulgare* to *Erysiphe graminis tritici*. *Aust. J. Biol. Sci.* 6, 335–346. doi: 10.1071/BI9530335

Rasheed, A., Wen, W., Gao, F., Zhai, S., Jin, H., Liu, J., et al. (2016). Development and validation of kasp assays for genes underpinning key economic traits in bread wheat. *Theor. Appl. Genet.* 129, 1843–1860. doi: 10.1007/s00122-016-2743-x

Sánchez-Martín, J., Steuernagel, B., Ghosh, S., Herren, G., Hurni, S., Adamski, N., et al. (2016). Rapid gene isolation in barley and wheat by mutant chromosome sequencing. *Genome Biol.* 17:221. doi: 10.1186/s13059-016-1082-1

Shah, L., Rehman, S., Ali, A., Yahya, M., Riaz, M. W., Si, H. Q., et al. (2018). Genes responsible for powdery mildew resistance and improvement in wheat using molecular marker-assisted selection. *J. Plant Dis. Protect.* 125, 145–158. doi: 10.1007/s41348-017-0132-6

Summers, R. W., and Brown, J. K. M. (2013). Constraints on breeding for disease resistance in commercially competitive wheat cultivars. *Plant Phothol.* 62:115.

Sun, H. G., Song, W., Sun, Y. L., Chen, X. M., Liu, J. J., Zou, J. W., et al. (2015a). Resistance to powdery mildew in the wheat cultivar Zhongmai 155: effectiveness and molecular detection of the resistance gene. *Crop Sci.* 55, 1017–1025. doi: 10.2135/cropsci2014.05.0355

Sun, Y. L., Zou, J. W., Sun, H. G., Song, W., Wang, X. M., and Li, H. J. (2015b). *PmLX66* and *PmW14*: new alleles of *Pm2* for resistance to powdery mildew in the Chinese winter wheat cultivars Liangxing 66 and Wennong 14. *Plant Dis.* 99, 1118–1124. doi: 10.1094/PDIS-10-14-1079-RE

William, H. M., Trethowan, R., and Crosby-Galvan, E. M. (2007). Wheat breeding assisted by markers: CIMMYT's experience. *Euphytica* 157, 307–319. doi: 10.1007/s10681-007-9405-7

Xu, H. X., Yi, Y. J., Ma, P. T., Qie, Y. M., Fu, X. Y., Xu, Y. F., et al. (2015). Molecular tagging of a new broad-spectrum powdery mildew resistance allele *Pm2c* in Chinese wheat landrace Niaomai. *Theor. Appl. Genet.* 128, 2077–2084. doi: 10.1007/s00122-015-2568-z

Zhang, D. Y., Zhu, K. Y., Dong, L. L., Liang, Y., Li, G. Q., Fang, T. L., et al. (2019). Wheat powdery mildew resistance gene *Pm64* derived from wild emmer (*Triticum turgidum* var. *dicoccoides*) is tightly linked in repulsion with stripe rust resistance gene *Yr5*. *Crop J.* 7, 761–770. doi: 10.1016/j.cj.2019.03.003

Conflict of Interest: The authors declare that the research was conducted in the absence of any commercial or financial relationships that could be construed as a potential conflict of interest.

Publisher's Note: All claims expressed in this article are solely those of the authors and do not necessarily represent those of their affiliated organizations, or those of the publisher, the editors and the reviewers. Any product that may

be evaluated in this article, or claim that may be made by its manufacturer, is not guaranteed or endorsed by the publisher.

frontiers | Frontiers in Plant Science

ORIGINAL RESEARCH
published: 02 June 2022
doi: 10.3389/fpls.2022.918508

Development and Characterization of *Triticum aestivum-Aegilops longissima* 6S^{l} Recombinants Harboring a Novel Powdery Mildew Resistance Gene *Pm6Sl*

Xiubin Tian[1,2], *Qifan Chen*[1,2], *Chao Ma*[1,2], *Wenqiang Men*[1,2], *Qianqian Liu*[1,2], *Yue Zhao*[1,2], *Jiajun Qian*[1,2], *Ziwei Fan*[1,2], *Jingnan Miao*[1,2], *Jinqiu He*[1,2], *Sunish K. Sehgal*[3], *Huanhuan Li*[1,2*] *and Wenxuan Liu*[1,2*]

[1] State Key Laboratory of Wheat and Maize Crop Science, Henan Agricultural University, Zhengzhou, China, [2] College of Life Sciences, Henan Agricultural University, Zhengzhou, China, [3] Department of Agronomy, Horticulture and Plant Science, South Dakota State University, Brookings, SD, United States

OPEN ACCESS

Edited by:
Cheng Liu,
Shandong Academy of Agricultural Sciences, China

Reviewed by:
Xiangyang Xu,
United States Department of Agriculture, United States
Huagang He,
Jiangsu University, China

***Correspondence:**
Huanhuan Li
lihuanhuanhappy@henau.edu.cn
Wenxuan Liu
liuwenxuan@henau.edu.cn

Specialty section:
This article was submitted to Plant Pathogen Interactions, a section of the journal Frontiers in Plant Science

Received: *12 April 2022*
Accepted: *02 May 2022*
Published: *02 June 2022*

Citation:
Tian X, Chen Q, Ma C, Men W, Liu Q, Zhao Y, Qian J, Fan Z, Miao J, He J, Sehgal SK, Li H and Liu W (2022) Development and Characterization of Triticum aestivum-Aegilops longissima 6S^{l} Recombinants Harboring a Novel Powdery Mildew Resistance Gene Pm6Sl. Front. Plant Sci. 13:918508. doi: 10.3389/fpls.2022.918508

Powdery mildew of wheat is a foliar disease that is spread worldwide. Cultivation of resistant varieties is the most effective, economical, and environmentally friendly strategy to curb this disease. Powdery mildew resistance genes (*Pm*) are the primary resources for resistance breeding, and new *Pm* genes are in constant demand. Previously, we identified *Aegilops longissima* chromosome 6S^{l}#3 as a carrier of powdery mildew resistance and designated the resistance gene as *Pm6Sl.* Here, we reported the design of 24 markers specific to 6S^{l}#3 on the basis of the full-length cDNA sequences of 6S^{l}#3 donor *Ae. longissma* accession TA1910, and the development of wheat-*Ae. longissima* 6S^{l}#3 introgression stocks by *ph1b*-induced homoeologous recombination. Further, 6S^{l}#3 introgression lines were identified and characterized by integration analysis of powdery mildew responses, *in situ* hybridization, and molecular markers and *Pm6Sl* was mapped to a distal interval of 42.80 Mb between markers Ael58410 and Ael57699 in the long arm of 6S^{l}#3. Two resistant recombinants, R43 (T6BS.6BL-6S^{l}#3L) and T27 (Ti6AS.6AL-6S^{l}#3L-6AL), contained segments harboring *Pm6Sl* with less than 8% of 6S^{l}#3 genomic length, and two markers were diagnostic for *Pm6Sl*. This study broadened powdery mildew resistance gene resources for wheat improvement and provided a fundamental basis for fine mapping and cloning of *Pm6Sl* to further understand its molecular mechanism of disease resistance.

Keywords: common wheat, *Ae. longissima*, 6S^{l}#3 recombinants, powdery mildew resistance, physical mapping

INTRODUCTION

Bread wheat (*Triticum aestivum* L., $2n = 6x = 42$; AABBDD) is a hexaploid species of the genus *Triticum* in the grass family *Poaceae* (or *Gramineae*). It is the most extensively grown and traded cereal crop with the highest monetary value and the second most-produced cereal after maize. Therefore, the sustainable production of wheat is essential for social progress and stability worldwide. Powdery mildew caused by the fungus *Blumeria graminis* f. sp. *tritici* (*Bgt*)

is one of the most damaging foliage diseases of wheat. Severe infection can cause yield loss of 5–30% and decrease grain quality in epidemic years (Fried et al., 1981; Bennett, 1984; Conner et al., 2003; Morgounov et al., 2012). The development and cultivation of resistant varieties is currently the most effective, economical, and environmentally friendly approach to constraining yield and grain quality losses caused by this disease (Wang et al., 2005). As resources for resistance breeding, many powdery mildew resistance genes (*Pm*) have been identified and introgressed into contemporary wheat varieties from landraces, ancestral species, and other wild relatives. Currently, at least 100 permanently and temporarily designated genes for powdery mildew resistance have been documented (McIntosh et al., 2017; Li et al., 2020; Zhang et al., 2020; He et al., 2021). Fourteen cataloged *Pm* genes have been cloned, including *Pm1*, *Pm2*, *Pm3*, *Pm4b*, *Pm5e*, *Pm8*, *Pm17*, *Pm21*, *Pm24*, *Pm38*, *Pm40*, *Pm41*, *Pm46*, and *Pm60* (Brunner et al., 2010; Hewitt et al., 2021; Sánchez-Martín et al., 2021; Yang et al., 2021). Only a fraction of the known *Pm* genes, such as *Pm2, Pm4b*, *Pm8*, *Pm13*, and *Pm21,* have been widely deployed in wheat production (Yang et al., 2013, 2021; Xing et al., 2018). A large number of *Pm* genes have been defeated by virulent races, and others could not be deployed in wheat breeding owing to either race-specificity or deleterious gene linkage drag (Klindworth et al., 2013; Tan et al., 2019). Consequently, new *Pm* genes for continuous improvement of wheat are still in demand.

Cultivated bread wheat has a large genome of 17 giga-base pairs (Gb) comprising three subgenomes, A, B, and D, which were contributed by *T. urartu* Tumanian ex Gandilyan ($2n = 2x = 14$, AA), *Ae. speltoides* Tausch ($2n = 2x = 14$, SS), and *Ae. tauschii* Coss. ($2n = 2x = 14$, DD) (Dubcovsky and Dvorak, 2007; El Baidouri et al., 2017). Wild species of common wheat serve as important gene resources for wheat improvement. Many of these species contain chromosomes that are not homologous to those of wheat, and the genes they bear are difficult to transfer to stable wheat lines. Since those chromosomes are functionally similar or homoeologous to wheat chromosomes, they can often be induced to pair and recombine with wheat chromosomes by suppression of strict bivalent formation, which is controlled by genes *Ph1* on chromosome arm 5BL and *Ph2* in homoeologous group 3 chromosomes (Riley et al., 1968; Sears, 1977; Qi et al., 2007). Other methods of achieving chromosome transfers include induction of centric fusion of unpaired wheat and foreign chromosomes by double monosomy (breakage and reunion) (Friebe et al., 2005; Liu et al., 2011, 2016) or radiation of seeds or pollen to induce random chromosome breaks and reunions (Sears, 1956; Liu et al., 1999). At least 15 cataloged *Pm* genes have been transferred into wheat from wild wheat relatives, including *Pm13* and *Pm66* from *Ae. longissima* Schweinf. & Muschl. ($2n = 2x = 14$, S^lS^l), *Pm29* probably from *Ae. geniculata* Roth. ($2n = 4x = 28$, $U^gU^gM^gM^g$), *Pm57* from *Ae. searsii* Feldman & Kislev ex Hammer ($2n = 2x = 14$, S^sS^s), *Pm7*, *Pm8*, *Pm17*, *Pm20*, and *Pm56* from *Secale cereale* L. ($2n = 2x = 14$, RR), *Pm21*(= *Pm31*), *Pm55*, *Pm62* and *Pm67* from *Dasypyrum villosum* (L.) P. Candargy ($2n = 2x = 14$, VV), *Pm51* from *Thinopyrum elongatum* (Host) D. R. Dewey ($2n = 2x = 14$, EE), and *Pm2b* from *Agropryron cristatum* (L.) Gaertn. ($2n = 2x = 14$, PP). Several of these *Pm* genes, such as *Pm8* on 1RS, and *Pm21* on 6VS, have been widely deployed in wheat resistance breeding programs across the world (He et al., 2018; Li et al., 2020; Zhang et al., 2020).

Ae. longissima Schweinf. & Muschl. ($2n = 2x = 14$, S^lS^l), an annual grass species native to the eastern Mediterranean basin is one of the five diploid *Aegilops* species carrying the S, or a modified S genome (Feldman et al., 1995; Friebe et al., 1996). *Ae. longissima* represents a valuable reservoir of genetic diversity for resistance to stem rust, stripe rust, powdery mildew, Septoria glume blotch, and eyespot (Ceoloni et al., 1992; Sheng et al., 2012; Wang et al., 2018; Xia et al., 2018). However, the potential of *Ae. longissima* in wheat improvement is far from being fully assessed; only powdery mildew resistance genes *Pm13* ($3S^lS$) and *Pm66* ($4S^lS$) have been used in wheat breeding programs (Li et al., 2021). Recently, genome sequences of *Ae. longissima* accession of TL05 (Li et al., 2022) and AEG-6782-2 (Avni et al., 2022) have been published. These genomic resources will accelerate the exploration and utilization of beneficial genes from this species.

Previously, we identified a Chinese Spring (CS)-*Ae. longissima* $6S^l$#3 disomic addition line TA7548 with resistance to wheat powdery mildew (Xia et al., 2018). In this study, we described the development of $6S^l$#3 recombinants conferring resistance to powdery mildew and the physical mapping of *Pm6Sl* in *Ae. longissima* chromosome $6S^l$#3.

MATERIALS AND METHODS

Plant Material

The plant material used in this study included common wheat CS, CS *ph1b* mutant TA3809 lacking pairing homologous gene *Ph1*, thereby permitting homoeologous recombination, CS-*Ae. longissima* $6S^l$#3 disomic addition line TA7548, where a pair of chromosomes $6S^l$#3 from *Ae. longissima* was added to CS background, $6S^l$#3 donor *Ae. longissima* accession TA1910, CS nulli-tetrasomic stocks N6AT6B (TA3152), N6BT6D (TA3155), and N6DT6A (TA3156), in which the chromosomes 6A, 6B and 6D pairs were respectively replaced by homoeologous pairs 6B, 6D, and 6A. The number following the chromosome designation ($6S^l$#3) indicated the origin of the alien chromosome derived from different *Ae. longissima* accessions (Raupp et al., 1995). All materials were provided by the Wheat Genetics Resource Center (WGRC), Kansas State University, USA, and increased in China at the Experimental Station of Henan Agricultural University.

Development of Populations Segregating for Chromosome $6S^l$#3

Two populations segregating for $6S^l$#3 were developed. Population 1 produced by crossing CS monosomic 6A (CSM6A, $20W'' + 6A'$) with TA7548 ($21W'' + 6S^l\#3''$) was used to develop compensating Robertsonian translocations (RobTs) involving wheat chromosome 6A and $6S^l$#3. F_1 plants with 42 chromosomes and positive for $6S^l$#3-specific markers were selected and self-pollinated.

Population 2 used to develop $6S^l$#3 recombinants was derived from the hybrid of CS *ph1b* mutant TA3809 crossed with TA7548. F_2 individuals with homozygous *ph1b* and monosomic $6S^l$#3 were selected using the *ph1b*-specific marker

TABLE 1 | Responses of TA7548 to 30 *Bgt* isolates.

Bgt-isolates	IT		*Bgt*-isolates	IT	
	CS	TA7548		CS	TA7548
A10	4	0	Y04	4	3
E05	4	0	Y15	4	1
E09	3	0	Y06	4	0
E31	3	0	Y07	4	0
E18	3	0	Y08	4	0
A3	4	0	Y09	4	0
E23-1	3	0	Y10	4	2
E20	3	0	Y11	4	2
E21	4	0	Y14	4	0
E26	4	0	Y16	4	0;
E32	4	0	Y17	4	0
E23	4	0	Y18	3	0
Y01	4	0	Y21	4	0
Y02	4	4	B18	4	0
Y03	3	0	GY-KDZ-1	4	1

ABC302.3 (Wang et al., 2002) and $6S^{l}$#3-specific markers. Self-pollinated progenies of these plants were used to screen putative $6S^{l}$#3 recombinants.

Individual plants of both populations were screened by a few $6S^{l}$#3-specific molecular markers to select the plants showing marker-disassociation as putative recombinants involving $6S^{l}$#3 and then verified by cytogenetic and molecular marker analyses.

Preparation, Sequencing, and Alignment of an *Ae. longissima* Full-Length cDNA Library

Preparation, sequencing and alignment of an *Ae. longissima* full-length cDNA library was performed by BGI Genomics (Shenzhen, China) with the Pacific Bioscience Sequel platform (Pacific Biosciences, Silicon Valley, California, USA). Briefly, the second leaves from *Ae. longissima* TA1910 were collected at 0, 12, 24, and 48 h post-inoculation with *Bgt* isolate E26 and equally mixed for total RNA extraction using a mirVana miRNA Isolation Kit (Cat. No. AM1561, Ambion, Thermo Fisher Scientific, Waltham, MA, USA) following the manufacturer's protocol. Total RNA was converted to first-strand cDNA using a SMARTer PCR cDNA Synthesis Kit (Cat. No. 634925, Clontech, Takara Biomedical Technology (Beijing) Co., Ltd., Beijing). After PCR optimization, a large-scale PCR was performed to synthesize second-strand cDNA. After another large-scale PCR, the DNA was ready for library template preparation by PacBio SMRTbell; selected fragments > 4 kb were sequenced by Pacific Biosciences Sequel. Sequencing data were processed by Single-Molecule, Real-Time (SMRT) sequencing analysis through reads of insert, classify, and cluster to obtain consensus full-length isoforms. Isoforms that could not be aligned to any database were predicted by TransDecoder version v3.0.1 (https://transdecoder.github.io).

Molecular Marker Analysis

Fifty-three markers were used in this study, of which 24 were $6S^{l}$#3-specific markers developed from full-length cDNA sequences of TA1910, and the other 29 simple sequence repeat (SSR) markers specific for wheat chromosomes 6A (15), 6B (8), and 6D (6) were obtained from GrainGenes. SSR marker details are listed in **Supplementary Table S1**. The genomic positions of the markers of $6S^{l}$#3-specificity were ordered using blastn alignment against both the CS reference genomic sequence (Wheat_IWGSC_RefSeq_v2.1) (Zhu et al., 2021) and *Ae. longissima* accession TL05 reference sequences (Li et al., 2022).

Genomic DNA (gDNA) was isolated from 5 to 10 cm segments of young leaves with a DNeasy Plant Mini Kit (Qiagen, Cat No. 69104) following the instructions. PCR reactions were conducted in a 15-μl volume containing 2.0 μl template gDNA (100 ng/μl), 1.0 μl of each primer (5.0 μmol/l), 7.5 μl Taq MasterMix (CW Bio Inc., China) and 3.5 μl ddH_2O. Using $6S^{l}$#3-specific primers, PCR amplifications were performed by Touchdown63 and by F50SSR using SSR markers (Liu et al., 2017). PCR products of $6S^{l}$#3-specific markers and SSR markers were resolved in 1.5% and 3.0% agarose gels and visualized by ethidium bromide staining under UV light.

Cytogenetic Analysis

Collection and nitrous oxide treatment of root tips, squash preparations, and genomic *in situ* hybridization (GISH) were performed following protocols described by Liu et al. (2017). *Ae. longissima* gDNA was labeled with fluorescein-12-dUTP. Common wheat CS gDNA was used as blocking. The ratio of gDNA of *Ae. longissima* to CS was 1:120. Fluorescence *in situ* hybridization (FISH) was performed with eight oligonucleotide probes, of which six were 6-carboxytetramethylrhodamine (TAMRA)-modified oligonucleotides (pAs1-1, pAs1-3, pAs1-4, pAs1-6, AFA-3, and AFA-4) and displayed red signals, and the other two were 6-carboxyfluorescein (FAM)-modified oligonucleotides (pSc119.2-1 and $(GAA)_{10}$), which fluoresced green (Du et al., 2017; Huang et al., 2018). After hybridization and slide washing, a drop (25–30 μl) of Vectashield mounting medium containing 1 μg/ml DAPI (Vector Laboratories Inc, Burlingame, CA, USA) was added to each slide and then covered with a 24 × 30 cm glass coverslip. Fluorescent images were observed under a Zeiss Axio Scope A1 fluorescence microscope (Jena, Germany) and captured with an AxioCam MRc5 CCD camera. Images were further processed with Adobe Photoshop CS3 (Version 10.0.1) (Adobe Systems Inc., San Jose, CA, USA).

Powdery Mildew Evaluation

Thirty single-pustule-derived *Bgt* isolates were collected from different regions in China and used to test TA7548. Isolate E26, kindly provided by the Nanjing Agricultural University and locally maintained, was used to test the $6S^{l}$#3 derivatives. The remaining 29 isolates were maintained at the University of Yantai, Shandong Province. The preparation of plant materials and *Bgt* inoculation followed protocols was described by Li et al. (2020). Infection types were recorded on a 0–4 scale at 10 days post inoculation, while conidia were fully developed on the first leaves

TABLE 2 | *Ae. longissima* 6S^{l}#3 specific markers developed in this study.

Maker name	Position (Mb)	Forward primer (5'-3')	Reverse primer (5'-3')	Tm (°C)	Product size (bp)
Ael69501	0.37	TGGGCCTTTGAGTAGAGC	ACTGACCACGATAGGTTTTT	63	197
Ael69148	3.97	TCGCCACCGCAGACCTT	TGGCTGGCTGCTTTGGG	63	111
Ael60640	7.21	GACCTGAAAGCGTCATACC	TTACAATACCGACGACAATG	63	410
Ael68035	9.04	GATTGCATGAATTATACTCTGG	AACAGACCCTCAACCGAAA	63	122
Ael67319	202.09	TATGTCTAGTGTATCTGTACGTGGC	ACTCATGTACAAGAGTAATCAGCAC	56.5	172
Ael63185	383.52	GAGCAGGCGTAGCCTCAGGAGCCTC	TTTTCTCTACCTAAGTGCATGGAAG	56.5	212
Ael65131	423.79	ACAGAACAATCGATGCGTAC	TCCTGTTACAAGATGCCCAG	63	543
Ael56039	433.79	CGAGAAAGGTGTATTGCCG	TCCAAACTGAATCCCAACA	63	305
Ael59504	440.43	AGTGGAACGCAGTGGCAA	CGGCGGGAGTAGTAGATTT	63	212
Ael68886	442.72	TGGCAGTGGCGGAGGAC	TTCTGCCATGACCTACTGACC	63	268
Ael63597	504.91	GCCGCTCTGTTTTACCTTC	AGATTTAGCAGCACTGTTCG	63	118
Ael59927	506.99	TTTGGATCGCGTGGGCA	GTGCACCGGCCAAGTAATG	63	195
Ael58062	511.11	ATCGTCATTCGTCGCCCT	GTCCACGCGCATCAGCA	63	376
Ael63981	526.76	GTCCGTCTACCTACCCTAGC	CAAAGAGGTACGGTACAAGC	63	168
Ael68067	527.64	ATCGTGGGAGAGGTGCAG	TTGGGTCGTGATCCATTG	63	408
Ael58468	580.44	CTGATCGACCGACCGATT	ATGCACATGGGCAAGAAC	63	249
Ael60368	580.44	CACAGAGAGGGAGAGAGATACT	AGGCCACCTGATACCAAC	63	143
Ael59300	580.44	GCTTGTCGACCGGGAGG	CTCTCATGCGTCTGCGTATT	63	240
Ael55917	608.24	CTCTCCGTCGTCGTCATG	TTCACCGGTTATTGACATCA	63	390
Ael58410	616.84	CATCGGGGGAGCGGTAC	CCCTAGCTACCAGATCACCC	60	159
Ael58120	620.73	TGTTCTGAGCATCACCATAC	TCATGCGAGTACATCAACC	55	261
Ael64341	621.98	CAAGTCTGTCAGCGTCTCG	CACAAGAGAGGAGGAATACGT	55	463
Ael57699	659.64	TACTGCAATGAGCTCAAGTCCAACA	TCGAGGAACACAACATCTTGCTGTT	67	183
Ael42958	659.64	GCCAACTGAGGTTAGTTTCGTTAAT	CTCACCTCACTAATCAGCCTTCACC	65	536

Position determined by synteny comparison with Ae. longissima TL05 6S^{l} reference genomic sequences. Tm: annealing temperature.

of susceptible control CS. Plants with ITs of 0–2 were considered to be resistant, whereas those with ITs of 3–4 were susceptible (Shi et al., 1987).

RESULTS

Response of TA7548 to a Panel of *Bgt* Isolates

Thirty *Bgt* isolates were used to test the *Bgt* response of TA7548 together with CS as a susceptible control when the first leaves were fully expanded. Seedling reactions 10 days post-inoculation indicated that 28 of 30 *Bgt* isolates were avirulent on TA7548, with ITs ranging from 0 to 2, and the other two isolates were virulent on TA7548 with ITs 3 and 4. CS, the susceptible control, was highly susceptible to all *Bgt*-isolates, with ITs 3-4 (**Table 1**). Thus, the gene(s) on chromosome 6S^{l}#3, designated as *Pm6Sl*, confers resistance to multiple *Bgt*-isolates.

Ae. longissima Full-Length cDNA Sequences

Sequenced by the Pacific Bioscience Sequel platform generated 2,136,574,821 bp CCS (reads of insert) data (1,161,885 reads), of which, 685,686 (59.01%) reads were full-length non-chimeric, with a mean length of 1,494.7 bp. After clustering and polishing the consensus with Quiver and removing redundancies, a total of 69,907 high-quality consensus isoforms were identified, covering a total length of 113,954,143 bp, with a mean length of 1,630 bp and N50 of 1,920 bp. The isoforms were further analyzed using TransDecoder software to identify candidate coding regions. The longest open reading frame (ORF) was then selected and blasted to the SwissProt and Hmmscan databases to search for Pfam protein homology sequences for CDS prediction, leading to the prediction of 62,761 (71,013,186 bp) CDS with lengths ranging from 297 to 5,913 bp were predicted.

Development of 6S^{l}#3-Specific Markers

By blasting the full-length sequences of 62,761 predicted CDS of *Ae. longissima* to CS reference genomic sequences (IWGSC RefSeq v2.1, IWGSC, 2021), a total of 8,461 (13.48%) CDS were uniquely assigned to homoeologous group 6. One hundred and thirty-four unique CDS with similarities of 80–90% to wheat group 6 genomic sequences were selected for further PCR primer design. Based on a comparison of these CDS sequences with those of CS, 134 PCR primer pairs were designed. The comparison of amplification of CS and CS-*Ae. longissima* 6S^{l}#3 disomic addition line TA7548 led to the identification of 24 (17.91%) markers specific to chromosome 6S^{l}#3 (**Table 2**).

Identification of RobTs Involving 6S^{l}#3

Four markers mapped to each arm of 6S^{l}#3 were used to select putative RobTs involving 6S^{l}#3 in Population 1. Markers Ael69501 and Ael42958 were distally located at opposite ends

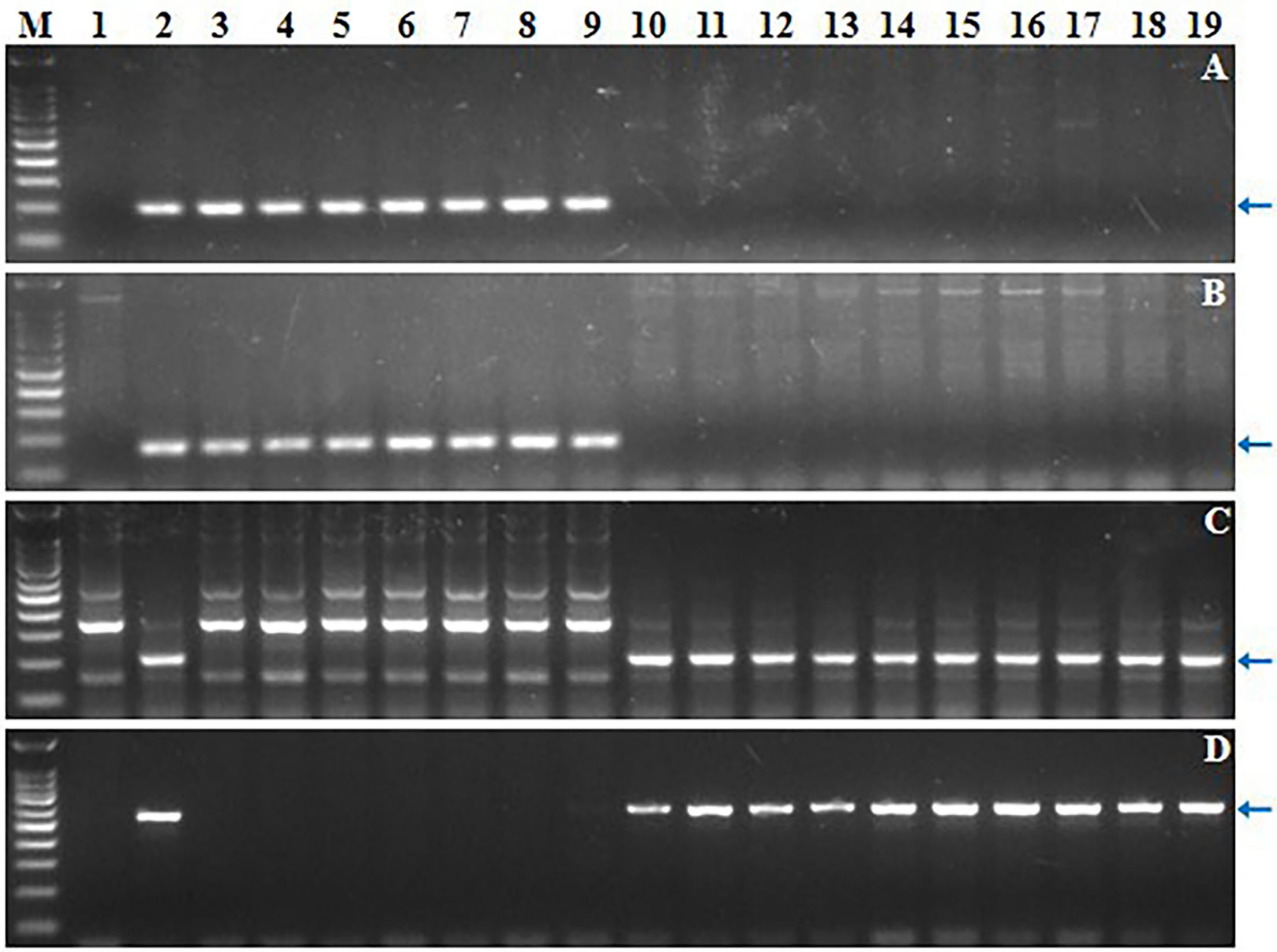

FIGURE 1 | Screening of 17 CS-*Ae. longissima* 6S^{l}#3 RobTs by molecular marker analysis. **(A–D)** Electrophoresis patterns of 6S^{l}#3-specific markers Ael69501, Ael67319, Ael63185 and Ael42958, respectively. M: 100 bp DNA Ladder Marker; 1: common wheat CS; 2: CS-*Ae. longissima* 6S^{l}#3 disomic addition line TA7548; 3-19: the newly developed CS-*Ae. longissima* 6S^{l}#3 RobTs and telosomes. Arrows pointed to the polymorphic bands of the chromosome 6S^{l}#3-specific molecular markers.

of 6S^{l}#3, whereas Ael67319 and Ael63185 occupied intermediate positions in the short and long arms. Plants lacking either the short arm- or long arm-specific marker(s) were selected as putative 6S^{l}#3 RobTs. From 608 plants in population 1, 17 (2.80%) showing disassociations of markers were selected as putative RobTs or having telosomes (Telos) for either 6S^{l}#3S or 6S^{l}#3L. Seven plants lacked long arm markers and 10 lacked short arm markers (**Figure 1**). GISH and FISH analyses of the seven plants lacking the long arm markers identified a compensating RobT T6S^{l}#3S.6AL (1S71), whereas the remaining plants were monotelosomic 6S^{l}#3S (**Figure 2**). The 10 plants with only long arm markers were all monotelosomic 6S^{l}#3L (represented by T42) (**Figure 2**). A powdery mildew test using *Bgt*-isolate E26 showed that the RobT T6S^{l}#3S.6AL and the six monotelosomic 6S^{l}#3S were susceptible, whereas all 10 monotelosomic 6S^{l}#3L were resistant with IT of 0 (**Figure 3**). Thus, *Pm6Sl* was located in the long arm of chromosome 6S^{l}#3.

Development of CS-*Ae. longissima* 6S^{l}#3L Recombinants

In order to develop CS-*Ae. longissima* recombinants with breakpoints at 6S^{l}#3L where *Pm6Sl* resides, four markers specific for 6S^{l}#3L were used to select putative recombinants in Population 2. Two markers (Ael65131 and Ael56039) were near the centromere of 6S^{l}#3L, whereas the other two, Ael58410 and Ael42958, were located at the distal region of 6S^{l}#3L. Fourteen plants (1.76%) displayed disassociations with the four markers and were selected as putative 6S^{l}#3L recombinants. These putative 6S^{l}#3L recombinants were further characterized using 24 6S^{l}#3-specific markers. Based on the presence of different markers, the 14 plants were grouped into four types: T31, T24, R43, and T27 (**Figure 4**).

T31 type lost six proximal and distal markers of 6S^{l}#3L (Ael55917, Ael58410, Ael58120, Ael64341, Ael57699, and Ael42958), which covered a distal segment of <81.77 Mb.

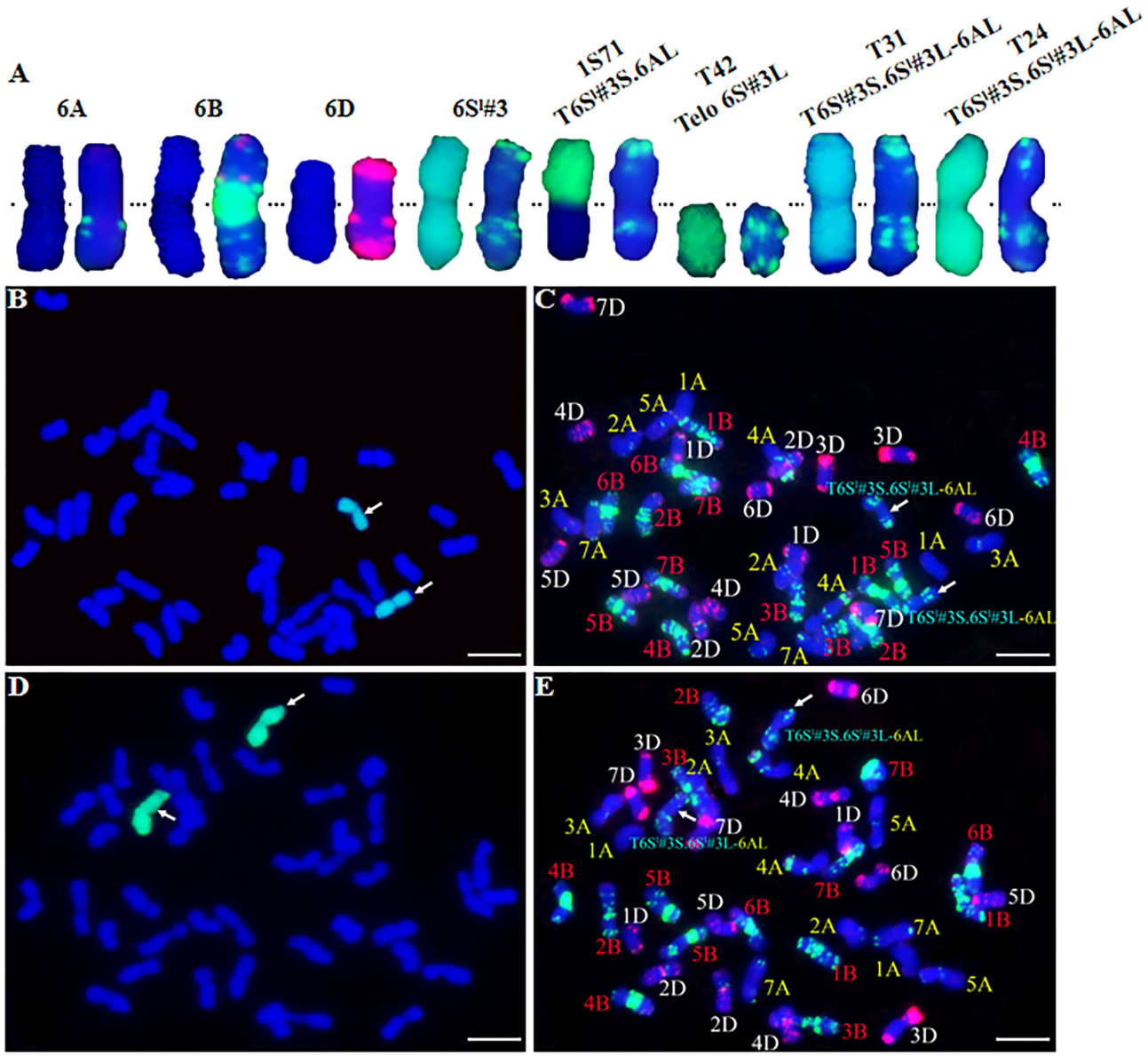

FIGURE 2 | GISH and FISH analysis of CS-*Ae. longissima* 6S^{l}#3 introgression lines. **(A)** From left to right, chromosome pairs of 6A, 6B, 6D, 6S^{l}#3, T6S^{l}#3S.6AL (1S71), 6S^{l}#3L telosome (T42), T6S^{l}#3S.6S^{l}#3L-6AL (T31), and T6S^{l}#3S.6S^{l}#3L-6AL (T24). The left and right chromosome of each pair is GISH and FISH, respectively. **(B–E)** GISH and FISH patterns of T31 **(B,C)** and T24 **(D,E)**. Arrows indicated the recombined chromosomes involving 6S^{l}#3. *Ae. longissima* chromatin is visualized by green florescence and wheat chromosomes are counterstained with DAPI and fluoresced blue in GISH. In FISH, TAMRA-modified oligonucleoties (pAs1-1, pAs1-3, pAs1-4, pAs1-6, AFA-3 and AFA-4) are in red color, FAM-modified pSc119.2-1 and $(GAA)_{10}$ are in green color. Scale bar = 10 μm.

T24 plants had all 6S^{l}#3-specific markers except two-terminal markers (Ael57699 and Ael42958), both at 659.64 Mb. The R43 type presented only four distal markers (Ael58120, Ael64341, Ael57699, and Ael42958) of 6S^{l}#3L covering a segment of <45.37 Mb. T27 was positive for only three distal markers of 6S^{l}#3L covering a segment of <51.40 Mb; however, both terminal markers of 6S^{l}#3L (Ael57699 and Ael42958) at 659.64 Mb were absent (**Figure 4**). Chromosome 6S^{l} segments in both recombinants R43 and T27 were < 8% of 6S^{l} genomic length.

Cytogenetic Analysis of 6S^{l}#3L Recombinants

GISH and FISH were performed to identify chromosome recombinants involving 6S^{l}#3L. GISH showed that type T31 contained a recombined 6S^{l}#3 chromosome with a terminal wheat segment consistent with 6AL (**Figures 2B,C**). Therefore, the T31 recombinants were identified as T6S^{l}#3S·6S^{l}#3L-6AL. Neither GISH nor FISH identified a wheat segment replacing distal 6S^{l}#3L in the T24 type despite positive

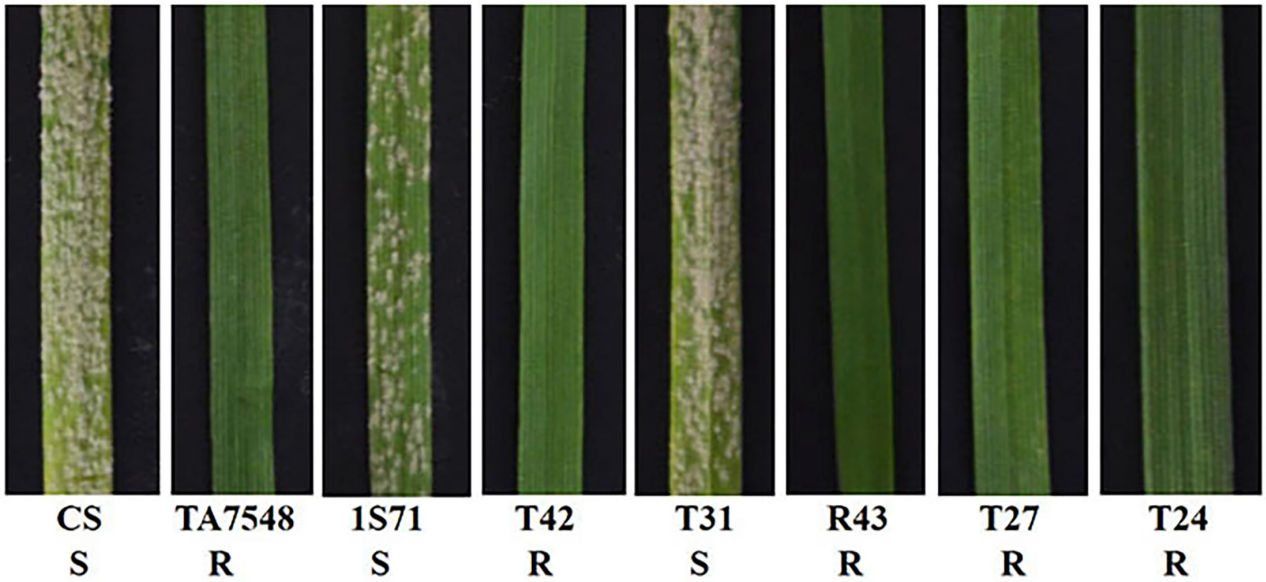

FIGURE 3 | Powdery mildew resistance evaluation of 6S^{l}#3 recombinants. 1S71: CS-*Ae. longissima* RobT T6S^{l}#3S.6AL; T42: 6S^{l}#3L telosome line; T31: CS-*Ae. longissima* T6S^{l}#3S.6S^{l}#3L-6AL recombinant; R43: CS-*Ae. longissima* T6BS.6BL-6S^{l}#3L recombinant; T27: CS-*Ae. longissima* Ti6AS.6AL-6S^{l}#3L-6AL recombinant; T24: CS-*Ae. longissima* T6S^{l}#3S.6S^{l}#3L-6AL recombinant. R: resistant to powdery mildew, S: susceptible to powdery mildew.

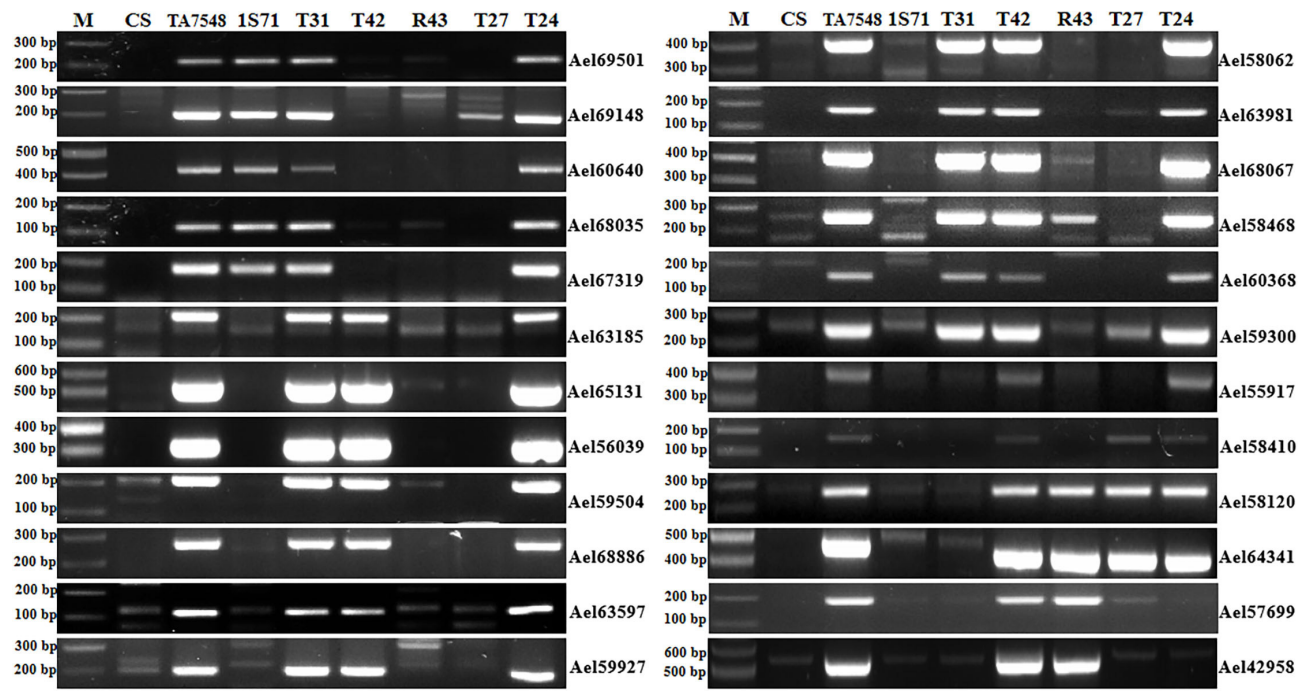

FIGURE 4 | PCR patterns of 6S^{l}#3 recombinants using 6S^{l}#3-specific markers. M: 100 bp DNA ladder marker.

indications from marker analysis (**Figures 2D,E**). The results indicated that those plants had a small distal segment of wheat replacing the 6S^{l}#3L counterpart. GISH of both R43 and T27 types failed to detect the green color for *Ae. longissima* chromatin, and FISH also failed to detect a difference from CS. This confirmed that any 6S^{l}#3 segments in these lines should be small and beyond the resolving power of these methods.

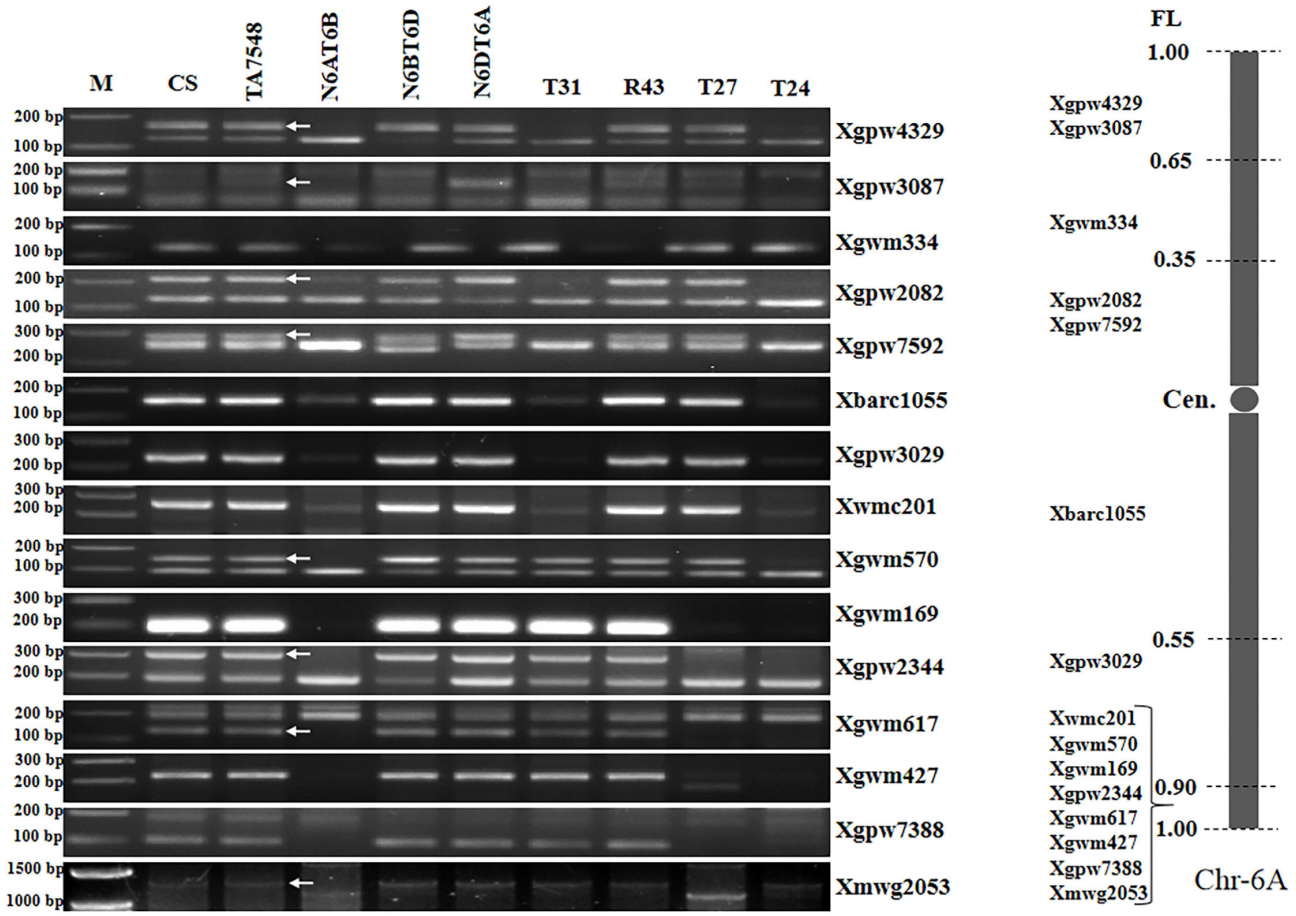

FIGURE 5 | Molecular markers analysis of 6S^{l}#3 recombinants using wheat 6A SSR markers. Arrows pointed to 6A-specific bands when two or more bands were amplified using a single primer pair. M: 100 bp DNA ladder marker.

Characterization of 6S^{l}#3L Recombinants by SSR Markers

The combined GISH, FISH patterns, and 6S^{l}#3-specific marker analyses indicated that all putative recombinants contained 6S^{l}#3L segments of various sizes, whereas the identities of the wheat segments in the other groups except T31 were unresolved. SSR markers were used to further characterize those 6S^{l}#3L recombinants. Twenty-nine SSR markers specific to chromosomes 6A (15), 6B (8) and 6D (6) were selected to perform PCR amplification (**Supplementary Table S1**). Compared with CS and TA7548, different PCR products were amplified from T31, T27, and T24 for 6A-SSRs, and R43 for 6B-SSRs.

Analyses of 15 6A-specific SSR markers displayed that recombinants of type T31 lacked all 6A-specific SSR markers except seven distal markers in chromosome bin 6AL8-0.90-1.00 (**Figure 5**; **Supplementary Table S2**), indicating that T31 lines had recombined chromosomes containing only small segments of 6AL, thus designated as T6S^{l}#3S.6S^{l}#3L-6AL (**Supplementary Figure S1**). Type T24 presented SSR patterns similar to those of T31 and was also designated as T6S^{l}#3S.6S^{l}#3L-6AL, but the wheat segment was smaller with just distal SSR marker Xmwg2053 (**Figure 5**; **Supplementary Table S2**). T27 recombinants lacked six distal markers in chromosome bin 6AL8-0.90-1.00, whereas they retained two proximal markers (Xwmc201 and Xgwm570) (**Figure 5**; **Supplementary Table S2**). By combining 6S^{l}#3 specific marker and SSR markers analyses, T27 should be an interstitial recombinant formed by proximal 6S^{l}#3L segments replaced 6AL counterparts, thus designated as Ti6AS.6AL-6S^{l}#3L-6AL (**Supplementary Figure S1**).

PCR patterns of eight 6B-specific SSR markers displayed that type R43 recombinants were negative for two of five markers (Xgwm219 and Xwmc417) in chromosome bin 6BL5-0.40-1.00 but positive for the remaining six markers (**Figure 6**; **Supplementary Table S2**). We concluded that the recombined chromosomes in R43 were formed by the 6S^{l}#3L distal segments substituting for distal counterparts of 6BL. Thus, R43 was designated T6BS.6BL-6S^{l}#3L (**Supplementary Figure S1**).

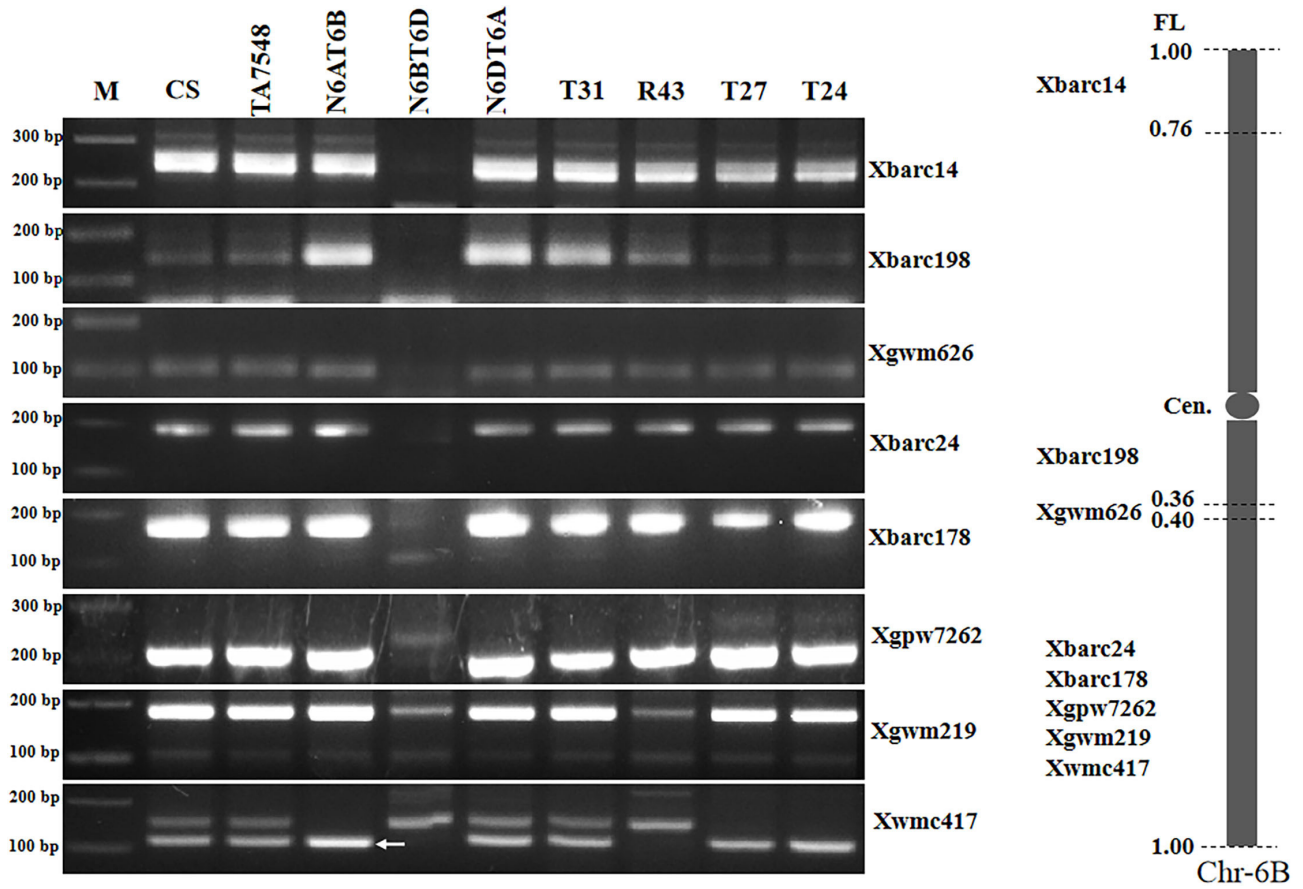

FIGURE 6 | Molecular markers analysis of 6S^{l}#3 recombinants using wheat 6B SSR markers. Arrows pointed to 6B-specific bands when two or more bands were amplified using a single primer pair. M: 100 bp DNA ladder marker.

Physical Mapping of *Pm6Sl*

The 6S^{l}#3L recombinants, together with susceptible control CS and resistant control TA7548, were assayed by inoculation of the *Bgt*-isolate E26. Infection types at 10 days post-inoculation indicated that recombinants of T24, R43, T27, and TA7548 were resistant (IT 0), whereas T31 plants and CS were susceptible (IT 4) (**Figure 3**). By integration of the *Bgt*-responsive assay and molecular marker analyses, *Pm6Sl* was physically mapped to a distal interval between markers Ael58410 and Ael42958 in the long arm of 6S^{l}#3, which spanned 42.8 Mb in *Ae. longissima* TL05 reference sequence (**Figure 7**).

Identification of Specific Markers for *Pm6Sl* in Wheat Genetic Backgrounds

Two markers developed in this study, Ael58120 and Ael64341, were close to *Pm6Sl*. PCR amplification was performed to determine whether they were diagnostic with four *Pm6Sl* stocks, including CS-*Ae. longissima* 6S^{l}#3 disomic addition line TA7548, recombinant R43, T24, and T27, and 23 wheat lines. The target bands were amplified from *Pm6Sl* stocks but were absent in those wheat varieties not containing *Pm6Sl* (**Figure 8**). Thus, both PCR markers can be used to assist the selection of *Pm6Sl* plants in the hybrid progeny of these *Pm6Sl* stocks in breeding programs.

DISCUSSION

in situ hybridization (GISH and FISH) provides a highly efficient approach to resolving alien chromosome segments in wheat (Li et al., 2019). The combined application of both techniques can display the size of both donor and recipient wheat chromosomes and the number and position of breakage points. However, the resolution of GISH is about 25 Mb (Mukai et al., 1993). Similarly, FISH can also fail to resolve chromosomes or segments unless there are presented abundant signal bands. In contrast, transcriptome sequencing can quickly and economically yield numerous sequences to facilitate the rapid and efficient development of molecular markers covering all the genomes of wild wheat relatives. Combined GISH/FISH with chromosome-specific markers has been widely used to accelerate the detection of alien chromatin harboring useful genes in wheat introgression and breeding programs (Wang et al., 2018; Zhang et al., 2019; Li et al., 2020). *Ae. longissima* belongs to the section *Sitopsis* in the genus *Aegilops*. The S or modified S

Markers	Genomic position (Mb)	CS	TA7548	T31	R43	T27	T24	
Ael69501	0.37	-	+	+	-	-	+	
Ael69148	3.97	-	+	+	-	-	+	
Ael60640	7.21	-	+	+	-	-	+	
Ael68035	9.04	-	+	+	-	-	+	
Ael67319	202.09	-	+	+	-	-	+	
Ael63185	383.52	-	+	+	-	-	+	
Ael65131	423.79	-	+	+	-	-	+	
Ael56039	433.79	-	+	+	-	-	+	
Ael59504	440.43	-	+	+	-	-	+	
Ael68886	442.72	-	+	+	-	-	+	
Ael63597	504.91	-	+	+	-	-	+	
Ael59927	506.99	-	+	+	-	-	+	
Ael58062	511.11	-	+	+	-	-	+	
Ael63981	526.76	-	+	+	-	-	+	
Ael68067	527.64	-	+	+	-	-	+	
Ael58468	580.44	-	+	+	-	-	+	
Ael60368	580.44	-	+	+	-	-	+	
Ael59300	580.44	-	+	+	-	-	+	
Ael55917	608.24	-	+	-	-	-	+	
Ael58410	616.84	-	+	-	-	+	+	
Ael58120	620.73	-	+	-	+	+	+	***Pm6Sl***
Ael64341	621.98	-	+	-	+	+	+	**42.80 Mb**
Ael57699	659.64	-	+	-	+	-	-	
Ael42958	659.64	-	+	-	+	-	-	
***Bgt* response**		**S**	**R**	**S**	**R**	**R**	**R**	

FIGURE 7 | Physical mapping of gene *Pm6Sl*. "+" indicated the presence of 6S^{l}#3-specific molecular markers, "**–**" indicated the absence of 6S^{l}#3-specific molecular marker. R indicated resistance to powdery mildew, S indicated susceptible to powdery mildew.

genomes of the section are genetically related to the wheat B and D genomes, thus resolving small segments of *Ae. longissima* chromatins introgressed into wheat by GISH is challenging. In this study, we successfully identified RobT lines with centric fusion T6S^{l}#3S.6AL (1S71), telosomes 6S^{l}#3S and 6S^{l}#3L, and recombinant T6S^{l}#3S.6S^{l}#3L-6AL (T31) by combining GISH and FISH, whereas other recombinants were unresolved. By integrating both 6S^{l}#3-specific and wheat SSR marker analyses, we identified recombinants T27 (Ti6AS.6AL-6S^{l}#3L-6AL), T24 (T6S^{l}#3S.6S^{l}#3L-6AL), and R43 (T6BS.6BL-6S^{l}#3L).

Mapping and cloning of genes from wild species still face tough challenges due to *Ph* gene-suppressed recombination between alien chromosomes and their wheat homoeologous counterparts, lack of reference genomic sequences for those wild species, and insufficient markers specific to alien chromosomes. In this study, we constructed a full-length cDNA sequence database of *Ae. longissima* accession TA1910, and designed PCR primers based on isoform sequence comparisons with CS reference genomic sequences. About 18% of molecular markers designed in the study gave polymorphic bands to distinguish *Ae. longissima* 6S^{l}#3 chromatin from wheat chromatin. This was much more efficient than the EST-PCR, SSR, and mapped-flcDNA-based marker development that we reported previously (Liu et al., 2016). By marker analysis and tests of powdery mildew

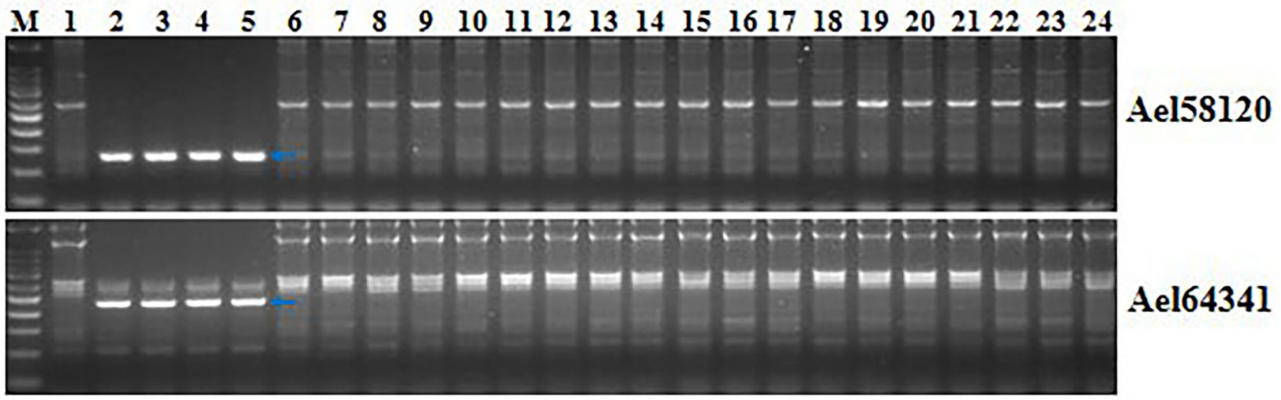

FIGURE 8 | Validation of the usefulness of two markers Ael58120 and Ael64341 closely linked to *Pm6Sl*. M: 100 bp DNA ladder; 1: CS; 2: CS-*Ae*. *longissima* $6S^{l}$#3 disomic addition line TA7548; 3-5: $6S^{l}$#3 recombinants R43, T24 and T27 with resistance to powdery mildew; 6: Bainong 207; 7: Bainong 64; 8: Aikang 58; 9: Zhoumai 16; 10: Zhoumai 18; 11: Zhoumai 22; 12: Zhoumai 28; 13: Pingan 0518; 14: Pingan 602; 15: Pingan 901; 16: Jimai 22; 17: Yanzhan 4110; 18: Shengxuan 6; 19: Yangmai 5; 20: Nannong 9918; 21: Linxuan 101; 22: Hua 5; 23: Ningmai 3; 24: Xinong 979. Arrows pointed to the polymorphic bands of the respective molecular markers linked to *Pm6Sl*.

response, *Pm6Sl* was located at the distal interval of 42.80 Mb flanked by markers Ael58410 and Ael57699 in the long arm of $6S^{l}$#3. The resistant recombinants with small $6S^{l}$#3 segments and the full-length cDNA sequence database of TA1910 developed in this study will help future fine mapping and cloning of *Pm6Sl*.

The transfer of favorable genes from wild relatives of common wheat is an effective approach to broadening the genetic base of modern wheat. Homoeologous recombination-based transfer is currently the best way to introgress desirable genes from wild species to common wheat. However, homoeologous recombination between alien chromatin and wheat homoeologous counterparts was restrained in the presence of *Ph* genes (Gyawali et al., 2019). The deletion mutant (*ph1b*) of the pairing homologous gene *Ph1* at 5BL is mostly deployed to promote homoeologous recombination between wild species and wheat. A lot of alien genes conferring disease and pest resistance have been transferred into wheat and mapped by *ph1b*-induced homoeologous recombination (Dong et al., 2020; Wan et al., 2020). In this study, 24 CS-*Ae*. *longissima* $6S^{l}$#3 recombinants were developed based on *ph1b*-induced homoeologous recombination. By integration of cytogenetic analyses and powdery mildew resistance evaluation, the novel powdery mildew resistance gene *Pm6Sl* was mapped to the distal interval of 42.8 Mb in the long arm of $6S^{l}$#3.

Ae. *longissima* has been reported to contain diverse biotic stress resistance genes. However, currently, very few genes from this species are deployed in wheat breeding programs, except *Pm13* (Ceoloni et al., 1992). In the present study, we developed two $6S^{l}$#3 recombinants, T27 (Ti6AS.6AL-$6S^{l}$#3L-6AL) and R43 (T6BS.6BL-$6S^{l}$#3L) by *ph1b*-induced homoeologous recombination. Both lines conferred broad-spectrum resistance to powdery mildew and harbored *Pm6Sl* in an *Ae. longissima* segment of <8% of the $6S^{l}$ genomic length. These resistant recombinants with tiny $6S^{l}$ segments will decrease the linkage drags and be potentially useful in wheat disease resistance breeding programs.

DATA AVAILABILITY STATEMENT

The original contributions presented in the study are included in the article/**Supplementary Material**, further inquiries can be directed to the corresponding author/s.

AUTHOR CONTRIBUTIONS

WL and HL conceived the research and wrote the paper. HL and SS performed *in situ* hybridization. XT, CM, and WM conducted full-length cDNA data analysis and molecular marker development. YZ, QC, and JM conducted molecular marker analysis. WM evaluated responses to *Bgt* isolates. JH, JQ, and ZF conducted SSR marker analyses. All authors contributed to the article and approved the submitted version.

FUNDING

This research was supported by the National Natural Science Foundation of China (Nos. 31971887 and 31801361), the Scientific and Technological Research Project of Henan Province of China (No. 212102110059), and the Topnotch Talents of Henan Agricultural University (30500939).

ACKNOWLEDGMENTS

The authors are thankful to Prof. Aizhong Cao from the College of Agronomy, Nanjing Agricultural

University, China, for kindly providing *Bgt* isolate E26.

SUPPLEMENTARY MATERIAL

The Supplementary Material for this article can be found online at: https://www.frontiersin.org/articles/10.3389/fpls.2022.918508/full#supplementary-material

Supplementary Figure S1 | Characterization of 6S^{l}#3 recombinants by wheat SSR markers and 6S^{l}#3-specific markers. Wheat 6A chromatins were represented by red column, 6B by purple and 6S^{l}#3 by green. Wheat 6A and 6B SSR markers were in red and purple italic, respectively, ordered by locating chromosome bin and primer-aligned CS reference genomic sequences in the same bin; 6S^{l}#3-specific markers in green bold, ordered by derived full-length cDNA sequence-aligned *Ae. longissima* TL05 reference genomic sequences. Bold black numbers on the right of 6A and 6B columns represented chromosome fragment length (FL). Based on analyses of SSR markers and 6S^{l}#3-specific markers, T31 was designated as T6S^{l}#3S.6S^{l}#3L-6AL, R43 as T6BS.6BL-6S^{l}#3L, T24 as T6S^{l}#3S.6S^{l}#3L-6AL, and T27 as Ti6AS.6AL-6S^{l}#3L-6AL.

Supplementary Table S1 | SSR primers used in this study.

Supplementary Table S2 | Characterization of 6S^{l}#3 recombinants using wheat SSR markers.

REFERENCES

Avni, R., Lux, T., Minz-Dub, A., Millet, E., Sela, H., Distelfeld, A., et al. (2022). Genome sequences of three *Aegilops* species of the section Sitopsis reveal phylogenetic relationships and provide resources for wheat improvement. *Plant J.* 110, 179–192. doi: 10.1111/tpj.15664

Bennett, F. (1984). Resistance to powdery mildew in wheat: a review of its use in agriculture and breeding programs. *Plant Pathol.* 33, 279–300. doi: 10.1111/j.1365-3059.1984.tb01324.x

Brunner, S., Hurni, S., Streckeisen, P., Mayr, G., Albrecht, M., Yahiaoui, N., et al. (2010). Intragenic allele pyramiding combines different specificities of wheat *Pm3* resistance alleles. *Plant J.* 64, 433–445. doi: 10.1111/j.1365-313X.2010.04342.x

Ceoloni, C., Signore, G., Ercoll, L., and Donini, P. (1992). Locating the alien chromatin segment in common wheat-*Aegilops longissima* mildew resistant transfers. *Hereditas* 116, 239–245. doi: 10.1111/j.1601-5223.1992.tb00830.x

Conner, R. L., Kuzyk, A. D., and Su, H. (2003). Impact of powdery mildew on the yield of soft white spring wheat cultivars. *Can. J. Plant Sci.* 83, 725–728. doi: 10.4141/P03-043

Dong, Z. J., Tian, X. B., Ma, C., Xia, Q., Wang, B. L., Chen, Q. F., et al. (2020). Physical mapping of *Pm57*, a powdery mildew resistance gene derived from *Aegilops searsii*. *Int. J. Mol. Sci.* 21, 322. doi: 10.3390/ijms21010322

Du, P., Zhuang, L. F., Wang, Y., Yuan, L., Wang, Q., Wang, D. R., et al. (2017). Development of oligonucleotides and multiplex probes for quick and accurate identification of wheat and *Thinopyrum bessarabicum* chromosomes. *Genome* 60, 93–103. doi: 10.1139/gen-2016-0095

Dubcovsky, J., and Dvorak, J. (2007). Genome plasticity a key factor in the success of polyploid wheat under domestication. *Science* 318, 393. doi: 10.1126/science.1143986

El Baidouri, M., Murat, F., Veyssiere, M., Molinier, M., Flores, R., Burlot, L., et al. (2017). Reconciling the evolutionary origin of bread wheat (*Triticum aestivum*). *New Phytol.* 213, 1477–1486. doi: 10.1111/nph.14113

Feldman, M., Lupton, F., and Miller, T. (1995). "Wheats," in *Evolution of Crop Plants, 2nd Edn*. Eds J. Smartt and N. W. Simmonds (London: Longman Scientific), 184–192.

Friebe, B., Jiang, J., Raupp, W. J., McIntosh, R. A., and Gill, B. (1996). Characterization of wheat-alien translocations conferring resistance to diseases and pest: current status. *Euphytica* 91, 59–87. doi: 10.1007/BF00035277

Friebe, B., Zhang, P., Linc, G., and Gill, B. S. (2005). Robertsonian translocations in wheat arise by centric misdivision of univalents at anaphase I and rejoining of broken centromeres during interkinesis of meiosis II. *Cytogenet. Genome Res.* 109, 293–297. doi: 10.1159/000082412

Fried, P., Mackenzie, D., and Nelson, R. (1981). Yield loss caused by *Erysiphe graminis* f. sp. *tritici* on single culms of "Chancellor" wheat and four multilines. *J. Plant. Dis. Prot.* 88, 256–264.

Gyawali, Y., Zhang, W., Chao, S., Xu, S., and Cai, X. W. (2019). Delimitation of wheat *ph1b* deletion and development of *ph1b*-specific DNA markers. *Theor. Appl. Genet.* 132, 195–204. doi: 10.1007/s00122-018-3207-2

He, H. G., Liu, R. K., Ma, P. T., Du, H. N., Zhang, H. H., Wu, Q. H., et al. (2021). Characterization of *Pm68*, a new powdery mildew resistance gene on chromosome 2BS of Greek durum wheat TRI 1796. *Theor. Appl. Genet.* 134, 53–62. doi: 10.1007/s00122-020-03681-2

He, H. G., Zhu, S. Y., Zhao, R. H., Jiang, Z. N., Ji, Y. Y., Ji, J., et al. (2018). *Pm21*, encoding a typical CC-NBS-LRR protein, confers broad-spectrum resistance to wheat powdery mildew disease. *Mol. Plant* 11, 879–882. doi: 10.1016/j.molp.2018.03.004

Hewitt, T., Muller, M. C., Molnar, I., Mascher, M., and Holušová, K., Šimková, H., et al. (2021). A highly differentiated region of wheat chromosome 7AL encodes a *Pm1a* immune receptor that recognizes its corresponding *AvrPm1a* effector from *Blumeria graminis*. *New Phytol.* 229, 2812–2826. doi: 10.1111/nph.17075

Huang, X. Y., Zhu, M. Q., Zhuang, L. F., Zhang, S. Y., Wang, J. J., Chen, X. J., et al. (2018). Structural chromosome rearrangements and polymorphisms identified in Chinese wheat cultivars by high-resolution multiplex oligonucleotide FISH. *Theor. Appl. Genet.* 131, 1967–1986. doi: 10.1007/s00122-018-3126-2

Klindworth, D. L., Hareland, G. A., Elias, E. M., and Xu, S. S. (2013). Attempted compensation for linkage drag affecting agronomic characteristics of durum wheat 1AS/1DL translocation lines. *Crop Sci.* 53, 422–429. doi: 10.2135/cropsci2012.05.0310

Li, H. H., Dong, Z. J., Ma, C., Tian, X. B., Qi, Z. J., Wu, N., et al. (2019). Physical mapping of stem rust resistance gene *Sr52* from *Dasypyrum villosum* based on *ph1b*-induced homoeologous recombination. *Int. J. Mol. Sci.* 20:4887. doi: 10.3390/ijms20194887

Li, H. H., Dong, Z. J., Ma, C., Xia, Q., Tian, X. B., Sehgal, S., et al. (2020). A spontaneous wheat-*Aegilops longissima* translocation carrying *Pm66* confers resistance to powdery mildew. *Theor. Appl. Genet.* 133, 1149–1159. doi: 10.1007/s00122-020-03538-8

Li, H. H., Tian, X. B., Pei, S. L., Men, W. Q., Ma, C., Sehgal, S., et al. (2021). Development of novel wheat-*Aegilops longissima* 3S^{l} translocations conferring powdery mildew resistance and specific molecular markers for chromosome 3S^{l}. *Plant Dis.* 105, 2938–2945. doi: 10.1094/PDIS-12-20-2691-RE

Li, L. F., Zhang, Z. B., Wang, Z. H., Li, N., Sha, Y., Wang, X. F., et al. (2022). Genome sequences of five Sitopsis species of *Aegilops* and the origin of polyploid wheat B subgenome. *Mol. Plant.* 15, 488–503. doi: 10.1016/j.molp.2021.12.019

Liu, W. X., Chen, P. D., and Liu, D. J. (1999). Development of *Triticum aestivum-Leymus racemosus* translocation lines by irradiating adult plants at meiosis. *Acta. Bot. Sin.* 41, 463–467.

Liu, W. X., Jin, Y., Rouse, M., Friebe, B., Gill, B. S., and Pumphery, M. O. (2011). Development and characterization of wheat-*Ae. searsii* Robertsonian translocations and a recombinant chromosome conferring resistance to stem rust. *Theor. Appl. Genet.* 122, 1537–1545. doi: 10.1007/s00122-011-1553-4

Liu, W. X., Koo, D. H., Friebe, B., and Gill, B. S. (2016). A set of *Triticum aestivum-Aegilops speltoides* Robertsonian translocation lines. *Theor. Appl. Genet.* 129, 2359–2368. doi: 10.1007/s00122-016-2774-3

Liu, W. X., Koo, D. H., Xia, Q., Li, C. X., Bai, F. Q., Song, Y. L., et al. (2017). Homoeologous recombination-based transfer and molecular cytogenetic mapping of powdery mildew-resistant gene *Pm57* from *Aegilops searsii* into wheat. *Theor. Appl. Genet.* 130, 841–848. doi: 10.1007/s00122-017-2855-y

McIntosh, R. A., Dubcovsky, J., Rogers, W. J., Morris, C., and Xia, X. C. (2017). Catalogue of gene symbols for wheat. 2017. *Supplement. Annu. Wheat. Newsl.* 53, 107–128.

Morgounov, A., Tufan, H. A., Sharma, R., Akin, B., Bagci, A., Braun, H. J., et al. (2012). Global incidence of wheat rusts and powdery mildew during 1969-2010

and durability of resistance of winter wheat variety Bezostaya 1. *Eur. J. Plant. Pathol.*132, 323–340. doi: 10.1007/s10658-011-9879-y

Mukai, Y., Friebe, B., Hatchet, J. H., Yamamoto, M., and Gill, B. S. (1993). Molecular cytogentic analysis of radiation-induced wheat-rye terminal and intercalary chromosomal translocations and the detection of rye chromatin specifying resistance to Hessian fly. *Chromosoma* 102, 88–95. doi: 10.1007/BF00356025

Qi, L. L., Friebe, B., Zhang, P., and Gill, B. S. (2007). Homoeologous recombination, chromosome engineering and crop improvement. *Chromosome Res.* 15, 3–19. doi: 10.1007/s10577-006-1108-8

Raupp, W. J., Friebe, B., and Gill, B. S. (1995). Suggested guidelines for the nomenclature and abbreviation of the genetic stocks of wheat, *Triticum aestivum* L. em Thell, and its relatives. *Wheat. Inf. Serv.* 81, 51–55.

Riley, R., Chapman, V., and Johnson, R. (1968). Introduction of yellow rust resistance of *Aegilops comosa* into wheat by genetically induced homoeologous recombination. *Nature* 217, 383–384. doi: 10.1038/217383a0

Sánchez-Martín, J., Widrig, V., Herren, G., Wicker, T., Zbinden, H., Gronnier, J., et al. (2021). Wheat *Pm4* resistance to powdery mildew is controlled by alternative splice variants encoding chimeric proteins. *Nat. Plants.* 7, 327–341. doi: 10.1038/s41477-021-00869-2

Sears, E. (1956). "The transfer of leaf rust resistance from *Aegilops umbellulata* to wheat, gentics in plant breeding," in *Brook-haven Symposia in Biology* (Upton, NY: Brookhaven National Laboratory), 1–22.

Sears, E. (1977). An induced mutant with homoeologous pairing in common wheat. *Can. J. Genet. Cytol.* 19, 585–593. doi: 10.1139/g77-063

Sheng, H. Y., See, D. R., and Murray, T. D. (2012). Mapping QTL for resistance to eyespot of wheat in *Aegilops longissima*. *Theor. Appl. Genet.* 125, 355–366. doi: 10.1007/s00122-012-1838-2

Shi, Q. M., Zhang, X. X., Duan, X. Y., and Sheng, B. Q. (1987). Identification of isolates of *Blumeria graminis* f. sp. *tritici*. *Sci. Agric. Sin.* 20, 64–70.

Tan, C. C., Li, G. Q., Cowger, C., Carver, B. F., and Xu, X. Y. (2019). Characterization of *Pm63*, a powdery mildew resistance gene in Iranian landrace PI 628024. *Theor. Appl. Genet.* 132, 1137–1144. doi: 10.1007/s00122-018-3265-5

Wan, W. T., Xiao, J., Li, M. L., Tang, X., Wen, M. X., Cheruiyot, A. K., et al. (2020). Fine mapping of wheat powdery mildew resistance gene *Pm6* using 2B/2G homoeologous recombinants induced by the *ph1b* mutant. *Theor. Appl. Genet.* 133, 1265–1275. doi: 10.1007/s00122-020-03546-8

Wang, K. Y., Lin, Z. S., Wang, L., Wang, K., Shi, Q. H., Du, L. P., et al. (2018). Development of a set of PCR markers specific to *Aegilops longissima* chromosome arms and application in breeding a translocation line. *Theor. Appl. Genet.* 131, 13–25. doi: 10.1007/s00122-017-2982-5

Wang, X. W., Lai, J. R., Liu, G. T., and Chen, F. (2002). Development of a Scar marker for the *Ph1* locus in common wheat and its application. *Crop Sci.* 42, 1365–1368. doi: 10.2135/cropsci2002.1365

Wang, Z. L., Li, L. H., He, Z. H., Duan, X. Y., Zhou, Y. L., Chen, X. M., et al. (2005). Seedling and adult plant resistance to powdery mildew in Chinese bread wheat cultivars and lines. *Plant Dis.* 89, 457–463. doi: 10.1094/PD-89-0457

Xia, Q., Mai, Y. N., Dong, Z. J., and Liu, W. X. (2018). Identification of powdery mildew resistance resources from wheat-wild relative disomic addition lines and development of molecular markers of alien chromosome-specialty. *J. Henan Agric. Sci.* 47, 64–69. doi: 10.15933/j.cnki.1004-3268.2018.06.012

Xing, L. P., Hu, P., Liu, J. Q., Witek, K., Zhou, S., Xu, J. F., et al. (2018). *Pm21* from *Haynaldia villosa* encodes a CC-NBS-LRR protein conferring powdery mildew resistance in wheat. *Mol. Plant.* 11, 874–878. doi: 10.1016/j.molp.2018.02.013

Yang, H., Zhong, S. F., Chen, C., Yang, H., Chen, W., Tan, F. Q., et al. (2021). Identification and cloning of a CC-NBS-NBS-LRR gene as a candidate of *Pm40* by integrated analysis of both the available transcriptional data and published linkage mapping. *Int. J. Mol. Sci.* 22, 10239. doi: 10.3390/ijms221910239

Yang, S. H., Li, J., Zhang, X. H., Zhang, Q. J., Huang, J., Chen, J. Q., et al. (2013). Rapidly evolving R genes in diverse grass species confer resistance to rice blast disease. *Proc. Natl. Acad. Sci. U. S. A.* 110, 18572–18577. doi: 10.1073/pnas.1318211110

Zhang, J. P., Zhang, P., Hewitt, T., Li, J. B., Dundas, I., Schnippenkoetter, W., et al. (2019). A strategy for identifying markers linked with stem rust resistance in wheat harboring an alien chromosome introgression from a non-sequenced genome. *Theor. Appl. Genet.* 132, 125–135. doi: 10.1007/s00122-018-3201-8

Zhang, R. Q., Xiong, C. X., Mu, H. Q., Yao, R. N., Meng, X. R., Kong, L. N., et al. (2020). *Pm67*, a new powdery mildew resistance gene transferred from *Dasypyrum villosum* chromosome 1V to common wheat (*Triticum aestivum* L.). *Crop J.* 9, 882–888. doi: 10.1016/j.cj.2020.09.012

Zhu, T. T., Wang, L., Rimbert, H., Rodriguez, J. C., Deal, K. R., Oliveira, R. D., et al. (2021). Optical maps refine the bread wheat *Triticum aestivum* cv. *Chinese Spring genome assembly*. *Plant J.* 107, 303–304. doi: 10.1111/tpj.15289

Conflict of Interest: The authors declare that the research was conducted in the absence of any commercial or financial relationships that could be construed as a potential conflict of interest.

Publisher's Note: All claims expressed in this article are solely those of the authors and do not necessarily represent those of their affiliated organizations, or those of the publisher, the editors and the reviewers. Any product that may be evaluated in this article, or claim that may be made by its manufacturer, is not guaranteed or endorsed by the publisher.

frontiers | Frontiers in Plant Science

ORIGINAL RESEARCH
published: 15 June 2022
doi: 10.3389/fpls.2022.931778

$Pm_{SN15218}$: A Potential New Powdery Mildew Resistance Gene on Wheat Chromosome 2AL

Meng Sun†, Qi Liu†, Yi Han, Guojun Liu, Jiajie Wu, Juan Qi, Fei Ni and Yinguang Bao**

State Key Laboratory of Crop Biology, College of Agronomy, Shandong Agricultural University, Tai'an, China

Powdery mildew, caused by *Blumeria graminis* f. sp. *tritici* (*Bgt*), is a devastating fungal disease that seriously damages the yield and quality of wheat in many regions of the world. Identifying new resistance genes and breeding new resistant varieties are effective methods to control this disease. The breeding line SN15218 shows good resistance against powdery mildew. We, therefore, developed an F_2 population and 287 $F_{2:3}$ families crossed between SN15218 and the powdery mildew susceptible cultivar Huixianhong (HXH). Genetic analysis indicated that a single dominant gene, designated herein $Pm_{SN15218}$, conferred resistance to the *Bgt* isolate E09 in SN15218. Bulked segregant RNA-Seq (BSR-Seq) analysis revealed that $Pm_{SN15218}$ is located in a ∼25-Mb interval on chromosome 2AL. Using the polymorphism information between SN15218 and HXH, we developed 13 polymerase chain reaction (PCR) markers and mapped this gene to a 0.5-cM genetic interval between the two flanking markers *PmM12* and *PmM14*, corresponding to a 6.01-Mb physical region in the Chinese Spring reference genome. The results of molecular marker analysis, allelic tests of resistance spectrum, and DNA resequencing indicated that $Pm_{SN15218}$ is distinct from the known resistance gene *Pm4b* on 2AL.

Keywords: wheat, powdery mildew, BSR-Seq, *Pm4* loci, $Pm_{SN15218}$

OPEN ACCESS

Edited by:
Handong Su,
Huazhong Agricultural University, China

Reviewed by:
Haiyan Jia,
Nanjing Agricultural University, China
Liu Dengcai,
Sichuan Agricultural University, China

****Correspondence:***
Fei Ni
nifei1998@sdau.edu.cn
Yinguang Bao
baoyinguang@163.com

†These authors have contributed equally to this work

Specialty section:
This article was submitted to Plant Pathogen Interactions, a section of the journal Frontiers in Plant Science

Received: *29 April 2022*
Accepted: *19 May 2022*
Published: *15 June 2022*

Citation:
Sun M, Liu Q, Han Y, Liu G, Wu J, Qi J, Ni F and Bao Y (2022) $Pm_{SN15218}$: A Potential New Powdery Mildew Resistance Gene on Wheat Chromosome 2AL. Front. Plant Sci. 13:931778. doi: 10.3389/fpls.2022.931778

INTRODUCTION

Wheat (*Triticum aestivum* L.) is an important food crop worldwide, providing about 20% of human calories (Ni et al., 2017). However, wheat quality and yield stability are frequently affected by fungal diseases. For example, powdery mildew caused by *Blumeria graminis* f. sp. *tritici* (*Bgt*), is a devastating wheat foliar disease. In recent decades, powdery mildew has led to severe yield losses of 5–8% during the years of average infection, and as high as 40% in some years, in China and other parts of the world (Singh et al., 2016). In addition to fungicides and other biological agents, the deployment of disease-resistant cultivars is the most economical and environmentally friendly method for managing this foliar disease (Fu et al., 2013; Qie et al., 2019). However, because frequent changes in pathogen populations often overcome the effects of available resistance genes (Yu et al., 2018), most reported powdery mildew resistance genes in wheat are race-specific and susceptible to resistance loss once they are widely deployed in commonly planted cultivars. Therefore, it is necessary for breeders to discover additional sources of powdery mildew resistance genes in breeding programs.

At present, more than 100 powdery mildew-resistance genes or alleles mapping to 63 different loci (*Pm1–Pm68*, *Pm18*/*Pm1c*, *Pm22*/*Pm1e*, *Pm23*/*Pm4c*, *Pm31*/*Pm21*, *Pm48*/*Pm46*, and *Pm17*/*Pm8*) have been reported, with the loci *Pm1*, *Pm3*, *Pm4*, *Pm5*, and *Pm24* having 5, 17, 8, 5, and 2 alleles, respectively (Li et al., 2020; McIntosh et al., 2020; He et al., 2021; Zhang et al., 2021; Wu et al., 2022). These include five resistance alleles, *Pm4a–Pm4e*, reported at the locus *Pm4*, located on the long arm of chromosome 2A. *Pm4a* was first identified in the emmer wheat cultivar Khapli and the durum wheat cultivar Yuma and was linked to marker *Xgwm356* (Ma et al., 2004). *Pm4b* was derived from the French common wheat cultivar VPM1, a lineage derived from a cross between *Aegilops ventricosa*, *Triticum turgidum* var. *carthlicum* (*Triticum persicum*), and the common wheat variety Marne (Bariana and McIntosh, 1994), and has been mapped to a 3.0-cM genetic interval between flanking markers *Xics43* and *Xics13* in chromosome 2AL (Wu et al., 2018). Over time, wheat cultivars carrying *Pm4a* have gradually lost resistance to powdery mildew in many countries and regions, such as the United States, the Middle East, and China, while *Pm4b*, which was identified over 30 years ago, still provides effective resistance in parts of China and the United States (El-Shamy et al., 2016; Cowger et al., 2017; Wu et al., 2018). *Pm4c* (also called *Pm23*) comes from the common wheat line 81-7241, which exhibits high resistance to powdery mildew and has a broad resistance spectrum. *Pm4c* is located at a 4.9-cM genetic interval between *Xbarc122* and *Xgwm356* on chromosome 2AL (Hao et al., 2008). *Pm4d* and *Pm4e* were identified from the common wheat introgression line Tm27d2, which inherited its resistance from the *Triticum monococcum* accession Tm27 and the Chinese landrace D29, respectively. *Pm4d* was mapped to a 6.7-cM genetic interval, while *Pm4e* was precisely mapped to a 0.19-cM interval corresponding to a 360-kb physical region (Schmolke et al., 2012; Ullah et al., 2018). Recently, researchers successfully cloned the *Pm4a-Fed* and *Pm4b-Fed* genes by sequencing related mutants from the wheat lines Fed-Pm4a and Fed-Pm4b (Fed refers to the common wheat cultivar "Federation"), respectively, and identified multiple resistant or susceptible haplotypes of *Pm4-Fed* simultaneously (Sánchez-Martín et al., 2021).

Novel powdery mildew resistance genes identified from modern cultivars are easier to use in breeding than those from wheat relatives or wild species. However, the powdery mildew resistance genes so far identified are almost from landraces or wild relatives and often have adverse factors or linkage drag of undesirable genes. Only a few, such as *Pm2a*, *Pm4a*, *Pm6*, *Pm8*, and *Pm21*, originated from modern cultivars and can be directly used in breeding programs (Qie et al., 2019). Moreover, of the 18 resistance genes (*Pm51–Pm68*) newly identified in recent years, only *Pm52*, *Pm54*, and *Pm65* originated from adapted cultivars (Liangxing99, Pioneer 26R61, and Xinmai208, respectively) (Zhao et al., 2013; Hao et al., 2015; Li et al., 2019; He et al., 2021; Zhang et al., 2021).

SN15218 is derived from a natural mutant plant of the cultivar Yannong 19 (YN19) in the seed production field. It shows a high level of resistance to powdery mildew at both seedling and adult stages, suggesting that it harbors a powdery mildew resistance gene that could be valuable for wheat breeding. In this study, we characterized the resistance gene in SN15218, temporarily named $Pm_{SN15218}$, through genetic analysis, molecular mapping, spectrum analysis, and allelic relationship comparison.

MATERIALS AND METHODS

Plant Materials

The materials used in this study included the winter wheat cultivars YN19 and Huixianhong (HXH) and powdery mildew resistant line, SN15218. YN19 and HXH are widely planted commercial cultivars and are susceptible to most *Bgt* isolates. SN15218 is a breeding line with a YN19 background. It is similar to common wheat and shows resistance to many powdery mildew races. To analyze the inheritance of powdery mildew resistance, SN15218 was crossed with HXH to construct a segregating population, and F_1, F_2, and $F_{2:3}$ materials were tested for resistance to the *Bgt* isolate E09, which is avirulent on SN15218 but virulent on HXH.

Tests of Powdery Mildew Resistance

SN15218, HXH, and their F_1 hybrids, F_2 populations, and $F_{2:3}$ families (25 seedlings for each line), as well as YN19 as a susceptible control, were tested for powdery mildew resistance using the *Bgt* isolate E09. Meanwhile, 23 single-spore-derived *Bgt* isolates and several wheat lines carrying known *Pm* genes were grown in a greenhouse at the Institute of Plant Protection, Chinese Academy of Agricultural Sciences, Beijing, to compare the reaction patterns of SN15218 and the other wheat lines with the different *Bgt* isolates. At the two-leaf stage, seedlings were inoculated with fresh spores and then transferred to a plant growth chamber at 15–18°C with 60% relative humidity and a 12 h light/12 h dark cycle to allow symptom development. Two weeks after the susceptible control materials HXH and YN19 were heavily infected, the plants were scored into infection types (ITs) according to a 0–4 scale (Tan et al., 2018). We classified the plants into two groups: resistant (R, IT = 0–2) and susceptible (S, IT = 3–4). Observed and expected segregation ratios were compared using the Chi-squared (χ^2) test for goodness of fit.

Bulked Segregant RNA-Seq Analysis

The $F_{2:3}$ families with contrasting resistance phenotypes against isolate *Bgt* E09 (30 homozygous resistant and 30 susceptible families) were used to construct sample pools. Leaves of similar quality were collected from five plants of each family. Resistant and susceptible leaves were pooled for RNA isolation. Two parents, SN15218 and HXH, were also processed as parental checks. Total RNA was extracted using TRIzol reagent (Tiangen Biotech Co., Beijing, China) according to the manufacturer's protocol. Library construction, high-throughput sequencing (Illumina NovaSeq 6000), and sequencing data qualification were performed by Berry Genomics Company (Beijing, China). Adapter sequences and low-quality bases were trimmed using fastp v0.19 with default paraments (Chen et al., 2018). High-quality reads were mapped to the Chinese Spring reference

TABLE 1 | Information of bulked segregant RNA-Seq (BSR-Seq) data.

Samples	Clean pairs	Clean bases (bp)	Read length (bp)	Mapping ratio (%)	Unique mapping ratio (%)	Note
Y2763	61,990,264	18,597,079,200	150	83.8	80.3	Resist parent SN15218
Y2764	62,628,016	18,788,404,800	150	83.6	79.9	Susceptible parent HXH
Y2765	63,695,851	19,108,755,300	150	85.9	81.9	Resistant pool
Y2766	58,922,100	17,676,630,000	150	84.0	80.1	Susceptible pool
Total	247,236,231	74,170,869,300	150	84.3	80.6	–

genome, RefSeq V1.0 (International Wheat Genome Sequencing Consortium, IWGSC), using Hisat2 v2.1.0 (Kim et al., 2019). Variant calling was performed using the HaplotypeCaller module in the GATK v3.8 toolkit (Poplin et al., 2018). Single-nucleotide polymorphism (SNP) filtration, sliding window analysis, and SNP-index plotting were conducted following a previously described protocol (Takagi et al., 2013). We excluded SNPs with read depth <5 from resistant and susceptible pools and two parent samples. SNP index values in the two pools were calculated using a custom perl script with SNPs of susceptible parent HXH as the reference, and the Δ(SNP-index) = (SNP-index of the resistant pool) − (SNP-index of the susceptible pool) was calculated for each SNP. Sliding window analysis was applied to ΔSNP-index plots with 1-Mb window size and 10-kb increment, and the average ΔSNP-index of SNPs was used for the sliding window plot (Takagi et al., 2013).

Genotyping and Linkage Analysis

Leaf tissue was collected from 2-week-old plants, and total genomic DNA was extracted using the cetyltrimethylammonium bromide (CTAB) method (Porebski et al., 1997). According to the variants data from bulked segregant RNA-Seq (BSR-Seq) analysis, four polymerase chain reaction (PCR) markers were developed based on SNPs (**Table 1**). These markers were used to genotype the 285 F_2 plants crossed with SN15218 and HXH and confirm the mapping result of BSR-Seq data. To develop more PCR markers, DNA resequencing and variants calling with two parents, SN15218 and HXH, were performed. The method of variant calling was similar to that described above for BSR-Seq, except that BWA v0.7.17[1] was used instead of Hisat2 for mapping. Based on DNA resequencing data and the Chinese Spring RefSeq v1.0 reference map, seven insertion/deletion (InDel) markers were newly developed (**Table 1**) for further genotyping. χ^2 tests of the F_2 and $F_{2:3}$ populations were used to evaluate the goodness of fit between observed data and expected segregation ratios. A genetic linkage map was constructed using the software JoinMap 4.0.[2] The recombination values were converted to genetic distance (cM) using the Kosambi mapping function.

De novo Assembly

DNA resequencing reads of the powdery mildew resistant line SN15218 were first aligned to the *Triticeae* repeat database mipsREdat 9.3p (PGSB Repeat Database) using BWA-mem v0.7.17 in order to filter out repeat noises. Non-mapped reads (which come from the genome region of non-repeat sequences) were fished using Samtools v1.9[3] and then used for *de novo* assembly using SPAdes v3.13[4] with default parameters.

[1] https://github.com/lh3/bwa

[2] https://www.kyazma.nl

RESULTS

SN15218 Powdery Mildew Resistance Is a Monogenic Inherited Trait

When inoculated with *Bgt* isolate E09, SN15218 was highly resistant (IT = 0) and HXH was highly susceptible to the fungus (IT = 4) (**Figure 1**). F_1 plants of SN15218 × HXH showed the same resistant phenotype as the parent SN15218, indicating the dominance of the powdery mildew resistance of SN15218. In the F_2 population, 216 individuals showed resistance (IT = 0–2) and 69 individuals showed susceptibility (IT = 3–4), indicating segregation of a single resistance gene ($\chi^2_{3:1} = 0.09$, $P_{1df} > 0.05$). All the 285 $F_{2:3}$ families derived from these two parents were also tested using the same *Bgt* isolate E09 in the climate chamber at the seedling stage. A total of 82 and 69 families were homozygous-resistant and homozygous-susceptible, respectively, and the remaining 134 families were segregated, confirming that

[3] http://www.htslib.org

[4] https://github.com/ablab/spades

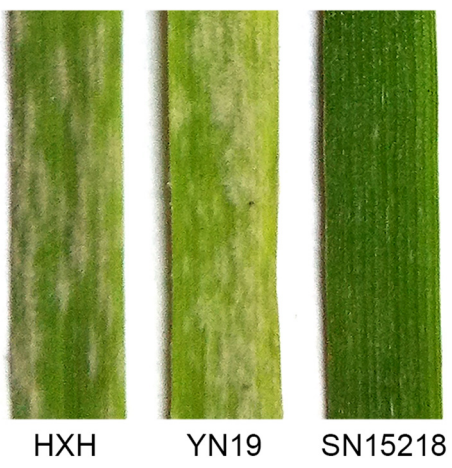

FIGURE 1 | Powdery mildew infection of seedling from susceptible materials Huixianhong (HXH), Yannong 19 (YN19), and resistant parent SN15218 at 15 dpi inoculated with *Blumeria graminis* f. sp. *tritici* (*Bgt*) isolate E09.

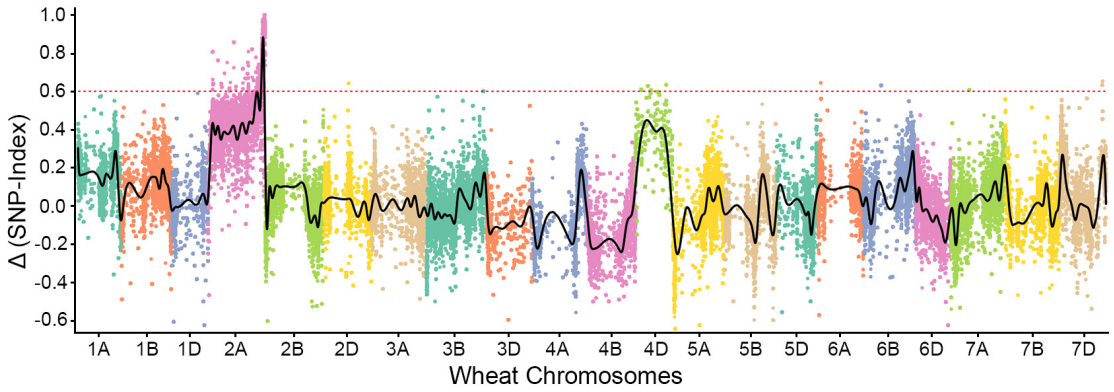

FIGURE 2 | Bulked segregant RNA-Seq (BSR-Seq) analysis of $Pm_{SN15218}$. $Pm_{SN15218}$ was localized at the distal end of the long arm of chromosome 2A.

TABLE 2 | Markers developed in this study.

Markers	Forward primer (5′ → 3′)	Reverse primer (5′ → 3′)	Tm (°)	Type[a]	Enz.[b]	Ploymorphic bands (bp)[c]
PmM1	GTGATGCTCGTATAACGCTTTCC	GTGGCTGCAATCATCAGCCTACC	60	CAPS	*Bsr*I	H (299); SN (248 + 51)
PmM4	TGCATGGAGTGCATCACCTAC	GATTTAGTTCTGTACTCATGAGTTG	60	CAPS	*Sty*I	H (233); SN (147 + 86)
PmM5	ACCCCAGCAAAACACGGAACAT	GCAAAAGGGGAATTGGGCCAT	60	CAPS	*Scr*FI	H (135 + 60); SN (195)
PmM6	TCATACTATGTGCTCAGCCAGA	AAGGAAGCGCAGCCTCGTGGT	58	InDel	–	H (234); SN (240)
PmM7	TGCAGAGGAAAATAGAGAATCAGGC	CATCGGTGGGTGCTGTTCCAT	54	dCSPS	*Nde*I	H (215); SN (193 + 22)
PmM8	GTGTAATTAGTGAGGTTGCTATAGC	CTACGCCGAAAGAATGTTCCTAC	58	InDel	–	H (371); SN (348)
PmM9	ACTCGGCGCACAGTCTGCTAT	GCCTCACGACATGGCTGGAT	58	InDel	–	H (178); SN (192)
PmM12	GGAGATACTCAAAGCAAAGCAAC	GTGCTACAAAGTGGGGAAATAATC	58	InDel	–	H (209); SN (226)
PmM13	GTCAGCTATCAGGACGAAATCGC	ACTCCTCAGTGCGTATTGCTG	58	InDel	–	H (185); SN (203)
PmM14	CCAAACCACAGCAACAGCCT	GGGATGATTAATTGGACGATCGA	58	InDel	–	H (155); SN (174)
PmM15	AAGATGGGCGCCGGGTAATG	GTCCTCAGAGCAAAATACTTCC	58	InDel	–	H (178); SN (199)
PmM16	GGGTATTCTGGTCATTTCTCGT	TAAGCGCCAGATAGGAGGC	58	InDel	–	H (203); SN (219)

[a] *Cleavage amplification polymorphism sequence (CAPS), degenerate cleavage amplification polymorphism sequence (dCAPS), insertion/deletion (InDel).*
[b] *Restriction enzymes (Enz.) used to digest the PCR product.*
[c] *Numbers within parentheses represent the size of diagnostic bands in HXH (H) and SN15218 (SN).*

the powdery mildew resistance of SN15218 was inherited as a single gene ($\chi^2_{1:2:1} = 2.2$, $P_{2df} > 0.05$). We temporarily named this resistance gene $Pm_{SN15218}$.

$Pm_{SN15218}$ Gene Is Localized on Chromosome 2AL

We sequenced the two parents (SN15218 and HXH) and two resistant and susceptible descendant pools in 150-bp paired-end mode, generating 58.9–63.7 million clean paired reads; the average read depth was more than 60 for each SNP after filtration (**Table 1**). Approximately, 84.3% of the clean reads from each parent or pool could be mapped to the reference, and 80.6% of them were uniquely mapped and used for variant calling. We identified 46,895 high-quality homozygous SNPs between the two parents. Meanwhile, there were 1,027 and 1,791 homozygous SNPs in the resistant and susceptible pools, respectively, most of which were located on chromosome 2A (255 SNPs in the resistant pool, 645 SNPs in the susceptible pool). Only a single sharp peak (ΔSNP-index > 0.8) was identified on the long arm of wheat chromosome 2A, and these SNPs were enriched in a ∼25-Mb interval (Chr2A: Mb 751-776) (**Figure 2**), suggesting that the powdery mildew resistance gene of SN15218 was located on chromosome 2AL.

$Pm_{SN15218}$ Maps to a 0.5-cM Genetic Interval

In the ∼25-Mb target region, we dispersedly selected five co-segregating SNPs/InDels identified from BSR-Seq data and converted them into cleaved amplified polymorphic sequences (CAPSs)/derived cleaved amplified polymorphic sequences (dCAPSs) markers (*PmM1*, *PmM4*, *PmM5*, and *PmM7*) or an InDel marker (*PmM6*) (**Table 2**). Using 90 F_2 plants from the offspring of hybridization between SNP15218 and HXH, we genotyped these five markers and found that they were all closely linked to $Pm_{SN15218}$, which confirmed the preliminary BSR-Seq mapping result. Based on DNA resequencing data, 6,172 SNPs/InDels were called in the ∼25-Mb target region, including 67 InDel sites larger than 10 bp between the 2 parents. We further created seven new InDel markers (**Table 2**) using the polymorphic information and reference data of Chinese Spring RefSeq v1.0 and mapped $Pm_{SN15218}$ to the 0.5-cM *PmM12–PmM14* interval using 287 F_2 plants, which

corresponded to a 6.01-Mb physical region (chr2A: Mb 764.093–770.104) (**Figure 3**).

Resistance Spectra

In addition to $Pm_{SN15218}$ from SN15218, several powdery mildew resistance genes, *Pm4a*, *Pm4b*, and *Pm4c*, that were previously identified from different wheat varieties or lines (Khapli, Armada, and 81-7241, respectively) were also mapped on chromosome 2AL. We evaluated the disease reactions of SN15218 and the above resistant landraces to 23 *Bgt* isolates. Line 81-7241, carrying *Pm4c*, showed high resistance to all of the isolates. Khapli, carrying *Pm4a*, showed resistance to most powdery mildew isolates but was susceptible to seven isolates. Armada, carrying *Pm4b*, showed a similar resistance spectrum to Khapli except for two isolates, E05 and E15 (**Table 3**). Line SN15218 exhibited better resistance than Khapli and Armada and was susceptible to only four *Bgt* isolates, E18, E20, E31, and E32 (**Table 3**). The results demonstrated that the resistance spectrum of $Pm_{SN15218}$ was distinct from that of *Pm4a*, *Pm4b*, or *Pm4c*.

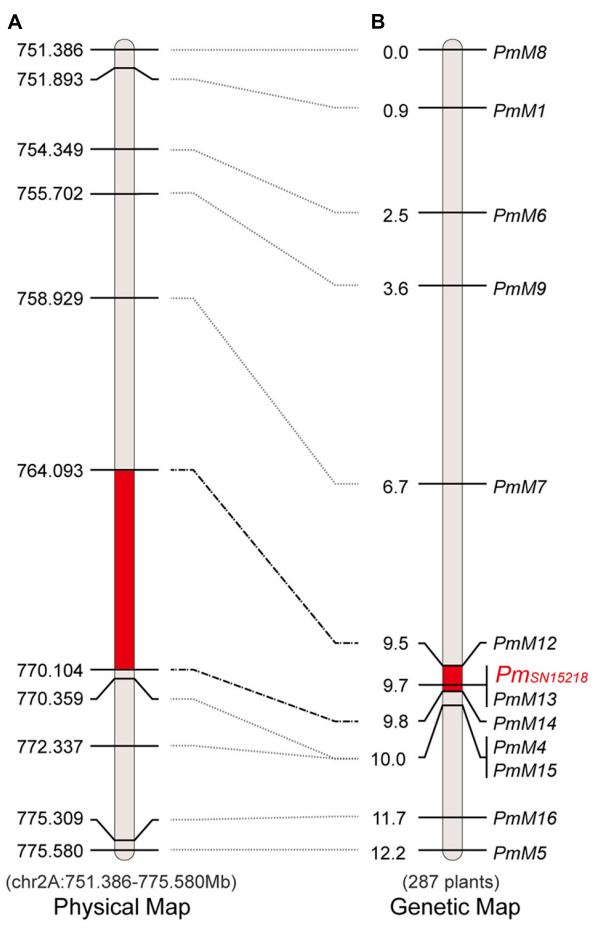

FIGURE 3 | Physical and genetic map of $Pm_{SN15218}$ region. **(A)** Physical map of chromosome 2AL 751.4–775.6 Mb. **(B)** The precision genetic map with 287 F_2 individuals. The map units were physical positions (Mb) or centimorgan (cM) that was labeled on the left sides of the map.

Allelic Relationship

To compare the physical locations of *Pm* genes at the *Pm4* locus, including *Pm4a* (Hao et al., 2008; Fu et al., 2013), *Pm4b-Fed* (Sánchez-Martín et al., 2021), *Pm4c* (*Pm23*) (Hao et al., 2008), *Pm4d* (Schmolke et al., 2012), *Pm4e* (Ullah et al., 2018), *Pm65* (Li et al., 2019), and $Pm_{SN15218}$, we integrated these tightly linked markers into chromosome 2AL of the Chinese Spring reference genome (IWGSC RefSeq v1.0) (**Supplementary Table 1**). These seven genes were located at the same physical interval: *Pm4a* was 4.8cM from marker *Xgwm365*, which was located in a region around Mb 762 of chromosome 2A; *Pm4b-Fed*, *Pm4c* (*Pm23*), *Pm4d*, *Pm4e*, *Pm65*, and $Pm_{SN15218}$ were located in the physical interval of Mb 760–770. Among them, the *Pm4b-Fed* gene, originating from tetraploid *T. carthlicum*, is not in the "Chinese Spring" genome reference but is most closely related to the gene *TraesCS2A01G557900* near Mb 761 of chromosome 2AL, the ancestor of which was duplicated and fused to form the kinase structural domain of *Pm4b-Fed* (Sánchez-Martín et al., 2021). To further confirm the relationship between $Pm_{SN15218}$ and *Pm4b-Fed*, we performed a PCR assay using three *Pm4*-specific PCR markers, *JS717* × *JS718*, *Pm4.1*, and *Pm4b-Fed-S* (newly developed in this study), and the results showed that SN15218 did not contain *Pm4*. We also performed *de novo* assembly using DNA resequencing data of SN15218 and found no *Pm4b-Fed* gene or fragment in the assembly database. In addition, we compared five other *Pm* genes, *PmX* (Fu et al., 2013), *PmLK906* (Niu et al., 2008), *PmPS5A* (Niu et al., 2010), *PmMl92145E8-9* (Yu et al., 2018), and *PmXMM* (Yao et al., 2022), which were also located on chromosome 2AL (**Supplementary Table 1**). Three of these, *PmX*, *PmLK906*, and *PmPS5A*, shared similar physical locations with $Pm_{SN15218}$, but *PmMl92145E8-9* and *PmXMM* were located in the proximal region of the *Pm4* locus.

DISCUSSION

Powdery mildew is a widespread fungal disease of wheat, which can infect wheat at both the seedling stage and adult stage and causes significant yield losses. Loss of resistance in wheat cultivars caused by the rapid evolution of this pathogenic fungus has prompted a continuing search for new sources of resistance. Here, we identified a single dominant resistance gene ($Pm_{SN15218}$) near the *Pm4* loci derived from the resistant mutant SN15218 through genetic analysis, molecular mapping, resistance spectrum investigation, and allelic relationship analysis. We tested different wheat genotypes against 23 *Bgt* isolates. The SN15218, carrying $Pm_{SN15218}$, displayed a different resistance pattern from wheat carrying *Pm4a*, *Pm4b*, or *Pm4c*. SN15218 was highly resistant to powdery mildew in fields and has the genetic background of common wheat. Therefore, it could serve as a good intermediate material for powdery mildew resistance breeding.

The $Pm_{SN15218}$ was mapped to a 0.5-cM genetic interval flanked by markers *PmM12* and *PmM14*, responding to the physical region of Mb 764.1–770.1 on chromosome 2A in the Chinese Spring RefSeq V1.0. One hundred and twenty-three genes were annotated in this region. Among them, 12 encode for NBS-LRR-like resistance proteins or disease-resistance proteins,

TABLE 3 | Resistance spectra of $Pm_{SN15218}$ and different *Pm4* genes.

Lines	Genes	*Bgt* isolates																					
		E01	E02	E05	E06	E07	E09	E11	E13	E15	E16	E17	E18	E20	E21	E23	E26	E30	E31	E32	E49	E50	E60	E69
Khapli	*Pm4a*	1 + 0;	0	0	0	4	0;	0	0	3	0	1	4	4	0;	0	0	3	4	4	0;	0	0	0
Armada	*Pm4b*	0;	0;	3 + 0;	0	4	0;	2 + 0;	0;	0;	0;	0;	3	3	0;	0;	0;	3	4	3	0	0	1 + 0;	0
81-7241	*Pm4c*	0;	0	0;	0;	0	0;	0	0	0;	0;	0;	0	1 + 0;	0;	0;	0;	0	0;	0	0;	0	0	0
SN15218	$Pm_{SN15218}$	0;	0;	0;	0;	0	0	0	0;	0;	0;	0	4	4	0	0;	0	1	4	4	0;	0	0;	0;

"0" and "0;" represent immune and near-immune, respectively.

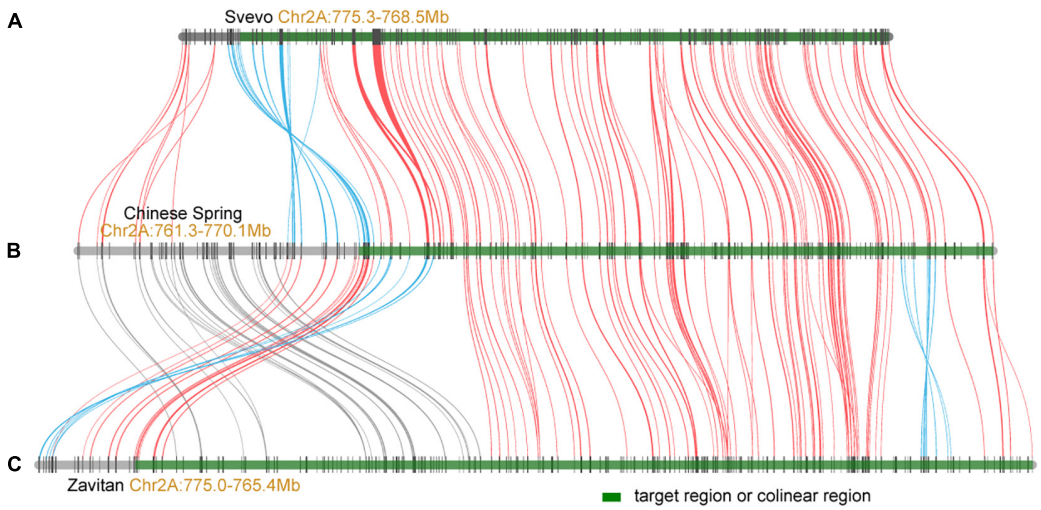

FIGURE 4 | Collinearity of $Pm_{SN15218}$ region between durum wheat Svevo **(A)**, common wheat Chinese Spring **(B)**, and wild emmer wheat Zavitan **(C)**. The green regions represent the colinear intervals of $Pm_{SN15218}$ gene.

and 11 encode for receptor-like kinases or protein kinases. Comparative genomics analysis indicated that most genes in the $Pm_{SN15218}$ region were conserved between the common wheat Chinese Spring (IWGSC), wild emmer wheat Zavitan (Avni et al., 2017), and durum wheat Seveo (Maccaferri et al., 2019; **Figure 4**). However, there were some inversions between Chinese Spring and Svevo or Zavitan and small chromosome fragment translocations between Chinese Spring and Zavitan in the upstream flanking region at the proximal side (**Figure 4**). These results indicate that the colinear genes located upstream of the target region should be considered when filtering candidate genes. In addition, more molecular markers and a larger segregation population need to be developed to enable further fine mapping and cloning of $Pm_{SN15218}$.

The *Pm4* loci for powdery mildew resistance in wheat are complex, and much research has focused on its localization, cloning, and breeding applications. Previous studies have shown that *Pm4b* is localized in the physical interval of Mb 771.887–779.732 on chromosome 2A (Wu et al., 2018; **Supplementary Table 1**). However, Sánchez-Martín et al. (2021) cloned the *Pm4b-Fed* gene from the wheat cultivar Federation using the MutChromSeq approach, and their analysis revealed that this gene was localized near Mb 761 on chromosome 2A. *Pm4b* is derived from the French cultivar VPM1, and VPM1 drives from a cross between *A. ventricosa*, *T. turgidum* var. *carthlicum*, and the common wheat (*T. aestivum*) variety Marne (Bariana and McIntosh, 1994). It was introduced to China from Europe in the 1980s for genetic improvement of wheat disease resistance breeding. *Pm4b-Fed* is derived from three wheat lines, Weihenstephan M1, ELS, and TP229, and was first named *Mle*, which was identified as an allele of *Pm4a* and then transferred to the Australian spring wheat variety Federation by backcrossing (Briggle, 1966; Wolfe, 1967; McIntosh and Bennett, 1979). Since the two genes have different donors, the contradictory localization results could be due to ectopic recombination that occurred during transfer to the common wheat background. To determine the allelic relationship of $Pm_{SN15218}$ and *Pm4b-Fed*, we tested *JS717* × *JS718* and *Pm4.1*, two specific markers for *Pm4b-Fed* (Sánchez-Martín et al., 2021; Yao et al., 2022), and a newly developed marker, *Pm4b-Fed-S* (**Supplementary Table 1**), and found that this gene was not present in HXH, YN19, or SN15218. In addition, we analyzed the closely linked markers of other *Pm* genes, including *PmX*, *Pm65*, *PmLK906*, *PmPS5A*, and *PmMl92145E8-9*, on chromosome 2AL using *in silico* PCR (**Supplementary Table 2**). These markers are either undetectable or differ in product size in the *de novo* assembly database of SN15218. Combining the results of the genetic map, resistance spectra, allelic relationship, and DNA resequencing data, we

speculate that $Pm_{SN15218}$ may be a potential new powdery mildew resistance gene, distinct from *Pm4*, on chromosome 2AL.

CONCLUSION

Herein, we identified a wheat powdery mildew resistance gene, $Pm_{SN15218}$, located on chromosome 2AL. It is distinct from the previously cloned *Pm4b*. This gene was derived from the breeding line SN15218 and could serve as a valuable genetic resource for wheat powdery mildew resistance breeding without any adverse factors or linkage drag of undesirable genes.

DATA AVAILABILITY STATEMENT

The original contributions presented in this study are included in the article/**Supplementary Material**, further inquiries can be directed to the corresponding authors.

AUTHOR CONTRIBUTIONS

YB, FN, and JW designed the project. MS, QL, YH, GL, and JQ performed the experiments. YB, FN, and JQ analyzed the data and wrote the manuscript. All authors discussed the results and reviewed the manuscript.

FUNDING

This research was funded by the Key R&D Program of Shandong Province (Major Science and Technology Innovation Project 2021LZGC009) and the Shandong Provincial Scientific Innovation Project for Young Scholars of Universities (2019KJF026).

SUPPLEMENTARY MATERIAL

The Supplementary Material for this article can be found online at: https://www.frontiersin.org/articles/10.3389/fpls.2022.931778/full#supplementary-material

Supplementary Table 1 | Closely linked markers for several reported powdery mildew resistance genes on chromosome 2AL.

Supplementary Table 2 | *In silico* polymerase chain reaction (PCR) analysis of selected powdery mildew resistance genes on chromosome 2AL.

REFERENCES

Avni, R., Nave, M., Barad, O., Baruch, K., Twardziok, S. O., Gundlach, H., et al. (2017). Wild emmer genome architecture and diversity elucidate wheat evolution and domestication. *Science* 357, 93–97. doi: 10.1126/science.aan0032

Bariana, H., and McIntosh, R. (1994). Characterisation and origin of rust and powdery mildew resistance genes in VPM1 wheat. *Euphytica* 76, 53–61.

Briggle, L. W. (1966). Transfer of resistance to *Erysiphe graminis* f. sp. tritici from khapli emmer and yuma durum to hexaploid wheat. *Crop Sci.* 6:crosci1966.

Chen, S., Zhou, Y., Chen, Y., and Gu, J. (2018). fastp: an ultra-fast all-in-one FASTQ preprocessor. *Bioinformatics* 34, i884–i890. doi: 10.1093/bioinformatics/bty560

Cowger, C., Mehra, L., Arellano, C., Meyers, E., and Murphy, J. P. (2017). Virulence differences in *Blumeria graminis* f. sp. tritici from the central and eastern united states. *Phytopathology* 108, 402–411. doi: 10.1094/PHYTO-06-17-0211-R

El-Shamy, M. M., Emara, H. M., and Mohamed, M. E. (2016). Virulence analysis of wheat powdery Mildew (*Blumeria graminis* f. sp. tritici) and effective genes in middle delta, egypt. *Plant Dis.* 100, 1927–1930.

Fu, B., Chen, Y., Li, N., Ma, H., Kong, Z., Zhang, L., et al. (2013). pmX: a recessive powdery mildew resistance gene at the Pm4 locus identified in wheat landrace *Xiaohongpi*. *Theor. Appl. Genet.* 126, 913–921. doi: 10.1007/s00122-012-2025-1

Hao, Y., Liu, A., Wang, Y., Feng, D., Gao, J., Li, X., et al. (2008). Pm23: a new allele of Pm4 located on chromosome 2AL in wheat. *Theor. Appl. Genet.* 117, 1205–1212. doi: 10.1007/s00122-008-0827-y

Hao, Y., Parks, R., Cowger, C., Chen, Z., Wang, Y., Bland, D., et al. (2015). Molecular characterization of a new powdery mildew resistance gene Pm54 in soft red winter wheat. *Theor. Appl. Genet.* 128, 465–476. doi: 10.1007/s00122-014-2445-1

He, H., Liu, R., Ma, P., Du, H., Zhang, H., Wu, Q., et al. (2021). Characterization of Pm68, a new powdery mildew resistance gene on chromosome 2BS of Greek durum wheat TRI 1796. *Theor. Appl. Genet.* 134, 53–62. doi: 10.1007/s00122-020-03681-2

Kim, D., Paggi, J. M., Park, C., Bennett, C., and Salzberg, S. L. (2019). Graph-based genome alignment and genotyping with HISAT2 and HISAT-genotype. *Nat. Biotechnol.* 37, 907–915. doi: 10.1038/s41587-019-0201-4

Li, G., Cowger, C., Wang, X., Carver, B. F., and Xu, X. (2019). Characterization of Pm65, a new powdery mildew resistance gene on chromosome 2AL of a facultative wheat cultivar. *Theor. Appl. Genet.* 132, 2625–2632. doi: 10.1007/s00122-019-03377-2

Li, H., Dong, Z., Ma, C., Xia, Q., Tian, X., Sehgal, S., et al. (2020). A spontaneous wheat-*Aegilops longissima* translocation carrying Pm66 confers resistance to powdery mildew. *Theor. Appl. Genet.* 133, 1149–1159. doi: 10.1007/s00122-020-03538-8

Ma, Z., Wei, J., and Cheng, S. (2004). PCR-based markers for the powdery mildew resistance gene Pm4a in wheat. *Theor. Appl. Genet.* 109, 140–145. doi: 10.1007/s00122-004-1605-0

Maccaferri, M., Harris, N. S., Twardziok, S. O., Pasam, R. K., Gundlach, H., Spannagl, M., et al. (2019). Durum wheat genome highlights past domestication signatures and future improvement targets. *Nat. Genet.* 51, 885–895. doi: 10.1038/s41588-019-0381-3

McIntosh, R., and Bennett, F. G. (1979). Cytogenetical studies in wheat. IX. monosomic analyses, telocentric mapping and linkage relationships of genes Sr21, Pm4 and Mle. *Austr. J. Biol. Sci.* 32, 115–126.

McIntosh, R., Dubcovsky, J., Rogers, J. W., Xia, X., and Raupp, W. (2020). *Catalogue of Gene Symbols for Wheat*. Available online at: https://wheat.pw.usda.gov/GG3/WGC (accessed December 31, 2021).

Ni, F., Qi, J., Hao, Q., Lyu, B., Luo, M. C., Wang, Y., et al. (2017). Wheat Ms2 encodes for an orphan protein that confers male sterility in grass species. *Nat. Commun.* 8:15121. doi: 10.1038/ncomms15121

Niu, J., Jia, H., Yin, J., Wang, B., Ma, Z., and Shen, T. (2010). Development of an STS marker linked to powdery mildew resistance genes PmLK906 and Pm4a by gene chip hybridization. *Agric. Sci. China* 9, 331–336.

Niu, J. S., Wang, B. Q., Wang, Y. H., Cao, A. Z., Qi, Z. J., and Shen, T. M. (2008). Chromosome location and microsatellite markers linked to a powdery mildew resistance gene in wheat line 'Lankao 90(6)'. *Plant Breed.* 127, 346–349.

Poplin, R., Ruano-Rubio, V., Depristo, M. A., Fennell, T. J., Carneiro, M. O., Van Der Auwera, G. A., et al. (2018). Scaling accurate genetic variant discovery to tens of thousands of samples. *bioRxiv* [Perprint]. bioRxiv, 201178,

Porebski, S., Bailey, L. G., and Baum, B. R. (1997). Modification of a CTAB DNA extraction protocol for plants containing high polysaccharide and polyphenol components. *Plant Mol. Biol. Rep.* 15, 8–15.

Qie, Y., Sheng, Y., Xu, H., Jin, Y., Ma, F., Li, L., et al. (2019). Identification of a new powdery mildew resistance gene pmDHT at or closely linked to the Pm5 locus in the Chinese wheat landrace dahongtou. *Plant Dis.* 103, 2645–2651. doi: 10.1094/PDIS-02-19-0401-RE

Sánchez-Martín, J., Widrig, V., Herren, G., Wicker, T., Zbinden, H., Gronnier, J., et al. (2021). Wheat Pm4 resistance to powdery mildew is controlled by

alternative splice variants encoding chimeric proteins. *Nat. Plants* 7, 327–341. doi: 10.1038/s41477-021-00869-2

Schmolke, M., Mohler, V., Hartl, L., Zeller, F. J., and Hsam, S. L. K. (2012). A new powdery mildew resistance allele at the Pm4 wheat locus transferred from einkorn (*Triticum monococcum*). *Mol. Breed.* 29, 449–456.

Singh, R. P., Singh, P. K., Rutkoski, J., Hodson, D. P., He, X., Jørgensen, L. N., et al. (2016). Disease impact on wheat yield potential and prospects of genetic control. *Ann. Rev. Phytopathol.* 54, 303–322. doi: 10.1146/annurev-phyto-080615-095835

Takagi, H., Abe, A., Yoshida, K., Kosugi, S., Natsume, S., Mitsuoka, C., et al. (2013). QTL-seq: rapid mapping of quantitative trait loci in rice by whole genome resequencing of DNA from two bulked populations. *Plant J.* 74, 174–183. doi: 10.1111/tpj.12105

Tan, C., Li, G., Cowger, C., Carver, B. F., and Xu, X. (2018). Characterization of Pm59, a novel powdery mildew resistance gene in afghanistan wheat landrace PI 181356. *Theor. Appl. Genet.* 131, 1145–1152. doi: 10.1007/s00122-018-3067-9

Ullah, K. N., Li, N., Shen, T., Wang, P., Tang, W., Ma, S., et al. (2018). Fine mapping of powdery mildew resistance gene Pm4e in bread wheat (*Triticum aestivum* L.). *Planta* 248, 1319–1328.

Wolfe, M. S. (1967). Physiologic specialization of *Erysiphe graminis* f. sp. tritici in the united kingdom, 1964–5. *Trans. Br. Mycol. Soc.* 50, 631–640.

Wu, L., Zhu, T., He, H., Cao, X., Li, H., Xu, H., et al. (2022). Genetic dissection of the powdery mildew resistance in wheat breeding line LS5082 using BSR-Seq. *Crop J.* doi: 10.1094/PDIS-12-21-2771-RE

Wu, P., Xie, J., Hu, J., Qiu, D., Liu, Z., Li, J., et al. (2018). Development of molecular markers linked to powdery mildew resistance gene Pm4b by combining SNP discovery from transcriptome sequencing data with bulked segregant analysis (BSR-Seq) in wheat. *Front. Plant Sci.* 9:95. doi: 10.3389/fpls.2018.00095

Yao, D., Ijaz, W., Liu, Y., Hu, J., Peng, W., Zhang, B., et al. (2022). Identification of a Pm4 allele as a powdery mildew resistance gene in wheat line xiaomaomai. *Int. J. Mol. Sci.* 2022:23. doi: 10.3390/ijms23031194

Yu, X., Ren, S., Zhao, L., Guo, J., Bao, Y., Ma, Y., et al. (2018). Molecular mapping of a novel wheat powdery mildew resistance gene Ml92145E8-9 and its application in wheat breeding by marker-assisted selection. *Crop J.* 6, 621–627.

Zhang, R., Xiong, C., Mu, H., Yao, R., Meng, X., Kong, L., et al. (2021). Pm67, a new powdery mildew resistance gene transferred from *Dasypyrum villosum* chromosome 1V to common wheat (*Triticum aestivum* L.). *Crop J.* 9, 882–888.

Zhao, Z., Sun, H., Song, W., Lu, M., Huang, J., Wu, L., et al. (2013). Genetic analysis and detection of the gene MlLX99 on chromosome 2BL conferring resistance to powdery mildew in the wheat cultivar liangxing 99. *Theor. Appl. Genet.* 126, 3081–3089. doi: 10.1007/s00122-013-2194-6

Conflict of Interest: The authors declare that the research was conducted in the absence of any commercial or financial relationships that could be construed as a potential conflict of interest.

Publisher's Note: All claims expressed in this article are solely those of the authors and do not necessarily represent those of their affiliated organizations, or those of the publisher, the editors and the reviewers. Any product that may be evaluated in this article, or claim that may be made by its manufacturer, is not guaranteed or endorsed by the publisher.

frontiers | Frontiers in Plant Science

ORIGINAL RESEARCH
published: 29 June 2022
doi: 10.3389/fpls.2022.928014

The Physical Location of Stripe Rust Resistance Genes on Chromosome 6 of Rye (*Secale cereale* L.) AR106BONE

Yanling Duan[1,2], *Jie Luo*[1,2], *Zujun Yang*[3], *Guangrong Li*[3], *Zongxiang Tang*[1,2]* and *Shulan Fu*[1,2]*

[1] College of Agronomy, Sichuan Agricultural University, Chengdu, China, [2] Provincial Key Laboratory for Plant Genetics and Breeding, Sichuan Agricultural University, Chengdu, China, [3] Center for Informational Biology, University of Electronic Science and Technology of China, Chengdu, China

It was reported that the chromosome 6R of rye (*Secale cereale* L.) carries stripe rust resistance gene *Yr83*, and the region with the candidate resistance gene(s) still needs to be narrowed down. This study confirmed that the chromosome 6RL^{Ar} derived from rye AR106BONE contains stripe rust resistance gene(s). A wheat-rye T6BS.6RL^{Ar} translocation chromosome, a wheat-rye small-segment translocation T6RL^{Ar}-6AS.6AL, and three kinds of deleted T6BS.6RL^{Ar} translocations, T6BS.6RL^{Ar}-1, T6BS.6RL^{Ar}-2, and T6BS.6RL^{Ar}-3, were identified. Translocations T6BS.6RL^{Ar}, T6BS.6RL^{Ar}-2, and T6RL^{Ar}-6AS.6AL were highly resistant to stripe rust and T6BS.6RL^{Ar}-1 and T6BS.6RL^{Ar}-3 were highly susceptible. The molecular markers specific to 6RL determined that the three regions of the 6RL^{Ar} arm from 732,999,830 bp to the telomere, from 735,010,030 to 848,010,414 bp, and from 848,011,262 bp to the telomere were deleted from T6BS.6RL^{Ar}-1, T6BS.6RL^{Ar}-2, and T6BS.6RL^{Ar}-3, respectively. T6BS.6RL^{Ar}-2 and T6RL^{Ar}-6AS.6AL contained the segment that was deleted in T6BS.6RL^{Ar}-3. Therefore, it can be concluded that about 37 Mb segment from 848,011,262 bp to the telomere carried stripe rust resistance gene(s), and it was smaller than that with the *Yr83* gene. Gene annotation indicated that about 37 Mb region contains 43 potential resistance genes, and 42 of them are nucleotide-binding site and leucine-rich repeat (NBS-LRR)-like resistance protein genes. The results in this study narrowed down the size of the region with candidate stripe rust resistance gene(s) on the 6RL arm, and the T6RL^{Ar}-6AS.6AL is a promising small-segment translocation for improvement of wheat cultivars.

Keywords: wheat, rye, stripe rust, 6R chromosome, small-segment translocation

OPEN ACCESS

Edited by:
Fangpu Han,
Institute of Genetics and Developmental Biology (CAS), China

Reviewed by:
Peng Zhang,
The University of Sydney, Australia
Andreas Houben,
Leibniz Institute of Plant Genetics and Crop Plant Research (IPK), Germany
Hongjie Li,
Institute of Crop Sciences (CAAS), China

***Correspondence:**
Zongxiang Tang
zxtang@sicau.edu.cn
Shulan Fu
fushulan@sicau.edu.cn

Specialty section:
This article was submitted to Plant Pathogen Interactions, a section of the journal Frontiers in Plant Science

Received: *25 April 2022*
Accepted: *23 May 2022*
Published: *29 June 2022*

Citation:
Duan Y, Luo J, Yang Z, Li G, Tang Z and Fu S (2022) The Physical Location of Stripe Rust Resistance Genes on Chromosome 6 of Rye (Secale cereale L.) AR106BONE. Front. Plant Sci. 13:928014. doi: 10.3389/fpls.2022.928014

INTRODUCTION

Wheat stripe rust is caused by *Puccinia striiformis* f. sp. *tritici* (Pst) and is one of the most serious diseases in wheat. Developing wheat cultivars with resistance to stripe rust is the most practical way to control this disease. More than 80 *Yr* (yellow rust resistance) genes were officially named; however, most of them lost their resistance because of variations in the prevalence of virulent pathotypes (Ren et al., 2022).

The resistance to stripe rust of 103 wheat lines was tested using pathogenic races CYR32, CYR33, and CYR34, which are currently prevalent in China, and only *Yr5*, *Yr15*, and *Yr45* exhibited all-stage resistance, and only *Yr41*, *Yr47*, and *Yr50* were adult plant resistant (Hu et al., 2022). The replacement of historically clonal *Pst* races by new ones occurred continually (Jamil et al., 2020; Bouvet et al., 2022). Therefore, it is important to explore new resistance genes to stripe rust and enrich the resource pool for wheat resistance breeding.

Wheat-related species contain abundant resistance genes. For example, rye (*Secale cereale* L.) is an important gene source for wheat disease resistance breeding (Spetsov and Daskalova, 2022). Stripe rust gene *Yr 9* located on the 1RS arm was successfully used in commercial wheat cultivars. Additionally, 2R, 4R, 5R, 6R, and 7R chromosomes also carry stripe rust-resistant genes (Lei et al., 2011; Li et al., 2016a, 2020a,b; Schneider et al., 2016; An et al., 2019; Xi et al., 2019; Johansson et al., 2020; Ren et al., 2020). Four of these reports indicated that rye chromosome 6R carried stripe rust resistance genes, and they were derived from different rye sources (Schneider et al., 2016; Johansson et al., 2020; Li et al., 2020a,b). A new stripe rust resistance gene on chromosome 6R was named *Yr83*, and it was located in a bin FL0.73-1.00 of 6RL (Li et al., 2020b). To clone the stripe rust resistance gene(s) on 6RL, it is necessary to narrow the segment with resistant gene(s). In this study, a wheat-rye $6R^{Ar}$ monosomic addition line ($MA6R^{Ar}$) with resistance to stripe rust, a $6RS^{Ar}$ monotelosomic addition line ($MTA6RS^{Ar}$), a $6RL^{Ar}$ monotelosomic addition line ($MTA6RL^{Ar}$), a $T6BS.6RL^{Ar}$ translocation line, and three kinds of deleted $T6BS.6RL^{Ar}$ translocation lines were used to locate the stripe rust resistance gene(s) on a smaller segment of $6RL^{Ar}$ arm, and some resistance protein genes in this segment were found.

MATERIALS AND METHODS

Plant Materials

Octoploid triticale lines Mianyang 11/AR106BONE-4 (MAR4) and Mianyang 11/Kustro (MK) were derived from common wheat (*Triticum aestivum* L.) Mianyang 11 (MY11) × *Secale cereale* L. AR106BONE and MY11 × *Secale cereale* L. Kustro, respectively. Crossing between MAR4 and a wheat line J1025 (*T. aestivum* L.) and between MK and MY11 was carried out. From the progenies of MAR4 × J1025 and MK × MY11, wheat-rye 6R monosomic addition lines $MA6R^{Ar}$ and $MA6R^{Ku}$ were identified, respectively. These monosomic addition lines were used to investigate the stripe rust resistance of the two kinds of 6R chromosomes. $MTA6RS^{Ar}$ and $MTA6RL^{Ar}$ were identified from the selfed progeny of $MA6R^{Ar}$. The seeds of $MA6R^{Ar}$ were irradiated with ^{60}Co-γ rays at a dosage of 200 Gy at Biotechnology and Nuclear Technology Research Institute, Sichuan Academy of Agricultural Sciences, China. From the progeny of irradiated $MA6R^{Ar}$, a wheat-rye $T6BS.6RL^{Ar}$ translocation line was obtained, and the seeds derived from this translocation line were also irradiated with ^{60}Co-γ rays and some deleted $T6BS.6RL^{Ar}$ translocation chromosomes were detected. The rye Kustro and AR106BONE and the common wheat MY11 and J1025 were kept in the seed store in our laboratory.

Cytological Analysis

The root-tip metaphase chromosomes of the materials used in this study were analyzed using non-denaturing fluorescence *in situ* hybridization (ND-FISH) technology. Oligo-pSc200, Oligo-pSc250 (Vershinin et al., 1995; Fu et al., 2015), Oligo-Ku (Xiao et al., 2017), Oligo-pSc119.2-1 (McIntyre et al., 1990; Tang et al., 2014), and Oligo-pTa535-1 (Komuro et al., 2013; Tang et al., 2014) were used as probes. Probes Oligo-pSc200, Oligo-pSc250, and Oligo-Ku were used to distinguish rye chromosomes from wheat (Fu et al., 2015; Xiao et al., 2017). Probes Oligo-pSc119.2-1 and Oligo-pTa535-1 were used to identify individual wheat chromosomes (Tang et al., 2014). Additionally, the different cytological structure of rye chromosomes was displayed by the combination of probes Oligo-pSc200, Oligo-pSc250, and Oligo-pSc119.2-1 (Fu et al., 2015). These oligonucleotide (oligo) probes were 5′ end-labeled with 6-carboxyfluorescein (6-FAM) or 6-carboxytetramethylrhodamine (TAMRA). The root-tip metaphase chromosomes were prepared according to the methods described by Han et al. (2006). The ND-FISH analysis was carried out following the methods described by Fu et al. (2015) and Xiao et al. (2017). Additionally, the genomic DNA of rye AR106BONE was used as a probe for the genomic *in situ* hybridization (GISH) analysis of the $T6RL^{Ar}$-6AS.6AL small-segment translocation. The GISH analysis was carried out according to the methods described by Fu et al. (2015).

Development of 6RL-Specific Markers

Primers were designed according to the 6RL sequence of rye Lo7 (Rabanus-Wallace et al., 2021) using Primer 3 software (version 4.0), and the optimal melting temperature and size values were set to 60°C and to 20 bases, respectively. In total, 423 pairs of primers were designed. Additionally, 124 developed $6RL^{Ku}$-specific length amplified fragment sequencing (SLAF-seq) markers (Li et al., 2016b) were also used. The PCR amplification and agarose gel electrophoresis were performed following the procedure described by Li et al. (2016b). Chinese Spring (CS), MY11, $T6BS.6RL^{Ar}$ translocation line, and rye AR106BONE were used to test the $6RL^{Ar}$ specificity of the 423 newly designed primer pairs and the 124 $6RL^{Ku}$-specific SLAF-seq markers. All the $6RL^{Ar}$-specific markers were physically mapped to specific regions of the $6RL^{Ar}$ arm using deleted $T6BS.6RL^{Ar}$ translocation lines. The sequences of the 124 SLAF-seq primer pairs were used for nucleotide Basic Local Alignment Search Tool (BLAST) searches against the 6R sequence of rye Lo7 (Rabanus-Wallace et al., 2021) using a BLAST tool in the Triticeae Multi-omics Center (http://202.194.139.32/), and the positions of these markers on 6RL arm were determined according to the BLAST results.

Cloning Partial Sequences of the Candidate Resistance Genes From $6RL^{Ar}$

To confirm that the candidate resistance genes on the 6RL arm of Lo7 are similar to that of $6RL^{Ar}$, the sequences of two candidate resistance genes *SECCE6Rv1G0449960.1* and *SECCE6Rv1G0453070.1* of Lo7 were randomly selected for

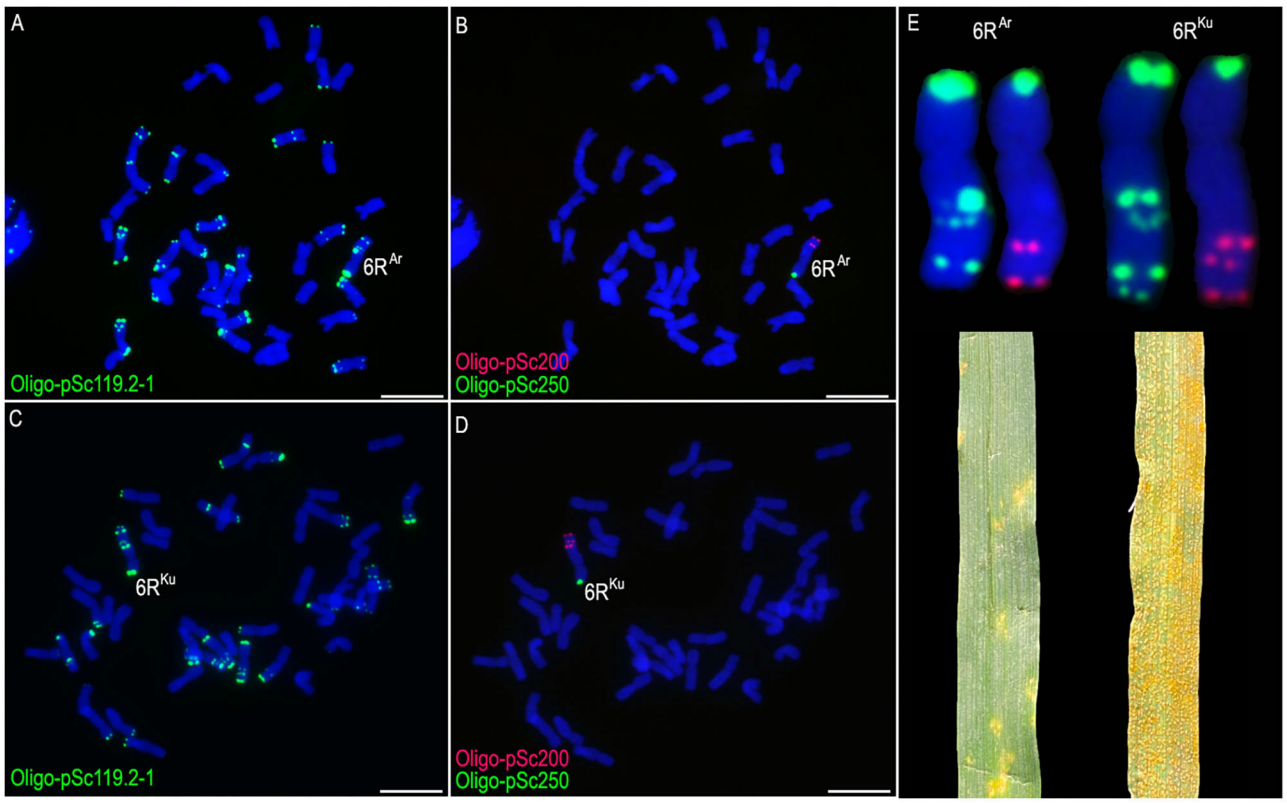

FIGURE 1 | The non-denaturing fluorescence *in situ* hybridization (ND-FISH) analysis of lines MA6R^{Ar} and MA6R^{Ku} using probes Oligo-pSc119.2-1 (green), Oligo-pSc200 (red), Oligo-pSc250 (green), and their stripe rust resistance test. **(A,B)** A root-tip metaphase cell of line MA6R^{Ar}. **(C,D)** A root-tip metaphase cell of line MA6R^{Ku}. **(E)** Cut-and-paste 6R^{Ar} and 6R^{Ku} chromosomes. 6R^{Ar} was highly resistant to stripe rust and 6R^{Ku} was susceptible. Scale bar: 10 μm.

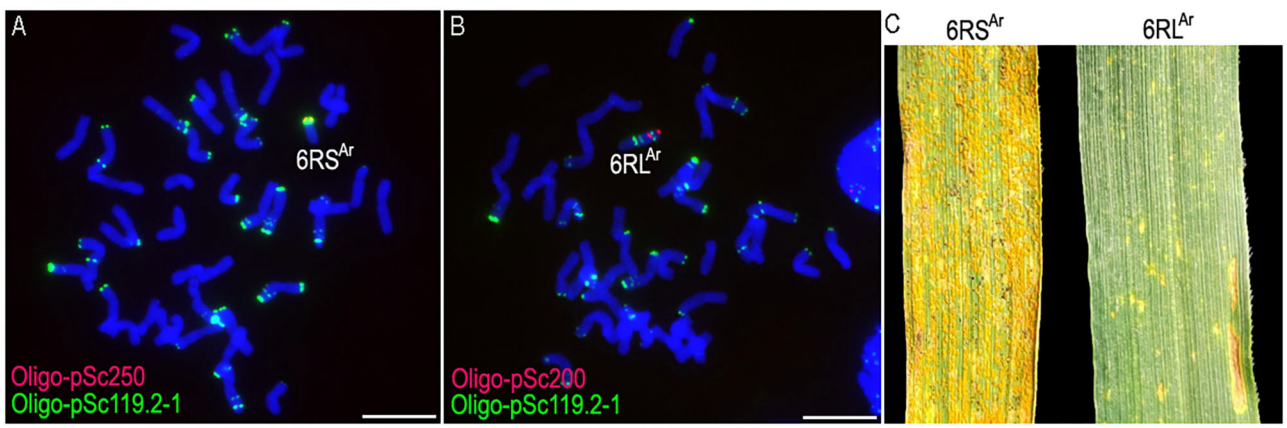

FIGURE 2 | The non-denaturing fluorescence *in situ* hybridization (ND-FISH) analysis of lines MTA6RS^{Ar} and MTA6RL^{Ar} using probes Oligo-pSc119.2-1 (green), Oligo-pSc200 (red), Oligo-pSc250 (red), and their stripe rust resistance test. **(A)** A root-tip metaphase cell of line MTA6RS^{Ar}. **(B)** A root-tip metaphase cell of line MTA6RL^{Ar}. **(C)** Line MTA6RS^{Ar} was susceptible to stripe rust and line MTA6RL^{Ar} was highly resistant. Scale bar: 10 μm.

designing primer pairs. Primer pairs of P60 (5′ TGGGG AATAG CTGGC ATTGG3′, 5′ TCGGT AGGGT AGACG GTGAG3′) and P70 (5′ AATGG GAGGA CTCTT GCGTG3′, 5′ CTGGG AATGA ACCGA CAGCT3′) were used to amplify the partial sequences of the two genes from 6RL^{Ar} arm. The PCR reactions and product separation were also performed according to the methods described by Li et al. (2016b), and the annealing temperature of the primer pairs was 60°C. The target products amplified by the two primer pairs, P60 and P70, were cloned and then sequenced by the Tsingke Biotechnology Co., Ltd.

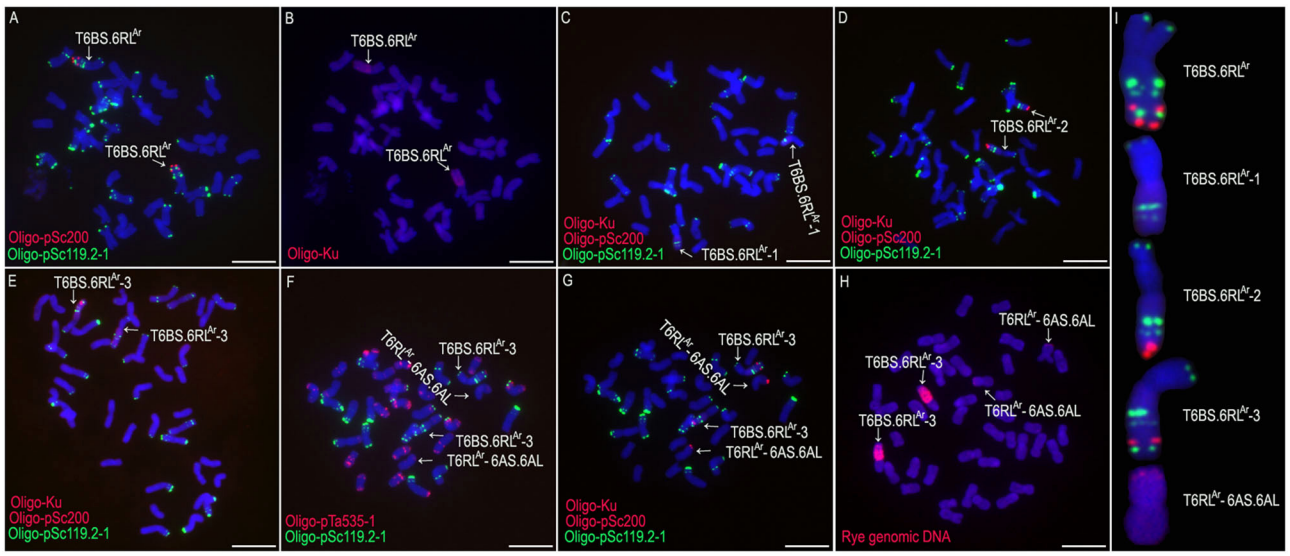

FIGURE 3 | The non-denaturing fluorescence *in situ* hybridization (ND-FISH) and genomic *in situ* hybridization (GISH) analyses of T6BS.6RL^{Ar} translocations and its deleted T6BS.6RL^{Ar} using probes Oligo-pSc119.2-1 (green), Oligo-pTa535-1 (red), Oligo-pSc200 (red), Oligo-Ku (red) and rye genomic DNA (red). **(A,B)** A root-tip metaphase cell of line 19T177-21. **(C)** A root-tip metaphase cell of line 21F1. **(D)** A root-tip metaphase cell of line 21F3. **(E)** A root-tip metaphase cell of line 21F7. **(F,G)** A root-tip metaphase cell of line 21F11. **(H)** GISH analysis of root-tip metaphase cell of line 21F11. **(I)** Cut-and-paste chromosomes of T6BS.6RL^{Ar} and deleted T6BS.6RL^{Ar}. Scale bar: 10 μm.

(Chengdu, China). Sequence alignment was performed using the software DNAMAN (Ver. 4.0, Lynnon Corp., Quebec, QC, Canada).

Stripe Rust Response Test

The response of parental wheat J1025, MY11, lines MA6R^{Ku}, MA6R^{Ar}, MTA6RS^{Ar}, MTA6RL^{Ar}, T6BS.6RL^{Ar}, and the deleted T6BS.6RL^{Ar} to stripe rust was evaluated. The mixed stripe rust prevalent isolates CYR32, CYR33, and CYR34 were used to inoculate seedlings in field according to the method described by Xi et al. (2019). A 0–9 numerical scale of infection types (IT) was scored according to the standard described by Wan et al. (2017) at the adult stage. The disease resistance of J1025, MY11, the lines MA6R^{Ku}, MA6R^{Ar}, MTA6RS^{Ar}, MTA6RL^{Ar}, and T6BS.6RL^{Ar} was evaluated in 2018–2019 in Qionglai, Sichuan Province, China and in 2019–2020, 2020–2021, and 2021–2022 in Wenjiang and Dayi, Sichuan Province, China. The disease resistance of the deleted T6BS.6RL^{Ar} and the T6RL^{Ar}-6AS.6AL translocation was evaluated in 2020–2021 and 2021–2022 in Wenjiang and Dayi. When the segment of 6RL^{Ar} with stripe rust resistance was identified, the candidate resistance genes were found according to the gene annotation of rye Lo7 (http://202.194.139.32/jbrowse.html) (Rabanus-Wallace et al., 2021).

RESULTS

Identification of Wheat-Rye 6R Addition and Translocation Lines

The ND-FISH based on oligo probes was used to analyze the progeny of wheat × rye. Wheat-rye 6R monosomic addition lines MA6R^{Ar} and MA6R^{Ku} were identified (**Figures 1A–D**). Both the short arms of the 6R^{Ar} and 6R^{Ku} chromosomes (6RS^{Ar} and 6RS^{Ku}) contained signals of Oligo-pSc119.2-1 and Oligo-pSc250, and no signals of Oligo-pSc250 were observed on their long arms (6RL^{Ar} and 6RL^{Ku}) (**Figure 1E**). The probe Oligo-pSc119.2-1 produced three and four signal bands on 6RL^{Ar} and 6RL^{Ku}, respectively (**Figure 1E**). Two and three signal bands of probe Oligo-pSc200 were observed on 6RL^{Ar} and 6RL^{Ku} arms, respectively (**Figure 1E**). The results indicated that the structure of the long arms of the 6R^{Ar} and 6R^{Ku} chromosomes is different. Line MA6R^{Ar} was highly resistant to stripe rust (IT = 1), whereas line MA6R^{Ku} was susceptible (IT = 9; **Figure 1E**).

From the selfed progeny of line MA6R^{Ar}, the 6RS^{Ar} and the 6RL^{Ar} monotelosomic addition lines, MTA6RS^{Ar} and MTA6RL^{Ar}, were identified (**Figures 2A,B**). Line MTA6RS^{Ar} was susceptible to stripe rust (IT = 9), and line MTA6RL^{Ar} displayed high resistance (IT = 1; **Figure 2C**). In total, 200 seeds of MA6R^{Ar} were irradiated. A plant 18T231-46 containing a wheat-rye T6BS.6RL^{Ar} translocation chromosome was identified from 1,182 M1 seeds, and a line 19T177-21 containing a pair of T6BS.6RL^{Ar} translocations was identified from 30 seeds of the selfed progeny of 18T231-46 (**Figures 3A,B**). Additionally, 104 seeds of the selfed progeny of 18T231-46 were also irradiated. Four lines, 21F1, 21F3, 21F7, and 21F11, were identified from the 1,090 seeds (M2) of the progeny of irradiated 18T231-46. In these lines, three kinds of deleted T6BS.6RL^{Ar} translocation chromosomes and a small-segment translocation T6RL^{Ar}-6AS.6AL were found (**Figures 3C–I**). Line 21F1 contained two deleted translocation chromosomes T6BS.6RL^{Ar}-1, on which the Oligo-pSc200 signals and the distal Oligo-pSc119.2-1 signals on the 6RL^{Ar} arms were disappeared (**Figures 3C,I**). Line 21F3 contained two deleted translocation chromosomes T6BS.6RL^{Ar}-2, carrying one Oligo-pSc200 signal band and two

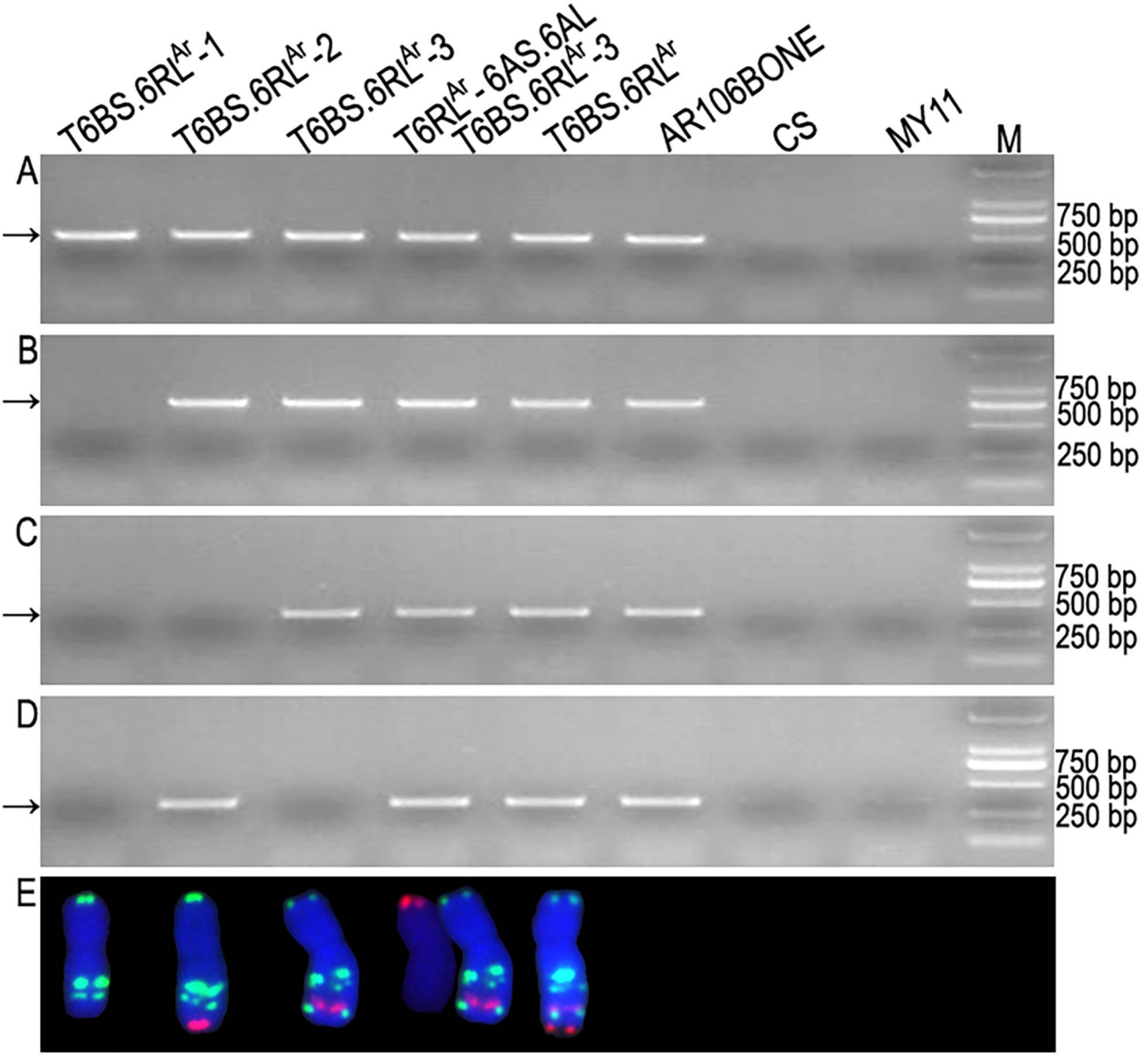

FIGURE 4 | Physically mapped 6RL^{Ar}-specific markers using deleted T6BS.6RL^{Ar} translocations. **(A)** Products amplified by primer pair Lo7.6RL-2 represent the markers located on T6BS.6RL^{Ar} and all the deleted T6BS.6RL^{Ar}. **(B)** Products amplified by primer pair Lo7.6RL-74 represent the markers located on T6BS.6RL^{Ar}, T6BS.6RL^{Ar}-2, and T6BS.6RL^{Ar}-3. **(C)** Products amplified by primer pair Ku.6RL-260 represent the markers located on T6BS.6RL^{Ar} and T6BS.6RL^{Ar}-3. **(D)** Products amplified by primer pair Lo7.6RL-183 represent the markers located on T6BS.6RL^{Ar}, T6BS.6RL^{Ar}-2, and T6RL^{Ar}-6AS.6AL. **(E)** Cut-and-paste translocation chromosomes corresponding to their amplified products in each electrophoresis lane. Arrows indicate the target bands amplified by 6RL^{Ar}-specific markers. Common wheat Chinese Spring (CS), Mianyang11 (MY11), and rye AR106BONE were used as controls. M: DNA marker.

intercalary Oligo-pSc119.2-1 signal bands (**Figures 3D,I**). Line 21F7 contained a pair of deleted translocation chromosomes T6BS.6RL^{Ar}-3, and the signals of Oligo-pSc200 on telomeric regions were disappeared (**Figures 3E,I**). In line 21F11, probe Oligo-pSc200 produced signals on the telomeric regions of the short arms of chromosomes 6A (**Figures 3F–I**). Therefore, line 21F11 contained a pair of small-segment translocations T6RL^{Ar}-6AS.6AL and a pair of T6BS.6RL^{Ar}-3 (**Figures 3F–I**). The weak GISH signals on the chromosomes T6RL^{Ar}-6AS.6AL indicated that the segment of 6RL^{Ar} involved in translocation is small (**Figures 3H,I**).

The Physical Location of 6RL^{Ar}-Specific Markers

Among the 423 newly designed primer pairs, 204 amplified specific bands from T6BS.6RL^{Ar} translocation line and rye AR106BONE, but not from CS and MY11, indicated that these 204 primer pairs are 6RL^{Ar}-specific markers (**Figure 4**

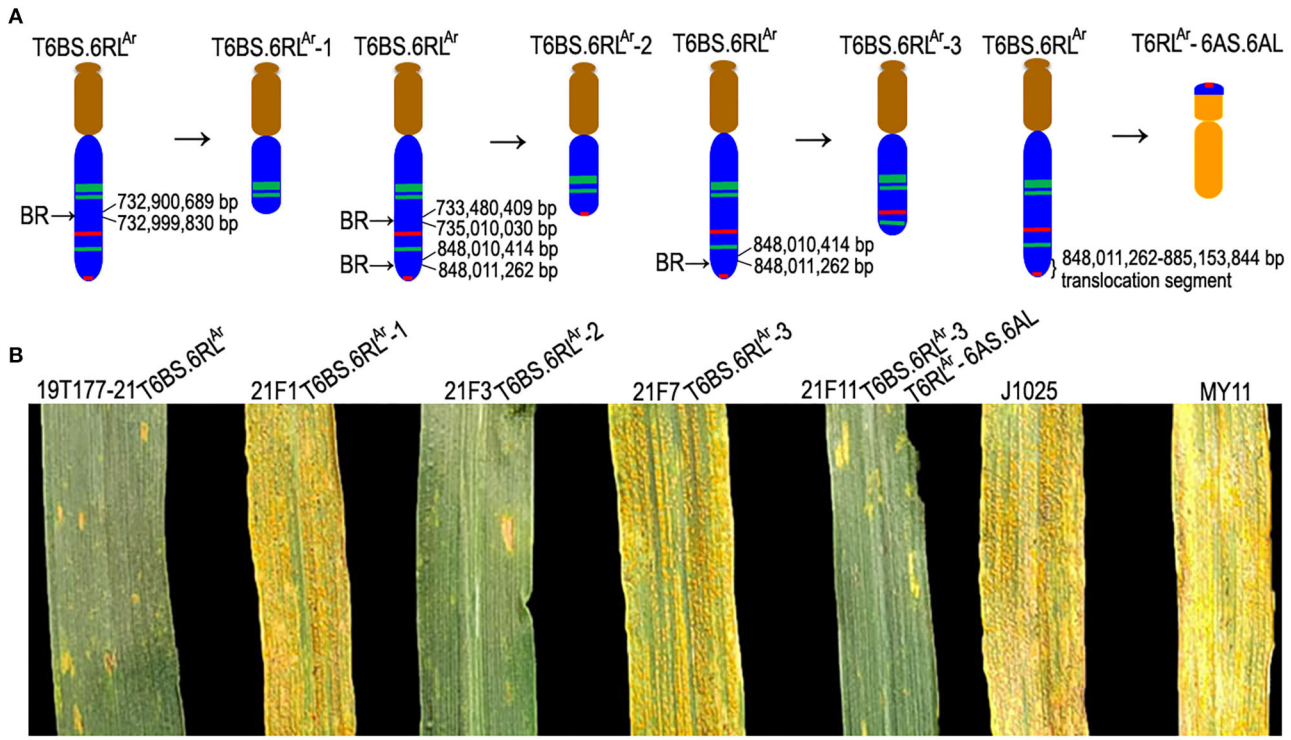

FIGURE 5 | Ideograms of wheat-rye 6RL translocation chromosomes and stripe rust response test. **(A)** Ideograms of T6BS.6RL^{Ar}, deleted T6BS.6RL^{Ar,} and the small-segment translocation T6RL^{Ar}-6AS.6AL. Brown, blue, and orange indicate segments of 6B, 6R, and 6A chromosomes, respectively. Green and red bands indicate the signals of Oligo-pSc119.2-1 and Oligo-pSc200, respectively. "BR" indicates a break point. The right brace indicates the 6RL^{Ar} segment that was transferred on the 6A chromosome. **(B)** Parental wheat J1025 and MY11 and lines 21F1 and 21F7 were highly susceptible to stripe rust and lines 19T177-21, 21F3, and 21F11 were highly resistant.

and **Supplementary Table S1**). Additionally, 95 of the 124 SLAF-seq markers amplified target bands from both T6BS.6RL^{Ar} and AR106BONE. A total of 299 (204 + 95) 6RL^{Ar}-specific markers were obtained, and their target amplification regions on the 6RL arm are listed in **Supplementary Table S1**. The breakpoints on the 6RL^{Ar} arms of T6BS.6RL^{Ar}-1, T6BS.6RL^{Ar}-2, and T6BS.6RL^{Ar}-3 were determined using the 299 markers. In total, 103 of the 299 markers amplified 6RL^{Ar}-specific bands from translocation T6BS.6RL^{Ar}-1 (**Figure 4A**), and these markers covered the region of 6RL from 333,302,151 to 732,900,689 bp (**Supplementary Table S1**). The first distal marker (Lo7.6RL-71) that did not amplify products from T6BS.6RL^{Ar}-1 occupied the region from 732,999,830 to 733,000,692 bp (**Supplementary Table S1**). Therefore, the breakpoint in T6BS.6RL^{Ar}-1 was located in the region of the 6RL^{Ar} arm between 732,900,689 and 732,999,830 bp (**Figure 5A** and **Supplementary Table S1**). Totally, 118 and 52 markers that were distributed into two regions of 6RL from 333,302,151 to 733,480,409 bp and from 848,011,262 to 885,003,466 bp, respectively amplified target bands from T6BS.6RL^{Ar}-2, and 129 markers that distributed the region of 6RL from 735,010,030 to 848,010,414 bp did not produce amplicons from this translocation chromosome (**Figures 4B–D** and **Supplementary Table S1**). It can be determined that the two breakpoints in T6BS.6RL^{Ar}-2 occurred in the two regions of 6RL^{Ar} arm between 733,480,409 and 735,010,030 bp and between 848,010,414 and 848,011,262 bp (**Figure 5A** and **Supplementary Table S1**). For T6BS.6RL^{Ar}-3 translocation, 247 markers that were distributed on the 6RL region from 333,302,151 to 848,010,414 bp amplified target bands, and the rest 52 markers, which were the same as those amplified products from T6BS.6RL^{Ar}-2, did not amplify amplicons (**Figure 4D** and **Supplementary Table S1**). According to the amplification of these markers, the breakpoint regions on 6RL^{Ar} in the three deleted T6BS.6RL^{Ar} translocations can be determined (**Figure 5A** and **Supplementary Table S1**). For the T6BS.6RL^{Ar}-3 chromosome, the breakpoint between 848,010,414 and 848,011,262 bp was the same as the second breakpoint in the T6BS.6RL^{Ar}-2 chromosome (**Figure 5A** and **Supplementary Table S1**). Therefore, the segments from 732,999,830 bp to telomere, from 735,010,030 to 848,010,414 bp, and from 848,011,262 bp to telomere of 6RL^{Ar} were deleted from T6BS.6RL^{Ar}-1, T6BS.6RL^{Ar}-2, and T6BS.6RL^{Ar}-3, respectively (**Figure 5A**). The 6RL^{Ar} segment deleted from T6BS.6RL^{Ar}-3 was transferred to T6RL^{Ar}-6AS.6AL (**Figures 4**, **5A**).

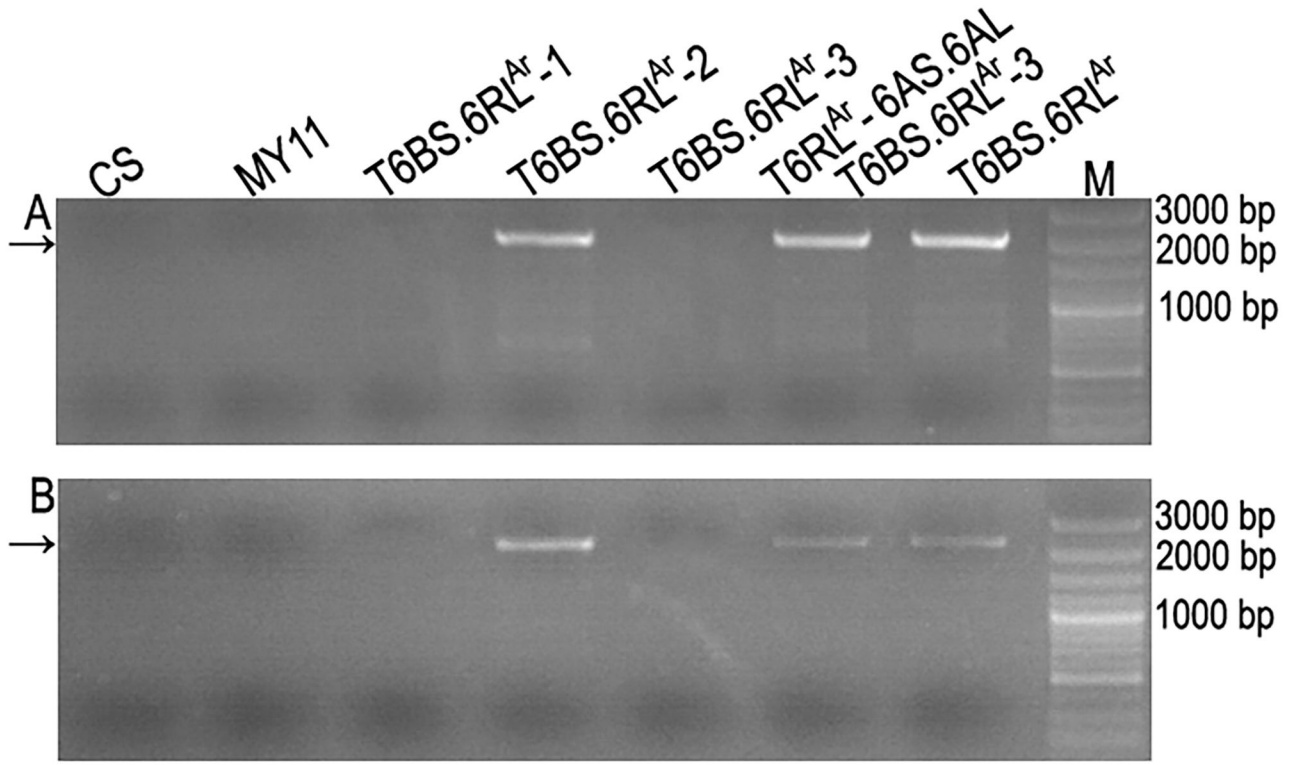

FIGURE 6 | Amplification of partial segments of genes *SECCE6Rv1G0449960.1* and *SECCE6Rv1G0453070.1*. **(A)** Products amplified by primer pair P60. **(B)** Products amplified by primer pair P70. Arrows indicate the target bands amplified by the two primer pairs. Common wheat Chinese Spring (CS) and Mianyang11 (MY11) were used as controls. M: DNA marker.

Location of Stripe Rust Resistance Genes on Segment of 6RL^{Ar}

Stripe rust response test indicated that translocation lines T6BS.6RL^{Ar}, 21F3 (T6BS.6RL^{Ar}-2), and 21F11 (T6BS.6RL^{Ar}-3 and T6RL^{Ar}-6AS.6AL) were highly resistant to stripe rust (IT = 1), and translocation lines 21F1 (T6BS.6RL^{Ar}-1) and 21F7 (T6BS.6RL^{Ar}-3) were highly susceptible (IT = 9; **Figure 5B**). According to the resistance of 21F3, 21F7, and 21F11, and the 6RL^{Ar} segments existed in T6BS.6RL^{Ar}-2, T6BS.6RL^{Ar}-3, and T6RL^{Ar}-6AS.6AL, it was determined that the 6RL^{Ar} segment in T6RL^{Ar}-6AS.6AL carried the stripe rust resistance gene. Therefore, it was determined that the 6RL^{Ar} region from 848,371,946 bp to the telomere (885,153,844 bp) carried the stripe rust resistance gene. Gene annotation indicated that there are 43 potential resistance genes located in the region from 848,011,885 to 885,153,844 bp of chromosome 6R (**Supplementary Table S2**). Only one of the 43 genes belongs to the kinase family protein gene and the other 42 genes are nucleotide-binding site and leucine-rich repeat (NBS-LRR)-like resistance protein genes (**Supplementary Table S2**).

The Similarity of the Candidate Genes on 6RL Arms of Lo7 and AR106BONE

The two primer pairs P60 and P70 amplified specific bands from translocation chromosomes T6BS.6RL^{Ar}, T6BS.6RL^{Ar}-2, and T6RL^{Ar}-6AS.6AL but not from T6BS.6RL^{Ar}-1 and T6BS.6RL^{Ar}-3 translocations (**Figure 6**). The two primer pairs also did not amplify products from CS and MY11 (**Figure 6**). The sequences amplified from T6RL^{Ar}-6AS.6AL were cloned and sequenced. The sequences amplified by primer pairs P60 and P70 were named Ar-60.1 (1,857 bp) and Ar-70.1 (2,423 bp), respectively (**Supplementary Figures S1**, **S2**). Sequences Ar-60.1 and Ar-70.1 had 99.03 and 99.50% similarity to the corresponding segments of genes *SECCE6Rv1G0449960.1* and *SECCE6Rv1G0453070.1*, respectively (**Supplementary Figures S1**, **S2**). These results indicated the conservation of resistance genes on the 6RL arms of Lo7 and AR106BONE.

DISCUSSION

Polymorphism of 6R Chromosomes

The complex cytological structure of the 6R chromosome has been reported. It was known that the long arm of the rye 6R chromosome contains homologous groups 3 and 7 segments in the distal region (Devos et al., 1993; Li et al., 2013). FISH signal patterns of tandem repeats pSc119.2 on *S. cereale* 6R and *S. africanum* 6R^{afr} were different, and this indicated the structural alteration between the two kinds of 6R chromosomes (Li et al., 2020a). In this study, the cytological structure of 6R chromosomes derived from rye AR106BONE and Kustro

is different. Some $6RL^{Ku}$-specific SLAF-seq markers that did not amplify products from $6R^{Ar}$ also exhibited the diversity between chromosomes $6R^{Ku}$ and $6R^{Ar}$. The 6RL arm with stripe rust resistance gene *Yr83* carried weak pSc119.2 signals in the intercalary and telomeric regions (Li et al., 2020b), and it is different from that of the $6RL^{Ar}$ arm. However, the pSc119.2 signal pattern of $6RL^{Ar}$ is similar to that on the 6RL arm of rye cv. Qinling (Hao et al., 2018). These results exhibited the abundant genetic diversity of chromosome 6R in the genus *Secale*. Therefore, it is necessary to continue to study the allelic variations of 6R chromosomes as they may enrich the genetic diversity of the resistance genes on them. Especially, the difference among the stripe rust resistance genes on different 6R chromosomes needs to be confirmed. Additionally, the results in this study make us think about whether the stripe rust resistance of the 6RL segment is controlled by a single gene or multiple genes.

Using 6R Deletions to Locate Stripe Rust Resistance Genes

Rye chromosome deletion lines are useful for the location of resistance genes. The powdery mildew resistance gene *Pm56* was located in the subtelomeric region of the 6RS arm using 6R deletion lines (Hao et al., 2018). The stripe rust resistance gene *Yr83* was mapped to the bin of FL0.73-1.00 of 6RL using deletion mapping (Li et al., 2020b). Similarly, 6R chromosome deletion and translocation lines were used to locate the powdery mildew resistance gene on the 6RL arm at FL0.85-1.00 and the stripe rust resistance gene on the 6RS arm at FL0.95-1.00 (Li et al., 2020a). However, the detailed information about the physical location of these reported resistance genes on 6R chromosomes is still unclear. In this study, 6RL-specific markers have been anchored to the exact physical positions on the 6R chromosome using reference genomic sequences of rye, and these markers combined with deleted T6BS.6RL translocation chromosomes were used to reveal that the 6RL segment with stripe rust resistance gene(s) is about 37 Mb. The primer sequences of the 33 markers that were located in the bin with the *Yr83* gene were used for nucleotide BLAST searches against the 6R sequence of rye Lo7 (Rabanus-Wallace et al., 2021) using a BLAST tool in the Triticeae Multi-omics Center (http://202.194.139.32/), and these markers covered the 6R segment between 743,894,430 and 880,064,740 bp. Therefore, in this study, the 6RL segment with stripe rust resistance is smaller than that reported by Li et al. (2020b), and this narrows down the candidate genes with stripe rust resistance on 6R chromosome. The high similarity of the candidate resistance gene sequences between rye Lo7 and AR106BONE indicated that the physical mapping based on the reference genome of rye Lo7 can be applied to $6RL^{Ar}$ arm. Additionally, the new markers developed in this study enrich the 6R-specific molecular markers. It is a pity that the effect of the $T6RL^{Ar}$-6AS.6AL chromosome on agronomic traits is unclear because it exists in a plant together with the $T6BS.6RL^{Ar}$-3 chromosome. To get rid of the $T6BS.6RL^{Ar}$-3, the cross between line 21F11 and some wheat lines that are susceptible to stripe rust has already been carried out. The $T6RL^{Ar}$-6AS.6AL chromosome is a promising small-segment translocation for the improvement of wheat cultivars.

DATA AVAILABILITY STATEMENT

The original contributions presented in the study are included in the article/**Supplementary Material**, further inquiries can be directed to the corresponding author/s.

AUTHOR CONTRIBUTIONS

ZT and SF conceived and designed the study, created the materials, analyzed the data, and wrote the manuscript. YD and JL performed the experiments and analyzed the data. ZY and GL created the materials. All authors read and approved the final manuscript.

FUNDING

This manuscript was provided by the National Natural Science Foundation of China (no. 31770373), the Open Project Program of the State Key Laboratory of Plant Cell and Chromosome Engineering, Institute of Genetics and Developmental Biology, China (no. PCCE-KF-2021-02), and the Sichuan Science and Technology Program (no. 2022ZDZX0014).

ACKNOWLEDGMENTS

The authors are thankful to Jie Zhang and Yun Jiang (Biotechnology and Nuclear Technology Research Institute, Sichuan Academy of Agricultural Sciences) for that they help us to irradiate the seeds used in this study.

SUPPLEMENTARY MATERIAL

The Supplementary Material for this article can be found online at: https://www.frontiersin.org/articles/10.3389/fpls.2022.928014/full#supplementary-material

Supplementary Figure S1 | Alignment between the sequence Ar-60.1 and Lo7-60.1. Ar-60.1 represents the sequence amplified by P60 from $T6RL^{Ar}$-6AS.6AL translocation. Lo7-60.1 represents the partial sequence of *SECCE6Rv1G0449960.1* of rye Lo7. Red arrows indicate the primer sequences.

Supplementary Figure S2 | Alignment between the sequence Ar-70.1 and Lo7-70.1. Ar-70.1 represents the sequence amplified by P70 from $T6RL^{Ar}$-6AS.6AL translocation. Lo7-70.1 represents the partial sequence of *SECCE6Rv1G0453070.1* of rye Lo7. Red arrows indicate the primer sequences.

REFERENCES

An, D., Ma, P., Zheng, Q., Fu, S., Li, L., Han, F., et al. (2019). Development and molecular cytogenetic identification of a new wheat-rye 4R chromosome disomic addition line with resistances to powdery mildew, stripe rust and sharp eyespot. *Theor. Appl. Genet.* 132, 257–272. doi: 10.1007/s00122-018-3214-3

Bouvet, L., Percival-Alwyn, L., Berry, S., Fenwick, P., Mantello, C. C., Sharma, R., et al. (2022). Wheat genetic loci conferring resistance to stripe rust in the face

of genetically diverse races of the fungus *Puccinia striiformis* f. sp. *tritici. Theor. Appl. Genet.* 135, 301–319. doi: 10.1007/s00122-021-03967-z

Devos, K. M., Atkinson, M. D., Chinoy, C. N., Francis, H. A., Harcourt, R. L., Koebner, R. M., et al. (1993). Chromosomal rearrangements in the rye genome relative to that of wheat. *Theor. Appl. Genet.* 85, 673–680. doi: 10.1007/BF00225004

Fu, S. L., Chen, L., Wang, Y. Y., Li, M., Yang, Z. J., Qiu, L., et al. (2015). Oligonucleotide probes for ND-FISH analysis to identify rye and wheat chromosomes. *Sci. Rep.* 5, 10552. doi: 10.1038/srep10552

Han, F. P., Lamb, J. C., and Birchler, J. A. (2006). High frequency of centromere inactivation resulting in stable dicentric chromosomes of maize. *Proc. Natl. Acad. Sci. U. S. A.* 103, 3238–3243. doi: 10.1073/pnas.0509650103

Hao, M., Liu, M., Luo, J., Fan, C., Yi, Y., Zhang, L., et al. (2018). Introgression of powdery mildew resistance gene *Pm56* on rye chromosome arm 6RS into wheat. *Front. Plant. Sci.* 9, 1040. doi: 10.3389/fpls.2018.01040

Hu, C. Y., Wang, F. T., Lang, X. W., Feng, J., Li, K. J., Lin, R. M., et al. (2022). Resistance analyses on wheat stripe rust resistance genes to the predominant races of *Puccinia striiformis* f. sp. *tritici in China. Sci. Agr. Sin.* 55, 491–502. https://doi.org/10.3864/j.issn.0578-1752.2022.03.006

Jamil, S., Shahzad, R., Ahmad, S., Fatima, R., Zahid, R., Anwar, M., et al. (2020). Role of genetics, genomics, and breeding approaches to combat stripe rust of wheat. *Front. Nutr.* 7, 580715. doi: 10.3389/fnut.2020.580715

Johansson, E., Henriksson, T., Prieto-Linde, M. L., Andersson, S., Ashraf, R., and Rahmatov, M. (2020). Diverse wheat-alien introgression lines as a basis for durable resistance and quality characteristics in bread wheat. *Front. Plant. Sci.* 11, 1067. doi: 10.3389/fpls.2020.01067

Komuro, S., Endo, R., Shikata, K., and Kato, A. (2013). Genomic and chromosomal distribution patterns of various repeated DNA sequences in wheat revealed by a fluorescence *in situ* hybridization procedure. *Genome* 56, 31–137. doi: 10.1139/gen-2013-0003

Lei, M., Li, G., Zhang, S., Liu, C., and Yang, Z. (2011). Molecular cytogenetic characterization of a new wheat Secale africanum 2Ra(2D) substitution line for resistance to stripe rust. *J. Genet.* 90, 283–287. doi: 10.1007/s12041-011-0081-y

Li, G. R., Gao, D., La, S. X., Wang, H. J., Li, J. B., He, W. L., et al. (2016a). Characterization of wheat-Secale africanum chromosome 5R(a) derivatives carrying Secale specific genes for grain hardness. *Planta* 243, 1203–1212. doi: 10.1007/s00425-016-2472-z

Li, G. R., Tang, L. R., Yin, Y., Zhang, A. H., Yu, Z. H., Yang, E. N., et al. (2020a). Molecular dissection of Secale africanum chromosome 6Rafr in wheat enabled localization of genes for resistance to powdery mildew and stripe rust. *BMC. Plant. Biol.* 20, 134. doi: 10.1186/s12870-020-02351-1

Li, J. B., Dundas, I., Dong, C. M., Li, G. R., Trethowan, R., Yang, Z. J., et al. (2020b). Identification and characterization of a new stripe rust resistance gene *Yr83* on rye chromosome 6R in wheat. *Theor. Appl. Genet.* 133, 1095–1107. doi: 10.1007/s00122-020-03534-y

Li, J. J., Endo, T. R., Saito, M., Ishikawa, G., Nakamura, T., and Nasuda, S. (2013). Homoeologous relationship of rye chromosome arms as detected with wheat PLUG markers. *Chromosoma* 122, 555–564. doi: 10.1007/s00412-013-0428-7

Li, M., Tang, Z. X., Qiu, L., Wang, Y. Y., Tang, S. Y., and Fu, S. L. (2016b). Identification and physical mapping of new PCR-based markers specific for the long arm of rye (*Secale cereale* L.) chromosome 6. *J. Genetics. Genomics.* 43, 209–216. doi: 10.1016/j.jgg.2015.11.005

McIntyre, C. L., Pereira, S., Moran, L. B., and Appels, R. (1990). New *Secale cereale* (rye) DNA derivatives for the detection of rye chromosome segments in wheat. *Genome* 33, 635–640. doi: 10.1139/g90-094

Rabanus-Wallace, M. T., Hackauf, B., Mascher, M., Lux, T., Wicker, T., Gundlach, H., et al. (2021). Chromosome-scale genome assembly provides insights into rye biology, evolution and agronomic potential. *Nat. Genet* 53, 564–573. doi: 10.1038/s41588-021-00807-0

Ren, T., Li, Z., Tan, F., Jiang, C., and Luo, P. (2022). "Advances in identifying stripe rust resistance genes in cereals," in *Achieving Durable Disease Resistance in Cereals*, ed R. Oliver (Cambridge: Burleigh Dodds Science Publishing), 39–80. doi: 10.19103/AS.2021.0092.04

Ren, T. H., Sun, Z. X., Ren, Z. L., Tan, F. Q., Luo, P. G., Tang, Z. X., et al. (2020). Molecular and cytogenetic characterization of a wheat-rye 7BS.7RL translocation line with resistance to stripe rust, powdery mildew, and fusarium head blight. *Phytopathology* 110, 1713–1720. doi: 10.1094/PHYTO-02-20-0061-R

Schneider, A., Rakszegi, M., Molnár-Láng, M., and Szakács, É. (2016). Production and cytomolecular identification of new wheat-perennial rye (Secale cereanum) disomic addition lines with yellow rust resistance (6R) and increased arabinoxylan and protein content (1R, 4R, 6R). *Theor. Appl. Genet.* 129, 1045–1059. doi: 10.1007/s00122-016-2682-6

Spetsov, P., and Daskalova, N. (2022). Resistance to pathogens in wheat-rye and triticale genetic stocks. *J. Plant. Pathol.* 104, 99–114. https://doi.org/10.1007/s42161-021-01019-5

Tang, Z. X., Yang, Z. J., and Fu, S. L. (2014). Oligonucleotides replacing the roles of repetitive sequences pAs1, pSc119.2, pTa-535, pTa71, CCS1, and pAWRC.1 for FISH analysis. *J. Appl. Genet.* 55, 313–318. doi: 10.1007/s13353-014-0215-z

Vershinin, A. V., Schwarzacher, T., and Heslop-Harrison, J. S. (1995). The large-scale genomic organization of repetitive DNA families at the telomeres of rye chromosomes. *Plant. Cell.* 7, 1823–1833. doi: 10.1105/tpc.7.11.1823

Wan, A., Wang, X., Kang, Z., and Chen, X. (2017). "Variability of the stripe rust pathogen," in *The Stripe Rust*, ed X. Chen (Van Godewijckstraat: Springer Nature), 35–154. doi: 10.1007/978-94-024-1111-9_2

Xi, W., Tang, Z., Luo, J., and Fu, S. (2019). Physical location of new stripe rust resistance gene(s) and PCR-based markers on rye (*Secale cereal* L.) chromosome 5 using 5R dissection lines. *Agronomy* 9, 498. doi: 10.3390/agronomy9090498

Xiao, Z. Q., Tang, S. Y., Qiu, L., Tang, Z. X., and Fu, S. L. (2017). Oligonucleotides and ND-FISH displaying different arrangements of tandem repeats and identification of *Dasypyrum villosum* chromosomes in wheat backgrounds. *Molecules* 22, 973. doi: 10.3390/molecules22060973

Conflict of Interest: The authors declare that the research was conducted in the absence of any commercial or financial relationships that could be construed as a potential conflict of interest.

Publisher's Note: All claims expressed in this article are solely those of the authors and do not necessarily represent those of their affiliated organizations, or those of the publisher, the editors and the reviewers. Any product that may be evaluated in this article, or claim that may be made by its manufacturer, is not guaranteed or endorsed by the publisher.

frontiers | Frontiers in Plant Science

ORIGINAL RESEARCH
published: 06 July 2022
doi: 10.3389/fpls.2022.918437

Genetic Analysis of Adult Plant Resistance to Stripe Rust in Common Wheat Cultivar "Pascal"

Bin Bai[1†], Zimeng Li[2†], Hongmei Wang[3], Xiaolin Du[1,4], Ling Wu[5], Jiuyuan Du[1] and Caixia Lan[2*]*

[1] Wheat Research Institute, Gansu Academy of Agricultural Sciences, Lanzhou, China, [2] Hubei Hongshan Laboratory, College of Plant Science and Technology, Huazhong Agricultural University, Wuhan, China, [3] Institute of Biotechnology, Gansu Academy of Agricultural Sciences, Lanzhou, China, [4] College of Life Science and Technology, Gansu Agricultural University, Lanzhou, China, [5] Crop Research Institute, Sichuan Academy of Agricultural Sciences, Chengdu, China

OPEN ACCESS

Edited by:
Cheng Liu,
Shandong Academy of Agricultural Sciences, China

Reviewed by:
Jindong Liu,
Institute of Crop Sciences (CAAS), China
Hongjie Li,
Institute of Crop Sciences (CAAS), China
Bhoja Raj Basnet,
International Maize and Wheat Improvement Center, Mexico

***Correspondence:**
Bin Bai
baibingaas@gsagr.cn
Caixia Lan
cxlan@mail.hzau.edu.cn

[†] These authors have contributed equally to this work and share first authorship

Specialty section:
This article was submitted to Plant Pathogen Interactions, a section of the journal Frontiers in Plant Science

Received: *12 April 2022*
Accepted: *09 June 2022*
Published: *06 July 2022*

Citation:
Bai B, Li Z, Wang H, Du X, Wu L, Du J and Lan C (2022) Genetic Analysis of Adult Plant Resistance to Stripe Rust in Common Wheat Cultivar "Pascal". Front. Plant Sci. 13:918437. doi: 10.3389/fpls.2022.918437

Wheat stripe rust is an important foliar disease that affects the wheat yield globally. Breeding for resistant wheat varieties is one of the most economically and environmentally effective ways to control this disease. The common wheat (*Triticum aestivum* L.) cultivar "Pascal" exhibited susceptibility to stripe rust at the seedling stage but it showed high resistance to stripe rust at the adult plant stage over 20 years in Gansu, a hotspot of the disease in northwestern China. To understand the genetic mechanism of stripe rust resistance in this cultivar, a 55K SNP array was used to analyze the two parents and the 220 recombinant inbred lines (RILs) derived from the cross of "Huixianhong" × "Pascal." We detected three new stripe rust adult plant resistance (APR) quantitative trait locus (QTL) contributed by Pascal, viz. *QYr.gaas-1AL*, *QYr.gaas-3DL,* and *QYr.gaas-5AS*, using the inclusive composite interval mapping method. They were flanked by SNP markers *AX-111218361—AX-110577861*, *AX-111460455—AX-108798599*, and *AX-111523523—AX-110028503*, respectively, and explained the phenotypic variation ranging from 11.0 to 23.1%. Bulked segregant exome capture sequencing (BSE-Seq) was used for fine mapping of *QYr.gaas-1AL* and selection of candidate genes, *TraesCS1A02G313700*, *TraesCS1A02G313800*, and *TraesCS1A02G314900* for *QYr.gaas-1AL*. KASP markers *BSE-1A-12* and *HXPA-3D* for *QYr.gaas-1AL* and *QYr.gaas-3DL* were developed for breeders to develop durable stripe rust-resistant wheat varieties.

Keywords: genetic mapping, quantitative traits, adult plant resistance, stripe rust, wheat

INTRODUCTION

Wheat stripe rust, also known as yellow rust, caused by the air-borne fungus *Puccinia striiformis* f. sp. *tritici* (*Pst*), is considered the primary biotic threat to wheat production globally (Todorovska et al., 2009). In 2017, 88% of the world's wheat production was susceptible to stripe rust, causing yield losses estimated to be 1 billion USD (Brandt et al., 2021), and a countrywide epidemic affected about 5.5 million ha of wheat in China (Zeng et al., 2022). It shows regional characteristics and occurs frequently in the southwestern and northwestern of China, especially in the southeastern Gansu, a stripe rust hotspot in northwestern of China (Bai et al., 2012). The management of

stripe rust includes the deployment of resistant wheat and the use of fungicide, and breeding resistant wheat cultivars is the most effective and economic strategy for controlling stripe rust (Wen et al., 2008).

Genetic resistance to stripe rust in wheat can be broadly divided into two phenotypically, mechanistically, and genetically distinct categories: (a) seedling resistance (all-stage resistance, ASR), which is detected at the seedling stage but is also expressed at all developmental stages. It usually shows a major effect and is race specific (Roberts and Caldwell, 1970; Lin and Chen, 2007); (b) adult plant resistance (APR), which is expressed at the adult plant stages and appears to be durable. Some APR genes are less characterized and are difficult to select phenotypically (Ren R. et al., 2012).

To date, most identified stripe rust resistance genes conferring "seedling resistance" encode classic nucleotide-binding site leucine-rich repeat (NBS-LRR) R proteins that recognize effectors and trigger a defense response to resist disease. While it is easy to overcome the recognition of a single classical R gene *via* a single genetic variation in an avirulence gene (Steuernagel et al., 2016; Schwessinger, 2017). The major epidemics causing severe economic losses have occurred in various regions of the world including United States, China, and Australia (Nsabiyera et al., 2018) due to virulence on seedling resistance genes including *Yr2*, *Yr6*, *Yr9*, *Yr17,* and *Yr27* (Wellings and McIntosh, 1990; Nsabiyera et al., 2018). Only a few seedling stripe rust resistance genes (i.e., *Yr5* and *Yr15*) are still effective to some *Pst* races in China, which drives the demand for persistent disease-resistant cultivars.

Adult plant resistance is generally known as more durable than ASR, since a single genetic variation appears insufficient to overcome this type of resistance in the asexual stage of *Pst* (Schwessinger, 2017). In general, APR delays infection and production of spore, leading to slow rusting phenotypes instead of complete immunity. This type of resistance gene usually encodes allele-specific protein variants that are molecularly unrelated to NBS-LRR proteins. In the case of these genes, *Yr18* and *Yr46* encode two types of transporters (Krattinger et al., 2009; Moore et al., 2015). In addition, *Yr36*, a chloroplast-localized kinase WKS1 regulating, reactive oxygen species production (Ellis et al., 2014; Gou et al., 2017). Since the durability of R genes is usually defined by the global genetic diversity of the pathogen, the combination of APR genes with ASR genes is the best way for a wheat breeder to develop the durable stripe rust resistant wheat variety at all plant stages. To date, more than 83 *Yr* genes or alleles (*Yr1–Yr83*) have been formally named in wheat (Li et al., 2020; Draz et al., 2021). Most of them are race-specific ASR genes, and only a few are APR genes. *Lr34/Yr18/Pm38/Sr57* (Dyck, 1991), *Lr46/Yr29/Pm39/Sr58* (Singh et al., 1998), and *Lr67/Yr46/Pm46/Sr55* (Herrera-Foessel et al., 2011) confer pleiotropic APR to stripe rust, leaf rust, powdery mildew, and stem rust. QTL analysis has been widely used to dissect complex traits through identifying the genomic location and effects of genes contributing to quantitative variation (Young, 1996). Over the past 20 years, more than 320 stripe rust resistance QTLs have been reported using different molecular markers, including diversity array technology (DArT), single sequence repeats (SSRs), and single-nucleotide polymorphisms (SNPs) (Lan et al., 2017); the genetic locations of these QTLs are continually being refined through fine mapping studies (Lan et al., 2017; Draz et al., 2021).

Various approaches can be used to identify genetic loci and genes in wheat. High-density SNP markers using gene-chip technology provide a superior approach for QTL mapping due to their high-throughput, efficiency, allele specificity, and high-resolution capacity (Yu et al., 2011; Draz et al., 2021). The Axiom wheat 55K SNP array with 53,063 SNP probes was selected from the wheat 660K SNP array, which is considered to be more appropriate for wheat genetic research (Ren et al., 2018; Huang et al., 2019). Based on the advantages of lower costs, higher accuracy, and its medium density, this SNP array has been widely used in QTL identification in wheat (Huang et al., 2019; Zhang et al., 2019). Also, whole-genome exome sequencing (WES) has been successfully applied for the identification of genetic loci and isolating genes in wheat (Henry et al., 2014; Mo et al., 2018). For instance, candidate natural variants were identified using a 110 Mb exome capture assay at the *Yr6* locus responsible for stripe rust resistance (Gardiner et al., 2016). A BSA-based exome capture sequencing pipeline for rapid gene cloning has been developed by Chengdu Tcuni Technology, which is an alternative method to effectively sequence coding regions with low cost in wheat (Dong et al., 2020). Therefore, SNP chip and WES approaches can be the effective strategies to find new genetic loci and candidate genes associated with important traits in wheat.

The Italian common winter wheat cv. Pascal (Lan Yin 1), introduced to Gansu Province of China in 1995, showed a high level of APR to stripe rust in the field but was susceptible to CYR32 and CYR33 at the seedling stage. However, the seedling gene locations and inheritance of APR to stripe rust in Pascal were not clear. Thus, the objectives of this study were to (1) map seedling stripe rust resistance gene in the Huixianhong/Pascal F_5 RIL population; (2) identify the APR to stripe rust in the same population; (3) determine the interaction effect between the identified resistance loci on stripe rust in the adult plant stage; and (4) develop molecular markers of new and stable resistance QTL for the wheat breeder to breed durable stripe rust-resistant wheat variety.

MATERIALS AND METHODS

Parent Materials

A population of 220 F_5 RILs was developed from a cross between "Huixianhong" and "Pascal." "Pascal" is a stripe rust-resistant parent, whereas the cultivar "Huixianhong" is highly susceptible to stripe rust in the field. Huixianhong was widely used as a susceptible spreader and negative control in the genetic analysis of wheat stripe rust resistance. A single seed descend method was used to develop the F_5 RIL population.

Seedling Test

The parents were evaluated for their reaction to stripe rust at the seedling stage using the *Pst* races CYR32 and CYR33 under greenhouse conditions at Huazhong Agricultural University, and

the reaction to CYR34 was tested in the Gansu Academy of Agricultural Sciences. The races of the pathogen were inoculated by spraying urediniospores suspended in mineral oil using an atomizer when wheat seedlings reached the two-leaf stage. The inoculated plants were left in an open area for 20 min to facilitate the evaporation of the oil and then placed in the dew chamber of 7°C for 24 h and back to the greenhouse. The infection types (ITs) were recorded approximately 2 weeks post-inoculation, based on a 0–9 scale modified from McNeal et al. (1971), and ITs with the scale of "0, 1, 2, 3, 4," "5, 6," and "7, 8, 9" are categorized as resistant, intermediate, and susceptible groups, respectively.

Adult Plant Stage of Field Test

The parents and RIL population were evaluated for APR to stripe rust in Qingshui Experimental Station of Gansu Academy of Agricultural Sciences during the 2017–2018 and the 2018–2019 growing seasons (GS2018 and GS2019), and in 2018–2019 growing season in Pidu Experimental Station of Sichuan Academy of Agricultural Sciences (SC2019).

Field plots consisted of 1.5-m rows planted with approximately fifty seeds of each line, and we used randomized complete block design with two replicates of the RIL population in each location. "Jinmai 47" was planted at every tenth plot of experimental materials and around the experiment as a susceptible check and spreader to ensure the maximum inoculum for disease development. Disease severity (DS) for the RILs and their parents in each environment was recorded one time or two times following the modified Cobb's scale (Peterson et al., 1948).

In 2018, we took the first rating when the susceptible check Huixianhong showed approximately 80% DS around 12 June, and the second rating about a week later when the DS of the susceptible check reached 90–100% in Gansu. In the other two environments, we investigated the phenotype once when the DS of susceptible check reached 90–100%. Combined with the natural infection, a mixture of *Pst* races CYR32, CYR33, and CYR34 was used to inoculate the spreaders at the jointing growth stage (around 2 months after planting). The lme4 package in Rstudio[1] was used to calculate the best linear unbiased prediction (BLUP).

Correlation Analysis of the Phenotypic Data

SAS 9.2 software (SAS Institute, Cary, NC) was used to calculate the correlations of final disease severity (FDS) for stripe rust in each season. The analysis of variance (ANOVA) was used to assess the significant effect of a single stripe rust resistance QTL and the interaction effect for multiple stripe rust resistance QTLs with the FDS values in each environment.

Genetic Linkage Map Construction and Quantitative Trait Locus Mapping

Deoxyribonucleic acid was extracted from about 20 plants of each line and parents using the cetyltrimethylammonium bromide (CTAB) method (Chatterjee et al., 2002). The 55K SNP array genotyping platform was used to genotype the parents and RIL population. A total of 55,000 SNP markers were obtained, of which 9,475 SNP markers were selected to make linkage groups by removing markers of distorted segregation ($p < 0.001$), monomorphic markers, and markers with more than 30% missing data. Genetic linkage groups were established using Joinmap 4.1 (Van, 2011) with a logarithm of odds (LODs) threshold of 10.0. MapChart (Voorrips, 2002) was used to draw genetic linkage maps. Software IciMapping 4.1 (Meng et al., 2015) was used to detect FDS-related QTL in each environment, BLUP and mean of final disease severity (MFDS) across each season to obtain the significant QTL position, LOD scores, phenotypic variance explained (PVE), and the additive effect of each locus. About one-thousand permutations were used to calculate LOD scores for each trait. The physical positions of identified QTL were compared with those previously reported on the same chromosome arm under different wheat lines, based on the wheat genome of (International Wheat Genome Sequencing Consortium [IWGSC], 2018).

Bulked Segregant Exome Capture Sequencing

The bulked segregant exome capture sequencing (BSE-Seq) was used for identifying causal mutations or candidate genes in this study. First, the genomic DNA of 33 extremely resistance (low FDS) lines and 43 extremely susceptible (high FDS) lines from the Huixianhong/Pascal F_5 population was extracted by CTAB method (Chatterjee et al., 2002) and then bulked in an equal amount of each line to generate the resistant-type bulked DNA pool and susceptible-type bulked DNA pool separately. The genomic DNA of Huixianhong and Pascal was also extracted using the same method as above. Therefore, the resistant-type bulked DNA pool, susceptible-type bulked DNA pool, resistant-type parent DNA, and susceptible-type parent DNA were used to Exome Capture Sequencing, which was developed by Chengdu Tcuni Technology.

The Euclidean Distance (ED) algorithm is a method using sequencing data to find significantly different markers between bulks and evaluates the region associated with the target trait (Hill et al., 2013).

$$ED = \sqrt{\begin{array}{l}(Amut - Awt)^2 + (Tmut - Twt)^2 + (Cmut - Cwt)^2 \\ \quad + \ (Gmut - Gwt)^2\end{array}}$$

In the formula, A, T, C, and G mut are the frequencies of A, T, C, and G bases in the mutant bulk, respectively; A, T, C, and G wt are the frequencies of A, T, C, and G bases in the wild-type bulk, respectively. Theoretically, the ED values of other loci should tend to 0 except for the target trait-related sites between the two mixed pools.

RESULTS

Phenotypic Analysis

Both Huixianhong and Pascal were susceptible after being inoculated by CYR32, CYR33, and CYR34 at the seedling stage (IT varied from 78 to 8) (**Figures 1A,B**). However, the MFDS

[1]https://CRAN.R-project.org/package=lme4

FIGURE 1 | The two parents Huixianhong (left) and Pascal (right) showed susceptible against stripe rust race CYR32 **(A)** and CYR33 **(B)** at the seedling stage. The response of susceptible parent Huixianhong **(C)** and the resistant parent Pascal **(D)** in the adult plant stage under Gansu province field test.

for Huixianhong and Pascal were 100 and 3%, respectively, in the adult plant stage (**Figures 1C,D**) over three environments. The frequency distributions of stripe rust severity among F_5 RILs showed a normal distribution (**Figure 2**), indicating a typical quantitative character for controlling stripe rust resistance in the Huixianhong/Pascal population. Pearson correlation coefficients (r) of stripe rust severity ranged from 0.66 to 0.85 over the environments (**Table 1**). In addition, it was estimated that there were around 3–4 stripe rust resistance genes with additive effects in the Huixianhong/Pascal RIL population based on the qualitative assessment of the Mendelian genetic segregation ratios (**Table 2**).

Genetic Linkage Map Construction

A genetic linkage map was constructed with a total of 9,475 markers and developed 28 linkage groups on the 21 wheat chromosomes. A total of three QTLs were identified for stripe rust resistance from "Pascal" and they were mapped on wheat chromosomes 1AL (*QYr.gaas-1AL*), 3DL (*QYr.gaas-3DL*), and 5AS (*QYr.gaas-5AS*) (**Table 3**). *QYr.gaas-1AL* was flanked by SNP markers *AX-111218361* and *AX-110577861* and located at 505.3–507.9 Mb based on IWGSC RefSeq v1.0 genome sequence information. It was stably detected in all tested environments with PVE values ranging from 11.3 to 23.1% (**Table 3**). *QYr.gaas-3DL* was closely linked to markers *AX-108798599*, *AX-109580758,* and *AX-111460455*. It was located around 354.6 Mb based on IWGSC RefSeq v1.0 genome sequence information and was also consistently detected in all three stripe rust field experiments explaining 16.1–20.6% total stripe rust variation (**Table 3**). The third QTL, *QYr.gaas-5AS*, was flanked by SNP markers *AX-111523523* and *AX-110028503* and mapped at the interval of 59.1–62.2 Mb based on IWGSC 1.0 with PVE values ranging from 11.0 to 17.3% (**Figure 3C** and **Table 3**).

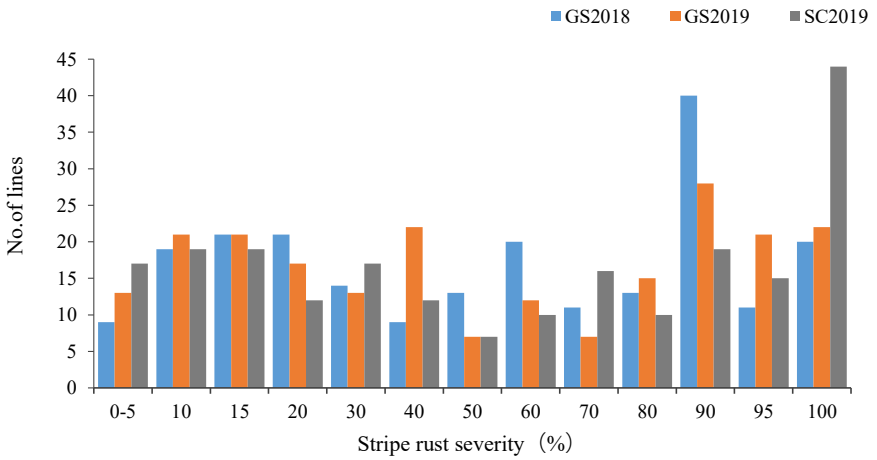

FIGURE 2 | Frequency distributions of 220 Huixianhong/Pascal F_5 recombinant inbred lines (RILs) for final disease severity of stripe rust in field traits at Gansu Province during 2017–2018 (GS2018), 2018–2019 (GS2019), and at Sichuan Province during 2018–2019 (SC2019).

Interactive Effects of Detected Resistance Loci

Based on the flanking molecular markers of detected three stripe rust resistance QTLs, we divided the F_5 RILs into 8 groups. The presence of parental alleles for each QTL was determined by markers inferred factorial combinations of the three stripe rust resistance QTLs.

There was a significantly different disease response between RILs carrying either *QYr.gaas-1AL* or *QYr.gaas-3DL* and RILs without any resistance loci ($p < 0.0001$), which explained 24.2 and 19.3% of the stripe rust variation, respectively (**Table 4**). The lines carrying *QYr.gaas-5AS* also showed a significantly different disease response from those without any resistance locus, but this locus only explained 8.5% of the stripe rust variation. This indicates that this third locus imparts a minor effect on stripe rust resistance than the other two loci (**Table 4**). A significant interaction ($p < 0.0001$) between *QYr.gaas-1AL* and *QYr.gaas-3DL* was observed across three environments as well as MFDS, which explained 3.3% of stripe rust variation based on MFDS. There were no significant differences among the average FDS of RILs carrying combinations of *QYr.gaas-1AL*Qyr.gaas-5AS*, *Qyr.gaas-3DL*Qyr.gaas-5AS*, and *QYr.gaas-1AL*QYr.gaas-3DL*QYr.gaas-5AS* ($p > 0.05$); however, the average FDS of RILs carrying combinations of three resistance QTLs was significantly lower than the average FDS of RILs carrying other combinations of two resistance QTLs ($p < 0.0001$) (**Table 4**).

TABLE 1 | Phenotypic Pearson's correlations for stripe rust (GS2018, GS2019, SC2019) in the Huixianhong/Pascal F_5 RIL population using the final disease severity for each season.

Environment	GS2018	GS2019	SC2019	YRM
GS2019	0.85**			
SC2019	0.66**	0.70**		
YRM	0.93**	0.91**	0.86**	
BLUP	0.91**	0.90**	0.87**	0.99**

*GS2018, final stripe rust severity during Gansu 2017–2018; GS2019, final stripe rust severity during Gansu 2018–2019; SC2019, final stripe rust severity during Sichuan 2018–2019; YRM, the mean final disease severity of each season. **Significant at p < 0.0001.*

TABLE 2 | The number of resistance genes that confer adult plant resistance to stripe rust calculated by Mendelian segregation ratios in Huixianhong/Pascal recombinant inbred lines population.

Category	GS2018	GS2019	SC2019	YRM	BLUP
HTPR[a]	9	13	15	8	4
HTPS[b]	20	22	30	9	11
Other[c]	188	184	173	203	205
In total	217	219	218	220	220
No. of genes	3	3	3	4	4
P-value	0.08*	0.32*	0.01	0.95*	0.21*

[a]*HPTR means homozygous parental type resistant (RILs showing a similar phenotype as the resistant parent).*
[b]*HPTS means homozygous parental type susceptible (RILs showing a similar phenotype as the susceptible parent).*
[c]*Other means RILs showing different responses from the above two categories.*
**Means p > 0.05.*

Bulked Segregant Exome Capture Sequencing

We filtered the data obtained by BSE-Seq with ref_Freq > 0.3, minDepth > 5 and ED = top 0.05 through the ED algorithm, and the results showed that there was a clear peak on chromosome 1AL, which is roughly around 506 Mb (**Figures 4A,B**). The SNPs between R bulk (same as resistance cultivar Pascal) and S bulk (same as susceptible cultivar Huixianhong) were filtered by AF < 0.2 or AF > 0.8, and the significant SNPs were found in a region of ∼506 Mb on chromosome 1A (**Figures 4C,D**). This result is also consistent with our mapping result, which indicates significant differences between two resistant and susceptible bulks and showed a high correlation between this region and stripe rust. Unfortunately, we failed to find high confidence SNPs

TABLE 3 | Position and effect of quantitative trait loci (QTL) that were detected for adult plant resistance (APR) to stripe rust (YR) in the test years, using each final disease severity, the mean of final disease severity (MFDS), best linear unbiased prediction (BLUP) for the Huixianhong/Pascal RIL population.

QTL	Traits	Chr	Pos (cM)	Marker interval	Phy pos (Mb)	LOD[a]	PVE (%)[b]	Add[c]
QYr.gaas-1AL	GS2018	1A	202	*AX-111218361—AX-110577861*	505.3–507.9	11.2	23.1	15.3
	GS2019	1A	202	*AX-111218361—AX-110577861*	505.3–507.9	4.8	11.3	9.9
	SC2019	1A	202	*AX-111218361—AX-110577861*	505.3–507.9	19.6	15.3	22.0
	YRM	1A	202	*AX-111218361—AX-110577861*	505.3–507.9	27.2	16.2	19.9
	BLUP	1A	202	*AX-111218361—AX-110577861*	505.3–507.9	27.2	15.9	17.3
QYr.gaas-3DL	SC2019	3D	350	*AX-111460455—AX-108798599*	354.6–360.5	17.4	16.1	19.0
	YRM	3D	350	*AX-111460455—AX-108798599*	354.6–360.5	18.4	20.6	15.9
	BLUP	3D	350	*AX-111460455—AX-108798599*	354.6–360.5	18.1	20.3	13.8
	GS2018	3D	351	*AX-108798599—AX-109580758*	339.7–354.6	13.1	16.4	15.3
	GS2019	3D	351	*AX-108798599—AX-109580758*	339.7–354.6	15.5	17.5	17.4
QYr.gaas-5AL	SC2019A	5A	197	*AX-111523523—AX-110028503*	59.1–62.2	5.4	11.0	12.8
	GS2018B	5A	198	*AX-111523523—AX-110028503*	59.1–62.2	4.9	13.2	10.3
	GS2019B	5A	198	*AX-111523523—AX-110028503*	59.1–62.2	6.9	15.7	12.6
	YRM	5A	198	*AX-111523523—AX-110028503*	59.1–62.2	6.3	15.8	11.3
	BLUP	5A	198	*AX-111523523—AX-110028503*	59.1–62.2	16.4	17.3	17.5

[a] *Logarithm of odds (LOD) score of QTL peak.*
[b] *Proportion of phenotypic variance explained by the QTL.*
[c] *Additive effect of phenotypic for each QTL.*

on chromosome 3D through BSE-Seq, which may be related to the collection stage of materials or different process of related gene expression.

For fine mapping *QYr.gaas-1AL*, we developed three Kompetitive allele-specific PCR (KASP) markers near *QYr.gaas-1AL* based on the SNP of BSE-Seq. *QYr.gaas-1AL* was 0.5–3.5 cM away from KASP marker *BSE-1A-12* (**Supplementary Table 1** and **Figure 3A**), which covered a physical interval of 505.3–506.8 Mb on chromosome 1A. There were 18 high confidence genes in this interval, whereas 13 genes have SNPs on their exon regions. *TraesCS1A02G313700* has 14 SNPs on its exon regions which encodes a dentin sialophosphoprotein-like protein. *TraesCS1A02G313800* and *TraesCS1A02G314900* encode early light-induced protein and metacaspase, respectively, which have 13 and 10 SNPs on their exon regions. The three candidate genes might have strong relationship with *QYr.gaas-1AL*.

The Distribution of *QYr.gaas-1AL* and *QYr.gaas-3DL*

Since *QYr.gaas-3DL* contributed stripe rust resistance in Pascal significantly, we converted SNP marker *AX-109580758* to a KASP marker and combined it with the phenotypic data for QTL mapping in 220 RIL families. The KASP marker *HXPA-3D* was 1.5–3.5 cm away from *QYr.gaas-3DL* (**Figure 3B**). This fact suggests that KASP marker *HXPA-3D* can be used as an effective marker to detect *QYr.gaas-3DL* for developing durable stripe rust resistant wheat varieties.

A total of two KASP markers *BSE-1A-12* and *HXPA-3D* for two stable loci were used to genotype a collection of 153 Chinese and global germplasm resources. In the global collection, *QYr.gaas-1AL* appears more frequently (69%), as compared to the Chinese wheat germplasm in which *QYr.gaas-1AL* appeared in 62%. Similarly, *QYr.gaas-3DL* is very common in foreign germplasm (75%), and it is significantly lower in Chinese wheat varieties and breeding lines (60%) (**Supplementary Table 2**). Our results suggest that Pascal could be a useful source of effective resistance against stripe rust in China.

DISCUSSION

"Pascal" was conferred by two recessive genes effective against two *Pst* races CYR 31 and CYR 32, respectively, at the seedling stage (Cao et al., 2006). In this study, we found both parents, Huixianhong and Pascal, susceptible to three *Pst* races of CYR32, CYR33, and CYR34 at the seedling stage (IT varied from 7 to 8). Most of the stripe rust resistance genes conferring seedling resistance can easily lose their effect since selection pressure favors the virulence in the pathogen population, which could explain that Pascal does not provide seedling resistance to stripe rust in this study. The constant evolution of pathogens and thus the breakdown of seedling resistance make our effort to continuously identify the sources of adult plant resistance increasingly important. We mapped three adult plant resistance QTLs for stripe rust in the Huixianhong/Pascal RIL population, and Pascal showed stable resistant over the last 50 years. There were five stripe rust resistance genes on chromosome 3D, viz. *Yr45* (Li et al., 2011), *Yr49* (Ellis et al., 2014), *Yr66* (Bariana et al., 2022), *Yr71* (Bariana et al., 2016), and *Yr73* (Dracatos et al., 2016). *Yr45*, *Yr71*, and *Yr73* were mapped on the 3DL, and the other two genes were mapped on 3DS. *Yr45* was discovered from a common spring wheat "PI181314," flanked by RGAP markers *wgp118*, *wgp115,* and two SSR markers *Xwmc656* and *Xbarc6*

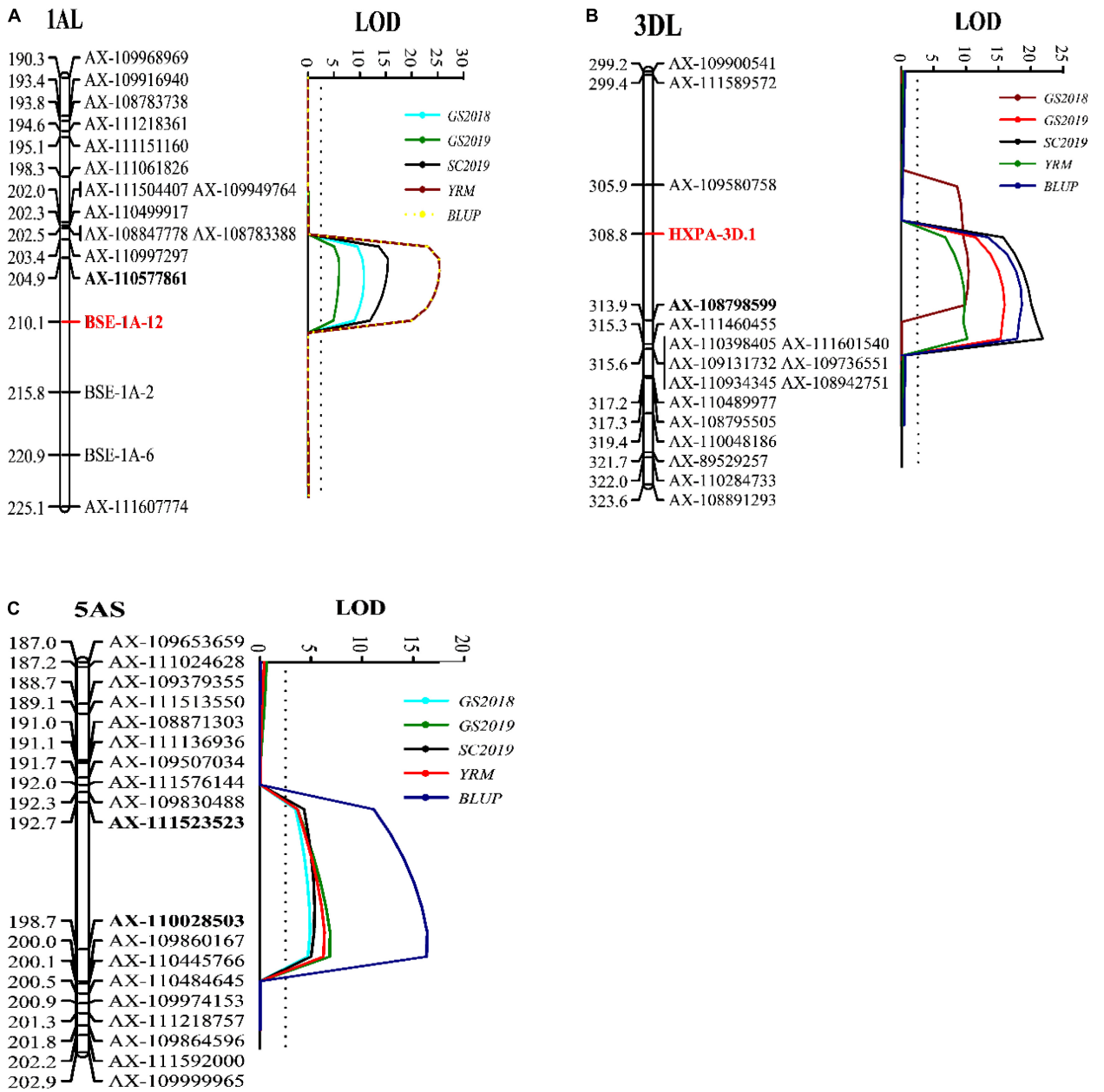

FIGURE 3 | Likelihood plots of quantitative trait loci (QTL) for adult plant resistance to stripe rust on chromosomes 1AL **(A)** after adding three KASP markers *BSE-1A-2*, *BSE-1A-6,* and *BSE-1A-12*, 3DL **(B)** after adding KASP marker *HXPA-3D* and 5AS **(C)** identified by IciMapping 4.1 in the Huixianhong/Pascal RIL population. The significant LOD threshold was based on 1,000 permutations. Positions (in cM) of the molecular markers along chromosomes are shown on the vertical axes using cumulated genetic distances. KASP markers *BSE-1A-2*, *BSE-1A-6,* and *BSE-1A-12* near *QYr.gaas-1AL* were designed based on the SNP of BSE-Seq in the interval of original marker *AX-111218361—AX-110577861*. New marker *BSE-1A-12* and SNP marker *AX-110577861* were closely linked with *QYr.gaas-1AL* identified in the present study. we converted SNP marker *AX-109580758* as a KASP marker named *HXPA-3D* to detect 220 RIL families. KASP marker *HXPA-3D* was closely linked with *QYr.gaas-3DL* identified in the present study. GS2018, final stripe rust severity during Gansu 2017–2018; GS2019, final stripe rust severity, during Gansu 2018–2019; SC2019, final stripe rust severity during Sichuan 2018–2019; YRM, the mean final disease severity of each season; BLUP, best linear unbiased prediction.

which were mapped 11.7 and 12.6 cM proximal to *Yr45*. We tried to test the two parents using markers *wgp115*, *Xwmc656,* and *Xbarc6* (Li et al., 2011). However, none of them are polymorphic, and the physical interval of *Yr45* was from 476.9 to 514.9 Mb on chromosome 3D, whereas *QYr.gaas-3DL* was located around 354.6 Mb on the same chromosome. Besides, *Yr45* is an all-stage resistant gene, whereas *QYr.gaas-3DL* was an APR locus in wheat, and therefore, *Yr45* could be different from *QYr.gaas-3DL*. *Yr71* is an adult plant resistance gene mapped on 3DL in the Australian cultivar Sunco, and the physical position of its flanking

TABLE 4 | Three-way factorial analysis of variance (ANOVA) of final disease severity (FDS) for stripe rust (YR) resistance loci, using years as blocks.

Source	No. of RILs	GS2018 FDS	GS2019 FDS	SC2019 FDS	MFDS[a]	DF	Type III SS	Mean square	*F*-value	Pr > F	Variation (%)
Year						2.0	1085.9	543.0	0.8	0.4	0.4
None	40.0	89.6A[b]	87.5A	80.9A	85.8A						
QYr.gaas-1AL	20.0	65.8BC	71.5AB	75.8A	70.8B	2.0	35459.6	17729.8	27.6	<0.0001	24.2
QYr.gaas-3DL	17.0	58.4BC	60.0BC	74.2A	61.5BC	3.0	41793.1	13931.0	21.7	<0.0001	19.3
QYr.gaas-5AS	20.0	67.4B	57.5BC	67.9A	66.4B	2.0	8755.1	4377.5	6.8	0.0	8.5
*QYr.gaas-1AL *QYr.gaas-5AS*	14.0	49.3CD	26.4D	45.6B	48.1C	2.0	5231.1	2615.5	4.1	0.0	0.5
*QYr.gaas-1AL *QYr.gaas-3DL*	31.0	38.8DE	31.4D	36.1BC	33.7D	4.0	19636.0	4909.0	7.6	<0.0001	3.3
*QYr.gaas-3DL *QYr.gaas-5AS*	7.0	33.2DE	17.7D	25.7C	27.4D	2.0	7184.2	3592.1	5.6	0.0	1.3
*QYr.gaas-1AL *QYr.gaas-3DL *QYr.gaas-5AS*	26.0	21.9E	21.5D	18.5C	20.4D	3.0	6082.8	2027.6	3.2	0.0	3.7

[a]*MFDS means the average of final disease severity over all tested environments, counted by the average YRM of RILs in each resistance genotype.*
[b]*Different letter in each columns means the significant difference between two values at $p < 0.01$.*
**Means the combination of two loci or three loci.*

marker *gwm114b* was at around 603.4 Mb (Bariana et al., 2016). KASP marker *Yr71_16434*, 1.8 cM distal to *Yr71*, was at 608 Mb on chromosome 3D. There was no polymorphic for *Xgwm114b* and *Yr71_16434A* in the "Huixianhong/Pascal" RILs population when we tried to detect the population, whereas *QYr.gaas-3DL* was located near the centromeric region of chromosome 3D. Another gene *Yr73*, a complementary gene on 3DL in the Australian cv. Avocet R, conferred seedling resistance to stripe rust. These results indicate that *QYr.gaas-3DL* is likely different from genes *Yr71* and *Yr73*.

The QTL *QYr/Lr.cim-3DC* for stripe rust near the centromeric region of chromosome 3D was identified in common wheat line UC1110 (Lan et al., 2017). It provided both of the leaf rust and stripe rust resistance in the population. *QYr.gaas-3DL* was also located near the centromeric region of chromosome 3D, but we did not detect the effect on leaf rust. *Qyrsicau-3DL*, a high-confidence APR locus was detected in a genome-wide association study (GWAS) in Sichuan wheat (Ye et al., 2019). The SNP marker *AX-109329567* closely linked with *Qyrsicau-3DL* was located at 595 Mb on chromosome 3D, which was about 240 Mb away from *QYr.gaas-3DL*. Huang et al. (2021) identified an APR QTL (*QYrsn.nwafu-3DL*) on 3DL explaining 5.8–12.2% of the phenotypic variation from Shannong 33 (SN33). The physical position of its flanking marker *AX-109582945* was around 407.4 Mb on chromosome 3D, which is around 52 Mb away from *QYr.gaas-3DL*. Furthermore, *QYrsn.nwafu-3DL* was present in 7.4% of a panel of 420 current Chinese wheat cultivars, which was much lower than the presence of *QYr.gaas-3DL* in a collection of 153 Chinese germplasm resources in our studies. Therefore, *QYrsn.nwafu-3DL* could be different from the APR resistance *QYr.gaas-3DL*.

The stripe rust resistance genes and QTL located on chromosome 5AS in the previous studies are extensive. A minor effect QTL (*QPst.jic-5A*) for field stripe rust resistance on chromosome 5AS was identified in a stripe rust susceptible winter wheat cv. Brigadier (Jagger et al., 2011). *QPst.jic-5A* was located between marker *Xwmc752* and *Xgwm786*, placing it near the centromere on the short arm of chromosome 5A. Since *QYr.gaas-5AS* was mapped at the interval of 59.1–62.2 Mb and far away from the centromere of chromosome 5A, *QPst.jic-5A* could be different from *QYr.gaas-5AS*. A major QTL, *QYr.cau-5AS*, exhibited 24.1–35.3% of PVE in winter wheat AQ24788-83 at the tillering growth stage (Quan et al., 2013). This QTL was flanked by markers *Xcfa2250* and *Xwmc705*, which were located around 245 Mb, suggesting this QTL was different from *QYr.gaas-5AS*.

QYr.cim-5AS was a minor APR QTL derived from Avocet and mapped near the SSR marker *Xcfa2104* and *Xbarc186* (Ren et al., 2017). The physical position of those SSR markers was around 22–46 Mb, placing near *QYr.gaas-5AS* in the present studies. However, it only explained 4.0–5.1% of YR variation, but *QYr.gaas-5AS* had PVE values ranging from 11.0 to 17.3%. It is possible that *QYr.gaas-5AS* is different from this QTL. However, this needs to be confirmed by allelism test in the future. *Qyrsicau-5AS*, a minor APR QTL with a PVE of 7.1–8.1%, were detected by the GWAS in Sichuan wheat (Ye et al., 2019). The SNP marker *AX-111623511* linked with *Qyrsicau-5AS* was located at 101 Mb on chromosome 5A, which was about 40 Mb from *QYr.gaas-5AS*, indicating *QYrsicau-5AS* could be different from the APR resistance *QYr.gaas-5AS*. Therefore, *QYr.gaas-5AS* is possibly a new QTL for APR to stripe rust.

Previous studies have detected several QTLs for stripe rust on chromosome 1AL in wheat. A minor APR QTL *QYr.sgi-1A* was located on chromosome 1A in the population of Kariega/Avocet S, contributing 6–12% to the phenotypic variance, and flanked by markers *s15m19D* and *s23m18E*, but was inconsistently detected across environments (Ramburan et al., 2004). Unfortunately, we failed to obtain the physical location of this QTL. Whereas *QYr.gaas-1AL* had PVE values ranging from 11.3 to 23.1%, it was stable across all environments in our studies, indicating that QTL *QYr.sgi-1A* was unlikely to be the same locus as *QYr.gaas-1AL*. Bariana et al. (2010) identified *QYr.sun-1A* controlling APR to stripe rust in Kukri/Janz-derived doubled haploid (DH)

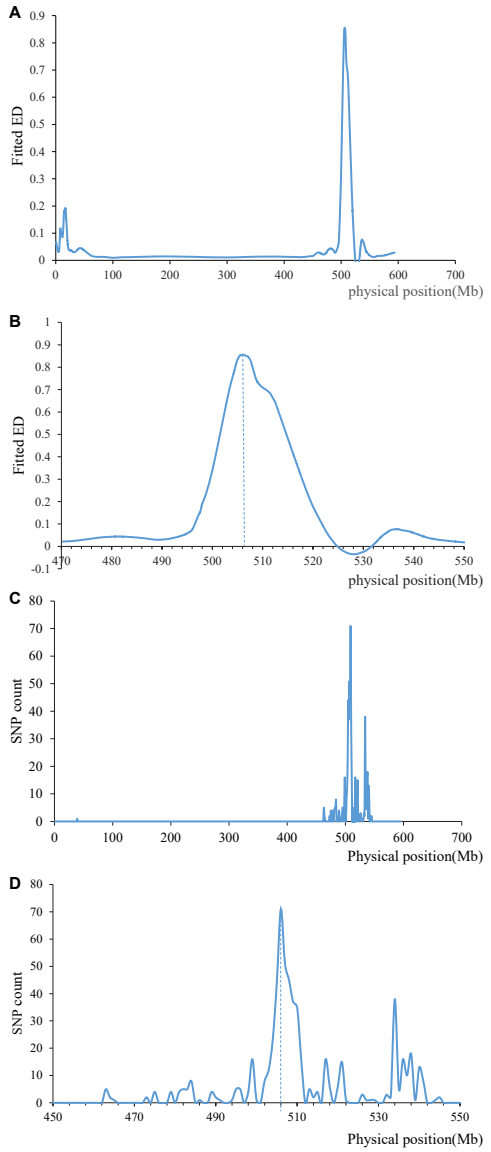

FIGURE 4 | Results of the BSE-Seq analysis method. Fitted ED on chromosome 1A **(A)** and ED after zooming in the area near the maximum **(B)**. SNP count between R bulk same as Pascal and S bulk same as Huixianhong on chromosome 1A **(C)**, and SNP count after zooming in the area near the maximum **(D)**.

population, which explained 6–7% phenotypic variation for stripe rust. This QTL was flanked by marker *Xgwm164* and its physical position was around 280.6 Mb. But *QYr.gaas-1AL* was located in the interval of 505.3–507.9 Mb, which indicated that *QYr.gaas-1AL* was different from *QYr.sun-1A*.

Ren Y. et al. (2012) identified a QTL (*QYr.caas-1AL*) contributed APR to stripe rust in German spring wheat cultivar Naxos. It was located in marker interval *XwPt-2406–Xwmc59* at 575.4 Mb, which was roughly 70 Mb away from *QYr.caas-1AL*. Besides, *QYr.caas-1AL* only explained 8.2% of the phenotypic variance in one environment, which showed lower effect and stability than *QYr.gaas-1AL*. *QYrid.ui-1A*, a minor high-temperature adult plant (HTAP) resistance QTL from the hard red winter wheat germplasm IDO444, were significant only for IT in single environment (Chen et al., 2012). *QYr.gaas-1AL* had high effect of stripe rust resistance and were stable across all environments. Gebrewahid et al. (2020) identified an APR QTL on chromosome 1A in spring wheat Fuyu 3 designated *QYr.hebau-1AL*, which was located on the interval of *AX-109403007* to *AX-110502416* around 286.6–289.3 Mb. This QTL should be different from *QYr.gaas-1AL* based on a physical distance of about 220 Mb between them. Grover et al. (2022) identified an ASR locus *Yraci* in the European winter wheat cultivar "Acienda" on the distal end of wheat chromosome 1A. Besides, two SNPs *AX-95162217* and *AX-94540853* linked with *Yraci* were mapped in the bin at 54.04 cM on chromosome 1A, whereas *QYr.gaas-1AL* covered a physical interval of 505.3–506.8 Mb on chromosome 1A was far away from *Yraci*. Therefore, *Yraci* and *QYr.gaas-1AL* were not the same QTL for strip rust. Further research is needed to determine the novelty of *QYr.gaas-1AL* from Pascal.

Combining BSA and the exome sequence strategy could accelerate gene mapping, especially in wheat with a large and complex genome. BSE-Seq is helpful for the construction of a linkage map across the whole genome, and it could be easily used to identify the linked interval regardless of the multiple gene copies and obtain most of the variations existing in the coding regions of genes (Dong et al., 2020). Using bulked segregant analysis and the exome sequence strategy, Mo et al. (2018) identified a clear peak region on chromosome 4BS associated with increased plant height. Harrington et al. (2019) identified a locus controlling an environmentally dependent chlorosis phenotype in the Durum wheat cv. Kronos. Martinez et al. (2020) finely mapped a novel *TaMKK3* allele conferring the wheat ERA8 ABA-hypersensitive germination phenotype in a wheat backcross population. In our studies, BSE-Seq helped us to confirm the reality of QTL and select candidate genes in QTL *QYr.gaas-1AL* region. *TraesCS1A02G313700*, *TraesCS1A02G313800,* and *TraesCS1A02G314900* had more than 10 SNPs on their exon regions. Of these genes, *TraesCS1A02G314900* encodes metacaspase, which has been reported to modulate autophagy to confine cell death to the target cells during Arabidopsis vascular xylem differentiation (Escamez et al., 2016), which suggests that this gene may be a strong candidate related to disease resistance. Further research is needed to determine the relationship between these genes and stripe rust resistance.

DATA AVAILABILITY STATEMENT

The original contributions presented in the study are included in the article/**Supplementary Material**, further inquiries can be directed to the corresponding author/s.

AUTHOR CONTRIBUTIONS

BB initiated the project, designed the experiment, and contributed to phenotype data. CL designed the experiment

and finalized the manuscript. ZL assisted in the data analysis and contributed to drafting the manuscript. HW and XD performed the sample preparation and DNA extraction. LW and JD contributed to the part of phenotype data in the field. All authors read and approved the final manuscript.

FUNDING

This work was supported by the National Natural Science Foundation of China (grant no. 31860379), Key R&D Program of Gansu Province (grant no. 21YF5NA146), the National Natural Science Foundation of China (grant no. 31860378), International Cooperation and Exchange of the National Natural Science Foundation of China (grant no. 31861143010), and the Hubei Hongshan Laboratory (grant no. 2022hspy001).

SUPPLEMENTARY MATERIAL

The Supplementary Material for this article can be found online at: https://www.frontiersin.org/articles/10.3389/fpls.2022.918437/full#supplementary-material

REFERENCES

Bai, B., Ren, Y., Xia, X., Du, J., and Zhou, G. (2012). Mapping of quantitative trait loci for adult plant resistance to stripe rust in German wheat cultivar Ibis. *J. Integr. Agric.* 11, 528–536. doi: 10.1016/S2095-3119(12)60039-2

Bariana, H., Bansal, U., Schmidt, A., Lehmensiek, J., Kaur, H., Miah, N., et al. (2010). Molecular mapping of adult plant stripe rust resistance in wheat and identification of pyramided QTL genotypes. *Euphytica* 176, 251–260. doi: 10.1007/s10681-010-0240-x

Bariana, H., Forrest, K., Qureshi, N., Miah, H., Hayden, M., and Bansal, U. (2016). Adult plant stripe rust resistance gene Yr71 maps close to Lr24 in chromosome 3D of common wheat. *Mol. Breed.* 36:98. doi: 10.1007/s11032-016-0528-1

Bariana, H., Kant, L., Qureshi, N., Forrest, K., Miah, H., and Bansal, U. (2022). Identification and characterisation of stripe rust resistance genes Yr66 and Yr67 in wheat cultivar VL Gehun 892. *Agronomy* 12:318. doi: 10.3390/agronomy12020318

Brandt, K., Chen, X., Tabima, J., See, D., Vining, K., and Zemetra, R. (2021). QTL analysis of adult plant resistance to stripe rust in a winter wheat recombinant inbred population. *Plants* 10:572. doi: 10.3390/plants10030572

Cao, S., Xie, Z., Jin, S., Jin, S., Jia, Q., Luo, H., et al. (2006). Inheritance analysis of resistance wheat cultivar Pascal to stripe rust. *J. Gansu Agric. Univ.* 2, 39–41. doi: 10.1016/S1872-2040(06)60047-9

Chatterjee, A., Moulik, S., Majhi, P., and Sanyal, S. (2002). Studies on surfactant-biopolymer interaction. I. Microcalorimetric investigation on the interaction of cetyltrimethylammonium bromide (CTAB) and sodium dodecylsulfate (SDS) with gelatin (Gn), lysozyme (Lz) and deoxyribonucleic acid (DNA). *Biophys. Chem.* 98, 313–327. doi: 10.1016/s0301-4622(02)00107-2

Chen, J., Chu, C., Souza, E., Guttieri, M., Chen, X., Xu, S., et al. (2012). Genome-wide identification of QTL conferring high-temperature adult-plant (HTAP) resistance to stripe rust (*Puccinia striiformis* f. sp. Tritici) in wheat. *Mol. Breed.* 29, 791–800. doi: 10.1007/s11032-011-9590-x

Dong, C., Zhang, L., Chen, Z., Xia, C., Gu, Y., Wang, J., et al. (2020). Combining a new exome capture panel with an effective varBScore algorithm accelerates BSA-Based gene cloning in wheat. *Front. Plant Sci.* 11:1249. doi: 10.3389/fpls.2020.01249

Dracatos, P., Zhang, P., Park, R., McIntosh, R., and Wellings, C. (2016). Complementary resistance genes in wheat selection 'Avocet R' confer resistance to stripe rust. *Theor. Appl. Genet.* 129, 65–76. doi: 10.1007/s00122-015-2609-7

Draz, I., Serfling, A., Muqaddasi, Q., and Röder, M. (2021). Quantitative trait loci for yellow rust resistance in spring wheat doubled haploid populations developed from the German Federal ex situ genebank genetic resources. *Plant Genome* 14:e20142. doi: 10.1002/tpg2.20142

Dyck, P. (1991). Genetics of adult-plant leaf rust resistance in 'chinese spring' and 'sturdy' wheats. *Crop Sci.* 31, 309–311.

Ellis, J., Lagudah, E., Spielmeyer, W., and Dodds, P. (2014). The past, present and future of breeding rust resistant wheat. *Front. Plant Sci.* 5:641. doi: 10.3389/fpls.2014.00641

Escamez, S., André, D., Zhang, B., Bollhöner, B., Pesquet, E., and Tuominen, H. (2016). METACASPASE9 modulates autophagy to confine cell death to the target cells during Arabidopsis vascular xylem differentiation. *Biol. Open* 5, 122–129. doi: 10.1242/bio.015529

Gardiner, L., Bansept-Basler, P., Olohan, L., Joynson, R., Brenchley, R., Hall, N., et al. (2016). Mapping-by-sequencing in complex polyploid genomes using genic sequence capture: a case study to map yellow rust resistance in hexaploid wheat. *Plant J.* 87, 403–419. doi: 10.1111/tpj.13204

Gebrewahid, T., Zhang, P., Zhou, Y., Yan, X., Xia, X., He, Z., et al. (2020). QTL mapping of adult plant resistance to stripe rust and leaf rust in a Fuyu 3/Zhengzhou 5389 wheat population. *Crop J.* 8, 655–665. doi: 10.1016/j.cj.2019.09.013

Gou, J., Li, K., Wu, K., Wang, X., Lin, H., Cantu, D., et al. (2017). Wheat stripe rust resistance protein WKS1 reduces the ability of the thylakoid-associated ascorbate peroxidase to detoxify reactive oxygen species. *Plant Cell.* 27, 1755–1770. doi: 10.1105/tpc.114.134296

Grover, G., Sharma, A., Mackay, I., Srivastava, P., Kaur, S., Kaur, J., et al. (2022). Identification of a novel stripe rust resistance gene from the European winter wheat cultivar 'Acienda': a step towards rust proofing wheat cultivation. *PLoS One* 17:e0264027. doi: 10.1371/journal.pone.0264027

Harrington, S., Cobo, N., Karafiátová, M., Doležel, J., Borrill, P., and Uauy, C. (2019). Identification of a dominant chlorosis phenotype through a forward screen of the *Triticum turgidum* cv. Kronos TILLING population. *Front. Plant Sci.* 10:963. doi: 10.3389/fpls.2019.00963

Henry, I., Nagalakshmi, U., Lieberman, M., Ngo, K., Krasileva, K., Vasquez-Gross, H., et al. (2014). Efficient genome-wide detection and cataloging of EMS-induced mutations using exome capture and next-generation sequencing. *Plant Cell* 26, 1382–1397. doi: 10.1105/tpc.113.121590

Herrera-Foessel, S., Lagudah, E., Huerta-Espino, J., Hayden, M., Bariana, H., Singh, D., et al. (2011). New slow-rusting leaf rust and stripe rust resistance genes Lr67 and Yr46 in wheat are pleiotropic or closely linked. *Theor. Appl. Genet.* 122, 239–249. doi: 10.1007/s00122-010-1439-x

Hill, J., Demarest, B., Bisgrove, B., Gorsi, B., Su, Y., and Yost, H. (2013). MMAPPR: mutation mapping analysis pipeline for pooled RNA-seq. *Genome Res.* 23, 687–697. doi: 10.1101/gr.146936.112

Huang, S., Liu, S., Zhang, Y., Xie, Y., Wang, X., Jiao, H., et al. (2021). Genome-wide wheat 55K SNP-based mapping of stripe rust resistance loci in wheat cultivar Shaannong 33 and their alleles frequencies in current Chinese wheat cultivars and breeding lines. *Plant Dis.* 105, 1048–1056. doi: 10.1094/PDIS-07-20-1516-RE

Huang, S., Wu, J., Wang, X., Mu, J., Xu, Z., Zeng, Q., et al. (2019). Utilization of the genomewide wheat 55K SNP array for genetic analysis of stripe rust resistance in common wheat line P9936. *Phytopathology* 109, 819–827. doi: 10.1094/PHYTO-10-18-0388-R

International Wheat Genome Sequencing Consortium [IWGSC] (2018). Shifting the limits in wheat research and breeding using a fully annotated reference genome. *Science* 361:eaar7191. doi: 10.1126/science.aar7191

Jagger, L., Newell, C., Berry, S., MacCormack, R., and Boyd, L. (2011). The genetic characterisation of stripe rust resistance in the German wheat cultivar Alcedo. *Theor. Appl. Genet.* 122, 723–733. doi: 10.1007/s00122-010-1481-8

Krattinger, S., Lagudah, E., Spielmeyer, W., Singh, R., Huerta-Espino, J., McFadden, H., et al. (2009). A putative ABC transporter confers durable resistance to multiple fungal pathogens in wheat. *Science* 323, 1360–1363. doi: 10.1126/science.1166453

Lan, C., Hale, I., Herrera-Foessel, S., Basnet, B., Randhawa, M., Huerta-Espino, J., et al. (2017). Characterization and mapping of leaf rust and stripe rust resistance loci in hexaploid wheat lines UC1110 and PI610750 under Mexican environments. *Front. Plant Sci.* 8:1450. doi: 10.3389/fpls.2017.01450

Li, J., Dundas, I., Dong, C., Li, G., Trethowan, R., Yang, Z., et al. (2020). Identification and characterization of a new stripe rust resistance gene Yr83 on rye chromosome 6R in wheat. *Theor. Appl. Genet.* 133, 1095–1107. doi: 10.1007/s00122-020-03534-y

Li, Q., Chen, X., Wang, M., and Jing, J. (2011). Yr45, a new wheat gene for stripe rust resistance on the long arm of chromosome 3D. *Theor. Appl. Genet.* 122, 189–197. doi: 10.1007/s00122-010-1435-1

Lin, F., and Chen, X. (2007). Genetics and molecular mapping of genes for race specific and all-stage resistance and non-specific high temperature adult-plant resistance to stripe rust in spring wheat cultivar Alpowa. *Theor. Appl. Genet.* 114, 1277–1287. doi: 10.1007/s00122-007-0518-0

Martinez, S., Shorinola, O., Conselman, S., See, D., Skinner, D., Uauy, C., et al. (2020). Exome sequencing of bulked segregants identified a novel TaMKK3-A allele linked to the wheat ERA8 ABA-hypersensitive germination phenotype. *Theor. Appl. Genet.* 133, 719–736. doi: 10.1007/s00122-019-03503-0

McNeal, F., Konzak, C., Smith, E., Tate, W., and Russell, T. (1971). *A Uniform System for Recording and Processing*. Washington, DC: Agricultural Research Service, 34–121.

Meng, L., Li, H., Zhang, L., and Wang, J. (2015). QTL IciMapping: integrated software for genetic linkage map construction and quantitative trait locus mapping in biparental populations. *Crop J.* 3, 269–283. doi: 10.1016/j.cj.2015.01.001

Mo, Y., Howell, T., Vasquez-Gross, H., Haro, L., Dubcovsky, J., and Pearce, S. (2018). Mapping causal mutations by exome sequencing in a wheat TILLING population: a tall mutant case study. *Mol. Genet. Genomics* 293, 463–477. doi: 10.1007/s00438-017-1401-6

Moore, J., Herrera-Foessel, S., Lan, C., Schnippenkoetter, W., Ayliffe, M., Huerta-Espino, J., et al. (2015). A recently evolved hexose transporter variant confers resistance to multiple pathogens in wheat. *Nat. Genet.* 47, 1494–1498. doi: 10.1038/ng.3439

Nsabiyera, V., Bariana, H., Qureshi, N., Wong, D., Hayden, M., and Bansal, U. (2018). Characterisation and mapping of adult plant stripe rust resistance in wheat accession Aus27284. *Theor. Appl. Genet.* 131, 1459–1467. doi: 10.1007/s00122-018-3090-x

Peterson, R., Campbell, A., and Hannah, A. (1948). A diagrammatic scale for estimating rust intensity on leaves and stems of cereals. *Can. J. Res.* 26c, 496–500. doi: 10.1139/cjr48c-033

Quan, W., Hou, G., Chen, J., Du, Z., Lin, F., Guo, Y., et al. (2013). Mapping of QTL lengthening the latent period of *Puccinia striiformis* in winter wheat at the tillering growth stage. *Eur. J. Plant Pathol.* 136, 715–727. doi: 10.1007/s10658-013-0201-z

Ramburan, V., Pretorius, Z., Louw, J., Boyd, L., Smith, P., Boshoff, W., et al. (2004). A genetic analysis of adult plant resistance to stripe rust in the wheat cultivar Kariega. *Theor. Appl. Genet.* 108, 1426–1433. doi: 10.1007/s00122-003-1567-7

Ren, R., Wang, M., Chen, X., and Zhang, Z. (2012). Characterization and molecular mapping of Yr52 for high-temperature adult-plant resistance to stripe rust in spring wheat germplasm PI 183527. *Theor. Appl. Genet.* 125, 847–857. doi: 10.1007/s00122-012-1877-8

Ren, T., Hu, Y., Tang, Y., Li, C., Yan, B., Ren, Z., et al. (2018). Utilization of a wheat 55K SNP array for mapping of major QTL for temporal expression of the tiller number. *Front. Plant Sci.* 9:333. doi: 10.3389/fpls.2018.00333

Ren, Y., He, Z., Li, J., Lillemo, M., Wu, L., Bai, B., et al. (2012). QTL mapping of adult-plant resistance to stripe rust in a population derived from common wheat cultivars Naxos and Shanghai 3/Catbird. *Theor. Appl. Genet.* 125, 1211–1221. doi: 10.1007/s00122-012-1907-6

Ren, Y., Singh, R., Basnet, B., Lan, C., Huerta-Espino, J., Lagudah, E., et al. (2017). Identification and mapping of adult plant resistance loci to leaf rust and stripe rust in common wheat cultivar kundan. *Plant Dis.* 101, 456–463. doi: 10.1094/PDIS-06-16-0890-RE

Roberts, J., and Caldwell, R. (1970). General resistance slow mildewing to *Erysiphe graminis* f. sp. tritici in knox wheat. *Phytopathology* 60:1310. doi: 10.1094/Phyto-60-1831

Schwessinger, B. (2017). Fundamental wheat stripe rust research in the 21st century. *New Phytol.* 213, 1625–1631. doi: 10.1111/nph.14159

Singh, R., Mujeeb-Kazi, A., and Huerta-Espino, J. (1998). Lr46: a gene conferring slow-rusting resistance to leaf rust in wheat. *Phytopathology* 88, 890–894. doi: 10.1094/PHYTO.1998.88.9.890

Steuernagel, B., Periyannan, S., Hernández-Pinzón, I., Witek, K., Rouse, M., Yu, G., et al. (2016). Rapid cloning of diseaseresistance genes in plants using mutagenesis and sequence capture. *Nat. Biotechnol.* 34, 652–655.

Todorovska, E., Christov, N., Slavov, S., Christova, P., and Vassilev, D. (2009). Biotic stress resistance in wheat—breeding and genomic selection implications. *Biotechnol. Equip.* 23, 1417–1426. doi: 10.2478/V10133-009-0006-6

Van, O. (2011). Multipoint maximum likelihood mapping in a full-sib family of an outbreeding species. *Genet Res.* 93, 343–349. doi: 10.1017/S0016672311000279

Voorrips, R. (2002). MapChart: software for the graphical presentation of linkage maps and QTLs. *J. Hered.* 93, 77–78. doi: 10.1093/jhered/93.1.77

Wellings, C., and McIntosh, R. (1990). *Puccinia striiformis* f. sp. Tritici in Australasia: pathogenic changes during the first 10 years. *Plant Pathol.* 39, 316–325. doi: 10.1111/j.1365-3059.1990.tb02509.x

Wen, W., Li, G., He, Z., Yang, W., Xu, M., and Xia, X. (2008). Development of an STS marker tightly linked to Yr26 against wheat stripe rust using the resistance gene-analog polymorphism (RGAP) technique. *Mol. Breed.* 22, 507–515. doi: 10.1007/s11032-008-9194-2

Ye, X., Li, J., Cheng, Y., Yao, F., Long, L., Yu, C., et al. (2019). Genome-wide association study of resistance to stripe rust (*Puccinia striiformis* f. sp. Tritici) in Sichuan wheat. *BMC Plant Biol.* 19:147. doi: 10.1186/s12870-019-1764-4

Young, N. (1996). QTL mapping and quantitative disease resistance in plants. *Annu. Rev. Phytopathol.* 34, 479–501. doi: 10.1146/annurev.phyto.34.1.479

Yu, H., Xie, W., Wang, J., Xing, Y., Xu, C., Li, X., et al. (2011). Gains in QTL detection using an ultra-high density SNP map based on population sequencing relative to traditional RFLP/SSR markers. *PLoS One* 6:e17595. doi: 10.1371/journal.pone.0017595

Zeng, Q., Zhao, J., Wu, J., Zhan, G., Han, D., and Kang, Z. (2022). Wheat stripe rust and integration of sustainable control strategies in China. *Front. Agr. Sci. Eng.* 9, 37-51. doi: 10.15302/J-FASE-2021405

Zhang, P., Li, X., Gebrewahid, T., Liu, H., Xia, X., He, Z., et al. (2019). QTL mapping of adult-plant resistance to leaf and stripe rust in wheat cross SW 8588/Thatcher using the wheat 55K SNP array. *Plant Dis.* 103, 3041–3049. doi: 10.1094/PDIS-02-19-0380-RE

Conflict of Interest: The authors declare that the research was conducted in the absence of any commercial or financial relationships that could be construed as a potential conflict of interest.

Publisher's Note: All claims expressed in this article are solely those of the authors and do not necessarily represent those of their affiliated organizations, or those of the publisher, the editors and the reviewers. Any product that may be evaluated in this article, or claim that may be made by its manufacturer, is not guaranteed or endorsed by the publisher.

frontiers | Frontiers in Plant Science

ORIGINAL RESEARCH
published: 25 July 2022
doi: 10.3389/fpls.2022.946700

Multi-Locus Genome-Wide Association Studies to Characterize Fusarium Head Blight (FHB) Resistance in Hard Winter Wheat

Jinfeng Zhang[1†], Harsimardeep S. Gill[1†], Jyotirmoy Halder[1], Navreet K. Brar[1], Shaukat Ali[1], Amy Bernardo[2], Paul St. Amand[2], Guihua Bai[2], Brent Turnipseed[1] and Sunish K. Sehgal[1]*

[1]Department of Agronomy, Horticulture and Plant Science, South Dakota State University, Brookings, SD, United States, [2]USDA-ARS, Hard Winter Wheat Genetics Research Unit, Manhattan, KS, United States

OPEN ACCESS

Edited by:
Cheng Liu,
Shandong Academy of Agricultural Sciences, China

Reviewed by:
Haiyan JIA,
Nanjing Agricultural University, China
Hongwei Wang,
Shandong Agricultural University, China
Fa Cui,
Ludong University, China

***Correspondence:**
Sunish K. Sehgal
sunish.sehgal@sdstate.edu

[†]These authors have contributed equally to this work

Specialty section:
This article was submitted to Plant Pathogen Interactions, a section of the journal Frontiers in Plant Science

Received: 17 May 2022
Accepted: 20 June 2022
Published: 25 July 2022

Citation:
Zhang J, Gill HS, Halder J, Brar NK, Ali S, Bernardo A, Amand PS, Bai G, Turnipseed B and Sehgal SK (2022) Multi-Locus Genome-Wide Association Studies to Characterize Fusarium Head Blight (FHB) Resistance in Hard Winter Wheat. Front. Plant Sci. 13:946700. doi: 10.3389/fpls.2022.946700

Fusarium head blight (FHB), caused by the fungus *Fusarium graminearum* Schwabe is an important disease of wheat that causes severe yield losses along with serious quality concerns. Incorporating the host resistance from either wild relatives, landraces, or exotic materials remains challenging and has shown limited success. Therefore, a better understanding of the genetic basis of native FHB resistance in hard winter wheat (HWW) and combining it with major quantitative trait loci (QTLs) can facilitate the development of FHB-resistant cultivars. In this study, we evaluated a set of 257 breeding lines from the South Dakota State University (SDSU) breeding program to uncover the genetic basis of native FHB resistance in the US hard winter wheat. We conducted a multi-locus genome-wide association study (ML-GWAS) with 9,321 high-quality single-nucleotide polymorphisms (SNPs). A total of six distinct marker-trait associations (MTAs) were identified for the FHB disease index (DIS) on five different chromosomes including 2A, 2B, 3B, 4B, and 7A. Further, eight MTAs were identified for Fusarium-damaged kernels (FDK) on six chromosomes including 3B, 5A, 6B, 6D, 7A, and 7B. Out of the 14 significant MTAs, 10 were found in the proximity of previously reported regions for FHB resistance in different wheat classes and were validated in HWW, while four MTAs represent likely novel loci for FHB resistance. Accumulation of favorable alleles of reported MTAs resulted in significantly lower mean DIS and FDK score, demonstrating the additive effect of FHB resistance alleles. Candidate gene analysis for two important MTAs identified several genes with putative proteins of interest; however, further investigation of these regions is needed to identify genes conferring FHB resistance. The current study sheds light on the genetic basis of native FHB resistance in the US HWW germplasm and the resistant lines and MTAs identified in this study will be useful resources for FHB resistance breeding *via* marker-assisted selection.

Keywords: FHB resistance, GBS, multi-locus GWAS, hard winter wheat, winter wheat breeding

INTRODUCTION

Fusarium head blight (FHB), also known as scab, is one of the most devastating diseases of wheat primarily caused by the fungus *Fusarium graminearum* Schwabe. FHB can cause severe losses in yield due to shriveled grains that lowers the test weight (Gilbert and Tekauz, 2000; Bai and Shaner, 2004). Further, *Fusarium* sp. produces harmful mycotoxins including deoxynivalenol (DON) that can accumulate in the infected grains and poses a serious threat to food and feed safety (Pestka, 2010; Ferrigo et al., 2016). In the US, FHB was first reported by Arthur (1891) in Indiana and since then, FHB has expanded its horizons to all major wheat-growing states in the US. This expansion of FHB is likely due to a suitable climate, increased acreage under no-till cultivation, and adoption of maize-wheat rotations over the last several decades, causing huge economic losses (Nganje et al., 2004; McMullen et al., 2012; Wilson et al., 2017). For instance, the US wheat producers suffered revenue losses worth $850 million due to FHB outbreaks in 2014 alone (Wilson et al., 2017).

Although fungicides are used for FHB prevention and control, the development of FHB-resistant varieties remains the most effective and economical approach to minimize the losses caused by this disease (Bai and Shaner, 2004; Gilbert and Haber, 2013). Genetic resistance to FHB is complex and controlled by multiple quantitative trait loci (QTLs) with small to medium effects. Further resistance expression is also significantly influenced by environmental conditions (Miedaner and Lauber et al., 2001; Buerstmayr et al., 2012). Several types of resistance mechanisms have been proposed, including resistance to the initial infection (Type I), resistance to the spread of infection within the spike (Type II), resistance to accumulation of mycotoxins such as DON (Type III), and resistance against damaged kernels (Type IV; Bai and Shaner, 2004; Gilbert and Haber, 2013), with Type II resistance being more stable and utilized in many wheat breeding programs. Nevertheless, type III and type IV resistance have also received attention in wheat breeding because they are associated with end-use quality and food safety, which is one of the biggest concerns of the growers and food industry (Mesterhazy, 2020). A large number of QTLs have been identified on all 21 wheat chromosomes (Liu et al., 2009; Venske et al., 2019), including seven cataloged FHB genes, *Fhb1* to *Fhb7* (Liu et al., 2009; Su et al., 2019; Venske et al., 2019; Ma et al., 2020). Most of those resistance QTLs originated from Asian germplasm such as the Chinese wheat cultivars 'Sumai-3' and 'Wangshuibai' or landraces (Bai et al., 1999; Anderson et al., 2001; Buerstmayr et al., 2009; Xue et al., 2010; Steiner et al., 2017) and wild relatives (*Fhb3*, *Fhb6*, and *Fhb7*; Qi et al., 2008; Cainong et al., 2015; Guo et al., 2015). Nevertheless, the transfer of resistance QTLs from wild relatives, landraces, or exotic materials is challenging due to linkage drag and adaptability issues. Thus, only a few QTLs with a major effect on FHB resistance, in particular *Fhb1*, have been successfully employed in wheat breeding programs (Bai et al., 2018). Contrarily, the majority of the germplasm from the hard winter wheat region of the US relies upon the variation in FHB resistance from native sources including cultivars 'Everest,' 'Overland,' 'Lyman,' and 'Expedition' (Clinesmith et al., 2019; Zhang et al., 2022). However, the identification of genomic regions underlying native resistance and the development of reliable markers are essential for pyramiding those QTLs to maintain an effective level of FHB resistance in locally adapted wheat backgrounds. Thus, it is important to determine the genetic basis of native FHB resistance in the germplasm from the HWW regions.

Though numerous QTLs for FHB resistance have been identified using traditional linkage mapping, this approach can encompass limited diversity. Genome-wide association study (GWAS) provides a good alternative by providing a much higher resolution to capture insights into the genetic architecture of complex traits because of historically accumulated mutations or recombination events (Scherer and Christensen, 2016; Sidhu et al., 2020). GWAS has been successfully used to dissect many traits of economic importance in wheat (Sukumaran et al., 2014; Sidhu et al., 2020; AlTameemi et al., 2021) including a several studies on FHB resistance (Kollers et al., 2013; Arruda et al., 2016; Wang et al., 2017; Tessmann et al., 2019; Larkin et al., 2020; Zhu et al., 2020). However, GWAS on FHB resistance has not been reported for the US hard winter wheat. Furthermore, recent developments in multi-locus GWAS (ML-GWAS) models have improved the power and reliability of this approach to identify causal loci for complex traits. For instance, more powerful methods like FarmCPU and BLINK have improved the ability of GWAS to detect the loci of smaller effects (Liu et al., 2016; Huang et al., 2019). Apart from these models, several important ML-GWAS models have been reported to outperform conventional single-locus GWAS models, which include the multi-locus random-SNP-effect mixed linear model (mrMLM), fast multi-locus random-SNP-effect mixed linear model (FASTmrMLM), fast multi-locus random-SNP-effect efficient mixed-model analysis (FASTmrEMMA), iterative modified-sure independence screening Expectation–Maximization-Bayesian least absolute shrinkage and selection operator (ISIS EM-BLASSO), polygenic-background-control based least angle regression plus empirical Bayes (pLARmEB), and pKWmEB (Wang et al., 2016; Tamba et al., 2017; Zhang et al., 2017; Ren et al., 2018; Wen et al., 2018). The ML-GWAS models are not only more reliable and efficient but also overcome the requirement of multiple testing correction that may result in false negatives (Zhang et al., 2019).

Majority of the GWAS studies make use of assembled diversity panels or landraces in various crop species (Ward et al., 2019). However, several studies effectively used the panels consisting of elite breeding lines to dissect the genetic basis of various traits of economic importance (Sukumaran et al., 2014, 2018). This approach permits identification, mapping, and the direct transfer and pyramiding of identified QTLs to the new backgrounds in the breeding programs without any linkage drag. Unfortunately, such studies have not been explored for FHB resistance in the US hard winter wheat breeding germplasm. Here we conducted such a study by genotyping a panel of elite lines from the South Dakota State University (SDSU) breeding program using

genotyping-by-sequencing (GBS) and phenotyped for FHB resistance in a controlled FHB field nursery for two years to uncover the genetic basis of native FHB resistance. The specific objectives of this study were to (i) evaluate the genetic basis of FHB resistance in hard winter wheat elite breeding material; (ii) identify markers associated with the QTLs to facilitate marker-assisted selection; (iii) identify putative candidate genes in the QTL regions that were significantly associated with FHB resistance.

MATERIALS AND METHODS

Plant Materials and FHB Evaluation

A set of 257 advanced and elite breeding lines from the SDSU winter wheat breeding program was evaluated for FHB resistance in a mist irrigated field nursery in the 2019 and 2020 winter wheat-growing seasons. Most of the evaluated breeding lines were at either $F_{4:7}$ or $F_{4:8}$ filial generations. Among these lines, 169 were screened in the 2019 nursery and 154 in the 2020 nursery, with an overlap of 58 lines between the two seasons. Owing to the missing genotypic data or inconsistent replications, eight lines from 2019 and one line from 2020 were removed, leaving 257 unique lines for downstream analysis.

The FHB nurseries were planted at Brookings, South Dakota (44.3114 °N, 96.7984 °W) in the fall of 2018 and 2019, respectively, using a randomized complete block design with 2 or 3 replicates for different sets of lines. 'Lyman' and 'Emerson' were used as resistant checks while 'Flourish' was used as the susceptible check in both experiments. Each experimental unit consisted of a 1-meter-long row plot with an inter-row spacing of 20 cm. The experimental plots were managed using the regional standard cultural practices. Days to heading (DTH) were recorded by calculating the Julian date when 50% of the plot had completely emerged heads. Plant height (PH) was measured from the soil surface to the top of spikes excluding awns at maturity.

The FHB nurseries were inoculated using corn kernel spawn and spraying a spore suspension of *F. graminearum* isolates (SD-FG1) as described in Halder et al. (2019). Briefly, the Fusarium-infected corn kernels (scabby corn inoculum) were scattered in the field at the boot stage (Feekes 10), followed by another round at the heading stage (Feekes 10.1) to ensure maximum infection in the FHB nursery. In addition, wheat plots were also inoculated by spraying a conidial suspension (100,000 spores/ml) at 50% anthesis to avoid any disease escape. The nursery was misted using an overhead mist irrigation system for two min with 15 min intervals from 19:00 to 7:00 h daily to maintain a humid micro-environment for disease infection. FHB disease incidence (INC) and severity (SEV) were scored for 20 spikes per genotype in each replication 21 days after anthesis using the scale described by Stack and McMullen (2011). The FHB disease index (DIS) was calculated as (INC × SEV)/100 (Stack and McMullen, 2011). The plots were harvested and threshed using a low air-speed thresher to prevent the loss of shriveled kernels. The harvested grain from each plot was visually scored for fusarium-damaged kernels percentage (FDK) by comparing each grain sample to a set of known FDK standards.[1]

Statistical Analysis

The phenotypic data from two seasons was analyzed to obtain the best linear unbiased estimates (BLUEs) for FHB traits using the following model:

$$y_{ijk} = \mu + E_i + R_{j(i)} + G_k + GE_{ik} + e_{ijk}$$

where y_{ijk} is the trait of interest, μ is the overall mean, E_i is the effect of the i^{th} environment, $R_{j(i)}$ is the effect of the j^{th} replicate nested within the i^{th} environment, G_k is the effect of the k^{th} genotype, GE_{ik} is the effect of the genotype × environment (G × E) interaction, and e_{ijk} is the residual error term. The broad-sense heritability (H^2) of a trait of interest in a combined environment analysis was assessed based on the variance estimates from the linear mixed model as follows:

$$H^2 = \frac{\sigma_g^2}{\sigma_g^2 + \sigma_{ge}^2 / nLoc + \sigma_e^2 / \left(nLoc \times nRep\right)}$$

where σ_g^2 and σ_e^2, are the genotype and error variance components, σ_{ge}^2 is the G × E interaction variance component and *nLoc* is the number of environments in the analysis. The analysis was performed in META-R (Alvarado et al., 2019) which is based on the 'lme4' (Bates et al., 2015) R package. The summary statistics, correlations, visualization, and comparison tests were performed in R (R Core Team, 2021).

Genotyping and Quality Control

The wheat panel was genotyped using the Genotyping-by-sequencing (GBS) procedure (Poland et al., 2012) at USDA Central Small Grain Genotyping Lab, Manhattan, KS. Briefly, the genomic DNA was extracted from leaf tissue at a three-leaf stage for each line using a cetyltrimethylammonium bromide (CTAB) method (Bai et al., 1999). GBS libraries were prepared by double restriction digestion with HF-*PstI* and *MspI* restriction enzymes (Poland et al., 2012) and sequenced in an Ion Proton sequencer (Thermo Fisher Scientific, Waltham, MA, United States). The Chinese Spring wheat genome reference RefSeq v2.0 (IWGSC, 2018; Zhu et al., 2021) was used to align the GBS reads with the default settings of Burrows-Wheeler Aligner v0.6.1.Single-nucleotide polymorphisms (SNPs) were called using the GBS v2.0 SNP discovery pipeline in TASSEL v5.0 (Bradbury et al., 2007). For quality control, unmapped SNPs and the SNPs with more than 30% missing values, minor allele frequency (MAF) of less than 5%, and more than 10% heterozygote frequency were filtered out. The

[1]https://agcrops.osu.edu/newsletter/corn-newsletter/2015-21/rating-fusarium-damaged-kernels-fdk-scabby-wheat

remaining 9,321 high-quality SNPs were imputed using BEAGLE v4.1 (Browning and Browning, 2007) for further analysis.

Population Structure and Linkage Disequilibrium Analysis

The principal component analysis (PCA) on the imputed SNP data of 257 lines was conducted to analyze the population structure using R (R Core Team, 2021) packages 'SNPRelate' (Zheng et al., 2012) and 'ggplot2' (Wickham, 2016). The population structure was also assessed using a Bayesian model-based clustering program, STRUCTURE v2.3.4 using an Admixture model (Pritchard et al., 2000) assuming 10 subgroups ($K = 1–10$) with 10 independent runs for each subgroup using a burn-in period of 10,000 iterations followed by 20,000 Monte Carlo iterations. The analysis was implemented in parallel using StrAuto v1.0 on the SDSU high-performance computing (HPC) cluster (Chhatre and Emerson, 2017; Tange, 2018). An *ad hoc* statistic (DeltaK) was used to infer the most likely number of subgroups using STRUCTURE HARVESTER (Evanno et al., 2005; Earl and vonHoldt, 2012). The linkage disequilibrium (LD) parameters (r^2) for the whole genome, as well as each sub-genome, were estimated separately in TASSEL v5.0 (Bradbury et al., 2007) by computing r^2 values for all pairwise markers using a sliding window size of 50 markers. LD decay over genetic distance was visualized by fitting a nonlinear model using the modified Hill and Weir method (Hill and Weir, 1988) in R (R Core Team, 2021).

Multi-Locus Genome-Wide Association Analysis

ML-GWAS was used to identify marker-trait associations (MTAs) using BLUEs for FHB traits obtained using the mixed model analysis and 9,321 high-quality SNPs. For association analysis, we compared a total of eight ML-GWAS models. Two models, FarmCPU (fixed and random model, circulating probability unification) and the BLINK (Bayesian-information and linkage-disequilibrium iteratively nested keyway), were implemented in genomic association and prediction integrated tool (GAPIT) v3.0 (Wang and Zhang, 2021) in the R environment. In addition, we used six recently developed ML-GWAS methods including mrMLM, FASTmrMLM, FASTmrEMMA, pLARmEB, ISIS EM-BLASSO, and pkWmEB. These six models were implemented in the R package 'mrMLM v4.0.2' (Zhang et al., 2020) using default parameters. The ML-GWAS models included the estimated kinship (K) and the first two principal components from PCA as covariates to account for relatedness and the population structure. Based on the comparison using quantile-quantile (QQ) plots for all the models, we decided to report the results generated from the FarmCPU model because it showed the best control of false positives and false negatives. Furthermore, we used a strict threshold based on false discovery rate correction (FDR adj. p value <0.05) for multiple testing. Though final results were reported from a single best model (FarmCPU), we used the results from the other seven ML-GWAS models to validate the FarmCPU MTAs as reliable, if they were also identified by other models. The Manhattan plots and QQ plots were generated using the R package 'CMPlot' to visualize the results from the FarmCPU analysis.

We also used a pairwise t-test to compare differences in trait means for different alleles of significant MTAs. For each MTA, mean trait values for two groups of alleles (resistant v/s susceptible) were compared using a t-test and visualized using boxplots with R package 'ggplot2' (Wickham, 2016). Furthermore, the allelic frequencies of significant MTAs were analyzed to compare the effect of the combination of resistance alleles for DIS and FDK. The 257 accessions were grouped based on the resistant alleles carried for each trait. These groups were compared using an FDR-adjusted pairwise t-test.

Candidate Gene Analysis

Two highly significant MTAs for FDK were subjected to candidate gene analysis to identify genes with putative functions of interest. Linkage blocks harboring these two MTAs were deduced using the confidence interval method in Haploview (Barrett et al., 2005). These MTAs were physically mapped to Chinese Spring RefSeq v2.1 using marker sequences of significant SNPs (IWGSC, 2018; Zhu et al., 2021). The high-confidence (HC) genes from IWGSC v2.1 RefSeq annotation were extracted from a flanking window around each MTA based on the LD decay in the respective region. The HC genes were annotated manually using Blast2GO (Conesa et al., 2005) for the identification of genes of interest. Further, a gene expression browser[2] and a thorough review of literature were used to exclude the unlikely candidates. For the gene expression browser, we used expression data from studies related to *Fusarium* infection in wheat (Borrill et al., 2016).

RESULTS

Observed Variation for FHB Traits

The BLUE values from two seasons exhibited a significant genotypic variation ($p < 0.001$) for DIS and FDK in the panel of 257 breeding lines. The variation for DIS ranged from 12.6 to 90.3, while the FDK ranged from 13.6 to 97.6 (**Table 1**). We observed a high broad-sense heritability ($H^2 = 0.85$) for DIS, whereas a moderate heritability for FDK (0.76). The BLUE values for the disease indices (DIS) were 36.3 and 31.6, for the moderately resistant checks, Emerson and Lyman, respectively, whereas 77.1 for the susceptible check Flourish. Similarly, the FDK percentage was 48.9 and 31.5% for Emerson and Lyman whereas 84.5% for 'Flourish.' Pearson's correlation coefficients between DIS and FDK estimated using the phenotypic BLUEs were significant ($r = 0.44$, $p < 0.001$; **Figure 1**). A significant negative correlation was observed between DIS and DTH ($r = 0.24$, $p < 0.001$) and between FDK and DTH ($r = 0.17$, $p < 0.01$). Further, DIS and FDK were not significantly correlated with PH (**Figure 1**).

[2]http://www.wheat-expression.com/

TABLE 1 | Phenotypic variation, variance estimates, and broad-sense heritability for studied FHB traits in the hard winter wheat panel of 257 breeding lines.

Trait	Genotypic variance[a]	Mean	Min	Max	CV[b]	H^2
DIS[b]	109.1***	45.4	12.6	90.3	20.7	0.85
FDK[b]	156.2***	70.6	13.6	97.6	16.3	0.76

[a]*Statistically significant differences are denoted by an asterisk (*), where ***$p \leq 0.001$.*

[b]*DIS, FHB disease index; FDK, Fusarium-damaged kernel percentage; CV, coefficient of variation; H^2, broad-sense heritability.*

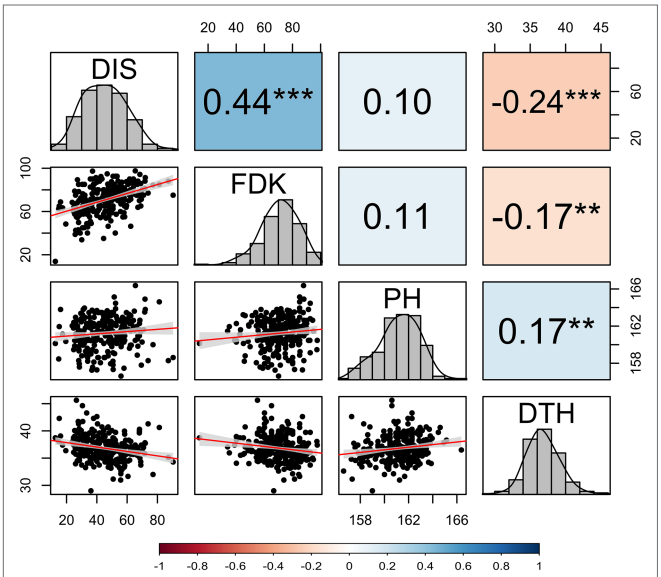

FIGURE 1 | Correlation coefficients among investigated FHB traits, PH, and DTH calculated by using the best linear unbiased estimates (BLUEs) obtained from a combined analysis of hard winter wheat panel of 257 breeding lines over two years. DIS, FHB disease index; FDK, Fusarium-damaged kernel percentage; PH, plant height; and DTH, days to heading. The diagonal of the pair plot elucidates the frequency distribution for four traits and lower triangle shows the bivariate scatterplots with fitted lines. Statistically significant differences are denoted by an asterisk (*), where **$p \leq 0.01$ and ***$p \leq 0.001$.

Genotyping, Population Structure, and Linkage Disequilibrium

Screening the panel using the GBS yielded 9,321 high-quality SNPs, with the B sub-genome having the highest SNP density (4,202; 45.1%) and the D sub-genome having the lowest SNP density (1,418; 15.2%; **Supplementary Table S1**). Among the 21 wheat chromosomes, 7A had the highest number of SNPs (796) whereas, chromosome 4D had the least (36 SNPs). The LD analysis revealed different patterns of LD decay among the three sub-genomes, with ~3.5 Mbp for the whole genome, and shorter LD decay distances for sub-genomes A and B than that for sub-genome D (Supplementary Figure S1). The population structure among 257 accessions was inferred using both PCA and STRUCTURE analysis (**Figure 2**). The DeltaK statistics based on STRUCTURE analysis revealed a major peak at $K = 2$, suggesting only two major groups in the panel (P1 and P2 for later reference; **Figure 2A**). The P1 comprised 138 accessions while the P2 consisted of 119 accessions. The subgroup P1 primarily consisted of breeding lines derived from the crosses involving parents from the southern HWW region of the US including breeding lines from Colorado, Kansas, Oklahoma, and Texas. Further, the P1 included important cultivars like Everest, Emerson, and Flourish, along with several breeding lines with Everest in its pedigree. In contrast, subgroup P2 was dominated by the cultivars from northern hard winter wheat region including Expedition, Ideal, Lyman, Overland, and Redfield, along with the breeding lines that have one these cultivars in their parentage. The results from PCA also showed considerable admixture in the population and suggested the presence of two subgroups in the panel in corroboration with STRUCTURE analysis (**Figures 2B,C**), with the first two principal components explaining around only 6.5 and 3.4% of the total variance, respectively.

Genomic Loci Associated With FHB Traits

Initial GWAS using eight different ML-GWAS models identified a total of 52 marker-trait associations (MTAs) for DIS and 53 MTAs for FDK (Supplementary Table S2). Nevertheless, we compared the QQ plots generated from those models and found FarmCPU fit best for the two traits in terms of controlling false positives and false negatives (**Supplementary Figure S2**). Thus, the FarmCPU model was used to report final MTAs for DIS and FDK (**Figure 3**).

A total of six distinct MTAs on five chromosomes were significant for DIS using the FarmCPU model based on FDR corrected threshold (FDR adj. value of $p < 0.05$; **Table 2**; **Figure 3A**). Among them, five were considered more reliable as they were significant in at least one other ML-GWAS model except for one MTA on chromosome 2B (*S2B_725552556*; **Table 2**). The most significant MTA (*S4B_40315424*) was identified on the short arm of chromosome 4B that was physically mapped at 40 Mbp, followed by *S3B_773516625* at 773 Mbp on chromosome 3B. For FDK, a total of eight unique MTAs were identified on six different chromosomes using the FarmCPU model (**Table 2**; **Figure 3B**), with one each on chromosomes 3B, 5A, 6D, and 7B, two each on 6B and 7A, respectively. Among them, four MTAs on chromosomes 3B (*S3B_768314878*), 5A (*S5A_619020400*), 6B (*S6B_718194425*), and 7B (*S7B_707550430*) were reliable MTAs as those were identified by another ML-GWAS model (**Table 2**). Among the 14 MTAs for DIS and FDK, only two MTAs (*S3B_768314878* and *S4B_647586119*) were significant for both the traits (**Supplementary Table S2**).

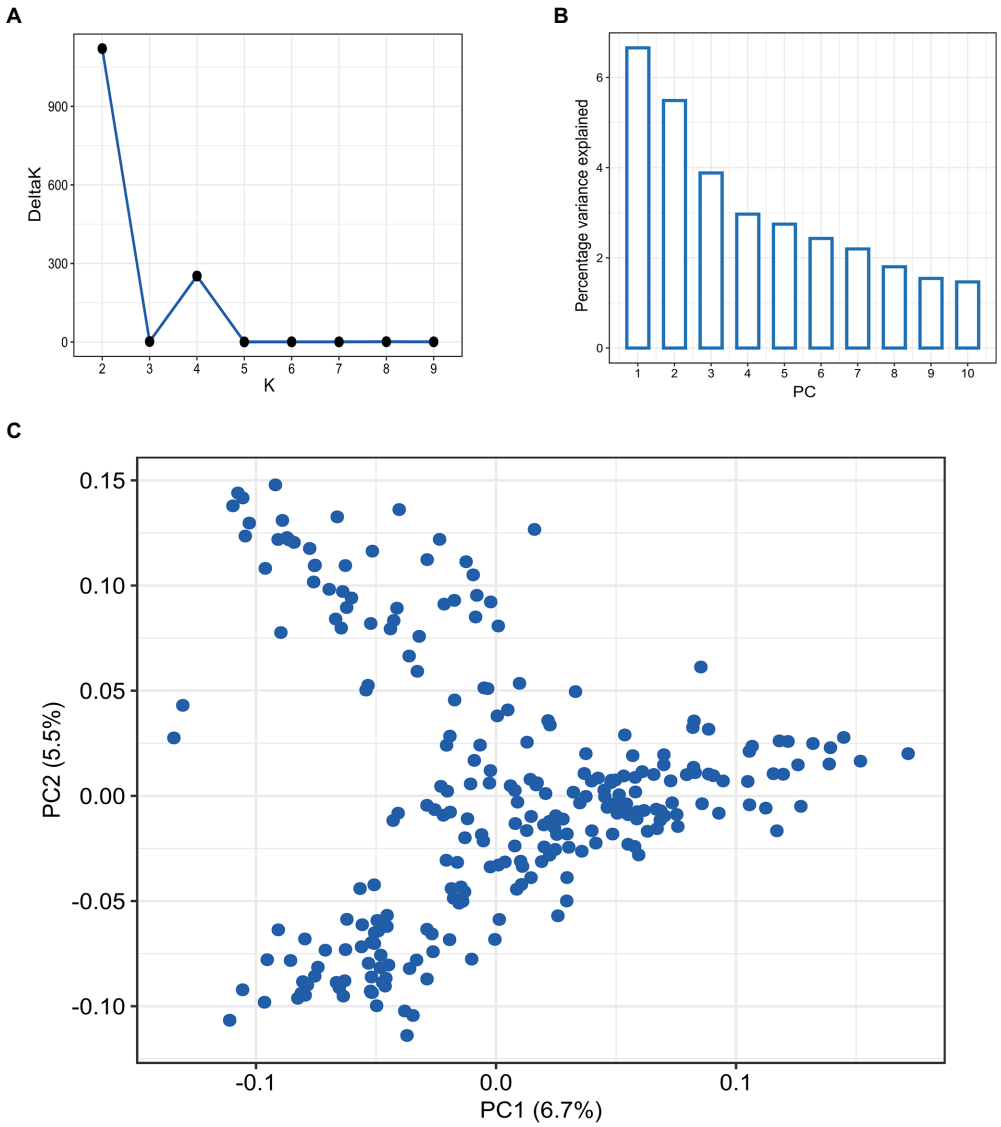

FIGURE 2 | Population structure analysis in hard winter wheat breeding panel of 257 lines based on the 9,321 SNPs, **(A)** Evanno plot of Delta-K statistic from the STRUCTURE analysis. **(B)** Scree plot for first 10 components obtained from principal component analysis (PCA). **(C)** Scatterplot for the first two components (PC1 and PC2) from PCA.

We compared trait means for DIS and FDK between the two alleles of the reliable MTAs (**Figure 4**). Of the five reliable MTAs for DIS, four exhibited a statistically significant difference in mean DIS scores between lines with the contrasting alleles (**Figure 4A**). The mean DIS score of the lines with resistance allele at *S3B_773516625* was 43.4%, significantly lower than those with susceptible allele (58.3%). Similarly, lines with a favorable allele at chromosome 4B (*S4B_40315424*) had a mean DIS score of 35.1% compared to 47.3% for lines carrying the susceptible allele. For FDK, all four reliable MTAs showed statistically significant differences in mean FDK percentage between lines carrying different alleles (**Figure 4B**). Intriguingly, favorable alleles at two MTAs (*S6B_718194425* and *S7B_707550430*) exhibited a decrease of around 13% of FDK over the unfavorable allele (**Figure 4B**).

Additive Effect of Identified MTAs on FHB Resistance

We investigated the effect of accumulating favorable alleles at reliable MTAs on DIS and FDK. The panel of 257 accessions was categorized into groups based on the number of favorable alleles carried by accessions. For DIS, we observed five groups with lines carrying one, two, three, four, or all five resistance alleles at the associated loci, with no line carrying zero favorable alleles. We observed a significant decrease in the mean DIS score as the number of resistance alleles increased (**Figure 5A**). The mean DIS for the group of accessions having only '1' resistance allele was 62.1, while the mean DIS for the group with all '5' resistance alleles was 31.5 (**Figure 5A**). Similarly, the mean FDK was significantly reduced with an increase in the number of resistance alleles (**Figure 5B**).

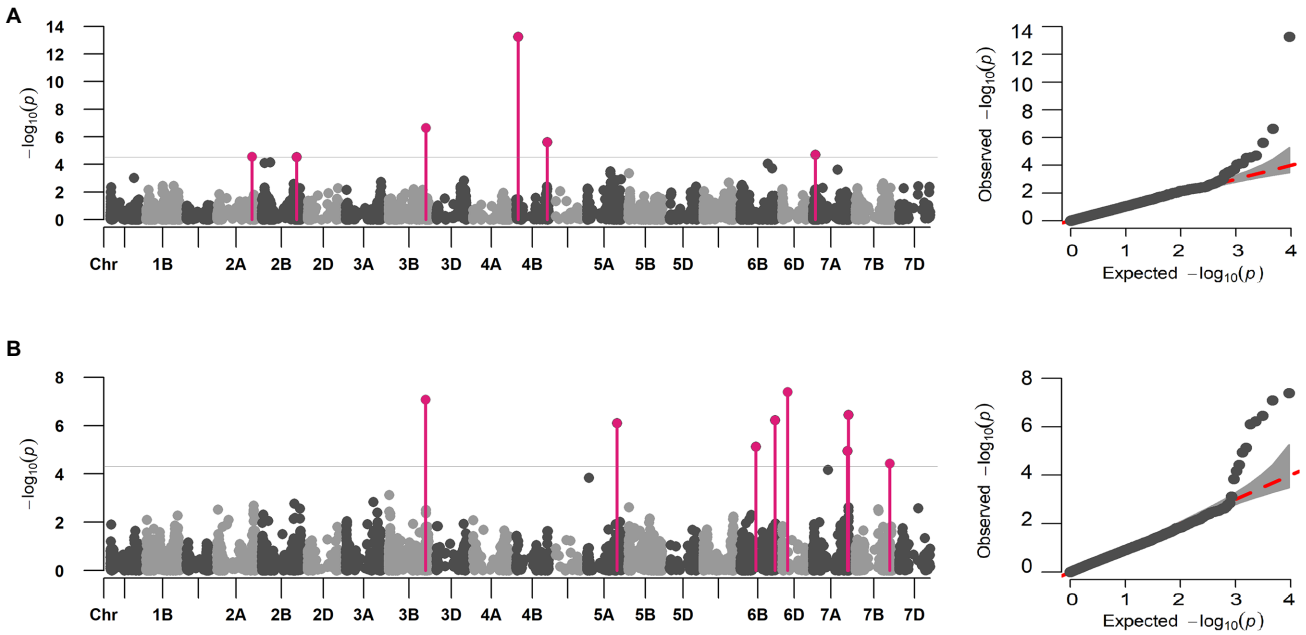

FIGURE 3 | Multi-locus marker-trait association for DIS and FDK in hard winter wheat breeding panel using the FarmCPU model. Manhattan and QQ plot for **(A)** DIS and **(B)** FDK showing the distinct peaks for identified MTAs. The significant associations (FDR $p < 0.05$) are elucidated using solid pink vertical lines.

TABLE 2 | Significant marker-trait associations (MTAs) identified by genome-wide association studies (GWAS) using the FarmCPU model for FHB disease index (DIS) and Fusarium-damaged kernels (FDK) in the hard winter wheat panel of 257 breeding lines.

Trait	SNP	Chr	Pos[a]	MAF[b]	SNP effect	*p* value	FDR-adj *p* value	Another model[c]
DIS	S2A_722857568	2A	722,857,568	0.17	3.70	2.72E-05	0.046	1,2,3,6
	S2B_725552556	2B	725,552,556	0.18	3.98	2.94E-05	0.046	
	S3B_773516625	3B	773,516,625	0.14	−5.47	2.29E-07	0.001	1,2,3,6,7
	S4B_40315424	4B	40,315,424	0.16	−7.00	5.46E-14	0.000	1,2,3,4,5,6,7
	S4B_647586119	4B	647,586,119	0.26	3.51	2.37E-06	0.007	1,4,5
	S7A_48708273	7A	48,708,273	0.07	−4.74	1.96E-05	0.047	7
FDK	S3B_768314878	3B	768,314,878	0.40	3.61	8.23E-08	0.000	1,2,3,4
	S5A_619020400	5A	619,020,400	0.13	4.63	7.83E-07	0.000	1,2,7
	S6B_320696398	6B	320,696,398	0.12	4.05	7.41E-06	0.012	
	S6B_718194425	6B	718,194,425	0.23	3.64	5.98E-07	0.001	1,2,3,4,5,6,7
	S6D_110313864	6D	110,313,864	0.06	−7.50	4.09E-08	0.000	
	S7A_713432647	7A	713,432,647	0.12	−4.44	1.13E-05	0.015	
	S7A_738859192	7A	738,859,192	0.34	2.87	3.51E-07	0.001	
	S7B_707550430	7B	707,550,430	0.30	−2.86	3.7E-05	0.043	1,2,6

The MTAs were declared significant based on a false discovery rate (FDR) corrected p value threshold of 0.05.

[a]*The physical position is based on IWGSC RefSeq v2.0 (IWGSC, 2018).*

[b]*MAF refers to minimum allele frequency for the corresponding MTA.*

[c]*This column enlists ML-GWAS model(s), which identified the corresponding MTA in addition to FarmCPU. The MTAs was referred to as 'reliable' if identified by at least two ML-GWAS models. Various ML-GWAS models are: 1, mrMLM; 2, FastmrMLM; 3, FastmrEMMA, 4, pLARmEB; 5, pKWmEB; 6, ISIS EM-BLASSO; and 7, BLINK.*

Relationship Between FHB and Height Genes

The most significant MTA for DIS (*S4B_40315424*) was identified at 40 Mbp on the short arm of chromosome 4B, where a semi-dwarfing gene *Rht1* is located. GWAS using the PH data of 257 accessions identified the most significant SNP at 40 Mbp (*S4B_40019966*) on chromosome 4B (**Supplementary Table S3**). Though the SNPs identified for DIS (*S4B_40315424*) and PH (*S4B_40019966*) were different, both the SNPs were 0.2 Mbp apart and in the same LD block, suggesting that this genomic region was associated with both traits in hard winter wheat. Further, we grouped the 257 accessions based on the allelic profile *S4B_40019966,* the MTA for PH in *Rht-B1* region. The two groups were compared using a t-test for differences in traits means for PH and DIS (**Supplementary Figure S3**). We observed significant differences (value of $p < 0.001$) in both PH and DIS among the two allelic groups. As expected, the allele associated with 'tall' phenotype had significantly lower

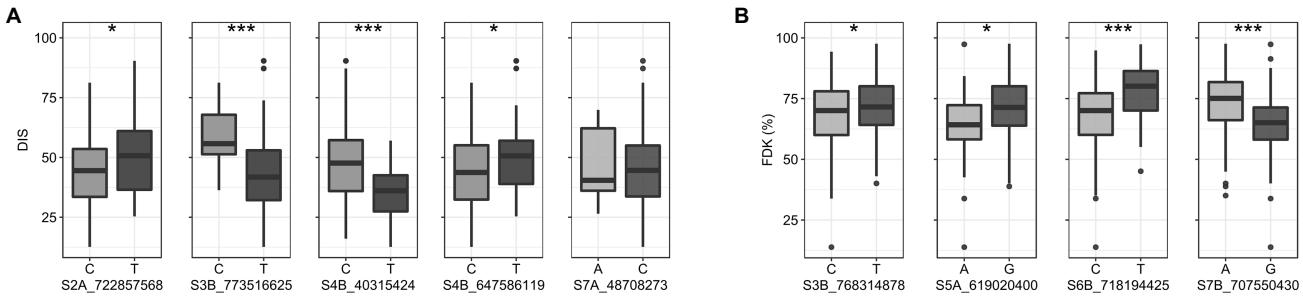

FIGURE 4 | Boxplots showing the effect of two alleles (favorable v/s unfavorable) of the reliable MTAs (enlisted in **Table 2**) on the trait means for **(A)** DIS **(B)** FDK in the hard winter wheat panel. Statistically significant differences are denoted by an asterisk (*), where *$p \leq 0.05$ and ***$p \leq 0.001$.

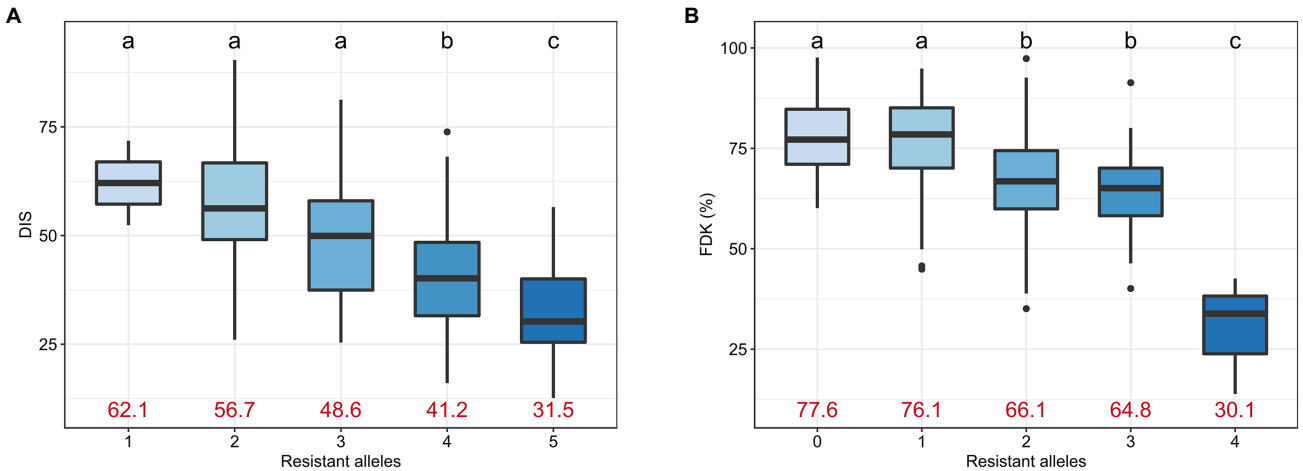

FIGURE 5 | Boxplots comparing the trait performance of the hard winter wheat lines carrying different numbers of resistant alleles for **(A)** DIS and **(B)** FDK, compared using an FDR-adjusted Least Significance Difference (LSD) test. Different letters on top of the boxplots denote statistically different groups. The mean trait value for DIS and FDK for the corresponding group is given using red text.

DIS compared to the allele associated with the 'dwarf' phenotype (**Supplementary Figure S3**).

Candidate Gene Analysis for Important Genomic Regions Associated With FDK

Candidate gene analysis was performed for two genomic regions (*S6B_718194425* and *S7B_707550430*) associated with FDK. The QTL associated with SNPs *S6B_718194425* and *S7B_707550430* were selected for candidate gene analysis as the LD blocks harboring these MTAs were identified to be smaller than 2.5 Mbp (**Supplementary Figure S4**). We identified a 1.7 Mbp LD block was identified harboring *S6B_718194425* (**Supplementary Figure S4a**). Similarly, a 2.3 Mbp long linkage block was identified for *S7B_707550430* (**Supplementary Figure S4b**). Based on Chinese Spring RefSeq v2.1, 28 and 20 high-confidence genes were retrieved from the 6B and 7B genomic regions, respectively (**Supplementary Table S4**). Further analysis using the wheat expression browser[3] with *Fusarium* specific studies, and comparison with literature identified 17 genes with putative functions of interest (**Table 3**). The functional annotation showed that several of these genes encode putative proteins of interest including cytochrome P450 714C2-like, aquaporin PIP1-5-like, disease resistance protein RGA5-like, NBS-LRR disease resistance protein, hydroquinone glucosyltransferase-like and others (**Table 3**). Among the 17 genes, four (*TraesCS6B02G448800, TraesCS6B02G450000, TraesCS6B02G450200,* and *TraesCS6B02G450500*) from 6B and three genes (*TraesCS7B02G417000*, *TraesCS7B02G429800* and *TraesCS7B02G430000*) from 7B were of specific interest as they exhibited a differential expression between mock and *Fusarium* inoculated spikes in Chinese Spring (**Supplementary Figures S5** and **S6**) and could be useful for further investigation of these QTL regions.

DISCUSSION

The utilization of host resistance to develop FHB-resistant wheat cultivars is the most economical and sustainable approach to manage FHB. This necessitates the continuous identification

[3]http://www.wheat-expression.com

TABLE 3 | Candidate genes identified for two QTLs for FDK, *S6B_718194425* and *S7B_707550430*, with putative functions of interest and their functional annotation.

Gene ID[a]	Previous ID[b]	Start position[c]	Annotation
TraesCS6B03G1247100	TraesCS6B02G448800	717,691,663	cytochrome P450 714C2-like
TraesCS6B03G1248900	TraesCS6B02G449400	718,124,729	nicotinate N-methyltransferase 1-like
TraesCS6B03G1249200	TraesCS6B02G449500	718,134,558	disease resistance protein RGA5-like
TraesCS6B03G1249300	TraesCS6B02G449600	718,142,603	disease resistance protein RGA5-like isoform X1
TraesCS6B03G1249800	TraesCS6B02G450000	718,403,799	aquaporin PIP1-5-like
TraesCS6B03G1250200	TraesCS6B02G450200	718,437,357	aquaporin PIP1-5-like
TraesCS6B03G1250700	TraesCS6B02G450500	718,634,434	50S ribosomal protein L9, chloroplastic
TraesCS6B03G1251200	TraesCS6B02G450700	718,948,307	acyl-CoA-binding domain-containing protein 4-like
TraesCS6B03G1252500	TraesCS6B02G451300	719,516,962	NAC domain-containing protein 78-like
TraesCS7B03G1160200	TraesCS7B02G417000	706,703,917	hypothetical protein CFC21_105377
TraesCS7B03G1160400	TraesCS7B02G417100	706,707,637	NBS-LRR disease resistance protein
TraesCS7B03G1161500	TraesCS7B02G417300	706,844,055	putative disease resistance protein RGA3
TraesCS7B03G1162000	TraesCS7B02G417400	706,905,895	probable LRR receptor-like serine/threonine-protein kinase
TraesCS7B03G1166000	TraesCS7B02G429700	708,194,926	hydroquinone glucosyltransferase-like
TraesCS7B03G1167100	TraesCS7B02G429800	708,341,181	uncharacterized methyltransferase At2g41040
TraesCS7B03G1167300	TraesCS7B02G430000	708,543,954	uncharacterized protein LOC119341039
TraesCS7B03G1167600	TraesCS7B02G430200	708,568,667	putative disease resistance RPP13-like protein 1 isoform X1

[a]*Gene ID based on the IWGSC RefSeq Annotation v2.1 (IWGSC, 2018; Zhu et al., 2021).*
[b]*Previous IDs for respective genes to the IDs used in IWGSC RefSeq Annotation v1.1 (IWGSC, 2018).*
[c]*Physical position of start points for respective genes are based on IWGSC RefSeq v2.0 (IWGSC, 2018).*

and validation of novel sources of FHB resistance and their utilization in breeding programs using marker-assisted selection. Thus, previous research efforts have resulted in the identification of several major and many minor QTLs for FHB resistance including *Fhb1*, and pyramiding them in various genetic backgrounds, particularly in spring wheat, has contributed significantly towards improved FHB resistance (Steiner et al., 2017; Bai et al., 2018; Ghimire et al., 2020). Nevertheless, using resistance genes from wild introgressions (*Fhb3*, *Fhb6*) or exotic sources, such as Sumai3, introduces the linkage drag or undesirable agronomic traits, making it difficult to incorporate these resistance genes into the US regional breeding programs. Thus, breeders still heavily rely on native sources for improving the FHB resistance in their breeding programs.

The majority of the HWW cultivars from the US Great Plains, including the SDSU winter wheat program, do not carry *Fhb1* likely due to yield drag, and 'TAM 205' is the only released HWW variety carrying *Fhb1* to date (Zhang et al., 2022). Fortunately, several HWW cultivars including Everest, Overland, Lyman, Heyne, Century, and Hondo that exhibit moderate FHB resistance but do not carry *Fhb1* have been released in the US HWW region (Jin et al., 2013; Bai et al., 2018; Clinesmith et al., 2019; Zhang et al., 2022), showing the importance of the native FHB resistance in the regional wheat breeding programs. Further, various studies have successfully identified QTLs for native resistance using cultivars such as 'Art,' Everest, and Lyman (Clinesmith et al., 2019; Hashimi, 2019). Thus, we used a set of advanced and elite breeding lines from the SDSU program with parentage from the US hard winter wheat region to identify genomic regions associated with FHB resistance, which could be readily employed in developing improved cultivars through marker-assisted breeding.

In this study, we evaluated a total of 257 breeding lines for FHB resistance in controlled disease nurseries over 2 years, with 58 lines being evaluated over both the years. The correlation for DIS evaluations from the two nurseries was 0.78, and the correlation among FDK evaluation over the years was 0.56. The significantly positive correlation among two nurseries, along with consistent performance of check cultivars suggests the reliability of phenotypic evaluation for GWAS. After evaluation of DIS and FDK in a panel of advanced breeding lines, we observed a significant variation for both the traits, with DIS from 12.6 to 90.3% and FDK from 13.6 to 97.6%. As majority of lines in the panel did not have *Fhb1* based on the parentage, the significant genotypic variation observed for the two traits was mainly contributed by native resistance genes. Furthermore, we observed a moderate to high heritability for DIS and FDK, which was in corroboration with several previous studies (Larkin et al., 2020; Xu et al., 2020; Zhu et al., 2020).

FarmCPU is an improved multi-locus model that eliminates the drawbacks of the conventional single-locus models by using associated markers as covariates to perform marker tests within a fixed-effect model. Later, this algorithm uses a separate random effect model for optimization of the association between tested markers and the trait (Liu et al., 2016). Several recent studies have reported better control of false positives and false negatives using FarmCPU compared to single-locus as well as other multi-locus models, as observed in our study. Hence, we employed FarmCPU for ML-GWAS that identified a total of six and eight genomic regions associated with DIS and FDK, respectively (**Table 2**). As previous studies used various types of marker systems to map FHB resistance and several are mapped to Chinese Spring RefSeq 1.0, it is difficult to precisely compare the MTAs

from the current study (mapped using Chinese Spring RefSeq 2.0) with previously identified regions. Therefore, we identified the approximate physical locations of previous QTLs and MTAs from the current study on Chinese Spring RefSeq 1.0 to facilitate the comparison and validation of the different loci for FHB resistance (**Supplementary Table S5**; IWGSC, 2018; Zhao et al., 2019).

Out of the six MTAs identified for DIS (**Table 2**), four were found in the proximity to previously reported loci for different types of FHB resistance, including type III and type IV resistance. One MTA identified at 718 Mbp on the long arm of chromosome 2A in the current study could be the same one (~709 Mbp) identified in a US soft winter wheat line 'VA00W-38' (Liu et al., 2012) for DON (type III) resistance. Another MTA on chromosome 3B (*S3B_773516625*) for DIS was mapped to 753 Mbp on RefSeq v1.0, which overlaps with the genomic region (~753 Mbp) for FHB type III resistance (DON) from a Canadian spring wheat cultivar 'AAC Tenacious,' validating the importance of this region (Dhariwal et al., 2020). Recently, a GWAS using soft red winter wheat germplasm from the US also reported a QTL in similar 3B region associated with both type II and type III resistance (Ghimire et al., 2022). Further, the MTA identified on 7AS (*S7A_48708273*) was mapped in a close proximity to a QTL for type III resistance (~50 Mbp) in soft red winter wheat germplasm from southern US (Larkin et al., 2020). In addition to this, several QTLs have been reported in this 7A genomic region (~28–68 Mbp) for different types of FHB resistance in previous studies (Zhang et al., 2010; Jiang et al., 2020; Thambugala et al., 2020).

Several studies have reported a co-localization of QTLs for FHB resistance with semi-dwarf genes such as *Rht-B1* and *Rht-D1*, with dwarfing alleles at these loci related to FHB susceptibility (Miedaner and Voss, 2008; Srinivasachary Gosman et al., 2008; Liu et al., 2012; Dhariwal et al., 2020; Thambugala et al., 2020; Goddard et al., 2021). In the current study, we identified a strong MTA for DIS on the short arm of chromosome 4B (37 Mbp), which co-localized with the *Rht-B1* region. Intriguingly, we did not observe a strong association between PH and any of the FHB traits based on Pearson's correlation (**Figure 1**). Further, we conducted a GWAS for PH using 257 accessions and identified the most significant SNP for PH at the same location as for DIS (37 Mbp; **Supplementary Table S3**), which co-localized with the location of *Rht-B1*. In corroboration with previous studies (Srinivasachary Gosman et al., 2008; Buerstmayr and Buerstmayr, 2016), our results suggest that the susceptibility associated with dwarfing allele of *Rht-B1* might be caused by a potential linkage of susceptible genes with the dwarfing genes. Thus, the identification of recombinants where the linkage between *Rht* genes and the FHB susceptible gene(s) is broken could be useful for the breeders. Except for these four MTAs for DIS, we did not find any previously reported QTL in the proximity of MTAs on chromosome 2BL (*S2B_725552556*) and 4BL (*S4B_647586119*). Thus, these two MTAs could represent novel QTLs for FHB resistance in hard winter wheat.

Among the eight MTAs identified for FDK (**Table 2**), six MTAs were found in genomic regions previously reported for harboring FHB resistance loci. The MTA *S3B_768314878* for FDK was about 5 Mbp away from MTA *S3B_773516625* that was identified for DIS in this study, suggesting a possible pleiotropic effect on both traits. As discussed earlier, previous studies also identified QTLs for different types of FHB resistance, including disease severity and DON at a similar position, suggesting this is an important region for FHB resistance on 3BL (Dhariwal et al., 2020; Larkin et al., 2020; Ghimire et al., 2022). Similarly, MTA *S5A_619020400* at 617 Mbp for FDK was found in the proximity of two previously reported QTLs, one for FDK mapped at ~596 Mbp in soft red winter wheat varieties AGS 2060 and AGS 2035 (Castro Aviles et al., 2020), and another for DON mapped at 621 Mbp in a Canadian spring wheat cultivar AAC Tenacious (Dhariwal et al., 2020). Further, two MTAs (*S6B_320696398* and *S6B_718194425*) identified for FDK were on the different arms of chromosome 6B at 314 Mbp and 708 Mbp, respectively (**Table 2**). The MTA (*S6B_718194425*) on 6BL aligned within the confidence interval of a meta-QTL for FHB resistance reported by Venske et al. (2019). However, we did not find any previously reported loci for FHB resistance around 314 Mbp on the 6BS. Another MTA (*S6D_110313864*) from this study was mapped on the short arm of 6D. Although a few studies reported QTLs for FHB resistance in this region, we were unable to compare their exact locations with *S6D_110313864* due to different marker systems used in these studies.

Two MTAs (*S7A_713432647* and *S7A_738859192*) for FDK identified in this study correspond to 707 Mbp and 731 Mbp on CS RefSeq v1.0 (**Table 2**). Several studies have reported QTLs for FHB resistance in the vicinity of these genomic regions. Among them, one QTL for FDK was mapped between 611 and 724 Mbp in the 'Nanda 2419×Wangshuibai' population (Li et al., 2008). Additionally, a recent GWAS using soft red winter wheat germplasm reported a QTL for type III and type IV resistance that was mapped at 738 Mbp, which perfectly co-localizes with the MTA from current study (Gaire et al., 2021). Previously, Larkin et al. (2020) also reported a QTL for type II resistance at 709 Mbp on chromosome 7A, which is in close proximity to the MTA *S7A_713432647* from this study. Other QTLs have also been reported for different FHB traits in the 7A region but their physical positions are not available for comparison with the newly identified MTAs (Li et al., 2012; Lu et al., 2013). Further, a significant MTA was identified at 698 Mbp on chromosome 7B, which is close to the QTL for DON mapped at ~718 Mbp in soft red winter wheat (Castro Aviles et al., 2020) and a QTL for FHB resistance was also mapped at ~683 Mbp from a cross of Ningmai-9×Yangmai-158 (Jiang et al., 2020). Two recent GWAS using soft red winter wheat germplasm from the US reported QTLs for type II resistance at around 716 Mbp (Larkin et al., 2020) and for DON at 723 Mbp on chromosome 7B (Gaire et al., 2021).

Overall, we identified 14 genomic regions associated with DIS and FDK in the current study. Out of these, 10 MTAs were co-localized with previously reported loci for different FHB traits, thus our study validates the previously reported QTLs in hard winter wheat germplasm with a higher mapping resolution. Further, the accessions harboring multiple FHB QTLs (**Supplementary Table S6**) could be directly employed in wheat breeding and the SNPs associated with these QTLs from the current study could be used to develop Kompetitive

allele specific PCR (KASP) markers to effectively track and pyramid these reliable FHB QTLs in diverse backgrounds using marker-assisted selection (Gill et al., 2019). We also identified four putative novel QTLs associated with FHB resistance that could be subjected to further investigation.

Further, we performed candidate gene analysis for two important genomic regions associated with FDK (*S6B_718194425* and *S7B_707550430*) to identify genes with putative functions of interest that could be used for further investigation of regions harboring these QTLs. We selected these two regions for candidate gene analysis based on the generation of LD blocks harboring significant SNPs. The LD analysis showed that the linkage blocks harboring these two SNPs were smaller than 2.5 Mbp, which seems to be appropriate region for identifying putative candidate genes. In wheat, the majority of cloned disease resistance genes encode intracellular immune receptors of the nucleotide-binding-site–leucine-rich repeat (NBS-LRR) family, receptor-like kinases (RLKs), or wall-associated kinases (WAKs) as the protein product (Keller et al., 2018). However, two recently characterized FHB resistance genes, *Fhb1* and *Fhb7*, were reported to have different mechanisms. Several candidates for *Fhb1* have been reported including a pore-forming toxin-like (PFT) gene encoding a chimeric lectin with two agglutinin domains (Rawat et al., 2016); and a mutation of a histidine-rich calcium-binding protein gene (Bai et al., 2018; Li et al., 2019; Su et al., 2019). Nevertheless, none of these genes share any conserved domains related to the disease-resistance gene cloned in plants (Li et al., 2019; Su et al., 2019). Recently, a gene encoding a glutathione S-transferase (GST) was determined as the *Fhb7*, which can detoxify pathogen-produced toxins by conjugating a glutathione (GSH) unit onto the epoxide moieties of the pathogenic molecule (Wang et al., 2020). Based on this information, we were able to identify several putative candidate genes for two genomic regions (**Table 3**), including several genes encoding putative disease resistance proteins such as LRR receptor-like serine/threonine-protein kinase, or nicotinate N-methyltransferase 1-like proteins (**Table 3**), that may play a role in the process of intracellular detection of pathogen-derived molecules and signal transduction (Zhou et al., 1995). Further, we analyzed expression data from *Fusarium*-infected spikes using a wheat expression browser (Borrill et al., 2016) and identified several differentially expressed genes in the target 6B and 7B regions between mock-inoculated and *Fusarium* inoculated spikes (**Supplementary Figures S5** and **S6**). These genes could be helpful in the further investigation of these genomic regions for their role in FHB resistance.

In summary, the current study provides new insights into the genetic basis of native FHB resistance in hard winter wheat germplasm from the US Great Plains region. The study validates the role of 10 genomic regions in FHB resistance in wheat including HWW germplasm, providing more confidence for the employment of these regions in breeding programs. Four putative novel QTLs and all reported SNP markers can facilitate the deployment of these QTLs through marker-assisted selection. Further, the information on genomic regions associated with FHB resistance could be useful for the breeders to improve the genomic selection models to select breeding lines with improved FHB resistance.

DATA AVAILABILITY STATEMENT

The datasets used for analysis in this study can be found in online repository. The names of the repository can be found in the article/**Supplementary Material**.

AUTHOR CONTRIBUTIONS

SS and JZ conceptualized the experiment and designed the methodology. JZ, NB, JH, and SA performed the investigation. HG and SS performed the data curation. HG and JZ performed the data analysis, visualization, and software implementation. AB, PA, and GB carried out genotyping and SNP discovery. JZ, HG, and SS wrote the original manuscript. GB, SA, and BT contributed to the interpretation of results. SS provided overall supervision. All authors contributed to manuscript revision and approved the final manuscript.

FUNDING

This project was collectively funded by the USDA hatch projects SD00H695–20, USDA-ARS agreement 59–0206–0-177 (USDA-USWBSI), and the USDA Agriculture and Food Research Initiative Competitive grants 2022–68013-36439 (Wheat-CAP) from the USDA National Institute of Food and Agriculture and South Dakota Wheat Commission grant 3X1340.

ACKNOWLEDGMENTS

The authors would like to thank the South Dakota Agriculture Experimental Station (Brookings, SD, United States) and South Dakota State University High-Performance Computing (HPC) team for providing the resources to conduct and analyze the experiments.

SUPPLEMENTARY MATERIAL

The Supplementary Material for this article can be found online at: https://www.frontiersin.org/articles/10.3389/fpls.2022.946700/full#supplementary-material

REFERENCES

AlTameemi, R., Gill, H. S., Ali, S., Ayana, G., Halder, J., Sidhu, J. S., et al. (2021). Genome-wide association analysis permits characterization of Stagonospora nodorum blotch (SNB) resistance in hard winter wheat. *Sci. Rep.* 11:12570. doi: 10.1038/s41598-021-91515-6

Alvarado, G., López, M., Vargas, M., Pacheco, Á., Rodríguez, F., Burgueño, J., et al. (2019). META-R (Multi Environment Trail Analysis with R for Windows) Version 6.04. Available at: https://data.cimmyt.org/dataset.xhtml?persistentId=hdl:11529/10201 (Accessed December 30, 2020).

Anderson, J. A., Stack, R. W., Liu, S., Waldron, B. L., Fjeld, A. D., Coyne, C., et al. (2001). DNA markers for Fusarium head blight resistance QTLs in two wheat populations. *Theor. Appl. Genet.* 102, 1164–1168. doi: 10.1007/s001220000509

Arruda, M. P., Brown, P., Brown-Guedira, G., Krill, A. M., Thurber, C., Merrill, K. R., et al. (2016). Genome-wide association mapping of Fusarium head blight resistance in wheat using genotyping-by-sequencing. *Plant Genome* 9:0028. doi: 10.3835/plantgenome2015.04.0028

Arthur, J. C. (1891). Wheat scab. *Indiana Agric. Exp. Stn. Bull.* 36, 129–138.

Bai, G., Kolb, F. L., Shaner, G., and Domier, L. L. (1999). Amplified fragment length polymorphism markers linked to a major quantitative trait locus controlling scab resistance in wheat. *Phytopathology* 89, 343–348. doi: 10.1094/PHYTO.1999.89.4.343

Bai, G., and Shaner, G. (2004). Management and resistance in wheat and barley to fusarium head blight. *Annu. Rev. Phytopathol.* 42, 135–161. doi: 10.1146/annurev.phyto.42.040803.140340

Bai, G., Su, Z., and Cai, J. (2018). Wheat resistance to Fusarium head blight. *Can. J. Plant Pathol.* 40, 336–346. doi: 10.1080/07060661.2018.1476411

Barrett, J. C., Fry, B., Maller, J., and Daly, M. J. (2005). Haploview: analysis and visualization of LD and haplotype maps. *Bioinformatics* 21, 263–265. doi: 10.1093/bioinformatics/bth457

Bates, D., Mächler, M., Bolker, B. M., and Walker, S. C. (2015). Fitting linear mixed-effects models using lme4. *J. Stat. Softw.* 67, 1–48. doi: 10.18637/jss.v067.i01

Borrill, P., Ramirez-Gonzalez, R., and Uauy, C. (2016). expVIP: a customizable RNA-seq data analysis and visualization platform. *Plant Physiol.* 170, 2172–2186. doi: 10.1104/pp.15.01667

Bradbury, P. J., Zhang, Z., Kroon, D. E., Casstevens, T. M., Ramdoss, Y., and Buckler, E. S. (2007). TASSEL: software for association mapping of complex traits in diverse samples. *Bioinformatics* 23, 2633–2635. doi: 10.1093/bioinformatics/btm308

Browning, S. R., and Browning, B. L. (2007). Rapid and accurate haplotype phasing and missing-data inference for whole-genome association studies by use of localized haplotype clustering. *Am. J. Hum. Genet.* 81, 1084–1097. doi: 10.1086/521987

Buerstmayr, H., Ban, T., and Anderson, J. A. (2009). QTL mapping and marker-assisted selection for Fusarium head blight resistance in wheat: A review. *Plant Breed.* 128, 1–26. doi: 10.1111/j.1439-0523.2008.01550.x

Buerstmayr, M., and Buerstmayr, H. (2016). The semidwarfing alleles Rht-D1b and Rht-B1b show marked differences in their associations with anther-retention in wheat heads and with fusarium head blight susceptibility. *Phytopathology* 106, 1544–1552. doi: 10.1094/PHYTO-05-16-0200-R

Buerstmayr, M., Huber, K., Heckmann, J., Steiner, B., Nelson, J. C., and Buerstmayr, H. (2012). Mapping of QTL for Fusarium head blight resistance and morphological and developmental traits in three backcross populations derived from *Triticum dicoccum* × *Triticum durum*. *Theor. Appl. Genet.* 125, 1751–1765. doi: 10.1007/s00122-012-1951-2

Cainong, J. C., Bockus, W. W., Feng, Y., Chen, P., Qi, L., Sehgal, S. K., et al. (2015). Chromosome engineering, mapping, and transferring of resistance to Fusarium head blight disease from Elymus tsukushiensis into wheat. *Theor. Appl. Genet.* 128, 1019–1027. doi: 10.1007/s00122-015-2485-1

Castro Aviles, A., Alan Harrison, S., Joseph Arceneaux, K., Brown-Guidera, G., Esten Mason, R., and Baisakh, N. (2020). Identification of QTLs for resistance to Fusarium head blight using a doubled haploid population derived from southeastern United States soft red winter wheat varieties AGS 2060 and AGS 2035. *Genes (Basel)* 11:699. doi: 10.3390/genes11060699

Chhatre, V. E., and Emerson, K. J. (2017). StrAuto: automation and parallelization of STRUCTURE analysis. *BMC Bioinfo.* 18:192. doi: 10.1186/s12859-017-1593-0

Clinesmith, M. A., Fritz, A. K., da Silva, C. L., Bockus, W. W., Poland, J. A., Dowell, F. E., et al. (2019). QTL mapping of fusarium head blight resistance in winter wheat cultivars 'art' and 'everest'. *Crop Sci.* 59, 911–924. doi: 10.2135/cropsci2018.04.0276

Conesa, A., Gotz, S., Garcia-Gomez, J. M., Terol, J., Talon, M., and Robles, M. (2005). Blast2GO: a universal tool for annotation, visualization and analysis in functional genomics research. *Bioinformatics* 21, 3674–3676. doi: 10.1093/bioinformatics/bti610

Dhariwal, R., Henriquez, M. A., Hiebert, C., McCartney, C. A., and Randhawa, H. S. (2020). Mapping of major fusarium head blight resistance from Canadian wheat cv. Aac tenacious. *Int. J. Mol. Sci.* 21, 1–24. doi: 10.3390/ijms21124497

Earl, D. A., and vonHoldt, B. M. (2012). STRUCTURE HARVESTER: a website and program for visualizing STRUCTURE output and implementing the Evanno method. *Conserv. Genet. Resour.* 4, 359–361. doi: 10.1007/s12686-011-9548-7

Evanno, G., Regnaut, S., and Goudet, J. (2005). Detecting the number of clusters of individuals using the software STRUCTURE: A simulation study. *Mol. Ecol.* 14, 2611–2620. doi: 10.1111/j.1365-294X.2005.02553.x

Ferrigo, D., Raiola, A., and Causin, R. (2016). Fusarium toxins in cereals: occurrence, legislation, factors promoting the appearance and their management. *Molecules* 21:0627. doi: 10.3390/molecules21050627

Gaire, R., Brown-Guedira, G., Dong, Y., Ohm, H., and Mohammadi, M. (2021). Genome-wide association studies for Fusarium head blight resistance and its trade-Off With grain yield in soft red winter wheat. *Plant Dis.* 105, 2435–2444. doi: 10.1094/PDIS-06-20-1361-RE

Ghimire, B., Mergoum, M., Martinez-Espinoza, A. D., Sapkota, S., Pradhan, S., Babar, M. A., et al. (2022). Genetics of Fusarium head blight resistance in soft red winter wheat using a genome-wide association study. *Plant Genome*:e20222. doi: 10.1002/tpg2.20222

Ghimire, B., Sapkota, S., Bahri, B. A., Martinez-Espinoza, A. D., Buck, J. W., and Mergoum, M. (2020). Fusarium head blight and rust diseases in soft red winter wheat in the Southeast United States: state of the art, challenges and future perspective for breeding. *Front. Plant Sci.* 11:1080. doi: 10.3389/fpls.2020.01080

Gilbert, J., and Haber, S. (2013). Overview of some recent research developments in fusarium head blight of wheat. *Can. J. Plant Pathol.* 35, 149–174. doi: 10.1080/07060661.2013.772921

Gilbert, J., and Tekauz, A. (2000). Review: recent developments in research on fusarium head blight of wheat in Canada. *Can. J. Plant Pathol.* 22, 1–8. doi: 10.1080/07060660009501155

Gill, H. S., Li, C., Sidhu, J. S., Liu, W., Wilson, D., Bai, G., et al. (2019). Fine mapping of the wheat leaf rust resistance gene Lr42. *Int. J. Mol. Sci.* 20:2445. doi: 10.3390/ijms20102445

Goddard, R., Steed, A., Scheeren, P. L., Maciel, J. L. N., Caierão, E., Torres, G. A. M., et al. (2021). Identification of Fusarium head blight resistance loci in two Brazilian wheat mapping populations. *PLoS One* 16:e0248184. doi: 10.1371/journal.pone.0248184

Guo, J., Zhang, X., Hou, Y., Cai, J., Shen, X., Zhou, T., et al. (2015). High-density mapping of the major FHB resistance gene Fhb7 derived from Thinopyrum ponticum and its pyramiding with Fhb1 by marker-assisted selection. *Theor. Appl. Genet.* 128, 2301–2316. doi: 10.1007/s00122-015-2586-x

Halder, J., Zhang, J., Ali, S., Sidhu, J. S., Gill, H. S., Talukder, S. K., et al. (2019). Mining and genomic characterization of resistance to tan spot, Stagonospora nodorum blotch (SNB), and Fusarium head blight in Watkins core collection of wheat landraces. *BMC Plant Biol.* 19, 480–415. doi: 10.1186/s12870-019-2093-3

Hashimi, A. (2019). *Mapping Quantitative Trait Loci for Fusarium Head Blight Resistance in US Winter Wheat*. Manhattan, KS: Kansas State University.

Hill, W. G., and Weir, B. S. (1988). Variances and covariances of squared linkage disequilibria in finite populations. *Theor. Popul. Biol.* 33, 54–78. doi: 10.1016/0040-5809(88)90004-4

Huang, M., Liu, X., Zhou, Y., Summers, R. M., and Zhang, Z. (2019). BLINK: A package for the next level of genome-wide association studies with both individuals and markers in the millions. *Gigascience* 8, 1–12. doi: 10.1093/gigascience/giy154

IWGSC (2018). Shifting the limits in wheat research and breeding using a fully annotated reference genome. *Science* 361:eaar7191. doi: 10.1126/science.aar7191

Jiang, P., Zhang, X., Wu, L., He, Y., Zhuang, W., Cheng, X., et al. (2020). A novel QTL on chromosome 5AL of Yangmai 158 increases resistance to Fusarium head blight in wheat. *Plant Pathol.* 69, 249–258. doi: 10.1111/ppa.13130

Jin, F., Zhang, D., Bockus, W., Baenziger, P. S., Carver, B., and Bai, G. (2013). Fusarium head blight resistance in U.S. winter wheat cultivars and elite breeding lines. *Crop Sci.* 53, 2006–2013. doi: 10.2135/cropsci2012.09.0531

Keller, B., Wicker, T., and Krattinger, S. G. (2018). Advances in wheat and pathogen genomics: implications for disease control. *Annu. Rev. Phytopathol.* 56, 67–87. doi: 10.1146/annurev-phyto-080516-035419

Kollers, S., Rodemann, B., Ling, J., Korzun, V., Ebmeyer, E., Argillier, O., et al. (2013). Whole genome association mapping of Fusarium head blight resistance

in European winter wheat (*Triticum aestivum* L.). *PLoS One* 8:e57500. doi: 10.1371/journal.pone.0057500

Larkin, D. L., Holder, A. L., Mason, R. E., Moon, D. E., Brown-Guedira, G., Price, P. P., et al. (2020). Genome-wide analysis and prediction of Fusarium head blight resistance in soft red winter wheat. *Crop Sci.* 60, 2882–2900. doi: 10.1002/csc2.20273

Li, T., Bai, G., Wu, S., and Gu, S. (2012). Quantitative trait loci for resistance to Fusarium head blight in the Chinese wheat landrace Huangfangzhu. *Euphytica* 185, 93–102. doi: 10.1007/s10681-012-0631-2

Li, G., Zhou, J., Jia, H., Gao, Z., Fan, M., Luo, Y., et al. (2019). Mutation of a histidine-rich calcium-binding-protein gene in wheat confers resistance to Fusarium head blight. *Nat. Genet.* 51, 1106–1112. doi: 10.1038/s41588-019-0426-7

Li, C., Zhu, H., Zhang, C., Lin, F., Xue, S., Cao, Y., et al. (2008). Mapping QTLs associated with Fusarium-damaged kernels in the Nanda 2419 × Wangshuibai population. *Euphytica* 163, 185–191. doi: 10.1007/s10681-007-9626-9

Liu, S., Christopher, M. D., Griffey, C. A., Hall, M. D., Gundrum, P. G., and Brooks, W. S. (2012). Molecular characterization of resistance to fusarium head blight in U.S. soft red winter wheat breeding line VA00W-38. *Crop Sci.* 52, 2283–2292. doi: 10.2135/cropsci2012.03.0144

Liu, S., Hall, M. D., Griffey, C. A., and McKendry, A. L. (2009). Meta-analysis of QTL associated with fusarium head blight resistance in wheat. *Crop Sci.* 49, 1955–1968. doi: 10.2135/cropsci2009.03.0115

Liu, X., Huang, M., Fan, B., Buckler, E. S., and Zhang, Z. (2016). Iterative usage of fixed and random effect models for powerful and efficient genome-wide association studies. *PLoS Genet.* 12:e1005767. doi: 10.1371/journal.pgen.1005767

Lu, Q., Lillemo, M., Skinnes, H., He, X., Shi, J., Ji, F., et al. (2013). Anther extrusion and plant height are associated with Type I resistance to Fusarium head blight in bread wheat line "Shanghai-3/Catbird.". *Theor. Appl. Genet.* 126, 317–334. doi: 10.1007/s00122-012-1981-9

Ma, Z., Xie, Q., Li, G., Jia, H., Zhou, J., Kong, Z., et al. (2020). Germplasms, genetics and genomics for better control of disastrous wheat Fusarium head blight. *Theor. Appl. Genet.* 133, 1541–1568. doi: 10.1007/s00122-019-03525-8

McMullen, M., Bergstrom, G., De Wolf, E., Dill-Macky, R., Hershman, D., Shaner, G., et al. (2012). Fusarium head blight disease cycle, symptoms, and impact on grain yield and quality frequency and magnitude of epidemics Since 1997. *Plant Dis.* 96, 1712–1728. doi: 10.1094/PDIS-03-12-0291-FE

Mesterhazy, A. (2020). Updating the breeding philosophy of wheat to fusarium head blight (FHB): Resistance components, QTL identification, and phenotyping - A review. *Plants (Basel).* 9:1702. doi: 10.3390/plants9121702

Miedaner, R., Lauber, S., and Geiger, H. H. (2001). Effects of genotype and genotype-environment interaction on deoxynivalenol accumulation and resistance to Fusarium head blight in rye, triticale, and wheat. *Plant Breed.* 120, 97–105. doi: 10.1046/j.1439-0523.2001.00580.x

Miedaner, T., and Voss, H.-H. (2008). Effect of dwarfing *Rht* genes on Fusarium head blight resistance in two sets of near-isogenic lines of wheat and check cultivars. *Crop Sci.* 48, 2115–2122. doi: 10.2135/cropsci2008.02.0107

Nganje, W. E., Kaitibie, S., Wilson, W. W., Leistritz, L. F., and Bangsund, D. A. (2004). *Economic Impacts of Fusarium Head Blight in Wheat and Barley: 1993–2001*. Agribusiness and Applied Economics Report No 538, North Dakota State University, Fargo. https://ageconsearch.umn.edu/record/23627?ln=en/ (Accessed 28 June, 2022).

Pestka, J. J. (2010). Toxicological mechanisms and potential health effects of deoxynivalenol and nivalenol. *World Mycotoxin J.* 3, 323–347. doi: 10.3920/WMJ2010.1247

Poland, J., Endelman, J., Dawson, J., Rutkoski, J., Wu, S., Manes, Y., et al. (2012). Genomic selection in wheat breeding using genotyping-by-sequencing. *Plant Genome* 5:0006. doi: 10.3835/plantgenome2012.06.0006

Pritchard, J. K., Stephens, M., and Donnelly, P. (2000). Inference of population structure using multilocus genotype data. *Genetics* 155, 945–959. doi: 10.1093/genetics/155.2.945

Qi, L. L., Pumphrey, M. O., Friebe, B., Chen, P. D., and Gill, B. S. (2008). Molecular cytogenetic characterization of alien introgressions with gene Fhb3 for resistance to Fusarium head blight disease of wheat. *Theor. Appl. Genet.* 117, 1155–1166. doi: 10.1007/s00122-008-0853-9

R Core Team. (2021). R: A language and environment for statistical computing. R Foundation for Statistical Computing, Vienna, Austria. Available at: https://www.R-project.org/ (Accessed 28 June, 2022).

Rawat, N., Pumphrey, M. O., Liu, S., Zhang, X., Tiwari, V. K., Ando, K., et al. (2016). Wheat Fhb1 encodes a chimeric lectin with agglutinin domains and a pore-forming toxin-like domain conferring resistance to Fusarium head blight. *Nat. Genet.* 48, 1576–1580. doi: 10.1038/ng.3706

Ren, W. L., Wen, Y. J., Dunwell, J. M., and Zhang, Y. M. (2018). PKWmEB: integration of Kruskal-Wallis test with empirical Bayes under polygenic background control for multi-locus genome-wide association study. *Heredity (Edinb).* 120, 208–218. doi: 10.1038/s41437-017-0007-4

Scherer, A., and Christensen, G. B. (2016). Concepts and relevance of genome-wide association studies. *Sci. Prog.* 99, 59–67. doi: 10.3184/003685016X14558068452913

Sidhu, J. S., Singh, D., Gill, H. S., Brar, N. K., Qiu, Y., Halder, J., et al. (2020). Genome-wide association study uncovers novel genomic regions associated With coleoptile length in hard winter wheat. *Front. Genet.* 10:1345. doi: 10.3389/fgene.2019.01345

Srinivasachary Gosman, N., Steed, A., Simmonds, J., Leverington-Waite, M., Wang, Y., et al. (2008). Susceptibility to Fusarium head blight is associated with the Rht-D1b semi-dwarfing allele in wheat. *Theor. Appl. Genet.* 116, 1145–1153. doi: 10.1007/s00122-008-0742-2

Stack, Robert W., and McMullen, Marcia P. (2011). A Visual Scale to Estimate Severity of Fusarium Head Blight in Wheat. Fargo Available at: www.ag.ndsu.edu/agcomm/creative-common. (Accessed April 23, 2021).

Steiner, B., Buerstmayr, M., Michel, S., Schweiger, W., Lemmens, M., and Buerstmayr, H. (2017). Breeding strategies and advances in line selection for Fusarium head blight resistance in wheat. *Trop. Plant Pathol.* 42, 165–174. doi: 10.1007/s40858-017-0127-7

Su, Z., Bernardo, A., Tian, B., Chen, H., Wang, S., Ma, H., et al. (2019). A deletion mutation in TaHRC confers Fhb1 resistance to Fusarium head blight in wheat. *Nat. Genet.* 51, 1099–1105. doi: 10.1038/s41588-019-0425-8

Sukumaran, S., Dreisigacker, S., Lopes, M., Chavez, P., and Reynolds, M. P. (2014). Genome-wide association study for grain yield and related traits in an elite spring wheat population grown in temperate irrigated environments. *Theor. Appl. Genet.* 128, 353–363. doi: 10.1007/s00122-014-2435-3

Sukumaran, S., Lopes, M., Dreisigacker, S., and Reynolds, M. (2018). Genetic analysis of multi-environmental spring wheat trials identifies genomic regions for locus-specific trade-offs for grain weight and grain number. *Theor. Appl. Genet.* 131, 985–998. doi: 10.1007/s00122-017-3037-7

Tamba, C. L., Ni, Y. L., and Zhang, Y. M. (2017). Iterative sure independence screening EM-Bayesian LASSO algorithm for multi-locus genome-wide association studies. *PLoS Comput. Biol.* 13:e1005357. doi: 10.1371/journal.pcbi.1005357

Tange, O. (2018). GNU Parallel 2018. Lulu.com [March 12, 2018].

Tessmann, E. W., Dong, Y., and Van Sanford, D. A. (2019). GWAS for Fusarium head blight traits in a soft red winter wheat mapping panel. *Crop Sci.* 59, 1823–1837. doi: 10.2135/cropsci2018.08.0492

Thambugala, D., Brûlé-Babel, A. L., Blackwell, B. A., Fedak, G., Foster, A. J., MacEachern, D., et al. (2020). Genetic analyses of native Fusarium head blight resistance in two spring wheat populations identifies QTL near the B1, Ppd-D1, Rht-1, Vrn-1, Fhb1, Fhb2, and Fhb5 loci. *Theor. Appl. Genet.* 133, 2775–2796. doi: 10.1007/s00122-020-03631-y

Venske, E., dos Santos, R. S., da Farias, D. R., Rother, V., da Maia, L. C., Pegoraro, C., et al. (2019). Meta-analysis of the QTLome of fusarium head blight resistance in bread wheat: refining the current puzzle. *Front. Plant Sci.* 10:727. doi: 10.3389/fpls.2019.00727

Wang, R., Chen, J., Anderson, J. A., Zhang, J., Zhao, W., Wheeler, J., et al. (2017). Genome-wide association mapping of Fusarium head blight resistance in spring wheat lines developed in the Pacific northwest and CIMMYT. *Phytopathology* 107, 1486–1495. doi: 10.1094/PHYTO-02-17-0073-R

Wang, S. B., Feng, J. Y., Ren, W. L., Huang, B., Zhou, L., Wen, Y. J., et al. (2016). Improving power and accuracy of genome-wide association studies via a multi-locus mixed linear model methodology. *Sci. Rep.* 6, 1–10. doi: 10.1038/srep19444

Wang, H., Sun, S., Ge, W., Zhao, L., Hou, B., Wang, K., et al. (2020). Horizontal gene transfer of Fhb7 from fungus underlies Fusarium head blight resistance in wheat. *Science* 368:5435. doi: 10.1126/science.aba5435

Wang, J., and Zhang, Z. (2021). GAPIT version 3: boosting power and accuracy for genomic association and prediction. *Genom. Proteomics Bioinfo.* 19, 629–640. doi: 10.1016/j.gpb.2021.08.005

Ward, B. P., Brown-Guedira, G., Kolb, F. L., Van Sanford, D. A., Tyagi, P., Sneller, C. H., et al. (2019). Genome-wide association studies for yield-related traits in soft red winter wheat grown in Virginia. *PLoS One* 14:e0208217. doi: 10.1371/journal.pone.0208217

Wen, Y.-J., Zhang, H., Ni, Y.-L., Huang, B., Zhang, J., Feng, J.-Y., et al. (2018). Methodological implementation of mixed linear models in multi-locus genome-wide association studies. *Brief. Bioinform.* 19, 700–712. doi: 10.1093/bib/bbw145

Wickham, H. (2016). ggplot2: Elegant Graphics for Data Analysis. Springer-Verlag: New York. Available at: https://cran.r-project.org/web/packages/ggplot2/citation.html (Accessed February 27, 2022).

Wilson, W. W., McKee, G., Nganje, W., Dahl, B., and Bangsund, D. (2017). Economic impact of USWBSI's scab initiative to reduce FHB. Agribusiness and Applied Economics Report No. 774, North Dakota State University, Fargo. https://ageconsearch.umn.edu/record/264672?ln=en (Accessed 28 June, 2022).

Xu, Q., Xu, F., Qin, D., Li, M., Fedak, G., Cao, W., et al. (2020). Molecular mapping of qtls conferring fusarium head blight resistance in chinese wheat cultivar Jingzhou 66. *Plan. Theory* 9, 1–15. doi: 10.3390/plants9081021

Xue, S., Li, G., Jia, H., Xu, F., Lin, F., Tang, M., et al. (2010). Fine mapping Fhb4, a major QTL conditioning resistance to Fusarium infection in bread wheat (*Triticum aestivum* L.). *Theor. Appl. Genet.* 121, 147–156. doi: 10.1007/s00122-010-1298-5

Zhang, J., Feng, J. Y., Ni, Y. L., Wen, Y. J., Niu, Y., Tamba, C. L., et al. (2017). PLARmEB: integration of least angle regression with empirical Bayes for multilocus genome-wide association studies. *Heredity (Edinb).* 118, 517–524. doi: 10.1038/hdy.2017.8

Zhang, J., Gill, H. S., Brar, N. K., Halder, J., Ali, S., Liu, X., et al. (2022). Genomic prediction of Fusarium head blight resistance in early stages using advanced breeding lines in hard winter wheat. *Crop J.* doi: 10.1016/j.cj.2022.03.010

Zhang, Y.-M., Jia, Z., and Dunwell, J. M. (2019). Editorial: The applications of new multi-locus GWAS methodologies in the genetic dissection of complex traits. *Front. Plant Sci.* 10:100. doi: 10.3389/fpls.2019.00100

Zhang, Y. W., Tamba, C. L., Wen, Y. J., Li, P., Ren, W. L., Ni, Y. L., et al. (2020). mrMLM v4.0.2: An R platform for multi-locus genome-wide association studies. *Genom. Proteomics Bioinfo.* 18, 481–487. doi: 10.1016/j.gpb.2020.06.006

Zhang, M., Zhang, R., Yang, J., and Luo, P. (2010). Identification of a new QTL for Fusarium head blight resistance in the wheat genotype "Wang shui-bai." *Mol. Biol. Rep.* 37, 1031–1035. doi: 10.1007/s11033-009-9809-7

Zhao, C., Sun, H., Guan, C., Cui, J., Zhang, Q., Liu, M., et al. (2019). Physical information of 2705 PCR-based molecular markers and the evaluation of their potential use in wheat. *J. Genet.* 98:69. doi: 10.1007/s12041-019-1114-1

Zheng, X., Levine, D., Shen, J., Gogarten, S. M., Laurie, C., and Weir, B. S. (2012). A high-performance computing toolset for relatedness and principal component analysis of SNP data. *Bioinformatics* 28, 3326–3328. doi: 10.1093/bioinformatics/bts606

Zhou, J., Loh, Y. T., Bressan, R. A., and Martin, G. B. (1995). The tomato gene Pti1 encodes a serine/threonine kinase that is phosphorylated by Pto and is involved in the hypersensitive response. *Cell* 83, 925–935. doi: 10.1016/0092-8674(95)90208-2

Zhu, Z., Chen, L., Zhang, W., Yang, L., Zhu, W., Li, J., et al. (2020). Genome-wide association analysis of Fusarium head blight resistance in Chinese elite wheat lines. *Front. Plant Sci.* 11:206. doi: 10.3389/fpls.2020.00206

Zhu, T., Wang, L., Rimbert, H., Rodriguez, J. C., Deal, K. R., De Oliveira, R., et al. (2021). Optical maps refine the bread wheat *Triticum aestivum* cv. Chinese Spring genome assembly. *Plant J.* 107, 303–314. doi: 10.1111/tpj.15289

Conflict of Interest: The authors declare that the research was conducted in the absence of any commercial or financial relationships that could be construed as a potential conflict of interest.

Publisher's Note: All claims expressed in this article are solely those of the authors and do not necessarily represent those of their affiliated organizations, or those of the publisher, the editors and the reviewers. Any product that may be evaluated in this article, or claim that may be made by its manufacturer, is not guaranteed or endorsed by the publisher.

frontiers | Frontiers in Plant Science

TYPE Original Research
PUBLISHED 09 August 2022
DOI 10.3389/fpls.2022.988641

OPEN ACCESS

EDITED BY
Handong Su,
Huazhong Agricultural University, China

REVIEWED BY
Guohao Han,
Institute of Genetics and Developmental Biology (CAS), China
Sung Un Huh,
Kunsan National University, South Korea
Shulan Fu,
Sichuan Agricultural University, China

*CORRESPONDENCE
Huagang He
hghe@ujs.edu.cn
Shanying Zhu
zhushanying@ujs.edu.cn

SPECIALTY SECTION
This article was submitted to Plant Pathogen Interactions, a section of the journal Frontiers in Plant Science

RECEIVED 07 July 2022
ACCEPTED 19 July 2022
PUBLISHED 09 August 2022

CITATION
He H, Guo R, Gao A, Chen Z, Liu R, Liu T, Kang X and Zhu S (2022) Large-scale mutational analysis of wheat powdery mildew resistance gene *Pm21*.
Front. Plant Sci. 13:988641.
doi: 10.3389/fpls.2022.988641

Large-scale mutational analysis of wheat powdery mildew resistance gene *Pm21*

Huagang He[1,2]*, Rui Guo[2], Anli Gao[3], Zhaozhao Chen[1], Renkang Liu[2], Tianlei Liu[1], Xusen Kang[3] and Shanying Zhu[4]*

[1]School of Life Sciences, Jiangsu University, Zhenjiang, China, [2]School of Food and Biological Engineering, Jiangsu University, Zhenjiang, China, [3]School of Life Sciences, Henan University, Kaifeng, China, [4]School of Environment, Jiangsu University, Zhenjiang, China

Wheat powdery mildew is a devastating disease leading to severe yield loss. The powdery mildew resistance gene *Pm21*, encoding a nucleotide-binding leucine-rich repeat receptor (NLR) protein, confers broad-spectrum resistance to powdery mildew and has great potential for controlling this disease. In this study, a large-scale mutagenesis was conducted on wheat cultivar (cv.) Yangmai 18 carrying *Pm21*. As a result, a total of 113 independent mutant lines susceptible to powdery mildew were obtained, among which, only one lost the whole *Pm21* locus and the other 112 harbored one- (107) or two-base (5) mutations in the encoding region of *Pm21*. From the 107 susceptible mutants containing one-base change, we found that 25 resulted in premature stop codons leading to truncated proteins and 82 led to amino acid changes involving in 59 functional sites. We determined the mutations per one hundred amino acids (MPHA) indexes of different domains, motifs, and non-domain and non-motif regions of PM21 protein and found that the loss-of-function mutations occurred in a tendentious means. We also observed a new mutation hotspot that was closely linked to RNBS-D motif of the NB-ARC domain and relatively conserved in different NLRs of wheat crops. In addition, we crossed all the susceptible mutants with Yangmai 18 carrying wild-type *Pm21*, subsequently phenotyped their F_1 plants and revealed that the variant E44K in the coiled-coil (CC) domain could lead to dominant-negative effect. This study revealed key functional sites of PM21 and their distribution characteristics, which would contribute to understanding the relationship of resistance and structure of *Pm21*-encoded NLR.

KEYWORDS

wheat powdery mildew, *Pm21*, nucleotide-binding leucine-rich repeat receptor (NLR), mutational analysis, mutation hotspot, dominant-negative effect

Introduction

Plants have developed a fine two-layered innate immune system to defense pathogens during long-time evolution. The first layer is pattern-triggered immunity (PTI) that is promoted *via* an activation of plasma membrane-resident pattern recognition receptors (PRRs) by perception of pathogen-associated molecular patterns (PAMPs). The second layer is effector-triggered immunity (ETI) that is elicited by pathogen effectors directly or indirectly recognized by intracellular nucleotide-binding leucine-rich repeat receptors (NLRs), commonly accompanied with hypersensitivity reaction (HR) leading to host cell death at the local site invaded by pathogens. It is considered that PTI contributes to basal defense and ETI provides race-specific resistance to pathogens (Dangl et al., 2013; Sun et al., 2020).

A typical plant NLR protein contains an N-terminal domain, a central nucleotide-binding (NB) domain, and a C-terminal leucine-rich repeat (LRR) domain. The variable N-terminus of NLR usually includes a Toll-interleukin 1 receptor (TIR) domain or a coiled-coil (CC) domain. Correspondingly, NLRs are classified into two types, TIR-type NLRs (TIR-NLRs) and CC-type NLRs (CC-NLRs) (Cui et al., 2015; Cesari, 2018). The central NB domain is highly conserved that works as a molecular switch to alter "off" and "on" state of NLR *via* binding adenosine diphosphate (ADP) and adenosine triphosphate (ATP) (Bernoux et al., 2016). The LRR domain participates in direct or indirect perception of effectors delivered into host cell by pathogens. The CC or TIR domains of many NLRs perform signal transduction and trigger cell death *via* homodimerization (Bernoux et al., 2011; Bai et al., 2012). Recently, it was found that TIR domain is a NADase that can cleave NAD^+ into nicotinamide and ADP-ribose and transduce signaling into cell death response (Horsefield et al., 2019; Wan et al., 2019). In a plant NLR protein, the above three different domains may interact intramolecularly each other, which can maintain NLR under the status of autoinhibition (Moffett et al., 2002; Wang et al., 2019a,b).

Wheat powdery mildew, caused by the biotrophic fungus *Blumeria graminis* f. sp. *tritici* (DC.) Speer (*Bgt*), is a devastating disease leading to severe yield losses. Up to date, over 80 formally designated wheat powdery mildew resistance genes/alleles have been characterized from wheat and its cultivated and wild relatives. Among them, several genes have been cloned (He et al., 2021a,b). *Pm21*, originated from wheat wild relative *Dasypyrum villosum* (L.) Candargy, confers broad-spectrum resistance to *Bgt* pathogen and displays a great value for controlling wheat powdery mildew. Recently, using a map-based cloning strategy, *Pm21* has been cloned that encodes a typical NLR protein (GenBank accession number: MF370199) (He et al., 2018). Transient expression assay suggests that PM21 protein is autoinhibited *via* intramolecular interactions of its different domains (Gao et al., 2020). Evolutionary analysis, based on a series of *Pm21* alleles isolated from different accessions of *D. villosum*, reveals that the LRR domain has higher genetic diversity than other domains and the solvent-exposed LRR residues have been undergone diversifying selection (dN/dS = 3.20), which is similar to the race-specific powdery mildew resistance genes *Pm3* from wheat and *Mla* from barley (He et al., 2020). In general, we know less about the characteristics of *Pm21* so far.

Mutational analysis is a powerful approach for uncovering structure and function of genes of interest. In the past years, several large-scale mutagenesis researches have been conducted on plant NLR genes, such as *Arabidopsis RPS2* (Tao et al., 2000) and *RPM1* (Tornero et al., 2002), both of which confer resistance against *Pseudomonas syringae*, and tobacco mosaic virus resistance gene *N* (Dinesh-Kumar et al., 2000). However, there is no systemic mutagenesis research focused on an NLR gene-derived wheat crops. Here, we report over a hundred *Bgt*-susceptible mutants of common wheat cv. Yangmai 18 carrying *Pm21 via* ethyl methanesulfonate (EMS) mutagenesis and identify dozens of mutated sites that lead to lose *Pm21* resistance. These mutations will contribute to understanding the molecular basis of PM21 protein.

Materials and methods

Plant materials and growth conditions

Wheat cv. Yangmai 18 is a common wheat-*D. villosum* translocation line that carries *Pm21* and confers effective resistance to powdery mildew. Yangmai 23, a susceptible wheat cv., was used as a negative control and a host for reproducing asexual spores of *Bgt*. Wheat plants were grown in the field or in a greenhouse.

Ethyl methanesulfonate treatment

About 8,000 seeds of Yangmai 18 carrying *Pm21* were soaked with 0.05 M phosphate buffer solution (PBS, pH 7.0) for 4 h. The seeds were then soaked with 0.8% EMS diluted in 0.05 M PBS (pH 7.0) and shook at 20°C for 12 h. The seeds treated with EMS were washed with running water for 4 h and then placed at 4°C for 3 days. After germination, the seeds were sowed in the field for generation. All seeds of each single plant were harvested as an M_2 family.

Preliminary screening of mutants susceptible to powdery mildew

About 100 seeds of each M_2 family were sowed in a pot. The plants at one-leaf stage were inoculated with *Bgt* isolate BgtYZ01

in a greenhouse with LED light under long-day condition (16-h light/8–h dark) at 24 ± 2°C. The powdery mildew responses were assessed at 7 days after inoculation. The susceptible individuals were kept and planted in the field. The responses of the harvested susceptible mutants were re-assessed with the same *Bgt* isolate at the seedling stage. Infection types (IT) were scored according to a 0–4 scale (He et al., 2021b).

Allelism test of candidate susceptible mutants

Each of the obtained candidate susceptible mutants was crossed with the mutant line Y18-S7, who carries a mutation site at position 834 (G to A) of *Pm21* leading to a premature stop codon and be completely susceptible to isolate BgtYZ01 at whole growth stages (He et al., 2018). The powdery mildew responses of the derived F_1 plants were detected with BgtYZ01 again to understand whether the mutation leading to susceptibility occurs in *Pm21*.

Detection of mutation sites

Total RNAs were extracted from leaves of each susceptible mutant using the TRIzol reagent (Life Technologies, Carlsbad, CA, United States), and 2 μg of total RNA was used to synthesize the first-strand cDNA using a PrimeScript™ II 1st Strand cDNA Synthesis Kit (TaKaRa, Shiga, Japan). The gene *Pm21* was PCR-amplified from the cDNA using the high fidelity PrimeSTAR Max Premix (TaKaRa, Shiga, Japan) and the primer pair (forward primer: 5′-TTACCCGGGCTCACCCGTTGGACTTGGACT-3′; reverse primer: 5′-CCCACTAGTCTCTCTTCGTTACATAATGTAGTG CCT-3′). PCR products were digested with *Sma*I and *Spe*I, inserted into the vector pAHC25-MCS1 (He et al., 2018) and sequenced. Each mutation site was further verified by sequencing the independent PCR products.

Annotation of domains and motifs of PM21 protein and statistical analysis of mutation frequency

In PM21 protein, the CC, NB-ARC, and LRR domains and LRR motifs were annotated based on our previous work (Gao et al., 2020; He et al., 2020). The nT motif in the CC domain was characterized as described by Bai et al. (2002). The motifs in the NB-ARC domain were identified as described by Meyers et al. (1999) and Dilbirligi and Gill (2003). Mutation frequency in full-length protein, different domains, and motifs was calculated by the index of mutations per one hundred amino acids, simply named MPHA index. Sequence logos were created by the WebLogo tool (Crooks et al., 2004) using different NLR proteins in wheat crops.

Screening and verification of susceptible mutants with dominant-negative phenotype

Yangmai 18 carrying wild-type *Pm21* was used as the female parent to cross, respectively, with different susceptible mutants. The powdery mildew responses of the generated F_1 plants were assessed by inoculation with BgtYZ01. The phenotypes of the F_2 plants derived from the susceptible F_1 were further tested with the same isolate. Chi-squared (χ^2) test was used to determine the goodness-of-fit of the observed segregation ratio to theoretical Mendelian ratio.

Results

A collection of loss-of-function of *Pm21* consists of 113 independent mutants

Ethyl methanesulfonate -induced mutagenesis was conducted on Yangmai 18 carrying *Pm21*. From derived 4,462 M_2 families, a total of 116 candidate mutants susceptible to *Bgt* isolate BgtYZ01 were identified. We also investigated the phenotypes of M_3 plants of the candidate mutants at the seedling stage and confirmed that all of them lost resistance completely. To exclude loss-of-function mutants caused by non-target mutations, all candidate mutants were crossed with Y18-S7 that had a premature stop codon (G834A) in *Pm21* leading to encode a 280-aa truncated protein and completely susceptible to BgtYZ01 at whole growth stages (He et al., 2018). The generated F_1 plants derived from 113 crosses were all susceptible whereas those from 3 crosses were resistant, suggesting that the susceptibility of the corresponding 113 susceptible mutants was truly caused by mutated *Pm21*. Of the 113 susceptible mutants, 58 were reported in our previous work (He et al., 2017, 2018) and 55 were newly obtained in this study (**Figure 1** and **Supplementary Table 1**). Except Y18-S6 that had a deletion of the *Pm21* locus, each of the other 112 contained one- (107) or two-base (5) changes in the encoding sequence of *Pm21*. Due to that it was unclear which change(s) led to loss the function in the 5 mutants harbored two mutation sites in *Pm21*, only the 107 susceptible mutants contained one mutation site were used for further statistical analysis.

In general, of the 107 mutation sites, 59 and 47 were involved in the transition of G to A (55.2%) and C to T (43.9%), respectively, and only one (Y18-S113) was involved in the transversion of A to T (0.9%). Of the 107 mutations of

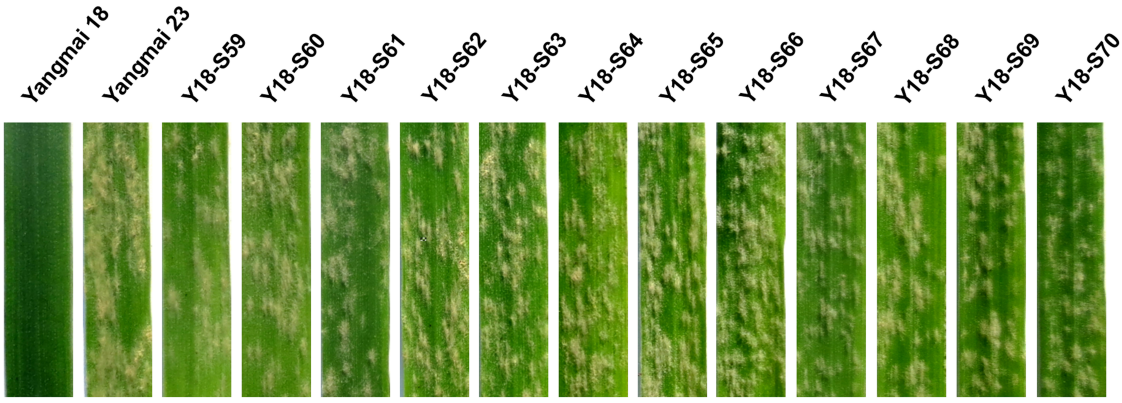

FIGURE 1
Powdery mildew responses of 12 representative susceptible mutants of Yangmai 18. Responses of the mutant lines Y18-S59∼Y18-S70 to *Bgt* isolate BgtYZ01 were assessed at one-leaf stage. Wheat cv. Yangmai 18 carrying wild-type *Pm21* and cv. Yangmai 23 were used as the resistant and susceptible controls, respectively.

Pm21, 25 resulted in premature stop codons leading to truncated proteins ranged from 178 to 843 aa. Compared with full-length PM21 protein that contains 16 LRR motifs as described in our previous work (He et al., 2020), the largest truncated protein (843 aa in Y18-S47) retained 13 LRR motifs, suggesting the importance of the last three LRR motifs (LRR14–LRR16) for resistance. Besides, 82 mutations of *Pm21* each led to a single amino acid change, of which, 59 mutations were unique and the other 23 were repetitive (**Figure 2** and **Supplementary Table 1**).

Loss-of-function mutations of *Pm21* occur in a tendentious means

In further study, the distribution characteristics of the above 59 distinctive mutations that led to single amino acid changes were analyzed using the index mutations per one hundred amino acids (MPHA). The data showed that the MPHA indexes of the CC (10.1) and NB-ARC (7.2) domains were higher than that of the full-length PM21 (6.5), whereas the MPHA index of the LRR domain (4.4) was lower than that of the full-length PM21. In addition, the MPHA indexes of the Linker 1 (the linker between the CC and NB-ARC domains) and the Linker 2 (the linker between the NB-ARC and LRR domains) were 11.1 and 4.5, which were similar to those of the CC and LRR domains, respectively (**Table 1**). It was indicated that the two linker regions also play the critical roles in powdery mildew resistance.

In the CC domain, the MPHA index of the nT motif (21.1) was obviously higher than that of non-motif region (8.6). In the NB-ARC domain, the MPHA index of motif region (19.6) was significantly higher than that of non-motif region (2.5). Strikingly, the MPHA indexes of Kinase-1a (also called P-loop or Walker A) and GLPL motifs reached 50.0 and 57.1, respectively, which were significantly higher than those of other motifs reported previously. Additionally, no mutation was observed in the motifs RNBS-A, Kinase-3a (also named RNBS-B), WIAEGF, and MHD. All the mutation sites in conserved motifs in the CC and NB-ARC domains are listed in **Table 2**. In the LRR domain, the MPHA indexes of the motifs LRR2, LRR3, LRR4, LRR6, LRR12, and LRR14 were obviously higher than that of the whole LRR domain (4.4). The MPHA indexes of the motifs LRR5, LRR10, and LRR11 were lower than the average value of the LRR domain, whereas there was no mutation observed in the remaining 7 LRR motifs (**Figure 3** and **Table 1**).

Taken together, these results indicated that the distribution of mutations that led to amino acid changes and loss-of-function of *Pm21* resistance is tendentious in some degrees.

LPLHLRP immediately close to RNBS-D motif is a new mutation hotspot

LPLHLRP at position 414–420 in PM21 protein was closely near to the N-terminus of RNBS-D motif in the NB-ARC domain. We observed that 7 susceptible mutants involved in 5 amino acid changes in this region, including L414F (Y18-S12), P415L (Y18-S59), L418F (Y18-S112), R419H (Y18-S58), and P420S (Y18-S19, Y18-S79, and Y18-S82). It meant that the MPHA index of LPLHLRP reached 71.4, significantly higher than those of any other motifs (**Table 1**). Obviously, LPLHLRP was a mutation hotspot that has not been reported previously. We compared 26 wheat and barley NLR proteins against different diseases and found that the seven amino acids were relatively conserved, with the consensus sequence LPx(H/N/Y/D)(L/M/I)(K/R/Q)(T/Q/P) (**Figure 4**). It was strongly suggested that this conserved sequence might play an important role(s) in NLR proteins.

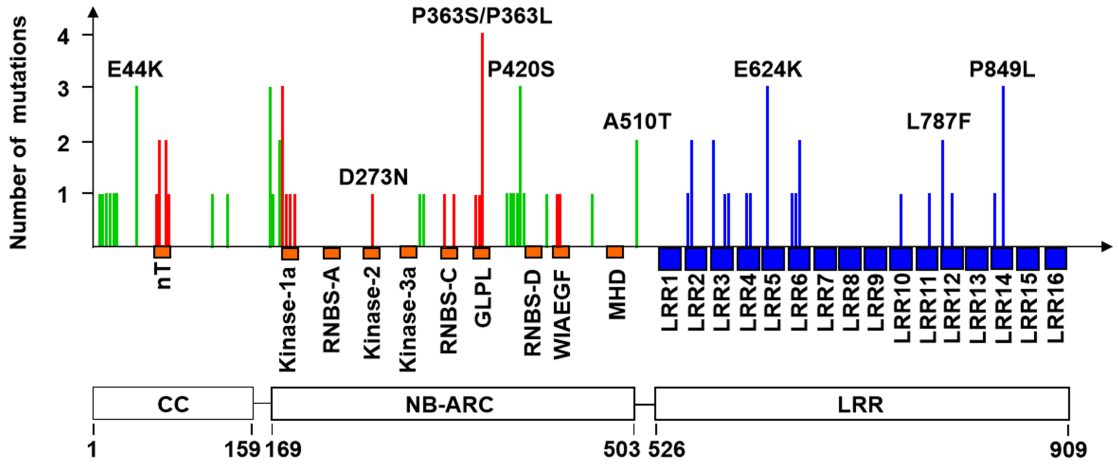

FIGURE 2
Frequency and distribution of 59 unique mutations leading to amino acid changes. The locations of the coiled-coil (CC), NB-ARC, and leucine-rich repeat (LRR) domains of PM21 are shown at bottom. The known conserved motifs (orange) of the CC and NB-ARC domains and 16 leucine-rich repeat motifs (blue) in the LRR domain are shown below the horizontal axis. The mutations in the motifs and non-motif regions of the CC and NB-ARC domains are shown as vertical red and green lines, respectively. The mutations in the LRR domain are shown as blue lines. A total of eight representative mutations are marked in the figure. More details of all mutation sites are listed in **Supplementary Table 1**.

The variant E44K in the coiled-coil domain leads to dominant-negative phenotype

All susceptible mutants were crossed with Yangmai 18 carrying wild-type *Pm21*, and the powdery mildew responses of the generated F_1 plants were then assessed. The results showed that all the F_1 plants derived from three crosses, Yangmai 18/Y18-S13, Yangmai 18/Y18-S23, and Yangmai 18/Y18-S100, were susceptible to BgtYZ01 (**Figure 5**), whereas all F_1 plants derived from other crosses were resistant. The susceptible and resistant individuals in the F_2 plants derived from the above three crosses were 116 and 35 (χ^2 = 0.267, p = 0.605), 145 and 46 (χ^2 = 0.086, p = 0.770), and 138 and 43 (χ^2 = 0.149, p = 0.699), respectively, which were all fit for the theoretical Mendelian segregation ratio 3:1 (**Table 3**). Interestingly, all the three independent susceptible mutants (Y18-S13, Y18-S23, and Y18-S100) contained the same mutation G to A at position 130, which led to the amino acid change E to K at position 44 in the CC domain. Therefore, it was strongly suggested that the mutation E44K could lead to dominant-negative phenotype.

Discussion

Pm21, originated from *D. villosum*, a wild relative of wheat, is one of the most valuable powdery mildew resistance genes that provides effective resistance to all tested isolates of *Bgt* (He et al., 2018; Zhang et al., 2019). Our recent research shows that *Pm21* encodes a CC-type NLR protein. Usually, disease resistance conferred by such kind of genes is subjected to be overcome by fast-evolved pathogen races. So, uncovering the molecular characteristic of PM21 protein will be very important for sustainable utilization of *Pm21* in wheat production. In this study, we performed large-scale mutagenesis on *Pm21* to find its key functional site. Nucleotide changes induced by EMS treatment widely occur in a genome, and some changes out of *Pm21*, such as changes in resistance signal components, may also impede *Pm21* resistance in some degrees. To exclude such non-target mutation leading to loss-of-function as possible, all the candidate susceptible mutants were crossed with Y18-S7, which carries a mutated *Pm21* only encoding very small fragment of PM21 protein and shows complete susceptibility at whole growth stages, and perform allelism tests. Finally, 113 stable susceptible mutants, whose variants leading to loss-of-function were considered to be occurred in the target gene *Pm21*, were identified. Among them, 82 independent mutants were involved in 59 different single amino acid substitutions, on which, we focused in this study.

In the CC domain of NLR, a core motif, EDVID motif (consensus sequence: VRELAYDAEDVID), was identified from the nT motif (consensus sequence: WVxxIRELAYDIEDIVDxY) originally predicted in rice (Bai et al., 2002; Rairdan et al., 2008). The EDVID motif, about 110–130 residues N-terminal to the P-loop motif of the NB-ARC domain, is conserved in most NLRs and required for the intramolecular interaction with the NB-ARC domain (Rairdan et al., 2008). Some mutations occurring in the residues in the EDVID motif can lead to lose cell death-inducing activity and disease resistance of potato Rx and barley MLA10 (Rairdan et al., 2008; Maekawa et al., 2011; Bai et al., 2012). In PM21 protein, a sequence,

WRDYVREMSYDMENCIDDF, similar to the EDVID motif, was characterized. In total, three variants, R73Q, E80K, and C82Y, could lead to loss-of-function of *Pm21*. Interestingly, our recent work showed that the CC domain containing any of the variants R73Q and E80K keeps the cell-death inducing activity but inhabits the autoactivation of PM21 (D491V) that harbors a mutation in the MHD motif (Gao et al., 2020). In addition, the variant R69K in the nT motif but not in the EDVID motif could also lead to loss-of-function of *Pm21*.

TABLE 1 Distribution and frequency of loss-of-function mutations altering amino acids in different domains and motifs of PM21.

Domain or motif	Position	Number of mutants	Number of mutations	MPHA index
FL	1–909	82	59	6.5
CC domain	1–159	21	16	10.1
Non-motif region	–	15	12	8.6
nT motif	68–86	6	4	21.1
Linker 1	160–168	3	1	11.1
NB-ARC domain	169–503	31	24	7.2
Non-motif region	–	8	7	2.5
Motif region	–	25	18	19.6
Kinase-1a (P-loop)	196–203	6	4	50.0
RNBS-A	215–227	0	0	0
Kinase-2	269–276	1	1	12.5
Kinase-3a (RNBS-C)	294–302	0	0	0
RNBS-C	319–338	2	2	10.0
GLPL	359–366	6	4	57.1
LPLHLRP	414–420	7	5	71.4
RNBS-D	421–431	1	1	9.1
WIAEGF	443–448	0	0	0
MHD	489–491	0	0	0
Linker 2	504–525	2	1	4.5
LRR domain	526–909	25	17	4.4
LRR1	526–546	0	0	0
LRR2	547–570	3	2	8.3
LRR3	571–596	4	3	11.5
LRR4	597–619	2	2	8.7
LRR5	620–641	3	1	4.8
LRR6	642–662	4	3	14.3
LRR7	663–685	0	0	0
LRR8	686–712	0	0	0
LRR9	713–739	0	0	0
LRR10	740–762	1	1	4.3
LRR11	763–786	1	1	4.2
LRR12	787–809	3	2	8.7
LRR13	810–832	0	0	0
LRR14	833–857	4	2	8.0
LRR15	858–887	0	0	0
LRR16	888–909	0	0	0

MPHA index, number of mutations per one hundred amino acids; FL, full-length protein; Linker 1, the linker between the CC and NB-ARC domains; Linker 2, the linker between the NB-ARC and LRR domains.

A recent research reported another motif, MADA motif, in the CC domain of NLR. The consensus sequence of MADA motif has been characterized as MADAxVSFxVxKLxxLLxxEx that lies in the N-terminus of the CC domain of ∼20% plant NLRs (Adachi et al., 2019). The MADA motif corresponds to the α1 helix of *Arabidopsis* ZAR1, which is a conformational switch during resistosome activation (Adachi et al., 2019; Wang et al., 2019a,b). Here, no similar sequence of the MADA motif could be found in PM21 protein. However, a mutation hotspot, ATMGAMNPLIGKL (from position 8–20), was observed in the N-terminus of the CC domain. In this hotspot, 7 variants involved in 6 sites could lead to lose *Pm21* resistance. So, it was speculated that this region might play the roles in PM21 resistosome activation.

The variant E44K in PM21 protein could lead to lose the cell death-inducing activity of the CC domain (Gao et al., 2020). Here, we found three independent mutants susceptible to powdery mildew that shows dominant-negative effect when crossed them with Yangmai 18 carrying wild-type *Pm21* gene. Surprisingly, each of the mutants contained the same mutation E44K in PM21 protein. It strongly indicated that E44K is responsible for this dominant-negative effect. In the previous research, two variants involved in the CC domain of *Arabidopsis* RPS2, a CC-NLR, can lead to dominant-negative effect. The first variant R2M1 has a truncated CC domain lacking of position 7–25. The second variant R2M2 has two amino acid substitutions, L38R and T40L (Tao et al., 2000).

Dominant-negative effect of NLR is thought to be caused by defective protein complex which consists of wild-type and mutated NLR (Dinesh-Kumar et al., 2000). Recently, plant NLR resistosome is confirmed to be a functional complex for disease resistance (Wang et al., 2019a,b). Therefore, for dominant-negative effect, one reasonable explanation is that mutated NLR could be integrated into resistosome with wild-type NLR and interfere the normal function of resistosome. In this study, a number of PM21 variants were identified; however, only E44K could cause dominant-negative effect, whereas other variants could not. This phenomenon suggested that most PM21 variants could not disturb the function of resistosome. It was also suggested that, in most situations, resistosome might possess strong fault-tolerance and maintain its resistance function when an abnormal peptide is incorporated into it.

The NB-ARC domain is a molecular switch for regulation of the activity of NLR (Bernoux et al., 2016). It consists of at least nine conserved motifs as reported previously (Meyers et al., 1999; Dilbirligi and Gill, 2003). Among them, the motifs P-loop, Kinase-2, and MHD are well known. P-loop, also called Kinase-1a or Walker A motif, has the consensus sequence GGLGKTTL and makes that NLR has the ability to bind ATP (Meyers et al., 1999; Tameling et al., 2002). Kinase-2, also called Walker B, shares the consensus sequence LIVLDDVW, in which, each

10.3389/fpls.2022.988641

TABLE 2 Mutation sites in conserved motifs in the coiled-coil (CC) and NB-ARC domains of PM21 protein.

Motif	Sequence in PM21	Consensus sequence	References
CC			
nT motif	WRDYVREMSYDMENCIDDF	WVxxIRELAYDIEDIVDxY	Bai et al., 2002
NB-ARC			
Kinase-1a	GGLGKTTL	GGLGKTTL	Dilbirligi and Gill, 2003
RNBS-A	FSCKIFFSVSQRP	FDLxAWVCVSQxF	Meyers et al., 1999
Kinase-2	LIVVDDLW	LIVLDDVW	Dilbirligi and Gill, 2003
Kinase-3a	GSRVIVTTR	GSKIIVTTR	Dilbirligi and Gill, 2003
RNBS-C	YRMEPLKEQDSRMLFCNRVF	YEVxxLSEDEAWELFCKxAF	Meyers et al., 1999
GLPL	CGGLPLA	CGGLPLA	Meyers et al., 1999
LPLHLRP*	LPLHLRP	LPx(H/N/Y/D)(L/M/I)(K/R/Q)(T/Q/P)	In this study
RNBS-D	CLLYFGMYPED	CFLYCALFPED	Meyers et al., 1999
WIAEGF	WVAEGF	WIAEGF	Dilbirligi and Gill, 2003
MHD	VHD	MHD	Dilbirligi and Gill, 2003

The amino acids marked by red were mutation sites found in PM21 protein.
*LPLHLRP, a mutation hotspot, was originally reported in this study.

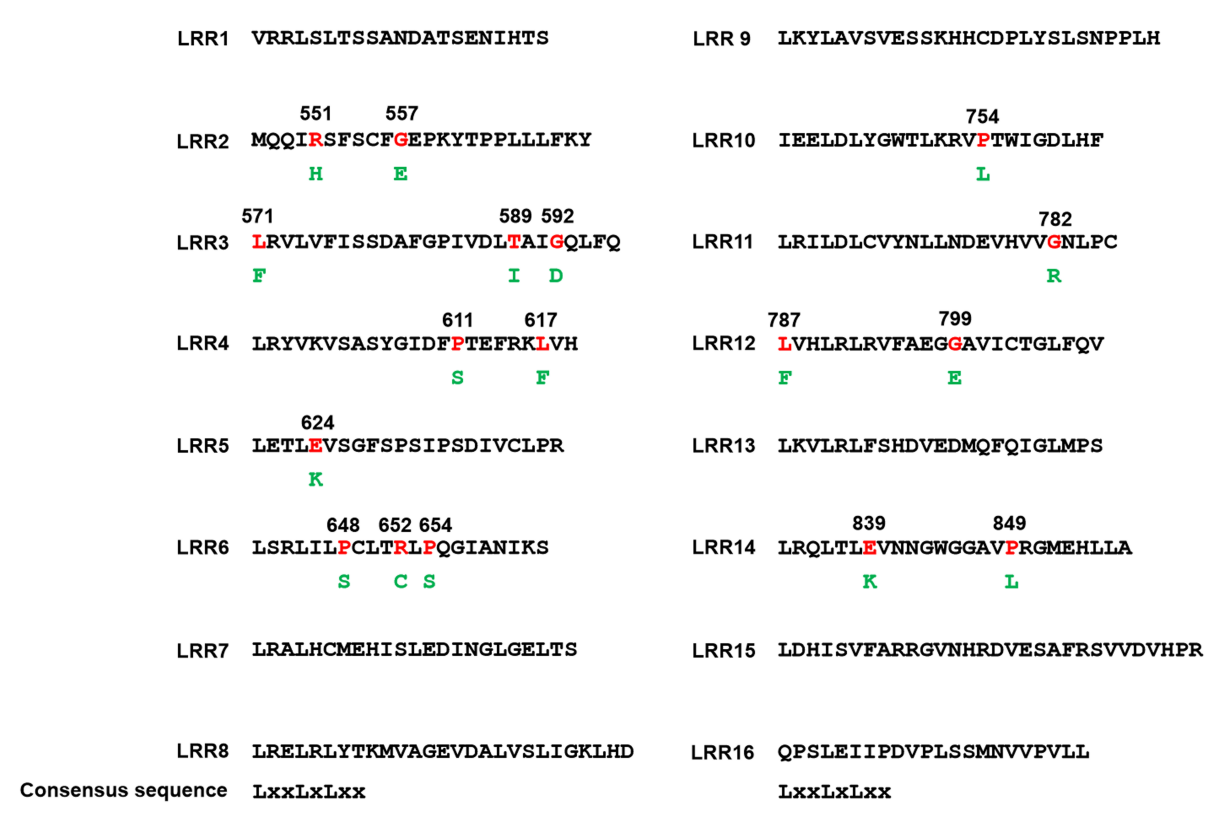

FIGURE 3
Mutation sites in the leucine-rich repeat (LRR) domain. The LRR domain of PM21 can be divided into 16 LRR motifs and their consensus sequence LxxLxLxx is given at the bottom of this figure. Substituted amino acids (green) and their positions are shown in the below and the above of the mutated ones (red), respectively.

aspartate (D) is almost conserved in all plant NLRs. The first D takes part in coordination of the Mg^{2+} ion in the catalytic site, and the second D acts as the catalytic site for ATP hydrolysis and activation of NLR (Meyers et al., 1999; Tameling et al., 2006). MHD lies in the C-terminus of the NB-ARC domain, which is known because the change aspartate (D) to valine (V) can enhance the binding between NLR and ATP and result in the autoactivation of many NLRs (Bendahmane et al., 2002;

10.3389/fpls.2022.988641

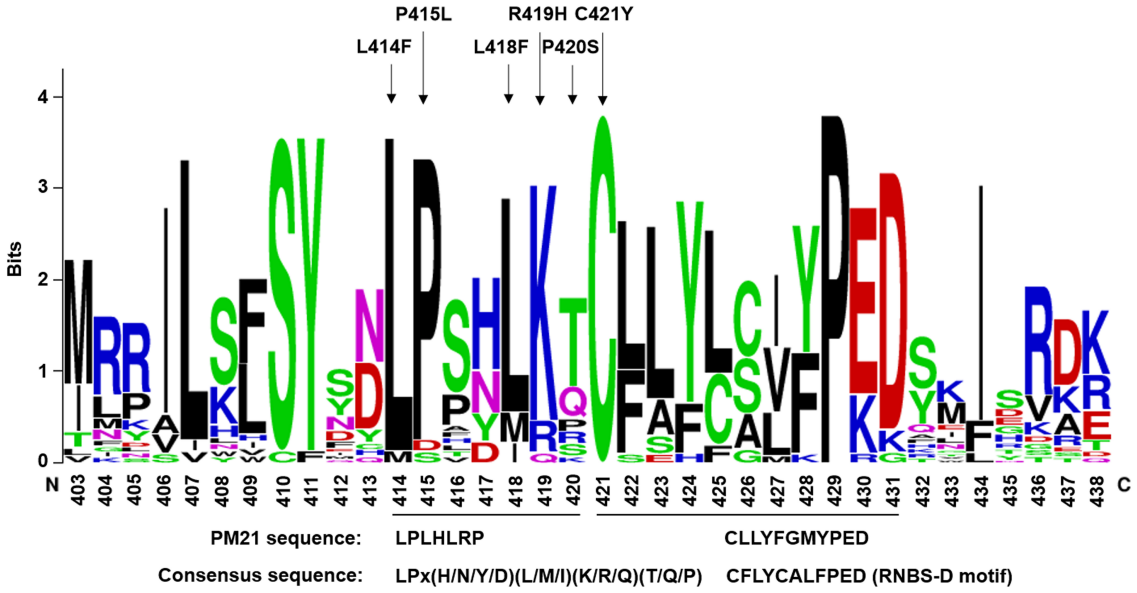

FIGURE 4
Sequence logos of the mutation hotspot LPLHLRP and its closely linked RNBS-D motif (CFLYCALFPED). Sequence logos were generated from 26 NLR proteins of wheat crops, including PM3, PM8, PM21, LR1, LR21, SR33, SR35, YR10, MLA1, MLA6, and so on. Arrows indicate amino acid changes leading to loss-of-function of PM21. The consensus sequences and the corresponding PM21 sequence are shown at the bottom.

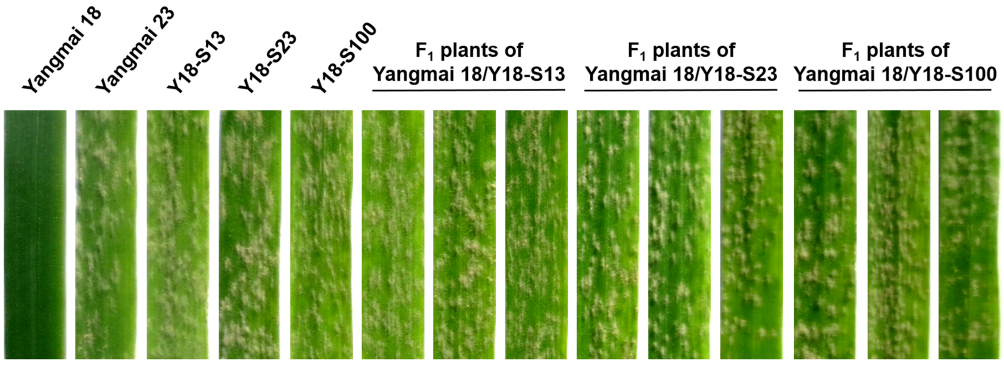

FIGURE 5
Powdery mildew responses of mutant lines and F_1 plants involving dominant-negative effect. Responses of the F_1 plants of the crosses Yangmai 18/Y18-S13, Yangmai 18/Y18-S23, and Yangmai 18/Y18-S100 were tested at one-leaf stage by inoculation with *Bgt* isolate BgtYZ01. Wheat cultivar (cv.) Yangmai 18, Yangmai 23, and the mutant lines Y18-S13, Y18-S23, and Y18-S100 were used as controls.

TABLE 3 Genetic data of three crosses showing dominant-negative effect.

Cross	Number of F_1 plants		Number of F_2 plants		$\chi^2_{3:1}$ ($P > 0.01$)
	Susceptible	Resistant	Susceptible	Resistant	
Yangmai 18/Y18-S13	28	0	116	35	0.267 (0.605)
Yangmai 18/Y18-S23	35	0	145	46	0.086 (0.770)
Yangmai 18/Y18-S100	22	0	138	43	0.149 (0.699)

Tameling et al., 2006; Gao et al., 2020). According to the result of sequence comparison, PM21 protein contains all the nine motifs. Our mutational analysis showed that 10 variants, leading to loss-of-function of PM21, were involved in amino acid substitutions in the core sites of 5 reported motifs of the NB-ARC domain (Table 2).

The sequence of PM21 P-loop motif is GGLGKTTL (position: 196–203), which well matches the consensus sequence of this motif. Mutational analysis showed that each of the six mutations such as G196R, G196E, G197D, G199D, L203F (occurring in P-loop), and G194E (near the N-terminus of P-loop) could lead to loss-of-function of PM21. Mutational research on tobacco N reveals that specific mutations, including G216A/E/V/R, G218R, G219D, K222E/N, and T223A/N, near or in the P-loop not only lead to lose N function but also result in dominant-negative effects (Dinesh-Kumar et al., 2000). However, in another research on *Arabidopsis* RPM1, no dominant-negative effect was detected in the mutant line rpm1-94 that carries the variant G200E corresponding to G216A/E/V/R of N (Tornero et al., 2002). Here, the variants G194E and G196R/E of PM21 corresponded to G216A/E/V/R and G218R of N, respectively. As our observation, all the F_1 plants derived from the crosses of the corresponding susceptible mutants with Yangmai 18 (harboring wild-type *Pm21*) showed complete resistance to powdery mildew, indicating that these variants could not interfere with PM21 function.

Previously, we found a susceptible natural accession of *D. villosum* that carries a non-functional *Pm21* allele with a transition A821G resulting in the amino acid change D274G in the Kinase-2 (Walker B) motif (He et al., 2020). Here, through EMS treatment, *Pm21* in the susceptible mutants Y18-S28 was identified to be containing a transition G817A resulting in the substitution D273N. The results suggested that the two D residues are important for Kinase-2 function and PM21 resistance, which is in accordance with the previous reports on *Arabidopsis* RPS2 (Tao et al., 2000), tobacco N (Dinesh-Kumar et al., 2000), and tomato I-2 (Tameling et al., 2006).

In the NB-ARC domain, the functions of another six motifs such as RNBS-A, RNBS-B (Kinase-3a), RNBS-C, GLPL, RNBS-D, and WIAEGF are not well known. It is believed that these motifs may play the roles in binding ATP for the regulation of NLR activity (Takken et al., 2006). Mutational analysis of *Arabidopsis* RPM1 shows that three variants, E340K, A341V, and L344F, respectively located in the 10th, 11th, and 14th residues in the RNBS-C motif, could result in RPM1 function defect (Tornero et al., 2002). Here, we demonstrated that two variants, L324F and S329L, occurred in the first and 11th residues in the RNBS-C motif could lead to lose PM21 resistance. S329L of PM21 and A341V of RPM1 situate in the same position of the RNBS-C motif, whereas L324F of PM21 is a new found functional site.

The GLPL motif has a conserved sequence CGGLPLA. Mutational analyses of flax rust resistance protein P2 (variant: G395E) (Dodds et al., 2001), maize Rp1-D21 (variant: P398L) (Wang et al., 2005), and RPM1 (variant: A379V) (Tornero et al., 2002) indicate the importance of the 3rd residue glycine (G), the 5th residue proline (P) and the last residue alanine (A). In this study, we obtained six independent susceptible mutants involved in four variants of three sites (C359Y, G361R, P363S, and P363L) in the GLPL motif. It was suggested that not only the 3rd residue G and the 5th residue P but also the first residues cysteine (C) are crucial for PM21 resistance.

The RNBS-D motif has a consensus sequence CFLYCALFPED. RPM1 variants (S439F and P442L) at the 6th and 9th residues in this motif result in loss-of-function (Tornero et al., 2002). Here, we revealed that replacement of the first residue cysteine (C) with tyrosine (Y) (C421Y) could lead to hampering PM21 resistance, indicating the importance of the cysteine residues in NLR. Interestingly, near the N-terminus of the RNBS-D motif, seven independent mutations, involved in five sites (L414F, P415L, L418F, R419H, and P420S), were observed in this study, suggesting that the sequence LPLHLRP of PM21 seems to be a mutation hotspot leading to loss-of-function. Comparative analysis showed that both the LPLHLRP-like sequences and the RNBS-D sequences are conserved in different NLRs. Due to that LPLHLRP is immediate before the reported motif RNBS-D, we propose that it should be considered as an extended functional region of the RNBS-D motif rather than as a new independent motif.

The LRR domain is more variant than other domains in NLR, which is usually considered as a sensor for specific recognition of pathogen effector by a direct or indirect means (Dangl et al., 2013). This is supported by several researches. For instance, a single amino acid difference can make that rice blast resistance gene *Pi-ta* differs from its susceptible allele (Bryan et al., 2000). A total of six amino acid changes can alter flax rust resistance gene *P2* to *P* specificities (Dodds et al., 2001). Natural variations in the LRR domain result in different powdery mildew responses of *Pm3* alleles (Srichumpa et al., 2005). A recent research showed that site-directed mutagenesis on the LRR domain of PM3A can obviously control response strength and resistance spectrum (Lindner et al., 2020). In this research, a total of 25 susceptible mutants involved in 17 amino acid changes were obtained. In our recent work, the LRR domain of PM21 has been divided into 16 LRR motif with the consensus sequence LxxLxLxx (where L represents a conserved leucine or other aliphatic residue and x represents any amino acid) (He et al., 2020). These variants were distributed in 9 LRR motifs (LRR2–LRR6, LRR10–LRR12, and LRR14), some of which have been confirmed to be under diversifying selection (He et al., 2020). Of 17 variants, 2 (L571F and L787F), 4 (R551H, E624K, P654S, and E839K), and other 11 occurred in the position of L, x, and the non-core region of LRR motif, respectively. It was suggested the importance of these sites for complete PM21 resistance. Whether the amino acid changes in the LRR domain alter recognition specificity for *Bgt* isolates needs further investigation.

In conclusion, we performed large-scale mutagenesis on wheat powdery mildew resistance gene *Pm21*, which revealed the distribution characteristics of variant amino acid residues and discussed their potential impacts on PM21 resistance. To our knowledge, some mutation sites have not been reported in

plant NLRs previously. Furthermore, two mutation hotspots, one near the N-terminus of the CC domain and the other immediately close to the N-terminus of RNBS-D motif of the NB-ARC domain and a variant resulting in dominant-negative effect, were identified. This study will contribute to understanding the relationship of resistance and structure of *Pm21*-encoded NLR, which would be useful for the development of durable resistance for efficiently controlling wheat powdery mildew.

Data availability statement

The datasets presented in this study can be found in online repositories. The names of the repository/repositories and accession number(s) can be found in the article/**Supplementary material**.

Author contributions

HH and SZ conceived and designed the experiments and wrote and revised the manuscript. HH, RG, ZC, RL, and XK screened the mutants and identified the mutation sites. HH performed allelism test. HH, AG, and TL analyzed the data. All authors contributed to the article and approved the submitted version.

Funding

This study was supported by the grants from National Natural Science Foundation of China (32171990 and U1604116), Key Research and Development Program of Zhenjiang (NY2021001), State Key Laboratory of Plant Cell and Chromosome Engineering (PCCE-KF-2021-05 and PCCE-KF-2022-07), and State Key Laboratory of Crop Biology in Shandong Agricultural University (2021KF01).

Conflict of interest

The authors declare that the research was conducted in the absence of any commercial or financial relationships that could be construed as a potential conflict of interest.

Publisher's note

All claims expressed in this article are solely those of the authors and do not necessarily represent those of their affiliated organizations, or those of the publisher, the editors and the reviewers. Any product that may be evaluated in this article, or claim that may be made by its manufacturer, is not guaranteed or endorsed by the publisher.

Supplementary material

The Supplementary Material for this article can be found online at: https://www.frontiersin.org/articles/10.3389/fpls.2022.988641/full#supplementary-material

References

Adachi, H., Contreras, M. P., Harant, A., Wu, C., Derevnina, L., Sakai, T., et al. (2019). An N-terminal motif in NLR immune receptors is functionally conserved across distantly related plant species. *Elife* 8:e49956. doi: 10.7554/eLife.49956

Bai, J., Pennill, L. A., Ning, J., Lee, S. W., Ramalingam, J., Webb, C. A., et al. (2002). Diversity in nucleotide binding site-leucine-rich repeat genes in cereals. *Genome Res.* 12, 1871–1884. doi: 10.1101/gr.454902

Bai, S., Liu, J., Chang, C., Zhang, L., Maekawa, T., Wang, Q., et al. (2012). Structure-function analysis of barley NLR immune receptor MLA10 reveals its cell compartment specific activity in cell death and disease resistance. *PLoS Pathog.* 8:e1002752. doi: 10.1371/journal.ppat.1002752

Bendahmane, A., Farnham, G., Moffett, P., and Baulcombe, D. C. (2002). Constitutive gain-of-function mutants in a nucleotide binding site-leucine rich repeat protein encoded at the Rx locus of potato. *Plant J.* 32, 195–204. doi: 10.1046/j.1365-313x.2002.01413.x

Bernoux, M., Burdett, H., Williams, S. J., Zhang, X., Chen, C., Newell, K., et al. (2016). Comparative analysis of the flax immune receptors L6 and L7 suggests an equilibrium-based switch activation model. *Plant Cell* 28, 146–159. doi: 10.1105/tpc.15.00303

Bernoux, M., Ve, T., Williams, S., Warren, C., Hatters, D., Valkov, E., et al. (2011). Structural and functional analysis of a plant resistance protein TIR domain reveals interfaces for self-association, signaling, and autoregulation. *Cell Host Microbe* 9, 200–211. doi: 10.1016/j.chom.2011.02.009

Bryan, G. T., Wu, K., Farrall, L., Jia, Y., Hershey, H. P., McAdams, S. A., et al. (2000). A single amino acid difference distinguishes resistant and susceptible alleles of the rice blast resistance gene Pi-ta. *Plant Cell* 12, 2033–2045. doi: 10.1105/tpc.12.11.2033

Cesari, S. (2018). Multiple strategies for pathogen perception by plant immune receptors. *New Phytol.* 219, 17–24. doi: 10.1111/nph.14877

Crooks, G. E., Hon, G., Chandonia, J. M., and Brenner, S. E. (2004). WebLogo: A sequence logo generator. *Genome Res.* 14, 1188–1190. doi: 10.1101/gr.849004

Cui, H., Tsuda, K., and Parker, J. E. (2015). Effector-triggered immunity: From pathogen perception to robust defense. *Annu. Rev. Plant Biol.* 66, 487–511. doi: 10.1146/annurev-arplant-050213-040012

Dangl, J. L., Horvath, D. M., and Staskawicz, B. J. (2013). Pivoting the plant immune system from dissection to deployment. *Science* 341, 746–751. doi: 10.1126/science.1236011

Dilbirligi, M., and Gill, K. S. (2003). Identification and analysis of expressed resistance gene sequences in wheat. *Plant Mol. Biol.* 53, 771–787. doi: 10.1023/B:PLAN.0000023663.55701.5f

Dinesh-Kumar, S. P., Tham, W. H., and Baker, B. J. (2000). Structure-function analysis of the tobacco mosaic virus resistance gene N. *Proc. Natl. Acad. Sci. U.S.A.* 97, 14789–14794. doi: 10.1073/pnas.97.26.14789

Dodds, P. N., Lawrence, G. J., and Ellis, J. G. (2001). Six amino acid changes confined to the leucine-rich repeat β-strand/β-turn motif determine the difference between the P and P2 rust resistance specificities in flax. *Plant Cell* 13, 163–178. doi: 10.1105/tpc.13.1.163

Gao, A., Hu, M., Gong, Y., Dong, R., Jiang, Y., Zhu, S., et al. (2020). Pm21 CC domain activity modulated by intramolecular interactions is implicated in cell death and disease resistance. *Mol. Plant Pathol.* 21, 975–984. doi: 10.1111/mpp.12943

He, H., Du, H., Liu, R., Liu, T., Yang, L., Gong, S., et al. (2021a). Characterization of a new gene for resistance to wheat powdery mildew on chromosome 1RL of wild rye Secale sylvestre. *Theor. Appl. Genet.* 134, 887–896. doi: 10.1007/s00122-020-03739-1

He, H., Liu, R., Ma, P., Du, H., Zhang, H., Wu, Q., et al. (2021b). Characterization of Pm68, a new broad-spectrum powdery mildew resistance gene on chromosome 2BS of Greek durum wheat TRI 1796. *Theor. Appl. Genet.* 134, 53–62. doi: 10.1007/s00122-020-03681-2

He, H., Ji, J., Li, H., Tong, J., Feng, Y., Wang, X., et al. (2020). Genetic diversity and evolutionary analyses reveal the powdery mildew resistance gene Pm21 undergoing diversifying selection. *Front. Genet.* 11:489. doi: 10.3389/fgene.2020.00489

He, H., Ji, Y., Zhu, S., Li, B., Zhao, R., Jiang, Z., et al. (2017). Genetic, physical and comparative mapping of the powdery mildew resistance gene Pm21 originating from *Dasypyrum villosum*. *Front. Plant Sci.* 8:1914. doi: 10.3389/fpls.2017.01914

He, H., Zhu, S., Zhao, R., Jiang, Z., Ji, Y., Ji, J., et al. (2018). Pm21, encoding a typical CC-NBS-LRR protein, confers broad-spectrum resistance to wheat powdery mildew disease. *Mol. Plant* 11, 879–882. doi: 10.1016/j.molp.2018.03.004

Horsefield, S., Burdentt, H., Zhang, X., Manik, M. K., Shi, Y., Chen, J., et al. (2019). NAD^+ cleavage activity by animal and plant TIR domains in cell death pathways. *Science* 365, 793–799. doi: 10.1126/science.aax1911

Lindner, S., Keller, B., Singh, S. P., Hasenkamp, Z., Jung, E., Müller, M. C., et al. (2020). Single residues in the LRR domain of the wheat PM3A immune receptor can control the strength and the spectrum of the immune response. *Plant J.* 104, 200–214. doi: 10.1111/tpj.14917

Maekawa, T., Cheng, W., Spiridon, L. N., Töller, A., Lukasik, E., Saijo, Y., et al. (2011). Coiled-coil domain-dependent homodimerization of intracellular barley immune receptors defines a minimal functional module for triggering cell death. *Cell Host Microbe* 9, 187–199. doi: 10.1016/j.chom.2011.02.008

Meyers, B. C., Dickerman, A. W., MIchelmore, R. W., Sivaramakrishnan, S., Sobral, B. W., and Young, N. D. (1999). Plant disease resistance genes encode members of an ancient and diverse protein family within the nucleotide-binding superfamily. *Plant J.* 20, 317–332. doi: 10.1046/j.1365-313x.1999.t01-1-00606.x

Moffett, P., Farnham, G., Peart, J., and Baulcombe, D. C. (2002). Interaction between domains of a plant NBS-LRR protein in disease resistance-related cell death. *EMBO J.* 21, 4511–4519. doi: 10.1093/emboj/cdf453

Rairdan, G. J., Collier, S. M., Sacco, M. A., Baldwin, T. T., Boettrich, T., and Moffett, P. (2008). The coiled-coil and nucleotide binding domains of the potato Rx disease resistance protein function in pathogen recognition and signaling. *Plant Cell* 20, 739–751. doi: 10.1105/tpc.107.056036

Srichumpa, P., Brunner, S., Keller, B., and Yahiaoui, N. (2005). Allelic series of four powdery mildew resistance genes at the Pm3 locus in hexaploid bread wheat. *Plant Physiol.* 139, 885–895. doi: 10.1104/pp.105.062406

Sun, Y., Zhu, Y., Balint-kurti, P. J., and Wang, G. (2020). Fine-tuning immunity: Players and regulators for plant NLRs. *Trends Plant Sci.* 25, 695–713. doi: 10.1016/j.tplants.2020.02.008

Takken, F. L. W., Albrecht, M., and Tameling, W. I. L. (2006). Resistance proteins: Molecular switches of plant defence. *Curr. Opin. Plant Biol.* 9, 383–390. doi: 10.1016/j.pbi.2006.05.009

Tameling, W. I. L., Elzinga, S. D., Darmin, P. S., Vossen, J. H., Takken, F. L. W., Haring, M. A., et al. (2002). The tomato R gene products I-2 and Mi-1 are functional ATP binding proteins with ATPase activity. *Plant Cell* 14, 2929–2939. doi: 10.1105/tpc.005793

Tameling, W. I. L., Vossen, J. H., Albrecht, M., Lengauer, T., Berden, J. A., Haring, M. A., et al. (2006). Mutations in the NB-ARC domain of I-2 that impair ATP hydrolysis cause autoactivation. *Plant Physiol.* 140, 1233–1245. doi: 10.1104/pp.105.073510

Tao, Y., Yuan, F., Leister, R. T., Ausubel, F. M., and Katagiri, F. (2000). Mutational analysis of the *Arabidopsis* nucleotide binding site-leucine-rich repeat resistance gene RPS2. *Plant Cell* 12, 2541–2554. doi: 10.1105/tpc.12.12.2541

Tornero, P., Chao, R. A., Luthin, W. N., Goff, S. A., and Dangl, J. L. (2002). Large-scale structure-function analysis of the *Arabidopsis* RPM1 disease resistance protein. *Plant Cell* 14, 435–450. doi: 10.1105/tpc.010393

Wan, L., Essuman, K., Anderson, R. G., Sasaki, Y., Monteiro, F., Chung, E., et al. (2019). TIR domains of plant immune receptors are NAD^+-cleaving enzymes that promote cell death. *Science* 365, 799–803. doi: 10.1126/science.aax1771

Wang, G., Ji, J., Ei-Kasmi, F., Dangl, J. L., Johal, G., and Balint-Kurti, P. J. (2005). Molecular and functional analyses of a maize autoactive NB-LRR protein identify precise structural requirements for activity. *PLoS Pathog.* 11:e1004674. doi: 10.1371/journal.ppat.1004674

Wang, J., Wang, J., Hu, M., Wu, S., Qi, J., Wang, G., et al. (2019a). Ligand-triggered allosteric ADP release primes a plant NLR complex. *Science* 364:eaav5868. doi: 10.1126/science.aav5868

Wang, J., Hu, M., Wang, J., Qi, J., Han, Z., Wang, G., et al. (2019b). Reconstitution and structure of a plant NLR ressitosome conferring immunity. *Science* 364:eaav5870. doi: 10.1126/science.aav5870

Zhang, D., Zhu, K., Dong, L., Liang, Y., Li, G., Fang, T., et al. (2019). Wheat powdery mildew resistance gene Pm64 derived from wild emmer (*Triticum turgidum* var. *dicoccoides*) is tightly linked in repulsion with stripe rust resistance gene Yr5. *Crop J.* 7, 761–770. doi: 10.1016/j.cj.2019.03.003

frontiers | Frontiers in Plant Science

TYPE Original Research
PUBLISHED 15 August 2022
DOI 10.3389/fpls.2022.984527

OPEN ACCESS

EDITED BY
Zuhua He,
Center for Excellence in Molecular Plant Sciences (CAS), China

REVIEWED BY
Jianbing Yan,
Huazhong Agricultural University, China
Jianfeng Weng,
Institute of Crop Sciences (CAAS), China

*CORRESPONDENCE
Mingliang Xu
mxu@cau.edu.cn

SPECIALTY SECTION
This article was submitted to Plant Pathogen Interactions, a section of the journal Frontiers in Plant Science

RECEIVED 02 July 2022
ACCEPTED 27 July 2022
PUBLISHED 15 August 2022

CITATION
Tong L, Yan M, Zhu M, Yang J, Li Y and Xu M (2022) *ZmCCT* haplotype *H5* improves yield, stalk-rot resistance, and drought tolerance in maize. *Front. Plant Sci.* 13:984527. doi: 10.3389/fpls.2022.984527

ZmCCT haplotype *H5* improves yield, stalk-rot resistance, and drought tolerance in maize

Lixiu Tong[1], Mingzhu Yan[1], Mang Zhu[1], Jie Yang[1,2], Yipu Li[1,3] and Mingliang Xu[1]*

[1]State Key Laboratory of Plant Physiology and Biochemistry, College of Agronomy and Biotechnology, National Maize Improvement Center, Center for Crop Functional Genomics and Molecular Breeding, China Agricultural University, Beijing, China, [2]Food Crops Research Institute, Xinjiang Academy of Agricultural Sciences, Urumqi, China, [3]Agricultural College, Inner Mongolia Agricultural University, Hohhot, China

The *ZmCCT* locus underlies both stalk-rot resistance and photoperiod sensitivity in maize (*Zea mays* L.). We previously introduced nine resistant *ZmCCT* haplotypes into seven elite but susceptible maize inbred lines (containing the haplotype *H1*) to generate 63 backcross families. Here, we continued backcrossing, followed by selfing, to develop 63 near-isogenic lines (NILs). We evaluated 22 of these NILs for stalk-rot resistance and flowering time under long-day conditions. Lines harboring the haplotype *H5* outperformed the others, steadily reducing disease severity, while showing less photoperiod sensitivity. To demonstrate the value of haplotype *H5* for maize production, we selected two pairs of NILs, $83B28^{H1}$/$83B28^{H5}$ and $A5302^{H1}$/$A5302^{H5}$, and generated F_1 hybrids with the same genetic backgrounds but different *ZmCCT* alleles: $83B28^{H1}$ × $A5302^{H1}$, $83B28^{H1}$ × $A5302^{H5}$, $83B28^{H5}$ ×$A5302^{H1}$, and $83B28^{H5}$ ×$A5302^{H5}$. We performed field trials to investigate yield/yield-related traits, stalk-rot resistance, flowering time, and drought/salt tolerance in these four hybrids. $83B28^{H5}$ ×$A5302^{H1}$ performed the best, with significantly improved yield, stalk-rot resistance, and drought tolerance compared to the control ($83B28^{H1}$ × $A5302^{H1}$). Therefore, the *ZmCCT* haplotype *H5* has great value for breeding maize varieties with high yield potential, stalk-rot resistance, and drought tolerance.

KEYWORDS

***ZmCCT*, hybrids, yield, stalk-rot resistance, drought tolerance**

Introduction

Increasing maize (*Zea mays* L.) output is crucial to meet the global demand for food security. However, both biotic and abiotic stress pose great threats to maize productivity. Breeding maize varieties with enhanced disease resistance and drought tolerance is the most effective and environmentally friendly way to ensure the security of maize production and supply.

Plants have evolved sophisticated defense responses against pathogens, including pattern-triggered immunity (PTI) and effector-triggered immunity (ETI). However, disease resistance is usually associated with a fitness penalty. In *Arabidopsis thaliana*, the *R* gene leads to a 5%–10% reduction in fitness in the absence of infection (Tian et al., 2003; Karasov et al., 2017). In crops, resistance (*R*) and susceptible (*S*) genes can play opposite roles in disease resistance and grain yield, with *S* genes decreasing disease resistance, but positively correlated with plant growth and development (Brown and Rant, 2013; Deng et al., 2017; Nelson et al., 2018). For example, *Mildew resistance locus O* (*mlo*) is derived from the loss of function of the dominant *S* gene (*MLO*), which confers durable, broad-spectrum resistance to powdery mildew in various species (Wang et al., 2014; Nekrasov et al., 2017). However, *mlo*-mediated resistance against powdery mildew is usually accompanied by a yield penalty (Büschges et al., 1997; Consonni et al., 2006), hampering the use of such resistance genes in crop breeding. Fortunately, the mildew-resistant mutant *Tamlo-R32* was recently created by genome editing and harbors an activated *Tonoplast monosaccharide transporter 3* (*TaTMT3B*) gene to rescue the *Tamlo*-related growth and yield penalty (Li et al., 2022). In addition, some ideal resistance genes appear to have no fitness cost and even increase yields (Li et al., 2017a; Wang et al., 2018). In rice, *IDEAL PLANT ARCHITECTURE 1* (*IPA1*) not only improves rice yields by reducing the formation of unproductive tillers to increase grains per panicle, but also enhances disease resistance by activating the pathogen defense gene *WRKY45* (*WRKY DNA-binding protein 45*; Wang et al., 2018). Thus, it is essential to evaluate the impact of a resistance gene on yield under normal and infected conditions before it can be appropriately applied for genetic improvement.

Pleiotropic genes are single genes (or a single locus) that affect two or more unrelated phenotypic traits (Solovieff et al., 2013) and numerous pleiotropic genes and QTLs have been reported in plants, whose functions range from growth and development to disease resistance (Liang et al., 2021). Most resistance genes in Arabidopsis have strong pleiotropic effects (Karasov et al., 2017). For example, the *Arabidopsis thaliana* typical coiled-coil (CC)-NBS-LRR (CNL) proteins *Resistance to Pseudomonas syringae 5* (*Rps5*) and *Resistance to P. syringae pv maculicola 1* (*Rpm1*) cause a fitness penalty when activated (Tian et al., 2003; Karasov et al., 2014). In maize, *ZmNF-Y3A* encodes a transcription factor that promotes early flowering and increases drought and heat stress tolerance by binding to different cis-elements in the promoters of various genes (Su et al., 2018).

In maize, a CCT (CONSTANS (CO), CO-LIKE, and TIMING OF CAB1) domain-containing transcription regulator gene, *ZmCCT*, was first reported to regulate flowering time under long-day conditions (Hung et al., 2012; Yang et al., 2013). Remarkably, *ZmCCT* was subsequently confirmed to be the causative gene at QTL-*qRfg1* associated with maize resistance to *Gibberella* stalk rot (Yang et al., 2010; Wang et al., 2017). The non-TE *ZmCCT* allele (lacking a transposable element [TE] in its promoter) is resistant to stalk rot and has photoperiod sensitivity under long-day conditions (Yang et al., 2013; Wang et al., 2017). In addition, the non-TE *ZmCCT* increases primary branch number, spike length (Xu et al., 2017), and crown root number (Zhang et al., 2018). A new *ZmCCT* allele was recently discovered that contains a 4.2-kilobase (kb) TE inserted in the intron of a non-TE *ZmCCT*; this allele shortens flowering time in low-latitude regions (Zhong et al., 2021). Phylogenetic analysis of genes encoding CCT proteins and their orthologs showed that the closest genes to *ZmCCT* are *Sb06g000570* in sorghum and *Ghd7* (*grain number, plant height, and heading date 7*) in rice (Xue et al., 2008; Yang et al., 2013). The CCT domain-containing gene *Ghd7* is involved in grain number, plant height, heading date (Xue et al., 2008), regulation of hormone metabolism, and biotic/abiotic stress responses (Weng et al., 2014). The finding that *ZmCCT* and *Ghd7* share highly similar genomic features prompted us to explore whether *ZmCCT* could also improve yield or other agronomic traits under various environmental conditions.

Marker-assisted selection (MAS) has been successfully used to breed disease-resistant lines (Zhao et al., 2012; Konlasuk et al., 2015; Xu et al., 2020). We previously introgressed nine non-TE *ZmCCT* haplotypes into seven elite inbred maize lines by MAS (Li et al., 2017b). In the current study, we selected 22 pairs of NILs derived from advanced backcross generations and evaluated their disease resistance and photoperiod sensitivity. We then focused on two pairs of NILs, $83B28^{H1}$/$83B28^{H5}$, and $A5302^{H1}$/$A5302^{H5}$, to prepare four F_1 hybrids with the same genetic backgrounds but different *ZmCCT* haplotypes. These F_1 hybrids were evaluated for their yield/yield-related traits, stalk-rot resistance, and flowering time under normal and biotic/abiotic stress conditions to assess the value of haplotype *H5* in the breeding of resistant maize varieties.

Materials and methods

Plant materials

We previously identified 15 haplotypes (*H1* to *H15*) at the *ZmCCT* locus. Of these, only haplotype *H1* contains a TE insertion in the promoter, whereas the other 14 lack a TE insertion (non-TE *ZmCCT*). Nine donor parents carrying different non-TE *ZmCCT* haplotypes (*H3*, *H4*, *H5*, *H6*, *H7*, *H12*, *H13*, *H14*, and *H15*) were previously crossed with and then backcrossed to seven elite inbred lines with haplotype *H1* (Zheng58, Chang7-2, 83B28, A5302, Jing24, F349, and Yu87-1) to generate 63 BC_5F_1 families (Li et al., 2017b). In the current study, we continued backcrossing twice to obtain 63 BC_7F_1 families, which were selfed and grown at the experimental station of China Agricultural University (Beijing, N39°54′, E116°24′). The BC_7F_2 families were planted in the Hainan winter nursery (Hainan, Sanya, N18°21′, E109°10′) in 2017/2018. After genotyping, BC_7F_2 plants from each family with homozygous haplotype *H1* or one of the non-TE *ZmCCT* haplotypes were continuously selfed to produce homozygous BC_7F_3 lines, which were grown at the experimental station of

China Agricultural University to develop pairs of near-isogenic lines (NILs).

Due to limited resources, we chose five haplotypes (*H3*, *H5*, *H6*, *H12*, and *H13*) in the Zheng58 and Chang7-2 backgrounds and six haplotypes (*H3*, *H5*, *H6*, *H7*, *H12*, and *H13*) in the 83B28 and A5302 backgrounds for further study. We used the GoldenGate 6KSNP chip to survey the genome-wide SNPs. The genomic identities of two pairs of NILs, $83B28^{H1}$/$83B28^{H5}$, and $A5302^{H1}$/$A5302^{H5}$, were estimated to be 96.86% and 93.71%, respectively. They were then crossed with one another to produce four F_1 hybrids with the same genetic backgrounds but different *ZmCCT* haplotypes, including $83B28^{H1} \times A5302^{H1}$, $83B28^{H1} \times A5302^{H5}$, $83B28^{H5} \times A5302^{H1}$, and $83B28^{H5} \times A5302^{H5}$.

Field experimental design

In 2018 and 2019, the NILs were grown in Beijing, China, and their stalk-rot resistance was investigated after artificial inoculation. Each pair of NILs was planted adjacent to each other, and different pairs of NILs were planted in a completely random design. Each NIL was planted in three rows, with 17 plants per row in three replicates. In 2020 and 2021, the 22 pairs of NILs were investigated for flowering time in Beijing, and due to the COVID-19 pandemic, each NIL was planted in two rows without replicates. For the four hybrids grown at different locations over the years, a randomized block design was implemented in the field trials with three replicates. Each hybrid was grown in three rows, with 17 plants per row.

Preparation of *Fusarium graminearum* inoculum, field inoculation, and scoring of symptoms

The preparation of *Fusarium graminearum* inoculum and field inoculation was previously described in detail (Yang et al., 2010). The six-scale scoring system (0, 0.2, 0.4, 0.6, 0.8, and 1) was applied to investigate symptoms in the field. A disease severity index (DSI) was used to assess the stalk-rot severity for each line or hybrid. The DSI was calculated using the disease scales of all plants in the same line or hybrid as follows: DSI (%) = [$\sum$(score × number of plants in score)]/total number of plants × 100.

Investigation of flowering time and other agronomic traits

We investigated three flowering-related traits per plant, including days to heading (DTH), days to anthesis (DTA), and days to silking (DTS) for the NILs and hybrids in 2020 and 2021 in Beijing. All hybrids were investigated for yield and yield-related traits from 2018 to 2020. At the harvest stage, ears were collected from healthy plants and dried in the sun for ~2 weeks. Five ear-related traits were then measured: ear length (EL), bare tip length (BTL), ear diameter (ED), kernel row number (KRN), and kernel number per row (KNPR). After threshing, the kernels were stored at room temperature for open-air drying for at least 2 weeks, and the hundred kernel weight (HKW) and kernel weight per ear (KWPE) were measured. Two plant morphological traits were also investigated from 2019 to 2021: plant height (PH) and ear height (EH).

Investigation of plant tolerance to drought and salt stress

The four hybrids were also planted in Xinjiang (from 2018 to 2020) and Ningxia (2018 and 2019), China to investigate yield and yield-related traits under drought and salt stress conditions, respectively. Xinjiang is an ideal place to test the drought tolerance of maize. Moreover, we employed drip irrigation under a mulch film, making it easy to control irrigation. For well-watered (control) conditions, the plants were irrigated regularly as needed. For drought stress conditions, the amount of irrigation water was reduced by half during the entire growth period compared to well-watered conditions, except for the first irrigation at the time of sowing. The Northeast of Ningxia Plain contains mostly alkaline soil, making it an excellent place to test plant tolerance to salt stress. We tested the soil salinity before sowing in 2018 and 2019. The salinity of 0–25-cm soil was 1.10% and 1.11% in 2018 and 2019, respectively, with a soil pH of 8.6 in 2019, indicating that the chosen site was an alkaline field with salt stress conditions.

Statistical analysis

For each pair of NILs, the two NILs differed solely at the *ZmCCT* locus, i.e., the resistant allele without the TE versus the susceptible allele with the TE insertion. Significant differences in DSI and flowering time between two NILs were analyzed by *t*-test. For the hybrids, all data were analyzed by one-way analysis of variance (ANOVA) with Duncan's test and Tamhane's test using IBM SPSS Statistics (version 21.0.0.0).

Results

Evaluation of stalk-rot resistance and flowering time in the NILs

We previously determined that all BC_3F_1 and BC_5F_1 plants with the non-TE *ZmCCT* showed dramatically reduced DSI (Li et al., 2017b). Of the NILs developed in the current study, we selected 22 lines to further examine stalk-rot resistance and flowering time in 2018 and 2019. Plants in the Zheng58 background with the non-TE *ZmCCT* haplotypes (except H13) showed DSI values of almost zero in both 2018 and 2019, i.e.,

almost no plants were diseased. By contrast, the haplotype *H13* decreased the DSI by 13.32% and 17.45% in 2018 and 2019, respectively (Figure 1A). In the Chang7-2 background, the non-TE *ZmCCT* haplotypes also dramatically decreased the DSI values, with average decreases of 9.43% and 23.38% in 2018 and 2019, respectively (Figure 1B). However, in the 83B28 and A5302 backgrounds, five non-TE *ZmCCT* haplotypes (*H5*, *H6*, *H7*, *H12*, and *H13*) tested in 2018 and six (*H3*, *H5*, *H6*, *H7*, *H12*, and *H13*) tested in 2019 showed a certain degree of variation in stalk-rot resistance (Figures 1C,D), with only haplotypes *H3* and *H5* steadily reducing the DSI. In 2019, haplotype *H3* reduced the DSI by 14.42% in the 83B28 background and 34.81% in the A5302 background. Likewise, in 2018 and 2019, haplotype *H5* reduced the DSI by 9.20% and 8.77% in the 83B28 background and 24.74% and 22.87% in the A5302 background, respectively (Figures 1C,D). These results indicate that the reduction in the severity of maize stalk-rot disease is determined by a combination of the genetic background and *ZmCCT* haplotype.

We also investigated the flowering-related traits DTH, DTA, and DTS in the same sets of NILs. In the Zheng58 background, all non-TE *ZmCCT* haplotypes were more sensitive to long-day conditions than the TE haplotype *H1* and delayed DTH, DTA, and DTS in Beijing by an average of 5.0, 7.0, and 10.6 days, respectively (Supplementary Figure 1A). Notably, the non-TE *ZmCCT* haplotypes in the Chang7-2 background were even more sensitive to long-day conditions than those in the Zheng58 background, resulting in further delays in DTH, DTA, and DTS by an average of 10.6, 11.6, and 13.3 days, respectively (Supplementary Figure 1B). By contrast, non-TE *ZmCCT* haplotypes in the 83B28 and A5302 backgrounds were less sensitive to long-day conditions in Beijing and did not show significant differences in most flowering-related traits. However, there were some subtle differences among the non-TE *ZmCCT* haplotypes, with haplotypes *H3* and *H5* showing no or less sensitivity to photoperiod in the 83B28 and A5302 backgrounds during 2020 and 2021 (Figures 2A,B).

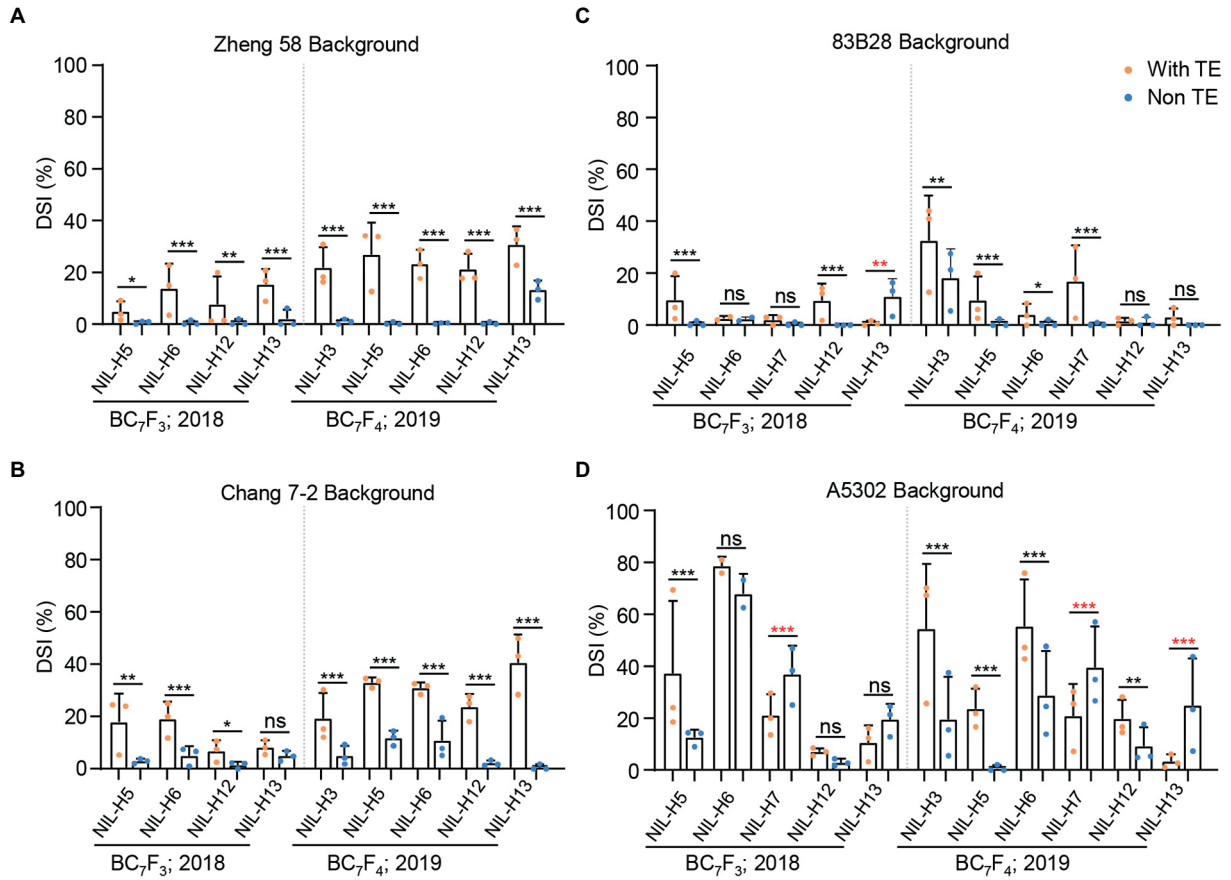

FIGURE 1
DSI of 22 NILs in four different backgrounds in 2018–2019 (Beijing). Five pairs of NILs include with TE *ZmCCT* homozygotes, and non-TE *ZmCCT* homozygotes in Zheng 58 **(A)**, Chang 7–2 **(B)**, 83B28 **(C)**, and A5302 **(D)** background were investigated for DSI. NILs include with TE *ZmCCT* homozygotes: *H1/H1*, and non-TE *ZmCCT* homozygotes: *H3/H3*, *H5/H5*, *H6/H6*, *H7/H7*, *H12/H12*, or *H13/H13* in different background were investigated for DSI. Values are mean±standard deviation (s.d.). Asterisks indicate significant differences between *H1/H1* plants and the other genotypes (two-tailed paired Student's *t-test*, **p* <0.05, ***p* <0.01, ****p* <0.001, ns, not significant).

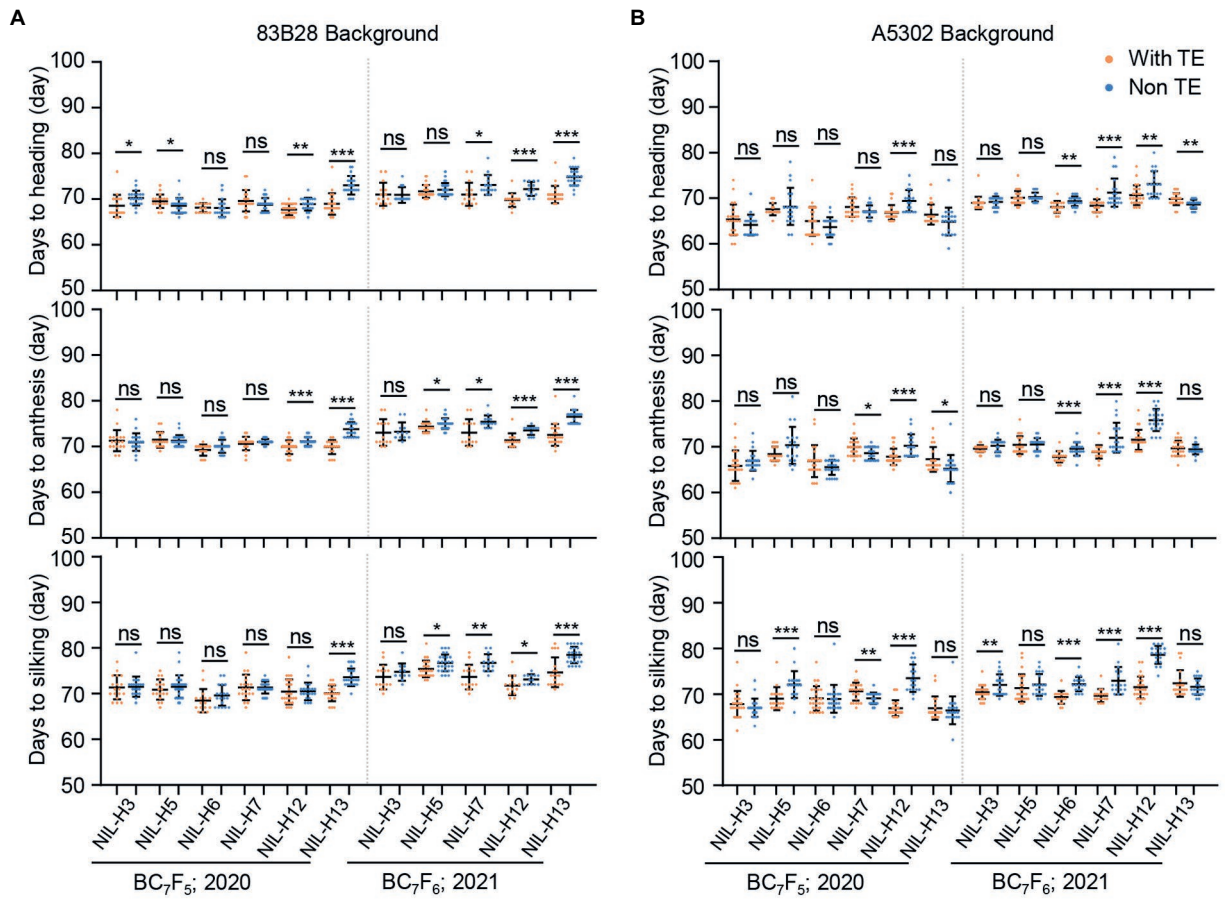

FIGURE 2
Twenty-two pairs of NILs in 83B28 **(A)** and A5302 **(B)** background were investigated for flowering time in 2020–2021 Beijing under long-day conditions. The genotypes of every pair of NILs were with TE *ZmCCT* homozygotes: *H1/H1*, and non-TE *ZmCCT* homozygotes: *H3/H3*, *H5/H5*, *H6/H6*, *H7/H7*, *H12/H12*, or *H13/H13*. Values are mean±standard deviation (s.d.). Asterisks indicate significant differences between *H1/H1* plants and the other genotypes (two-tailed paired Student's *t-test*, *p <0.05, **p <0.01, ***p <0.001, ns, not significant).

Of the non-TE *ZmCCT* haplotypes tested, *H5* performed the best, with high and stable stalk-rot resistance as well as less or no photoperiod sensitivity in the 83B28 and A5302 backgrounds, suggesting it would be valuable for breeding stalk-rot-resistant varieties.

Stalk-rot resistance and flowering times of four F_1 hybrids

We used two pairs of NILs, $83B28^{H1}$/$83B28^{H5}$ and $A5302^{H1}$/$A5302^{H5}$, to generate four F_1 hybrids. Overall, the F_1 hybrids exhibited higher stalk-rot resistance than the parental lines in both 2018 and 2019, presumably due to heterosis. Among the four F_1 hybrids, $83B28^{H5} \times A5302^{H1}$ and $83B28^{H5} \times A5302^{H5}$ only produced a few diseased plants. Compared to $83B28^{H1} \times A5302^{H1}$, these two hybrids showed significantly lower DSI values, with an average reduction of 6.98% and 8.68%, respectively (Figure 3A; Table 1). However, there was no significant difference in the DSI values between $83B28^{H1} \times A5302^{H5}$ and $83B28^{H1} \times A5302^{H1}$ (Figure 3A). These findings suggest that the maternal parental line plays a decisive role in stalk-rot resistance and that the homozygous *ZmCCT* haplotype *H5/H5* does not further increase stalk-rot resistance compared to the heterozygous *ZmCCT* haplotype *H5/H1*.

We also investigated the flowering-related traits of the four hybrids under long-day (Beijing, 2020) and short-day (Hainan, 2020/2021) conditions. In Beijing, the *H5*-containing parental lines $83B28^{H5}$ and $A5302^{H5}$ did not show detectible photoperiod sensitivity (Figures 2A,B), whereas the hybrids $83B28^{H5} \times A5302^{H1}$ and $83B28^{H5} \times A5302^{H5}$ showed 1.4- and 1.8-day delays in flowering time (average of DTH, DTA, and DTS), respectively, compared to $83B28^{H1} \times A5302^{H1}$. By contrast, the three flowering-related traits of the $83B28^{H1} \times A5302^{H5}$ hybrid did not significantly differ from those of $83B28^{H1} \times A5302^{H1}$ (Figure 3B; Supplementary Figure 2). In Hainan, the hybrid with two *H5* alleles ($83B28^{H5} \times A5302^{H5}$) showed earlier flowering times than the hybrids with a single *H5* ($83B28^{H5} \times A5302^{H1}$ and $83B28^{H1} \times A5302^{H5}$), while $83B28^{H1} \times A5302^{H1}$ showed the latest flowering time (Figure 3B; Supplementary Figure 2). Taken together, these results indicate that hybrids with the heterozygous genotype at *ZmCCT* (*H5/H1*) can

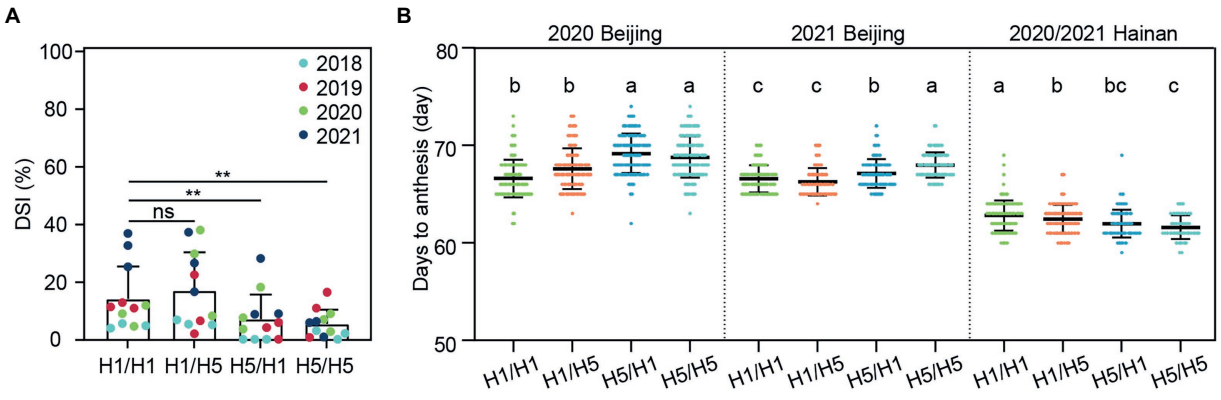

FIGURE 3
Evaluation of DSI and flowering time of four hybrids. In 2018–2021, the DSI **(A)** was investigated after artificial inoculated, each spot represents one replication of field trial (two-tailed paired Student's t-test, $^{**}p$ <0.01, ns, not signifcant). The flowering time **(B)** of four hybrids was investigated in 2020–2021 Beijing and 2020/2021 Hainan, which represents long-day conditions and short-day conditions, respectively. H1/H1, H1/H5, H5/H1, and H5/H5 are genotypes of four hybrids representing $83B28^{H1} \times A5302^{H1}$, $83B28^{H1} \times A5302^{H5}$, $83B28^{H5} \times A5302^{H1}$, and $83B28^{H5} \times A5302^{H5}$, respectively. Values are mean±standard deviation (s.d.). Different letters indicate significant differences among hybrids (p <0.05, one-way ANOVA, Tamhane test).

TABLE 1 Two-way ANOVA of DSI among different genotypes and years.

Source	SS	*df*	MS	F	*p*-value	F crit
Genotype	1107.882	3	369.29	7.58	5.73E-04	2.90
Year	1700.355	3	566.78	11.64	2.56E-05	2.90
Interact	1097.664	9	121.96	2.50	2.69E-02	2.19
Interclass	1558.021	32	48.69			
Total	5463.922	47				

help meet the breeding goal of improved maize stalk-rot resistance with little or no photoperiod sensitivity under long-day conditions.

The genetic effects of *H5* on yield of the hybrids under infected conditions

To test the genetic effect of the haplotype *H5* on yield under infected conditions, we planted the four hybrids in Beijing and performed artificial inoculation in the field, with no inoculation as a control. In 2018, hybrids $83B28^{H5} \times A5302^{H1}$ and $83B28^{H5} \times A5302^{H5}$ had significantly higher kernel weight per ear (KWPE) than $83B28^{H1} \times A5302^{H1}$ under infected conditions, with increases of 16.6% and 11.4%, respectively, whereas the KWPE of $83B28^{H1} \times A5302^{H5}$ did not significantly differ from that of $83B28^{H1} \times A5302^{H1}$ (Figure 4). To confirm these findings, we repeated the experiment in Beijing in 2019 and added a no inoculation control. Compared to $83B28^{H1} \times A5302^{H1}$, $83B28^{H5} \times A5302^{H1}$ showed a significantly higher KWPE under both infected and non-infected conditions, increasing by 7.4% and 8.0%, respectively. By contrast, the other two hybrids, $83B28^{H1} \times A5302^{H5}$ and $83B28^{H5} \times A5302^{H5}$, did not show significant improvements in KWPE. In 2020, the KWPE of $83B28^{H5} \times A5302^{H1}$ was not significantly improved compared with $83B28^{H1} \times A5302^{H1}$, likely due to environmental effects (Figure 4).

Consistent with its yield, the $83B28^{H5} \times A5302^{H1}$ hybrid generally performed better than the control ($83B28^{H1} \times A5302^{H1}$) for yield-related traits, including ear length (EL), bare tip length (BTL), ear diameter (ED), kernel row number (KRN), kernel number per row (KNPR), and hundred kernel weight (HKW). In 2018, $83B28^{H5} \times A5302^{H1}$ had greater EL, KNPR, and ED values than those of $83B28^{H1} \times A5302^{H1}$ (Supplementary Figure 3). The hybrid $83B28^{H5} \times A5302^{H5}$ had better BTL, ED, and KRN but worse HKW values than the control (Supplementary Figure 3). In 2019, $83B28^{H5} \times A5302^{H1}$ had greater ED and HKW values than $83B28^{H1} \times A5302^{H1}$ under normal conditions but showed no significant differences in any yield-related traits compared to $83B28^{H1} \times A5302^{H1}$ under infected conditions (Supplementary Figure 3). By contrast, $83B28^{H1} \times A5302^{H5}$ and $83B28^{H5} \times A5302^{H5}$ showed better BTL and KRN but worse EL, KPR, and HKW values than the control under both infected and normal conditions (Supplementary Figure 3). In 2020, $83B28^{H5} \times A5302^{H1}$ had higher EL and KPR values but lower ED, KRN, and HKW values than those of $83B28^{H1} \times A5302^{H1}$, resulting in no difference in KWPE (Supplementary Figure 3; Figure 4). Taken together, these findings indicate that $83B28^{H5} \times A5302^{H1}$ performed better than the other hybrids in terms of yield and yield-related traits.

The genetic effects of *H5* on yield under abiotic stress conditions

We tested the yield and yield-related traits of the hybrids under drought stress conditions in Xinjiang from 2018 to 2020 and salt stress conditions in Ningxia in 2018 and 2019. Under normal irrigation conditions in Xinjiang from 2018 to 2020, $83B28^{H5} \times A5302^{H1}$ and $83B28^{H5} \times A5302^{H5}$ showed significantly higher KWPE compared to $83B28^{H1} \times A5302^{H1}$ and $83B28^{H1} \times A5302^{H5}$ (Figure 5). Under drought stress,

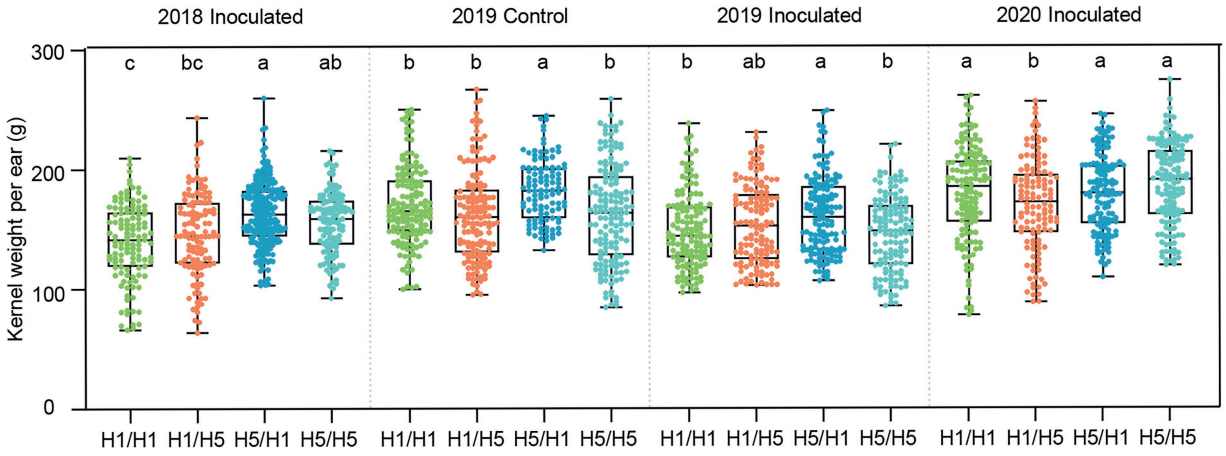

FIGURE 4
The kernel weight per ear of hybrids in Beijing under control and biotic stress. H1/H1, H1/H5, H5/H1, and H5/H5 are genotypes of four hybrids represent 83B28^{H1} × A5302^{H1}, 83B28^{H1} × A5302^{H5}, 83B28^{H5} × A5302^{H1}, and 83B28^{H5} × A5302^{H5}, respectively. Boxes show mean and quartile, whiskers represent max to min. Different letters indicate significant differences among hybrids (p <0.05, one-way ANOVA, Tamhane's test and Duncan's test).

83B28^{H5} × A5302^{H1} showed the best KWPE among the four hybrids in 2018, with an increase of 9.7% compared to the control (83B28^{H1} × A5302^{H1}), but with no significant difference in this value in 2019 and 2020. The hybrid 83B28^{H5} × A5302^{H5} showed a higher KWPE value in 2018 but lower values in 2019 and 2020 compared to the control. The KWPE of 83B28^{H1} × A5302^{H5} did not significantly differ from the control value from 2018 to 2019 but was lower than the control value in 2020 (Figure 5). Overall, 83B28^{H5} × A5302^{H1} performed the best among the four hybrids.

Under salt stress in Ningxia, 83B28^{H5} × A5302^{H1} and 83B28^{H5} × A5302^{H5} had lower KWPE values in 2018 but higher values in 2019 compared to 83B28^{H1} × A5302^{H1}. The KWPE of 83B28^{H1} × A5302^{H5} did not significantly differ from the control in 2018 but was higher than the control value in 2019 (Figure 6). Unlike under *F. graminearum* inoculation and drought stress conditions, 83B28^{H1} × A5302^{H5} showed the best performance under salt stress conditions, suggesting that the haplotype *H5* employs different mechanisms in response to different stress conditions.

When comparing yield-related traits among the four hybrids in Xinjiang, each hybrid showed similar trends under normal and drought conditions (Supplementary Figure 4). In 2018, 83B28^{H5} × A5302^{H1} had significantly higher EL, lower BTL, and higher KPR than 83B28^{H1} × A5302^{H1} under both normal and drought conditions (Supplementary Figure 4). Similarly, 83B28^{H5} × A5302^{H5} showed better EL, BTL, KPR, and ED values, whereas 83B28^{H1} × A5302^{H5} only showed improved ED and KRN values (Supplementary Figure 4). In 2019, 83B28^{H5} × A5302^{H1} showed higher HKW than 83B28^{H1} × A5302^{H1} under drought stress but no significant improvements in any other yield-related trait (Supplementary Figure 4). In 2020, 83B28^{H5} × A5302^{H1} had higher EL, lower BTL, and higher HKW but lower ED compared to 83B28^{H1} × A5302^{H1} under drought stress, while 83B28^{H5} × A5302^{H5} showed higher EL and lower BTL but lower ED vs. the control (Supplementary Figure 4). Finally, 83B28^{H1} × A5302^{H5} had a similar performance for yield-related traits compared to the control (83B28^{H1} × A5302^{H1}; Supplementary Figure 4).

We also compared the yield-related traits of the hybrids under salt stress in Ningxia. The hybrid 83B28^{H5} × A5302^{H1} had significantly smaller ED than 83B28^{H1} × A5302^{H1}, and 83B28^{H1} × A5302^{H5} had significantly higher KRN than 83B28^{H1} × A5302^{H1} (Supplementary Figure 5). For the remaining yield-related traits, no significant differences were detected among the four hybrids in 2018 and 2019 (Supplementary Figure 5). These yield-related traits underlie the KWPE performance of the four hybrids.

Morphological traits of the hybrids

To better understand the genetic effects of haplotype *H5* on plant morphological traits, we investigated the plant height (PH) and ear height (EH) of the hybrids under different environmental conditions. In 2019, 83B28^{H5} × A5302^{H1} had significantly higher PH and EH than 83B28^{H1} × A5302^{H1} in Beijing (normal and infected conditions), Xinjiang (normal conditions), and Ningxia (salt stress; Figure 7). In Beijing and Xinjiang in 2020, 83B28^{H5} × A5302^{H1} and 83B28^{H5} × A5302^{H5} had significantly higher PH than 83B28^{H1} × A5302^{H1} and 83B28^{H1} × A5302^{H5} (Supplementary Figure 6). Finally, 83B28^{H5} × A5302^{H1} had significantly higher EH than 83B28^{H1} × A5302^{H5}, while the EH values of 83B28^{H5} × A5302^{H5} and 83B28^{H1} × A5302^{H1} fell between those of 83B28^{H5} × A5302^{H1} and 83B28^{H1} × A5302^{H5} (Supplementary Figure 6). In conclusion, haplotype *H5* significantly increased PH and EH in the hybrid 83B28^{H5} × A5302^{H1}.

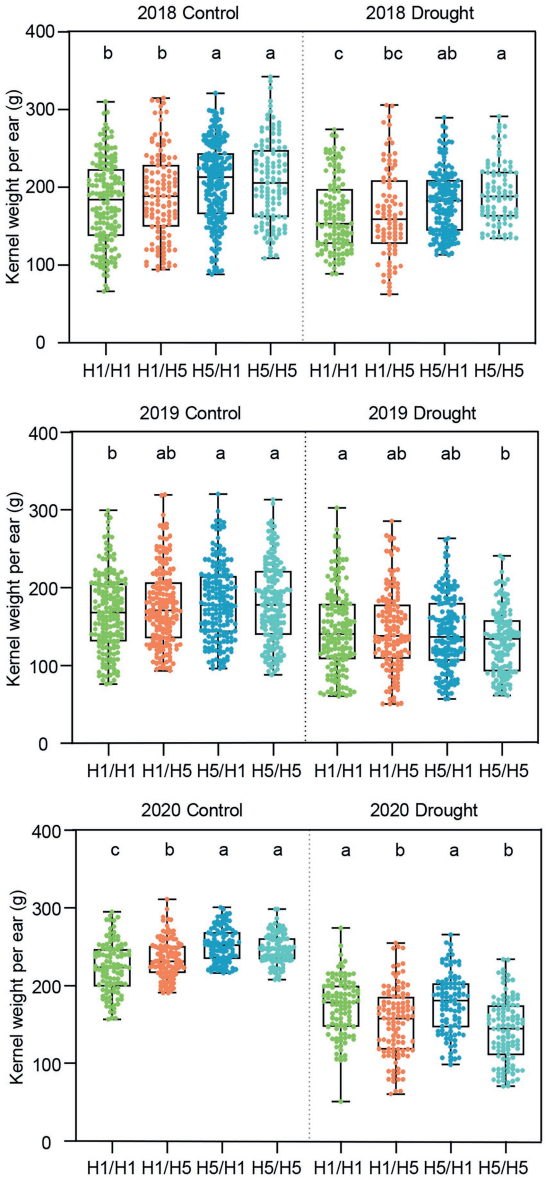

FIGURE 5
The kernel weight per ear of hybrids in 2018–2020 Xinjiang under control and drought stress. Figures above show the KWPE of hybrids in 2018, 2019, and 2020, respectively. H1/H1, H1/H5, H5/H1, and H5/H5 are genotypes of four hybrids represent 83B28^{H1} × A5302^{H1}, 83B28^{H1} × A5302^{H5}, 83B28^{H5} × A5302^{H1}, and 83B28^{H5} × A5302^{H5}, respectively. Boxes show mean and quartile, whiskers represent max to min. Different letters indicate significant differences among hybrids (p <0.05, one-way ANOVA, Duncan's test, and Tamhane's test).

Discussion

CCT domain genes are associated with crop yield

Increasing the resilience of crops is important in light of the changing climate (Juliana et al., 2019). Plant disease resistance usually compromises plant fitness (Brown, 2002; Yang et al., 2012; Li et al., 2016). The pleiotropic effects of *ZmCCT* on disease resistance and delayed flowering make it possible to have no yield penalty. We previously examined the performance of the progeny of a cross between 83B28$^{H5/H1}$ and A5302$^{H4/H1}$, whose F_1 hybrids could be divided into non-TE (*H4* and *H5*), TE (*H1*), and heterozygous genotypes at *ZmCCT* (Li et al., 2017b). This experiment did not clearly explain the genetic effects of *H5* or *H4*, and the test was only conducted for 1 year. In the current study, to explore the use of *H5* for maize resistance breeding, we obtained four hybrids by single crossing among two pairs of NILs: 83B28^{H1}/83B28^{H5} and A5302^{H1}/A5302^{H5}. The use of four hybrids allowed us to clearly observe the specific effects of different combinations of alleles under various conditions. The DSI values were significantly lower for 83B28^{H5} × A5302^{H1} and 83B28^{H5} × A5302^{H5} compared to the other two hybrids. Moreover, 83B28^{H5} × A5302^{H1} had significantly higher KWPE than the other three hybrids under both normal and infected conditions. In Xinjiang, 83B28^{H5} × A5302^{H1} and 83B28^{H5} × A5302^{H5} had higher KWPE values than the other two hybrids under well-watered conditions, while 83B28^{H5} × A5302^{H1} had no yield penalty compared to 83B28^{H1} × A5302^{H1} under drought stress. Overall, 83B28^{H5} × A5302^{H1} showed the best performance among the four hybrids.

ZmCCT expression is induced in roots in response to *F. graminearum*, confers stalk-rot resistance, and exhibits photoperiod sensitivity in leaves to delay flowering time (Yang et al., 2013; Wang et al., 2017). We propose that *ZmCCT* has different inducers in different tissues (leaves or roots), similar to the transcription factor gene *IPA1*. This may partly explain why the haplotype *H5* has no yield penalty compared to other disease resistance genes, or in some cases (like 83B28^{H5} × A5302^{H1}) even increases yield, like *IPA1* (Wang et al., 2018). The haplotype *H5* was slightly sensitive to photoperiod in the 83B28 and A5302 backgrounds; the underlying mechanism deserves further investigation. In wheat, the CCT domain gene *TaCol-B5* also has pleiotropic effects: It increases the number of spikelet nodes per spike, as well as the number of tillers and spikes, leading to increased grain yield (Zhang et al., 2022). CCT domain genes have obvious convergent effects in rice (*Ghd7*), maize (*ZmCCT*), and wheat (*TaCol-B5*), all of which are pleiotropic genes that regulate plant growth, development, stress responses, yield performance, and other agronomic traits (Xue et al., 2008; Weng et al., 2014; Zhang et al., 2022).

83B28^{H5} × A5302^{H1} and 83B28^{H1} ×A5302^{H5} show opposite effects

Among the four hybrids, 83B28^{H5} × A5302^{H1} had better KWPE values than the others under both pathogen-infected and drought conditions, while 83B28^{H1} × A5302^{H5} showed better performance under salt stress conditions. In all circumstances, the effects of 83B28^{H5} × A5302^{H1} on yield-related traits were opposite those of 83B28^{H1} × A5302^{H5}. Whereas 83B28^{H5} × A5302^{H1} tended

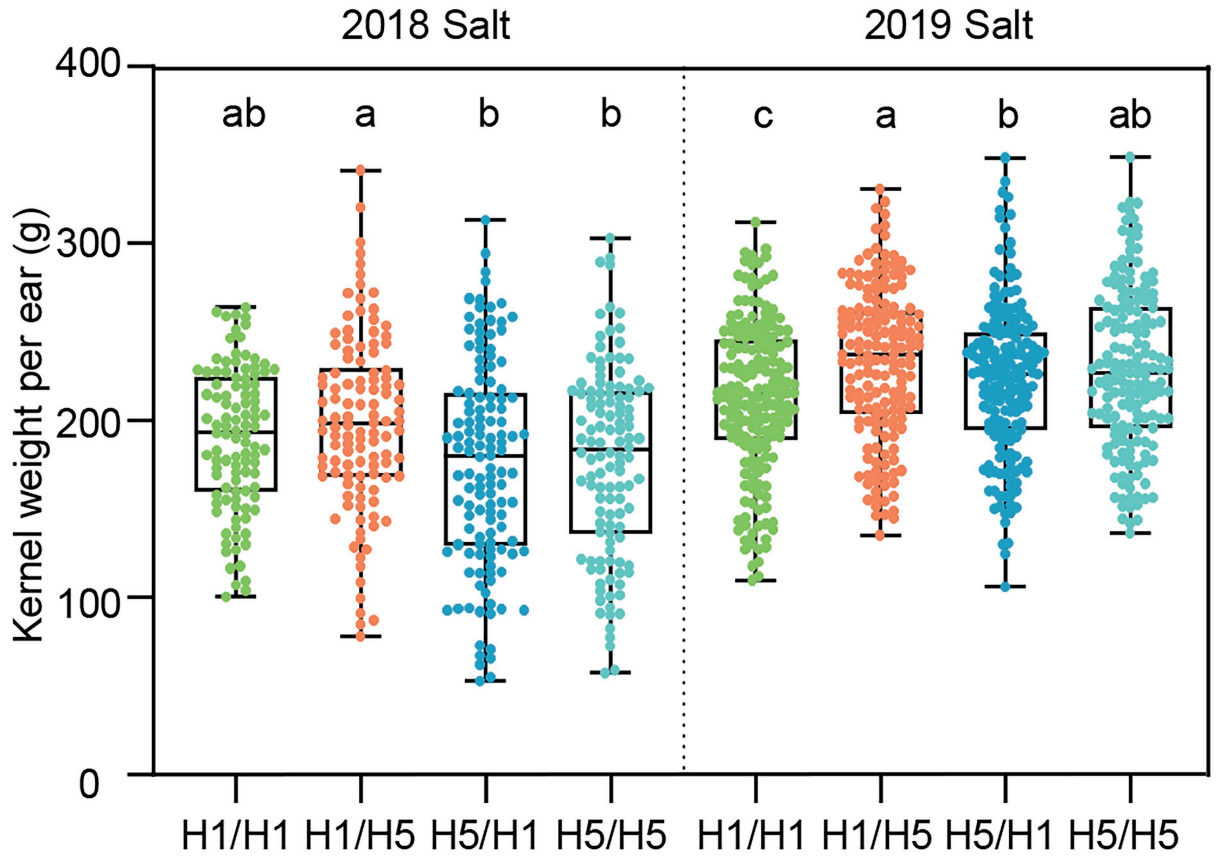

FIGURE 6
The yield-related traits of hybrids in 2018–2019 Ningxia under salt stress conditions. H1/H1, H1/H5, H5/H1, and H5/H5 are genotypes of four hybrids represent 83B28^{H1} × A5302^{H1}, 83B28^{H1} × A5302^{H5}, 83B28^{H5} × A5302^{H1}, and 83B28^{H5} × A5302^{H5}, respectively. Boxes show mean and quartile, whiskers represent max to min. Different letters indicate significant differences among hybrids (p <0.05, one-way ANOVA, Duncan's test, and Tamhane's test).

to show higher EL and KNPR values, 83B28^{H1} × A5302^{H5} tended to show higher KRN. In addition, the plant architecture traits of 83B28^{H5} × A5302^{H1} were opposite those of 83B28^{H1} × A5302^{H5}. Compared to 83B28^{H1} × A5302^{H1}, 83B28^{H5} × A5302^{H1} showed significantly greater PH, while 83B28^{H1} × A5302^{H5} generally showed lower PH. The flowering time of 83B28^{H5} × A5302^{H1} was significantly delayed in Beijing in 2020 and 2021, whereas that of 83B28^{H1} × A5302^{H5} was not. Why do these two hybrids exhibit such different characteristics even though they contain the same single haplotype *H5*? A recent study indicated that maternal and cytoplasmic effects influence multiple traits in durum wheat, such as resistance to *Zymoseptoria tritici*, plant height, and thousand kernel weight (Hassine et al., 2022). Therefore, perhaps, the haplotype *H5* has maternal effects on the hybrids.

The relationships of flowering time, plant height, and yield

Alleles that delay flowering time generally increase plant height, such as *Ghd7* and *DTH8* (*Days to heading 8*) in rice (Xue et al., 2008; Wei et al., 2010), *gmap1* (homozygous quadruple mutant of *APETALA 1*) in soybean (Chen et al., 2020), and *lfy1* (*leafy* 1), *ZmCCT9*, and *ZmMADS69* (*MADS-box transcription factor*) in maize (Cui et al., 2017; Huang et al., 2018; Liang et al., 2019). In some cases, alleles that increase plant height also increase yield, as in *Ghd7* and *OsMPH1* (*MYB-like gene of plant height 1*; Zhang et al., 2017). It is reasonable to associate a longer vegetative stage with more biomass: The taller the plant, the higher the grain yield. However, in other cases, such as *zmm28* (AP1-FUL-Like MADS-Box Gene) in maize, increased yield is independent of plant height (Wu et al., 2019). In a study of 280 genotypic combinations within the same population, earlier flowering times were generally associated with reduced plant height and ear weight, although 11 optimal genotypic combinations were also identified (Xiao et al., 2021). In the current study, 83B28^{H5} × A5302^{H1} showed delayed flowering time under long-day conditions and increased PH and KWPE under all conditions except salt stress. These traits conferred by the haplotype *H5* must be intrinsically related.

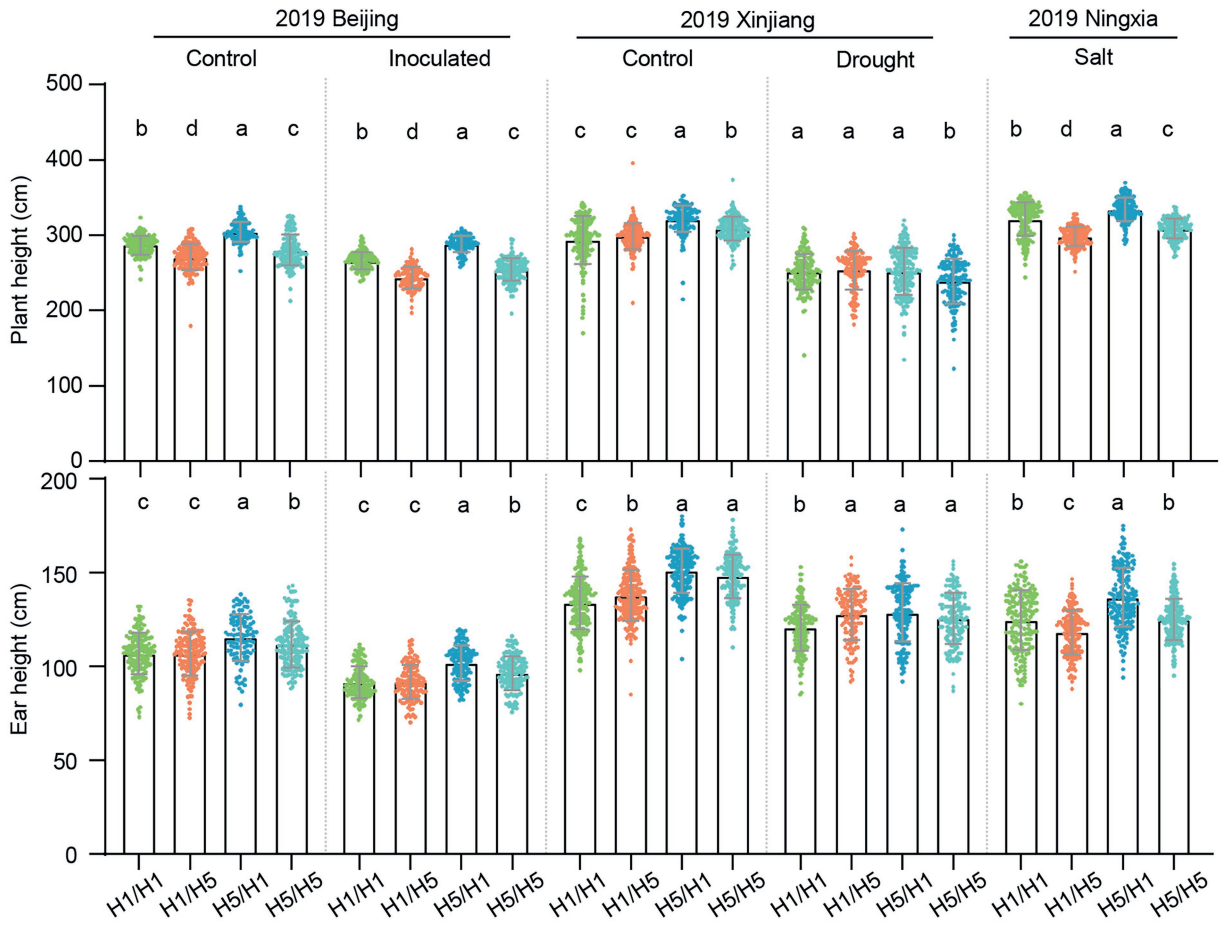

FIGURE 7
Plant architecture traits of hybrids in 2019 under control, inoculated, drought, and salt conditions. H1/H1, H1/H5, H5/H1, and H5/H5 are genotypes of four hybrids representing 83B28^{H1} × A5302^{H1}, 83B28^{H1} × A5302^{H5}, 83B28^{H5} × A5302^{H1}, and 83B28^{H5} × A5302^{H5}, respectively. Values are mean±standard deviation (s.d.). Different letters indicate significant differences (p <0.05, one-way ANOVA, Tamhane's test, and Duncan's test).

The haplotype *H5* of *ZmCCT* is a versatile maize resistance gene

In summary, the hybrid 83B28^{H5} ×A5302^{H1} with a single haplotype *H5* showed an ~2-day delay in flowering time, increased stalk-rot resistance, and improved yield and yield-related traits under both biotic and abiotic stress conditions. From the perspective of maize breeding, an ~2-day delay in flowering time has little impact on farmers, but the yield and resilience of this crop under different conditions are important. Therefore, the haplotype *H5* is valuable due to its ability to optimize the trade-off between stress resistance and plant growth. However, the haplotype *H5* did not lead to better performance under salt stress, reminding us of the limits of using the haplotype *H5* in maize breeding.

In the current study, we also generated four hybrids from the cross between Zheng58^{H1}/Zheng58^{H5} and Chang7-2^{H1}/Chang7-2^{H5}. However, the hybrids with the haplotype *H5* exhibited much stronger photoperiod sensitivity than their parental lines and were therefore excluded from further study. While conducting this study, the haplotype *H5* was introgressed into a number of elite maize inbred lines in China. The stalk-rot resistance of these lines greatly improved, and grain yield routinely increased by 5%–10%. For example, the original maize variety MC812 (developed by the Beijing Academy of Agricultural and Forestry Sciences) had a diseased plant rate of 19.25% and a yield of 12,936 kg per hectare, in contrast to the improved MC812, with a diseased plant rate of 1.79% and a yield of 13,818 kg per hectare. In conclusion, the haplotype *H5* will be quite valuable for maize breeding for stalk-rot resistance and improved grain yield. This is a good example to exploit natural genetic variation to uncouple growth and defense trade-offs (He et al., 2022).

Data availability statement

The original contributions presented in the study are included in the article/Supplementary material, further inquiries can be directed to the corresponding author.

Author contributions

MX and LT designed the study, analyzed, and interpreted the data, and wrote and revised the manuscript. LT conducted the experiments. MY, MZ, and JY participated in field experiments and partial traits data collection. MZ helped in data analysis and data visualization. YL provided the seed resources. MX supervised the project. All authors contributed to the article and approved the submitted version.

Funding

This study was supported by Jiangsu province's Seed Industry Revitalization project [JBGS(2021)002] and Yunnan Provincial Science and Technology Department (202005AF150026).

Acknowledgments

We extend our thanks to the Crop Functional Genomics and Molecular Breeding Center of China Agricultural University for their strong support in the field trial of salt tolerance.

Conflict of interest

The authors declare that the research was conducted in the absence of any commercial or financial relationships that could be construed as a potential conflict of interest.

Publisher's note

Supplementary material

The supplementary material for this article can be found online at: https://www.frontiersin.org/articles/10.3389/fpls.2022.984527/full#supplementary-material

References

Brown, J. K. (2002). Yield penalties of disease resistance in crops. *Curr. Opin. Plant Biol.* 5, 339–344. doi: 10.1016/s1369-5266(02)00270-4

Brown, J. K. M., and Rant, J. C. (2013). Fitness costs and trade-offs of disease resistance and their consequences for breeding arable crops. *Plant Pathol.* 62, 83–95. doi: 10.1111/ppa.12163

Büschges, R., Hollricher, K., Panstruga, R., Simons, G., Wolter, M., Frijters, A., et al. (1997). The barley Mlo gene: a novel control element of plant pathogen resistance. *Cell* 88, 695–705. doi: 10.1016/s0092-8674(00)81912-1

Chen, L., Nan, H., Kong, L., Yue, L., Yang, H., Zhao, Q., et al. (2020). Soybean AP1 homologs control flowering time and plant height. *J. Integr. Plant Biol.* 62, 1868–1879. doi: 10.1111/jipb.12988

Consonni, C., Humphry, M. E., Hartmann, H. A., Livaja, M., Durner, J., Westphal, L., et al. (2006). Conserved requirement for a plant host cell protein in powdery mildew pathogenesis. *Nat. Genet.* 38, 716–720. doi: 10.1038/ng1806

Cui, M., Jia, B., Liu, H., Kan, X., Zhang, Y., Zhou, R., et al. (2017). Genetic mapping of the leaf number above the primary ear and its relationship with plant height and flowering time in maize. *Front. Plant Sci.* 8:1437. doi: 10.3389/fpls.2017.01437

Deng, Y., Zhai, K., Xie, Z., Yang, D., Zhu, X., Liu, J., et al. (2017). Epigenetic regulation of antagonistic receptors confers rice blast resistance with yield balance. *Science* 355, 962–965. doi: 10.1126/science.aai8898

Hassine, M., Bnejdi, F., Bahri, B. A., Tissaoui, S., Mougou-Hamdane, A., Guesmi, M., et al. (2022). Detection of maternal and cytoplasmic effects on resistance to *Zymoseptoria tritici* in durum wheat. *Biomed. Res. Int.* 2022, 8497417–8497416. doi: 10.1155/2022/8497417

He, Z., Webster, S., and He, S. Y. (2022). Growth-defense trade-offs in plants. *Curr. Biol.* 32, R634–R639. doi: 10.1016/j.cub.2022.04.070

Huang, C., Sun, H., Xu, D., Chen, Q., Liang, Y., Wang, X., et al. (2018). ZmCCT9 enhances maize adaptation to higher latitudes. *Proc. Natl. Acad. Sci. U. S. A.* 115, E334–E341. doi: 10.1073/pnas.1718058115

Hung, H. Y., Shannon, L. M., Tian, F., Bradbury, P. J., Chen, C., Flint-Garcia, S. A., et al. (2012). ZmCCT and the genetic basis of day-length adaptation underlying the postdomestication spread of maize. *Proc. Natl. Acad. Sci. U. S. A.* 109, E1913–E1921. doi: 10.1073/pnas.1203189109

Juliana, P., Poland, J., Huerta-Espino, J., Shrestha, S., Crossa, J., Crespo-Herrera, L., et al. (2019). Improving grain yield, stress resilience and quality of bread wheat using large-scale genomics. *Nat. Genet.* 51, 1530–1539. doi: 10.1038/s41588-019-0496-6

Karasov, T. L., Chae, E., Herman, J. J., and Bergelson, J. (2017). Mechanisms to mitigate the trade-Off between growth and defense. *Plant Cell* 29, 666–680. doi: 10.1105/tpc.16.00931

Karasov, T. L., Kniskern, J. M., Gao, L., DeYoung, B. J., Ding, J., Dubiella, U., et al. (2014). The long-term maintenance of a resistance polymorphism through diffuse interactions. *Nature* 512, 436–440. doi: 10.1038/nature13439

Konlasuk, S., Xing, Y. X., Zhang, N., Zuo, W. L., Zhang, B. Q., Tan, G. Q., et al. (2015). ZmWAK, a quantitative resistance gene to head smut in maize, improves yield performance by reducing the endophytic pathogen *Sporisorium reiliana*. *Mol. Breed.* 35:174. doi: 10.1007/s11032-015-0325-2

Li, S., Lin, D., Zhang, Y., Deng, M., Chen, Y., Lv, B., et al. (2022). Genome-edited powdery mildew resistance in wheat without growth penalties. *Nature* 602, 455–460. doi: 10.1038/s41586-022-04395-9

Li, Y., Tong, L., Deng, L., Liu, Q., Xing, Y., Wang, C., et al. (2017b). Evaluation of ZmCCT haplotypes for genetic improvement of maize hybrids. *Theor. Appl. Genet.* 130, 2587–2600. doi: 10.1007/s00122-017-2978-1

Li, X., Yang, D. L., Sun, L., Li, Q., Mao, B., and He, Z. (2016). The systemic acquired resistance regulator OsNPR1 attenuates growth by repressing Auxin signaling through promoting IAA-Amido synthase expression. *Plant Physiol.* 172, 546–558. doi: 10.1104/pp.16.00129

Li, W., Zhu, Z., Chern, M., Yin, J., Yang, C., Ran, L., et al. (2017a). A natural allele of a transcription factor in Rice confers broad-Spectrum blast resistance. *Cell* 170, 114.e15-126.e15. doi: 10.1016/j.cell.2017.06.008

Liang, Y., Liu, Q., Wang, X., Huang, C., Xu, G., Hey, S., et al. (2019). ZmMADS69 functions as a flowering activator through the ZmRap2.7-ZCN8 regulatory module and contributes to maize flowering time adaptation. *New Phytol.* 221, 2335–2347. doi: 10.1111/nph.15512

Liang, Y., Liu, H. J., Yan, J., and Tian, F. (2021). Natural variation in crops: realized understanding, continuing promise. *Annu. Rev. Plant Biol.* 72, 357–385. doi: 10.1146/annurev-arplant-080720-090632

Nekrasov, V., Wang, C., Win, J., Lanz, C., Weigel, D., and Kamoun, S. (2017). Rapid generation of a transgene-free powdery mildew resistant tomato by genome deletion. *Sci. Rep.* 7:482. doi: 10.1038/s41598-017-00578-x

Nelson, R., Wiesner-Hanks, T., Wisser, R., and Balint-Kurti, P. (2018). Navigating complexity to breed disease-resistant crops. *Nat. Rev. Genet.* 19, 21–33. doi: 10.1038/nrg.2017.82

Solovieff, N., Cotsapas, C., Lee, P. H., Purcell, S. M., and Smoller, J. W. (2013). Pleiotropy in complex traits: challenges and strategies. *Nat. Rev. Genet.* 14, 483–495. doi: 10.1038/nrg3461

Su, H., Cao, Y., Ku, L., Yao, W., Cao, Y., Ren, Z., et al. (2018). Dual functions of ZmNF-YA3 in photoperiod-dependent flowering and abiotic stress responses in maize. *J. Exp. Bot.* 69, 5177–5189. doi: 10.1093/jxb/ery299

Tian, D., Traw, M. B., Chen, J. Q., Kreitman, M., and Bergelson, J. (2003). Fitness costs of R-gene-mediated resistance in *Arabidopsis thaliana*. *Nature* 423, 74–77. doi: 10.1038/nature01588

Wang, Y., Cheng, X., Shan, Q., Zhang, Y., Liu, J., Gao, C., et al. (2014). Simultaneous editing of three homoeoalleles in hexaploid bread wheat confers heritable resistance to powdery mildew. *Nat. Biotechnol.* 32, 947–951. doi: 10.1038/nbt.2969

Wang, C., Yang, Q., Wang, W., Li, Y., Guo, Y., Zhang, D., et al. (2017). A transposon-directed epigenetic change in ZmCCT underlies quantitative resistance to Gibberella stalk rot in maize. *New Phytol.* 215, 1503–1515. doi: 10.1111/nph.14688

Wang, J., Zhou, L., Shi, H., Chern, M., Yu, H., Yi, H., et al. (2018). A single transcription factor promotes both yield and immunity in rice. *Science* 361, 1026–1028. doi: 10.1126/science.aat7675

Wei, X., Xu, J., Guo, H., Jiang, L., Chen, S., Yu, C., et al. (2010). DTH8 suppresses flowering in rice, influencing plant height and yield potential simultaneously. *Plant Physiol.* 153, 1747–1758. doi: 10.1104/pp.110.156943

Weng, X., Wang, L., Wang, J., Hu, Y., Du, H., Xu, C., et al. (2014). Grain number, plant height, and heading date 7 is a central regulator of growth, development, and stress response. *Plant Physiol.* 164, 735–747. doi: 10.1104/pp.113.231308

Wu, J., Lawit, S. J., Weers, B., Sun, J., Mongar, N., Van Hemert, J., et al. (2019). Overexpression of zmm28 increases maize grain yield in the field. *Proc. Natl. Acad. Sci. U. S. A.* 116, 23850–23858. doi: 10.1073/pnas.1902593116

Xiao, Y., Jiang, S., Cheng, Q., Wang, X., Yan, J., Zhang, R., et al. (2021). The genetic mechanism of heterosis utilization in maize improvement. *Genome Biol.* 22:148. doi: 10.1186/s13059-021-02370-7

Xu, Z., Hua, J., Wang, F., Cheng, Z., Meng, Q., Chen, Y., et al. (2020). Marker-assisted selection of qMrdd8 to improve maize resistance to rough dwarf disease. *Breed. Sci.* 70, 183–192. doi: 10.1270/jsbbs.19110

Xu, G., Wang, X., Huang, C., Xu, D., Li, D., Tian, J., et al. (2017). Complex genetic architecture underlies maize tassel domestication. *New Phytol.* 214, 852–864. doi: 10.1111/nph.14400

Xue, W., Xing, Y., Weng, X., Zhao, Y., Tang, W., Wang, L., et al. (2008). Natural variation in Ghd7 is an important regulator of heading date and yield potential in rice. *Nat. Genet.* 40, 761–767. doi: 10.1038/ng.143

Yang, Q., Li, Z., Li, W., Ku, L., Wang, C., Ye, J., et al. (2013). CACTA-like transposable element in ZmCCT attenuated photoperiod sensitivity and accelerated the postdomestication spread of maize. *Proc. Natl. Acad. Sci. U. S. A.* 110, 16969–16974. doi: 10.1073/pnas.1310949110

Yang, D. L., Yao, J., Mei, C. S., Tong, X. H., Zeng, L. J., Li, Q., et al. (2012). Plant hormone jasmonate prioritizes defense over growth by interfering with gibberellin signaling cascade. *Proc. Natl. Acad. Sci. U. S. A.* 109, E1192–E1200. doi: 10.1073/pnas.1201616109

Yang, Q., Yin, G., Guo, Y., Zhang, D., Chen, S., and Xu, M. (2010). A major QTL for resistance to Gibberella stalk rot in maize. *Theor. Appl. Genet.* 121, 673–687. doi: 10.1007/s00122-010-1339-0

Zhang, X., Jia, H., Li, T., Wu, J., Nagarajan, R., Lei, L., et al. (2022). TaCol-B5 modifies spike architecture and enhances grain yield in wheat. *Science* 376, 180–183. doi: 10.1126/science.abm0717

Zhang, Y., Yu, C., Lin, J., Liu, J., Liu, B., Wang, J., et al. (2017). OsMPH1 regulates plant height and improves grain yield in rice. *PLoS One* 12:e0180825. doi: 10.1371/journal.pone.0180825

Zhang, Z., Zhang, X., Lin, Z., Wang, J., Xu, M., Lai, J., et al. (2018). The genetic architecture of nodal root number in maize. *Plant J.* 93, 1032–1044. doi: 10.1111/tpj.13828

Zhao, X., Tan, G., Xing, Y., Wei, L., Chao, Q., Zuo, W., et al. (2012). Marker-assisted introgression of qHSR1 to improve maize resistance to head smut. *Mol. Breed.* 30, 1077–1088. doi: 10.1007/s11032-011-9694-3

Zhong, S. Y., Liu, H. Q., Li, Y., and Lin, Z. W. (2021). Opposite response of maize ZmCCT to photoperiod due to transposon jumping. *Theor. Appl. Genet.* 134, 2841–2855. doi: 10.1007/s00122-021-03862-7

frontiers | Frontiers in Plant Science

TYPE Original Research
PUBLISHED 19 August 2022
DOI 10.3389/fpls.2022.992016

OPEN ACCESS

EDITED BY
Cheng Liu,
Shandong Academy of Agricultural Sciences, China

REVIEWED BY
Pengtao Ma,
Yantai University, China
Diaoguo An,
Institute of Genetics and Developmental Biology (CAS), China

*CORRESPONDENCE
Tianheng Ren
renth@sicau.edu.cn
Zhi Li
lizhi@sicau.edu.cn

†These authors have contributed equally to this work

SPECIALTY SECTION
This article was submitted to Plant Pathogen Interactions, a section of the journal Frontiers in Plant Science

RECEIVED 12 July 2022
ACCEPTED 29 July 2022
PUBLISHED 19 August 2022

CITATION
Ren T, Sun Z, Hu Y, Ren Z, Tan F, Luo P and Li Z (2022) Molecular cytogenetic identification of new wheat-rye 6R, 6RS, and 6RL addition lines with resistance to stripe rust and powdery mildew. *Front. Plant Sci.* 13:992016. doi: 10.3389/fpls.2022.992016

Molecular cytogenetic identification of new wheat-rye 6R, 6RS, and 6RL addition lines with resistance to stripe rust and powdery mildew

Tianheng Ren[1,2*†], Zixin Sun[1,2†], Yuling Hu[1,2], Zhenglong Ren[1,2], Feiquan Tan[1,2], Peigao Luo[1,2] and Zhi Li[1,2*]

[1]State key Laboratory of Crop Gene Exploration and Utilization in Southwest China, Sichuan Agricultural University, Chengdu, China, [2]College of Agronomy, Sichuan Agricultural University, Chengdu, China

Stripe rust and powdery mildew are devastating diseases that have severe effects on wheat production. Introducing resistant genes/loci from wheat-related species into the wheat genome is an important method to improve wheat resistance. Rye (*Secale cereale* L.) is a cross-pollinating plant and is the most important related species for wheat genetic improvement. In this study, we developed three 6RS ditelosomic addition lines, three 6RL ditelosomic addition lines, and two 6R disomic addition lines by crossing common wheat cultivar Chuannong 25 and rye inbred line QL2. The chromosome composition of all new lines was confirmed by non-denaturing fluorescence *in situ* hybridization (ND-FISH) and molecular marker analyses. Disease responses to different *Puccinia striiformis* f. sp. *tritici* (*Pst*) races and *Blumeria graminis* f. sp. *tritici* (*Bgt*) isolates and cytogenetic analysis showed that the resistance of the new lines was derived from the rye chromosome 6R of QL2, and both arms (6RS and 6RL) may harbor resistance genes against *Pst* and *Bgt*. These new lines could be used as a promising bridging parent and valuable genetic resource for wheat disease resistance improvement.

KEYWORDS

***Triticum aestivum*, *Secale cereale*, chromosome addition, resistance, genetic resource**

Introduction

Wheat (*Triticum aestivum* L.) is one of the most important food crops in the world and provides ~20% of the protein and calories for human beings (Chaves et al., 2013). However, stripe rust (caused by *Puccinia striiformis* f. sp. *tritici*, *Pst*) and powdery mildew (*Blumeria graminis* f. sp. *tritici*, *Bgt*) are typically devastating diseases and are very detrimental to wheat production in subtropical agricultural zones (Duveiller et al., 2007). Stripe rust and powdery mildew result in the loss of ~5% of production. However, in some of the most

prevalent areas, stripe rust and powdery mildew can increase the loss to 20%–30% of production (Ren et al., 2009; Chen et al., 2014). For example, serious outbreaks of stripe rust resulted in a 25% yield loss in the United States from 1958 to 2014 (Chen, 2005, 2014). In China, stripe rust is epidemic almost every year and causes significant yield losses (Wan et al., 2007; Ren et al., 2022). In recent years, with the change in global climate, powdery mildew has affected wheat production more (Huo et al., 2002). For example, in 1990 and 1991, more than 12 million hectares of wheat were attacked by *Bgt* in China, causing 1.4 million and 0.7 million tons of yield losses, respectively (Hou et al., 2000).

Breeding disease-resistant wheat cultivars represent the most economical, environmentally friendly, and effective control measures at present. Related species of wheat, such as rye (*Secale cereale*; Schlegel and Korzun, 1997), *Haynaldia villosa* (Chen et al., 1995), *Elytrigia intermedium* (Luo et al., 2009), and *Agropyron cristatum* (Wang et al., 2022), contain a large number of resistance genes and have been used in wheat disease resistance breeding for a long time. Among them, the most valuable related species is rye (Schlegel and Korzun, 1997; Ren et al., 2022). Disease-resistance genes for *Pst* and *Bgt,* such as *Yr9*, *Pm8*, and *Pm17,* were introduced into the wheat genome *via* T1RS·1BL or T1RS·1AL translocation (Mater et al., 2004; Mago et al., 2005). However, due to the changes in the prevalent pathogens, these resistance genes were overcome by new pathogens at the end of the last century (Ren et al., 2009). In the past 10 years, several new 1RS chromosomes have been introduced into the wheat genome and have exhibited resistance to the new *Pst* and *Bgt* pathogens (Ren et al., 2017a, 2018, 2022; Han et al., 2020). Additionally, 2R, 4R, 5R, 6R, and 7R chromosomes are also introduced into the wheat genome in the form of chromosome translocation, addition, and substitution, and several of these newly developed lines exhibit resistance to stripe rust or powdery mildew (An et al., 2015, 2019; Li et al., 2016; Schneider et al., 2016; Ren et al., 2017b, 2020; Johansson et al., 2020; Han et al., 2022).

In this study, eight new addition lines, including three 6RS ditelosomic addition lines, three 6RL ditelosomic addition lines, and two 6R disomic addition lines, were developed and selected from a cross between the rye inbred line QL2 and wheat cultivar CN25. All eight addition lines showed high resistance to both *Pst* and *Bgt*. The results indicated that both the long arm and short arm of QL2 may contain resistance genes for *Pst* and *Bgt*. These eight new lines could represent valuable genetic resources for wheat disease resistance breeding programs in the future.

Materials and methods

Plant materials

Chuannong 25 (CN25) is a high-yield wheat cultivar that was approved by the Sichuan Provincial Variety Examination and Committee in 2007 and has been widely planted in southwestern China. The pure genetic stocks of CN25 used in this study were bred by single-spike descent over several generations. Rye Qinling was collected by our lab in the 1990s. An inbred line of Qinling rye, QL2, was used in this study. CN25 was crossed directly with QL2 to produce hybrid F_1 seeds. Then, the F_1 seedlings were treated with 0.05% colchicine plus 3% dimethyl sulfoxide for 8 h to produce the amphidiploid (C_1). The C_1 plants were backcrossed with wheat parent CN25 twice to produce the BC_2F_1 plants. From now on, only the plants that showed resistance to diseases in the field were harvested and reproduced in the generations BC_2F_1 to BC_2F_4. In the generation BC_2F_5, the chromosome composition of the plants was examined by non-denaturing fluorescence *in situ* hybridization (ND-FISH), and then, the plants were transplanted into the field. In this generation, several plants with rye 6R chromosomes were identified. The seeds of these plants were harvested and reproduced by selfing. In BC_2F_6, 50 seeds were randomly selected from each line and cultured in the lab first, and the chromosome composition of the plants was determined by ND-FISH. Then, all surviving plants were transplanted into the field. From BC_2F_6 to BC_2F_8, 6R disomic addition plants, 6RS ditelosomic addition plants, and 6RL ditelosomic addition plants were identified.

Cytogenetic and molecular analyses

ND-FISH was used to identify the chromosome composition of the plant materials. Five oligonucleotide probes, Oligo-pSc119.2-1, Oligo-pTa535-1, Oligo-Ku, Oligo-pSc200, and Oligo-pSc250, were used in this study (Tang et al., 2014; Ren et al., 2019). The sequences and chromosomes that could be identified by these five probes are listed in Table 1. The wheat and rye chromosomes could be accurately distinguished by the combination of these five probes in one cell. Moreover, the

TABLE 1 The sequences of the oligonucleotide probes for ND-FISH used in this study.

Probes	Chromosome or location	Sequences
Oligo-pSc119.2-1	4A, 5A, 1B-7B, 2D, 3D, 4D	6-FAM-5′-ccgttttgtggactattactcaccgctttgggtcccatagctat-3′
Oligo-pTa535-1	1A, 2A, 3A, 4A, 6A, 7A, 3B, 6B, 7B, 1D-7D	Tamra-5′-aaaaacttgacgcacgtcacgtacaaattggacaaactctttcggagtatcagggtttc-3′
Oligo-Ku	1R-7R	Tamra-5′-gatcgagacttctagcaataggcaaaaatagtaatggtatccgggttcg-3′
Oligo-pSc200	1R-7R	Tamra-5′-ctcacttgctttgagagtctcgatcaattcggactctaggttgatttttgtattttct-3′
Oligo-pSc250	1R-7R	Tamra-5′-tgtgttgttcttggacaaaacaatgcataccatctcttctac-3′
Oligo-CCS1	Wheat and rye centromere	6-FAM-5′-ccgtttgatagaggcaaaggtgtcccgtctttgatgaga-3′
Oligo-PAWRC.1	Rye centromere	6-FAM-5′-ccgtttgatagaggcaaaggtgtcccgtctttgatgaga-3′
Oligo-Telo	Telomere	Tamra-5′-tttagggtttagggtttaggg-3′

Cuadrado and Jouve (2010), Tang et al. (2014), Ren et al. (2019).

centromeric-specific probe Oligo-CCS1, rye centromeric-specific probe Oligo-PAWRC.1, and telomere-specific probe Oligo-Telo were mixed and used in another ND-FISH experiment (Cuadrado and Jouve, 2010; Tang et al., 2014). Cell images were captured using an epifluorescence microscope (model BX51, Olympus, Center Valley, PA, United States) equipped with a cooled charge-coupled device camera and operated with the software program HCIMAGE Live (version 2.0.1.5, Hamamatsu Corp., Sewickley, PA, United States). The processes of sample preparation (root tips), probe labeling, and ND-FISH were performed according to Tang et al. (2014) and Ren et al. (2019). Molecular markers specific to 6RL and 6RS were also used to confirm the chromosome. The genomic DNA of the plant materials was isolated from young leaves using the surfactant cetyltrimethylammonium bromide (CTAB; Doyle and Doyle, 1987). Two primer pairs, KU88 and KU291, which were specific for the rye 6RS chromosome arm, and two primer pairs, KU86 and KU153, which were specific for the rye 6RL chromosome arm, were used (Qiu et al., 2016; Table 2). These primers can detect rye 6RS or 6RL chromosome arms in the wheat genetic background and can amplify specific ~400-bp fragment bands (Qiu et al., 2016). PCR and electrophoresis were performed according to Qiu et al. (2016).

Stripe rust and powdery mildew tests

The *Pst* races CYR32 (virulent to *Yr1, 2, 3, 4, 6, 7, 8, 9, 17, 25, 27, 28, 31, 32, 43, 44, A, Alba, Cle, Gaby, Res, SD, SO, Exp2, SK*, and *SP*), CYR33 (virulent to *Yr1, 2, 3, 4, 6, 7, 8, 9, 17, 25, 28, 31, 32, A*, and *Su*), and CYR34 [virulent to *Yr1, 2, 3, 4, 6, 7, 8, 9, 10, 17, 19, 24(=26), 25, 27, 28, 31, 32, 43, 44, Exp2, SP, A*, and *Sk*] were used in this experiment (Ren et al., 2022). These three *Pst* races were considered the most virulent and frequent *Pst* races occurring in China and were used in stripe rust resistance tests at the seedling stage (Ren et al., 2022). The inoculation of *Pst* on wheat seedlings was performed according to Ren et al. (2020). Two *Bgt* isolates, E20 and No. 15, were used in the powdery mildew resistance tests at the seedling stage. Both *Bgt* isolates have been virulent to many newly released cultivars in China in recent years (Ren et al., 2017a; Yang et al., 2021). The inoculation of *Bgt* on wheat seedlings was performed according to Yang et al. (2021). The three *Pst* races were provided by the Plant Protection Institute, Gansu Academy of Agricultural Sciences, China. The *Bgt* isolate E20 was provided by the Department of Plant Protection, Sichuan Agricultural University. The *Bgt* isolate No. 15 was collected by our lab in Ya'an City, Sichuan, China (Ren et al., 2018). The inoculation of *Pst* and *Bgt* on wheat seedlings was performed with three replications in the greenhouse. In addition, the disease resistance of all materials identified in this study was tested in the field under severe natural *Pst* and *Bgt* infection at the Qionglai Research Station of Sichuan Agricultural University in Cheng Plain, Southwest China (30°25′N, 103°28′E) from 2020 to 2022. The field experiments were performed according to the methods described previously (Ren et al., 2020, 2022). The wheat parent CN25, rye parent QL2, wheat cultivar Mianyang 11, and RT1104-1 were served as controls. Stripe rust reactions were scored at the grain filling stage as infection types (ITs) based on a 0–9 scale as described by Wan et al. (2004) and Ren et al. (2022). Powdery mildew reactions were scored at the heading stage as ITs based on a 0–4 scale as described by Xie et al. (2004) and Ren et al. (2020).

Results

Development of disomic addition lines

The pedigrees of the 6R disomic addition lines, 6RS ditelosomic addition lines, and 6RL ditelosomic addition lines are displayed in Figure 1. The wheat parent CN25 ($2n = 42$, 21″WW) was directly crossed with QL2 ($2n = 14$, 7″RR), and several F_0 seeds ($2n = 28$, 21″W + 7″R) were obtained. The chromosome

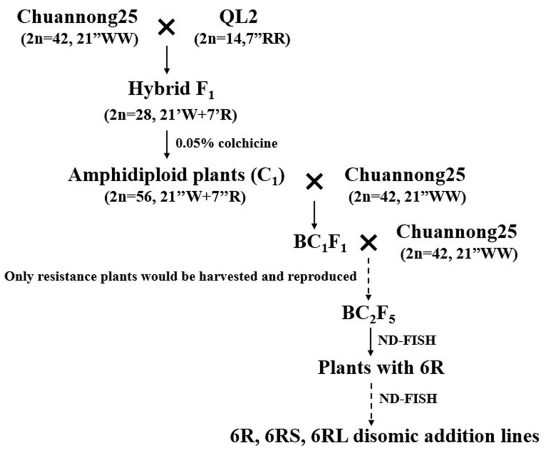

FIGURE 1
The pedigree of the new 6R, 6RS, and 6RL addition lines.

TABLE 2 The sequences of the specific molecular markers for PCR used in this study.

Markers	Forward (5′–3′)	Reverse (5′–3′)	Chromosome
KU88	caggatatcccacaacacaaga	atgggttgtatttgccgaaa	6RS
KU291	gagactacccgtcgaaggac	ggggcttcatcgacaatcta	6RS
KU86	acagccaagctcaaagtggt	tcagtgcagacggtgatagc	6RL
KU153	tggaacttccctttgaatgc	tggaagaaatgtgcagataaaca	6RL

Qiu et al. (2016).

10.3389/fpls.2022.992016

numbers of F_1 plants were doubled by colchicine treatment to produce amphidiploid (C_0) seeds ($2n = 56$, 21″WW + 7″RR; Figure 2A). The amphidiploid plants were then backcrossed with the wheat parent CN25 twice to produce the BC_2F_1 plants. The continued generations were reproduced by selfing, and only the plants that exhibited resistance to diseases were harvested and bred. In the BC_2F_5 generation, the chromosome composition of the plants was examined by ND-FISH during the seedling stage, and then, the plants were transplanted into the field. In this generation, several plants with rye 6R or partial 6R were identified, and these plants also showed resistance in the field. The seeds of these plants containing alien chromatin were harvested and reproduced by selfing. The seedlings of BC_2F_6 were also identified by ND-FISH. In this generation, several homozygous 6R disomic addition lines, 6RS ditelosomic addition lines, and 6RL ditelosomic addition lines were identified. On the other hand, several plants were heterozygous or missed the 6R chromosomes. When plants missed the 6R, they also lose disease resistance in the field. The homozygous addition lines were harvested and reproduced the next generation by selfing. The heterozygous plants were also harvested, and we continued to screen the homozygous plants in their progeny in the generation of BC_2F_7 to BC_2F_8. Finally, three 6RS ditelosomic addition lines (46-13-3, 46-13-11, and 46-13-16), three 6RL ditelosomic addition lines (48-9-2, 48-9-5, and 48-9-6), and two 6R disomic addition lines (48-9-8 and 48-9-10) were selected.

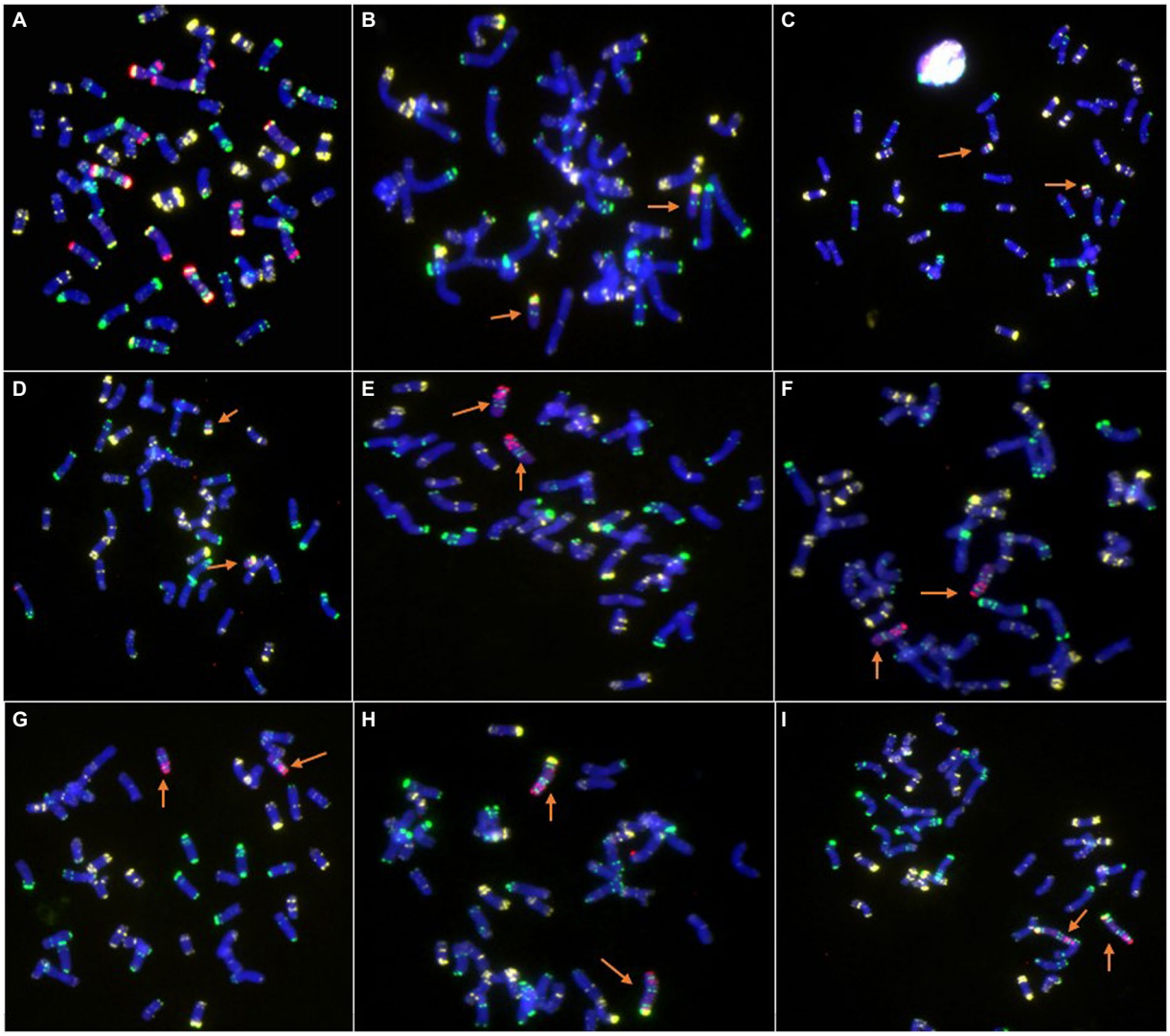

FIGURE 2
Cytogenetic analysis of new wheat-rye lines by ND-FISH. **(A)** Amphidiploid plants (2*n*=56, 21″WW+7″RR). **(B)** 46-13-3, 6RS ditelosomic addition line. **(C)** 46-13-11, 6RS ditelosomic addition line. **(D)** 46-13-16, 6RS ditelosomic addition line. **(E)** 48-9-2, 6RL ditelosomic addition line. **(F)** 48-9-5, 6RL ditelosomic addition line. **(G)** 48-9-6, 6RL ditelosomic addition line. **(H)** 48-9-8, 6R disomic addition line. **(I)** 48-9-10, 6R disomic addition line. The arrows show the 6R, 6RL, or 6RS chromosomes. Oligo-pSc119.2-1: green; Oligo-pTa535-1: white; Oligo-Ku, Oligo-pSc200, and Oligo-pSc250: red.

Chromosome identification

The combination of the five probes Oligo-pSc119.2-1, Oligo-pTa535-1, Oligo-Ku, Oligo-pSc200, and Oligo-pSc250 can easily and accurately distinguish wheat and rye chromosomes in one cell. The ND-FISH results indicated that three lines, 46-13-3, 46-13-11, and 46-13-16, contained a pair of 6RS chromosome arms (Figures 2B–D). Three lines, 48-9-2, 48-9-5, and 48-9-6, contained a pair of 6RL chromosome arms (Figures 2E–G). Two lines, 48-9-8 and 48-9-10, contained a pair of 6R chromosomes (Figures 2H,I).

The centromere and telomere structure of the new lines was identified using the combinations of the probes Oligo-CCS1, Oligo-PAWRC.1, and Oligo-Telo. The Oligo-CCS1 probe can detect both wheat and rye centromeres, whereas Oligo-PAWRC.1 can detect only rye centromeres. Therefore, the centromere of the 6R chromosome showed both signal patterns of Oligo-PAWRC.1 and Oligo-CCS1 (Figures 3E,F). The probe Oligo-Telo can detect the structure of the telomere and can also detect the telocentric chromosome. Therefore, the centromere of the 6RS and 6RL chromosome arms can show both signal patterns of the probes Oligo-PAWRC.1 and Oligo-Telo. The ND-FISH results showed that both 6RS and 6RL chromosomes showed complex signal patterns of Oligo-PAWRC.1 and Oligo-Telo (Figures 3A–D).

The chromosome composition of all lines was also confirmed by specific molecular markers. Two primer pairs, KU88 and KU291, were specific for the rye 6RS chromosome arm and amplified a specific band of ~400 bp. The PCR results showed that all DNA of the 6RS ditelosomic and 6R disomic addition lines amplified the expected bands at ~400 bp, whereas the bands were absent from the DNA of the 6RL ditelosomic addition lines and wheat CN25 (Figures 4A,B). On the other hand, the primer pairs KU86 and KU153 were specific for the rye 6RL chromosome arm and could also amplify a specific band at ~400 bp. The PCR results showed that all DNA of 6RL ditelosomic and 6R disomic addition lines can amplify the expected bands of ~400 bp, whereas the bands were absent from the DNA of 6RS ditelosomic addition lines and wheat CN25 (Figures 4C,D; Table 2).

Resistance to stripe rust and powdery mildew

The wheat parent CN25 was intermediately resistant to two *Pst* races (CYR32 and 34) and highly susceptible to the *Bgt* isolate E20 and No. 15. CN25 also exhibited intermediate resistance to stripe rust and was highly susceptible to powdery mildew in the field

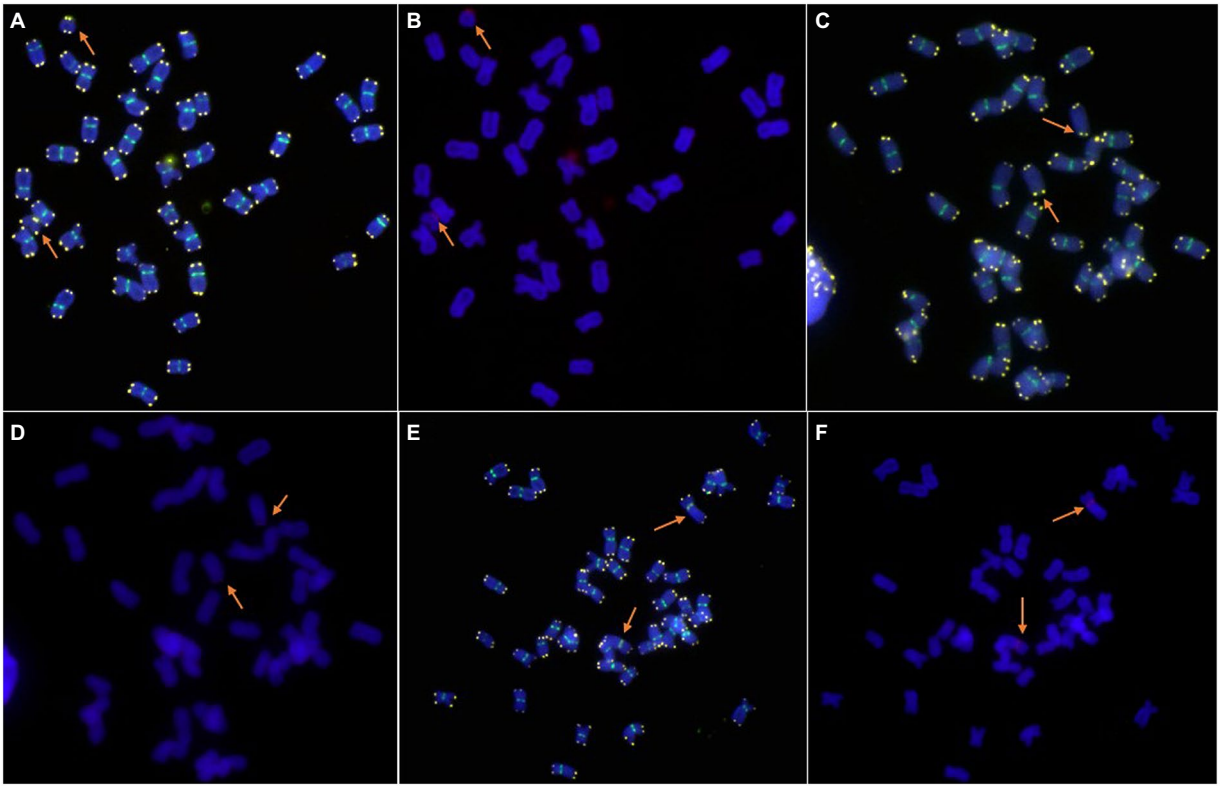

FIGURE 3
Cytogenetic analysis of the telomeres and centromeres of new lines by ND-FISH. **(A,B)**: 6RS ditelosomic addition line. The signal patterns were derived from one cell. **(C,D)**: 6RL ditelosomic addition line. The signal patterns were derived from one cell. **(E,F)**: 6R disomic addition line. The signal patterns were derived from one cell. Oligo-CCS1 (green), Oligo-PAWRC.1 (red), and Oligo-Telo (white). The arrows show the 6RS, 6RL, or 6R chromosomes.

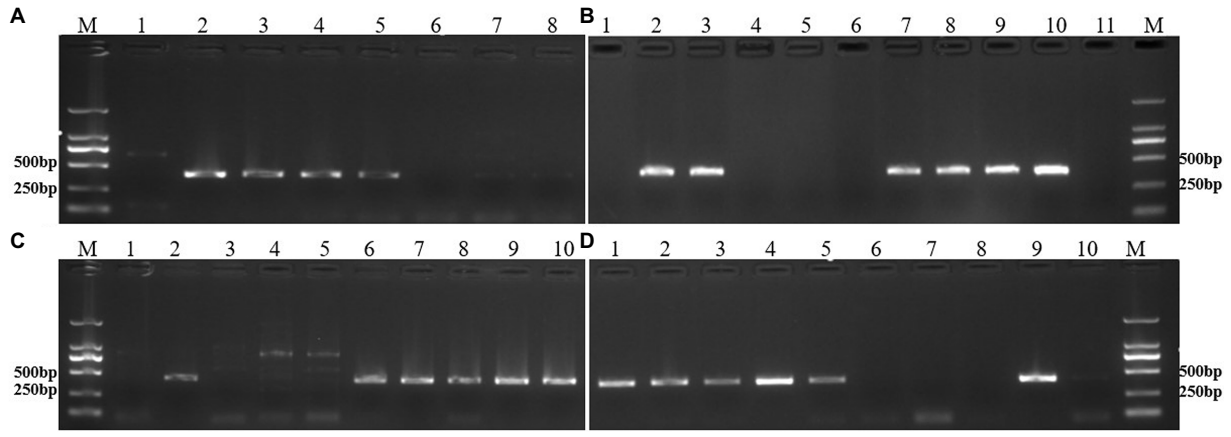

FIGURE 4
PCR results of specific molecular markers. **(A)** PCR results of the primer pair KU88. Lane 1: CN25, Lane 2: 46-13-3 (6RS), Lane 3: 46-13-11 (6RS), Lane 4: 46-13-16 (6RS), Lane 5: rye QL2, Lane 6: 48-9-2 (6RL), Lane 7: 48-9-5 (6RL), Lane 8: 48-9-6 (6RL). **(B)** PCR results of the primer pair KU291. Lane 1: CN25, Lane 2: 48-9-8 (6R), Lane 3: 48-9-10 (6R), Lane 4: 48-9-2 (6RL), Lane 5: 48-9-5 (6RL), Lane 6: 48-9-6 (6RL), Lane 7: 46-13-3 (6RS), Lane 8: 46-13-11 (6RS), Lane 9: 46-13-16 (6RS), Lane 10: rye QL2, Lane 11: CN25. **(C)** PCR results of the primer pair KU86. Lane 1: CN25, Lane 2: rye QL2, Lane 3: 46-13-3 (6RS), Lane 4: 46-13-11 (6RS), Lane 5: 46-13-16 (6RS), Lane 6: 48-9-2 (6RL), Lane 7: 48-9-5 (6RL), Lane 8: 48-9-6 (6RL), Lane 9: 48-9-8 (6R), Lane 10: 48-9-10 (6R). **(D)** PCR results of the primer pair KU153. Lane 1: 48-9-2 (6RL), Lane 2: 48-9-5 (6RL), Lane 3: 48-9-6 (6RL), Lane 4: 48-9-8 (6R), Lane 5: 48-9-10 (6R), Lane 6: 46-13-3 (6RS), Lane 7: 46-13-11 (6RS), Lane 8: 46-13-16 (6RS), Lane 9: rye QL2, Lane 10: CN25. Lane M: DNA marker DL2000. 6RS: 6RS ditelosomic addition lines; 6RL: 6RL ditelosomic addition lines; 6R: 6R disomic addition lines.

(Table 3). On the other hand, inbred rye line QL2 was highly resistant to three *Pst* races and two *Bgt* isolates. QL2 also exhibited high resistance to stripe rust and powdery mildew in the field (Table 3). The control Mianyang 11 was highly susceptible to three *Pst* races and two *Bgt* isolates, and also exhibited susceptible to stripe rust and powdery mildew in the field. The control RT1104-1 exhibited resistance to three *Pst* races and two *Bgt* isolates, and also showed resistance in the field (Table 3). The 6R disomic, 6RS ditelosomic, and 6RL ditelosomic addition lines showed a high level of resistance to three *Pst* races and two *Bgt* isolates at the seedling stages. In addition, these eight lines also showed high resistance to stripe rust and powdery mildew in the field at the adult stage (Table 3).

Moreover, in addition to these homozygous 6R, 6RS, and 6RL disomic or ditelosomic addition lines, several other types, such as 6R monosomic addition (Figure 5A), 6RL monotelosomic addition (Figure 5B), and 6RS monotelosomic addition (Figure 5C), and several plants that missed 6R, 6RL, or 6RS (Figure 5D), were also identified in the generation of BC_2F_7–BC_2F_8. Without exception, plants exhibit disease resistance as long as they have 6R, 6RS, or 6RL in their genome, but disease resistance was lost when 6R, 6RS, or 6RL was missed (Table 4).

Discussion

6R chromosome of Qinling rye provides resistance to *Pst* and *Bgt*

Related species of wheat are very important for the improvement of wheat genetics (Friebe et al., 1996), and rye is the most important species. According to Weining rye genome sequencing data, 1,909 disease resistance-associated (DRA) genes were identified in the rye genome (Li et al., 2021). Several useful resistance genes were introduced into the wheat genome through wheat-rye distance crosses. For example, *Yr9*, *Pm8*, *Pm17*, *Sr31*, and *Lr26* were derived from the 1RS chromosome arm through T1RS·1BL or T1RS·1AL chromosome translocation (Mago et al., 2005). *Sr59* and *H21* were derived from the 2RL chromosome arm through T2RL.2BS or T2RL.2DS chromosome translocation (Friebe et al., 1990; Rahmatov et al., 2016). *Sr27* was derived from the 3RS chromosome arm through the T3RS.3BL chromosome translocation (Marais and Marais, 1994). Many other rye chromosomes with resistance have been introduced into the wheat genome. For example, Ren et al. reported (Ren et al., 2020) a T7RL.7BS translocation line with resistance to *Pst*, *Bgt,* and *Fusarium* head blight. An et al. reported (An et al., 2019) a 4R disomic addition line with resistance to *Pst*, *Bgt*, and sharp eyespot. The 6R chromosome of rye also contains many excellent resistance genes and plays an important role in wheat genetic improvement. According to Weining rye genome sequencing data, 287 disease resistance-associated genes mapped to the 6R chromosome (Li et al., 2021). To date, stripe rust resistance gene *Yr83* has been mapped on the 6RL chromosome arm (Li et al., 2020), and powdery mildew stripe rust gene *Pm56* has been mapped on the 6RS chromosome arm (Hao et al., 2018). Several other 6R chromosomes have been introduced into the wheat genome. For example, Han et al. (2022) reported a 6R addition line originating from a cross between octoploid triticale and common wheat that exhibited resistance to powdery mildew. Duan et al. (2022) reported a T6RL.6BS translocation line with

TABLE 3 Analysis of resistance to stripe rust and powdery mildew when inoculated with prevalent races/isolates of stripe rust and powdery mildew.

Lines	Chromosome	*Pst* analysis				*Bgt* analysis		
		CYR32	CYR33	CYR34	In field	E20	No.15	In field
Chuannong 25	21″WW	4	3	5	5	4	4	4
46-13-3	21″WW + 1″6RS	0	0	0	0	0	0	0
46-13-11	21″WW + 1″6RS	0	0	0	0	0	0	0
46-13-16	21″WW + 1″6RS	0	0	0	0	0	0	0
48-9-2	21″WW + 1″6RL	0	0	0	0	0	0	0
48-9-5	21″WW + 1″6RL	0	0	0	0	0	0	0
48-9-6	21″WW + 1″6RL	0	0	0	0	0	0	0
48-9-8	21″WW + 1″6R	0	0	0	0	0	0	0
48-9-10	21″WW + 1″6R	0	0	0	0	0	0	0
Rye QL2	7″RR	0	0	0	0	0	0	0
Mianyang 11	21″WW	8	8	9	9	4	4	4
RT1104-1	T1RS.1BL	0	0	0	0	0	0	0

For *Pst* analysis: 0: no visible symptoms; 1: necrotic flecks; 2: necrotic areas without sporulation; 3: necrotic and chlorotic areas with restricted sporulation; 4–6: moderate uredinia with necrosis and chlorosis; 7–8: abundant uredia with chlorosis; 9: without chlorosis For *Bgt* analysis: 0: no visible symptoms; 0;: hypersensitive necrotic flecks; 1: minute colonies with few conidia produced; 2: colonies with moderately developed hyphae, but few conidia; 3: colonies with well-developed hyphae and abundant conidia, but colonies not joined together; 4: colonies with well-developed hyphae and abundant conidia, and colonies mostly joined together.

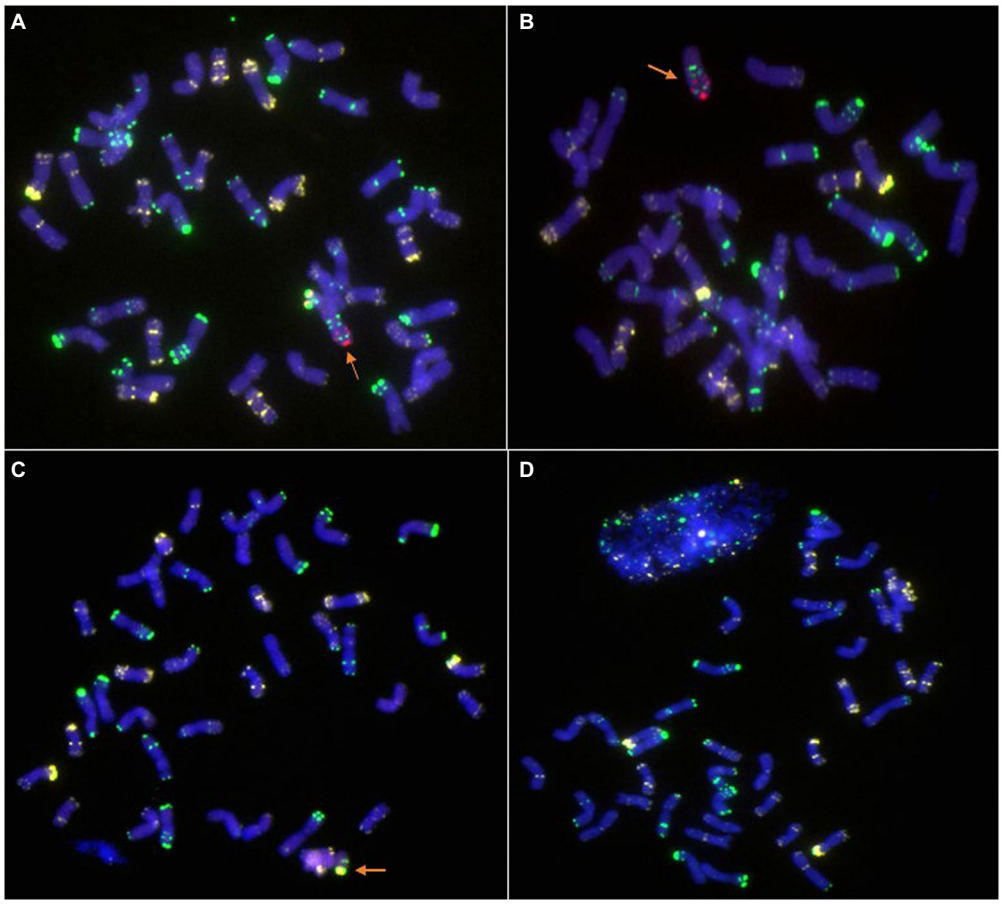

FIGURE 5
Lines with other types identified by ND-FISH. **(A)** 6R monosomic addition. **(B)** 6RL monotelosomic addition. **(C)** 6RS monotelosomic addition. **(D)** Lines that missed 6R. The arrows show the 6R, 6RL, or 6RS chromosomes. Oligo-pSc119.2-1: green; Oligo-pTa535-1: white; Oligo-Ku, Oligo-pSc200, and Oligo-pSc250: red.

TABLE 4 Relationship between resistance and chromosome types.

Types	Chromosome	Resistance to *Pst*	Resistance to *Bgt*
6R disomic addition line	21″WW + 1″6R	0	0
6R monosomic addition line	21″WW + 1′6R	0	0
6RS ditelosomic addition line	21″WW + 1″6RS	0	0
6RS monotelosomic addition line	21″WW + 1′6RS	0	0
6RL ditelosomic addition line	21″WW + 1″6RL	0	0
6RL monotelosomic addition line	21″WW + 1′6RL	0	0
Lines missed rye chromatin	21″WW	5	4
CN25	21″WW	5	4

For *Pst* analysis: 0: no visible symptoms; 5: moderate uredinia with necrosis and chlorosis. For *Bgt* analysis: 0: no visible symptoms; 4: colonies with well-developed hyphae and abundant conidia, and colonies mostly joined together.

resistance to stripe rust and originating from rye AR106BONE. Du et al. (2018) reported a 6RL/6D small segment translocation line with powdery mildew resistance that originated from rye Kustro. Schneider et al. (2016) reported a 6R disomic addition line with resistance to stripe rust originating from *Secale cereanum*. An et al. (2015) reported a 6R disomic addition line with resistance to powdery mildew originating from the rye cultivar., German White. However, most of these new lines were resistant to only one disease. A few new lines exhibit resistance to both stripe rust and powdery mildew. In this study, three 6RS ditelosomic addition lines, three 6RL ditelosomic addition lines, and two 6R disomic addition lines were selected from the cross between wheat CN25 and rye QL2 (Figures 1–3). All eight new lines exhibited high resistance to both stripe rust and powdery mildew (Table 3). Once 6RS or 6RL chromosome arms were added to the wheat genome, resistance to stripe rust and powdery mildew was demonstrated. If 6R chromosomes were missed in the offspring, the resistance was also lost (Figure 5; Table 4). The results indicated that both the 6RS and 6RL chromosome arms of QL2 contained gene(s) associated with resistance to stripe rust and powdery mildew.

Genetic diversity of rye resistance genes

Rye has great potential as a source for favorable genes, such as genes supporting higher yield, stress resistance, disease resistance, and other agronomic traits desirable for wheat genetic improvement (Ren et al., 2011). Rye is a wind-pollinated plant, and high levels of genetic diversity are found not only between cultivars originating from different regions but also within the same cultivar (Persson and von Bothmer, 2002; Ren et al., 2011). A large number of disease resistance genes may also be present in the rye genome (Ren et al., 2022). The results of genome sequencing of Weining rye also revealed that there were many DRA genes that existed in the rye genome and were distributed to seven chromosomes with NBS (nucleotide-binding site), RLK (receptor-like kinase), RLP (receptor-like protein), and CC-TM (coiled-coil plus transmembrane receptor) types (Li et al., 2021). The numbers of these DRA genes along the seven assembled chromosomes of Weining rye (1R to 7R) were 242, 296, 301, 301, 255, 287, and 227, respectively (Li et al., 2021). Considering the crucial importance of DRA genes in plant responses to biotic adversities (Kourelis and van der Hoorn, 2018; Li et al., 2021), they may facilitate efficient genetic studies and molecular improvement of disease resistance in wheat. For example, Ren et al. (2022) reported 166 different T1RS·1BL translocation lines, which originated from three rye cultivars. These T1RS·1BL translocation lines exhibited different resistance patterns when they were tested by different *Pst* races. The stripe rust resistance gene *Yr9* originated from Petkus rye (Mago et al., 2005). Shi et al. (2001) found an allele of *Yr9* that exhibited different resistance patterns to the tested *Pst* pathotypes from a T1RS·1BL line Weique, which also originated from Petkus rye. Ren et al. (2009) reported the *Pst* resistance gene *YrCn17* from the T1RS·1BL cultivar CN17, which originated from an inbred line of Petkus rye, L155. The powdery mildew resistance gene *Pm8* was derived from Petkus rye (Mater et al., 2004), and another *Bgt* resistance gene *Pm17* was also mapped on the 1RS chromosome of Amigo, which originated from rye Insave (Mater et al., 2004). Ren et al. (2009) also reported a *Bgt* resistance gene, *PmCn17,* from cultivar CN17. In recent years, more 1RS chromosomes have carried more disease-resistance genes into the wheat genome and played a positive role in wheat disease-resistance breeding. Similar to 1RS chromosomes, the other six chromosomes of rye (2R–6R) also contain a large number of DRA genes (Li et al., 2021), which has great potential in wheat disease-resistance breeding in the future. To date, the stripe rust resistance gene *Yr83* has been mapped to 6RL, and the powdery mildew resistance gene *Pm56* has been mapped to 6RS (Hao et al., 2018; Li et al., 2020). Obviously, there is also abundant genetic diversity on the 6R chromosome, which may contain more disease-resistance genes for wheat genetic improvement. In this study, six monotelosomic addition lines and two disomic addition lines were identified from the distance cross between rye line QL2 and wheat cultivar CN25. The resistance analysis showed that all new lines exhibited high resistance to *Pst* and *Bgt*. This finding indicated that similar to 1RS, high genetic diversity of resistance genes existed on the 6RS or the 6RL chromosome arms. The genetic diversity of resistance genes on alien chromosomes could be transferred into the wheat genome

to increase the genetic diversity of resistance genes in wheat (Ren et al., 2022). Further utilization of the genetic diversity of resistance genes is an important method to further utilize rye resources to improve wheat genetics. These new lines could be used as a promising bridging parent and valuable genetic resource for wheat disease resistance improvement.

Data availability statement

The original contributions presented in the study are included in the article/supplementary material, further inquiries can be directed to the corresponding authors.

Author contributions

TR and ZL: conceived and designed the study. TR and ZR: created the materials. TR, ZR, and ZL: analyzed the data. TR: wrote the manuscript. ZS, YH, FT, and PL: performed the experiments and analyzed the data. All authors contributed to the article and approved the submitted version.

Funding

This work was supported by the National Natural Science Foundation of China (31801357) and the Foundation of Sichuan Province Science and Technology Support Program (2019YJ0510, 2021YJ0509, and 2021JDRC0127).

Conflict of interest

The authors declare that the research was conducted in the absence of any commercial or financial relationships that could be construed as a potential conflict of interest.

Publisher's note

All claims expressed in this article are solely those of the authors and do not necessarily represent those of their affiliated organizations, or those of the publisher, the editors and the reviewers. Any product that may be evaluated in this article, or claim that may be made by its manufacturer, is not guaranteed or endorsed by the publisher.

References

An, D., Ma, P., Zheng, Q., Fu, S., Li, L., Han, F., et al. (2019). Development and molecular cytogenetic identification of a new wheat-rye 4R chromosome disomic addition line with resistances to powdery mildew, stripe rust and sharp eyespot. *Theor. Appl. Genet.* 132, 257–272. doi: 10.1007/s00122-018-3214-3

An, D. G., Zheng, Q., Luo, Q. L., Ma, P. T., Zhang, H. X., Li, L. H., et al. (2015). Molecular cytogenetic identification of a new wheat-rye 6R chromosome disomic addition line with powdery mildew resistance. *PLoS One* 10:e0134534. doi: 10.1371/journal.pone.0134534

Chaves, M. S., Martinelli, J. A., Wesp-Guterres, C., Graichen, F. A., Brammer, S. P., Scagliusi, S. M., et al. (2013). The importance for food security of maintaining rust resistance in wheat. *Food Secur.* 5, 157–176. doi: 10.1007/s12571-013-0248-x

Chen, X. M. (2005). Epidemiology and control of stripe rust (*Puccinia striiformis* f. sp. *tritici*) on wheat. *Can. J. Plant Pathol.* 27, 314–337. doi: 10.1080/07060660509507230

Chen, X. M. (2014). Integration of cultivar resistance and fungicide application for control of wheat stripe rust. *Can. J. Plant Pathol.* 36, 311–326. doi: 10.1080/07060661.2014.924560

Chen, P. D., Qi, L. L., Zhou, B., Zhang, S. Z., and Liu, D. J. (1995). Development and molecular cytogenetic analysis of wheat-*Haynaldia villosa* 6VS/6AL translocation lines specifying resistance to powdery mildew. *Theor. Appl. Genet.* 91, 1125–1128. doi: 10.1007/BF00223930

Chen, W. Q., Wellings, C., Chen, X. M., Kang, Z. S., and Liu, T. G. (2014). Wheat stripe (yellow) rust caused by *Puccinia striiformis* f. sp. *tritici*. *Mol. Plant Pathol.* 15, 433–446. doi: 10.1111/mpp.12116

Cuadrado, Á., and Jouve, N. (2010). Chromosomal detection of simple sequence repeats (SSRs) using nondenaturing FISH (ND-FISH). *Chromosoma* 119, 495–503. doi: 10.1007/s00412-010-0273-x

Doyle, J. J., and Doyle, J. L. (1987). A rapid DNA isolation procedure from small quantities of fresh leaf tissues. *Phytochem. Bull.* 19, 11–15.

Du, H., Tang, Z., Duan, Q., Tang, S., and Fu, S. (2018). Using the 6RL^{Ku} minichromosome of rye (*Secale cereale* L.) to create wheat-rye 6D/6RL^{Ku} small segment translocation lines with powdery mildew resistance. *Int. J. Mol. Sci.* 19, 3933. doi: 10.3390/ijms19123933

Duan, Y., Luo, J., Yang, Z., Li, G., Tang, Z., and Fu, S. (2022). The physical location of stripe rust resistance genes on chromosome 6 of Rye (*Secale cereale* L.) AR106BONE. *Front. Plant Sci.* 13:928014. doi: 10.3389/fpls.2022.928014

Duveiller, E., Singh, R. P., and Nicol, J. M. (2007). The challenges of maintaining wheat productivity: pests, diseases, and potential epidemics. *Euphytica* 157, 417–430. doi: 10.1007/s10681-007-9380-z

Friebe, B., Hatchett, J. H., Sears, R. G., and Gill, B. S. (1990). Transfer of hessian fly resistance from 'Chaupon' rye to hexaploid wheat via a 2BS/2RL wheat-rye chromosome translocation. *Theor. Appl. Genet.* 79, 385–389. doi: 10.1007/BF01186083

Friebe, B., Jiang, J., Raupp, W. J., McIntosh, R. A., and Gill, B. S. (1996). Characterization of wheat-alien translocations conferring resistance to diseases and pests: current status. *Euphytica* 91, 59–87. doi: 10.1007/BF00035277

Han, G. H., Liu, S. Y., Wang, J., Jin, Y. L., Zhou, Y. L., Luo, Q. L., et al. (2020). Identification of an elite wheat-rye T1RS.1BL translocation line conferring high resistance to powdery mildew and stripe rust. *Plant Dis.* 104, 2940–2948. doi: 10.1094/PDIS-02-20-0323-RE

Han, G., Yan, H., Wang, J., Cao, L., Liu, S., Li, X., et al. (2022). Molecular cytogenetic identification of a new wheat-rye 6R addition line and physical localization of its powdery mildew resistance gene. *Front. Plant Sci.* 13:889494. doi: 10.3389/fpls.2022.889494

Hao, M., Liu, M., Luo, J., Fan, C., Yi, Y., Zhang, L., et al. (2018). Introgression of powdery mildew resistance gene *Pm56* on rye chromosome arm 6RS into wheat. *Front. Plant Sci.* 9:1040. doi: 10.3389/fpls.2018.01040

Hou, Z. G., Liu, W. C., Shao, Z. R., and Jiang, R. Z. (2000). On developing long-term meteorological prediction research of crops pests and diseases prevailing in China. *J. Nat. Disasters* 9, 117–121.

Huo, Z., Ye, C., Qian, S., Chen, L., and Liu, W. (2002). Relationship between climatic anomaly and prevailing of the wheat powdery mildew in China. *J. Nat. Disasters* 11, 85–90.

Johansson, E., Henriksson, T., Prieto-Linde, M. L., Andersson, S., Ashraf, R., and Rahmatov, M. (2020). Diverse wheat-alien introgression lines as a basis for durable resistance and quality characteristics in bread wheat. *Front. Plant Sci.* 11:1067. doi: 10.3389/fpls.2020.01067

Kourelis, J., and van der Hoorn, R. A. L. (2018). Defended to the nines: 25 years of resistance gene cloning identifies nine mechanisms for R protein function. *Plant Cell* 30, 285–299. doi: 10.1105/tpc.17.00579

Li, J. B., Dundas, I., Dong, C. M., Li, G. R., Trethowan, R., Yang, Z. J., et al. (2020). Identification and characterization of a new stripe rust resistance gene *Yr83* on rye chromosome 6R in wheat. *Theor. Appl. Genet.* 133, 1095–1107. doi: 10.1007/s00122-020-03534-y

Li, G. R., Gao, D., La, S. X., Wang, H. J., Li, J. B., He, W. L., et al. (2016). Characterization of wheat-Secale *africanum* chromosome 5R(a) derivatives carrying *Secale* specific genes for grain hardness. *Planta* 243, 1203–1212. doi: 10.1007/s00425-016-2472-z

Li, G., Wang, L., Yang, J., He, H., Jin, H., Li, X., et al. (2021). A high-quality genome assembly highlights rye genomic characteristics and agronomically important genes. *Nat. Genet.* 53, 574–584. doi: 10.1038/s41588-021-00808-z

Luo, P. G., Luo, H. Y., Chang, Z. J., Zhang, H. Y., Zhang, M., and Ren, Z. L. (2009). Characterization and chromosomal location of *Pm40*, in common wheat: A new gene for resistance to powdery mildew derived from *elytrigia intermedium*. *Theor. Appl. Genet.* 118, 1059–1064. doi: 10.1007/s00122-009-0962-0

Mago, R., Miah, H., Lawrence, G. J., Wellings, C. R., Spielmeyer, W., Bariana, H. S., et al. (2005). High-resolution mapping and mutation analysis separate the rust resistance genes *Sr31*, *Lr26* and *Yr9* on the short arm of rye chromosome 1. *Theor. Appl. Genet.* 112, 41–50. doi: 10.1007/s00122-005-0098-9

Marais, G. F., and Marais, A. S. (1994). The derivation of compensating translocations involving homoeologous group 3 chromosomes of wheat and rye. *Euphytica* 79, 75–80. doi: 10.1007/BF00023578

Mater, Y., Baenziger, S., Gill, K., Graybosch, R., Whitcher, L., Baker, C., et al. (2004). Linkage mapping of powdery mildew and greenbug resistance genes on recombinant 1RS from 'amigo' and 'Kavkaz' wheat-rye translocations of chromosome 1RS.1AL. *Genome* 47, 292–298. doi: 10.1139/g03-101

Persson, K., and von Bothmer, R. (2002). Genetic diversity amongst landraces of rye (*Secale cereale* L.) from northern Europe. *Hereditas* 136, 29–38. doi: 10.1034/j.1601-5223.2002.1360105.x

Qiu, L., Tang, Z., Li, M., and Fu, S. (2016). Development of new PCR-based markers specific for chromosome arms of rye (*Secale cereale* L.). *Genome* 59, 159–165. doi: 10.1139/gen-2015-0154

Rahmatov, M., Rouse, M. N., Nirmala, J., Danilova, T., Friebe, B., Steffenson, B. J., et al. (2016). A new 2DS·2RL Robertsonian translocation transfers stem rust resistance gene *Sr59* into wheat. *Theor. Appl. Genet.* 129, 1383–1392. doi: 10.1007/s00122-016-2710-6

Ren, T. H., Chen, F., Zou, Y. T., Jia, Y. H., Zhang, H. Q., Yan, B. J., et al. (2011). Evolutionary trends of microsatellites during the speciation process and phylogenetic relationships within the genus *Secale*. *Genome* 54, 316–326. doi: 10.1139/g10-121

Ren, T., He, M., Sun, Z., Tan, F., Luo, P., Tang, Z., et al. (2019). The polymorphisms of oligonucleotide probes in wheat cultivars determined by ND-FISH. *Molecules* 24, 1126. doi: 10.3390/molecules24061126

Ren, T. H., Jiang, Q., Sun, Z., Zhao, L., Peng, W., Ren, Z., et al. (2022). Development and molecular cytogenetic characterization of novel primary wheat-rye 1RS.1BL translocation lines from multiple rye sources with resistance to stripe rust. *Plant Dis.* 106, 2191–2200. doi: 10.1094/PDIS-11-21-2605-RE

Ren, T., Li, Z., Yan, B., Tan, F., Tang, Z., Fu, S., et al. (2017b). Targeted segment transfer from Rye chromosome 2R to wheat chromosomes 2A, 2B, and 7B. *Cytogenet. Genome Res.* 151, 50–59. doi: 10.1159/000458743

Ren, T., Ren, Z., Yang, M., Yan, B., Tan, F., Fu, S., et al. (2018). Novel source of 1RS from Baili rye conferred high resistance to diseases and enhanced yield traits to common wheat. *Mol. Breed.* 38, 101. doi: 10.1007/s11032-018-0856-4

Ren, T., Sun, Z., Ren, Z., Tan, F., Luo, P., Tang, Z., et al. (2020). Molecular and cytogenetic characterization of a wheat-rye 7BS.7RL translocation line with resistance to stripe rust, powdery mildew and *Fusarium* head blight. *Phytopathology* 110, 1713–1720. doi: 10.1094/PHYTO-02-20-0061-R

Ren, T., Tang, Z., Fu, S., Yan, B., Tan, F., Ren, Z., et al. (2017a). Molecular cytogenetic characterization of novel wheat-rye T1RS.1BL translocation lines with high resistance to diseases and great agronomic traits. *Front. Plant Sci.* 8:799. doi: 10.3389/fpls.2017.00799

Ren, T. H., Yang, Z. J., Yan, B. J., Zhang, H. Q., Fu, S. L., and Ren, Z. L. (2009). Development and characterization of a new 1BL.1RS translocation line with resistance to stripe rust and powdery mildew of wheat. *Euphytica* 169, 207–213. doi: 10.1007/s10681-009-9924-5

Schlegel, R., and Korzun, V. (1997). About the origin of 1RS.1BL wheat-rye chromosome translocations from Germany. *Plant Breed.* 116, 537–540. doi: 10.1111/j.1439-0523.1997.tb02186.x

Schneider, A., Rakszegi, M., Molnár-Láng, M., and Szakács, É. (2016). Production and cytomolecular identification of new wheat-perennial rye (Secale *cereanum*) disomic addition lines with yellow rust resistance (6R) and increased arabinoxylan and protein content (1R, 4R, 6R). *Theor. Appl. Genet.* 129, 1045–1059. doi: 10.1007/s00122-016-2682-6

Shi, Z. X., Chen, X. M., Line, R. F., Leung, H., and Wellings, C. R. (2001). Development of resistance gene analog polymorphism markers for the *Yr9* gene resistance to wheat stripe rust. *Genome* 44, 509–516. doi: 10.1139/g01-028

Tang, Z., Yang, Z., and Fu, S. (2014). Oligonucleotides replacing the roles of repetitive sequences pAs1, pSc119.2, pTa-535, pTa71, CCS1, and pAWRC.1 for FISH analysis. *J. Appl. Genet.* 55, 313–318. doi: 10.1007/s13353-014-0215-z

Wan, A. M., Chen, X. M., and He, Z. H. (2007). Wheat stripe rust in China. *Aus. J. Agri. Res.* 58, 605–619. doi: 10.1071/AR06142

Wan, A., Zhao, Z., Chen, X., He, Z., Jin, S., Jia, Q., et al. (2004). Wheat stripe rust epidemic and virulence of *Puccinia striiformis* f. sp. *tritici* in China in 2002. *Plant Dis.* 88, 896–904. doi: 10.1094/PDIS.2004.88.8.896

Wang, X., Han, B., Sun, Y., Kang, X., Zhang, M., Han, H., et al. (2022). Introgression of chromosome 1P from *Agropyron cristatum* reduces leaf size and plant height to improve the plant architecture of common wheat. *Theor. Appl. Genet.* 135, 1951–1963. doi: 10.1007/s00122-022-04086-z

Xie, C. J., Sun, Q. X., Ni, T., Nevo, E., and Fahima, F. (2004). Identification of resistance gene analogue markers closely linked to wheat powdery mildew resistance gene *Pm31*. *Plant Breed.* 123, 198–200. doi: 10.1046/j.1439-0523.2003.00940.x

Yang, H., Zhong, S., Chen, C., Yang, H., Chen, W., Tan, F., et al. (2021). Identification and cloning of a CC-NBS-NBS-LRR gene as a candidate of *Pm40* by integrated analysis of both the available transcriptional data and published linkage mapping. *Int. J. Mol. Sci.* 22:10239. doi: 10.3390/ijms221910239

frontiers | Frontiers in Plant Science

TYPE Original Research
PUBLISHED 30 August 2022
DOI 10.3389/fpls.2022.1006409

OPEN ACCESS

EDITED BY
Cheng Liu,
Shandong Academy of Agricultural Sciences, China

REVIEWED BY
Shuanghe Cao,
Institute of Crop Sciences (CAAS), China
Junming Li,
Center for Agricultural Resources Research, IGDB (CAS), China

*CORRESPONDENCE
Hui Li
zwslihui@163.com
Yingjun Zhang
zhangyingjun1977@163.com

†These authors have contributed equally to this work

SPECIALTY SECTION
This article was submitted to Plant Pathogen Interactions, a section of the journal Frontiers in Plant Science

RECEIVED 29 July 2022
ACCEPTED 12 August 2022
PUBLISHED 30 August 2022

CITATION
Sun L, Lv L, Zhao J, Hu M, Zhang Y, Zhao Y, Tang X, Wang P, Li Q, Chen X, Li H and Zhang Y (2022) Genome-wide identification and expression analysis of the *TaRRA* gene family in wheat (*Triticum aestivum* L.). *Front. Plant Sci.* 13:1006409. doi: 10.3389/fpls.2022.1006409

Genome-wide identification and expression analysis of the *TaRRA* gene family in wheat (*Triticum aestivum* L.)

Lijing Sun†, Liangjie Lv†, Jie Zhao, Mengyun Hu, Yelun Zhang, Yun Zhao, Xiaodong Tang, Peinan Wang, Qianying Li, Xiyong Chen, Hui Li* and Yingjun Zhang*

Laboratory of Crop Genetics and Breeding of Hebei, Institute of Cereal and Oil Crops, Hebei Academy of Agriculture and Forestry Sciences, Shijiazhuang, China

Cytokinin is an important endogenous hormone in plants performing a wide spectrum of biological roles. The *type-A response regulators (RRAs)* are primary cytokinin response genes, which are important components of the cytokinin signaling pathway and are involved in the regulation of plant growth and development. By analysis of the whole genome sequence of wheat, we identified 20 genes encoding RRAs which were clustered into eight homologous groups. The gene structure, conserved motifs, chromosomal location, and *cis*-acting regulatory elements of the *TaRRAs* were analyzed. Quantitative real-time polymerase chain reaction (qRT-PCR) results showed that the expression levels of most of the *TaRRAs* increased rapidly on exogenous cytokinin application. Moreover, the *TaRRA* family members displayed different expression profiles under the stress treatments of drought, salt, cold, and heat. This study provides valuable insights into the *RRA* gene family in wheat and promotes the potential application of these genes in wheat genetic improvement.

KEYWORDS

type-A response regulators, gene family, wheat (*Triticum aestivum* L.), expression pattern, cytokinin, abiotic stress

Introduction

Cytokinin is a vital phytohormone responsible for regulating numerous aspects of plant growth and development, including cell division and differentiation, apical dominance, leaf senescence, photomorphogenesis, fertility, and seed development (Werner and Schmülling, 2009; Hwang et al., 2012; Schaller et al., 2015; Wybouw and De Rybel, 2019). In addition, cytokinin plays an important role in plant response to many environmental stresses such as drought, salt, cold, and heat (Ha et al., 2012; Pavlů et al., 2018; Liu et al., 2020). Cytokinin signal transduction is mediated by a multistep two-component system (TCS) involving a His-Asp-His-Asp phosphorelay from histidine

kinase receptors (HKs) and histidine-containing phosphotransfer proteins (HPs) to downstream response regulators (RRs) (Argueso et al., 2010; El-Showk et al., 2013; Kieber and Schaller, 2018).

The response regulators are classified into four distinct groups based on phylogenetic and conserved domain analysis, namely, type-A response regulators (RRAs), type-B response regulators (RRBs), type-C response regulators (RRCs), and circadian clock-related pseudo response regulators (PRRs) (Heyl et al., 2013), all with a conserved N-terminal receiver domain and a variable-length C-terminal. The C-terminal of RRAs is short and has yet to be assigned any specific function. RRBs have a large C-terminal extension containing Myb-like DNA binding, nuclear localization, and transcription activation domains (Sakai et al., 2000; Hosoda et al., 2002). The C-terminal of RRCs is also short; however, they are not grouped in the same class as RRAs. PRRs lack the highly conserved Asp residue required for phosphorylation and have a C-terminal including a CCT domain (CO, CO-LIKE, TOC1) (Makino et al., 2000; Schaller et al., 2008). RRBs are transcription factors that mediate the transcriptional response to cytokinin (Argyros et al., 2008). RRAs are transcriptionally induced in response to cytokinin *via* direct activation by RRBs and are responsible for repressing cytokinin signaling *via* a negative feedback loop (Hwang et al., 2012).

Many reports have established that RRAs play a critical role in plant growth and development. In *Arabidopsis*, 10 *RRAs* have been reported (*ARR3-ARR9* and *ARR15-ARR17*) (D'Agostino et al., 2000), of which *ARR3* and *ARR4* act redundantly in the determination of the circadian rhythm (Salomé et al., 2006). ARR4 interacts with phytochrome B, modulating red light signaling by stabilizing the active Pfr form of phytochrome B (Sweere et al., 2001; Mira-Rodado et al., 2007). *ARR7* negatively influences meristem size through regulation of its expression by WUSCHEL (Leibfried et al., 2005). Moreover, *ARR7*, together with *ARR15*, also participates in the cytokinin–auxin hormonal control of the shoot stem-cell niche (Zhao et al., 2010). In addition, *ARR16* has been reported to be involved in *Arabidopsis* seedling development *via* regulation of its expression by MYC2 (Srivastava et al., 2019).

Accumulating evidence indicates that RRAs are involved in abiotic stress responses. Dehydration stress transiently induces the expression of *ARR5*, *ARR7*, and *ARR15*, but reduces the expression of *ARR8* and *ARR17* (Kang et al., 2012). Also, the phosphorylation of ARR5 Ser residues by SnRK2s enhances its stability and plant drought tolerance (Huang et al., 2018). The expression of a variety of *RRAs*, including *ARR5*, *ARR6*, *ARR7*, and *ARR15*, are induced by cold (Jeon et al., 2010). However, *ARR-OE* plants (*ARR5-OE*, *ARR7-OE*, and *ARR15-OE*) and *arr* mutants (*arr5*, *arr6*, and *arr7*) show similar enhanced freezing tolerance, indicating that RRAs play a complex role in regulating cold stress response (Jeon et al., 2010; Shi et al., 2012). In rice, the expression of type-A *OsRR6* is induced by salt, dehydration, and low-temperature treatments (Jain et al., 2006), and overexpression of *OsRR6* enhances seedling drought and salinity tolerance (Bhaskar et al., 2021); whereas, *OsRR9* and *OsRR10* negatively regulate rice salinity tolerance (Wang et al., 2019). Recently, *ZmRR1*, a maize type-A RR, has been demonstrated to positively regulate maize chilling tolerance by modulating the expression of *ZmDREB1s* and *ZmCesAs*. The phosphorylation of ZmRR1 Ser residues by ZmMPK8 accelerates its degradation, thereby reducing the chilling tolerance (Zeng et al., 2021).

RRAs have been widely studied in *Arabidopsis* and rice, however, limited information is available for RRAs in wheat. The completion of the wheat whole genome sequence and further improvements of the wheat genome database have immensely contributed to decoding the wheat genome at the molecular level. In the present study, we systematically performed a genome-wide analysis of the wheat *RRA* gene family and investigated their gene structures, conserved motifs, chromosomal locations, *cis*-acting regulatory elements, and expression patterns in response to cytokinin treatment and various stresses. This work provides valuable information on the wheat *RRA* gene family and lays a foundation for further functional analysis of this gene family.

Materials and methods

Identification of *TaRRA* genes in wheat

Whole-genome and protein sequence data of wheat (IWGSC Assembly GCA_900519105.1) and the hidden Markov model (HMM) file for the response regulator receiver domain (PF00072) were downloaded from the EnsemblPlants database[1] and Pfam database,[2] respectively. A wheat-specific HMM file was established by the alignment of the response regulator receiver domain HMM file with the wheat protein sequences (E-value $< 1e^{-20}$). The wheat-specific HMM file was then used as bait to search against the local reference genome database to identify candidate wheat RRs (E-value < 0.01). Redundant genes were removed, and the longest representative transcripts were selected for further analysis. The identified proteins were then submitted to Pfam (see text footnote 2), SMART,[3] and NCBI conserved domains search tool[4] to further check the receiver domain as well as other conserved domains. The protein sequence of RRs in wheat, *Arabidopsis*, and rice was used to carry out multiple sequence

1 https://plants.ensembl.org/index.html
2 https://pfam.xfam.org
3 http://smart.embl.de/
4 https://www.ncbi.nlm.nih.gov/Structure/cdd/wrpsb.cgi

alignment using ClustalX 2.1 software (Larkin et al., 2007). The phylogenetic tree was established using MEGA 7.0 based on the neighbor-joining (NJ) method with 1,000 bootstrap replicates (Kumar et al., 2016), and RRs were named according to the standard nomenclature for the plant TCS elements (Heyl et al., 2013).

Characterization of *TaRRAs*

Information about the *TaRRA* gene family, such as chromosomal localization, number of exons, and cDNA and protein length, was obtained from the EnsemblPlants. The protein sequence of TaRRAs was analyzed in the Expasy server[5] to obtain the theoretical isoelectric point (PI) and molecular weight (MW).

Gene structure and motif analysis of *TaRRAs*

The gene structure of *TaRRAs* was constructed by the gene structure display server (GSDS 2.0[6]) using the coding sequence (CDS) and corresponding genomic sequence retrieved from the EnsemblPlants database. Conserved motifs of TaRRAs were predicted using the Multiple Em for Motif Elicitation (MEME 5.4.1[7]), with the following parameters: maximum number of 10 motifs and optimum motif widths of 6-50 residues.

Collinearity relationship of *TaRRAs*

The wheat genomic sequence and genome annotation files downloaded from the EnsemblPlants database were used to generate a graph of chromosomal location and collinearity relationship of *TaRRAs* by TBtools software (Chen et al., 2020). The synteny relationship of *RRAs* between wheat and rice was constructed using the Dual Systeny Plot for MCscanX.[8]

Cis-acting elements analysis of *TaRRAs*

The promoter region, 1,500 bp upstream of the initiation code (ATG), of all of the *TaRRAs*, was obtained from the EnsemblPlants database and the *cis*-acting regulatory elements were predicted by PlantCARE.[9]

5 https://web.expasy.org/compute_pi/
6 http://gsds.gao-lab.org/
7 https://meme-suite.org/meme/tools/meme
8 https://github.com/CJ-Chen/TBtools
9 http://bioinformatics.psb.ugent.be/webtools/plantcare/html/

Gene expression analysis of *TaRRAs*

The expression data in various tissues were downloaded from the WheatOmics 1.0 (Ma et al., 2021). The transcripts per million (TPM) values were used to create a heat map by using Heatmap (see text footnote 8).

Jimai325, a high-yielding and water-saving wheat variety cultivated by our lab, was used for qRT-PCR analysis. Ten-day-old hydroponically grown seedlings were exposed to 50 μM 6-BA, 20% PEG-6000 (drought stress), 200 mM NaCl (salt stress), 4°C (cold stress), or 40°C (heat stress) for 0, 1, 3, 6, 12, and 24 h, and samples were then collected. Total RNA was isolated using TRNzol Universal reagent (TIANGEN) according to the manufacturer's instructions, and 1 μg of total RNA was used as the template for cDNA synthesis. Real-time PCR was subsequently performed to quantify the cDNA using SYBR Premix Ex Taq (TaKaRa) in a CFX96^{TM} real-time PCR detection system (BIO-RAD). *TaActin* was used as an internal control to normalize all data. The primers used were listed in **Supplementary Table 1**.

Results

Identification and classification of *TaRRA* genes in wheat

The wheat-specific HMM file for the response regulator receiver domain was aligned with the whole protein sequences in wheat, and 151 non-redundant *TaRR* genes in wheat were identified after receiver domain confirmation. An unrooted phylogenetic tree was generated by using the conserved receiver domain and incorporating the well-established family members from *Arabidopsis* and rice for the subfamily classification of *TaRR*s (**Figure 1**; Heyl et al., 2013). To confirm the subfamily classification, the protein sequences of all TaRRs were further analyzed for conserved domains, including the receiver domain, Myb-like DNA binding domain of RRBs, and CCT domain of PRRs. Among the 151 *TaRR* genes, there were 20 *TaRRAs*, 71 *TaRRBs*, 43 *TaRRCs*, and 17 *TaPRRs* (**Supplementary Table 2**), and each type of *TaRR* gene in wheat was found to be more abundant than the corresponding type of *RR* genes in *Arabidopsis* and rice (**Table 1**).

Further phylogenetic analysis using the full-length protein sequence of type-A RRs in wheat clustered the 20 *TaRRA* genes into eight homologous groups (**Figure 2A**), which were named *TaRRA1* to *TaRRA8*. *TaRRA1*, *2*, *3*, *6*, and *7* had three orthologous genes (*TaRRA1-A/B/D*, *TaRRA2-A/B/D*, *TaRRA3-A/B/D*, *TaRRA6-A/B/D*, and *TaRRA7-A/B/D*), while *TaRRA4* and *8* contained two orthologous genes (*TaRRA4-B/D* and *TaRRA8-A/D*) and *TaRRA5* possessed only one gene copy (*TaRRA5-B*). All the proteins encoded by

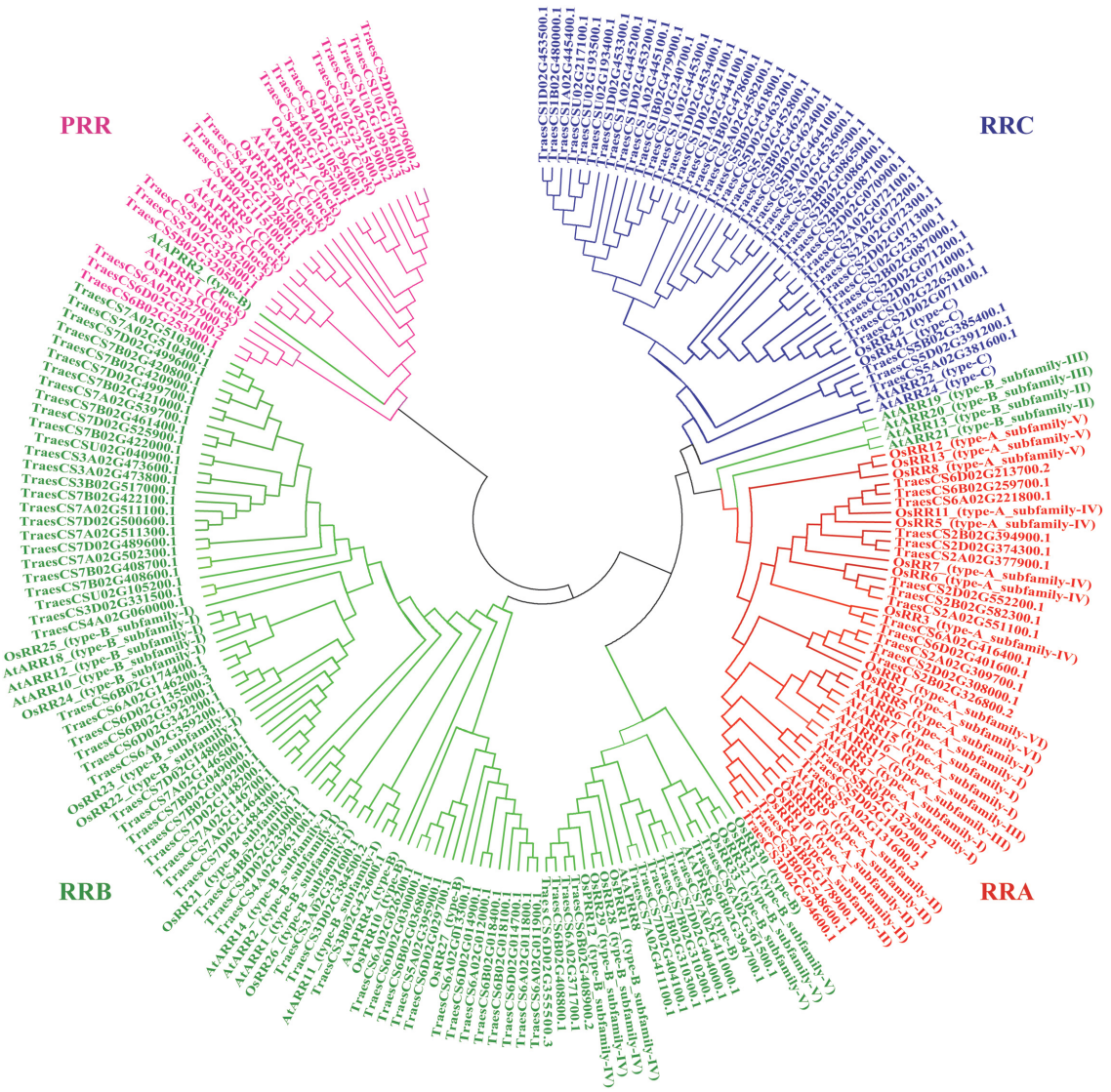

FIGURE 1
Phylogenetic analysis of RR proteins among the wheat, *Arabidopsis*, and rice. All RR proteins were allocated into four clades. Red, green, blue, and pink represent RRA, RRB, RRC, and PRR, respectively. The unrooted tree was established by the neighbor-joining method using the MEGA7.0 software with 1,000 bootstrap replicates.

TaRRA genes varied from 108 to 269 amino acids with predicted molecular weights (MW) ranging from 12.22 to 28.89 kDa and the isoelectric points (PI) ranging from 5.05 to 8.48 (Table 2).

Gene structure and conserved motifs of *TaRRAs*

To gain further insights into the *TaRRA* gene members, we surveyed the gene structure and conserved motifs of each *TaRRA*. Although the lengths of genomic DNA varied from 859 to 3,709 bp in different *TaRRAs*, orthologous genes at each *TaRRA* locus usually had similar genomic DNA lengths. For instance, genomic DNA length of *TaRRA7-A*, *TaRRA7-B*, and *TaRRA7-D* was 888, 859, and 932 bp, respectively, while genomic DNA length of *TaRRA4-B* and *TaRRA4-D* was 3,709 and 3,604 bp, respectively (Figure 2B). Additionally, the number of exons, ranging from 2 to 6 in different *TaRRAs*, was generally the same in orthologous genes at each *TaRRA* locus. For example, *TaRRA3-A*, *TaRRA3-B*, and *TaRRA3-D* all harbored 2 exons, while *TaRRA1-A*, *TaRRA1-B*, and *TaRRA1-D* all contained 6 exons (Figure 2B and Table 2).

Using the MEME tool to predict the conserved protein motifs of the TaRRA family, 10 conversed motifs were identified (Figure 2C and Supplementary Table 3). Except for TaRRA5-B

10.3389/fpls.2022.1006409

TABLE 1 Summary of the RR superfamily in wheat, *Arabidopsis*, and rice.

Classification	Wheat	*Arabidopsis*	Rice
RRA	20	10	13
RRB	71	14	16
RRC	43	2	2
PRR	17	5	5
RR (for potential new clades)	0	1	0
Total	151	32	36

and TaRRA7-A, all TaRRAs contained motif 1, motif 2, motif 3, and motif 4. Additionally, TaRRA1-A, TaRRA1-B, and TaRRA1-D also possessed motif 5 and motif 8 (both unique in this group). TaRRA3-A, TaRRA3-B, and TaRRA3-D also had motif 6, while TaRRA4-B and TaRRA4-D had an added motif 9. TaRRA6-A, TaRRA6-B, and TaRRA6-D additionally contained motif 6, motif 7 (unique in this group), and motif 9. Likewise, TaRRA8-A and TaRRA8-D had motif 10 (unique in this group). In addition, all TaRRAs contained the highly conserved Lys and two Asp residues (D-D-K) in the receiver domain, except for TaRRA5-B and TaRRA7-A, which lacked the Lys and the first Asp respectively (**Supplementary Figure 1**). It is worth mentioning that all the 20 TaRRAs contained the predicted Asp phosphorylation site (the second Asp in the conserved D-D-K motif), which was embedded in a conserved TDY sequence. The above results indicate that orthologous *TaRRA* genes in the A, B, and D wheat subgenomes were usually similar in gene structure and encoding protein motifs, suggesting that *TaRRA* genes were conserved during evolution.

Chromosomal distribution and synteny analysis of *TaRRAs*

Chromosomal localization analysis showed that the 20 *TaRRA* genes were unevenly distributed on 12 of the 21 wheat chromosomes (**Figure 3**), with the number of *TaRRA* genes on each chromosome ranging from 1 (3B, 3D, 4B, 5A, 5B, 5D, and 6B) to 3 (2A, 2B, and 2D). Chromosomal group II harbored 9 (45.0%) *TaRRA* genes, the largest number, followed by chromosomal groups VI, V, III, and IV, which contained 5 (25.0%), 3 (15.0%), 2 (10.0%), and 1 (5.0%) *TaRRA* genes, respectively (**Figure 3**). Whereas, there was no *TaRRA*

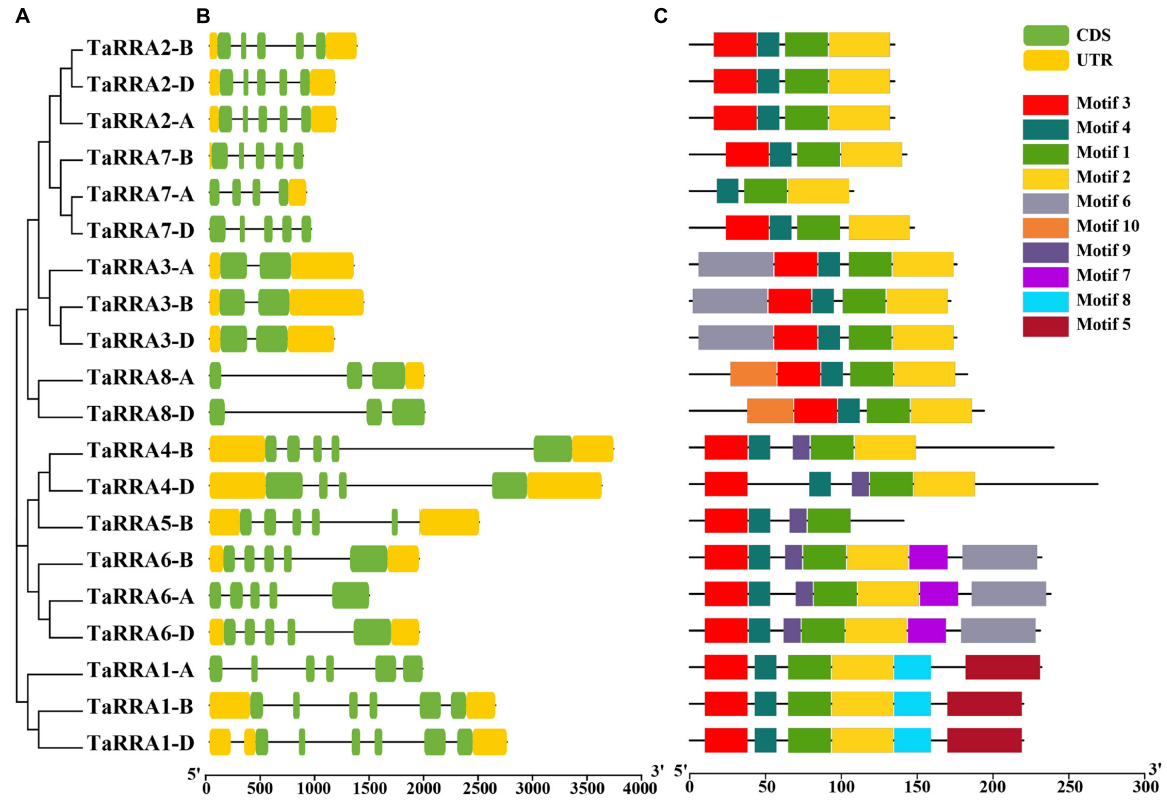

FIGURE 2
Phylogenetic analysis, gene structure, and conserved motifs of TaRRAs. **(A)** The phylogenetic tree was constructed based on the full-length amino acid sequence of TaRRAs. **(B)** Gene structure analysis of *TaRRA* genes. Yellow boxes represent UTR regions; green boxes indicate exons; black lines represent introns. **(C)** Conserved domain structures identified in the TaRRAs. Different color boxes show different motifs.

TABLE 2 Information of the *TaRRA* gene members in wheat.

Gene name	ID	Chromosome location	Exon	cDNA (bp)	Protein (aa)	MW (kDa)	PI
TaRRA1-A	TraesCS2A02G309700.1	2A:532865797-532867753	6	699	232	25.49	6.74
TaRRA1-B	TraesCS2B02G326800.2	2B:467870720-467873343	6	1,305	220	24.09	8.48
TaRRA1-D	TraesCS2D02G308000.1	2D:394798248-394800977	6	1,276	220	24.06	8.48
TaRRA2-A	TraesCS2A02G377900.1	2A:620212372-620213537	5	728	135	14.72	7.77
TaRRA2-B	TraesCS2B02G394900.1	2B:559553430-559554782	5	768	135	14.72	7.77
TaRRA2-D	TraesCS2D02G374300.1	2D:477627271-477628424	5	735	135	14.72	7.77
TaRRA3-A	TraesCS2A02G551100.1	2A:758102501-758103826	2	1,210	176	19.12	5.90
TaRRA3-B	TraesCS2B02G582300.1	2B:769949352-769950767	2	1,293	172	18.72	5.50
TaRRA3-D	TraesCS2D02G552200.1	2D:627582838-627583982	2	1,061	176	19.12	5.90
TaRRA4-B	TraesCS3B02G548600.1	3B:784040014-784043723	5	1,616	240	25.90	5.33
TaRRA4-D	TraesCS3D02G494600.1	3D:587200633-587204237	4	2,013	269	28.89	5.88
TaRRA5-B	TraesCS4B02G178900.1	4B:392001595-392004069	6	1,248	141	15.36	5.55
TaRRA6-A	TraesCS5A02G131600.2	5A:296468274-296469739	5	717	238	26.24	5.61
TaRRA6-B	TraesCS5B02G132900.2	5B:247665062-247666984	5	1,116	232	25.36	5.14
TaRRA6-D	TraesCS5D02G140200.1	5D:223887585-223889509	5	1,088	231	25.36	5.05
TaRRA7-A	TraesCS6A02G221800.1	6A:412848604-412849492	4	493	108	12.22	6.58
TaRRA7-B	TraesCS6B02G259700.1	6B:469707108-469707967	5	451	143	15.39	7.88
TaRRA7-D	TraesCS6D02G213700.2	6D:303981610-303982542	5	447	148	15.91	5.85
TaRRA8-A	TraesCS6A02G416400.1	6A:615462243-615464213	3	727	183	20.10	6.31
TaRRA8-D	TraesCS6D02G401600.1	6D:470632933-470634909	3	585	194	21.29	8.45

gene located in the rest two chromosomal groups (I and VII). Collinear relationship displayed the homology between *TaRRAs* (**Figure 3**), which was consistent with the phylogenetic analysis (**Figure 2**).

Synteny analysis between the wheat and rice was conducted and 30 orthologous *RRA* gene pairs were found (**Figure 4** and **Supplementary Table 4**), with a close similarity to the phylogenetic analysis (**Figure 1**), indicating that these syntenic gene pairs were relatively conserved during the evolution of gramineous species.

Prediction of *Cis*-acting regulatory elements in the promoter of *TaRRAs*

The *cis*-acting elements in the promoter region play important roles in gene transcription regulation. The *RRAs* are cytokinin response genes that are targets of RRB transcription factors in *Arabidopsis* (To et al., 2004). Therefore, the 1,500 bp DNA sequence upstream of *TaRRAs* was analyzed for BA-dependent (+BA) and BA-independent (-BA) RRB binding *cis*-acting elements (**Figure 5A** and **Supplementary Table 5**; Xie et al., 2018). Both the BA-dependent and BA-independent RRB binding *cis*-acting elements were distributed widely throughout all of the *TaRRA* genes, suggesting that transcription of *TaRRAs* was probably regulated in part by RRBs.

To fully understand the potential role of *TaRRAs*, the 1,500 bp promoter region of *TaRRAs* was further analyzed in the PlantCARE database for more *cis*-acting elements. A total of 43 types of *cis*-acting elements with known functions were identified in the *TaRRAs* promoter region, which were divided into three different categories, i.e., growth and development response elements, biotic/abiotic stress response elements, and phytohormone response elements (**Figure 5B** and **Supplementary Tables 6, 7**). Among the growth and development response *cis*-elements, CAAT-box (common *cis*-acting element in promoter and enhancer regions) and TATA-box (core promoter element around -30 of transcription start) were highly enriched in all the *TaRRA* promoters. In addition, O2-site involved in zein metabolism regulation, RY-element involved in seed-specific regulation, and CAT-box related to meristem expression were identified in some of the *TaRRA* promoters. Among the biotic/abiotic stress response *cis*-elements, the proportion of light-response elements was large, including 19 *cis*-regulatory factors, such as G-box, Sp1, and TCCC-motif. Additionally, ARE and GC-motif involved in anaerobic induction and LTR and MBS elements involved in low-temperature and drought responsiveness, respectively, were found in several *TaRRA* promoters. In the phytohormone response category, ABRE in ABA response and CGTCA-motif and TGACG-motif in MeJA response were distributed in most of the *TaRRA* promoters. Moreover, GARE-motif, P-box, and TATC-box implicated in gibberellin response, AuxRR-core and TGA-element in auxin response, and TCA-element in salicylic acid response were also distributed in several *TaRRA* promoters. The presence of different numbers and types of *cis*-acting

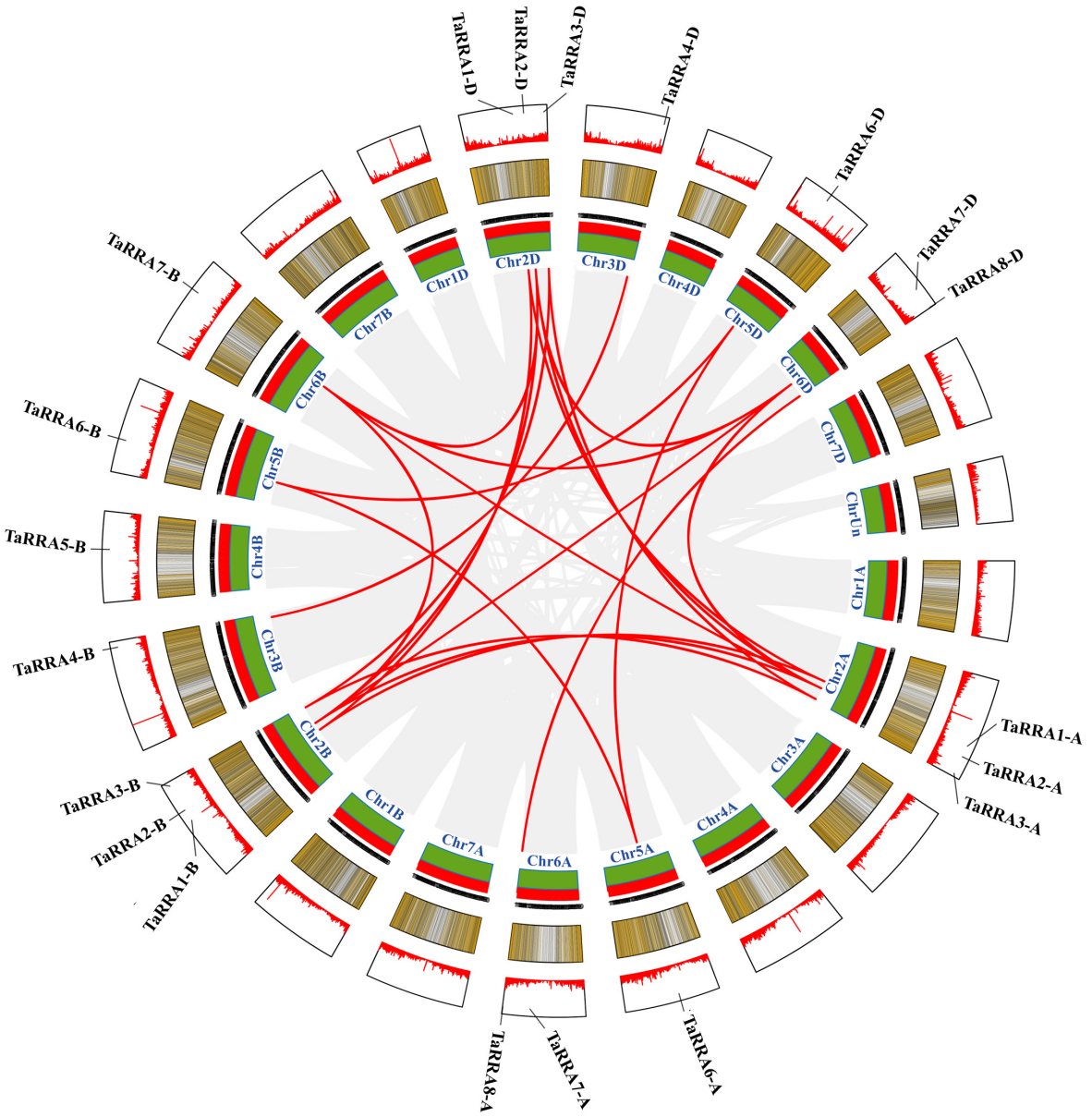

FIGURE 3
Schematic diagram of the inter-chromosomal relationships of *TaRRA* genes. Gray lines indicate all syntenic blocks in the wheat genome, and red lines indicate the presence of *TaRRA* genes.

elements in *TaRRA* promoters indicates that these genes may be involved in different regulatory mechanisms.

Expression pattern of *TaRRAs* in different tissues and response to cytokinin

To characterize the expression profiles of the *TaRRA* gene family, we analyzed the RNA-seq data downloaded from the WheatOmics 1.0 (Ma et al., 2021). Notably, *TaRRA2-A/B/D* and *TaRRA7-A/B/D* were hardly detected in any of the tissues tested, while other *TaRRAs* showed relatively high expression in the root, except for *TaRRA1-A/B/D* with higher expression in the stem (**Figure 6A**).

Since most of the *RRAs* are rapidly induced by exogenous cytokinin in monocots and dicots (D'Agostino et al., 2000; Jain et al., 2006), we investigated the expression profiles of *TaRRAs* in response to cytokinin treatment by qRT-PCR (**Figure 6B**). In the root, 10 out of 13 detectable *TaRRAs* were up-regulated after 1 h BA treatment and displayed an increasing expression trend afterward. Most of the *TaRRAs* reached maximal induction

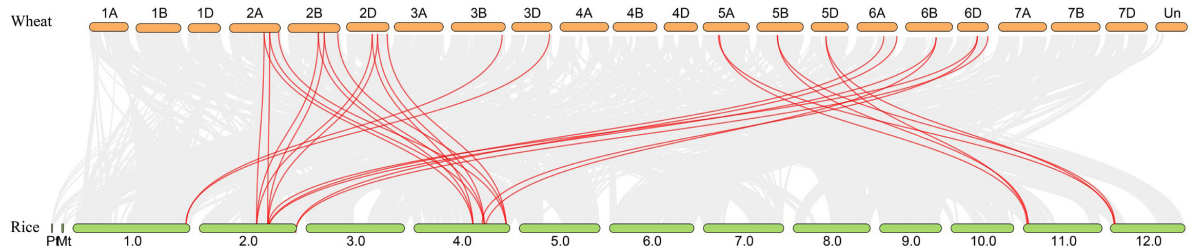

FIGURE 4
Synteny analysis of *RRA* genes in wheat and rice. Gray lines in the background indicate all syntenic blocks within the two genomes, while red lines highlight the syntenic *RRA* gene pairs.

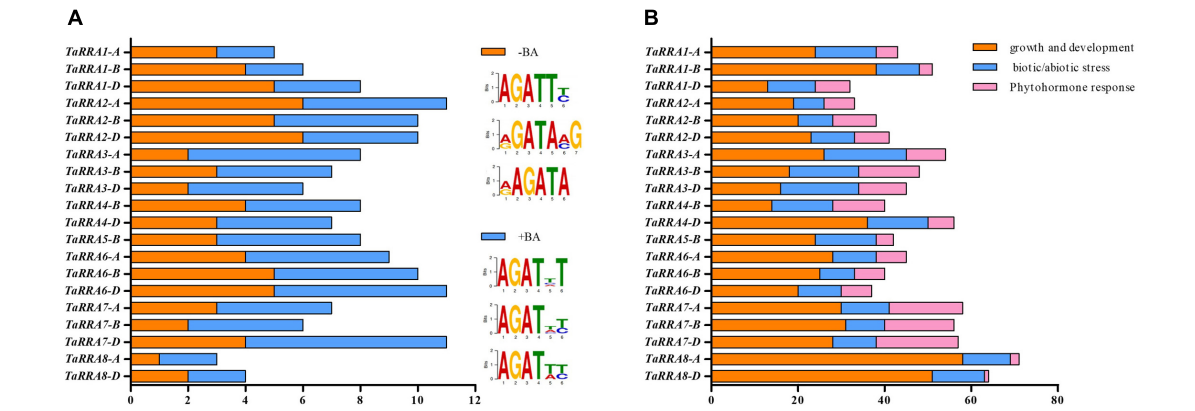

FIGURE 5
Prediction of *cis*-acting elements in the promoter region of *TaRRAs*. **(A)** BA-dependent (+BA) and BA-independent (-BA) RRB binding *cis*-acting elements in the promoter of *TaRRAs*. **(B)** Growth and development, biotic/abiotic stress, and phytohormone responses *cis*-acting elements in the promoter of *TaRRAs*.

at 12 h, except for *TaRRA5-B* and *TaRRA6-A*, which were maximally induced at 6 h, and *TaRRA1-B*, *TaRRA4-D*, and *TaRRA8-D*, which were maximally induced at 24 h. Although all the 13 detectable *TaRRAs* were cytokinin-induced, their fold-change varied greatly after BA treatment, ranging from 2.6 (*TaRRA5-B*, 6 h) to 47.3 (*TaRRA1-D*, 12 h) times compared with the control (0 h). It is worth noting that expression levels of orthologous genes at each *TaRRA* locus could differ significantly after BA treatment. For instance, *TaRRA1-D* was up-regulated by 47.3 times at 12 h, whereas *TaRRA1-A* was up-regulated by 5.5 times. In the leaf, 9 out of 13 detectable *TaRRAs* displayed an obvious increase in the transcription level after 6 h BA treatment and showed maximal induction at 12 h. However, there was no increase in the transcription levels of *TaRRA5-B* and *TaRRA8-A*, and a decrease was observed in the transcription levels of *TaRRA1-A* and *TaRRA8-D*. The above results showed that most *TaRRAs* responded more rapidly and strongly to BA treatment in the root than that in the leaf. However, we could hardly detect the expression of *TaRRA2-A/B/D* and *TaRRA7-A/B/D* by qRT-PCR, which was consistent with previous RNA-seq data (Figure 6A).

Expression pattern of *TaRRAs* under different stresses

To further evaluate the potential function of *TaRRAs* in response to abiotic stress, the *TaRRA* gene expression patterns were analyzed by qRT-PCR under drought, salt, cold, and heat stress treatments (Figures 7, 8). The results showed that under drought stress, the expression levels of *TaRRA1-B*, *TaRRA3-B*, *TaRRA3-D*, *TaRRA4-D*, and *TaRRA8-A* decreased continuously from 0 to 6 h and later increased marginally at 12 and 24 h (Figure 7A). *TaRRA8-D* was exclusively up-regulated by drought stress, while the expression of the rest of the *TaRRAs* showed insignificant changes under drought stress. Under salt stress, the expression levels of most *TaRRAs* were up-regulated at least at one time point (Figure 7B). Notably, *TaRRA1-D*, *TaRRA3-D*, *TaRRA6-B*, and *TaRRA6-D* were induced at each time point compared with the control (0 h). Inversely, *TaRRA5-B* was gradually down-regulated by salt stress. Under cold stress, the expression of 8 *TaRRAs* increased after 6 h treatment, among which the expression of *TaRRA1-D*, *TaRRA4-B*, *TaRRA6-A*, *TaRRA6-B*, and *TaRRA6-D* continued to increase till 12 h,

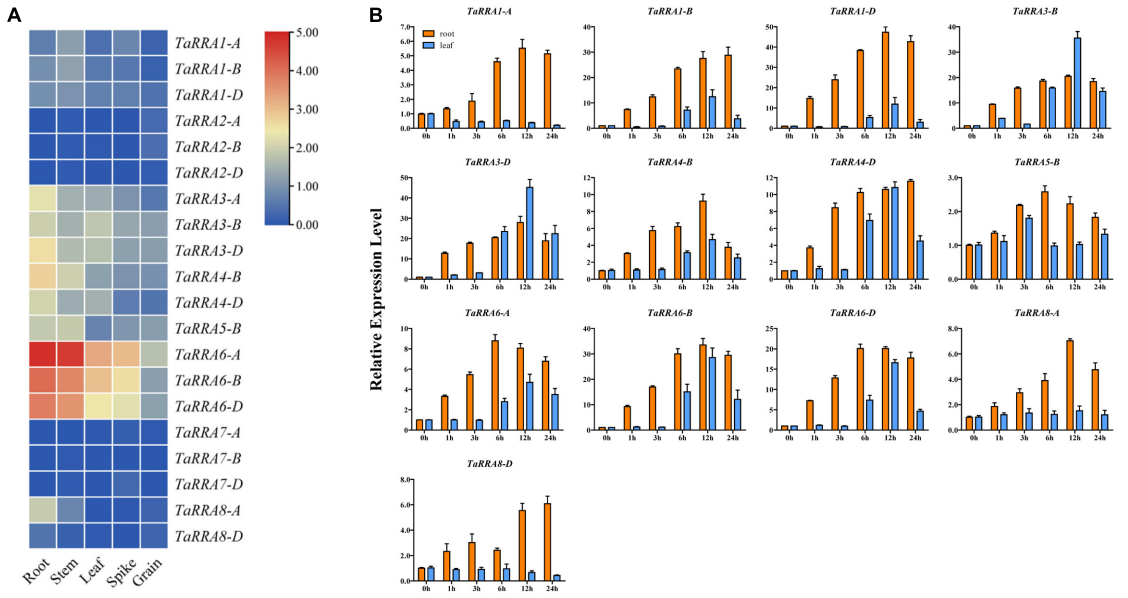

FIGURE 6
Expression analysis of *TaRRA* genes. **(A)** Expression profiles of *TaRRA* genes in various tissues. The RNA-sequence data was obtained from leaf, root, stem, spike, and grain of Chinese Spring (International Wheat Genome Sequencing Consortium [IWGSC], 2014). **(B)** Quantitative RT-PCR analysis of *TaRRA* genes in response to cytokinin treatment. Leaves and roots of 10-day-old seedlings were sampled after 50 μM 6-BA treatment for 0, 1, 3, 6, 12, and 24 h. The data are given as means ± SE of three biological replicates.

whereas the expression of *TaRRA3-B*, *TaRRA3-D*, and *TaRRA8-D* was reduced subsequently (**Figure 8A**). Heat significantly inhibited the expression of most *TaRRAs* after 3 h treatment, except for that of *TaRRA8-A* and *TaRRA8-D*, which increased after 1 h treatment (**Figure 8B**).

It is worth noting that some orthologous genes at each *TaRRA* locus (*TaRRA3-B/D* and *TaRRA6-A/B/D*) exhibited similar expression patterns in response to abiotic stress, indicating that they may have similar biological functions under stress conditions. On the contrary, *TaRRA8-A* and *TaRRA8-D* showed different expression patterns under drought and cold stress, suggesting that they could play different roles under some abiotic stresses. In general, all the *TaRRAs* showed significant changes in response to at least one abiotic stress.

Discussion

RRAs are rapidly induced by exogenous cytokinin and are thus considered to be primary cytokinin response genes (D'Agostino et al., 2000; Jain et al., 2006). The *RRA* gene family, a subfamily of the *RR* gene family, is relatively small in higher plants, with only 10, 13, 21, and 18 members in *Arabidopsis*, rice, maize, and soybean, respectively (Mochida et al., 2010; Chu et al., 2011; Heyl et al., 2013). In this study, we performed a systematic genome-wide analysis of the wheat *RRA* gene family by combining two different approaches. First, we performed phylogenetic analysis by using the conserved receiver domain of 151 TaRRs, and simultaneously adding the well-established family members from *Arabidopsis* and rice into the analysis (**Figure 1**; Heyl et al., 2013). Second, we analyzed the conserved domains of all the TaRRs to further confirm whether they contain a Myb-like DNA binding domain or a CCT domain in addition to the receiver domain. We used the protein sequence of the longest transcript of each TaRR for domain analysis to avoid domain missing of the shorter transcript. According to the above method, we identified 20 *RRAs*, 71 *RRBs*, 43 *RRCs*, and 17 *PRRs* from the wheat reference genome (**Table 1**). However, in a previous study, 41 *RRAs*, 2 *RRBs*, and 2 *PRRs* have been identified in wheat (Gahlaut et al., 2014). Given that RRAs only carry a receiver domain, while RRBs contain an additional Myb-like DNA binding domain and PRRs have an extra CCT domain, some truncated RRBs and PRRs may be identified as RRAs due to the earlier incomplete wheat reference genome. In recent years, great progress has been made in genome sequencing, assembly, and annotation of wheat (International Wheat Genome Sequencing Consortium [IWGSC], 2018; Alonge et al., 2020; Zhu et al., 2021), which provides a high-quality reference genome for the study of the *TaRRA* gene family. The 20 *TaRRA* genes belonging to 8 homologous groups were unequally distributed on 12 wheat chromosomes (**Figure 3**). As wheat is an allohexaploid (AABBDD), most *TaRRA* genes had homologs in the A, B, and D subgenomes due to polyploidization, sharing similar gene structures and protein motifs within the homologous group (**Figure 2**).

10.3389/fpls.2022.1006409

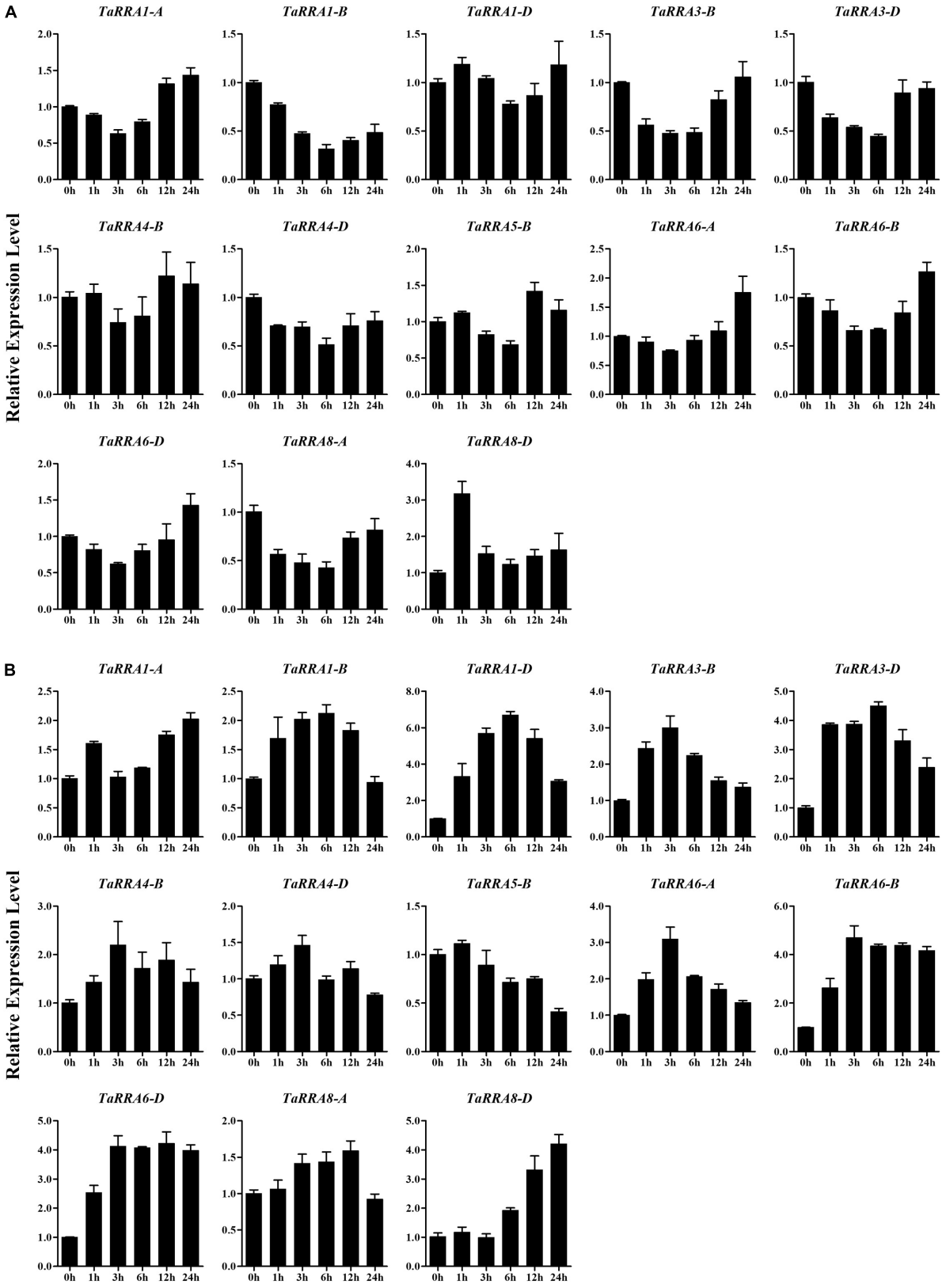

FIGURE 7
Quantitative RT-PCR analysis of *TaRRA* genes under drought and salt stress. Roots of 10-day-old seedlings were sampled after 0, 1, 3, 6, 12, and 24 h drought stress **(A)** and salt stress **(B)**. The data are given as means ± SE of three biological replicates.

10.3389/fpls.2022.1006409

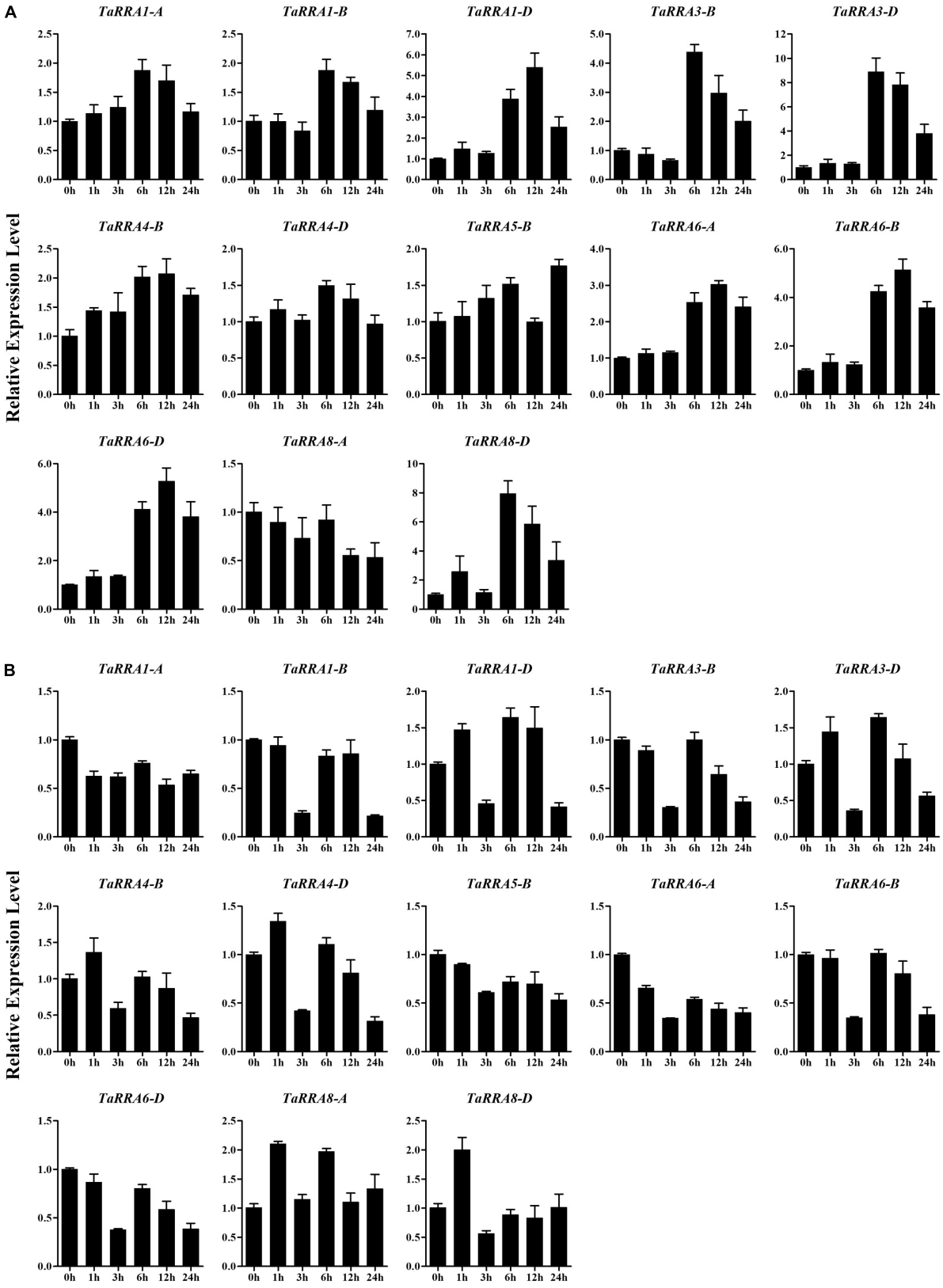

FIGURE 8
Quantitative RT-PCR analysis of *TaRRA* genes under cold and heat stress. Roots of 10-day-old seedlings were sampled after 0, 1, 3, 6, 12, and 24 h cold stress **(A)** and heat stress **(B)**. The data are given as means ± SE of three biological replicates.

Most of the *RRAs* are rapidly induced by exogenous cytokinin in plants (D'Agostino et al., 2000; Asakura et al., 2003; Jain et al., 2006). Consistent with previous results, the transcription levels of most detectable *TaRRAs* displayed an obvious increase after BA treatment in both the root and leaf (**Figure 6B**). However, the transcripts of most *TaRRAs* reached a maximal induction at 12 h cytokinin treatment, while most *RRAs* in *Arabidopsis* and rice showed maximal induction within 1 h cytokinin treatment and then gradually declined (D'Agostino et al., 2000; Jain et al., 2006). Although *TaRRA1-A*, *TaRRA5-B*, *TaRRA8-A*, and *TaRRA8-D* were induced by cytokinin in the root, their transcription levels were unchanged or even decreased in the leaf after cytokinin treatment (**Figure 6B**), indicating their potential function differentiation between root and leaf. Similarly, there is no significant change in the transcript abundance of a few *RRAs* in *Arabidopsis* and rice following cytokinin treatment, including *ARR8*, *ARR9*, *OsRR3*, and *OsRR8* (D'Agostino et al., 2000; Jain et al., 2006). The rapid induction of *RRAs* by exogenous cytokinin has been shown to mediate a feedback mechanism, probably by competing with RRBs for the phosphotransfer from HPs. Phosphorylation of RRAs increases their protein stability (To et al., 2007), whereas phosphorylation of RRBs enables them to bind to DNA, thus initiating transcription of downstream targets (Kim et al., 2006; Zubo et al., 2017). Double and higher-order type-A *arr* mutants, rather than the single *arr* mutants, show increasing sensitivity to cytokinin, indicating that RRAs act as negative regulators of cytokinin signaling with partially redundant functions (To et al., 2007).

Cytokinin signaling components are widely involved in plant response to abiotic stress. A series of *Arabidopsis* mutants, including *ahk2,3*, *ahp2,3,5*, and *arr1,10,12*, show significantly increased drought and salt tolerance, indicating that HKs, HPs, and RRBs are negative regulators of these stress responses (Tran et al., 2007; Nishiyama et al., 2013; Nguyen et al., 2016; Abdelrahman et al., 2021). In contrast, plants overexpressing *ARR5* exhibit enhanced drought tolerance, suggesting that type-A ARR5 is a positive regulator of drought tolerance (Huang et al., 2018). Functional analysis of the single and double *ahk* mutants indicates that HKs function partially redundantly as negative regulators of the cold stress adaptation response (Jeon et al., 2010). However, type-B ARR1 is a positive factor in cold signaling, because *arr1* shows reduced cold resistance, whereas *ARR1* overexpression increases plant cold resistance (Jeon and Kim, 2013). Additionally, RRAs also play important roles in cold stress signaling (Jeon et al., 2010; Shi et al., 2012).

Given that the expression pattern of genes has a correlation with its function, we monitored the expression profiles of *TaRRA* family members under multiple stresses. Drought stress reduced the expression of *TaRRA1-B*, *TaRRA3-B*, *TaRRA3-D*, *TaRRA4-D*, and *TaRRA8-A*, but induced the expression of *TaRRA8-D* (**Figure 7A**). Similarly, drought stress reduces the expression of *ARR8* and *ARR17*, whereas induces the expression of *ARR5*, *ARR7*, and *ARR15* in *Arabidopsis* (Kang et al., 2012). We identified 8 *TaRRAs* with significantly up-regulated expression under cold stress (**Figure 8A**), which is consistent with the cold-induced changes in *ARR5*, *ARR6*, *ARR7*, and *ARR15* expression in *Arabidopsis* (Jeon et al., 2010). Furthermore, overexpression of *ARR5*, *ARR7*, and *ARR15* enhances the freezing tolerance of plants, while *arr5*, *arr6*, and *arr7* also lead to higher freezing tolerance (Jeon et al., 2010; Shi et al., 2012). These different results suggest the complexity of the molecular mechanism involved and hence further research is warranted. In addition, a considerable number of *TaRRAs* were shown to respond to salt and heat stress (**Figures 7B**, **8B**), suggesting that they are promising regulators for salt and heat response in wheat. *TaRRA3-B/D*, orthologs of drought and salt positive regulator *OsRR6*, and *TaRRA6-A/B/D*, orthologs of salt negative regulator *OsRR9* and *OsRR10* (**Supplementary Table 4**), showed responses to salt, cold, and heat stress, which may be important candidate genes for genetic improvement of stress tolerance in wheat.

In conclusion, this study provided comprehensive insights into the *TaRRA* gene family in wheat. The systematical identification and investigation of the *TaRRA* gene family will inevitably contribute to further elucidation of the biological function and genetic improvement application of *TaRRAs* in wheat.

Data availability statement

The original contributions presented in this study are included in the article/**Supplementary material**, further inquiries can be directed to the corresponding authors.

Author contributions

HL and YJZ designed the experiments. LS, LL, JZ, MH, YLZ, YZ, XT, PW, QL, and XC performed the experiments and analyzed the data. LS and LL wrote the manuscript. All authors reviewed and approved the manuscript.

Funding

This work was funded by the S&T Program of Hebei (C2019301089 and 20326345D), the HAAFS Science and Technology Innovation Special Project (2022KJCXZX-LYS-1), the Basic Research Funds of Hebei Academy of Agriculture and Forestry Sciences (2018060304), the Hebei Modern Agricultural Industrial Technology System (HBCT2018010201), and the Project for Hebei Scientific and Technological Innovation Team of Modern Wheat Seed Industry (21326318D).

Conflict of interest

The authors declare that the research was conducted in the absence of any commercial or financial relationships that could be construed as a potential conflict of interest.

Publisher's note

All claims expressed in this article are solely those of the authors and do not necessarily represent those of their affiliated organizations, or those of the publisher, the editors and the reviewers. Any product that may be evaluated in this article, or claim that may be made by its manufacturer, is not guaranteed or endorsed by the publisher.

Supplementary material

The Supplementary Material for this article can be found online at: https://www.frontiersin.org/articles/10.3389/fpls.2022.1006409/full#supplementary-material

References

Abdelrahman, M., Nishiyama, R., Tran, C. D., Kusano, M., Nakabayashi, R., Okazaki, Y., et al. (2021). Defective cytokinin signaling reprograms lipid and flavonoid gene-to-metabolite networks to mitigate high salinity in *Arabidopsis*. *Proc. Natl. Acad. Sci. U.S.A.* 118:e2105021118. doi: 10.1073/pnas.2105021118

Alonge, M., Shumate, A., Puiu, D., Zimin, A. V., and Salzberg, S. L. (2020). Chromosome-scale assembly of the bread wheat genome reveals thousands of additional gene copies. *Genetics* 216, 599–608. doi: 10.1534/genetics.120.303501

Argueso, C. T., Raines, T., and Kieber, J. J. (2010). Cytokinin signaling and transcriptional networks. *Curr. Opin. Plant Biol.* 13, 533–539. doi: 10.1016/j.pbi.2010.08.006

Argyros, R. D., Mathews, D. E., Chiang, Y. H., Palmer, C. M., Thibault, D. M., Etheridge, N., et al. (2008). Type B response regulators of *Arabidopsis* play key roles in cytokinin signaling and plant development. *Plant Cell* 20, 2102–2116. doi: 10.1105/tpc.108.059584

Asakura, Y., Hagino, T., Ohta, Y., Aoki, K., Yonekura-Sakakibara, K., Deji, A., et al. (2003). Molecular characterization of His-Asp phosphorelay signaling factors in maize leaves: Implications of the signal divergence by cytokinin-inducible response regulators in the cytosol and the nuclei. *Plant Mol. Biol.* 52, 331–341. doi: 10.1023/a:1023971315108

Bhaskar, A., Paul, L. K., Sharma, E., Jha, S., Jain, M., and Khurana, J. P. (2021). OsRR6, a type-A response regulator in rice, mediates cytokinin, light and stress responses when over-expressed in *Arabidopsis*. *Plant Physiol. Biochem.* 161, 98–112. doi: 10.1016/j.plaphy.2021.01.047

Chen, C., Chen, H., Zhang, Y., Thomas, H. R., Frank, M. H., He, Y., et al. (2020). TBtools: An integrative toolkit developed for interactive analyses of big biological data. *Mol. Plant* 13, 1194–1202. doi: 10.1016/j.molp.2020.06.009

Chu, Z. X., Ma, Q., Lin, Y. X., Tang, X. L., Zhou, Y. Q., Zhu, S. W., et al. (2011). Genome-wide identification, classification, and analysis of two-component signal system genes in maize. *Genet. Mol. Res.* 10, 3316–3330. doi: 10.4238/2011.December.8.3

D'Agostino, I. B., Deruère, J., and Kieber, J. J. (2000). Characterization of the response of the *Arabidopsis* response regulator gene family to cytokinin. *Plant Physiol.* 124, 1706–1717. doi: 10.1104/pp.124.4.1706

El-Showk, S., Ruonala, R., and Helariutta, Y. (2013). Crossing paths: Cytokinin signalling and crosstalk. *Development* 140, 1373–1383. doi: 10.1242/dev.086371

Gahlaut, V., Mathur, S., Dhariwal, R., Khurana, J. P., Tyagi, A. K., Balyan, H. S., et al. (2014). A multi-step phosphorelay two-component system impacts on tolerance against dehydration stress in common wheat. *Funct. Integr. Genomics* 14, 707–716. doi: 10.1007/s10142-014-0398-8

Ha, S., Vankova, R., Yamaguchi-Shinozaki, K., Shinozaki, K., and Tran, L. S. (2012). Cytokinins: Metabolism and function in plant adaptation to environmental stresses. *Trends Plant Sci.* 17, 172–179. doi: 10.1016/j.tplants.2011.12.005

Heyl, A., Brault, M., Frugier, F., Kuderova, A., Lindner, A. C., Motyka, V., et al. (2013). Nomenclature for members of the two-component signaling pathway of plants. *Plant Physiol.* 161, 1063–1065. doi: 10.1104/pp.112.213207

Hosoda, K., Imamura, A., Katoh, E., Hatta, T., Tachiki, M., Yamada, H., et al. (2002). Molecular structure of the GARP family of plant Myb-related DNA binding motifs of the *Arabidopsis* response regulators. *Plant Cell* 14, 2015–2029. doi: 10.1105/tpc.002733

Huang, X., Hou, L., Meng, J., You, H., Li, Z., Gong, Z., et al. (2018). The antagonistic action of abscisic acid and cytokinin signaling mediates drought stress response in *Arabidopsis*. *Mol. Plant* 11, 970–982. doi: 10.1016/j.molp.2018.05.001

Hwang, I., Sheen, J., and Müller, B. (2012). Cytokinin signaling networks. *Annu. Rev. Plant Biol.* 63, 353–380. doi: 10.1146/annurev-arplant-042811-105503

International Wheat Genome Sequencing Consortium [IWGSC] (2014). A chromosome-based draft sequence of the hexaploid bread wheat (*Triticum aestivum*) genome. *Science* 345:1251788. doi: 10.1126/science.1251788

International Wheat Genome Sequencing Consortium [IWGSC] (2018). Shifting the limits in wheat research and breeding using a fully annotated reference genome. *Science* 361:eaar7191. doi: 10.1126/science.aar7191

Jain, M., Tyagi, A. K., and Khurana, J. P. (2006). Molecular characterization and differential expression of cytokinin-responsive type-A response regulators in rice (*Oryza sativa*). *BMC Plant Biol.* 6:1. doi: 10.1186/1471-2229-6-1

Jeon, J., and Kim, J. (2013). *Arabidopsis* response regulator1 and *Arabidopsis* histidine phosphotransfer protein2 (AHP2), AHP3, and AHP5 function in cold signaling. *Plant Physiol.* 161, 408–424. doi: 10.1104/pp.112.207621

Jeon, J., Kim, N. Y., Kim, S., Kang, N. Y., Novák, O., Ku, S. J., et al. (2010). A subset of cytokinin two-component signaling system plays a role in cold temperature stress response in *Arabidopsis*. *J. Biol. Chem.* 285, 23371–23386. doi: 10.1074/jbc.M109.096644

Kang, N. Y., Cho, C., Kim, N. Y., and Kim, J. (2012). Cytokinin receptor-dependent and receptor-independent pathways in the dehydration response of *Arabidopsis thaliana*. *J. Plant Physiol.* 169, 1382–1391. doi: 10.1016/j.jplph.2012.05.007

Kieber, J. J., and Schaller, G. E. (2018). Cytokinin signaling in plant development. *Development* 145:dev149344. doi: 10.1242/dev.149344

Kim, H. J., Ryu, H., Hong, S. H., Woo, H. R., Lim, P. O., Lee, I. C., et al. (2006). Cytokinin-mediated control of leaf longevity by AHK3 through phosphorylation of ARR2 in *Arabidopsis*. *Proc. Natl. Acad. Sci. U.S.A.* 103, 814–819. doi: 10.1073/pnas.0505150103

Kumar, S., Stecher, G., and Tamura, K. (2016). MEGA7: Molecular evolutionary genetics analysis version 7.0 for bigger datasets. *Mol. Biol. Evol.* 33, 1870–1874. doi: 10.1093/molbev/msw054

Larkin, M. A., Blackshields, G., Brown, N. P., Chenna, R., McGettigan, P. A., McWilliam, H., et al. (2007). Clustal W and Clustal X version 2.0. *Bioinformatics* 23, 2947–2948. doi: 10.1093/bioinformatics/btm404

Leibfried, A., To, J. P., Busch, W., Stehling, S., Kehle, A., Demar, M., et al. (2005). WUSCHEL controls meristem function by direct regulation of cytokinin-inducible response regulators. *Nature* 438, 1172–1175. doi: 10.1038/nature04270

Liu, Y., Zhang, M., Meng, Z., Wang, B., and Chen, M. (2020). Research progress on the roles of cytokinin in plant response to stress. *Int. J. Mol. Sci.* 21:6574. doi: 10.3390/ijms21186574

Ma, S., Wang, M., Wu, J., Guo, W., Chen, Y., Li, G., et al. (2021). WheatOmics: A platform combining multiple omics data to accelerate functional genomics studies in wheat. *Mol. Plant* 14, 1965–1968. doi: 10.1016/j.molp.2021.10.006

Makino, S., Kiba, T., Imamura, A., Hanaki, N., Nakamura, A., Suzuki, T., et al. (2000). Genes encoding pseudo-response regulators: Insight into His-to-Asp

phosphorelay and circadian rhythm in *Arabidopsis thaliana*. *Plant Cell Physiol.* 41, 791–803. doi: 10.1093/pcp/41.6.791

Mira-Rodado, V., Sweere, U., Grefen, C., Kunkel, T., Fejes, E., Nagy, F., et al. (2007). Functional cross-talk between two-component and phytochrome B signal transduction in *Arabidopsis*. *J. Exp. Bot.* 58, 2595–2607. doi: 10.1093/jxb/erm087

Mochida, K., Yoshida, T., Sakurai, T., Yamaguchi-Shinozaki, K., Shinozaki, K., and Tran, L. S. (2010). Genome-wide analysis of two-component systems and prediction of stress-responsive two-component system members in soybean. *DNA Res.* 17, 303–324. doi: 10.1093/dnares/dsq021

Nguyen, K. H., Ha, C. V., Nishiyama, R., Watanabe, Y., Leyva-González, M. A., Fujita, Y., et al. (2016). *Arabidopsis* type B cytokinin response regulators ARR1, ARR10, and ARR12 negatively regulate plant responses to drought. *Proc. Natl. Acad. Sci. U.S.A.* 113, 3090–3095. doi: 10.1073/pnas.1600399113

Nishiyama, R., Watanabe, Y., Leyva-Gonzalez, M. A., Van Ha, C., Fujita, Y., Tanaka, M., et al. (2013). *Arabidopsis* AHP2, AHP3, and AHP5 histidine phosphotransfer proteins function as redundant negative regulators of drought stress response. *Proc. Natl. Acad. Sci. U.S.A.* 110, 4840–4845. doi: 10.1073/pnas.1302265110

Pavlů, J., Novák, J., Koukalová, V., Luklová, M., Brzobohatý, B., and Černý, M. (2018). Cytokinin at the crossroads of abiotic stress signalling pathways. *Int. J. Mol. Sci.* 19:2450. doi: 10.3390/ijms19082450

Sakai, H., Aoyama, T., and Oka, A. (2000). *Arabidopsis* ARR1 and ARR2 response regulators operate as transcriptional activators. *Plant J.* 24, 703–711. doi: 10.1111/j.1365-313X.2000.00909.x

Salomé, P. A., To, J. P., Kieber, J. J., and McClung, C. R. (2006). *Arabidopsis* response regulators ARR3 and ARR4 play cytokinin-independent roles in the control of circadian period. *Plant Cell* 18, 55–69. doi: 10.1105/tpc.105.037994

Schaller, G. E., Bishopp, A., and Kieber, J. J. (2015). The yin-yang of hormones: Cytokinin and auxin interactions in plant development. *Plant Cell* 27, 44–63. doi: 10.1105/tpc.114.133595

Schaller, G. E., Kieber, J. J., and Shiu, S. H. (2008). Two-component signaling elements and histidyl-aspartyl phosphorelays. *Arabidopsis Book* 2008:e0112. doi: 10.1199/tab.0112

Shi, Y., Tian, S., Hou, L., Huang, X., Zhang, X., Guo, H., et al. (2012). Ethylene signaling negatively regulates freezing tolerance by repressing expression of *CBF* and type-A *ARR* genes in *Arabidopsis*. *Plant Cell* 24, 2578–2595. doi: 10.1105/tpc.112.098640

Srivastava, A. K., Dutta, S., and Chattopadhyay, S. (2019). MYC2 regulates *ARR16*, a component of cytokinin signaling pathways, in *Arabidopsis* seedling development. *Plant Direct* 3:e00177. doi: 10.1002/pld3.177

Sweere, U., Eichenberg, K., Lohrmann, J., Mira-Rodado, V., Bäurle, I., Kudla, J., et al. (2001). Interaction of the response regulator ARR4 with phytochrome B in modulating red light signaling. *Science* 294, 1108–1111. doi: 10.1126/science.1065022

To, J. P., Deruère, J., Maxwell, B. B., Morris, V. F., Hutchison, C. E., Ferreira, F. J., et al. (2007). Cytokinin regulates type-A *Arabidopsis* response regulator activity and protein stability via two-component phosphorelay. *Plant Cell* 19, 3901–3914. doi: 10.1105/tpc.107.052662

To, J. P., Haberer, G., Ferreira, F. J., Deruère, J., Mason, M. G., Schaller, G. E., et al. (2004). Type-A *Arabidopsis* response regulators are partially redundant negative regulators of cytokinin signaling. *Plant Cell* 16, 658–671. doi: 10.1105/tpc.018978

Tran, L. S., Urao, T., Qin, F., Maruyama, K., Kakimoto, T., Shinozaki, K., et al. (2007). Functional analysis of AHK1/ATHK1 and cytokinin receptor histidine kinases in response to abscisic acid, drought, and salt stress in *Arabidopsis*. *Proc. Natl. Acad. Sci. U.S.A.* 104, 20623–20628. doi: 10.1073/pnas.0706547105

Wang, W. C., Lin, T. C., Kieber, J., and Tsai, Y. C. (2019). Response Regulators 9 and 10 negatively regulate salinity tolerance in rice. *Plant Cell Physiol.* 60, 2549–2563. doi: 10.1093/pcp/pcz149

Werner, T., and Schmülling, T. (2009). Cytokinin action in plant development. *Curr. Opin. Plant Biol.* 12, 527–538. doi: 10.1016/j.pbi.2009.07.002

Wybouw, B., and De Rybel, B. (2019). Cytokinin – a developing story. *Trends Plant Sci.* 24, 177–185. doi: 10.1016/j.tplants.2018.10.012

Xie, M., Chen, H., Huang, L., O'Neil, R. C., Shokhirev, M. N., and Ecker, J. R. (2018). A B-ARR-mediated cytokinin transcriptional network directs hormone cross-regulation and shoot development. *Nat. Commun.* 9:1604. doi: 10.1038/s41467-018-03921-6

Zeng, R., Li, Z., Shi, Y., Fu, D., Yin, P., Cheng, J., et al. (2021). Natural variation in a type-A response regulator confers maize chilling tolerance. *Nat. Commun.* 12:4713. doi: 10.1038/s41467-021-25001-y

Zhao, Z., Andersen, S. U., Ljung, K., Dolezal, K., Miotk, A., Schultheiss, S. J., et al. (2010). Hormonal control of the shoot stem-cell niche. *Nature* 465, 1089–1092. doi: 10.1038/nature09126

Zhu, T., Wang, L., Rimbert, H., Rodriguez, J. C., Deal, K. R., De Oliveira, R., et al. (2021). Optical maps refine the bread wheat *Triticum aestivum* cv. Chinese Spring genome assembly. *Plant J.* 107, 303–314. doi: 10.1111/tpj.15289

Zubo, Y. O., Blakley, I. C., Yamburenko, M. V., Worthen, J. M., Street, I. H., Franco-Zorrilla, J. M., et al. (2017). Cytokinin induces genome-wide binding of the type-B response regulator ARR10 to regulate growth and development in *Arabidopsis*. *Proc. Natl. Acad. Sci. U.S.A.* 114, E5995–E6004. doi: 10.1073/pnas.1620749114

frontiers | Frontiers in Plant Science

TYPE Original Research
PUBLISHED 06 September 2022
DOI 10.3389/fpls.2022.1005627

OPEN ACCESS

EDITED BY
Handong Su,
Huazhong Agricultural University, China

REVIEWED BY
Jindong Liu,
Institute of Crop Sciences (CAS), China
Zhu-Qing Shao,
Nanjing University, China
Ping Lu,
Institute of Genetics and Developmental Biology (CAS), China

*CORRESPONDENCE
Pengtao Ma
ptma@ytu.edu.cn
Guohao Han
ghhan@ms.sjziam.ac.cn
Jiangchun Wang
yt-wjc@163.com

†These authors have contributed equally to this work

SPECIALTY SECTION
This article was submitted to Plant Pathogen Interactions, a section of the journal Frontiers in Plant Science

RECEIVED 28 July 2022
ACCEPTED 15 August 2022
PUBLISHED 06 September 2022

CITATION
Mu Y, Gong W, Qie Y, Liu X, Li L, Sun N, Liu W, Guo J, Han R, Yu Z, Xiao L, Su F, Zhang W, Wang J, Han G and Ma P (2022) Identification of the powdery mildew resistance gene in wheat breeding line Yannong 99102-06188 *via* bulked segregant exome capture sequencing.
Front. Plant Sci. 13:1005627.
doi: 10.3389/fpls.2022.1005627

Identification of the powdery mildew resistance gene in wheat breeding line Yannong 99102-06188 *via* bulked segregant exome capture sequencing

Yanjun Mu[1†], Wenping Gong[2†], Yanmin Qie[3†], Xueqing Liu[4], Linzhi Li[4], Nina Sun[4], Wei Liu[4], Jun Guo[2], Ran Han[2], Ziyang Yu[1], Luning Xiao[1], Fuyu Su[1], Wenjing Zhang[1], Jiangchun Wang[4*], Guohao Han[5*] and Pengtao Ma[1*]

[1]College of Life Sciences, Yantai University, Yantai, China, [2]Crop Research Institute, Shandong Academy of Agricultural Sciences, Jinan, China, [3]Institute of Cereal and Oil Crops, Hebei Academy of Agricultural and Forestry Sciences/Hebei Laboratory of Crop Genetic and Breeding, Shijiazhuang, China, [4]Institute of Grain and Oil Crops, Yantai Academy of Agricultural Sciences, Yantai, China, [5]Center for Agricultural Resources Research, Institute of Genetics and Developmental Biology, Chinese Academy of Sciences, Shijiazhuang, China

Powdery mildew of wheat (*Triticum aestivum*), caused by *Blumeria graminis* f.sp. *tritici* (*Bgt*), is a destructive disease that seriously threatens the yield and quality of its host. Identifying resistance genes is the most attractive and effective strategy for developing disease-resistant cultivars and controlling this disease. In this study, a wheat breeding line Yannong 99102-06188 (YN99102), an elite derivative line from the same breeding process as the famous wheat cultivar Yannong 999, showed high resistance to powdery mildew at the whole growth stages. Genetic analysis was carried out using *Bgt* isolate E09 and a population of YN99102 crossed with a susceptible parent Jinhe 13–205 (JH13–205). The result indicated that a single recessive gene, tentatively designated *pmYN99102*, conferred seedling resistance to the *Bgt* isolate E09. Using bulked segregant exome capture sequencing (BSE-Seq), *pmYN99102* was physically located to a ~33.7 Mb (691.0–724.7 Mb) interval on the chromosome arm 2BL, and this interval was further locked in a 1.5 cM genetic interval using molecular markers, which was aligned to a 9.0 Mb physical interval (699.2–708.2 Mb). Based on the analysis of physical location, origin, resistant spectrum, and inherited pattern, *pmYN99102* differed from those of the reported powdery mildew (*Pm*) resistance genes on 2BL, suggesting *pmYN99102* is most likely a new *Pm* gene/allele in the targeted interval. To transfer *pmYN99102* to different genetic backgrounds using marker-assisted selection (MAS), 18 closely linked markers were tested for their availability in different genetic backgrounds for MAS, and all markers expect for *YTU103-97* can be used in MAS for tracking *pmYN99102* when it transferred into those susceptible cultivars.

KEYWORDS

wheat powdery mildew, *pmYN99102*, MAS, BSE-Seq, molecular mapping

Introduction

Common wheat (*Triticum aestivum*) is one of the most important crops to food security for it provides ∼20% of the calories consumed by humans (Isham et al., 2021). With an estimated global population of more than nine billion by 2050, wheat production is needed an ∼70% growth to meet the food demands (International Wheat Genome Sequencing Consortium (IWGSC), 2014). However, powdery mildew, a global devastating wheat disease caused by *Blumeria graminis* f. sp. *tritici* (*Bgt*), can significantly reduce wheat yield and affect flour quality (Li et al., 2019; Wang et al., 2021). It typically decreases wheat yield by 10–15% and up to 62% in severe cases (Singh et al., 2016).

To control this disease, utilization of host resistance is regarded as the most effective, and environmentally friendly way (Chen, 2013; Ma et al., 2015). Nevertheless, it cannot be ignored that *Bgt* isolates have complex and highly variable virulence structures, so their frequent evolution will lead to the continuous breakdown of resistance genes, particularly in the areas where race-specific resistance genes were widely used. A well-known example was the "boom-bust" of *Pm8*, which led to severe epidemics after extended periods of use in the main wheat production regions of China (He et al., 2011, 2015; An et al., 2019). On the other hand, despite more than 80 formally designated *Pm* genes (*Pm1-Pm68*, noting that *Pm8=Pm17*, *Pm18=Pm1c*, *Pm22=Pm1e*, *Pm23=Pm4c*, and *Pm31=Pm21*) having been reported (Li H. H. et al., 2020; McIntosh et al., 2020; He et al., 2021), most of them cannot be directly applied in wheat production due to undesirable linkage drag, such as a broad-spectrum gene *Pm16* which caused up to 15% yield loss when introduced into wheat backgrounds (Summers and Brown, 2013; Tan et al., 2018). In the modern wheat breeding programs of China, only a few *Pm* genes including *Pm2*, *Pm4*, *Pm5*, *Pm8,* and *Pm21* have been extensively applied in wheat improvement (Jia et al., 2020; Jin et al., 2021), making them face huge selective pressure. Therefore, unceasingly exploring and utilizing the novel *Pm* genes/alleles that could balance the broad resistance and comprehensive agronomic performance is an ongoing and essential process.

Once the effective gene was identified, its accurate and rapid transfer or pyramiding is the key point in breeding practice. In comparison to conventional breeding based on phenotypic selection, marker-assisted selection (MAS) is more effective because it combines both genotypic and phenotypic identification. Using the tightly linked or diagnostic markers, the targeted genes could be selected or excluded in fewer generations and thus promote the breeding process (Jiang et al., 2016). Therefore, the isolation of target genes/loci and the development of their tightly linked markers are the two key factors for MAS. Recent advances in the whole-genome sequencing of wheat and corresponding high-throughput sequencing techniques have significantly accelerated the identification and isolation of the resistance genes (Zhu et al., 2020; Ma et al., 2021). A newly-developed strategy bulked segregant exome capture sequencing (BSE-Seq), which combines bulked segregant analysis (BSA) and the exome sequence strategy, has great potential to accelerate gene mapping, particularly in polyploid species with large and complex genome properties such as common wheat. BSE-Seq could effectively identify the linked interval which is not limited to the multiple gene copies, high similarity among the homoeologs, and various types of mapping segregant populations. More importantly, most of the variations obtained from BSE-Seq are existed in the coding regions, making it an economical but effective method for constructing linkage maps and also analyzing the differentially expressed genes associated with the targeted traits (Dong et al., 2020).

Wheat genotypes carrying high-resistance genes but with poor agronomic performance will be greatly limited in breeding because of multigeneration of backcrossing needed, which is not preferred by breeders (Summers and Brown, 2013; Yu et al., 2022). Genes identified in wheat cultivars/breeding lines can be more easily applied in breeding practice compared with those originated from wheat relatives or landraces (Xu et al., 2015). In this case, wheat breeding lines are of high breeding priority as the donor to improve powdery mildew resistance. Yannong 99102-06188 (YN99102), is an elite wheat breeding line developed by the Yantai Academy of Agricultural Sciences (Yantai, China). It exhibited both high resistance to powdery mildew and elite agronomic traits for consecutive years of observation in the field. To better clarify and use the powdery mildew resistance in YN99102, the objectives of this study were to (i) assess the powdery mildew resistance of YN99102 and determine its inheritance; (ii) rapidly map the *Pm* gene(s) using BSE-Seq; (iii) evaluate and develop the tightly linked markers suitable for MAS.

Materials and methods

Plant materials

Wheat breeding line YN99102, a derivative line from the same breeding process as the elite wheat cultivar Yannong 999, was derived from the multiple crosses of Lumai 14 and Lin 9,511 through space mutation breeding (Supplementary Figure 1). YN99102 showed high resistance to powdery mildew at both seedling and adult plant stages. To determine the genetic analysis and map the *Pm* gene(s) at the seedling stage in YN99102, the wheat line Jinhe 13–205 (JH13–205) was used as the susceptible parent to cross with YN99102 to generate F_1 hybrids, F_2 populations, and $F_{2:3}$ families. Wheat cultivar Mingxian 169 without any known *Pm* gene, was used as the susceptible control for phenotypic evaluation and served as the *Bgt* inoculum

spreader. Eight wheat genotypes with known *Pm* genes on chromosome 2BL, Coker 747 (with *Pm6*) (Wan et al., 2020), Am9/3 (with *Pm33*) (Zhu et al., 2005), CH7086 (with *Pm51*) (Zhan et al., 2014), Liangxing 99 (with *Pm52*) (Zhao et al., 2013), WE35 (with *Pm64*) (Zhan et al., 2014), LS5082 (with *PmLS5082*) (Wu et al., 2019), KN0816 (with *PmKN0816*) (Wang et al., 2021) and Qingxinmai (with *PmQ*) (Li Y. H. et al., 2020) were tested with different *Bgt* isolates in order to compare their reactions with that of YN99102 (Table 1). Forty-two susceptible wheat cultivars from different regions of China were used to evaluate the usefulness of the closely linked markers for MAS of the *Pm* gene(s) in YN99102 (Supplementary Table 1).

Phenotypic assessment of reactions to powdery mildew

At the adult stage, YN99102 was inoculated with a mixture of 11 *Bgt* isolates including A3, A10, E05, E09, E18, E20, E21, E23–1, E32, E23, and E31 in the field nurseries with three replicates. The assessments were performed from 2018 to 2021 at Yantai University, Yantai City, Shandong Province, China (121.39'E, 37.52'N). For each replicate, YN99102 was planted with 30 seeds per row in four 1.2-m rows, with Mingxian 169 planted on each side of YN99102 as susceptible control and inoculum spreader. When Mingxian 169 showed severe disease symptoms, the disease reaction of YN99102 was assessed using a 0–9 scale for infection types (ITs), in which 0–4 were considered resistant and 5–9 were susceptible (Sheng and Duan, 1991). Each plant was assessed twice for confirmation.

To determine the inheritance of the powdery mildew resistance in YN99102 at the seedling stage, the *Bgt* isolate E09, which is prevalent in the main wheat producing regions of North China (Zhou et al., 2005), was used to inoculate YN99102, susceptible parent JH13–205, and their F_1 hybrids, F_2 population, and $F_{2:3}$ families at the one-leaf stage. Each of the $F_{2:3}$ families was tested with 30 seeds to confirm the phenotypic reaction of the F_2 plants. The resistance assessment was carried out in a greenhouse in a high humidity environment with a daily cycle of 14 h of light at 22°C and 10 h of darkness at 18°C. The tested seeds were planted in rectangular trays (54 × 28 × 4.2 cm) with 128 wells (3.2 × 3.2 × 4.2 cm) and then inoculated at one leaf stage by dusting the fresh conidia of *Bgt* isolate E09, and Mingxian 169 was planted randomly in the trays as the susceptible control. When the pustules were fully developed on the first leaf of Mingxian 169 about 14–15 days after inoculation, each plant was assessed on a 0–4 scale, plants with ITs 0–2 were regarded as resistant and those with ITs 3 and 4 as susceptible (Sheng, 1988; Wang et al., 2005). Goodness-of-fit was analyzed using the chi-square (χ^2) test to investigate deviations of the observed phenotypic data of F_2 populations and $F_{2:3}$ families from theoretically expected segregation ratios.

BSE-Seq

BSE-Seq was used to rapidly located *Pm* gene(s) in the targeted interval by Oebiotech (Shanghai, China). After the susceptible control Mingxian 169 showed serious powdery mildew symptoms on the first leaf, equal leaf tissues from 30 homozygous resistant and 30 homozygous susceptible $F_{2:3}$ plants of YN99102 × JH13–205, respectively, were randomly collected to construct resistant and susceptible bulks. These two DNA bulks were subjected to exome capture sequencing with deep coverage (∼70 ×). The construction, assessment, and sequencing of the libraries were performed as described by (Dong et al., 2020).

Raw sequence reads were filtered using Fastp (v0.12.4) to remove the low-quality reads and adapters used. The high-quality reads were then aligned to IWGSC RefSeq v1.0 genome. After that, raw cohort vcf was worked out with GATK (v4.0.10.1) (McCormick et al., 2015). The minimum-mapping-quality parameter was set as 30 for only high-quality alignment reads used to call variants. SNP calling and density analysis were carried out using sliding window calculation based on the reference of Takagi et al. (2013) The data filtering parameters were set as AF (Allele Frequence) <0.3 or >0.7. Bcftools (v1.9) (Narasimhan et al., 2016) was performed for variants quality filtering with "QUAL > 30" and "DP ≥5." The statistical model varBScore was carried out to determine the candidate interval. SnpEff (v4.3T) (Cingolani et al., 2012) was used to generate customized databases containing IWGSC v1.1 HC/LC genes for the annotation of the variants.

Molecular markers analysis

Based on the candidate interval obtained from BSE-Seq, 98 molecular markers linked to the known *Pm* genes in the candidate interval were firstly used to test for polymorphisms between resistant and susceptible parents and bulks (Table 2). Then, the polymorphic markers between the parents and the bulks were used to genotype the $F_{2:3}$ families of YN99102 × JH13–205 for a preliminary mapping of the *Pm* gene(s) in YN99102. Moreover, 70 new markers in the target interval were developed based on the simple sequence repeat (SSR) and small insertion-deletion (InDel) that were discovered by BSE-Seq (Supplementary Table 2).

PCR amplification was performed as described by Han et al. (2022a,b) with minor modification. The PCR products were then separated in 8% non-denaturing polyacrylamide gels with a 29:1 ratio of acrylamide and bisacrylamide, finally visualized by silver staining.

TABLE 1 Comparative responses of Yannong 99102-06188 and wheat genotypes with known powdery mildew resistance genes on chromosome arm 2BL to 11 isolates of *Blumeria graminis* f. sp. *tritici* (*Bgt*) with different virulence.

Genotypes	*Pm* gene	A3	A10	E05	E09	E18	E20	E21	E23-1	E32	E23	E31
Yannong 99102-06188	*pmYN99102*	3	1	1	0	1	0	2	0	0	0	0
Jinhe 13–205	–	4	4	4	4	4	4	4	4	4	4	4
Coker747	*Pm6*	0	0	0	3	3	0	3	0	0	0	2
Am9/3	*Pm33*	4	0	0	0	3	0	2	0	0	0	4
CH7086	*Pm51*	0	0	0	0	0	0	4	0	0	0	0
Liangxing 99	*Pm52*	3	0	0	0	0	0	0	0	0	0	0
WE35	*Pm64*	0	0	0	0	0	0	0	4	0	0	0
LS5082	*PmLS5082*	3	0*	0	0	3	0	0	0	0	0	0
KN0816	*PmKN0816*	0	0	0	0	0	0	0	0	0	0	0
Qingxinmai	*PmQ*	0	4	4	3	3	4	0	4	0	4	3

0–4 scale was used to scored the infection types: 0, 0; 1 and 2 were regarded as resistant phenotypes and 3 and 4 were susceptible phenotypes.

Map construction and functional annotation

After obtaining phenotyping data from the evaluation of disease resistance and the genotyping data of the $F_{2:3}$ families from molecular marker analysis, the linkage map of the *Pm* gene in YN99102 was constructed using MAPMAKER 3.0 (Lincoln et al., 1992) and the Kosambi function as reported previously (Kosambi, 1944). Functional annotation was performed based on the information from IWGSC RefSeq [version 1.0; The International Wheat Genome Sequencing Consortium (IWGSC, 2018)].

Comparison with the known *Pm* genes on the chromosome arm 2BL

Considering that the *Pm* gene in YN99102 was assigned to the chromosome 2BL, YN99102 and eight wheat genotypes also carrying known *Pm* genes on chromosome 2BL, including Coker 747 (with *Pm6*), Am9/3 (with *Pm33*), CH7086 (with *Pm51*), Liangxing 99 (with *Pm52*), WE35 (with *Pm64*), LS5082 (with *PmLS5082*), KN0816 (with *PmKN0816*) and Qingxinmai (with *PmQ*), were tested against 11 *Bgt* isolates that were collected from the diseased wheat fields in different wheat growing areas of China to compare their resistance spectrum (Table 1). Each isolate was developed through single-spore purification and separately stored in glass tubes with three layers of gauzes. The methods of inoculation and incubated conditions were described previously (Wu et al., 2019).

To further distinguish the *pmYN99102* from the documented *Pm* genes on chromosome arm 2BL at the level of genetic diversity, 98 markers closely linked to those *Pm* genes were tested for polymorphisms between resistant and susceptible parents and bulks derived from the $F_{2:3}$ families of YN99102 × JH13–205 to investigate the genetic diversity of the candidate interval of *Pm* gene in YN99102 and the known *Pm* genes in chromosome arm 2BL (Table 2).

Evaluation of the closely linked markers for MAS

To evaluate the applicability of the markers for MAS breeding, 42 susceptible wheat cultivars from different regions of China were tested with the closely linked or co-segregated markers. The markers which were able to consistently amplify polymorphic band(s) between YN99102 and these susceptible cultivars were regarded as effective for MAS in those genetic backgrounds (Supplementary Table 1). To transfer the *Pm* gene(s) in YN99102 to applicable backgrounds, these cultivars were crossed with YN99102 to construct BC_1F_2 and F_3 segregation populations for MAS.

Results

Evaluation and inheritance of powdery mildew resistance in YN99102

For the adult plant investigations with powdery mildew in the field, YN99102 showed high resistance with ITs 0–1 to the *Bgt* mixture including *Bgt* isolates A3, A10, E05, E09, E18, E20, E21, E23–1, E32, E23 and E31 over the consecutive growing seasons from 2018 to 2021.

Then, the *Bgt* isolate E09 was used to determine the inheritance of powdery mildew resistance in YN99102 at the seedling stage. When inoculated with this isolate, YN99102 was highly resistant with IT 0, whereas JH13–205 was highly susceptible with IT 4. All the 10 F_1 plants of the cross YN99102 × JH13–205 were susceptible with IT 4, indicating the resistance

TABLE 2 Polymorphic and linkage analyses of the markers linked to the powdery mildew resistance genes located on chromosome arm 2BL using the mapping population derived from the cross of Yannong 99102-06188 × Jinhe 13–205.

Marker	Resistance genes	Physical location (Mb)	Polymorphism		Linkage to *pmYN99102*	References
			Parents	$F_{2:3}$ bulks		
CIT02g-1	*Pm6*	711.0	-	-	-	Wan et al., 2020
CIT02g-2	*Pm6*	722.1	+	+	+	Wan et al., 2020
CIT02g-3	*Pm6*	699.2	+	+	+	Wan et al., 2020
CIT02g-4	*Pm6*	730.2	-	-	-	Wan et al., 2020
CIT02g-5	*Pm6*	724.8	-	-	-	Wan et al., 2020
CIT02g-6	*Pm6*	694.1	-	-	-	Wan et al., 2020
CIT02g-7	*Pm6*	694.1	-	-	-	Wan et al., 2020
CIT02g-8	*Pm6*	710.3	-	-	-	Wan et al., 2020
CIT02g-9	*Pm6*	710.3	-	-	-	Wan et al., 2020
CIT02g-10	*Pm6*	722.1	-	-	-	Wan et al., 2020
CIT02g-11	*Pm6*	709.1	-	-	-	Wan et al., 2020
CIT02g-12	*Pm6*	722.3	-	-	-	Wan et al., 2020
CIT02g-13	*Pm6*	708.2	+	+	+	Wan et al., 2020
CIT02g-14	*Pm6*	694.1	-	-	-	Wan et al., 2020
CIT02g-15	*Pm6*	722.1	+	+	+	Wan et al., 2020
CIT02g-16	*Pm6*	709.8	-	-	-	Wan et al., 2020
CIT02g-17	*Pm6*	697.7	+	+	+	Wan et al., 2020
CIT02g-18	*Pm6*	698.3	+	+	+	Wan et al., 2020
CIT02g-19	*Pm6*	731.0	-	-	-	Wan et al., 2020
CIT02g-20	*Pm6*	699.2	+	+	+	Wan et al., 2020
CIT02g-21	*Pm6*	730.9	-	-	-	Wan et al., 2020
CIT02g-22	*Pm6*	715.6	-	-	-	Wan et al., 2020
CISSR02g-1	*Pm6*	704.2	-	-	-	Wan et al., 2020
CISSR02g-2	*Pm6*	701.8	-	-	-	Wan et al., 2020
CISSR02g-3	*Pm6*	701.1	-	-	-	Wan et al., 2020
CISSR02g-5	*Pm6*	699.1	-	-	-	Wan et al., 2020
CISSR02g-6	*Pm6*	700.4	+	+	+	Wan et al., 2020
CINAU117	*Pm6*	614.9	-	-	-	Qin et al., 2011
CINAU118	*Pm6*	-	-	-	-	Qin et al., 2011
CINAU119	*Pm6*	-	-	-	-	Qin et al., 2011
CINAU120	*Pm6*	-	-	-	-	Qin et al., 2011
CINAU121	*Pm6*	-	-	-	-	Qin et al., 2011
CINAU122	*Pm6*	-	-	-	-	Qin et al., 2011
CINAU125	*Pm6*	653.3	-	-	-	Qin et al., 2011
CINAU126	*Pm6*	-	-	-	-	Qin et al., 2011
CINAU127	*Pm6*	677.3	-	-	-	Qin et al., 2011
CINAU128	*Pm6*	-	-	-	-	Qin et al., 2011
CINAU129	*Pm6*	-	-	-	-	Qin et al., 2011
CINAU131	*Pm6*	689.1	-	-	-	Qin et al., 2011
CINAU132	*Pm6*	-	-	-	-	Qin et al., 2011
CINAU133	*Pm6*	-	-	-	-	Qin et al., 2011
CINAU134	*Pm6*	-	-	-	-	Qin et al., 2011
CINAU135	*Pm6*	690.2	-	-	-	Qin et al., 2011
CINAU136	*Pm6*	695.8	-	-	-	Qin et al., 2011

(Continued)

TABLE 2 (Continued)

Marker	Resistance genes	Physical location (Mb)	Polymorphism		Linkage to *pmYN99102*	References
			Parents	$F_{2:3}$ bulks		
CINAU137	*Pm6*	-	-	-	-	Qin et al., 2011
CINAU138	*Pm6*	-	-	-	-	Qin et al., 2011
CINAU139	*Pm6*	753.0	-	-	-	Qin et al., 2011
CINAU140	*Pm6*	747.2	-	-	-	Qin et al., 2011
CINAU141	*Pm6*	710.9	-	-	-	Qin et al., 2011
CINAU142	*Pm6*	723.0	-	-	-	Qin et al., 2011
CINAU143	*Pm6*	715.0	-	-	-	Qin et al., 2011
CINAU144	*Pm6*	710.9	-	-	-	Qin et al., 2011
NAU/STSBCD135-2	*Pm6*	738.6	-	-	-	Qin et al., 2011; Tan et al., 2018
CINAU123	*Pm6*	-	-	-	-	Qin et al., 2011
CINAU124	*Pm6*	-	-	-	-	Qin et al., 2011
Xicscl172	*Pm52*	595.7	+	+	-	Wu et al., 2019
Xicscl174	*Pm52*	595.7	+	+	-	Wu et al., 2019
Xicsl326	*Pm52*	581.0	+	+	-	Wu et al., 2019
Xicscl795	*Pm52*	585.0	-	-	-	Wu et al., 2019
Xicsl163	*Pm52*	596.4	-	-	-	Wu et al., 2019
Xicsl224	*Pm52*	556.6	-	-	-	Wu et al., 2019
Xicsl275	*Pm52*	382.9	-	-	-	Wu et al., 2019
Xicsl306	*Pm52*	607.2	-	-	-	Wu et al., 2019
Xicsl34	*Pm52*	564.8	-	-	-	Wu et al., 2019
Xicsl62	*Pm52*	556.6	-	-	-	Wu et al., 2019
Xicsl90	*Pm52*	603.6	-	-	-	Wu et al., 2019
Xicsl234	*Pm52*	596.6	+	+	-	Wu et al., 2019
Xgwm120	*Pm52*	615.7	-	-	-	Zhao et al., 2013
Xwmc175	*Pm52, Pm63*	670.6	-	-	-	Zhao et al., 2013; Tan et al., 2018
Xgwm120	*Pm52, Pm63*	615.8	-	-	-	Zhao et al., 2013; Tan et al., 2018
Xwmc441	*Pm52, Pm63*	598.0	-	-	-	Zhao et al., 2013; Tan et al., 2018
WGGBH1212	*Pm64*	656.6	-	-	-	Zhang et al., 2019
WGGBH1260	*Pm64*	695.1	-	-	-	Zhang et al., 2019
WGGBH134	*Pm64*	670.6	-	-	-	Zhang et al., 2019
WGGBH1364	*Pm64*	695.4	-	-	-	Zhang et al., 2019
WGGBH218	*Pm64*	699.2	-	-	-	Zhang et al., 2019
WGGBH252	*Pm64*	732.3	-	-	-	Zhang et al., 2019
WGGBH612-5	*Pm64*	710.3	-	-	-	Zhang et al., 2019
WGGBH686	*Pm64*	680.0	-	-	-	Zhang et al., 2019
WGGBH913	*Pm64*	715.0	-	-	-	Zhang et al., 2019
WGGBH1099	*Pm64*	705.5	-	-	-	Zhang et al., 2019
stars419	*Pm63*	710.3	-	-	-	Tan et al., 2019
Xbcd135-2	*Pm63*	723.4	-	-	-	Tan et al., 2019
BE405017	*Pm51*	767.1	-	-	-	Zhan et al., 2014
BE444894	*Pm51*	765.3	-	-	-	Zhan et al., 2014

(Continued)

TABLE 2 (Continued)

Marker	Resistance genes	Physical location (Mb)	Polymorphism		Linkage to *pmYN99102*	References
			Parents	$F_{2:3}$ bulks		
BQ246670	*Pm51*	709.8	-	-	-	Zhan et al., 2014
Cos66	*Pm51*	747.2	-	-	-	Zhan et al., 2014
Xbarc159	*Pm51*	793.0	-	-	-	Zhan et al., 2014
Xwmc332	*Pm51, Pm63*	739.4	-	-	-	Zhan et al., 2014; Tan et al., 2018
Xwmc332	*Pm51, Pm63*	739.4	-	-	-	Zhan et al., 2014; Tan et al., 2018
Xgwm526	*Pm33*	774.1	-	-	-	Zhu et al., 2005
Xwmc317	*Pm33*	784.3	-	-	-	Zhu et al., 2005
Xicsq10	*PmQ*	750.0	-	-	-	Li H. H. et al., 2020
Xicsq129	*PmQ*	740.3	-	-	-	Li H. H. et al., 2020; Li Y. H. et al., 2020
Xicsq253	*PmQ*	730.6	-	-	-	Li H. H. et al., 2020
Xicsq347	*PmQ*	720.9	-	-	-	Li H. H. et al., 2020
Xicsq405	*PmQ*	710.7	-	-	-	Li H. H. et al., 2020
Xicsq453	*PmQ*	730.8	-	-	-	Li Y. H. et al., 2020

In the polymorphism column, "+" represents polymorphic or linked, and "–" represents non-polymorphic or unlinked, and in physical location, "–" represents no data.

of YN99102 to *Bgt* isolate E09 was controlled by recessive *Pm* gene(s). The F_2 populations segregated in 31 resistant plants scored as IT 0, and 77 susceptible plants scored as IT 4, which fits a theoretical ratio of 1:3 for the monogenic segregation ($\chi^2 = 0.79$; $P = 0.37$). Subsequently, all the 108 F_2 plants were transplanted in the field to generate $F_{2:3}$ families for the confirmation of the homozygous or heterozygous genotype of the susceptible F_2 plants. The 108 $F_{2:3}$ families segregated with 31 homozygous resistant (rr), 52 segregating (Rr), and 25 homozygous susceptible (RR), and the phenotypic result of $F_{2:3}$ families further confirmed the ratio of monogenic inheritance of the powdery mildew resistance 1:2:1 ($\chi^2 = 0.48$; $P = 0.49$) (Table 3). Therefore, it suggested that the resistance to *Bgt* isolate E09 in YN99102 was controlled by a single recessive gene, tentatively designated as *pmYN99102*.

SNP calling and confirmation of candidate interval

To confirm the genetic position of *pmYN99102*, the resistant and susceptible DNA bulks were genotyped using BSE-Seq. Based on the results of BSE-Seq, a total of 32,711 high-quality SNPs were identified between the resistant and susceptible bulks by ΔSNP index analysis, which was distributed on all of the wheat chromosomes (Figure 1). Among them, 10,731 (32.8%) SNPs were detected on chromosome arm 2B, 2,978 (27.8%) SNPs enriched on chromosome arm 2BL 691.0–724.7 Mb with varBScore analysis (Figure 2), indicating that the *pmYN99102* was likely located in this 33.7 Mb interval on chromosome arm 2BL.

Molecular mapping of *PmYN99102* and prediction of the candidate genes

With the candidate interval confirmed, 98 previously reported markers linked to the candidate interval on 2BL (Table 2) and 70 newly developed markers based on the results of BSE-Seq (Supplementary Table 2) were used to screen polymorphism between the resistant and susceptible parents and bulks. Among them, 19 markers, including 10 newly developed markers (Table 4), amplified consistent polymorphisms between the resistant and susceptible parents and bulks, which were used to genotype the $F_{2:3}$ families of the cross of YN99102 × JH13–205 to construct the linkage map and further narrow down the candidate interval of *pmYN99102* (Figure 3). The result showed that *pmYN99102* was flanked by markers *CIT02g-3*/*CIT02g-20* and *CIT02g-13*/*CIT02g-2*/*CIT02g-15* with genetic distances of 0.5 and 1.0 cM, corresponding to 699.2–708.2 Mb physical interval, and co-segregated with *CISSR02g-6* (700.4 Mb) according to the IWGSC Chinese Spring reference genome v1.0 (Figure 4). In this interval, we obtained a total of 76 high confidence genes based on the gene annotation results. Among them, four genes *TraesCS2B01G505200*, *TraesCS2B01G507000*, *TraesCS2B01G507100* and *TraesCS2B01G509000* were related to disease resistance and were regarded as the candidate genes of *pmYN99102* (Supplementary Table 3).

TABLE 3 Segregation ratios of F_2 and $F_{2:3}$ generations of Yannong 99102-06188 (YN) and Jinhe 13-205 (JH) following inoculation with *Blumeria graminis* f. sp. *tritici* (*Bgt*) isolate E09 at the seedling stage.

Parent and cross[a]	Generation[b]	Observed ratio[c]	Expected ratio	χ^2	*P*
YN	RP	R:S=10:0			
JH	SP	R:S=0:10			
YN × JH F_1	F_1	R:S=0:10			
YN × JH F_2	F_2	R:S=31:77	1:3	0.79	0.37
YN × JH F_3	$F_{2:3}$	HR:Seg:HS=31:52:25	1:2:1	0.48	0.49

[a] YN, Yannong 99102-06188; JH, Jinhe 13–205 [b] RP, Resistant parent; SP, Susceptible parent. [c] R, Resistant; S, Susceptible; HR, homozygous resistant; Seg, segregating; HS, homozygous susceptible.

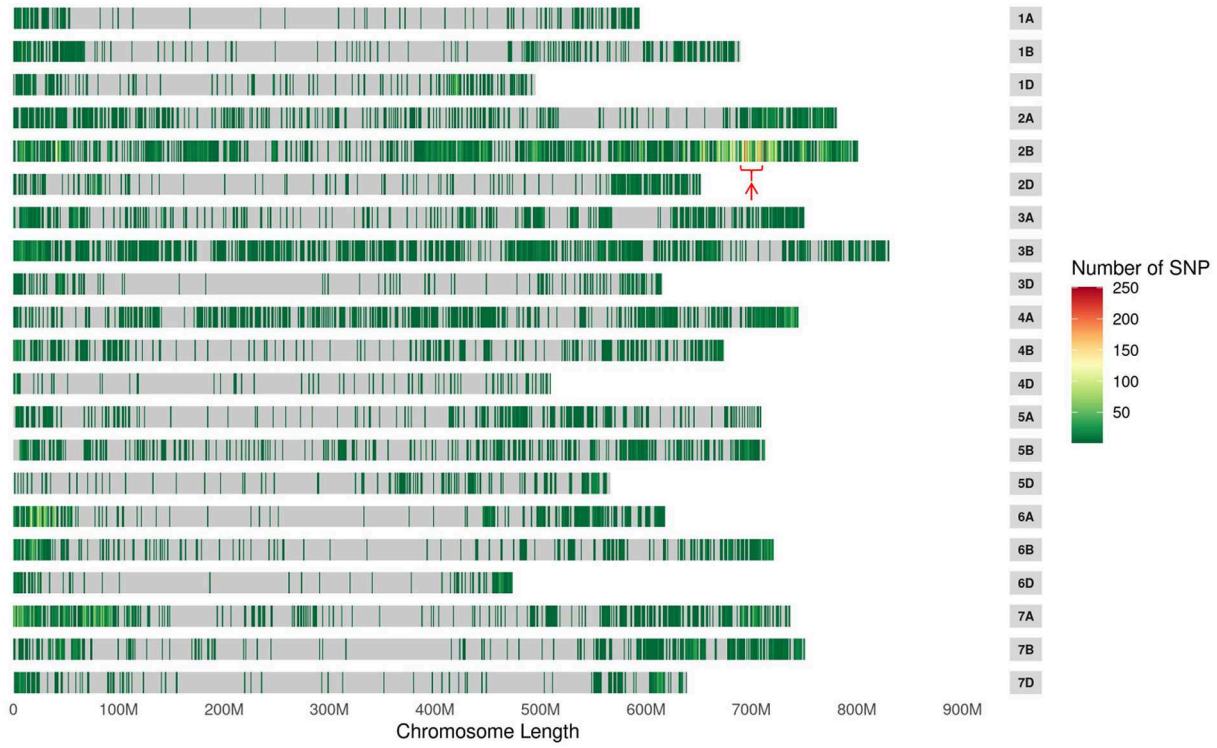

FIGURE 1
The distribution of single nucleotide polymorphisms (SNPs) and significant candidate intervals (indicated with red arrow) across the 21 wheat chromosomes.

Comparisons of *PmYN99102* and the known *Pm* genes on chromosome arm 2BL

To identify the relationship between *pmYN99102* and the known *Pm* genes on chromosome arm 2BL, YN99102 (with *pmYN99102*), Coker747 (with *Pm6*), Am9/3 (with *Pm33*), CH7086 (with *Pm51*), Liangxing99 (with *Pm52*), WE35 (with *Pm64*), LS5082 (with *PmLS5082*), KN0816 (with *PmKN0816*) and Qingxinmai (with *PmQ*) were tested against 11 *Bgt* isolates to evaluate their resistance spectrum. The results showed that YN99102 was resistant to 10 of 11 (90.9%) isolates, while Coker747, Am9/3, CH7086, Liangxing99, WE35, LS5082, KN0816 and Qingxinmai was resistant to 8 of 11 (72.7%), 8 of 11 (72.7%), 10 of 11 (90.9%), 10 of 11 (90.9%), 10 of 11 (90.9%), 9 of 11 (81.8%), 11 of 11 (100%), 3 of 11 (27.2%), respectively (Figure 5 ; Table 1). Even though YN99102, CH7086, and Liangxing 99 were all resistant to 10 out of 11,

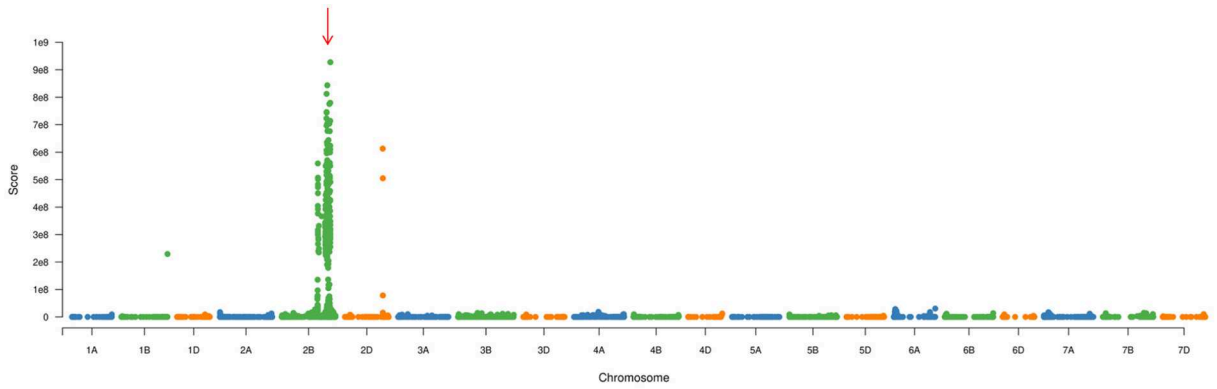

FIGURE 2
Manhattan plot of the varBScore across the 21 wheat chromosomes for analyzing the candidate region (indicated with red arrow).

TABLE 4 *pmYN99102*-linked markers developed by bulked segregant exome capture sequencing (BSE-Seq).

Marker	Location	FORWARD PRIMER1 (5'-3')	REVERSE PRIMER1 (5′ − 3′)
YTU103-26	chr2B:680042044-680043045	TGTCGCTGTCACTTGCTGAT	TCACCAGCACATGAGTCACC
YTU103-41	chr2B:680805143-680806144	AGCTTGAACTTGCCGGCTAT	CAGCTTCATGGACAGGCTCA
YTU103-54	chr2B:696080372-696081373	AGGGCAAAAGATGGAGGTCG	TCGTTCAAGGGCATCAGCAT
YTU103-69	chr2B:698301932-698302933	CGAGCGTGATGTAGACCTCC	GTTTTTCCAGGCCAGCAAGG
YTU103-71	chr2B:698963503-698964504	CTCGTCGCCAAATGCTGATG	AGGCGGTTGATAGAGCACAC
YTU103-87	chr2B:697993507-697994508	AGCCGTTCCTTGATGTCAGG	ACTCCCATCGAGGATCCACA
YTU103-88	chr2B:698590771-698591772	CTCGCGCAAGAACACACAAA	ACCTGCTCTGGATGCTTGAC
YTU103-97	chr2B:680597479-680598480	CTAGGGCTGGACCAGTTTGG	AGTTGTGGAAATCGGCGGAT
YTU103-108	chr2B:692161592-692162593	GTCAGGCCTGGGAGGAATTC	CCATGGAAGGAGGAGGAGGA
YTU103-113	chr2B:695372385-695373386	CTGCTGACAGTACGGTGTGT	CGCCAGCAGATTAACCATGC

they showed significantly different phenotypes against different isolates. Therefore, YN99102 had different resistance spectrum from the known *Pm* genes on 2BL.

To further distinguish *pmYN99102* from the known *Pm* genes on 2BL, 98 previously reported markers that were closely linked to the documented *Pm* genes on chromosome arm 2BL were test the polymorphisms between the resistant and susceptible bulks derived from the $F_{2:3}$ families of YN99102 × JH13–205 (Table 2). Among them, 12 markers, including eight markers for *Pm6* (*CIT02g−2*, *CIT02g−3*, *CIT02g−13*, *CIT02g−15*, *CIT02g−17*, *CIT02g−18*, *CIT02g−20*, *CISSR02g−2*) and four markers for *Pm52* (*Xicscl172*, *Xicscl174*, *Xicsl326,* and *Xicsl234*) amplified polymorphisms between the resistant and susceptible parents and bulks, while other 86 markers showed no polymorphism. Four markers closely linked to *Pm52* were not linked to *pmYN99102* (Table 2). Molecular markers analysis combined with different resistance spectrum demonstrated that *pmYN99102* is most likely different from the known *Pm* genes on chromosome arm 2BL.

Molecular markers for MAS

To better use *pmYN99102* in MAS, 18 markers closely linked to *pmYN99102* were tested for their availability in the 42 susceptible wheat cultivars for MAS (Figure 6; Supplementary Table 1). All markers except for *YTU103–97* could amplify polymorphic bands between YN99102 and most of the 42 susceptible cultivars, suggesting that these markers can be used in MAS for tracking *pmYN99102* when transferred into those cultivars. *YTU103–97* amplified consistent bands in 38 out of 42 susceptible cultivars, meaning that these two markers were less appropriate for MAS of *pmYN99102*.

Discussion

In the present study, using genetic analysis, BSE-Seq, and molecular marker analysis, we accurately and rapidly

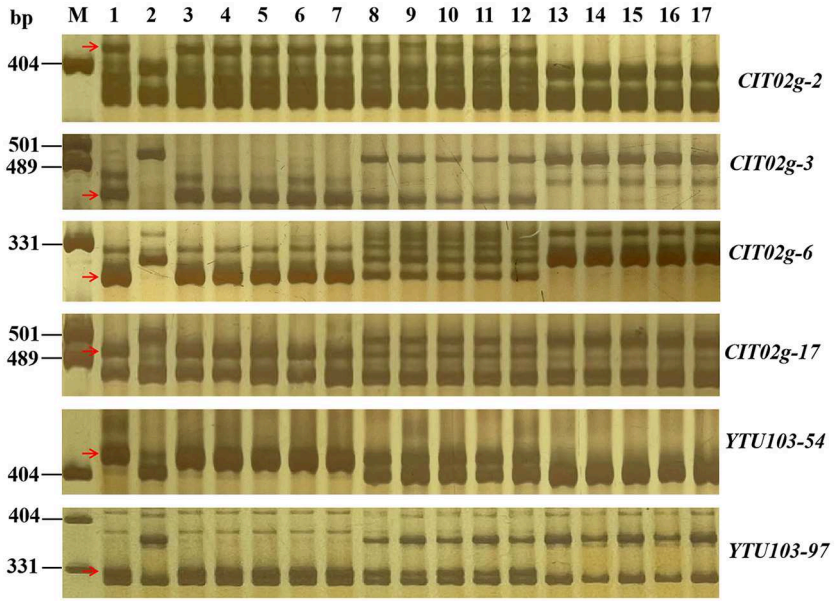

FIGURE 3
Amplification patterns of *pmYN99102*-linked markers *CIT02g-2* (A), *CIT02g-3* (B), *CIT02g-6* (C), *CIT02g-17* (D), *CIT02g-54* (E) and *YTU103-97* in genotyping resistant parent Yannong 99102-06188 (YN99102), susceptible parent Jinhe13–205 (JH13–205) and randomly selected $F_{2:3}$ families of YN99102 × JH13–205. Lane M, pUC18 *Msp* I; lanes 1–2, YN99102 and JH13–205; lanes 3–7, homozygously resistant $F_{2:3}$ families; lanes 8–12, heterozygously $F_{2:3}$ families; lanes 13–17, homozygously susceptible $F_{2:3}$ families. The red arrows were used to indicate the polymorphic bands linked to *pmYN99102*.

identified a recessive *Pm* gene *pmYN99102* in YN99102 and localized it to a 0.9 Mb interval (699.2–708.2 Mb) on chromosome arm 2BL, an enrichment region carrying many *Pm* genes (Wu et al., 2019). Eleven *Pm* genes have been reported to be located on chromosome arm 2BL from various gene donors, including *Pm6* from *Triticum timopheevii* (Wan et al., 2020), *Pm33* from *T. persicum* Vav. (Zhu et al., 2005), *Pm51* from a *Thinopyrum ponticum* introgression line (Zhan et al., 2014), *Pm52* from Chinese wheat cultivar Liangxing 99 (Wu et al., 2019), *Pm63* from Iranian wheat landrace PI 628024 (Tan et al., 2019), *Pm64* from wild emmer (Zhang et al., 2019), *PmQ* from Chinese wheat landrace Qingxinmai (Li H. H. et al., 2020), *MlZec1* and *MlAB10 both from T. dicoccoides* (Mohler et al., 2005; Maxwell et al., 2010), *PmKN0816* from the Chinese wheat breeding line KN0816 (Wang et al., 2021) and *PmLS5082* from the Chinese wheat breeding line LS5082 (Wu et al., 2019), suggesting chromosome arm 2BL is a potential R gene-rich region and complex molecular modules and mechanisms may be involved in the chromosome arm 2BL. Compared with those documented genes, *pmYN99102* (699.2–708.2 Mb) could be clearly distinguished from eight of them: *Pm33* (773.2–784.3 Mb), *Pm51* (709.8–739.4 Mb), *Pm52* (581.0–585.0 Mb), *Pm63* (710.3–723.4 Mb), *PmQ* (710.7–714.7 Mb), *MlZec1* and *MlAB10* (both 796.7–780.0 Mb), and *PmLS5082* (710.3–711.0 Mb) based on their physical locations and/or origins. However, the physical intervals of three genes *Pm6* (698.3–699.2 Mb), *Pm64* (699.2–710.3 Mb), and *PmKN0816* (700.4–710.3 Mb) overlapped that of *pmYN99102* (699.2–708.2 Mb) and hence it is necessary to clarify their relationships.

T. timopheevii derived *Pm6* was the first *Pm* gene identified on chromosome 2BL and was transferred into the wheat genetic background in the form of wheat-*T. timopheevii* 2B/2G introgression lines (Jorgensen and Jensen, 1973; Bennett, 1984; Ji et al., 2008). The 2G chromosome introgression segment carrying *Pm6* has strong recombination suppression in the wheat genome, so seven of the eight *Pm6*-linked markers used in this study had no recombination between the 2G chromosome introgression segment carrying *Pm6* and the corresponding wheat segment, while they showed normal recombination frequency as common wheat in the *pmYN99102* interval. Moreover, only 8 of 55 *Pm6*-linked markers showed polymorphisms between YN99102 and JH13–205, and their derivative $F_{2:3}$ resistant and susceptible bulks (Table 2), which revealed a distinct genetic diversity between the intervals of *pmYN99102* and *Pm6*. Meanwhile, YN99106 had a broader resistance spectrum than Coker 747 (with *Pm6*). Critically, YN99106 was resistant to *Bgt* isolate E09 and *pmYN99102* was identified by inoculating the *Bgt* isolate E09, whereas Coker 747 (with *Pm6*) was susceptible to the *Bgt* isolate

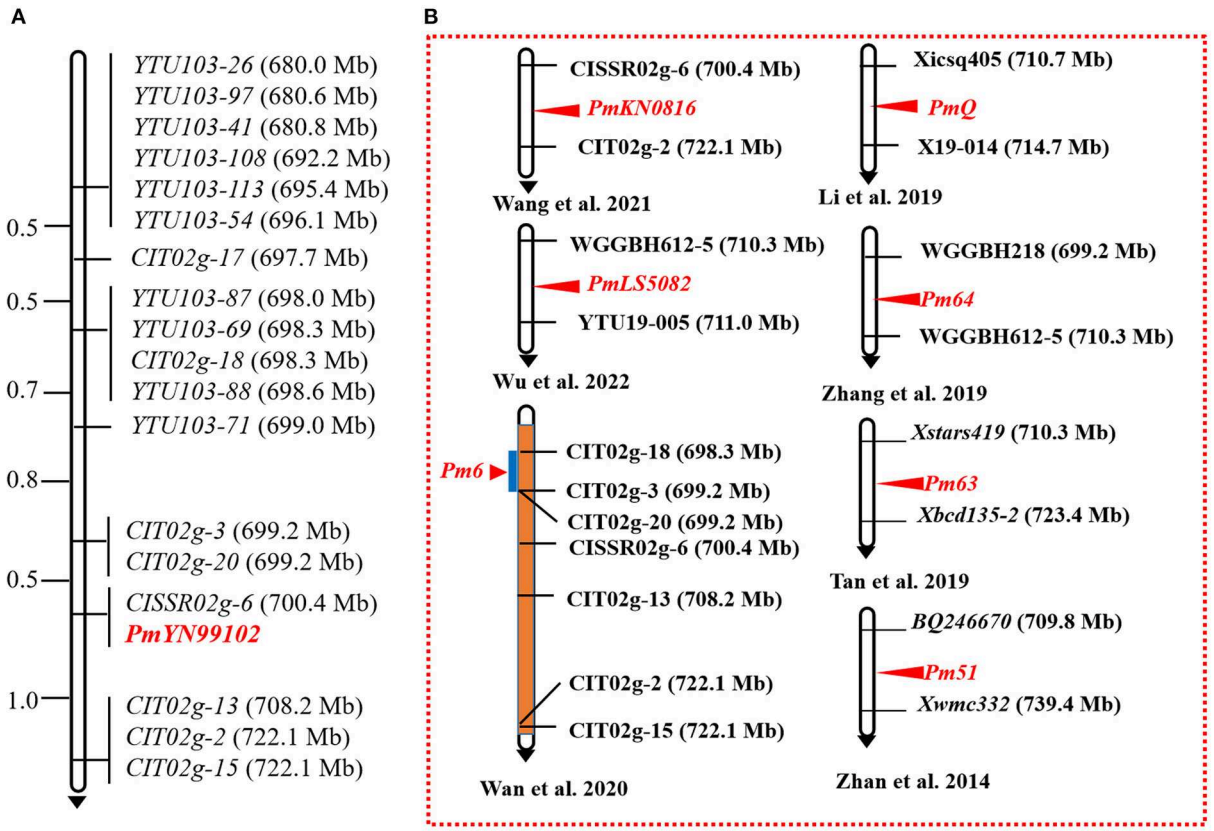

FIGURE 4
Linkage map of *pmYN99102* using the $F_{2:3}$ families of Yannong 99102-06188 × Jinhe13–205 (A) and the physical locations of cataloged *Pm* genes on chromosome arm 2BL (B). Genetic distances in cM are showed to the left. The black arrows point to the centromere.

E09 (Table 1). It was reported that Coker 747 was moderate effectiveness at the one-leaf stage to the two-leaf stage, but showed gradually increased resistance from the third leaf stage and reached complete resistance at the fourth leaf stage and later (Qin et al., 2011). Whereas, YN99102 exhibited high resistance to *Bgt* isolates from the one-leaf stage and continued through all growth stages. Therefore, the combined evidence indicated that *pmYN99102* was different from *Pm6*. *Pm64*, derived from a wheat-*T. dicoccoides* introgression line showed a different resistance spectrum from *pmYN99102* (Table 1). When tested with 10 *Pm64*-linked markers, none of them amplified polymorphisms in YN99102 and JH03–125 and their mapping population. *PmKN0816* was a broad-spectrum resistance gene and also discovered in a Chinese wheat breeding line, and its donor KN0816 was resistant to all the 11 tested *Bgt* isolates, but YN99102 was susceptible to the *Bgt* isolate A03. In addition, all of the three *Pm* genes *Pm6*, *Pm64*, and *PmKN0816* followed dominant inheritance pattern, while *pmYN99102* was distinctively recessive. Taken together, *pmYN99102* is most likely a new gene different from the cataloged *Pm* genes on chromosome 2BL based on their origins, chromosome intervals, resistance spectrum, and inheritance pattern. Of course, allelism tests and cloning of these genes are necessary in the future to finally determine their relationships in such a mysterious interval containing multiple and complex resistance genes. Further validation on the four candidate genes of *pmYN99102* that was directly related to disease resistance (Supplementary Table 3) will be our focus in the near future.

When a resistance gene was identified, less linkage drag is the critical factor associated with its easy use in wheat breeding programs, but often, disease resistance is at the expense of some agronomic traits and reduced plant adaptation (Deng et al., 2017; Ma et al., 2018; Han et al., 2022b). Fortunately, YN99102 is an elite derivative line from the same breeding process as a famous wheat cultivar Yannong 999 in China, which is the first wheat cultivar to exceed 800 kilograms per mu yield in China. In the breeding process of Yannong 999, two prominent breeding lines, Yannong 99102-06072 and Yannong 99102-06188 (YN99102) were selected as the candidate

lines. Of the two lines, Yannong 99102-06072 has favorable synergy between yield and quality, making it the current Yannong 999 official registration which met the breeding goal of high yield and quality; whereas YN99102 has the advantages of both powdery mildew resistance and high yield, making it a valuable resistance resource for both wheat breeding and genetic study. To facilitate the transfer of *pmYN99102* in MAS, we evaluated the applicability of 17 markers including 10 newly developed markers and seven reported markers in 42 susceptible cultivars (Supplementary Table 1). The results showed that all markers except for *YTU103–97* were polymorphic between YN99102 and most of the 42 susceptible cultivars, suggesting that these markers can be used in MAS for detecting *pmYN99102* once it was introduced to those susceptible cultivars. In fact, we have obtained the BC_1F_2 and F_3 segregation populations from the cross of some applicable cultivars and YN99102 currently. We believe that *pmYN99102* will release its full potential following the selection for resistance and agronomic performance in wheat breeding programs.

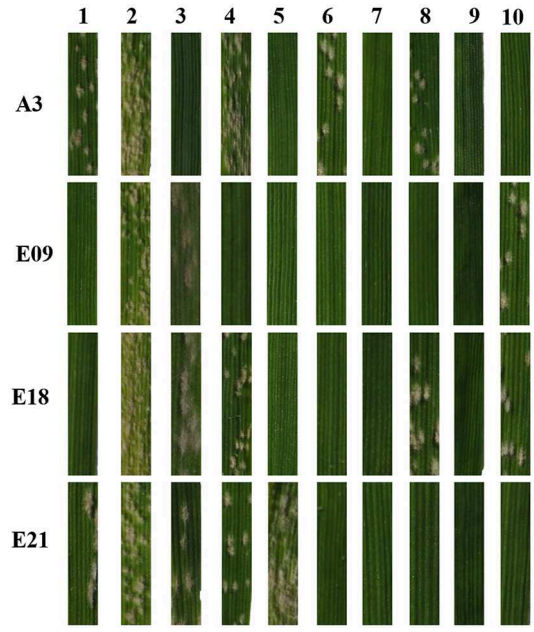

FIGURE 5
Reaction patterns of wheat breeding line Yannong 99102-06188 (YN99102) and the resistant donors with cataloged *Pm* genes on 2BL chromosome to selected *Blumaria graminis* f. s. *tritici* isolates A3, E09, E18, and E21. 1: YN99102; 2: susceptible parent Jinhe13-205 (JH13–205); 3: Coker747 (*Pm6*); 4: Am9/3 (*Pm33*); 5: CH7086 (*Pm51*); 6: Liangxing 99 (*Pm52*); 7: WE35 (*Pm64*); 8: LS5082 (*PmLS5082*); 9: KN0816 (*PmKN0816*); 10: Qingxinmai (*PmQ*).

Conclusion

In conclusion, using BSE-Seq and molecular markers, we identified a powdery mildew resistance gene *pmYN99102* in the wheat breeding line YN99102. Based on the analysis of physical location, origin, resistant spectrum, and inherited pattern, *pmYN99102* is most likely a new *Pm* gene. Molecular markers available for marker-assisted selection were also selected for tracking *pmYN99102* in breeding. Our study can be valuable for enhancing the genetic diversity of powdery mildew resistance in breeding.

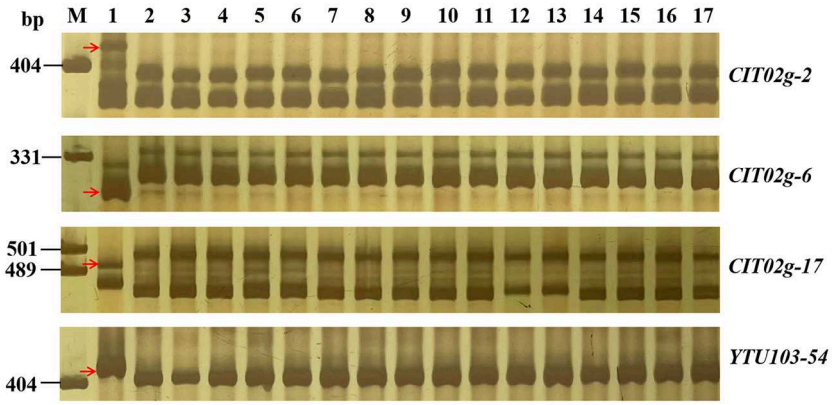

FIGURE 6
Amplification patterns of *pmYN99102*-linked markers *CIT02g-2* (A) and *CIT02g-6* (B), *CIT02g-17* (C) and *YTU103-54* (D) in Yannong 99102-06188 (YN99102), Jinhe13–205 (JH13–205), and 15 wheat cultivars/breeding lines susceptible to powdery mildew. M, DNA marker pUC18 *Msp* I; lanes 1 and 2, YN99102 and JH13–205; and lanes 3–17: Shannong 1,538, Hanmai 13, Huaimai 0,226, Zhoumai 27, Xinong 979, Lumai 185, Zhongyu 1,311, Jimai 268, Tainong 1,014, Jimai 229, Jimai 21, Jimai 20, Daimai 2,173, Zhoumai 1,751, Jinan 17. The white arrows indicate the polymorphic bands in YN99102.

Data availability statement

The datasets presented in this study can be found in online repositories. The names of the repository/repositories and accession number(s) can be found in the article/Supplementary material.

Author contributions

PM, GH, and JW conceived the research. YM, WG, YQ, ZY, LX, FS, and WZ performed the experiments. JW and XL developed the experimental materials. NS and WL performed the phenotypic assessment. GH, JG, and RH analyzed the data. PM wrote the manuscript. All authors read and approved the final manuscript.

Funding

This research was financially supported by the National Natural Science Foundation of China (32072053, 31971874) and the Key Research and Development Project of Shandong Province (2020CXGC010805, 2021LZGC009).

Acknowledgments

We are grateful to Prof. Emerita Paula E. Jameson, University of Canterbury, financially supported by Double Hundred Plan for Foreign Experts in Shandong Province, China, for critically reviewing and editing this manuscript.

Conflict of interest

The authors declare that the research was conducted in the absence of any commercial or financial relationships that could be construed as a potential conflict of interest.

Publisher's note

Supplementary material

The Supplementary Material for this article can be found online at: https://www.frontiersin.org/articles/10.3389/fpls.2022.1005627/full#supplementary-material

SUPPLEMENTARY FIGURE 1
Genealogy of the wheat breeding line Yannong 99102-06188 and its relationship with the wheat cultivar Yannong 999.

SUPPLEMENTARY TABLE 1
Validation of *pmYN99102*-linked markers on 42 Chinese wheat cultivars/breeding lines in marker-assisted selection (MAS) breeding.

SUPPLEMENTARY TABLE 2
Molecular markers developed by bulked segregant exome capture sequencing (BSE-Seq).

SUPPLEMENTARY TABLE 3
Gene annotation in the candidate interval of wheat powdery mildew resistance gene *pmYN99102*.

References

An, D. G., Ma, P. T., Zheng, Q., Fu, S. L., Li, L. H., Han, F. P., et al. (2019). Development and molecular cytogenetic identification of a new wheat-rye 4R chromosome disomic addition line with resistances to powdery mildew, stripe rust and sharp eyespot. *Theor. Appl. Genet.* 132, 257–272. doi: 10.1007/s00122-018-3214-3

Bennett, F. G. A. (1984). Resistance to powdery mildew in wheat: a review of its use in agriculture and breeding programmes. *Plant Pathol.* 33, 279–300. doi: 10.1111/j.1365-3059.1984.tb01324.x

Chen, X. M. (2013). Review article: high-temperature adult-plant resistance, key for sustainable control of stripe rust. *Am. J. Plant Sci.* 4, 608–627. doi: 10.4236/ajps.2013.43080

Cingolani, P., Platts, A., Wang, L. L., Coon, M., Nguyen, T., Wang, L., et al. (2012). A program for annotating and predicting the effects of single nucleotide polymorphisms, SnpEff: SNPs in the genome of Drosophila melanogaster strain w1118; iso-2; iso-3. *Fly (Austin).* 6, 80–92. doi: 10.4161/fly.19695

Deng, Y. W., Zhai, K. R., Xie, Z., Yang, D. Y., Zhu, X. D., Liu, J. Z., et al. (2017). Epigenetic regulation of antagonistic receptors confers rice blast resistance with yield balance. *Science* 355, 962–965. doi: 10.1126/science.aai8898

Dong, C. H., Zhang, L. C., Chen, Z. X., Xia, C., Gu, Y. Q., Wang, J. R., et al. (2020). Combining a new exome capture panel with an effective varBScore algorithm accelerates BSA-based gene cloning in wheat. *Front. Plant Sci.* 11, 1249. doi: 10.3389/fpls.2020.01249

Han, G. H., Yan, H. W., Gu, T. T., Cao, L. J., Zhou, Y. L., Wei, L., et al. (2022a). Identification of a wheat powdery mildew dominant resistance gene in the *Pm5* locus for high-throughput marker-assisted selection. *Plant Dis.* doi: 10.1094/PDIS-07-22-1545-RE. [Epub ahead of print].

Han, G. H., Yan, H. W., Wang, J., Cao, L. J., Liu, S. Y., Li, X. Q., et al. (2022b). Molecular cytogenetic identification of a new wheat-rye 6R addition line and physical localization of its powdery mildew resistance gene. *Front. Plant Sci.* 13, 889494. doi: 10.3389/fpls.2022.889494

He, H. G., Liu, R. K., Ma, P. T., Du, H. N., Zhang, H. H., Wu, Q. H., et al. (2021). Characterization of *Pm68*, a new powdery mildew resistance gene on chromosome 2BS of greek durum wheat TRI 1796. *Theor. Appl. Genet.* 134, 53–62. doi: 10.1007/s00122-020-03681-2

He, Z. H., Xia, X. C., Chen, X. M., Zhang, Y., Zhang, Y., Yan, J., et al. (2015). "Application of molecular markers in plant quality and disease resistance breeding". *In the Proceedings of the Seventh National Symposium on Wheat Genetics and Breeding*. Zhengzhou.

He, Z. H., Xia, X. C., Chen, X. M., and Zhuang, Q. S. (2011). Progress of wheat breeding in China and the future perspective. *Acta Agron. Sin*. 37, 202–215. doi: 10.3724/SP.J.1006.2011.00202

International Wheat Genome Sequencing Consortium (IWGSC) (2014). A chromosome-based draft sequence of the hexaploid bread wheat (Triticum aestivum) genome. *Science* 345, 1251788. doi: 10.1126/science.1251788

Isham, K., Wang, R., Zhao, W., Wheeler, J., Klassen, N., Akhunov, E., et al. (2021). QTL mapping for grain yield and three yield components in a population derived from two high-yielding spring wheat cultivars. *Theor. Appl. Genet*. 134, 2079–2095. doi: 10.1007/s00122-021-03806-1

IWGSC. (2018). Shifting the limits in wheat research and breeding using a fully annotated reference genome. *Science* 361, eaar7191. doi: 10.1126/science.aar7191

Ji, J. H., Qin, B., Wang, H. Y., Cao, A. Z., Wang, S. L., Chen, P. D., et al. (2008). STS markers for powdery mildew resistance gene *Pm6* in wheat. *Euphytica* 163, 159–165. doi: 10.1007/s10681-007-9578-0

Jia, M. S., Xu, H. X., Liu, C., Mao, R. X., Li, H. S., Liu, J. J., et al. (2020). Characterization of the powdery mildew resistance gene in the elite wheat cultivar Jimai 23 and its application in marker-assisted selection. *Front. Genet*. 11, 241. doi: 10.3389/fgene.2020.00241

Jiang, Y., Schulthess, A. W., Rodemann, B., Ling, J., Plieske, J., Kollers, S., et al. (2016). Validating the prediction accuracies of marker-assisted and genomic selection of fusarium head blight resistance in wheat using an independent sample. *Theor. Appl. Genet*. 130, 471–482. doi: 10.1007/s00122-016-2827-7

Jin, Y. L., Shi, F. Y., Liu, W. H., Fu, X. Y., Gu, T. T., Han, G. H., et al. (2021). Identification of resistant germplasm and detection of genes for resistance to powdery mildew and leaf rust from 2,978 wheat accessions. *Plant Dis*. 105, 3900–3908. doi: 10.1094/PDIS-03-21-0532-RE

Jorgensen, J. H., and Jensen, C. J. (1973). Gene *Pm6* for resistance to powdery mildew in wheat. *Euphytica* 22, 423–423. doi: 10.1007/BF00022656

Kosambi, D. D. (1944). The estimation of map distances from recombination values. *Ann. Hum. Genet*. 12, 172–175. doi: 10.1111/j.1469-1809.1943.tb02321.x

Li, H. H., Dong, Z. J., Ma, C., Xia, Q., Tian, X. B., Sehgal, S., et al. (2020). A spontaneous wheat-aegilops longissima translocation carrying *Pm66* confers resistance to powdery mildew. *Theor. Appl. Genet*. 133, 1149–1159. doi: 10.1007/s00122-020-03538-8

Li, H. J., Murray, T. D., Mcintosh, R. A., and Zhou, Y. (2019). Breeding new cultivars for sustainable wheat production. *Crop J.* 7, 715–717. doi: 10.1016/j.cj.2019.11.001

Li, Y. H., Shi, X. H., Hu, J. H., Wu, P. P., Qiu, D., Qu, Y. F., et al. (2020). Identification of a recessive gene *PmQ* conferring resistance to powdery mildew in wheat landrace Qingxinmai using BSR-Seq analysis. *Plant Dis.* 104, 743–751. doi: 10.1094/pdis-08-19-1745-re

Lincoln, S. E., Daly, M. J., Lander, E. S., Lincoln, S., Daly, M., and Lander, E. (1992). *Constructing Genetics Maps With MAPMAKER/EXP 3.0. Whitehead Institute Technical Report,* 3rd Edn. Cambridge, MA: Whitehead Institute.

Ma, P. T., Wu, L. R., Xu, Y. F., Xu, H. X., Xu, Z., Zhang, X., et al. (2021). Bulked segregant RNA-Seq provides distinctive expression profile against powdery mildew in the wheat genotype YD588. *Front. Plant Sci*. 12, 764978. doi: 10.3389/fpls.2021.764978

Ma, P. T., Xu, H. X., Xu, Y. F., Li, L. H., Qie, Y. M., Luo, Q. L., et al. (2015). Molecular mapping of a new powdery mildew resistance gene *Pm2b* in Chinese breeding line KM2939. *Theor. Appl. Genet*. 128, 613–622. doi: 10.1007/s00122-015-2457-5

Ma, P. T., Xu, H. X., Xu, Y. F., Song, L. P., Liang, S. S., Sheng, Y., et al. (2018). Characterization of a powdery mildew resistance gene in wheat breeding line 10V-2 and its application in marker-assisted selection. *Plant Dis.* 102, 925–931. doi: 10.1094/pdis-02-17-0199-re

Maxwell, J. J., Lyerly, J. H., Srnic, G., Parks, R., Cowger, C., Marshall, D., et al. (2010). MlAB10: A *Triticum turgidum* subsp. *Dicoccoides derived powdery mildew resistance gene identified in common wheat. Crop Sci*. 50, 2261. doi: 10.2135/cropsci2010.04.0195

McCormick, R. F., Truong, S. K., and Mullet, J. E. (2015). RIG: recalibration and interrelation of genomic sequence data with the GATK. *G3 (Bethesda)*. 5, 655–665. doi: 10.1534/g3.115.017012

McIntosh, R. A., Dubcovsky, J., Rogers, W. J., Xia, X. C., and Raupp, W. J. (2020). *Catalogue of Gene Symbols For Wheat 2020 Supplement*. Available online at: https://wheat.pw.usda.gov/GG3/WGC

Mohler, V., Zeller, F. J., Wenzel, G., and Hsam,. S. L. K. (2005). Chromosomal location of genes for resistance to powdery mildew in common wheat (*Triticum aestivum* L. em Thell.). 9. Gene *MlZec1* from the *Triticum dicoccoides*-derived wheat line Zecoi-1. *Euphytica* 142, 161–167. doi: 10.1007/s10681-005-1251-x

Narasimhan, V., Danecek, P., Scally, A., Xue, Y., Tyler-Smith, C., and Durbin, R. (2016). BCFtools/RoH: a hidden markov model approach for detecting autozygosity from next-generation sequencing data. *Bioinformatics* 32, 1749–1751. doi: 10.1093/bioinformatics/btw044

Qin, B., Cao, A., Wang, H., Chen, T., You, F. M., Liu, Y., et al. (2011). Collinearity-based marker mining for the fine mapping of *Pm6*, a powdery mildew resistance gene in wheat. *Theor. Appl. Genet*. 123, 207–218. doi: 10.1007/s00122-011-1577-9

Sheng, B. Q. (1988). Wheat powdery mildew was recorded using infection type in seedling stage. *Plant Prot*. 14:49.

Sheng, B. Q., and Duan, X. Y. (1991). Improvement of scale 0-9 method for scoring adult plant resistance to powdery mildew of wheat. *Beijing Agr. Sci*. 1, 38–39.

Singh, R. P., Singh, P. K., Rutkoski, J., Hodson, D. P., He, X., Jørgensen, L. N., et al. (2016). Disease impact on wheat yield potential and prospects of genetic control. *Annu. Rev. Phytopathol*. 54, 303–322. doi: 10.1146/annurev-phyto-080615-095835

Summers, R. W., and Brown, J. K. M. (2013). Constraints on breeding for disease resistance in commercially competitive wheat cultivars. *Plant Phothol*. 62, 115–121. doi: 10.1111/ppa.12165

Takagi, H., Uemura, A., Yaegashi, H., Tamiru, M., Abe, A., Mitsuoka, C., et al. (2013). MutMap-Gap: whole-genome resequencing of mutant F2 progeny bulk combined with de novo assembly of gap regions identifies the rice blast resistance gene Pii. *New Phytol*. 200, 276–283. doi: 10.1111/nph.12369

Tan, C. C., Li, G. Q., Cowger, C., Carver, B. F., and Xu, X. Y. (2018). Characterization of *Pm59*, a novel powdery mildew resistance gene in Afghanistan wheat landrace PI 181356. *Theor. Appl. Genet*. 131, 1145–1152. doi: 10.1007/s00122-018-3067-9

Tan, C. C., Li, G. Q., Cowger, C., Carver, B. F., and Xu, X. Y. (2019). Characterization of *Pm63*, a powdery mildew resistance gene in Iranian landrace PI 628024. *Theor. Appl. Genet*. 132, 1137–1144. doi: 10.1007/s00122-018-3265-5

Wan, W. T., Xiao, J., Li, M. L., Tang, X., Wen, M. X., Cheruiyot, A. K., et al. (2020). Fine mapping of wheat powdery mildew resistance gene *Pm6* using 2B/2G homoeologous recombinants induced by the ph1b mutant. *Theor. Appl. Genet*. 133, 1265–1275. doi: 10.1007/s00122-020-03546-8

Wang, W. R., He, H. G., Gao, H. M. , Xu, H. X., Song, W. Y., Zhang, X., et al. (2021). Characterization of the powdery mildew resistance gene in wheat breeding line KN0816 and its evaluation in marker-assisted selection. *Plant Dis*. 105, 4042–4050. doi: 10.1094/pdis-05-21-0896-re

Wang, Z. L., Li, L. H., He, Z. H., Duan, X. Y., Zhou, Y. L., Chen, X. M., et al. (2005). Seedling and adult plant resistance to powdery mildew in Chinese bread wheat cultivars and lines. *Plant Dis*. 89, 457–463. doi: 10.1094/pd-89-0457

Wu, P. P., Hu, J. H., Zou, J. W., Qiu D., Qu, Y. F., Li, Y. H., et al. (2019). Fine mapping of the wheat powdery mildew resistance gene Pm52 using comparative genomics analysis and the Chinese Spring reference genomic sequence. *Theor. Appl. Genet*. 132, 1451–1461. doi: 10.1007/s00122-019-03291-7

Xu, H. X., Yi, Y. J., Ma, P. T., Qie, Y. M., Fu, X. Y., Xu, Y. F., et al. (2015). Molecular tagging of a new broad-spectrum powdery mildew resistance allele *Pm2c* in Chinese wheat landrace Niaomai. *Theor. Appl. Genet*. 128, 2077–2084. doi: 10.1007/s00122-015-2568-z

Yu, Z. Y., Xiao, L. N., Su, F. Y., Liu, W., Luo, F. Y., Han, R., et al. (2022). Mining of wheat *Pm2* alleles for goal-oriented marker-assisted breeding. *Front. Plant Sci*. 13, 912589. doi: 10.3389/fpls.2022.912589

Zhan, H. X., Li, G. R., Zhang, X. J., Li, X., Guo, H. J., Gong, W. P., et al. (2014). Chromosomal location and comparative genomics analysis of powdery mildew resistance gene *Pm51* in a putative wheat-*Thinopyrum ponticum* introgression line. *PLoS ONE*. 9, e113455. doi: 10.1371/journal.pone.0113455

Zhang, D. Y., Zhu, K. Y., Dong, L. L., Liang, Y., Li, G. Q., Fang, T. L., et al. (2019). Wheat powdery mildew resistance gene *Pm64* derived from wild emmer (*Triticum turgidum var. dicoccoides*) is tightly linked in repulsion with stripe rust resistance gene *Yr5*. *Crop J*. 7, 761–770. doi: 10.1016/j.cj.2019.03.003

Zhao, Z. H., Sun, H. G., Song, W., Lu, M., Huang, J., Wu, L. F., et al. (2013). Genetic analysis and detection of the gene *MlLX99* on chromosome 2BL conferring resistance to powdery mildew in the wheat cultivar Liangxing 99. *Theor. Appl. Genet*. 126, 3081–3089. doi: 10.1007/s00122-013-2194-6

Zhou, R. H., Zhu, Z. D., Kong, X. Y., Huo, N. X., Tian, Q. Z., Li, P., et al. (2005). Development of wheat near-isogenic lines for powdery mildew resistance. *Theor. Appl. Genet*. 110, 640–648. doi: 10.1007/s00122-004-1889-0

Zhu, T., Wu, L. R., He, H. G., Song, J. C., Jia, M. S., Liu, L. C., et al. (2020). Bulked segregant RNA-Seq reveals distinct expression profiling in Chinese wheat cultivar Jimai 23 responding to powdery mildew. *Front. Genet*. 11, 474. doi: 10.3389/fgene.2020.00474

Zhu, Z. D., Zhou, R. H., Kong, X. Y., Dong, Y. C., and Jia, J. Z. (2005). Microsatellite markers linked to 2 powdery mildew resistance genes introgressed from *Triticum carthlicum* accession PS5 into common wheat. *Genome* 48, 585–590. doi: 10.1139/G05-016

frontiers | Frontiers in Plant Science

TYPE Original Research
PUBLISHED 09 September 2022
DOI 10.3389/fpls.2022.968924

OPEN ACCESS

EDITED BY
Handong Su,
Huazhong Agricultural University, China

REVIEWED BY
Vikas Venu Kumaran,
Indian Agricultural Research Institute (ICAR), India
Ping Yang,
Institute of Crop Sciences (CAAS), China

*CORRESPONDENCE
Min Jiang
jm3192@126.com
Yanbo Wang
lnwangyanbo@163.com

†PRESENT ADDRESS
Xue Gong,
Guangxi Academy of Agricultural Sciences,
Nanning, China

‡These authors have contributed equally to this work

SPECIALTY SECTION
This article was submitted to Plant Pathogen Interactions, a section of the journal Frontiers in Plant Science

RECEIVED 14 June 2022
ACCEPTED 25 August 2022
PUBLISHED 09 September 2022

CITATION
Zhu M, Ma J, Liu X, Guo Y, Qi X, Gong X, Zhu Y, Wang Y and Jiang M (2022) High-resolution mapping reveals a *Ht3*-like locus against northern corn leaf blight. *Front. Plant Sci.* 13:968924. doi: 10.3389/fpls.2022.968924

High-resolution mapping reveals a *Ht3*-like locus against northern corn leaf blight

Mang Zhu[2‡], Jun Ma[1‡], Xinfang Liu[1‡], Yanling Guo[3], Xin Qi[1], Xue Gong[1†], Yanbin Zhu[2,3], Yanbo Wang[1*] and Min Jiang[1*]

[1]Liaoning Academy of Agricultural Sciences, Shenyang, China, [2]State Key Laboratory of Plant Physiology and Biochemistry, College of Agronomy and Biotechnology, National Maize Improvement Center, Center for Crop Functional Genomics and Molecular Breeding, China Agricultural University, Beijing, China, [3]Liaoning Dongya Agricultural Development Co., Ltd., Shenyang, China

Northern corn leaf blight (NCLB), caused by the fungal pathogen *Exserohilum turcicum*, poses a grave threat to maize production worldwide. The resistance gene in A619*Ht3*, discovered decades ago, is an important genetic resource for NCLB control. By using a pair of near-isogenic lines (NILs) A619*Ht3* and A619, together with the resistant and susceptible bulks derived from the cross of A619*Ht3* and L3162 lines, we initially detected a *Ht3*-like (*Ht3L*) locus in bin 8.06 that was closely associated with NCLB resistance. We then performed five rounds of fine-mapping, which ultimately delimited the *Ht3L* locus to a 577-kb interval flanked by SNP markers KA002081 and KA002084. Plants homozygous for the *Ht3L*/*Ht3L* genotype exhibited an average reduction in diseased leaf area (DLA) by 16.5% compared to plants lacking *Ht3L locus*. The *Ht3L* locus showed extensive variation in genomic architecture among different maize lines and did not appear to contain any genes encoding canonical cell wall-associated kinases against NCLB. Moreover, the *Ht3L* locus was located ~2.7 Mb away from the known *Htn1* locus. We speculate that the *Ht3L* locus may contain a bona fide *Ht3* gene or a novel NCLB resistance gene closely linked to *Ht3*. In practice, the *Ht3L* locus is a valuable resource for improving maize resistance to NCLB.

KEYWORDS

***Ht3*, northern corn leaf blight (NCLB), maize (*Zea mays* L.), maize disease, fine-mapping**

Introduction

Northern corn leaf blight (NCLB), caused by the hemibiotrophic fungus *Exserohilum turcicum* (Chang and Fan, 1986), is one of the most devastating foliar diseases in most maize-growing areas worldwide. Maize (*Zea mays* L.) grown in areas with high humidity and moderate temperatures is more prone to NCLB

outbreaks. During the grain-filling period, NCLB causes leaf necrosis and thus abolishes photosynthetic output, leading to lower grain yield (Raymundo and Hooker, 1981). The development and deployment of resistant maize varieties is the most environmentally friendly and cost-effective way to reduce yield loss caused by NCLB.

Maize resistance to NCLB is a very complex trait, including both qualitative and quantitative resistance. Several qualitative resistance genes against NCLB have been discovered. The first locus, *Helminthosporium turcium resistance l* (*Ht1*), was identified in the inbred line 'GE440' and 'Ladyfinger' popcorn in 1959; this locus shows a partially dominant inheritance pattern and maps to chromosome 2L (Bentolila et al., 1991). *Ht1* substantially inhibits the formation of conidia in chlorosis (Hilu and Hooker, 1964, 1965). The *Ht2* locus displays a similar resistance performance and genetic architecture to *Ht1* and maps to chromosome 8L (Hooker, 1977). *Ht3*, a dominant single gene identified independently of *Ht1* and *Ht2*, was introgressed into the maize genome from the wild maize relative Florida gamagrass (*Tripsacum floridanum*) (Hooker, 1981). *Ht2* and *Ht3* were recently shown to be identical and allelic to the previously cloned *Htn1* gene (Yang et al., 2021). At the maturity stage, plants harboring *Ht2* or *Ht3* display necrotic and chlorotic lesions, respectively, while plants with *Htn1* show a delay in lesion formation (Hooker, 1977, 1981; Welz and Geiger, 2000). This observation suggests that other genes may be linked to *Htn1* and contribute to the response against NCLB. Moreover, histological studies revealed that plants with different resistance genes (*Ht1*, *Ht2*, *Ht3*, or *Htn1*) show different symptoms, indicating that resistance mechanisms conferred by these genes are not equivalent (Navarro et al., 2020).

Previous studies have shown that quantitative trait loci (QTLs) for resistance to NCLB are dispersed over all 10 chromosomes in maize (Welz and Geiger, 2000; Wisser et al., 2006; Balint-Kurti et al., 2010; Zwonitzer et al., 2010). Although many QTLs associated with resistance against NCLB have been identified in different populations, few have been fine-mapped or their causal genes even cloned. For instance, a major QTL was detected on chromosome 8 from a cross derived from two near-isogenic lines (NILs) with contrasting performance for NCLB resistance and fine-mapped to a 460-kb region containing 12 annotated genes (Chung et al., 2010). Another major QTL, designated *qNLB1.06*, was anchored to a 3.6-Mb region and narrowed down to two putative candidate genes by joint linkage and association mapping (Jamann et al., 2014). The QTL *qNCLB7.02* was mapped to chromosome 7 by linkage mapping and validated in chromosome segment substitution lines (CSSLs) (Wang et al., 2018). Single-marker and haplotype-based association mapping studies identified 12 and 10 loci, respectively, that were significantly associated with NCLB resistance (Ding et al., 2015). A total of 29 resistance QTLs against NCLB were identified using a nested association mapping (NAM) population with 5,000 recombinant inbred lines (RILs) (Poland et al., 2011). To date, the gene *ZmWAK-RLK1* (*Wall-associated-receptor-like kinase 1*) at the *Htn1* locus is the only resistance QTL against NCLB that has been cloned through map-based cloning (Hurni et al., 2015). Further investigation revealed that NCLB resistance mediated by ZmWAK-RLK1 correlates with reduced benzoxazinoid contents (Yang et al., 2019).

Although the *Htn1* locus is effective against most prevalent NCLB races, NCLB isolates with virulence in *Htn1*-bearing plants have been reported (Weems and Bradley, 2018; Jindal et al., 2019). Thus, there is an urgent need to explore novel loci conferring NCLB resistance. Quantitative disease resistance has been widely utilized in resistance breeding programs due to its moderate effectiveness and the durable and non-race-specific resistance it confers (Ayliffe et al., 2008; Poland et al., 2009). Introgression of both qualitative and quantitative resistance loci into inbred lines via marker-assisted backcrossing (MABC) is a powerful means to control diseases in maize (Zhao et al., 2012; Li et al., 2017).

Bulked-segregant analysis (BSA) is a rapid, technically simple method to identify markers linked to specific genes (Michelmore et al., 1991), which has been widely used in rice (*Oryza sativa*) (Venuprasad et al., 2009), wheat (*Triticum aestivum*) (Shen et al., 2003) and maize (Cai et al., 2003; Li et al., 2018). Another powerful strategy to narrow down a QTL interval is sequential QTL fine-mapping based on the genotypes and phenotypes of progeny derived from recombinants (Yang et al., 2012). Many quantitative disease-resistance genes have been cloned using this strategy (Zuo et al., 2015; Leng et al., 2017; Liu et al., 2017, 2020; Wang et al., 2017; Ye et al., 2019). In the current study, we conducted QTL identification and high-resolution mapping of the *Ht3*-like (*Ht3L*) locus in the resistant line A619*Ht3* by combining NIL analysis, BSA and sequential QTL fine-mapping. Our results lay the foundation for the future map-based cloning of the causal gene at the *Ht3L* locus. The molecular markers on or adjacent to *Ht3L* described here can also be used for MABC to improve maize resistance to NCLB in breeding programs.

Materials and methods

Plant materials

The pair of near-isogenic lines (NILs) A619*Ht3* and A619 was obtained from the Eastern Cereal and Oilseed Research Centre of Agriculture and Agri-Food Canada. While A619*Ht3* is highly resistant to NCLB, A619 is highly susceptible to NCLB, and both NILs share ~98.84% genomic homozygosity (Ma et al., 2014). The elite but susceptible inbred line L3162 is the male parent of the hybrids Liaodan565 and Liaodan566 widely grown in China. From a cross between A619*Ht3* (donor parent) and L3162 (recurrent parent), multiple backcross populations

were developed for initial QTL detection and fine-mapping. In 2016, the two parental lines (A619*Ht3* and L3162) and their BC_2F_1 backcross population comprising 362 individuals were grown at the Shenyang experimental station (41°46′N, 123°26′E) in China for artificial inoculation. Twenty-nine highly susceptible and 29 highly resistant plants were selected to form the susceptible and resistant bulks, respectively, for initial mapping of the *Ht3L* locus. Subsequently, the BC_3F_1 progeny from recombination events in the mapped *Ht3L* region were identified and backcrossed to L3162 (Hainan winter nursery, 18°39′N and 109°21′E) to produce BC_4F_1 progeny for fine-mapping. In the following five rounds of fine-mapping from 2017 to 2021, newly-occurring recombinants were screened in Shenyang and then backcrossed twice to L3162 in Shenyang and Hainan to generate progeny. All offspring were investigated for NCLB resistance at the Shenyang experimental station. A619*Ht3* and L3162 were planted annually in each experimental block as resistant and susceptible controls, respectively.

Artificial inoculation and northern corn leaf blight disease evaluation

Exserohilum turcicum (mixed races 0, 1, 2, 3N, 12N, and 23N) was cultured on potato dextrose agar (PDA) medium for 15 days at 25°C and then stored in the dark at room temperature. Plant materials were artificially inoculated at the V8-V10 leaf stages with ∼5 mL of spore suspension (1×10^5-10^6 conidia per mL in 0.02% [v/v] Tween 20) per plant. Spray irrigation was then performed for 2 days following inoculation, three to four times a day, to maintain a humid environment. Four weeks after inoculation, NCLB lesions were prominent and suitable for first scoring, followed by two more scorings over the next 14 days. Diseased leaf area (DLA) was examined for three leaves (ear leaf and its upper and lower leaves) based on standards listed in **Supplementary Figure 1**. Average DLA was used to represent NCLB severity.

Genotyping

Fresh leaf tissue at the five-leaf seedling stage was harvested for high-throughput extraction of genomic DNA in 96-well plates. Plant genomic DNA was extracted according to the method described previously (Murray and Thompson, 1980). The Maize3K Chip was used to genotype the NILs (A619*Ht3* and A619) and the two parental lines (A619*Ht3* and L3162). The Maize6K Chip was used to genotype each plant in the selected susceptible and resistant bulks. Kompetitive Allele-Specific PCR (KASP) markers, developed in the target *Ht3L* region, were subjected to automated genotyping with the QuantStudio 12 K Flex Real-Time PCR System (Applied Biosystems by Life Technologies).

Bulk-based association analysis and statistical analysis

The single-nucleotide polymorphism (SNP) index was calculated based on the heterozygosity at each SNP within a given bulk. For each SNP, the Δ(SNP-index) value was calculated using the following formula: Δ(SNP-index) = SNP-index in the resistant bulk – SNP-index in the susceptible bulk (Takagi et al., 2013). The Δ(SNP-index) value was used to identify candidate regions for *Ht3L*. The average Δ(SNP-index) value of the SNPs located in each genomic interval was calculated using a sliding window with a window size of 10 Mb and 10-kb steps. The distribution of Δ(SNP-index) along the chromosomes was plotted using R software. SNP markers in the candidate *Ht3L* regions were also used to conduct regional association analyses. For each SNP marker, the significant difference in SNP-index between two bulks was determined by chi-squared test.

Genomic structure analysis

Markers in the *Ht3L* region were identified according to the B73 reference genome sequence and were projected onto the 25 founders of the NAM population to define their corresponding *Ht3L* regions. The sequence information and annotated genes in the *Ht3L* regions were then retrieved from MaizeGDB[1]. The gene distribution in susceptible and resistant founders was plotted using R software.

Results

A619*Ht3* exhibits a distinct resistance spectrum to *Exserohilum turcicum* races

To determine the A619*Ht3* resistance spectrum, we conducted virulence testing on the five near-isogenic lines containing the different *Ht* loci (A619, A619*Ht1*, A619*Ht2*, A619*Ht3* and A619*HtN*) by inoculating designated physiological races of *Exserohilum turcicum* (1,2,3, and 123N) in growth chamber. The results showed that A619*Ht3* exhibits susceptible to races 3 and 123N, while resistant to races 1 and 2 (**Table 1**), which was consistent with the resistance spectrum of the *Ht3* locus in OH43 and HZS genetic backgrounds (Guo, 2015). We thus named the resistance gene in A619*Ht3* as *Ht3*-like (*Ht3L*) to distinguish it from the recently reported *Ht3* allele that is identical to *Ht2* and allelic to *Htn1* (Yang et al., 2021).

1 http://www.maizegdb.org/

TABLE 1 Virulence testing on the five different *Ht* genes by designating physiological races of *Exserohilum turcium*.

Race	Response				
	A619	**A619*Ht1***	**A619*Ht2***	**A619*Ht3***	**A619*HtN***
1	S	S	R	R	R
2	S	R	S	R	R
3	S	R	R	S	R
123N	S	S	S	S	S

R: resistant, no necrosis, or chlorotic lesions surrounded by chlorosis; S: susceptible, necrotic lesions without chlorotic border.

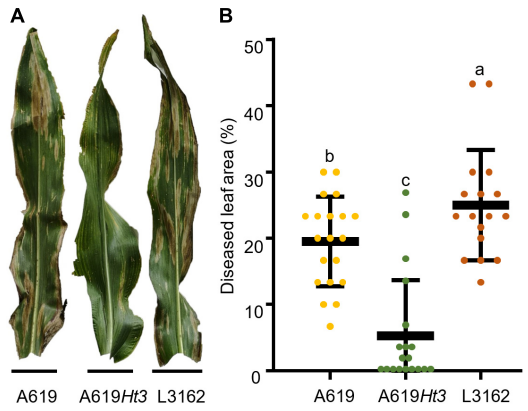

FIGURE 1
Performances of three maize inbred lines A619, A619*Ht3*, and L3162 against NCLB at nearly 6 weeks after inoculation in 2021. A619*Ht3* exhibited highly resistant to NCLB, while A619 and L3162 show highly susceptible to NCLB. **(A)** Symptoms of NCLB on leaves; **(B)** Diseased leaf area (DLA).

Preliminary mapping of the *Ht3L* locus

The NILs A619 and A619*Ht3* differ considerably in their resistance to NCLB, with A619 being highly susceptible and A619*Ht3* extremely resistant (Figures 1A,B). We genotyped the A619 and A619*Ht3* NILs using the Maize3K Chip to identify chromosomal region(s) potentially covering the *Ht3L* locus. We detected three segments with stretches of polymorphisms between the two NILs in bins 3.08 (6 SNPs), 7.03/7.04 (12 SNPs) and 8.06 (12 SNPs) (Table 2), which we considered candidate *Ht3L* regions.

To determine which segment harbors the *Ht3L* locus, we selected the susceptible line L3162 that is genetically distinct from A619*Ht3* to generate mapping populations. We genotyped A619*Ht3* and L3162 with the Maize3K Chip, which returned 493 SNPs distributed over all maize chromosomes, numbers sufficient for an initial mapping of *Ht3L* (Supplementary Table 1). Within the frames of three *Ht3L* candidate regions defined by two NILs, we searched for SNPs between two parental lines A619*Ht3* and L3162 to define the cognate *Ht3L* candidate regions.

From a BC_2F_1 population derived from a cross between A619*Ht3* and L3162, we selected 29 highly resistant and 29 susceptible individuals to prepare two bulks. We then used the Maize6K Chip to genotype each BC_2F_1 individual from the two bulks and calculated the Δ(SNP-index) for each SNP in the resistant and susceptible bulks. This analysis revealed a prominent peak on chromosome 8 (Figure 2A). We also calculated the SNP-index values for those SNPs mapping to the three *Ht3L* candidate regions defined above between the two bulks. We detected no significant difference for SNP-index values between the two bulks within bins 3.08 or 7.03/7.04 (Figure 2B and Supplementary Table 2). By contrast, the SNP-index value for every SNP in bin 8.06 was significantly higher in the resistant bulk than in the susceptible bulk, indicating that the *Ht3L* locus might lie within bin 8.06 (Figure 2B and Table 3). Taken together, we concluded that the *Ht3L* locus maps to bin 8.06, which was flanked by SNP markers PZE-108095959 and PZE-108110343 and represented a physical distance of 11.23 Mb based on the B73 physical map (AGPv5).

Development of high-density molecular markers in the *Ht3L* region

We developed high-density molecular markers over the *Ht3L* region to saturate the target region. Accordingly, we retrieved the SNP markers in the *Ht3L* region between A619*Ht3* and L3162 from the genotype data of the Maize6K Chip. We then converted all SNPs located in the *Ht3L* region into KASP markers and tested them against A619*Ht3* and L3162. Totally, we obtained 18 effective KASP markers for fine-mapping (Supplementary Table 3).

Sequential fine-mapping of the *Ht3L* locus

We used a sequential fine-mapping strategy based on recombinant-derived progeny to narrow down the location of the *Ht3L* locus. In the first round of fine-mapping, we used six KASP markers (A001802, A000823, A001155, A001807, A000827, and A001808) to detect recombination events in the

TABLE 2 Three candidate *Ht3*-like regions associated with NCLB resistance.

Chr.	Flanking markers		Bins	Physical position (bp, AGPv5)		Number of SNPs	Magnitude (bp)
				Start point	End point		
3	PZE-103160158	SYN8639	3.08	216,799,618	222,134,027	6	5,334,409
7	PUT-163a-76010550-3720	PZE-107107154	7.03/7.04	154,680,564	167,990,718	12	13,310,154
8	PZE-108096541	PZE-108110136	8.06	156,678,533	169,300,416	12	12,621,883

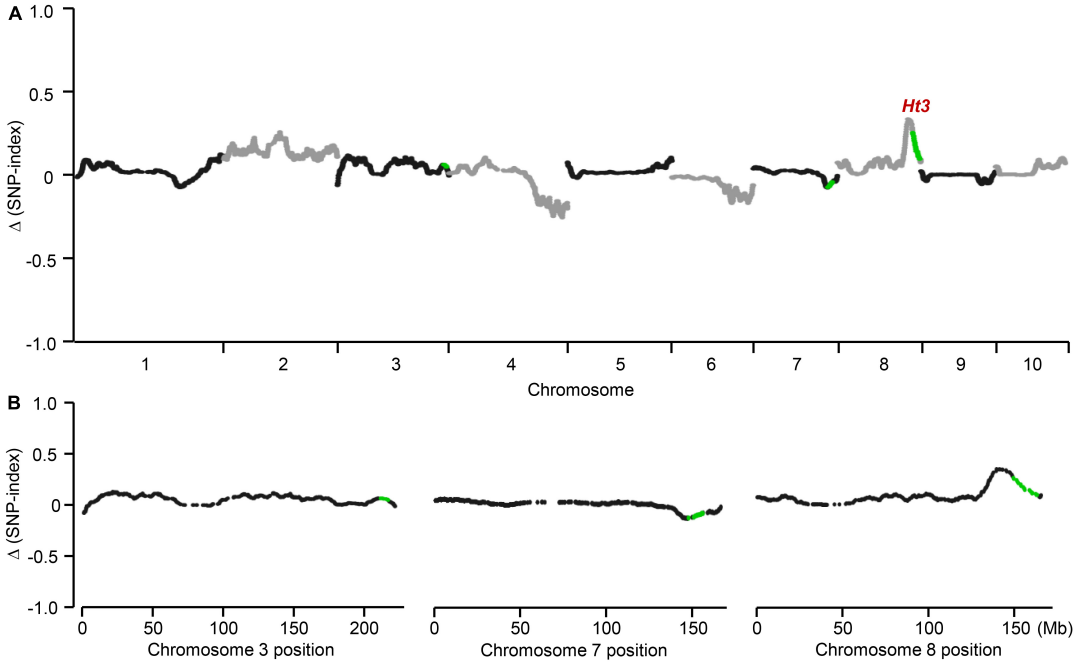

FIGURE 2
Initial detection of the *Ht3L* locus. In the BC_2F_1 segregating population, highly resistant and susceptible individuals were selected to prepare two blocks. SNP-index value which represents the heterozygosity was estimated for each SNP. **(A)** Genome-wide association mapping of *Ht3L* locus. **(B)** *Ht3L* was located in bin 8.06. Difference in SNP-index between two bulks, Δ(SNP-index), was calculated for all SNPs and used for genome-wide association. The average Δ(SNP-index) was calculated using a sliding window analysis with 10-Mb window size and 10-kb increments. Each plot represents a SNP marker, and the green plots correspond to the significantly associated SNPs in NILs analysis. The *Ht3L* locus was identified as a peak of the Δ(SNP-index) in bin 8.06.

11.23-Mb *Ht3L* region from the BC_2F_1 population obtained in 2016. We identified seven BC_2F_1 recombinants, which we backcrossed twice to the susceptible parent L3162 to produce their corresponding BC_4F_1 populations. With an additional five newly-developed KASP markers (A007452, A007453, A007455, A007456, and A007457), we determined the precise recombination breakpoint for each recombinant. To this end, we grew 1,678 plants from the BC_4F_1 progeny in the field and scored them for their extent of diseased leaf area (DLA) in Shenyang in 2017 (Figure 3A). In parallel, the marker in the heterozygous *Ht3L* region was used to genotype all individuals to distinguish homozygous (L3162/L3162) from heterozygous (A619*Ht3*/L3162) BC_4F_1 plants. With the both genotypic and phenotypic data, an average DLA value can be estimated for both homozygous and heterozygous genotypes in each BC_4F_1 progeny. Significant difference in DLA between two genotypes indicated the presence of the *Ht3L* locus in the A619*Ht3* donor segment; otherwise, there is no *Ht3L* locus. As shown, recombinants I to V showed a significant difference ($P < 0.05$) in their DLA values between homozygous and heterozygous genotypes in their BC_4F_1 progeny, indicating that they carried the *Ht3L* locus in the A619*Ht3* donor segment (Figure 3A), while recombinants VI and VII exhibited no significant difference ($P > 0.05$), and thus lacked the *Ht3L* locus. Recombinants V (with *Ht3L*) and VII (without *Ht3L*) defined the left boundary of the mapping interval to marker A007452, while recombinants I (with *Ht3L*) and VI (without *Ht3L*) marked the right boundary with marker A007455. The

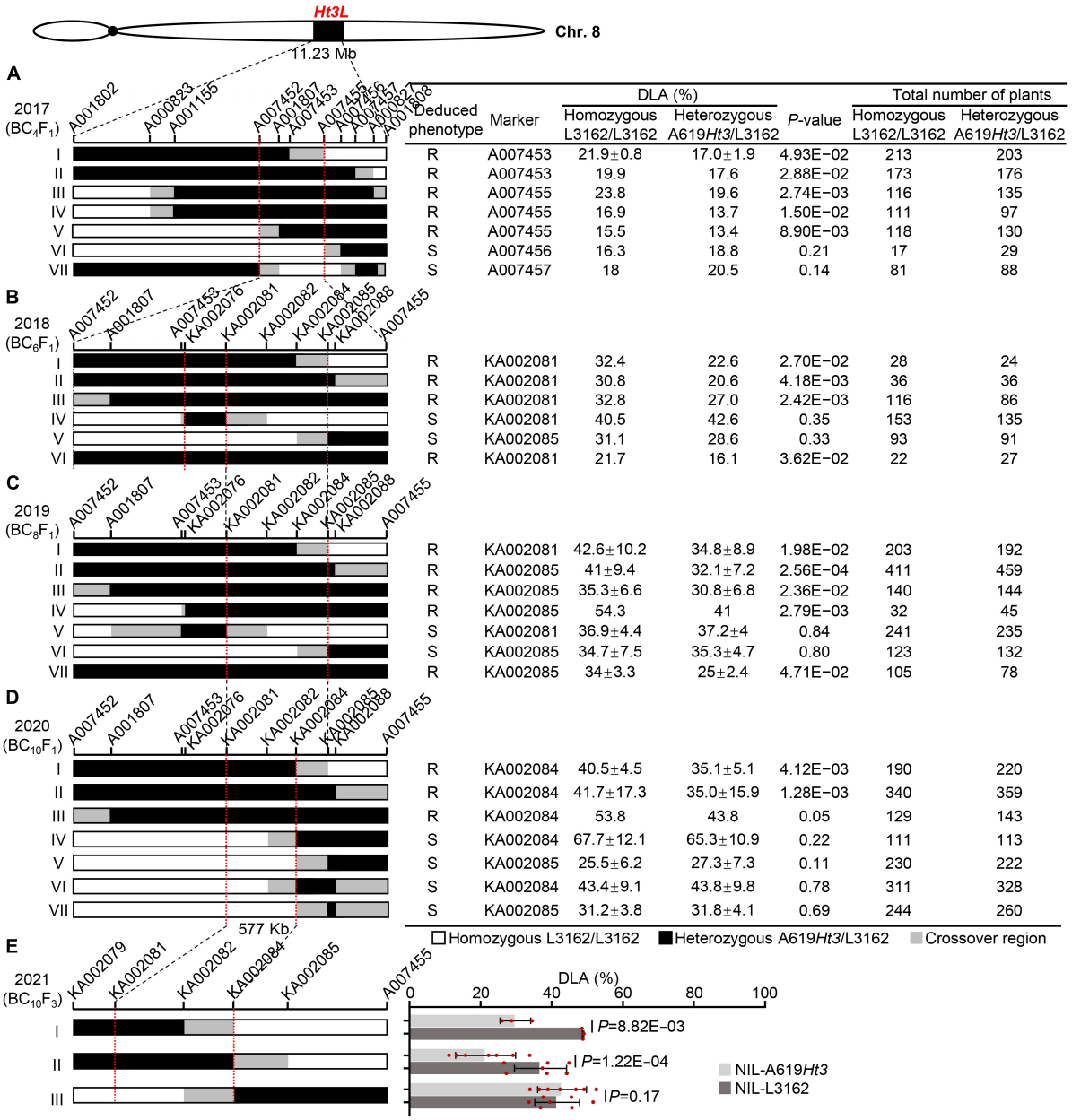

	Deduced phenotype	Marker	DLA (%) Homozygous L3162/L3162	DLA (%) Heterozygous A619*Ht3*/L3162	*P*-value	Total number of plants Homozygous L3162/L3162	Total number of plants Heterozygous A619*Ht3*/L3162
A							
I	R	A007453	21.9±0.8	17.0±1.9	4.93E−02	213	203
II	R	A007453	19.9	17.6	2.88E−02	173	176
III	R	A007455	23.8	19.6	2.74E−03	116	135
IV	R	A007455	16.9	13.7	1.50E−02	111	97
V	R	A007455	15.5	13.4	8.90E−03	118	130
VI	S	A007456	16.3	18.8	0.21	17	29
VII	S	A007457	18	20.5	0.14	81	88
B							
I	R	KA002081	32.4	22.6	2.70E−02	28	24
II	R	KA002081	30.8	20.6	4.18E−03	36	36
III	R	KA002081	32.8	27.0	2.42E−03	116	86
IV	S	KA002081	40.5	42.6	0.35	153	135
V	S	KA002085	31.1	28.6	0.33	93	91
VI	R	KA002081	21.7	16.1	3.62E−02	22	27
C							
I	R	KA002081	42.6±10.2	34.8±8.9	1.98E−02	203	192
II	R	KA002085	41±9.4	32.1±7.2	2.56E−04	411	459
III	R	KA002085	35.3±6.6	30.8±6.8	2.36E−02	140	144
IV	R	KA002085	54.3	41	2.79E−03	32	45
V	S	KA002081	36.9±4.4	37.2±4	0.84	241	235
VI	S	KA002085	34.7±7.5	35.3±4.7	0.80	123	132
VII	R	KA002085	34±3.3	25±2.4	4.71E−02	105	78
D							
I	R	KA002084	40.5±4.5	35.1±5.1	4.12E−03	190	220
II	R	KA002084	41.7±17.3	35.0±15.9	1.28E−03	340	359
III	R	KA002084	53.8	43.8	0.05	129	143
IV	S	KA002084	67.7±12.1	65.3±10.9	0.22	111	113
V	S	KA002085	25.5±6.2	27.3±7.3	0.11	230	222
VI	S	KA002084	43.4±9.1	43.8±9.8	0.78	311	328
VII	S	KA002085	31.2±3.8	31.8±4.1	0.69	244	260

FIGURE 3
Sequential fine-mapping of the *Ht3L* locus by using the recombinant-derived progeny. The vertical bars mark the sites of key molecular markers. The red dotted lines indicate the left and right boundaries of the mapped *Ht3L*. The chromosomal composition at *Ht3L* is depicted as black, white, and gray rectangles, representing heterozygous A619*Ht3*/L3162, homozygous L3162/L3162, and recombination breakpoint regions, respectively. The total number of plants refers to all progeny of a given recombinant. The significant difference in DLA among genotypes was calculated using *t*-test. A significant difference in DLA ($P < 0.05$) between heterozygous and homozygous offsprings indicated the presence of *Ht3L* in the A619*Ht3* donor region, and the corresponding parental recombinants were deduced to be NCLB resistance (R). A *P*-value > 0.05 indicates that no significant difference in DLA between heterozygous and homozygous offsprings, suggesting the absence of *Ht3L* in the donor region, and the corresponding recombinants were deduced to be NCLB susceptibility (S). *Ht3L* was narrowed from an ~11.23-Mb to an ~577-kb region flanked by the markers KA002081 and KA002084 through five rounds of fine-mapping process. **(A)** *Ht3L* was initially mapped in bin 8.06 with the physical distance of 11.23-Mb and fine-mapped to an ~2.17-Mb interval with seven BC_4F_1 recombinants. **(B)** *Ht3L* was localized into either A007452/KA002076 or KA002081/KA002085 intervals by using six BC_6F_1 recombinants. **(C)** *Ht3L* was confirmed to be located into the 838-kb KA002081/KA002085 interval by using seven BC_8F_1 recombinants. **(D)** *Ht3L* was narrowed down to a 577-kb interval flanked by markers KA002081 and KA002084 by using seven $BC_{10}F_1$ recombinants. **(E)** *Ht3L* was further confirmed to be in a 577-kb interval by using three pairs of NILs.

10.3389/fpls.2022.968924

TABLE 3 SNP markers in bin 8.06 significantly associated with NCLB resistance.

Chr.	Marker	Bins	Physical position (bp, AGPv5)	SNP-index (%)		χ^2	*P*-value
				Resistant bulk	Susceptible bulk		
8	PZE-108095959	8.06	156,276,743	0.62	0.28	5.6	0.0083
	PZE-108097802	8.06	157,706,869	0.62	0.28	5.6	0.0083
	PZE-108097921	8.06	157,881,029	0.62	0.28	5.6	0.0083
	PZE-108098977	8.06	159,229,224	0.59	0.28	4.5	0.0170
	PZE-108099332	8.06	159,625,544	0.62	0.28	5.6	0.0083
	PZE-108099526	8.06	159,865,570	0.62	0.28	5.6	0.0083
	PZE-108099959	8.06	160,066,656	0.62	0.28	5.6	0.0083
	PZE-108103023	8.06	164,969,666	0.59	0.31	3.4	0.0347
	PZE-108103951	8.06	165,599,868	0.59	0.31	3.4	0.0347
	PZE-108105699	8.06	166,329,198	0.59	0.31	3.4	0.0347
	SYN32657	8.06	166,526,926	0.59	0.31	3.4	0.0347
	PZE-108106737	8.06	166,828,537	0.59	0.31	3.4	0.0347
	SYN10384	8.06	168,773,685	0.59	0.31	3.4	0.0347
	SYN13369	8.06	169,143,087	0.59	0.31	3.4	0.0347
	PZE-108110343	8.06	169,514,058	0.59	0.31	3.4	0.0347

resulting interval spanned a region of 2.17 Mb (AGPv5) (Figure 3A).

Based on the results shown in Figure 3A, we selected those recombinants with crossovers within the 2.17-Mb mapping interval for the next round of fine-mapping, as such recombinants were still valuable to resolve the *Ht3L* locus with high-density markers. Thus, we backcrossed recombinants I and V to L3162 twice to produce their BC_6F_1 progeny. We also identified another three new recombinants within the 2.17-Mb region from the BC_4F_1 progeny, which, together with a heterozygous plant (as a positive control), were backcrossed twice to L3162 to produce BC_6F_1 progeny. We genotyped the five resulting BC_6F_1 progeny consisting of 847 individuals, grown in the field for NCLB testing in 2018, with 11 markers spanning the 2.17-Mb region, including seven newly-developed markers. We also tested the markers against the heterozygous *Ht3L* region to distinguish homozygous from heterozygous BC_6F_1 progeny. We detected a significant difference ($P < 0.05$) in DLA for recombinants I, II and III, together with the positive control (VI in Figure 3B), between the two genotypes in their BC_6F_1 progeny, but not for recombinants IV or V. Thus, the recombinant III defines a new left boundary of the mapping interval with marker A007452, and the recombinants I and V define a new right boundary with marker KA002085. Notably, recombinant IV appeared to harbor two crossovers that allowed us to exclude the region between markers KA002076 and KA002081 for the *Ht3L* locus, thus delineating the *Ht3L* locus to either the A007452-KA002076 or KA002081-KA002085 interval (Figure 3B).

From the BC_6F_1 populations, we isolated one new recombinant that, along with six existing BC_6F_1 recombinants, was backcrossed twice to L3162 to produce seven BC_8F_1 populations comprising 2,540 individuals. With this third round of fine-mapping, we observed that the new recombinant (IV in Figure 3C) shows a significant difference in DLA between the homozygous and heterozygous BC_8F_1 offspring. This recombinant carried a heterozygous region downstream of marker KA002076, which excluded the A007452-KA002076 interval as the candidate region (Figure 3C). The other six BC_8F_1 progeny derived from previous recombinants exhibited similar results, with recombinants I to III harboring the *Ht3L* locus in their heterozygous region, but not recombinants V or VI. Taken together, this third round of fine-mapping delimited the *Ht3L* locus to the region flanked by markers KA002081 and KA002085, with a physical length of 838 kb (AGPv5).

In the summer of 2020, we planted 3,200 $BC_{10}F_1$ plants corresponding to seven recombinants in Shenyang for further fine-mapping. Of them, two new recombinants (IV and VI in the Figure 3D) with breakpoints between KA002082 and KA002084 showed no significant difference ($P > 0.05$) in DLA between the $BC_{10}F_1$ homozygous and heterozygous genotypes, indicating the A619*Ht3* donor region lacked *Ht3L*. Based on these two recombinants, we moved the right boundary from marker KA002085 to marker KA002084. Phenotypic scorings for NCLB severity in the field indicated that the progeny from recombinants I-III showed a significant difference ($P < 0.05$) in DLA between the homozygotes and heterozygotes in their $BC_{10}F_1$ progeny, whereas the progeny from recombinants IV–VII did not show this difference. Thus, we ultimately

anchored *Ht3L* to a 577-kb interval flanked by markers KA002081 and KA002084 (AGPv5).

From the $BC_{10}F_1$ progeny, we selfed heterozygous recombinants to develop three pairs of NILs, which were planted in the summer of 2021 to evaluate their DLA values. The first two pairs of NILs (I and II in **Figure 3E**) displayed significant differences in the DLA scores between NILs with and without A619*Ht3* donors, but the third pair did not (**Figure 3E**). These results confirmed that *Ht3L* maps to the 577-kb interval flanked by markers KA002081 and KA002084 (AGPv5).

The genetic effect of *Ht3L* locus in resistance to northern corn leaf blight

We calculated the genetic effect of the *Ht3L/ht3l* genotype as the difference in the DLA values between heterozygous and homozygous genotypes for each of the BC_4F_1, BC_6F_1, BC_8F_1 and $BC_{10}F_1$ progeny. For the *ht3l/ht3l* and *Ht3L/ht3l* genotypes, we estimated the average DLA values to be 20.3% and 16.5% in BC_4F_1, 29.4% and 21.6% in BC_6F_1, 40.5% and 32.1% in BC_8F_1 and 42.2% and 35.9% in $BC_{10}F_1$, respectively (**Figure 4**). As expected, the *Ht3L/ht3l* heterozygotes had lower DLA values than *ht3l/ht3l* homozygotes. We also estimated the genetic effect of *Ht3L/ht3l* relative to *ht3l/ht3l*: 3.8% in BC_4F_1, 7.9% in BC_6F_1, 8.4% in BC_8F_1 and 6.3% in $BC_{10}F_1$ progeny, respectively. For the three pairs of NILs, the average DLA values of the susceptible NILs (with *ht3l/ht3l*) and resistant NILs (with *Ht3L/Ht3L*) were 40.4% and 23.9%, respectively. Thus, the genetic effect of the homozygous *Ht3L/Ht3L* genotype was 16.5% (**Figure 4**).

Exploration of the annotated genes in the mapped *Ht3L* region across various maize lines

Bin 8.06 is associated with several *Ht* genes, such as *Ht2* and *Htn1*. The identified resistance genes belong to the cell wall-associated-like kinase gene family and exhibit extensive variation in their genomic structure (Yang et al., 2021). Within the current 577-kb mapping interval of *Ht3L* locus, we detected 15 annotated genes according to the B73 reference genome sequence (RefGen_v5, **Figure 5** and **Table 4**). To our surprise, we identified no *WAK-like* gene within this interval, which appeared inconsistent with a recent report (Yang et al., 2021). Three of these genes encoded proteins of unknown function, while the remaining 12 genes encoded, among others, a VIVIPAROUS1 (VP1)-like transcription factor (Zm00001eb361390), a K^+ exchanger-like protein (Zm00001eb361440), a zinc knuckle (CCHC-type) protein (Zm00001eb361470), two violaxanthin de-epoxidases (Zm00001eb361480 and Zm00001eb361490), a brassinosteroid-insensitive protein (Zm00001eb361520), a potassium channel KAT protein (Zm00001eb361550) and a phosphatidylinositol kinase (Zm00001eb361560).

We also retrieved the corresponding regions for the mapped 577-kb *Ht3L* region from 25 sequenced founders of the NAM population (see text footnote 1). Of these 25 lines, seven were highly susceptible and another ten were highly resistant to NCLB, based on a previous report (Poland et al., 2011). The inbred lines Oh7B and M162W were the most susceptible and resistant lines, respectively (**Table 4**). The *Ht3L* region exhibited considerable variation in its length across inbred lines, varying from 383 kb to 590 kb (**Supplementary Figure 2**). Again, none of the annotated genes in these inbred lines encoded a cell wall-associated kinase. Further fine-mapping and functional testing will be required to identify the *Ht3L* causative gene conferring NCLB resistance.

Discussion

Rapid and reliable mapping of *Ht3L* locus

We initially genotyped the two NILs, A619*Ht3* and A619, which share ~98.84% of their genome sequences and yet differ widely in NCLB resistance. We rapidly identified three chromosomal segments possibly associated with NCLB resistance based on the presence of SNPs between the two NILs. To narrow down the position of the *Ht3L* locus and improve NCLB resistance, we crossed the donor A619*Ht3* to the elite but highly susceptible inbred line L3162 as a recurrent parental line. The genomes of the donor A619*Ht3* and the recurrent parental line L3162 differed by sufficient SNPs to allow fine-mapping of *Ht3L*. With A619*Ht3* as the parental line, we could quickly project the three potential *Ht3L* segments from A619*Ht3*/A619 to A619*Ht3*/L3162. Given that two bulks consisted of highly resistant and susceptible individuals, respectively, we calculated the SNP-index values and looked for a region characterized by a higher index value in the resistant bulk compared to the susceptible bulk. This allowed us to detect a QTL peak on bin 8.06, which was confirmed by regional analysis using SNP-index over the three *Ht3L* candidate segments. We then attempted to continuously narrow down the *Ht3L* location by sequential fine-mapping based on recombinant-derived progeny testing (Yang et al., 2012), reaching a final interval of 577 kb.

The deployment of multiple controls ensured the accuracy of the fine-mapping results

Stable onset of symptoms and accurate phenotypic assessment are particularly critical for QTL mapping related to NCLB resistance. Considering the uncertainty associated

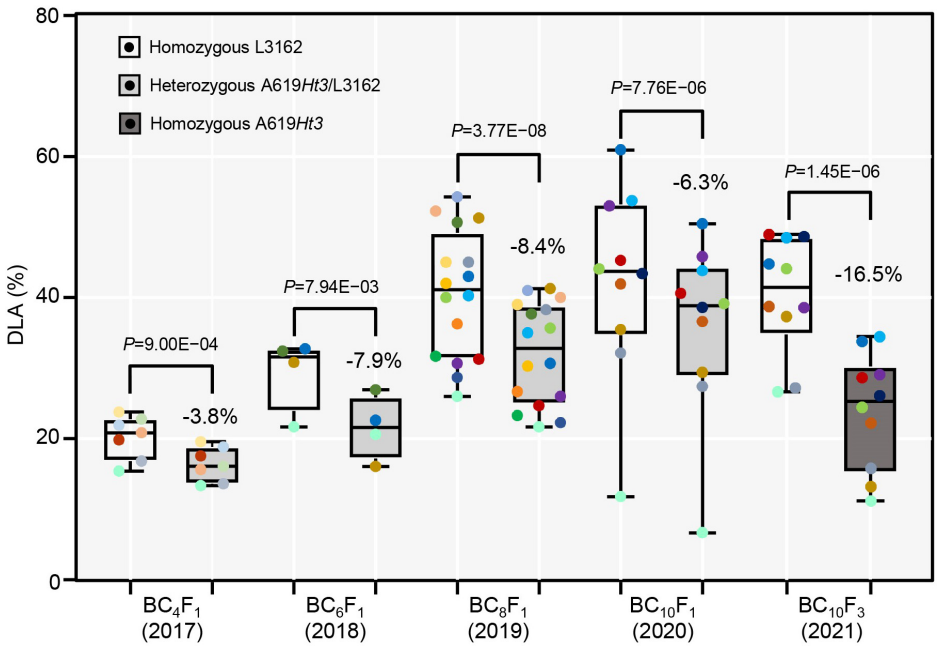

FIGURE 4
The genetic effect of the *Ht3L* locus. The DLAs are shown for both homozygous and heterozygous genotypes at *Ht3L* in the BC_4F_1, BC_6F_1, BC_8F_1, $BC_{10}F_1$ populations. The difference in DLA homozygous *ht3l/ht3l* and heterozygous *Ht3L/ht3l* genotypes was calculated for each generation. In the last two columns, the DLAs were calculated for two homozygous genotypes *ht3l/ht3l* and *Ht3L/Ht3L* of NIL-I and NIL-II. The *P* values between two genotypes were calculated by paired two-tailed *t*-test and indicated. *P*-value < 0.05 indicates significant difference; *P*-value > 0.05 indicates no significant difference.

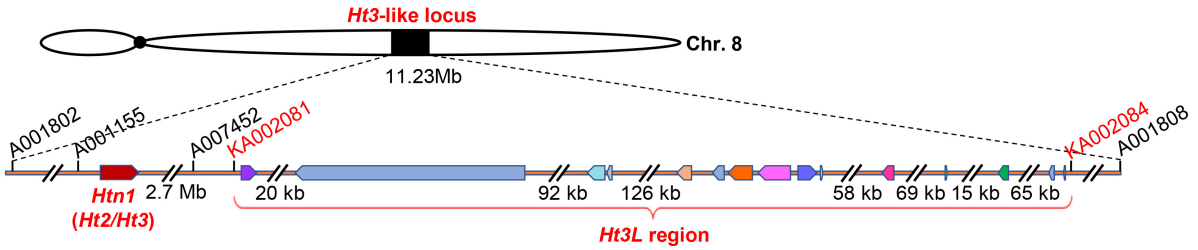

FIGURE 5
The *Ht3L* locus is independent from *Htn1*. The mapped *Ht3L* region encompassing 15 annotated genes, which was located 2.7-Mb to the right of *Htn1*.

with natural infections, we adopted an artificial inoculation method to ensure stable and uniform environmental conditions conducive to NCLB occurrence. We therefore uniformly sprayed plants with a spore suspension, followed by spray irrigation for two days, three to four times a day, to maintain high humidity. To obtain reliable phenotypic data, we assessed DLA three times in the field four weeks after artificial inoculation, using three leaves around the ear leaf. Moreover, we planted the resistant and susceptible parental lines, along with test materials, every year as controls, which allowed us to judge the stable occurrence of NCLB. In light of the performance of the positive and negative controls in terms of resistance, we believe that our artificial inoculation method was successful and reliable.

At least four major genes and numerous QTLs have been reported for resistance to NCLB in maize (Yang et al., 2017; Zhu et al., 2021). Symptom development is influenced by both genetic factors and environmental conditions. We therefore undertook a sequential fine-mapping strategy based on recombinant-derived progeny testing (Yang et al., 2012). To minimize the influence of genetic backgrounds, we conducted five rounds of QTL fine-mapping from families derived from four to ten generations of backcrosses to ensure that each individual had an almost identical genetic background outside

TABLE 4 Predicted candidate genes within the *Ht3*-like region.

B73		Oh7B		M162W	
Gene ID	**Predicted function**	**Gene ID**	**Predicted function**	**Gene ID**	**Predicted function**
Zm00001eb361390	VP1-transcription factor	Zm00038ab369880	VP1-transcription factor	Zm00033ab382990	VP1-transcription factor
Zm00001eb361410	Myosin family protein with Dil domain	Zm00038ab369900	Myosin family protein with Dil domain	Zm00033ab383010	Myosin family protein with Dil domain
Zm00001eb361420	Mitochondrial fission protein ELM1	Zm00038ab369920	Hypothetical protein	Zm00033ab383030	NA
Zm00001eb361440	K-exchanger-like protein			Zm00033ab383040	K-exchanger-like protein
Zm00001eb361450	PLASTID MOVEMENT IMPAIRED 1-RELATED	Zm00038ab369930	PLASTID MOVEMENT IMPAIRED 1-RELATED	Zm00033ab383060	PLASTID MOVEMENT IMPAIRED 1-RELATED
Zm00001eb361460	Ras-related protein Rab7	Zm00038ab369940	Ras-related protein Rab7	Zm00033ab383070	Ras-related protein Rab7
Zm00001eb361470	zinc knuckle (CCHC-type) family protein	Zm00038ab369950	zinc knuckle (CCHC-type) family protein	Zm00033ab383080	zinc knuckle (CCHC-type) family protein
		Zm00038ab369960	uncharacterized protein	Zm00033ab383100	uncharacterized protein
Zm00001eb361480	uncharacterized protein	Zm00038ab369970	uncharacterized protein	Zm00033ab383110	uncharacterized protein
Zm00001eb361490	Violaxanthin de-epoxidase	Zm00038ab369980	Violaxanthin de-epoxidase	Zm00033ab383120	Violaxanthin de-epoxidase
Zm00001eb361500	Violaxanthin de-epoxidase			Zm00033ab383130	Violaxanthin de-epoxidase
Zm00001eb361520	Brassinosteroid insensitive	Zm00038ab369990	Brassinosteroid insensitive	Zm00033ab383140	Brassinosteroid insensitive
Zm00001eb361540	uncharacterized protein	Zm00038ab370000	uncharacterized protein	Zm00033ab383150	uncharacterized protein
Zm00001eb361550	Potassium channel KAT	Zm00038ab370010	Potassium channel KAT	Zm00033ab383160	Potassium channel KAT
Zm00001eb361560	Phosphatidylinositol kinase				
Zm00001eb361570	Hypothetical protein				

10.3389/fpls.2022.968924

of the *Ht3L* region (**Supplementary Figure 3**). We planted all progeny derived from the same recombinant in the same plot to ensure that they experienced very similar environmental conditions. As the heterozygous and homozygous plants of the same progeny were randomly distributed in the testing plot, the difference in DLA between these two genotypes should minimally reflect any environmental influence. Generally, we backcrossed each recombinant twice to the susceptible inbred L3162 to increase the size of the mapping progeny, to further minimize both background noise and any environmental influence. In addition, we evaluated key recombinants for NCLB resistance over several years; although disease severity varied over the years, the difference in DLA between two genotypes was very stable for all key recombinants, which underscores the accuracy of the fine-mapping data presented in the current study.

A high density of molecular markers is also key to effective QTL mapping. The wide availability of genome sequences for multiple maize germplasms has driven SNP marker-based genetic mapping and QTL analysis (Chen et al., 2015; Ding et al., 2015). In the current study, we used the Maize3K and Maize6K Chips to obtain useful SNPs, from which we developed high-density KASP markers over the target *Ht3L* region. The developed markers were easy to use in each fine-mapping step and are characterized by positional accuracy, low genotyping errors, relatively low cost, and scalable flexibility in applications (Semagn et al., 2013).

The *Ht3L* locus is independent from *Htn1*

Bin 8.05/8.06 is a hotspot for NCLB resistance, as *Ht2*, *Ht3*, *Htn1* and other QTLs against NCLB also map to this genomic interval. Recently, *Ht2* and *Ht3* were reported to be identical and allelic to *Htn1* (Yang et al., 2021). We initially anchored the *Ht3L* locus to a genomic segment of 11.23 Mb (AGPv5) in bin 8.06, flanked by the SNP markers PZE-108095959 and PZE-108110343. Notably, this 11.23-Mb segment overlapped with the known location of the *Htn1* locus. After five rounds of fine-mapping, we delineated the *Ht3L* locus to a 577-kb interval. To our surprise, the *Ht3L* locus was located ∼2.7 Mb away from *Htn1* (**Figure 5**). Intriguingly, when looking back over the resistance performance of different recombinants, we failed to observe any genetic contribution of the *Htn1* locus to NCLB resistance. For instance, the BC_2F_1 recombinant VII, which carried only the *Htn1* locus and lacked the *Ht3L* locus, did not exhibit a significant difference in DLA between its BC_4F_1 offspring heterozygous and homozygous for *Htn1*. Likewise, BC_2F_1 recombinants (No. I and II) with two loci (*Ht3L* and *Htn1*) did not display a lower DLA score than those BC_2F_1 recombinants (No. V) only harboring the *Ht3L* locus. The lack of phenotypic variation associated with the *Htn1* locus between A619*Ht3* and L3162 thus indicated that both lines have the same susceptible *Htn1* allele. The other possibility is that *Htn1* may lose its NCLB-resistance function due to the presence of an unidentified suppressor or the absence of a co-receptor in the L3162 background. For example, a dominant suppressor inhibiting the expression of *Ht2* was found in lines related to 'B14' (Ceballos and Gracen, 1989).

The *Ht3L* locus shows extensive variation

We detected extensive genomic variation within the 577-kb *Ht3L* interval in the 25 founders of the NAM population, with a size varying from 383 kb to 590 kb. Surprisingly, no gene in this *Ht3L* region was annotated as encoding a canonical cell wall-associated kinase, in contrast to the *Ht2*/*Ht3*/*Htn1* locus (Yang et al., 2021). In field trials across multiple years, A619*Ht3* always exhibited highly resistance to NCLB, in sharp contrast to the highly susceptible lines A619 and L3162. Given that A619*Ht3* harbors both the resistant *Ht3L* and *Htn1* loci, we propose two possible explanations for the results of the current study: 1) the 577-kb *Ht3L* locus interval may contain a bona fide *Ht3* gene that is located ∼2.7 Mb away from the known *Ht2*/*Ht3*/*Htn1* locus; or 2) A619*Ht3* harbors a *Ht3* gene that is allelic to *Htn1*, as claimed by Yang et al. (2021), in which case the mapped *Ht3L* locus must contain a novel NCLB resistance gene. In this alternative scenario, we speculate that A619*Ht3* is unlikely to harbor another resistant allele at the reported *Ht2*/*Ht3* or *Htn1* loci, as only one resistance QTL was detected in our mapping populations. Since the detailed genomic sequence of the parental line A619*Ht3* is not currently available, we are still uncertain about the relationship between the currently mapped *Ht3L* locus and the reported *Ht2*/*Ht3*/*Htn1* locus. In addition, the genetic backgrounds clearly have pronounced effects on *Ht3L*-conferred NCLB resistance, as we observed wide variation in DLA scores between homozygotes and heterozygotes in the fine-mapping progeny of different parental recombinants.

Toward the application of a novel locus in northern corn leaf blight-resistant breeding

Exserohilum turcicum shows clear physiological differentiation as a function of the resistance performance of inbred lines and differences of climatic conditions. Moreover, the distribution of physiological races is also complex. Twelve physiological races have been identified in China, of which races 0 and 1 are dominant (Gao et al., 2011). Because of the apparent physiological differentiation of the fungus causing NCLB, the rapid evolution of pathogen populations must be considered in NCLB-resistance breeding programs. Several resistance loci

should be pyramided via marker-assisted backcrossing (MABC) to breed more resistant varieties that can combat multiple physiological races of NCLB. MABC was shown to be effective to improve the resistance of inbred lines. For example, all 63 converted lines produced through MABC by introducing nine resistant *ZmCCT* (*CONSTANS* [*CO*], *CO-like*, *TIMING OF CAB2 EXPRESSION 1* [*TOC1*]) haplotypes into seven elite maize inbred lines exhibited enhanced resistance to maize stalk rot (Li et al., 2017). The current study reveals a distinct *Ht3L* locus for NCLB resistance. Considering the substantial annual yield loss caused by NCLB, the *Ht3L* locus will be valuable in future breeding programs of NCLB-resistant maize.

Conclusion

Mining and utilizing resistant loci/genes can greatly promote the development of resistant varieties, which will decrease yield losses and improve grain quality. With the availability of high-density SNP markers, we delimited *Ht3L* to an interval of 577kb via five rounds of sequential fine-mapping. The homozygous *Ht3L/Ht3L* genotype reduced DLA by 16.5% compared to that in lines without *Ht3L*. Our results will facilitate the cloning of the causative gene underlying the *Ht3L* locus and accelerate application of *Ht3L* in the breeding of NCLB-resistant maize varieties.

Data availability statement

The original contributions presented in this study are included in the article/**Supplementary material**, further inquiries can be directed to the corresponding author/s.

Author contributions

MJ and YW designed the experiments. JM, XL, XQ, XG, and MJ were responsible for the field tests. YG, YZ, and XL conducted genotyping. MZ and YG analyzed the data. MZ, JM, and MJ wrote the manuscript. MJ and YW supervised the project. MZ, JM, and MJ revised the manuscript in response to the reviewers. All authors read and approved the manuscript.

Funding

This study was supported by the National Key Research and Development Project of China (2021YFD1201003) and Modern Agricultural Industry System Construction Project of China (CARS-02-52).

Acknowledgments

We are thankful to Zhiyan Cao (Hebei Agricultural University) for providing *E. turcicum* isolates. We also gratefully acknowledge editor and reviewers for thoughtful suggestion on our manuscript.

Conflict of interest

YG and YZ were employed by Liaoning Dongya Agricultural Development Co., Ltd.

The remaining authors declare that the research was conducted in the absence of any commercial or financial relationships that could be construed as a potential conflict of interest.

Publisher's note

All claims expressed in this article are solely those of the authors and do not necessarily represent those of their affiliated organizations, or those of the publisher, the editors and the reviewers. Any product that may be evaluated in this article, or claim that may be made by its manufacturer, is not guaranteed or endorsed by the publisher.

Supplementary material

The Supplementary Material for this article can be found online at: https://www.frontiersin.org/articles/10.3389/fpls.2022.968924/full#supplementary-material

References

Ayliffe, M., Singh, R., and Lagudah, E. (2008). Durable resistance to wheat stem rust needed. *Curr. Opin. Plant Biol.* 11, 187–192. doi: 10.1016/j.pbi.2008.02.001

Balint-Kurti, P. J., Yang, J., Van Esbroeck, G., Jung, J., and Smith, M. E. (2010). Use of a maize advanced intercross line for mapping of QTL for Northern leaf blight resistance and multiple disease resistance. *Crop Sci.* 50, 458–466. doi: 10.2135/cropsci2009.02.0066

Bentolila, S., Guitton, C., Bouvet, N., Sailland, A., Nykaza, S., and Freyssinet, G. (1991). Identification of an RFLP marker tightly linked to the Ht1 gene in maize. *Theor. Appl. Genet.* 82, 393–398. doi: 10.1007/BF00588588

Cai, H. W., Gao, Z. S., Yuyama, N., and Ogawa, N. (2003). Identification of AFLP markers closely linked to the rhm gene for resistance to Southern corn leaf blight

in maize by using bulked segregant analysis. *Mol. Genet. Genomics* 269, 299–303. doi: 10.1007/s00438-003-0837-z

Ceballos, H., and Gracen, V. E. (1989). A dominant inhibitor gene inhibits the expression of Ht2 against Exserohilum turcicum race 2 in corn inbred lines related to B14. *Plant Breed.* 102, 35–44.

Chang, H. S., and Fan, K. C. (1986). Comparative studies ou some biology and pathology of corn and broom corn isolates of Exserohilum turcicum (Pass) Leonard & Suggs. *Bot. Bull. Acad. Sin.* 27, 209–218.

Chen, G., Wang, X., Long, S., Jaqueth, J., Li, B., Yan, J., et al. (2015). Mapping of QTL conferring resistance to northern corn leaf blight using high-density SNPs in maize. *Mol. Breed.* 36:4. doi: 10.1007/s11032-015-0421-3

Chung, C. L., Jamann, T., Longfellow, J., and Nelson, R. (2010). Characterization and fine-mapping of a resistance locus for northern leaf blight in maize bin 8.06. *Theor. Appl. Genet.* 121, 205–227. doi: 10.1007/s00122-010-1303-z

Ding, J., Ali, F., Chen, G., Li, H., Mahuku, G., Yang, N., et al. (2015). Genome-wide association mapping reveals novel sources of resistance to northern corn leaf blight in maize. *BMC Plant Biol.* 15:206. doi: 10.1186/s12870-015-0589-z

Gao, J., Lu, S., Gao, Z., Zhuang, J., Zhang, X., and Zhang, S. (2011). Identification and dynamic analysis on physiological race of Exserohilum turcicum in Northeastern China in 2009. *J. Maize Sci.* 19, 138–140.

Guo, L. (2015). *Genetic diversity and mating type distribution of Setosphaeria turcica in China*. Hebei: Hebei Agricultural University.

Hilu, H. M., and Hooker, A. L. (1964). Host-pathogen relationship of Helminthosporium turcicum in resistant and susceptible corn seedlings. *Phytopathology* 54, 570–575.

Hilu, H. M., and Hooker, A. L. (1965). Localized infection by Helminthosporium turcium on corn leaves. *Phytopathology* 55, 189–192.

Hooker, A. L. (1977). A second major locus in corn for chlortic-lesion resistance to helmintbosporium turcicum. *Crop Sci.* 17, 132–135.

Hooker, A. L. (1981). Resistance to Helminthosporium turcium from Tripsacum floridanum incorporated into maize. *Maize Genet. Crop Newsl.* 55, 87–88.

Hurni, S., Scheuermann, D., Krattinger, S. G., Kessel, B., Wicker, T., Herren, G., et al. (2015). The maize disease resistance gene Htn1 against northern corn leaf blight encodes a wall-associated receptor-like kinase. *Proc. Natl. Acad. Sci. U.S.A.* 112, 8780–8785. doi: 10.1073/pnas.1502522112

Jamann, T. M., Poland, J. A., Kolkman, J. M., Smith, L. G., and Nelson, R. J. (2014). Unraveling genomic complexity at a quantitative disease resistance locus in maize. *Genetics* 198, 333–344. doi: 10.1534/genetics.114.167486

Jindal, K. K., Tenuta, A. U., Woldemariam, T., Zhu, X., Hooker, D. C., and Reid, L. M. (2019). Occurrence and distribution of physiological races of exserohilum turcicum in ontario. *Can. Plant Dis.* 103, 1450–1457. doi: 10.1094/PDIS-06-18-0951-SR

Leng, P., Ji, Q., Asp, T., Frei, U. K., Ingvardsen, C. R., Xing, Y., et al. (2017). Auxin binding protein 1 reinforces resistance to sugarcane mosaic virus in maize. *Mol. Plant* 10, 1357–1360. doi: 10.1016/j.molp.2017.07.013

Li, P., Du, C., Zhang, Y., Yin, S., Zhang, E., Fang, H., et al. (2018). Combined bulked segregant sequencing and traditional linkage analysis for identification of candidate gene for purple leaf sheath in maize. *PLoS One* 13:e0190670. doi: 10.1371/journal.pone.0190670

Li, Y., Tong, L., Deng, L., Liu, Q., Xing, Y., Wang, C., et al. (2017). Evaluation of ZmCCT haplotypes for genetic improvement of maize hybrids. *Theor. Appl. Genet.* 130, 2587–2600. doi: 10.1007/s00122-017-2978-1

Liu, Q., Deng, S., Liu, B., Tao, Y., Ai, H., Liu, J., et al. (2020). A helitron-induced RabGDIalpha variant causes quantitative recessive resistance to maize rough dwarf disease. *Nat. Commun.* 11:495. doi: 10.1038/s41467-020-14372-3

Liu, Q., Liu, H., Gong, Y., Tao, Y., Jiang, L., Zuo, W., et al. (2017). An atypical thioredoxin imparts early resistance to sugarcane mosaic virus in maize. *Mol. Plant* 10, 483–497. doi: 10.1016/j.molp.2017.02.002

Ma, J., Wang, Y., KLiu, X., Li, M., Gong, X., Qi, X., et al. (2014). SNP gene chip analysis of near-isogenic lines to northern corn leaf blight. *J. Maize Sci.* 22, 153–158.

Michelmore, R., Paran, I., and Kesseli, R. (1991). Identification of markers linked to disease-resistance genes by bulked segregant analysis: Arapid method to detect markers in specific genomic regions by using segregating populations. *Proc. Natl. Acad. Sci. U.S.A.* 88, 9828–9832. doi: 10.1073/pnas.88.21.9828

Murray, M. G., and Thompson, W. F. (1980). Rapid isolation of high molecular weight plant DNA. *Nucleic Acids Res.* 8, 4321–4325.

Navarro, B. L., Hanekamp, H., Koopmann, B., and von Tiedemann, A. (2020). Diversity of expression types of Ht genes conferring resistance in maize to exserohilum turcicum. *Front. Plant. Sci.* 11:607850. doi: 10.3389/fpls.2020.607850

Poland, J. A., Balint-Kurti, P. J., Wisser, R. J., Pratt, R. C., and Nelson, R. J. (2009). Shades of gray: The world of quantitative disease resistance. *Trends Plant Sci.* 14, 21–29. doi: 10.1016/j.tplants.2008.10.006

Poland, J. A., Bradbury, P. J., Buckler, E. S., and Nelson, R. J. (2011). Genome-wide nested association mapping of quantitative resistance to northern leaf blight in maize. *Proc. Natl. Acad. Sci. U.S.A.* 108, 6893–6898. doi: 10.1073/pnas.1010894108

Raymundo, A. D., and Hooker, A. L. (1981). Measuring the relationship between northern corn leaf blight and yield losses. *Plant Dis.* 65, 325–327.

Semagn, K., Babu, R., Hearne, S., and Olsen, M. (2013). Single nucleotide polymorphism genotyping using Kompetitive Allele Specific PCR (KASP): Overview of the technology and its application in crop improvement. *Mol. Breed.* 33, 1–14. doi: 10.1007/s11032-013-9917-x

Shen, X., Zhou, M., Lu, W., and Ohm, H. (2003). Detection of Fusarium head blight resistance QTL in a wheat population using bulked segregant analysis. *Theor. Appl. Genet.* 106, 1041–1047. doi: 10.1007/s00122-002-1133-8

Takagi, H., Abe, A., Yoshida, K., Kosugi, S., Natsume, S., Mitsuoka, C., et al. (2013). QTL-seq: Rapid mapping of quantitative trait loci in rice by whole genome resequencing of DNA from two bulked populations. *Plant J.* 74, 174–183. doi: 10.1111/tpj.12105

Venuprasad, R., Dalid, C. O., Del Valle, M., Zhao, D., Espiritu, M., Sta Cruz, M. T., et al. (2009). Identification and characterization of large-effect quantitative trait loci for grain yield under lowland drought stress in rice using bulk-segregant analysis. *Theor. Appl. Genet.* 120, 177–190. doi: 10.1007/s00122-009-1168-1

Wang, C., Yang, Q., Wang, W., Li, Y., Guo, Y., Zhang, D., et al. (2017). A transposon-directed epigenetic change in ZmCCT underlies quantitative resistance to *Gibberella* stalk rot in maize. *New Phytol.* 215, 1503–1515. doi: 10.1111/nph.14688

Wang, J., Xu, Z., Yang, J., Lu, X., Zhou, Z., Zhang, C., et al. (2018). qNCLB7.02, a novel QTL for resistance to northern corn leaf blight in maize. *Mol. Breed.* 38:54. doi: 10.1007/s11032-017-0770-1

Weems, J. D., and Bradley, C. A. (2018). exserohilum turcicum race population distribution in the North Central United States. *Plant Dis.* 102, 292–299. doi: 10.1094/PDIS-01-17-0128-RE

Welz, H., and Geiger, H. (2000). Genes for resistance to northern corn leaf blight in diverse maize populations. *Plant Breed.* 119, 1–14.

Wisser, R., Balint-Kurti, P., and Nelson, R. (2006). The genetic architecture of disease resistance in maize: A synthesis of published studies. *Phytopathology* 96, 120–129. doi: 10.1094/PHYTO-96-0120

Yang, P., Praz, C., Li, B., Singla, J., Robert, C. A. M., Kessel, B., et al. (2019). Fungal resistance mediated by maize wall-associated kinase ZmWAK-RLK1 correlates with reduced benzoxazinoid content. *New Phytol.* 221, 976–987. doi: 10.1111/nph.15419

Yang, P., Scheuermann, D., Kessel, B., Koller, T., Greenwood, J. R., Hurni, S., et al. (2021). Alleles of a wall-associated kinase gene account for three of the major northern corn leaf blight resistance loci in maize. *Plant J.* 106, 526–535. doi: 10.1111/tpj.15183

Yang, Q., Balint-Kurti, P., and Xu, M. (2017). quantitative disease resistance: Dissection and adoption in maize. *Mol. Plant* 10, 402–413. doi: 10.1016/j.molp.2017.02.004

Yang, Q., Zhang, D., and Xu, M. (2012). A sequential quantitative trait locus fine-mapping strategy using recombinant-derived progeny. *J. Integr. Plant Biol.* 54, 228–237. doi: 10.1111/j.1744-7909.2012.01108.x

Ye, J., Zhong, T., Zhang, D., Ma, C., Wang, L., Yao, L., et al. (2019). The auxin-regulated protein ZmAuxRP1 coordinates the balance between root growth and stalk rot disease resistance in maize. *Mol. Plant* 12, 360–373. doi: 10.1016/j.molp.2018.10.005

Zhao, X., Tan, G., Xing, Y., Wei, L., Chao, Q., Zuo, W., et al. (2012). Marker-assisted introgression of qHSR1 to improve maize resistance to head smut. *Mol. Breed.* 30, 1077–1088. doi: 10.1007/s11032-011-9694-3

Zhu, M., Tong, L., Xu, M., and Zhong, T. (2021). Genetic dissection of maize disease resistance and its applications in molecular breeding. *Mol. Breed.* 41, 1–22. doi: 10.1007/s11032-021-01219-y

Zuo, W., Chao, Q., Zhang, N., Ye, J., Tan, G., Li, B., et al. (2015). A maize wall-associated kinase confers quantitative resistance to head smut. *Nat. Genet.* 47, 151–157. doi: 10.1038/ng.3170

Zwonitzer, J., Coles, N., Krakowsky, M., Arellano, C., Holland, J., McMullen, M., et al. (2010). Mapping resistance QTL for three foliar diseases in a maize RIL population-evidence for multiple disease resistance. *Phytopathology* 100, 72–79.

frontiers | Frontiers in Plant Science

TYPE Original Research
PUBLISHED 13 September 2022
DOI 10.3389/fpls.2022.954546

OPEN ACCESS

EDITED BY
Mingliang Xu,
China Agricultural University, China

REVIEWED BY
Lukasz Stepien,
Polish Academy of Sciences, Poland
Manje S. Gowda,
The International Maize and Wheat Improvement Center (CIMMYT), Kenya

*CORRESPONDENCE
Jianfeng Weng
wengjianfeng@caas.cn
Canxing Duan
duancanxing@caas.cn

SPECIALTY SECTION
This article was submitted to Plant Pathogen Interactions, a section of the journal Frontiers in Plant Science

RECEIVED 27 May 2022
ACCEPTED 11 August 2022
PUBLISHED 13 September 2022

CITATION
Xia Y, Wang B, Zhu L, Wu W, Sun S, Zhu Z, Li X, Weng J and Duan C (2022) Identification of a Fusarium ear rot resistance gene in maize by QTL mapping and RNA sequencing.
Front. Plant Sci. 13:954546.
doi: 10.3389/fpls.2022.954546

Identification of a Fusarium ear rot resistance gene in maize by QTL mapping and RNA sequencing

Yusheng Xia[1], Baobao Wang[1,2], Lihong Zhu[1], Wenqi Wu[1], Suli Sun[1], Zhendong Zhu[1], Xinhai Li[1], Jianfeng Weng[1]* and Canxing Duan[1]*

[1]National Key Facility for Crop Gene Resources and Genetic Improvement, Institute of Crop Sciences, Chinese Academy of Agricultural Sciences, Beijing, China, [2]Shijiazhuang Academy of Agricultural and Forestry Sciences, Shijiazhuang, China

Fusarium ear rot (FER) caused by *Fusarium verticillioides* is a prevalent maize disease. To comprehensively characterize the genetic basis of the natural variation in FER resistance, a recombinant inbred line (RIL) population was used to map quantitative trait loci (QTL) for FER resistance. A total of 17 QTL were identified by linkage mapping in eight environments. These QTL were located on six chromosomes and explained 3.88–15.62% of the total phenotypic variation. Moreover, *qFER1.03* had the strongest effect and accounted for 4.98–15.62% of the phenotypic variation according to analyses of multiple environments involving best linear unbiased predictions. The chromosome segment substitution lines (CSSLs) derived from a cross between Qi319 (donor parent) and Ye478 (recurrent parent) were used to verify the contribution of *qFER1.03* to FER resistance. The line CL171, which harbored an introgressed *qFER1.03*, was significantly resistant to FER. Further fine mapping of *qFER1.03* revealed that the resistance QTL was linked to insertion/deletion markers InDel 8 and InDel 2, with physical distances of 43.55Mb and 43.76Mb, respectively. Additionally, *qFER1.03* differed from the previous resistance QTL on chromosome 1. There were three annotated genes in this region. On the basis of the RNA-seq data, which revealed the genes differentially expressed between the FER-resistant Qi319 and susceptible Ye478, *GRMZM2G017792* (MPK3) was preliminarily identified as a candidate gene in the *qFER1.03* region. The Pr-CMV-VIGS system was used to decrease the *GRMZM2G017792* expression level in CL171 by 34–57%, which led to a significant decrease in FER resistance. Using RIL and CSSL populations combined with RNA-seq and Pr-CMV-VIGS, the candidate gene can be dissected effectively, which provided important gene resource for breeding FER-resistant varieties.

KEYWORDS

maize, ear rot, *Fusarium verticillioides*, resistance gene, QTL mapping, RNA sequencing

Introduction

Maize (*Zea mays* L.) is widely grown from the Northeast Plain to the Yunnan–Guizhou Plateau in the southwestern part of China. It is an important food crop, feed crop, and a source of energy in China, making it a key contributor to agricultural production and the national economy. Ear rot caused by many pathogenic fungi is one of the most destructive diseases of maize, and often leads to a considerable decrease in yield and quality (Duan et al., 2016; Lanubile et al., 2017; Zhou et al., 2018). The previous researches identified the *Fusarium verticillioides* and *Fusarium graminearum* species complex as the dominant pathogens responsible for maize ear rot in China (Shi and Bai, 1992; Qin et al., 2014; Zhou et al., 2016; Xiao et al., 2017; Sun et al., 2017a,b; Du et al., 2019; Wei et al., 2019). Maize ear rot caused by *F. verticillioides* (FER) is widespread in temperate and semitropical areas, including Asian, American, and European maize-growing areas. *F. verticillioides* can produce dangerous fumonisins that are toxic for humans and animals (Munkvold, 2003; Duan et al., 2016). This fungus overwinters in soil, seeds, and plant residues and spreads to maize grains through the roots and the air (Morales-Rodríguez et al., 2007; Chen et al., 2016). Additionally, it typically grows as white–pink mycelia on the seeds and/or silk. Infected kernels may also exhibit "starburst" symptoms, in which white stripes radiate from the silk-attachment site at the cap or from the base of the kernel (Lanubile et al., 2017).

The most economical and effective method for controlling FER involves the breeding and cultivation of resistant varieties (Duan et al., 2015a). Introducing disease resistance-related quantitative trait loci (QTL) or genes from donors into superior maize germplasm is a feasible strategy for developing disease-resistant germplasm and commercial hybrids (Nankam and Pataky, 1996). Some studies have shown that maize resistance to FER is typically a quantitative trait (Duan et al., 2015b). Screening resistant resources and mapping resistance genes or QTL are the basis for resistance breeding. The considerable abundance of genetic material and the strong influence of environmental factors have delayed the accurate localization of QTL, which has had a detrimental effect on the efficiency of marker-assisted selection (MAS) during breeding (Robertson-Hoyt et al., 2006). Increasing the population size and the number of molecular markers, improving the accuracy of the phenotype-based identification of ear rot, and integrating data from multiple environments will help overcome such limitations. Identifying and mapping resistance genes or QTL that can be stably expressed in different environments is critical for developing disease-resistant varieties. Several of the studies on FER that have been conducted over the past 30 years identified effective QTL for FER resistance (Yang et al., 2010; Xiang et al., 2012). Studies on the genetic structures and variations associated with complex maize traits have usually involved linkage analyses. However, most of the available genetic maps were constructed on the basis of low-throughput and low-density molecular markers, which has limited the efficiency and accuracy of QTL mapping as well as the coverage of genetic markers (Holland, 2007). Compared with simple sequence repeat (SSR) markers used for mapping, next-generation sequencing technology for genotyping is a powerful tool for developing single nucleotide polymorphism (SNP) markers and constructing high-density genetic maps. Using recombinant inbred line (RIL) populations with ultra-high-density genetic maps is an effective method for identifying QTL for complex agronomic traits (Zhou et al., 2016; Zhang et al., 2017). Accordingly, they have been widely used for mapping stress resistance QTL/genes in maize (Ding et al., 2008; Wang et al., 2018). However, the genetic background of a RIL population can be complex and easily affected by environmental factors (Eshed and Zamir, 1994; Alonso-Blanco and Koornneef, 2000). Chromosome segment substitution lines (CSSLs) can minimize the interference from the genetic background, making them suitable for mapping, confirming, and cloning target genes and QTL. A CSSL can also improve the accuracy of QTL mapping by separating single or several chromosomal fragments from the donor parent with the same genetic background as the recurrent parent. Additionally, CSSLs have been used to detect QTL with relatively small additive effects that have been masked by QTL with larger additive effects in primary populations (Shim et al., 2010).

Combined with QTL mapping, transcriptome sequencing is a useful technique for identifying candidate genes and validating loci for quantitative traits (Korte and Farlow, 2013). Combining these methods has enabled researchers to overcome the limitations of either method performed alone (Brachi et al., 2010).

Virus-induced gene silencing (VIGS) exploits RNA-mediated antiviral defense mechanisms, namely RNA interference and post-transcriptional gene silencing, to downregulate gene expression, which often results in a "functional deficit" phenotype in plants (Vance and Vaucheret, 2001; Becker and Lange, 2010). Although several VIGS vectors have been developed for maize, their utility is limited because of several factors (e.g., inefficient viral infection, unstable insertion, relatively short gene-silencing period, inappropriate inoculation methods, and abnormal growth temperature requirements). A maize gene-silencing system was recently established on the basis of the cucumber mosaic virus (CMV) to overcome many of the limitations of existing VIGS systems developed to silence maize genes (Li et al., 2021).

Most previously reported QTLs and candidate genes exhibit a minor effect on FER resistance in maize. This indicates that pyramiding of QTLs or genes from different resources would be an effective approach to improve FER resistance. Therefore, exploration of more effective and stable QTLs that impart FER resistance is necessary to provide resources for molecular breeding of resistant varieties of maize. In the present study, the maize inbred lines Qi319 and Ye478 were selected as the resistant and susceptible parents, respectively, to generate a RIL population for QTL mapping. An ultra-high-density bin map

with 4,183 SNP markers was constructed along with the RIL population (Zhou et al., 2016). The relevant CSSLs were developed for fine mapping and for evaluating FER resistance to confirm and refine mapped region. The aims of this study were to finely map FER resistance gene in Qi319 and obtain the candidate gene in the targeted QTL region. The results will provide new molecular markers and genetic resource to aid in the breeding of FER-resistant varieties.

Materials and methods

Plant materials and pathogen

A RIL population consisting of 300 F_{11} lines was developed by single-seed descent from a cross between maize inbred lines Qi319 and Ye478 (Zhou et al., 2016). Inbred line Qi319 was developed from the FER-resistant maize hybrid 78,599 by the Shandong Academy of Agricultural Sciences (Tian et al., 2014). In contrast, Ye478 is a FER-susceptible inbred line with excellent agronomic traits and high general combining ability. Additionally, CSSLs were constructed using Qi319 and Ye478 as the donor and receptor parents, respectively (Lu et al., 2020). After back-crossing for five generations and self-crossing for three generations, the following 12 CSSLs were selected to verify the FER resistance QTL on chromosome 1: CL160, CL171, CL9, CL172, CL173, CL82, CL14, CL174, CL45, CL61, CL28, and CL21 (i.e., Types 1–12). Type 2 (CL171) was the CSSL with the candidate FER resistance-related gene. The F_2 hybrid generation and the F_3 selfing generation derived from CL171 and Ye478 were used for the subsequent gene mapping, whereas CL171 was used for the VIGS-based silencing of the candidate FER resistance-related gene.

The FER pathogen *F. verticillioides* strain used for inoculation, FVHN-10, was isolated from Zhumadian, Henan Province, and then was purified and stored in the laboratory of the Institute of Crop Sciences, Chinese Academy of Agricultural Sciences (Duan et al., 2016). FVHN-10 was proved be strong virulence to susceptible maize ears, such as Ye478, B73, and Ye107.

Phenotypic evaluation of maize for FER resistance

In May 2019, 300 RIL materials were grown in Changping (Beijing), Shunyi (Beijing), and Xinxiang (Henan). In May 2020, they were grown repeatedly in Changping (Beijing) and Xinxiang (Henan). In May 2021, they were grown in Shunyi and Changping (Beijing) and Xinxiang (Henan). Each material was grown in a row (5 m long), with 0.6 m separating rows and 0.25 m separating plants. Each row comprised 25 plants. As controls, Qi319 (resistant) and Ye478 (susceptible) were acted as controls for every 50 rows. To produce the inoculum, *F. verticillioides* was grown on potato dextrose agar (PDA) medium in plates, which were incubated in darkness. A substantial abundance of conidia was produced in about 10 days. Six days before plants were inoculated, the PDA medium covered with mycelium and conidia was cut into small pieces in an ultra-clean platform and transferred to sterilized potato dextrose broth (PDB) medium for the subsequent propagation. The filtered *F. verticillioides* conidial suspension was diluted to 1×10^6 spores/mL. The silk channel injection method was used to inoculate maize ears at 5–7 days after silk emergence when silks are elongated, pollinated, and may have some tip browning but are not dry (Duan et al., 2022). Briefly, the continuous syringe was adjusted and then inserted along the side of the corn silk to inject 2 ml conidial suspension into each ear through the silk channel. At about 40 days after the inoculation, maize ears were hand husked and removed line by line. FER incidence and severity were surveyed and resistance scales were evaluated (Wang, 2005; Duan et al., 2022). In this study, the severity of FER was accurately determined on the basis of the diseased ear area, which was calculated using the Automatic Imaging System for Ear Rot (customized by the National Agricultural Information Engineering Technology Research Center). The average diseased ear area (%) of each line was used for further analyses.

Analysis of phenotypic data and heritability

All descriptive statistics (mean, range, skewness, and kurtosis) of the parental lines and RILs across the eight environments were analyzed using the Statistical Product and Service Solutions (SPSS) software v20.0. The generalized heritability (H2) of FER resistance in the eight environments was analyzed using the method of Wang (2017). Standard analysis of variance with the general linear model procedure (PROC GLM) was adopted to estimate all variance in Excel. We used the following genetic model: $H^2 = \sigma_G^2/(\sigma_G^2 + \sigma_{G\varepsilon}^2/e + \sigma_\varepsilon^2/er)$, where σ_G^2 is the genetic variance reflecting the blocking effect, σ_ε^2 is the error variance, $\sigma_{G\varepsilon}^2$ is the genotype × environment interaction, and e and r are the number of environments and repeats, respectively (Knapp et al., 1985). Inclusive composite interval mapping (ICIM) was used to locate QTL (Wang, 2009).

QTL mapping for FER resistance in the RIL population

The QTL for FER resistance were analyzed using the ICIM method in the QTL IciMapping software (version 4.0; Wang, 2009). The ICIM method can exclude the influence of QTL outside the current interval. Specifically, this method involves a two-step strategy to effectively separate the cofactor selection from the interval mapping process, thereby controlling the background

additive and dominance effects more effectively than compound interval mapping and improving the identification of QTL with additive effects (Zeng, 1993). The best linear unbiased prediction (BLUP) values were calculated with the following model: BLUP = (μ1 + …… + μ8)/*e*, where μ1–μ8 are the average performances in E1 (2019 in Shunyi), E2 (2019 in Changping), E3 (2019 in Xinxiang), E4 (2020 in Xinxiang), E5 (2020 in Changping), E6 (2021 in Shunyi), E7 (2021 in Changping), and E8 (2021 Xinxiang), respectively, and *e* is the number of environments (Wang, 2017). For each dataset, the significance threshold for affirming a putative QTL was obtained from 1,000 permutations was as follows: $p < 0.05$ with a logarithm of odds (LOD) score > 3.5 (Doerge and Churchill, 1996).

Validation of the FER resistance loci in CSSL populations

After generating a CSSL population with elite inbred line Qi319 as the donor and Ye478 as the receptor, we obtained 200 CSSLs covering all maize chromosomes, from which 12 CSSLs (CL160, CL171, CL9, CL172, CL173, CL82, CL14, CL174, CL45, CL61, CL28, and CL21) covering chromosome 1 were selected to identify *qFER1.03*.

To accurately locate the FER resistance-related gene on chromosome 1, insertion/deletion (InDel) markers were designed to increase the marker density between 40.0 and 50.0 Mb (B73 RefGen_v3). A PCR amplification was performed using the GeneAmp 9,700 PCR System (ABI, Norwalk, CT, United States). The 20-μL reaction volume consisted of 50 ng genomic DNA, 0.2 μm primer mix, 1.5 U Taq DNA polymerase, 0.2 mm dNTPs, and 2.0 μl 10 × buffer. The PCR program was as follows: 94°C for 4 min; 35 cycles of 94°C for 1 min, 50–60°C for 1 min, and 72°C for 1 min; 72°C for 10 min.

RNA-seq analysis

Total RNA was isolated from the ears of Qi319 and Ye478 plants inoculated with *F. verticillioides* (12 and 72 h) and the uninoculated controls (0 h, CK) using the TRIzol Kit (Invitrogen, Carlsbad, CA, United States) and then purified using the RNeasy kit (Qiagen, Germany). Three replicates were prepared for each sample. The purified RNA was used to construct a cDNA library using the NEBNext Ultra RNA Library Prep kit. The 18 libraries were subsequently sequenced using the Illumina HiSeq 2,500 system. After removing adapter sequences and low-quality reads, the high-quality paired-end reads were mapped to the maize reference genome (B73_v3) using the spliced read mapper TopHat (version 2.0.12; Kim et al., 2013). A principal component analysis was performed using the default settings of the prcomp function in the R software to interpret the relatedness among all replicates for each genotype. Significant differentially expressed genes (DEGs) were determined on the basis of a 2-fold expression-level change and a false discovery rate < 0.05 using the Cuffdiff module of Cufflinks (Trapnell et al., 2012).

Construction of target gene VIGS vectors

The Pr-CMV-VIGS system was used to silence the target gene (Li et al., 2021). Briefly, the target gene (150–200 bp) was amplified by RT-PCR using primers containing LIC adapters. The PCR product was purified and treated with T4 DNA polymerase (Thermo Scientific) in the presence of 5 mm dATP (Promega) at 37°C for 30 min before inactivating the T4 DNA polymerase at 75°C for 20 min. The pCMVZ2$_{2bN81}$-LIC vector was digested with *Apa*I and then similarly treated with T4 DNA polymerase in the presence of 5 mm dTTP (Promega). The T4 DNA polymerase-treated PCR product and pCMVZ2$_{2bN81}$-LIC vector were mixed and incubated at 70°C for 10 min and then at 22°C for 30 min. The mixture was subsequently used to transform *Escherichia coli* DH5α competent cells according to a heat shock method. The transformants were verified by sequencing, which was performed by the Genomic Sciences Laboratory at Sangon Biotech. The amplified product and two other CMV RNA sequences were inserted into *Agrobacterium tumefaciens* GV3101 cells, which were then grown overnight at 28°C in LB medium containing 50 mg/l kanamycin and 50 mg/l rifampicin. Equal amounts of GV3101 cells containing CMV RNA 1, 2, and 3 constructs were mixed, collected by centrifugation, and resuspended in infiltration buffer (10 mm $MgCl_2$, 10 mm MES pH 5.6, and 0.2 mm As) for an optical density at 600 nm of 1.0. The cell solutions were left undisturbed at room temperature for 3 h. They were then injected into the unfolded leaves of 5-week-old *Nicotiana benthamiana* plants using a syringe. The plants were incubated in darkness for 48 h and then placed under light. At 7 days after the inoculation, *N. benthamiana* leaves were collected, juiced, and used to inoculate the heart leaves of maize seedlings at the two-leaf and one-heart stage by rubbing. The inoculated leaves were covered with plastic wrap and then the maize seedlings were incubated in darkness for 48 h. The plastic wrap was removed and seedlings were transferred to the field and cultivated normally (Li et al., 2021).

Validation of the RNA silencing effect by quantitative real-time PCR (qRT-PCR)

Total RNA samples served as the template for a reverse transcription using the SuperScript III RT kit (Invitrogen) to synthesize cDNA. A qRT-PCR analysis of three replicates of the cDNA samples was performed using the SYBR Green Master Mix (Applied Biosystems, Foster City, CA, United States) and the CFX96 Real-Time System (Bio-Rad, Hercules, CA, United States).

Results

Variation in FER resistance among RILs

A total of 300 RILs were evaluated in terms of their FER resistance under field conditions in 2019, 2020, and 2021 in Changping, Shunyi, Xinxiang. The phenotypic variations are listed in Table 1. Transgressive segregation of FER resistance was observed in the RILs, and a wide range of variations was detected among families. The FER resistance among lines, which ranged from completely susceptible to highly resistant, was almost normally distributed, suggesting FER resistance is a quantitatively inherited trait. An analysis of the contributions of environmental and genetic factors to FER resistance revealed H^2 was as high as 95.46%, implying that the phenotypic variance in the RIL population was predominantly controlled by genetic factors (Table 2).

Mapping of QTL for FER resistance in the RIL population

Seventeen QTL were identified in eight environments (Table 3). The QTL, which were located on six chromosomes, explained 3.88–15.62% of the phenotypic variation, tentatively designated as *qFER1.03*, *qFER1.05*, *qFER1.06*, *qFER1.07*, *qFER3.06*, *qFER4.07*, *qFER5.05*, *qFER7.02*, *qFER8.05*. Among the FER resistance QTL, *qFER1.03* had the strongest effect and the highest LOD value, which was detected in Shunyi, Changping, Xinxiang in 2019, Changping in 2020 and Shunyi in 2021, could explain 4.99% to 15.4 of the phenotypic variation. *qFER4.07* was detected in Xinxiang in 2019 and Shunyi in 2021, explaining 4.5% of the phenotypic variation. *qFER1.05* was detected in Xinxiang in 2020 and Shunyi in 2021, explaining 9.2% of the phenotypic variation. *qFER1.06*, detected in Shunyi in 2019 and Xinxiang in 2020, explained 4.6 to 5.8% of the phenotypic variation. Moreover, using a LOD threshold of 3.0 and a 95% confidence interval, two QTL, on average, were detected on chromosome 1. *qFER1.03* had LOD value of 6.49 and accounted for as high as 15.62% of the phenotypic variation. Based on the B73 RefGen_v3 sequence, *qFER1.03* was localized in the 41–49 Mb intervals.

Validation and mapping of the *qFER1.03* locus using a CSSL population

The effect of *qFER1.03* was investigated using a CSSL population (derived from a cross between Qi319 and Ye478) that covered the whole chromosome 1 segments. The 12 selected CSSLs were obtained using the MAS method (BC_5F_3) by backcrossing for five generations and self-crossing for three generations. These 12 CSSLs had average background recovery rates of 97–99%. The QTL mapping results for the RIL population and 12 CSSLs covering chromosome 1 were used to map *qFER1.03*. The genotypes of the 12 CSSLs are presented in Figure 1, whereas the phenotypic data are provided in Table 4.

Line CL171 was significantly more resistant to FER than the susceptible parent Ye478. The localization of the resistance locus was consistent with the interval revealed by the analysis of the RIL population, confirming that *qFER1.03* contributes to maize FER resistance. The fragment carrying *qFER1.03* was narrowed to 40–50 Mb on chromosome 1, flanked by markers between mk194 and mk210. On the basis of the whole-genome resequencing data for the two parents, primer pairs were designed for 243 InDel markers between mk194 and mk210, of which five (InDel 1–InDel 5) specific for one of the two parents were selected to detect the target interval. The F_2 progeny obtained from the self-crossing of Ye 478 and CL171 were used for fine mapping. Additionally, 53 genotypes were identified. Finally, seven individual plants (Type 1–Type 7) were selected for a phenotypic analysis. The target fragment was located between 42.17 Mb and 43.76 Mb of chromosome 1 and was flanked by markers InDel 1 and InDel 2 (Figure 2). The F_3 families derived from the selfing of Type 1 were used to further narrow the target interval. Three polymorphic InDel markers (InDel 6–InDel 8) were detected between 42.17 Mb and 43.76 Mb. Three individual plants were selected for a

TABLE 1 Phenotype of parental lines and a recombinant inbred lines (RIL) population based on eight replicates.

Sites	Qi319	Ye478	RILs					
			Mean ± SD	Diseased area	Skewness	Kurtosis	CV%	H^2%
E1	0.27	0.37	0.25613 ± 0.006424	0.031–0.687	1.04	1.52	2.51	95.46
E2	0.22	0.54	0.39357 ± 0.008269	0.098–0.877	0.63	0.35	2.1	
E3	0.21	0.68	0.24527 ± 0.007687	0.035–0.701	0.83	0.44	3.13	
E4	0.29	0.72	0.24517 ± 0.007687	0.01–0.687	1.8	5.02	3.52	
E5	0.11	0.45	0.16113 ± 0.005668	0.118–0.9	0.15	0.57	1.88	
E6	0.2	0.6	0.26781 ± 0.006705	0.027–0.647	0.87	0.5	2.5	
E7	0.16	0.38	0.28497 ± 0.006172	0.082–0.774	0.93	1.41	2.17	
E8	0.18	0.39	0.26235 ± 0.006131	0.035–0.643	0.8	0.88	2.34	

SD = standard deviation, CV = coefficient of variation, and H^2 = generalized heritability.

TABLE 2 Analysis of variance of Fusarium ear rot resistance.

Source	df	SS	MS	*F* value	*Pr* > *F*	H^2 (%)
Genotype (G)	364	42.92806984	0.117934258	7.796953017	2.4687E-229	95.46%
Environment (E)	7	16.32332348	2.331903355	154.168443	3.4342E-190	
G × E	2,548	700.7287705	0.275011291	1202.044106	0	
Residuals error	2,919	38.5402462	0.015125685			

df = degree of freedom, SS = sum of squares, MS = mean square deviation, and H^2 = generalized heritability.

TABLE 3 Quantitative trait loci (QTL) mapping for Fusarium ear rot resistance using a recombinant inbred line population derived from Qi319 and Ye478.

E	Chromosome	[a]Peak position	[b]Interval (B73_V3, Mb)	LOD	[c]PVE (%)	Add
E1	1	43.5	43–44	6.1735	10.8112	0.0536
E2	1	43.5	43–44	9.8834	15.4031	0.0467
	3	187.6	187.1–188.1	3.5259	5.2438	0.0264
E3	1	43.5	43–44	4.3553	4.9804	0.0279
	1	187.5	187–188	4.0032	4.5815	0.0261
	4	169.35	168.85–169.85	3.9803	4.5449	0.0262
	8	161.95	161.45–162.45	3.6001	4.1217	0.0245
	1	208.5	208–209	6.0969	8.3916	0.035
E4	1	41.5	41–42	4.0072	5.9042	0.0281
	1	129.5	125–138	6.0185	9.1556	0.0339
E5	1	85.5	85–86	6.118	9.2149	0.032
	1	193.5	192–194	3.8964	5.7595	0.0256
E6	1	43.5	43–44	9.8594	10.9206	0.0505
	4	168.35	166.85–168.85	4.3667	4.6294	0.0322
	5	178.45	177.95–178.95	3.6582	3.8835	0.0291
E7	1	48.5	48–49	9.2732	13.571	0.05
E8	7	108.35	107.85–108.85	4.4657	6.1587	−0.0368
BLUP	1	40.5	40–41	6.491	15.625	0.0262
	1	187.5	187–188	4.889	11.571	0.0218

[a]Peak position = position with the highest logarithm of odds (LOD) value.
[b]Interval = interval between two markers in the B73 RefGen_v3 genome sequence.
[c]PVE = phenotypic variance explained by a single QTL; ADD = additive effects of a QTL.

phenotypic analysis (Type 8–Type 10). Finally, *qFER1.03* was located between markers InDel 8 and InDel 2, with physical distances of 43.55 and 43.76 Mb, respectively (Figure 2).

Integration of DEG and QTL data

Seven annotated genes were detected in the target interval between 43.55 Mb and 43.76 Mb on chromosome 1 following a search of MaizeGDB. According to the RNA-seq analysis, only one gene (*GRMZM2G017792*) was differentially expressed between Ye478 and Qi319. In MaizeGDB, *GRMZM2G017792* is named *mpk3* (MAP kinase 3). Additionally, its transcription and the activity of the encoded protein are upregulated by ABA and H_2O_2. Therefore, *GRMZM2G017792* was identified as a potential candidate gene for FER resistance. The STRING online program and RNA-seq data revealed an interaction between the proteins encoded by *GRMZM2G017792* and *GRMZM2G164405*, which is annotated in MaizeGDB as a 1-aminocyclopropane-1-carboxylic acid synthase 2 gene that is involved in limiting ethylene biosynthesis. Therefore, *GRMZM2G017792* may be related to ethylene synthesis.

GRMZM2G017792 was confirmed as a FER resistance-related gene by VIGS

To confirm its contribution to FER resistance, *GRMZM2G017792* was silenced in maize plants by VIGS. An analysis of FER incidence and severity in Sanya (Hainan) at 3 week post-inoculation indicated that all examined corn kernels were infected with *F. verticillioides*, with mycelia covering the cobs of CL171-1, CL171-2, and CL171-3, which differed regarding the extent of gene silencing. The grains were shriveled at the inoculation site in line CL171, but mycelial growth was restricted (Figure 3). Furthermore, CL171 was significantly more resistant

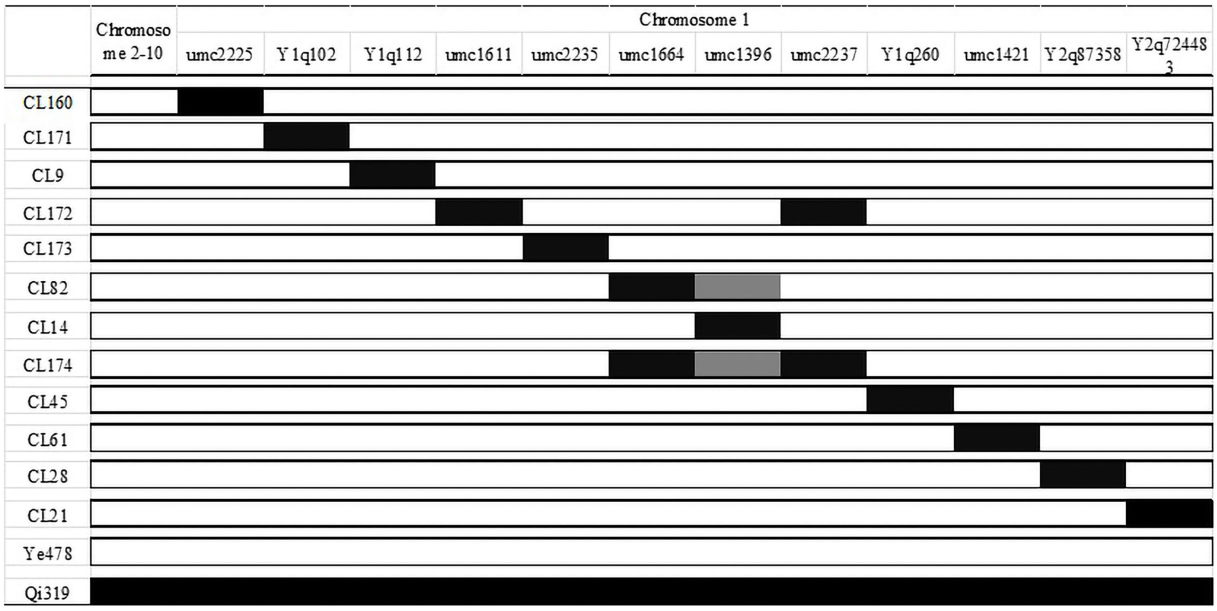

FIGURE 1
Identification of FER resistance QTL in the CSSL population.

to FER than CL171-1, CL171-2, and CL171-3, in which *GRMZM2G017792* was silenced. More specifically, the average RNA expression was significantly smaller ($p = 0.024$) for CL171 than for the gene-silenced materials (Figure 4).

Discussion

Nowadays, Fusarium ear rot has been one of the most important diseases on maize in China. The breeding for FER resistance is pressing and has been an indispensable target trait. The mining of stable FER resistance genes/loci will facilitate resistance breeding. The accuracy of phenotypic value has a great influence on gene mapping. The performance of precise identification of maize resistance to ear rot was proven to be a difficult issue because of the genetic complexity and sensitive dependence of FER on environmental conditions. Therefore, all plants were artificially inoculated with pathogen spore suspension 5–7 days after silking to ensure that pathogen infection occurred at almost the same stage of kernel development among all individuals, and the Automatic Imaging System for Ear Rot was used to analyze the diseased area of inoculated ears. Compared with previous researches on the incidence and severity of maize ear rot on the basis of visual observations and estimations, the Automatic Imaging System for Ear Rot enabled a more accurate calculation of the diseased ear area. Using this method, we ensured that experimental uniformity and pathogen infection occurred at almost the same stage of kernel development among individuals.

Although some studies have reported FER-resistant loci derived from various inbred lines and mapped at different intervals (Zhang et al., 2007; Ding et al., 2008; Li et al., 2011). However, the newly identified genes/loci insensitivity to environments are needed for FER-resistant breeding. In this study, nine QTL associated with FER resistance overlapped regions in bins 1.03, 1.05 to 1.07, 3.06, 4.07, 5.05, 7.02 and 8.05. Among the intervals of bin 1.03, 3.06, 4.07, 7.02 overlapped with those reported in previous studies (Zhang et al., 2007; Chen et al., 2016; Wen et al., 2021), the major QTL at bin1.03 detected in five different environments explained the phenotypic variation as high as 15.4% Therefore, this QTL was selected for further fine mapping.

A combined analysis of RILs and CSSLs is a powerful approach for dissecting the QTL for FER resistance in maize. The CSSLs with the same genetic background can be used to mendelize QTL and substantially improve the localization of individual QTL. After preliminarily localizing QTL in a RIL population, we more precisely mapped QTL using CSSLs. This approach is useful for detecting FER resistance-related genes. The isolated QTL can be quickly localized by identifying QTL-linked markers in a CSSL population (Yung et al., 2012). We used SSR markers to select 12 CSSLs with different genetic backgrounds for chromosome 1, but identical backgrounds for the remaining chromosomes, to eliminate the effects of other FER resistance-related genes. These CSSLs were used for reconfirming and precisely localizing the newly identified major QTL *qFER1.03*. Line CL171 was resistant to FER, whereas the other CSSLs were susceptible. Therefore, CL171 may be used to construct a secondary backcross population for the fine mapping and cloning of the gene mediating FER resistance. Therefore, CL171 can be used to construct a secondary backcross population for fine positioning and cloning of

10.3389/fpls.2022.954546

TABLE 4 Comparison of the FER resistance between the CSSLs and the susceptible control line Ye478.

CSSL	Background recovery	Diseased area	Resistance Growth (%)	Bin	Marker
CL160	0.98	0.63	0.07	1.02	bnlg1614-umc2225
CL171		0.35	0.45	1.03	Y1q25-bumc1144
CL9	0.99	0.71	−0.04	1.04	Y1q102-Y1q112
CL172		0.81	−0.19	1.05	umc1076-umc1611
CL173		0.66	0.03	1.05, 1.06	umc1611-umc1590
CL82	0.98	0.88	−0.29	1.06	umc2235
CL14	0.99	0.94	−0.38	1.06	umc1664-umc1709
CL174		0.67	0.01	1.06, 1.07	umc1254-umc2237
CL45	0.97	0.88	−0.29	1.07, 1.08	umc2505-umc2240
CL61	0.98	0.69	−0.01	1.09	Y1q260-Y1q272
CL28	0.98	0.69	−0.01	1.11	umc1421-bnlg2123
CL21	0.98	0.89	−0.31	1.11	Y2q87358-Y2q724483
Ye478		0.68			

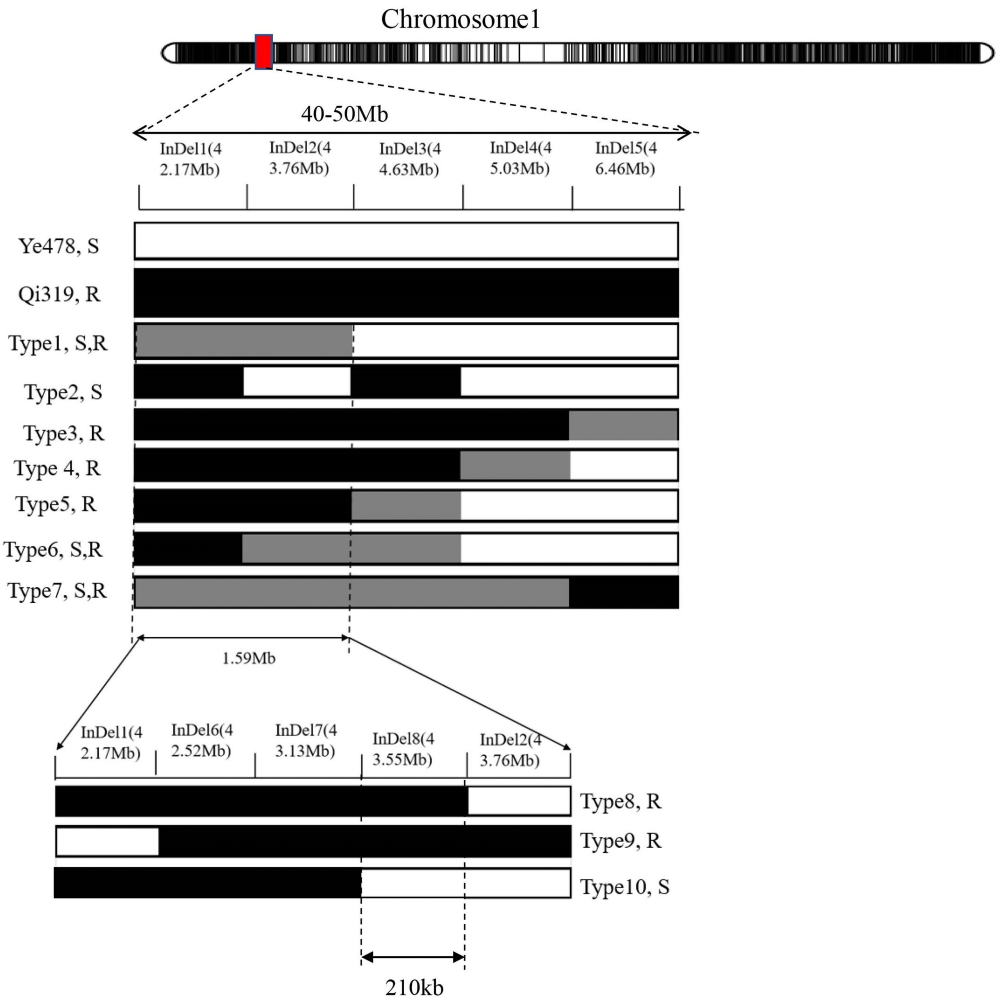

FIGURE 2
(A) Narrowing of the *qFER1.03* interval using an F_2 hybrid generation derived from a cross between CL171 and Ye478. Black and gray rectangles represent homozygous Qi319 alleles and homozygous Ye478 alleles, respectively. Light gray indicates heterozygous alleles of Qi319 and Ye478. S and R refer to susceptible and resistant, respectively. **(B)** Narrowing of the *qFER1.03* interval using an F_3 inbred generation derived from the selfing of Type 1.

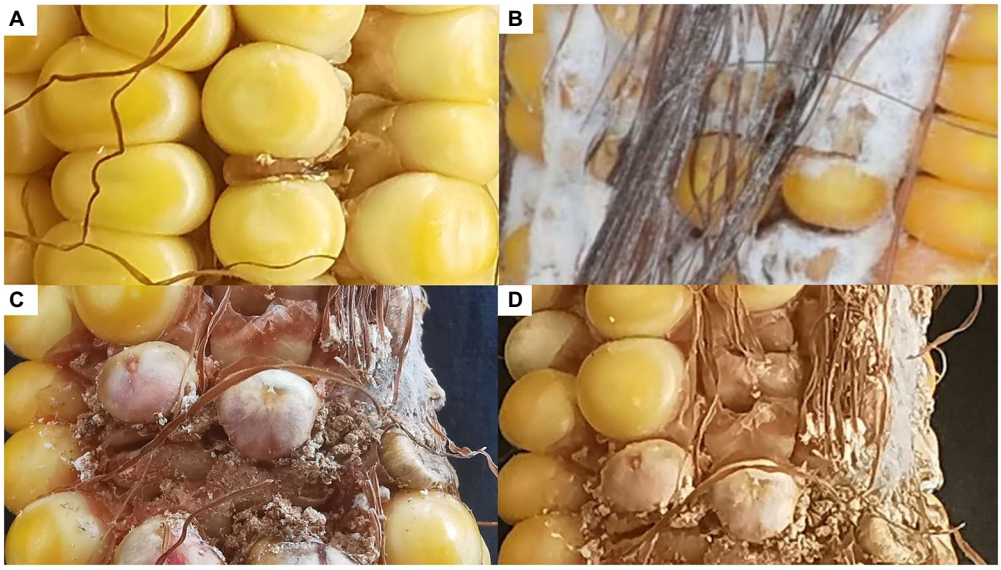

FIGURE 3
Incidence and severity of FER among CL171 and the gene-silenced materials. **(A)** CL171; **(B)** CL171-1; **(C)** CL171-2; **(D)** CL171-3.

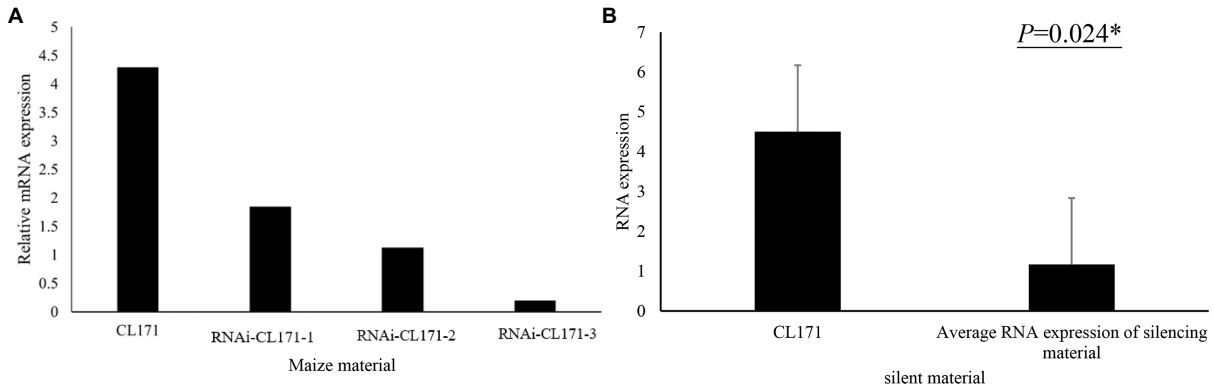

FIGURE 4
(A) Expression of *GRMZM2G017792* in CL171 and gene-silenced materials. **(B)** Significant difference (p=0.024) in the RNA expression between CL171 and the gene-silenced materials (average).

the significant gene for FER resistance. This strategy was feasible for laying a foundation in FER resistance breeding.

Transcriptomic data provide researchers with important information for mining candidate genes for maize ear rot resistance. In the current study, only one gene (*GRMZM2G017792*) in the QTL region was differentially expressed between the parents susceptible (Ye478) and resistant (Qi319) to FER. The mitogen-activated protein kinase cascade is a signal transduction pathway that is common in eukaryotes. It plays an important role in plant responses to biotic and abiotic stresses. Recent studies on *Arabidopsis thaliana* confirmed that MPK3 and MPK6 are important for leaf stomatal development, petal shedding, and ovule development. Moreover, they are activated by various stimuli (e.g., salt stress and pathogen infection) during the regulation of diverse defense responses, making them crucial for plant disease resistance. Meng et al. (2013) reported that MPK3/MPK6 in *A. thaliana* phosphorylate ERF6 (ethylene-responsive factor), thereby activating defense-related gene expression and enhancing the resistance to *Botrytis cinerea*. Li et al. (2021) observed that MPK3/6 phosphorylates ERF72 to regulate the transcriptional activation of *PAD3*, *CYP71A12*, and *WRKY33*.

In a previous study involving CMV-ZMBJ-based VIGS in maize line B73, a vascular puncture inoculation method resulted in a viral infection rate of approximately 59%, but only about 60% of the infected plants exhibited different degrees of gene silencing. Moreover, the gene-silencing efficiency in five young systemic leaves varied from 25 to 78% among individual plants over 60 days (Wang et al., 2016). The relatively low viral infection rate associated with the vascular puncture inoculation method is not unique to

CMV, with similar results obtained for other VIGS vectors (e.g., BSMV and MRFV; Jarugula et al., 2018; Mlotshwa et al., 2020). In contrast, the Pr-CMV-VIGS system can silence the target gene in maize for relatively long periods. More specifically, Pr CMV: *ZmIspH* was used for the highly efficient and durable silencing of *ZmIspH* (59.4–87.3%) for over 105 days, which is the longest period of VIGS in maize reported to date (Li et al., 2021).

In the present study, we silenced the candidate gene *GRMZM2G017792* using the Pr-CMV-VIGS system, which resulted in a distinct decrease in the FER resistance of CL171. Pyramiding several disease resistance-related genes in a single variety and developing multiline cultivars are the most effective methods for increasing the durability of maize FER resistance. In this study, *GRMZM2G017792* was identified as a candidate FER resistance-related gene, which may be useful for maize breeding. More specifically, it may be exploited to decrease the incidence and severity of FER outbreaks. Future studies will need to clone and functionally characterize the candidate gene. Furthermore, clarifying the molecular mechanism underlying FER resistance in maize will enhance the breeding of superior inbred lines and FER-resistant hybrids.

Data availability statement

The data presented in the study are deposited in the NCBI repository, accession numbers are SAMN29837145, SAMN29837146, SAMN29837147, SAMN29837148, SAMN29837149, SAMN29837150, SAMN29837151, SAMN29837152, SAMN29837153, SAMN29837154, SAMN29837155, SAMN29837156, SAMN29837157, SAMN29837158, SAMN29837159, SAMN29837160, SAMN29837161, SAMN29837162, SAMN29837163, SAMN29837164, and SAMN29837165.

Author contributions

YX, JW, and CD conceived and designed the experiments. XL discussed experimental scheme and revised the article. YX, BW, LZ, and ZZ performed RILs phenotype data collecting. YX, LZ, XL, and SS analyzed the RILs data and conducted the QTL identification and further fine mapping. YX, JW, XL, and LZ constructed the sequence library of the Ye478 and Qi319. YX, WW, and CD analyzed the data and discussed the article. YX and CD wrote the paper. All authors contributed to the article and approved the submitted version.

Funding

This project was supported by the National Key Research and Development Program of China (2021YFD1200702 and 2016YFD0100103), the Project of Sanya Yazhou Bay Science and Technology City (SKJC-2020-02-001), and Agricultural Science and Technology Innovation Project of Chinese Academy of Agricultural Sciences (CAAS-ASTIP-2017-ICS).

Acknowledgments

We thank Prof. Liu Yule (Tsinghua University) and Zhou Tao (China Agricultural University) for providing the VIGS vectors. We also thank Liwen Bianji (Edanz; www.liwenbianji.cn) for editing the English text of a draft of this manuscript.

Conflict of interest

The authors declare that the research was conducted in the absence of any commercial or financial relationships that could be construed as a potential conflict of interest.

Publisher's note

Supplementary material

The Supplementary material for this article can be found online at: https://www.frontiersin.org/articles/10.3389/fpls.2022.954546/full#supplementary-material

References

Alonso-Blanco, C., and Koornneef, M. (2000). Naturally occurring variation in *Arabidopsis*: an underexploited resource for plant genetics. *Trends Plant Sci.* 5, 22–29. doi: 10.1016/S1360-1385(99)01510-1

Becker, A., and Lange, M. (2010). VIGS-genomics goes functional. *Trends Plant Sci.* 15, 1–4. doi: 10.1016/j.tplants.2009.09.002

Brachi, B., Faure, N., Horton, M., Flahauw, E., Vazquez, A., Nordborg, M., et al. (2010). Linkage and association mapping of *Arabidopsis thaliana* flowering time in nature. *PLoS Genet.* 6:e1000940. doi: 10.1371/journal.pgen.1000940

Chen, J., Shrestha, R., Ding, J., Zheng, H., Mu, C., Wu, J., et al. (2016). Genome-wide association study and QTL mapping reveal genomic loci associated with Fusarium ear rot resistance in tropical maize germplasm. *G3 (Bethesda)* 6, 3803–3815. doi: 10.1534/g3.116.034561

Ding, J. Q., Wang, X. M., Chander, S., Yan, J. B., and Li, J. S. (2008). QTL mapping of resistance to Fusarium ear rot using a RIL population in maize. *Mol. Breed.* 22, 395–403. doi: 10.1007/s11032-008-9184-4

Doerge, R. W., and Churchill, G. A. (1996). Permutation tests for multiple loci affecting a quantitative character. *Genetics* 142, 285–294. doi: 10.1007/BF00132588

Du, Q., Tang, Z. L., Li, S. C., Shang, G. L. L., Li, H. J., and Duan, C. X. (2019). Composition of *Fusarium* species causing maize ear rot and analysis of toxigenic chemotype in Guangxi. *Sci. Agric. Sin.* 52, 1895–1907. doi: 10.3864/j.issn.0578-1752.2019.11.005

Duan, C. X., Cui, L. N., Xia, Y. S., Dong, H. Y., Yang, Z. H., Hu, Q. Y., et al. (2022). Precise characterization and analysis of maize germplasm resources for resistance to Fusarium ear rot and Gibberella ear rot. *Acta Agron. Sin.* 48, 2155–2167.

Duan, C. X., Qin, Z. H., Yang, Z. H., Li, W. X., Sun, S. L., Zhu, Z. D., et al. (2016). Identification of pathogenic *Fusarium* spp. causing maize ear rot and potential mycotoxin production in China. *Toxins* 8:186. doi: 10.3390/toxins8060186

Duan, C. X., Wang, X. M., Song, F. G., Sun, S. L., Zhou, D. N., and Zhu, Z. D. (2015b). Research progress in maize resistance to ear rot. *Sci. Agric. Sin.* 48, 2152–2164. doi: 10.3864/j.issn.0578-1752.2015.11.007

Duan, C. X., Wang, X. M., Wu, X. F., Yang, Z. H., Song, F. G., Zhao, L. P., et al. (2015a). Resistance analysis of maize germplasm and new varieties to Pythium stalk rot and Fusarium ear rot. *J. Plant Genet. Resour.* 16, 947–954. doi: 10.13430/j.cnki.jpgr.2015.05.004

Eshed, Y., and Zamir, D. (1994). A genomic library of *Lycopersicon pennellii* in *L. esculentum*: a tool for fine mapping of genes. *Euphytica* 79, 175–179. doi: 10.1007/BF00022516

Holland, J. B. (2007). Genetic architecture of complex traits in plants. *Curr. Opin. Plant Biol.* 10, 156–161. doi: 10.1016/j.pbi.2007.01.003

Jarugula, S., Willie, K., and Stewart, L. R. (2018). Barley stripe mosaic virus (BSMV) as a virus-induced gene silencing vector in maize seedlings. *Virus Genes* 54, 616–620. doi: 10.1007/s11262-018-1569-9

Kim, D., Pertea, G., Trapnell, C., Pimentel, H., Kelley, R., and Salzberg, S. L. (2013). TopHat2: accurate alignment of transcriptomes in the presence of insertions, deletions and gene fusions. *Genome Biol.* 14, R36. doi: 10.1186/gb-2013-14-4-r36

Knapp, S. J., Stroup, T. W. W., and Ross, W. M. (1985). Exact confidence intervals for heritability on a progeny mean basis. *Crop Sci.* 25, 192–194.

Korte, A., and Farlow, A. (2013). The advantages and limitations of trait analysis with GWAS: a review. *Plant Methods* 9, 29. doi: 10.1186/1746-4811-9-29

Lanubile, A., Maschietto, V., Borrelli, V. M., Stagnati, L., Logrieco, A. F., and Marocco, A. (2017). Molecular basis of resistance to Fusarium ear rot in maize. *Front. Plant Sci.* 8:1774. doi: 10.3389/fpls.2017.01774

Li, Z. M., Ding, J. Q., Wang, R. X., Chen, J. F., Sun, X. D., Chen, W., et al. (2011). A new QTL for resistance to Fusarium ear rot in maize. *J. Appl. Genet.* 52, 403–406. doi: 10.1007/s13353-011-0054-0

Li, H., Zhang, D. F., Xie, K., Wang, Y., Liao, Q. S., Hong, Y. G., et al. (2021). Efficient and high-throughput pseudo recombinant-chimeric *cucumber mosaic virus*-based VIGS in maize. *Plant Physiol.* 187, 2865–2876. doi: 10.1093/plphys/kiab443

Lu, L., Xu, Z. N., Sun, S. L., Du, Q., Zhu, Z. D., Weng, J. F., et al. (2020). Discovery and fine mapping of *qSCR6.01*, a novel major QTL conferring southern rust resistance in maize. *Plant Dis.* 104, 1918–1924. doi: 10.1094/PDIS-01-20-0053-RE

Meng, X., Xu, J., He, Y., Yang, K. Y., Mordorski, B., Liu, Y., et al. (2013). Phosphorylation of an ERF transcription factor by Arabidopsis MPK3/MPK6 regulates plant defense gene induction and fungal resistance. *Plant Cell* 25, 1126–1142. doi: 10.1105/tpc.112.109074

Mlotshwa, S., Xu, J., Willie, K., Khatri, N., Marty, D., and Stewart, L. R. (2020). Engineering *maize rayado fino virus* for virus-induced gene silencing. *Plant Direct* 4, 1–15. doi: 10.1002/pld3.224

Morales-Rodríguez, I., Yanez-Morales, M. D. J., Silva-Rojas, H. V., Garcia-de-Los-Santos, G., and Guzman-de-Pena, D. A. (2007). Biodiversity of *Fusarium* species in Mexico associated with ear rot in maize, and their identification using a phylogenetic approach. *Mycopathologia* 163, 31–39. doi: 10.1007/s11046-006-0082-1

Munkvold, G. P. (2003). Epidemiology of *Fusarium* diseases and their mycotoxins in maize ears. *Eur. J. Plant Pathol.* 109, 705–713. doi: 10.1023/A:1026078324268

Nankam, C., and Pataky, J. K. (1996). Resistance to kernel infection by *Fusarium moniliforme* in the sweet corn inbred IL125b. *Plant Dis.* 80, 593–598. doi: 10.1094/PD-80-0593

Qin, Z. H., Ren, X., Jiang, K., Wu, X. F., Yang, Z. H., and Wang, X. M. (2014). Identification of *Fusarium* species and *F. graminearum* species complex causing maize ear rot in China. *Acta Phytophy. Sin.* 41, 589–596. doi: 10.13802/j.cnki.zwbhxb.2014.05.032

Robertson-Hoyt, L. A., Jines, M. P., Balint-Kurti, P. J., Kleinschmidt, C. E., White, D. G., Payne, G. A., et al. (2006). QTL mapping for Fusarium ear rot and fumonisin contamination resistance in two maize populations. *Crop Sci.* 46, 1734–1743. doi: 10.1186/s12870-017-0970-1

Shi, X. R., and Bai, L. (1992). Investigation on the pathogens of different types of maize population ear and kernel rot. *Acta Phytophy. Sin.* 18, 28–29.

Shim, R. A., Angeles, E. R., Ashikari, M., and Takashi, T. (2010). Development and evaluation of *Oryza glaberrima* Steud. Chromosome segment substitution lines (CSSLs) in the background of *O. sativa* L. cv. 'Koshihikari'. *Breed. Sci.* 60, 613–619. doi: 10.1270/jsbbs.60.613

Sun, H., Guo, N., Shi, J., Zhang, H. J., Ma, H. X., and Liu, S. S. (2017a). Characterization of the maize ear rot pathogens and genetic diversity analysis of dominant species in Hainan. *Sci. Agric. Sin.* 47, 577–583. doi: 10.13926/j.cnki.apps.000032

Sun, H., Zhang, H. J., Guo, N., Shi, J., Chen, D., and Ma, H. X. (2017b). Isolation and identification of pathogenic bacteria of corn ear rot in Hainan and genetic diversity analysis of dominant species. *Acta Phytophy. Sin.* 44, 796–802. doi: 10.13802/j.cnki.zwbhxb.2017.2016078

Tian, Y. J., Zhao, S. G., Zhang, J., Wang, Q. Y., Huang, L. H., and Chen, H. D. (2014). Research progress on maize rust in China. *Chin. Agric. Sci. Bull.* 30, 226–231. doi: 10.11924/j.issn.1000-6850.2013-1232

Trapnell, C., Roberts, A., Goff, L., Pertea, G., Kim, D., Kelley, D. R., et al. (2012). Differential gene and transcript expression analysis of RNA-seq experiments with TopHat and cufflinks. *Nat. Protoc.* 7, 562–578. doi: 10.1038/nprot.2012.016

Vance, V., and Vaucheret, H. (2001). RNA silencing in plants-defense and counterdefense. *Science* 292, 2277–2280. doi: 10.1126/science.1061334

Wang, X. M. (2005). Series of lectures on knowledge of maize diseases and insect pests (III) identification and investigation technology of maize disease and insect resistance. *Crop J.* 21, 53–55. doi: 10.16035/j.issn.1001-7283.2005.06.026

Wang, J. K. (2009). Complete interval mapping method for quantitative trait genes. *Acta Phytophy. Sin.* 35, 239–245. doi: 10.3724/SP.J.1006.2009.00239

Wang, J. K. (2017). *Quantitative Genetics*. Beijing, China: Science Press.

Wang, J. J., Xu, Z. N., Yang, J., Lu, X. H., Zhou, Z. Q., Zhang, C. S., et al. (2018). *qNCLB7.02*, a novel QTL for resistance to northern maize leaf blight in maize. *Mol. Breed.* 38:54. doi: 10.1007/s11032-017-0770-1

Wang, R., Yang, X., Wang, N., Liu, X., Nelson, R. S., Li, W., et al. (2016). An efficient virus-induced gene silencing vector for maize functional genomics research. *Plant J.* 86, 102–115. doi: 10.1111/tpj.13142

Wei, Q., Liao, L. L., Chen, L., and Qi, Y. X. (2019). Isolation and identification of the main fusarium species causing maize ear rot in Anhui province. *Acta Phytophy. Sin.* 45, 221–225. doi: 10.16688/j.zwbh.2018362

Wen, J., Shen, Y. Q., Xing, Y. X., Wang, Z. Y., Han, S. P., Li, S. J., et al. (2021). QTL mapping of Fusarium ear rot resistance in maize. *Plant Dis.* 105, 558–565. doi: 10.1094/PDIS-02-20-0411-RE

Xiang, K. L., Reid, M., Zhang, Z. M., Zhu, X. Y., and Pan, G. T. (2012). Characterization of correlation between grain moisture and ear rot resistance in maize by QTL meta-analysis. *Euphytica* 183, 185–195. doi: 10.1007/s10681-011-0440-z

Xiao, S. Q., Xu, J. N., Yan, L. B., Sui, Y. H., Xue, C. S., and Chen, J. (2017). Identification and distribution of the pathogen of maize Fusarium ear rot in Liaoning Province. *Acta Phytophy. Sin.* 44, 803–808. doi: 10.13802/j.cnki.zwbhxb.2017.2016056

Yang, Q., Yin, G., Guo, Y., Zhang, D., Chen, S., and Xu, M. (2010). A major QTL for resistance to *Gibberella* stalk rot in maize. *Theor. Appl. Genet.* 121, 673–687. doi: 10.1007/s00122-010-1339-0

Yung, L., Ding, D., Li, W. H., Xie, H. L., Tang, J. H., and Fu, Z. Y. (2012). Construction of single segment substitution lines (SSSLs) of elite inbred lines in 514 maizes. *J. Maize Sci.* 20, 52–55. doi: 10.13597/j.cnki.maize.science.2012.02.010

Zeng, Z. B. (1993). Theoretical basis for separation of multiple linked gene effects in mapping quantitative trait loci. *P. Natl. Acad. Sci. USA* 90, 10972–10976. doi: 10.1073/pnas.90.23.10972

Zhang, F., Wan, X. Q., and Pan, G. T. (2007). QTL mapping for resistance to ear and kernel rot in maize. *Acta Agron. Sin.* 33, 491–496. doi: 10.3321/j.issn:0496-3490.2007.03.021

Zhang, C. S., Zhou, Z. Q., Yong, X. C., Hao, Z. F., Zhang, F. J., Li, M. S., et al. (2017). Analysis of the genetic architecture of maize ear and grain morphological traits by combined linkage and association mapping. *Theor. Appl. Genet.* 130, 1011–1029. doi: 10.1007/s00122-017-2867-7

Zhou, D. N., Wang, X. M., Chen, G. K., Sun, S. L., Yang, Y., Zhu, Z. D., et al. (2018). The major Fusarium species causing maize ear and kernel rot and their toxigenicity in Chongqing, China. *Toxins* 10, 90. doi: 10.3390/toxins10020090

Zhou, D. N., Wang, X. M., Li, D. N., Yang, Y., Chen, G. K., and Duan, C. X. (2016). Isolation and identification of the pathogenic Fusarium of maize ear rot in Chongqing and surrounding areas. *Acta Phytophy. Sin.* 43, 782–788. doi: 10.13802/j.cnki.zwbhxb.2016.05.011

frontiers | Frontiers in Plant Science

TYPE Original Research
PUBLISHED 13 October 2022
DOI 10.3389/fpls.2022.1008624

OPEN ACCESS

EDITED BY
Cheng Liu,
Shandong Academy of Agricultural Sciences, China

REVIEWED BY
Baojian Guo,
Yangzhou University, China
Xueju Yang,
Agricultural University of Hebei, China
Pengtao Ma,
Yantai University, China

*CORRESPONDENCE
Aiju Zhao
zhaoaiju81@126.com
Yuping Liu
ypliu2008@126.com

SPECIALTY SECTION
This article was submitted to Plant Pathogen Interactions, a section of the journal Frontiers in Plant Science

RECEIVED 01 August 2022
ACCEPTED 26 August 2022
PUBLISHED 13 October 2022

CITATION
Lv L, Chen X, Li H, Huang J, Liu Y and Zhao A (2022) Different adaptive patterns of wheat with different drought tolerance under drought stresses and rehydration revealed by integrated metabolomic and transcriptomic analysis.
Front. Plant Sci. 13:1008624.
doi: 10.3389/fpls.2022.1008624

Different adaptive patterns of wheat with different drought tolerance under drought stresses and rehydration revealed by integrated metabolomic and transcriptomic analysis

Liangjie Lv, Xiyong Chen, Hui Li, Jinan Huang, Yuping Liu* and Aiju Zhao*

Crop Genetics and Breeding Laboratory of Hebei, Institute of Cereal and Oil Crops, Hebei Academy of Agriculture and Forestry Sciences, Shijiazhuang, China

Wheat as a staple food crop is enduring ever-frequent intermittent and changing drought with the climate change. It is of great significance to highlight the adaptive approaches under such variable conditions at multiple levels to provide a comprehensive understanding of drought tolerance and facilitate the genetic breeding of wheat. Therefore, three wheat lines with different drought tolerance (drought-tolerant mutant *Mu*>common wheat CK>drought susceptible mutant *mu*) were analyzed under moderate and severe drought stresses as well as rehydration. Samples were subjected to transcriptomic and metabolomic profiling in combination with physiological and biochemical determination. The moderate drought stress rendered 198 and 115 differentially expressed metabolites (DEMs) in CK and *Mu*, respectively. The severe drought stress rendered 166, 151 and 137 DEMs in CK, *Mu* and *mu*, respectively. The rehydration rendered 150 and 127 DEMs in CK and *Mu*. 12,557 and 10,402 differentially expressed genes (DEGs) were identified for CK and *Mu* under moderate drought stress, respectively. 9,893, 7,924, and 9,387 DEGs were identified for CK, *Mu*, and *mu* under severe drought stress, respectively. 13,874 and 14,839 were identified in CK and Mu under rehydration, respectively. Metabolomics results showed that amino acid was the most differentially expressed metabolites, followed by phenolic acids. Flavonoids played an important role in drought tolerance. Most enriched pathways under drought included biosynthesis of secondary metabolites, metabolic pathways and photosynthesis. Metabolites and genes involved in osmotic regulation, antioxidase activities, and ABA signaling were more enriched in *Mu* than in CK and mu. Various drought-responsive genes and metabolites in *Mu* showed different trends with those in CK and *mu*. Increased amino acids biosynthetic capability and ROS scavenging ability resulted from higher antioxidase activities and increased flavonoids may be the mechanisms underlying the drought tolerance characteristic of *Mu*. Recovery from reversible ROS damage and rapid amino acid biosynthesis may contribute to the rapid recovery of *Mu*.

The present study provides new insights for mechanisms of wheat under complex drought conditions.

KEYWORDS

wheat, drought, rehydration, metabolome, transcriptome

Introduction

Drought is one of the most important environmental factors and severely impact crop growth, yield and quality (Krasensky and Jonak, 2012; Zhang et al., 2014; Tatar et al., 2020). After long terms of evolution, plants have developed various strategies to cope with deleterious effects of drought, which deserves in-depth investigation. The main coping strategies to drought employed by plants can be summarized as drought escape, drought avoidance, and drought tolerance (Du et al., 2018; Osmolovskaya et al., 2018; Li et al., 2021). The escape strategy generally involves a seasonal response, including life or growth cycle adjustment (Basu et al., 2016). In the drought avoidance strategy, plants enhance water uptake and reduce water loss. Drought tolerance is mediated by osmotic adjustment (such as accumulation of osmotin and protective proteins), extension of antioxidant capacity (including enzymatic and non-enzymatic activities), and development of desiccation tolerance (such as cell wall hardening; Zhang, 2007).

Wheat is one of the staple crops in the world and endures frequent drought stresses. Drought tolerance strategies have also been documented in wheat. Like other plants, wheat under drought synthesizes and accumulates more osmotic regulatory substances, such as proline, betaine, and other inorganic ions (Francki and Appels, 2002). Genetically modified engineering confirmed that genes encoding delta1-pyrroline-5-carboxylate synthetase (P5CS; Vendruscolo et al., 2007) and 1-phosphate mannitol dehydrogenase (mlt D; Abebe et al., 2003) could result in drought tolerance improvement of wheat. Protective proteins also play a role in the drought tolerance process of wheat. Sivamani et al. (2000) introduced *HVA1*, the gene encoding barley group 3 LEA protein, into wheat, and found that under drought conditions, the biomass and water use efficiency of transgenic wheat were increased, and the survival rate was improved. Moreover, wheat transcription factors such as *DREB2* (Morran et al., 2011), *WRKY2* (Gao et al., 2018), and *NAC69* (Xue et al., 2011) are also reported to be related to drought tolerance of wheat. The expression of *TaFER-5B* was induced by drought. Overexpression of this gene improved the drought resistance, heat resistance, oxidation resistance and high iron resistance of wheat plants, which was mainly due to the improved ability to scavenge reactive oxygen species, increased catalase (CAT) and glutathione reductase (GR) activities, and decreased H_2O_2 content (Zang et al., 2017).

Plants are often grown in a changing environment with alternating dry and wet conditions, especially for crops with artificial interference (Yang et al., 2022), such as wheat. In other words, intermittent drought occurs more frequently in actual production. The rapid recovery ability of plants after rehydration, on the one hand, can quickly reduce the damage caused by drought stress, and at the same time reduce the impact of drought on plant yield with different degrees of compensation effect, which is of great significance to plant production. However, reports addressing responses to progressive drought and recovery upon rehydration are relatively limited (Abid et al., 2018).

OMICS techniques including metabolomics, transcriptomics, proteomics, and ionomics, provide a wider scope of mechanisms underlying the biological process compared with conventional methods (Budak et al., 2015). They contribute a lot to the identification and characterization of genes, proteins, metabolites, and ions involved in signaling pathways of interest. With the progress in methodology and the decrease in cost, these techniques have been widely adopted in drought-related researches (Wilkins et al., 2010; You et al., 2019; Xu et al., 2021). Great progress in investigations into wheat under drought stresses have also been made (Xiao et al., 2012; Reddy et al., 2014; Zhan et al., 2014). Proteomics and metabolomics of leaf tissues from spring-wheat showed that photosynthetic proteins and enzymes involved in sugar and nitrogen metabolism, as well as capacity of detoxifying harmful molecules were of significance during drought response of wheat. Ma et al. (2019) adopted transcriptome to investigate the differentially expressed genes and enriched pathways during drought-sensitive period under field conditions in bread wheat, and pointed out that genes encoding tubulins, 6-phosphogluconate dehydrogenase (PGD6), cuticular wax-associated proteins, and heat shock proteins were greatly involved. Li et al. (2022) revealed a novel regulation of drought resistance during germination in wheat by integrated metabolome and transcriptome. They showed that the DEGs that participated in the mTOR and alpha-linolenic acid metabolism pathways were considered candidate DEGs related to drought resistance.

Overall, we contend that drought stress studies should be extended to explore the differences of cultivars/lines with as many approaches as possible, and drought intensities as well as rehydration should be taken into consideration to gain more insights of wheat under complex drought situations. Therefore, the present study was carried out to characterize the physiological, biochemical, metabolomic and transcriptomic responses of three wheat lines with different drought tolerance to different intensities of drought as well as rehydration. Our study may provide a

comprehensive understanding of the underlying mechanisms of wheat response to drought and rehydration, and facilitate the breeding of drought-tolerant cultivars.

Materials and methods

Plant materials and treatments

The common wheat cultivar Jimai 418, designated as CK, and its two ethyl methane sulfonate (EMS)-induced mutants, namely drought-tolerant mutant *Mu* and drought-susceptible mutant *mu*, were taken as experimental materials. The details of the EMS mutagenesis can be found in our previous study (Lv et al., 2020). The experiment was carried out in an incubation room of the Institute of Grain and Oil Crops, Hebei Academy of Agriculture and Forestry Sciences (114.38°, 38.23° E N, 50 m). All wheat plants were grown in a greenhouse under 23°C/14 h light and 15°C/10 h dark. Seeds of the three lines were surface-sterilized with 0.2% $HgCl_2$ for 20 min, followed by rinsing thoroughly with distilled water, and dried on filter papers. The seeds were planted in free-draining plastic pots filled with clay loam soil. Three pots were prepared for each line with different treatments. The moisture was kept at 70–80% field capacity by irrigating with tap water until the drought stress treatments. Thirty-five days after the planting (tillering stage), wheat seedlings of CK and *Mu* were subjected to normal irrigation (about 70–80% field capacity), moderate drought (about 50–60% field capacity) and severe drought (about 30–40% field capacity) for 10 days, respectively (seedlings undergone the treatments were designated as CK1, CK2, CK3, *Mu*1, *Mu*2, and *Mu*3). Wheat seedlings of *mu* were subjected to normal irrigation and severe drought stress (designated as *mu*1 and *mu*3). Rehydration was carried out for CK3 and *Mu*3 to allow a 3-day recovery (seedlings undergone the rehydration were designated as CK4 and *Mu*4, respectively). At the end of each treatment, fresh leaves were collected for physiological and biochemical analysis, or immediately frozen in liquid nitrogen and stored at −80°C for further metabolomic and transcriptomic analysis.

Determination of soluble sugar content, soluble protein content and enzymic antioxidant activities

Fresh leaves (0.5 g) were homogenized at 4°C in 100 mM potassium phosphate buffer (pH 7.0) supplemented with 1 mM EDTA and 1% polyvinylpyrrolidone (*w*/*v*). The homogenates were centrifuged at 13,000 × *g* for 10 min. The soluble sugar content was determined according to Wood (Wood, 2002). The soluble sugar content was determined by the Coomassie brilliant blue G250 method (Pierce and Suelter, 1977). The catalase (CAT) activity was measured by the hydrogen peroxide reduction method and the peroxidase (POD) activity was measured by the guaiacol method (Chance and Maehly, 1955); the superoxide dismutase (SOD) activity was measured by nitrous blue Tetrazole photoreduction method (Giannopolitis and Ries, 1977); malondialdehyde (MDA) was determined using a detection kit for MDA (Nanjing Jiancheng Bioengineering institute, Nanjing, China) according to the manufacturer's instructions.

RNA extraction and sequencing

TRIzol reagent (Invitrogen, CA, United States) was used to extract total RNA of the leaves. The RNA was quantified with a Qubit fluorometer (Invertrogen) and its integrity was verified by an Agilent 2100 Bioanalyzer (Agilent, CA, United States) and polyacrylamide gel electrophoresis. Sequencing libraries were generated using NEBNext®Ultra™ RNA Library Prep Kit for Illumina® (NEB, United States) following the manufacturer's instructions. The libraries were quality-controlled, pooled, and subjected to sequencing on an Illumina Hiseq Xten platform (Illumina, United States). Sequences containing adaptors, and those with more than 10% unknown nucleotides and 50% low-quality sequences (*Q* value ≤ 20) were removed from the data sets to obtain clean reads. These clean reads were then mapped to the wheat reference genome of "Chinese spring"[1] by HISAT2. Mapped reads and transcript length were normalized and gene expression were estimated by fragments per kilobase of transcript per million fragments mapped (FPKM). Differential expressed genes (DEGs) of two groups were identified with the DESeq2 R package (Love et al., 2014; Varet et al., 2016) using the standard of false discovery rate (FDR) < 0.01 and fold change (FC) > 2 or < 0.5. DEGs were then annotated based on the KO (KEGG Orthologue database),[2] and Gene Ontology (GO).[3] We used KOBAS (Xie et al., 2011) software to test the statistical enrichment of differential expression genes in KEGG pathways. The R packages pheatmap version 1.0.12 and VennDiagram version 1.7 were used to generate the heatmaps and Venn diagrams.

Identification and analysis of metabolites

The frozen leaves were grounded to powder and 100 mg powder was extracted overnight at 4°C with 0.6 ml 70% aqueous methanol, centrifuged at 10,000 g for 10 min, absorbed in CNWBOND Carbon-GCB SPE Cartridge (250 mg, 3 ml; ANPEL, Shanghai, China) and filtrated with a 0.22 μm SCAA-104 (ANPEL, Shanghai, China). The obtained extracts were then subjected to metabolites analysis with an ultra-performance liquid chromatography (UPLC)-ESI-MS/MS system (UPLC, ExionLC

1 ftp://ftp.ensemblgenomes.org/pub/plants/release-31/fasta/triticum_aestivum/dna/

2 https://www.genome.jp/kegg/

3 http://www.geneontology.org/

AD; MS, Applied Biosystems 6,500 Triple Quadrupole). The parameters were set as previously described (Zhu et al., 2017), and a mixture of supernatant from each biological sample was used as a quality control (QC) sample to evaluate the stability of the system. The data was scaled and subjected to principal component analysis (PCA). Metabolites with variable important in projection (VIP) greater than or equal to 1 and absolute Log_2FC (fold change) greater than or equal to 1 were deemed as significantly regulated and annotated against the KEGG database. *K*-means clustering was carried out with R software.

Quantitative real-time PCR analysis

The RNA was transcribed into cDNA using the Reverse Transcription System (Promega, United States), and qRT-PCR was carried out with the SYBR Premix Ex Taq (TAKARA, Japan) on a LightCycler480 instrument (Rotkreuz, Switzerland). The expression was calculated using the $2^{-\Delta\Delta Ct}$ method (Livak and Schmittgen, 2001) and normalized to ACTIN. Primers used are summarized in Supplementary Table S1.

Statistical analysis

The physiological and biochemical parameters, as well as the qRT-PCR data were analyzed using IBM SPSS Statistics version 23.0 (IBM, NY, United States). The data were presented as means ± standard error. Significant differences were identified using one-way ANOVA followed by the Duncan's multiple range test ($p < 0.05$).

Results

Physiological and physiochemical changes during drought and recovery periods

Soluble sugar and protein are among the two important osmotic regulatory substances. A significant increase in soluble sugar only occurred in CK under severe drought stress, while the content of soluble sugar in *Mu* decreased both under drought stresses and rehydration, and the decrease reached significant ($p < 0.01$) under rehydration, as compared to *Mu*1 (Figure 1A). As for the soluble protein, *Mu* exhibited significant increase under drought stresses, and *mu* showed a significant decrease under severe drought (Figure 1B). During drought stresses, the activities of SOD and POD increased in all the wheat lines, except that the POD activity of *mu* remained unchanged (Figures 1C,D). No significant change was observed in the CAT activity of all wheat lines, except that the CAT activity in CK increased significantly under severe drought (Figure 1E). The MDA content increased significantly in both CK and *mu* under drought, but decreased significantly in *Mu* under moderate drought stress and rehydration (Figure 1F).

Metabolic dynamics during drought stresses and recovery in wheat

The metabolic dynamics of the three lines during moderate and severe drought stresses and rehydration were analyzed. The metabolites were detected by UPLC–ESI-MS/MS. A total of 553 metabolites for 30 samples were obtained, including 50 alkaloids, 74 amino acids and derivatives, 100 flavonoids, 21 lignans and coumarins, 77 lipids, 46 nucleotides and derivatives, 40 organic acids, 97 phenolic acids, and so on (Supplementary Table S2). To reveal the clear separation among the 10 groups of the three lines under different treatments, principal component analysis (PCA) was adopted. It was showed that the first principal component (PC1) explained 29.86% of the variation, which distinguished the untreated samples from samples under drought stresses and rehydration (Figure 2A). The second principle component (PC2) explained 18.65% of the variation, which separated *mu* with other samples. The biological replicates clustered together, suggesting a good correlation of replicates.

To identify key metabolites responding to drought stresses and rehydration, differentially expressed metabolites (DEMs) were screened under a standard of fold change ≥ 2 or ≤ 0.5 and VIP ≥ 1. The moderate drought stress rendered 198 and 115 DEMs in CK and *Mu*, respectively. The severe drought stress rendered 166, 151 and 137 DEMs in CK, *Mu* and *mu*, respectively. 150 and 127 DEMs were found in CK and *Mu* during rehydration, respectively, as compared to CK1 and *Mu*1 (Supplementary Table S3). The percentage of each kind of DEM is shown in Figure 2B. Under moderate drought stress, more amino acids and derivatives (22.6%) and phenolic acids (22.6%) were differentially accumulated in *Mu* than in CK (20.2 and 16.2%). During severe drought stress and rehydration, the situation was similar to that under moderate drought stress, that is, more amino acids and derivatives were differentially accumulated in *Mu* than in CK. Among the amino acids, L-proline plays an important role in drought tolerance. It increased in all the three lines during drought stresses, and recovered in CK but did not recover in *Mu* after rehydration (Supplementary Figure S1). Soluble sugars including sucrose, trehalose anhydrous, isomaltulose, and melibiose in *Mu* decreased during drought stresses and did not recover after rehydration, as compared with those in *Mu*1 (Supplementary Table S2).

Next, *K*-means clustering was performed to identify the metabolites that might contribute to the drought tolerance differences of the three lines. The metabolites were clustered into 16 sub classes. Most metabolites in the three lines showed similar responses to drought stresses and rehydration, but their fold changes were different. Among these sub classes, sub classes 6 and 13 were of particular interest, since metabolites in sub class 6

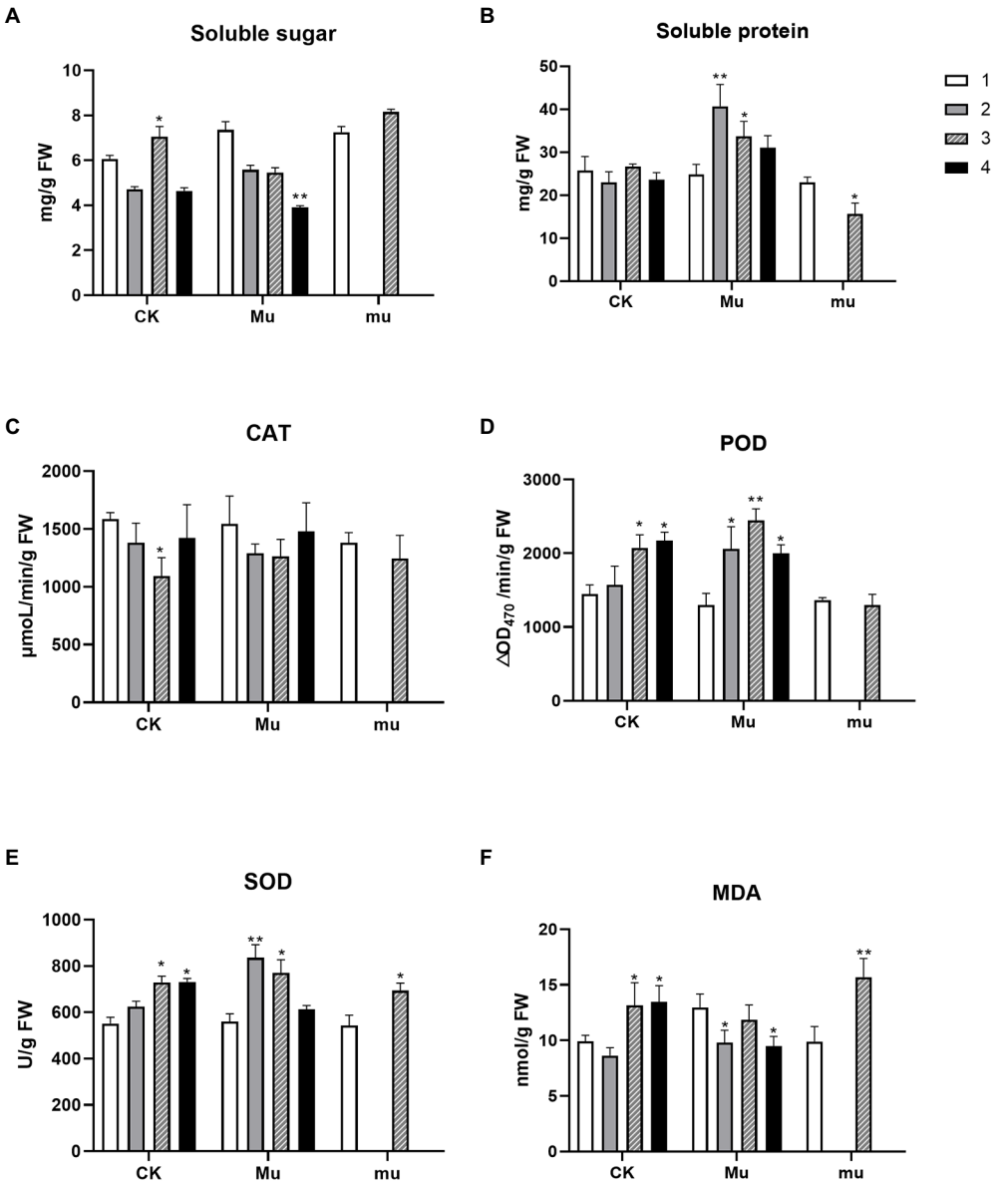

FIGURE 1
Physiological and biochemical changes of the three wheat lines during drought stresses and rehydration. Contents of soluble sugar **(A)**, soluble protein **(B)**, and MDA **(F)** and enzymic activities of CAT **(C)**, POD **(D)**, and SOD **(E)** of wheat under different treatments. The number 1–4 indicate different treatment. 1, pre-treatment; 2, moderate drought stress; 3, severe drought stress; 4, rehydration. Stars on the bar indicate significant difference as compared to the stage before drought. *p<0.05, **p<0.01.

showed a dramatic increase under moderate drought stress and that in sub class 13 remained highly accumulated. Metabolites in the two sub classes included 14 phenolic acids and 9 flavonoids (Supplementary Table S4).

Overall transcriptomic analysis of wheat during drought stresses and rehydration

To investigate how wheat lines with different drought tolerances cope with drought stresses and rehydration at transcriptomic levels, the samples were subjected to next-generation sequencing. A total of 2.73 billion clean reads were obtained for 30 samples, with over 11 Gb for each sample on average and the Q30 value reached as high as 93% (Supplementary Table S5). To validate the accuracy of the sequencing, quantitative real-time PCR (qRT-PCR) was carried out with 12 genes of interest. It was showed that the R^2 was 0.904 (Figure 3A), suggesting the consistency of qRT-PCR and RNA-sequencing. Raw reads were uploaded to NCBI and the SRA accession number was PRJNA801431 and PRJNA800468. PCA was adopted to analyze the clear separation. The results

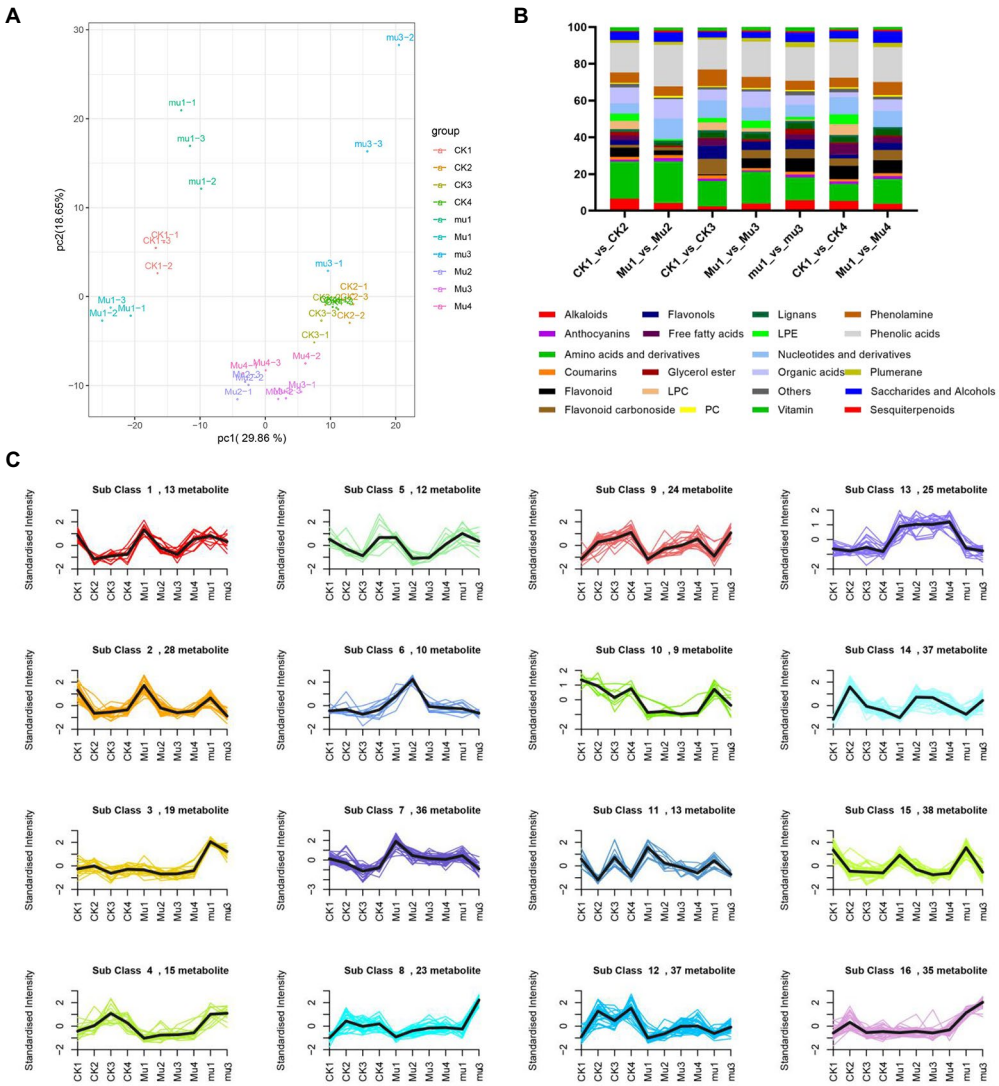

FIGURE 2
Metabolic dynamics during drought stresses and recovery in wheat. **(A)** PCA analysis of all samples. **(B)** Percentage of each kind of differentially expressed metabolites. **(C)** K-means clustering analysis of all the metabolites.

were slightly different with that of metabolome, where samples under severe drought stress were separated with others, with the PC1 explaining 19.89% of the variation (Supplementary Figure S2). DEGs were then identified under the standard of FDR < 0.01 and FC > 2 or < 0.5. The moderate drought stress each rendered 12,557 and 10,402 DEGs in CK and *Mu*, compared with CK1 and *Mu*1, respectively. The severe drought stress each rendered 9,893, 7,924, and 9,387 DEGs in CK, *Mu*, and *mu*, as compared with CK1, *Mu*1 and *mu*1, respectively. There were 13,874 and 14,839 DEGs in CK1_vs_CK4, and *Mu*1_vs_*Mu*4 groups, respectively (Figure 3B). Thousand and three hundred and ninety DEGs were commonly expressed in all the three lines under drought stresses (Figure 3C), and 4,831 DEGs were identified to be common in CK1_vs_CK4, and *Mu*1_vs_*Mu*4 groups (Figure 3D).

Differentially expressed genes involved in osmotic regulation

Osmotic regulation is an important approach adopted by plants during drought stresses and rehydration. To investigate how the osmotic regulation was carried out in different wheat lines at transcriptomic levels, DEGs involved in this process were identified (Figure 4). It was showed that genes encoding major intrinsic protein (MIP, also known as aquaporin), Delta-1-pyrroline-5-carboxylate synthase (P5CS), trehalose-phosphate synthase (TPS), betaine aldehyde dehydrogenase (BADH), and fructan 1-fructosyltransferase (FFT) were differentially expressed in all the three lines during drought stresses and rehydration, and it seemed that *Mu*3 had higher expression of the above genes than CK3 and *mu*3 (Figure 4; Supplementary Table S6). It is noted that

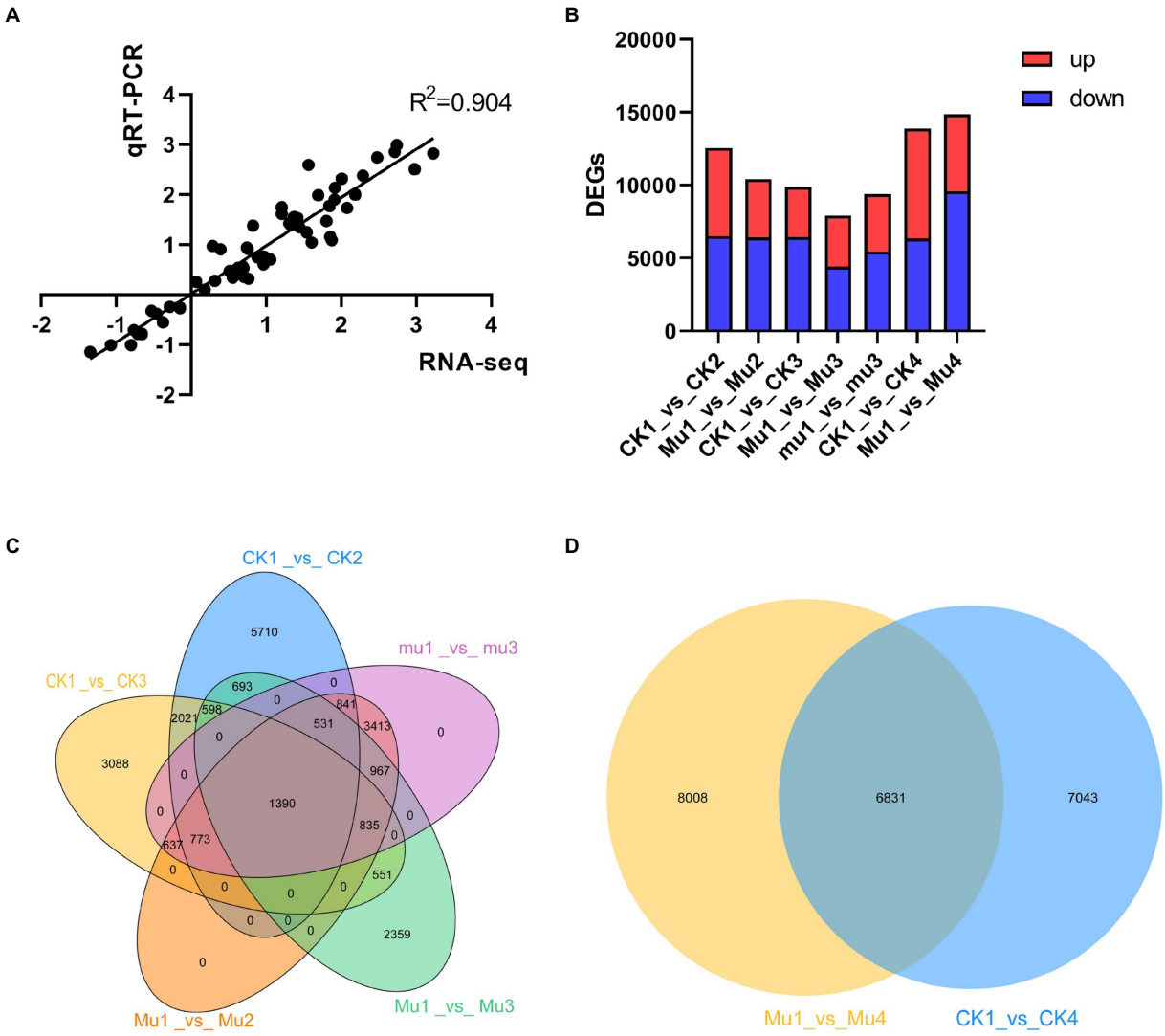

FIGURE 3
Overall transcriptomic analysis of wheat during drought stresses and recovery. **(A)** Correlation analysis of qRT-PCR and RNA seq results. **(B)** Statistics of DEGs during moderate and severe drought stresses and rehydration. **(C)** Venn diagram of DEGs during moderate and severe drought stresses. **(D)** Venn diagram of DEGs after rehydration.

genes encoding MIP in *Mu* had higher expression during rehydration than in other treatments.

Differentially expressed genes involved in enzymic antioxidation

Genes relevant to antioxidase (FPKM > 1), including genes encoding CAT, POD, and SOD were found to be differentially expressed as expected (Figure 5 and Supplementary Table S7). Their overall expression was almost consistent with the activities of the enzymes they encoded. However, genes encoding different isozymes or subunits of the same antioxidase had different expression patterns. For example, although both *TraesCS6A02G041700* and *TraesCS6D02G048300* belonged to catalase, *TraesCS6A02G041700* was highly expressed in CK2, and *TraesCS6D02G048300* was highly expressed in CK3.

Differentially expressed genes involved in flavonoids synthesis

The metabolomics results showed that flavonoids were highly accumulated in *Mu*. To determine genes contributing to the accumulated flavonoids, we analyzed the expression profile of genes (FPKM > 1) involved in the general flavonoids biosynthesis pathway in plants (Figure 6 and Supplementary Table S8). It was showed that *Mu*2 and *Mu*3 had the highest expression in terms of DEGs encoding chalcone synthase (CHS), chalcone isomerase (CHI), flavanone 3-hydroxylase (F3H), flavonol synthase (FLS),

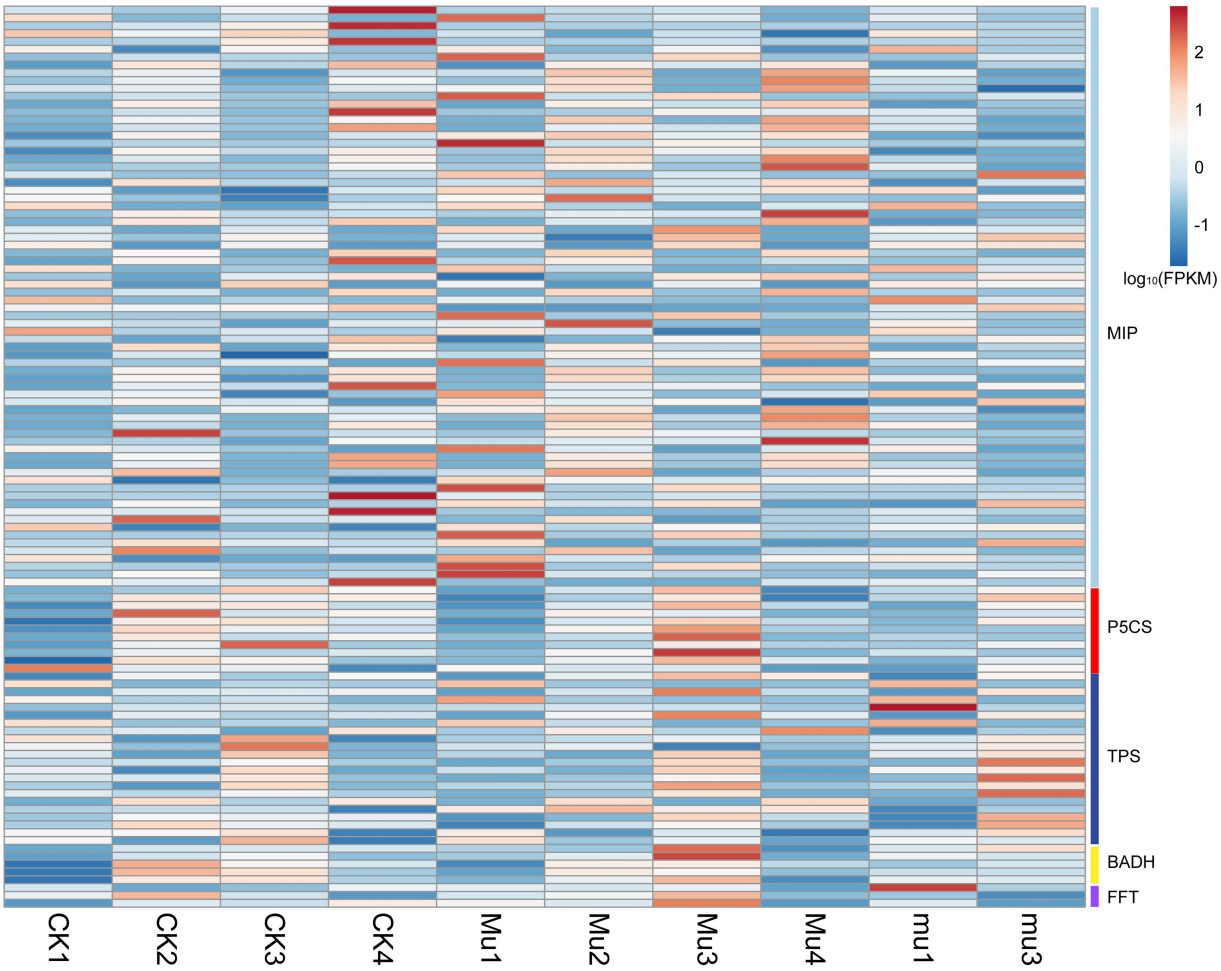

FIGURE 4
Heatmap showing the expression of DEGs related to osmotic regulation. Gene expression is normalized using FPKM and represents the means of three biological replicates. Expression values are presented as FPKM normalized log10-transformed counts. The color represents relative gene expression levels. While the horizontal direction shows the sample names, the vertical direction shows the names of genes involved in osmotic regulation. MIP: major intrinsic protein, P5CS: Delta-1-pyrroline-5-carboxylate synthase, TPS: trehalose-phosphate synthase, BADH: betaine aldehyde dehydrogenase, FFT: fructan 1-fructosyltransferase.

dihydroflavonol-4-reductase (DFR). The trend was especially clear for CHS and CHI. Genes encoding flavone synthase (FNS) was not found to be differentially expressed.

Differentially expressed genes involved in ABA signaling

Abscisic acid (ABA) is a sensitive indicator for drought and rehydration. It was up-regulated under drought in all the three lines, but the pattern was different. It increased with the drought degree in *Mu*, but increased then slightly decreased with the increasing drought degree in CK (Figure 7). Figure 7 shows a typical signaling pathway and representative expression pattern of genes encoding pyrabactin resistance 1-like 4 (PYL4), mitogen protein kinase 3 (MPK3), protein phosphatases 2C (PP2C), sucrose nonfermenting-1 (SNF1) related kinase 2 s (snRK2), and ABA-responsive element-binding factors (ABF). In *Mu*, the gene encoding PYL4 showed opposite trend with that encoding MPK3, which was consistent with the negative relationship of the two genes. The expression trends of the genes in *Mu* under different degrees of drought were quite different from that in CK and *mu*, which highlighted its drought tolerance.

Differentially expressed genes involved in photosynthesis

A lot of DEGs participating PSI, PSII, cytochrome b6/f complex, photosynthetic electron transport, F-type ATPase, and light harvesting chlorophyll II protein complex were identified (Supplementary Figure S3, only *Mu*3_vs_*Mu*1 was showed as representatives, since the situation was similar in other groups). After rehydration, it was found that less photosynthetic genes were

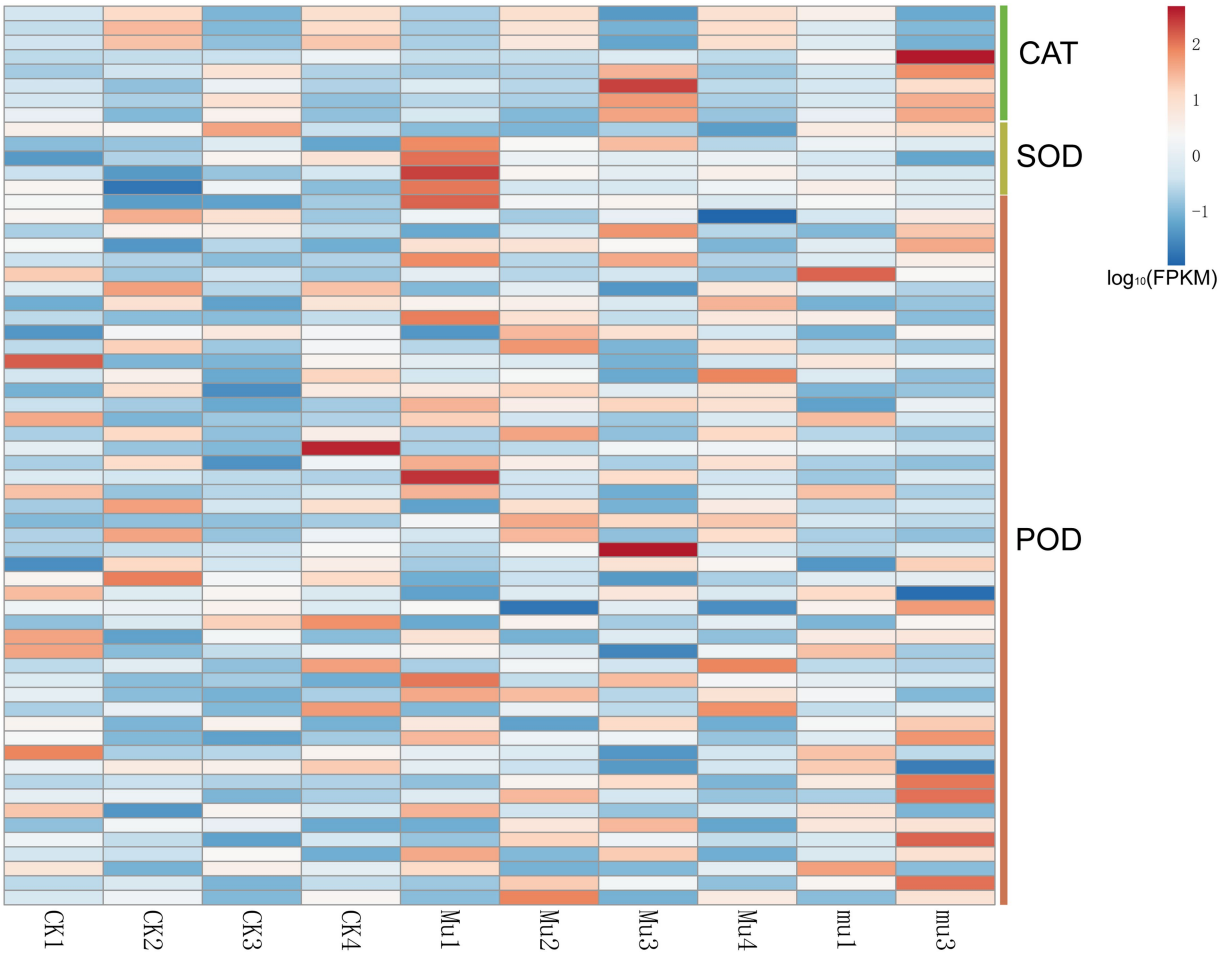

FIGURE 5
Heatmap showing the expression of DEGs related to enzymic antioxidant. Gene expression is normalized using FPKM and represents the means of three biological replicates. Expression values are presented as FPKM normalized log10-transformed counts. The color represents relative gene expression levels. While the horizontal direction shows the sample names, the vertical direction shows the names of genes involved in osmotic regulation. DEGs involved direct to those encoding catalase, superoxide dismutase, peroxidase, and glutathione peroxidase.

significantly down-regulated in *Mu* than in CK (Figure 8). The expression of genes encoding photosynthesis-antenna protein was almost totally recovered from drought after rehydration.

Kyoto encyclopedia of genes and genomes and GO enrichment of DEGs during drought stresses and rehydration

Kyoto encyclopedia of genes (KEGG) and genomes and GO enrichment of the DEGs was performed to gain more insights into the expression profile of the three lines during drought stresses and rehydration. The KEGG enrichment showed that biosynthesis of secondary metabolites (ko01110), metabolic pathway (ko01100), glyoxylate and dicarboxylate metabolism (ko00630), and carbon metabolism (ko01200) were among the common and most enriched pathways among all the three lines during drought stresses. The most enriched pathways in CK during rehydration were biosynthesis of secondary metabolites (ko01110), metabolic pathway (ko01100), glyoxylate and dicarboxylate metabolism (ko00630), starch and sucrose metabolism (ko00500), etc. The most enriched pathways in *Mu* during rehydration were ribosome (ko03010), biosynthesis of secondary metabolites (ko01110), carotenoid biosynthesis (ko00906), etc. (Figure 9A).

The GO enrichment results showed that GO terms involved in photosynthesis, including photosystem II oxygen evolving complex (GO: 0009654), photosystem I (GO: 0009522), photosystem (GO: 0009521), thylakoid lumen (GO: 0031977) and photosystem II (GO: 0009523), were among the most enriched in the three lines during drought stresses, with the enrich factors varied among different mutants. GO enrichment patterns were quite different between CK and *Mu* during rehydration. Amyloplast (GO: 0009501), cytoplasmic stress granule (GO: 0010494), and extracellular matrix (GO: 0031012) were among the most enriched GO terms in CK, while ribosomal related terms, such as cytosolic ribosome (GO: 0022626), cytosolic large

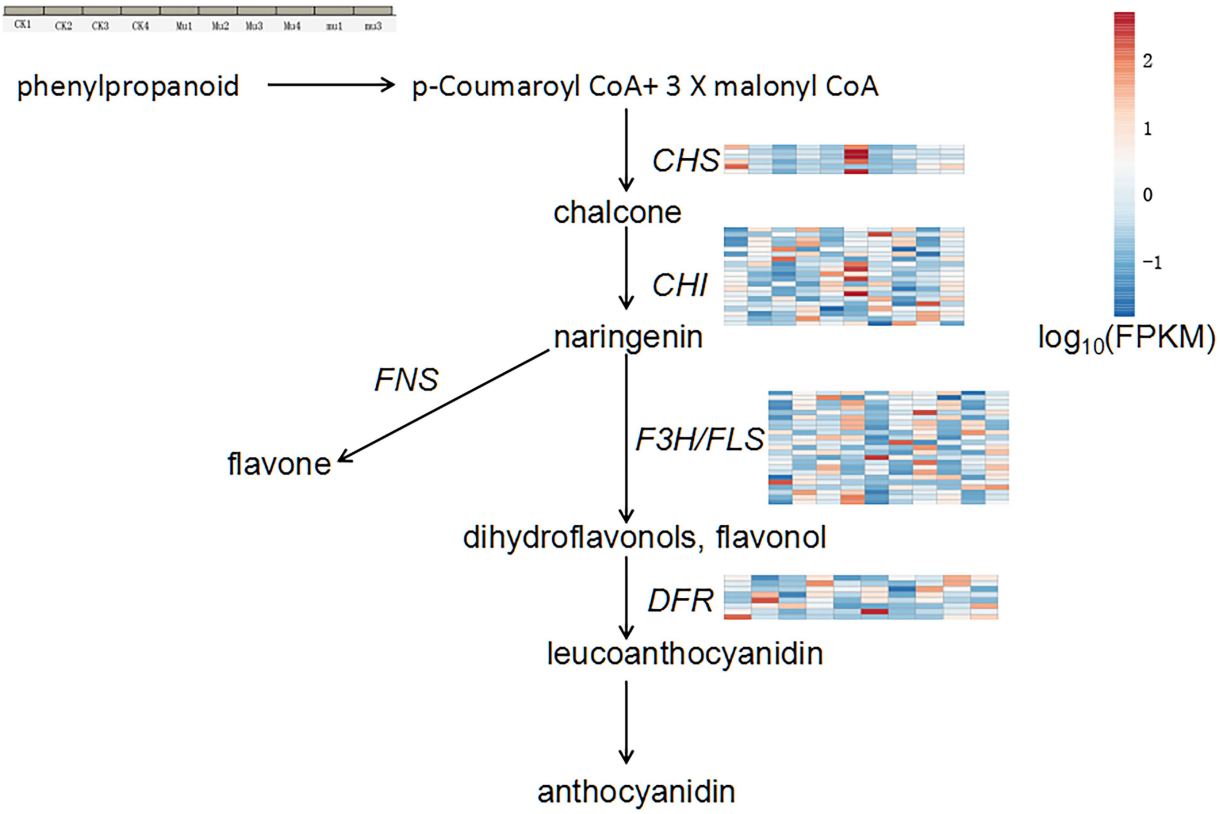

FIGURE 6
General anthocyanidin synthesis pathway and expression profile of DEGs involved in the pathway. Gene expression is normalized using FPKM and represents the means of three biological replicates. Expression values are presented as FPKM normalized log10-transformed counts. The color represents relative gene expression levels. While the horizontal direction shows the sample names, the vertical direction shows the names of genes involved in osmotic regulation. CHS, chalcone synthase; CHI, chalcone isomerase, F3H, flavanone 3-hydroxylase; FNS, flavone synthase; FLS, flavonol synthase; DFR, dihydroflavonol-4-reductase.

ribosomal unit (GO: 0022625) and large ribsomal unit (GO: 0015934) were among the most enriched GO terms in *Mu* (Figure 9B).

Correlation analysis of metabolome and transcriptome

To screen key pathways and genes involved in the response to drought and rehydration, we performed correlation analysis of metabolome and transcriptome. The co-regulated pathways are summarized in Table 1. No significant co-regulated pathway was found in CK1_vs_CK3, CK4_vs_*Mu*4, and *Mu*1_vs_*Mu*4. It was showed that Biosynthesis of secondary metabolites (ko01110), Biosynthesis of amino acids (ko01230), Cyanoamino acid metabolism (ko00460), Phenylalanine, tyrosine and tryptophan biosynthesis (ko00400), and Tropane, piperidine and pyridine alkaloid biosynthesis (ko00960) etc., were the significantly co-regulated pathways ($p < 0.01$). A network related to these pathways was constructed. The network revealed that various amino acids and their derivatives including shikimic acid (mws0154), L-phenylalanine (pme0021) and N-Acetyl-L-glutamic acid (pme0075) were positively correlated with genes encoding fructose-biphosphate aldolase (*TraesCS7B02G283000*), P5CS (*TraesCS3A02G363700*), and citrate synthase (*TraesCS5B02G416700*) (Figure 10).

Discussion

Although various strategies for wheat to cope with drought stress and rehydration have been characterized (Osmolovskaya et al., 2018), these strategies vary and are even contradict sometimes. It is believed that these variations may be due to the differences in cultivars, depth of investigation and strength of drought stresses, etc. Taking into consideration of the fact that wheat is enduring ever-frequent intermittent drought, we for the first time took advantage of a commonly planted wheat cultivar and its drought-tolerant mutant and drought susceptible mutant to study their physiological, biochemical, metabolomic and transcriptomic responses to different intensities of drought and rehydration after severe drought stress. The present study provides a comprehensive understanding of plant under complicated drought conditions

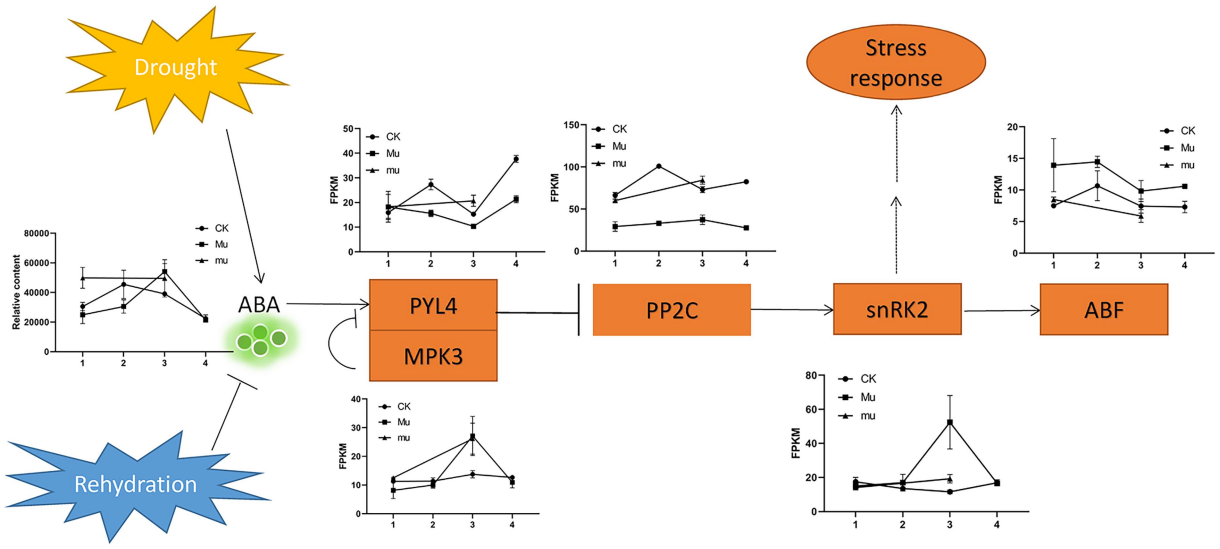

FIGURE 7
Expression pattern of DEGs involved in ABA signaling. PYL4, pyrabactin resistance 1-like 4; MPK3, mitogen protein kinase 3; PP2C, protein phosphatases 2C; snRK2, sucrose nonfermenting-1 (SNF1) related kinase 2; ABF, ABA-responsive element-binding factors. Rectangles indicate genes, Oval indicates biological process, arrows indicate promotion, bars (T) indicate inhibition, and dashed lines indicate postulated regulation.

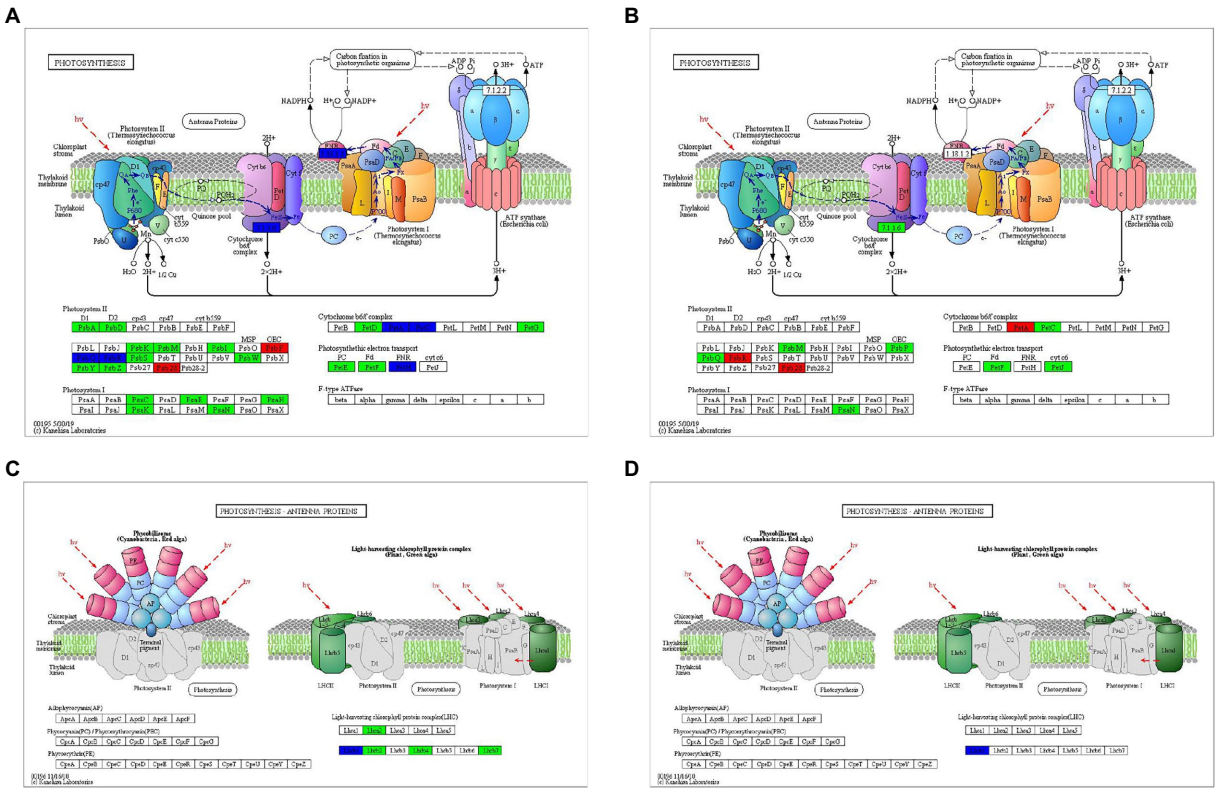

FIGURE 8
DEGs involved in photosynthesis during rehydration. DEGs involved in the "photosynthesis" pathway after rehydration in CK **(A)** and *Mu* **(B)**. DEGs involved in the "photosynthesis-antenna proteins" pathway after rehydration in CK **(C)** and *Mu* **(D)**.

and is expected to facilitate the genetic breeding of wheat with excellent drought tolerance.

Generally, plants having poor drought tolerance are more prone to be disturbed by drought due to absence of homeostasis

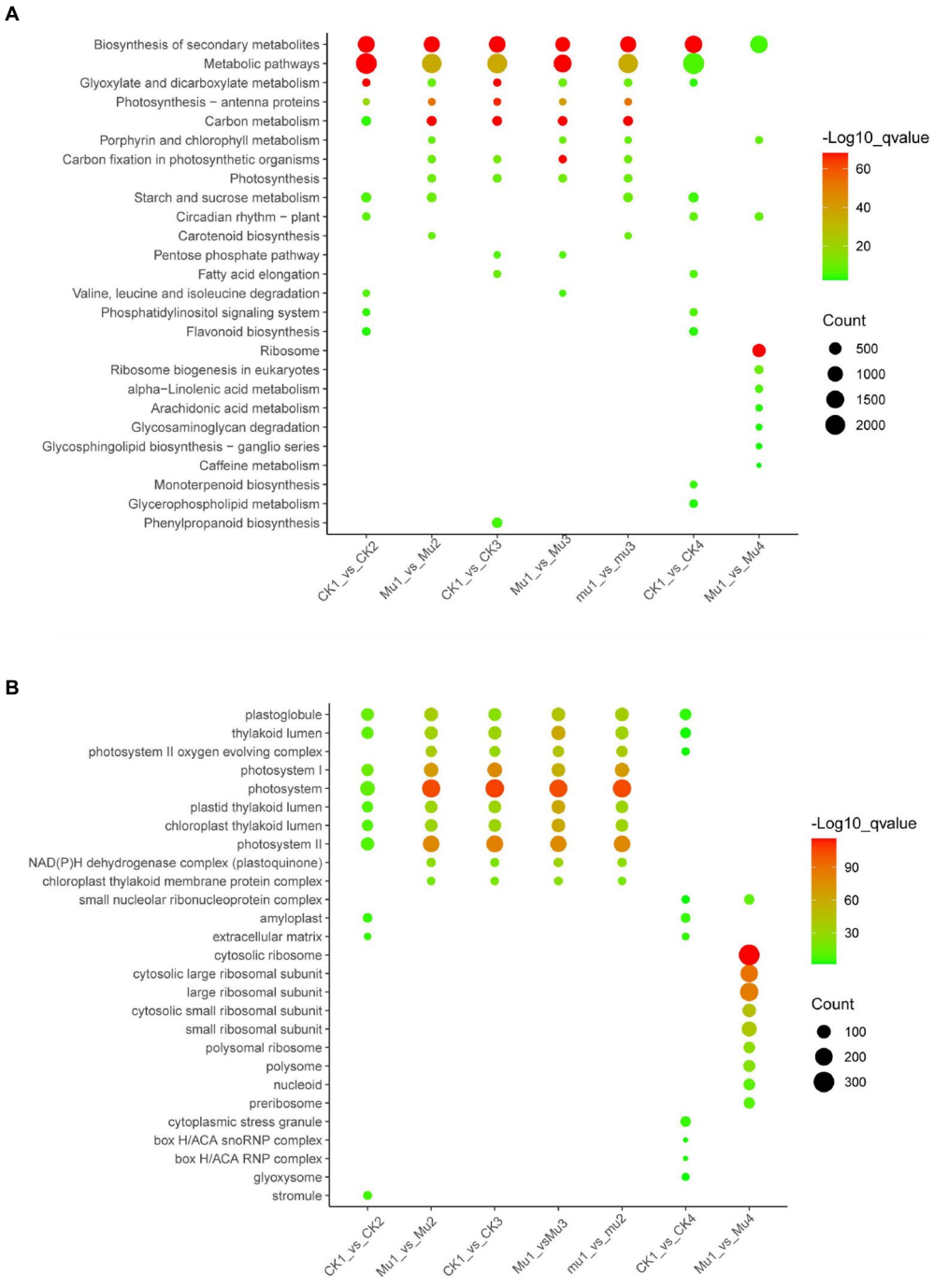

FIGURE 9
KEGG and GO enrichment of DEGs during drought stresses and rehydration. The most enriched top10 pathways and GO terms are displayed. **(A)** KEGG enrichment of DEGs during drought stresses and rehydration. **(B)** GO enrichment of DEGs during drought stresses and rehydration.

mechanisms to mitigate the impact of water deficit (You et al., 2019). The overall results of transcriptome and metabolome in the present study showed that there were less genes and metabolites to be changing in *Mu* than in CK and *mu*, suggesting the disturbance existed at both transcriptional and metabolic levels. The hyper-responsive to abiotic stress at the molecular level in susceptible genotype was also reported in other plant species (Ma et al., 2016; Muthusamy et al., 2016; Svoboda et al., 2016).

Osmotic adjustment is a critical process for maintaining water status and physiological activity of plant cells (Krasensky and Jonak, 2012; Gurrieri et al., 2020). Osmotically active substances including soluble sugars, amino acids (especially proline), soluble protein, betaine, and organic acid have been well documented to

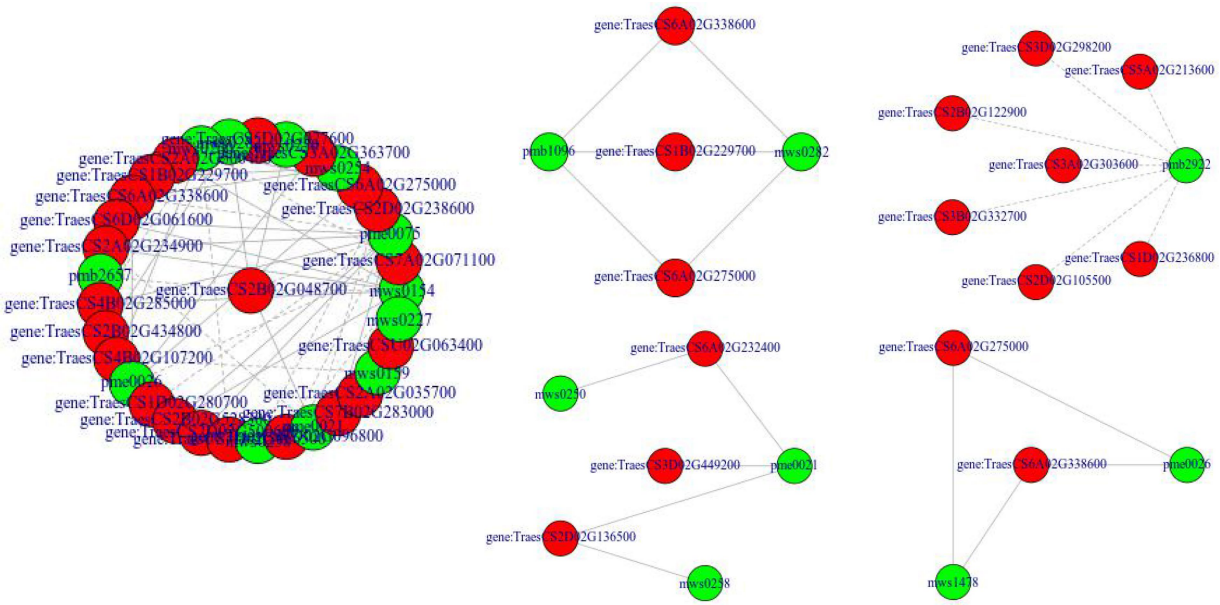

FIGURE 10
Network constructed based on the co-regulated pathways of metabolome and transcriptome. Red indicates genes, green indicates metabolites, solid line indicates positive relationship, and dash line indicates negative relationship.

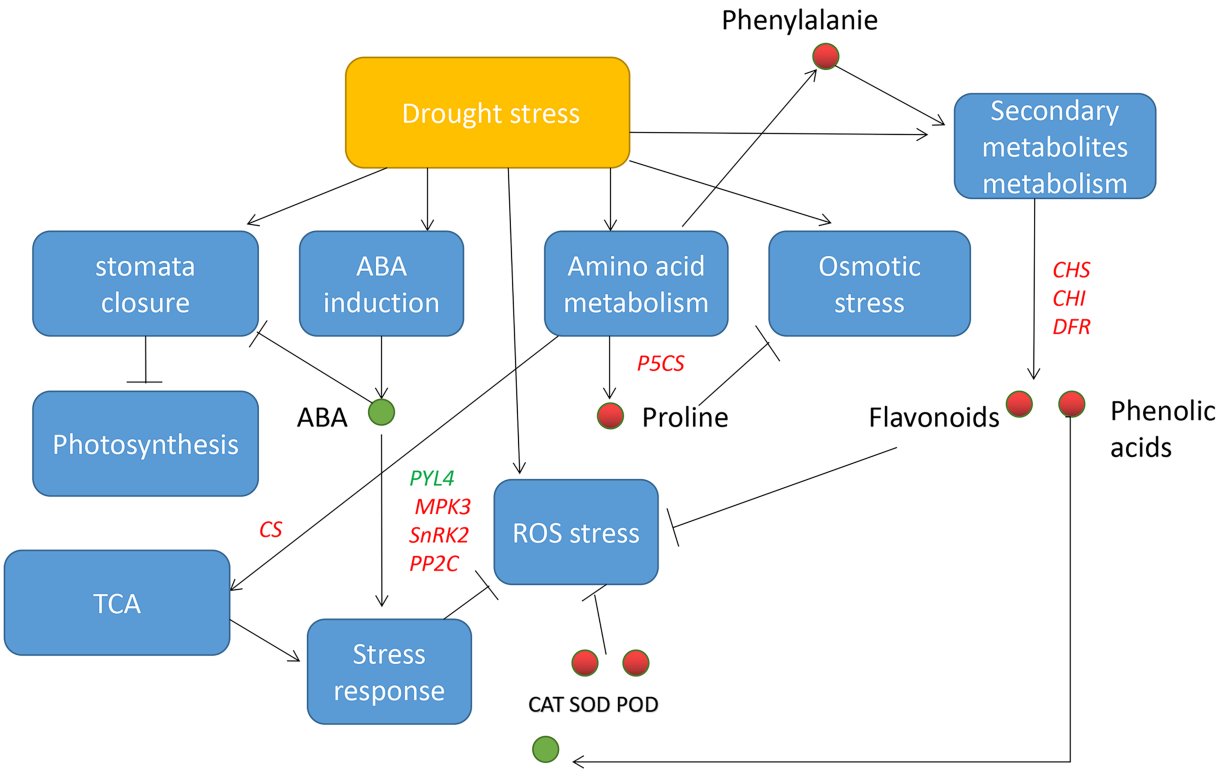

FIGURE 11
Drought tolerance model based on the present study. Blue rectangle indicates biological process, red/green circle indicates increased/decreased substances, red/green words indicates up-/down-regulated genes, line (T) indicates inhibition, and arrows indicates induction.

be changing under drought stress (Paudel et al., 2016; Tschaplinski et al., 2019). These substances bring about stabilization of membranes, proteins, and other subcellular structures under osmotic stress. In the present study, the contents of proline in all

TABLE 1 Co-regulated pathways according to the metabolome and transcriptome analysis.

Group	KEGG_pathway	ko_id	*p*-Value_gene	*p*-Value_meta	Gene count	Meta count
Ck1_vs_CK2	Biosynthesis of secondary metabolites	ko01110	0	0.049517903	1,309	53
	Glycerophospholipid metabolism	ko00564	9.96304E-05	0.007050157	105	10
	Cyanoamino acid metabolism	ko00460	0.000405749	0.029054387	90	6
	Phenylalanine, tyrosine and tryptophan biosynthesis	ko00400	0.001741824	0.002373248	37	9
	Tropane, piperidine and pyridine alkaloid biosynthesis	ko00960	0.004636233	0.012961524	28	7
	Ether lipid metabolism	ko00565	0.016238155	0.016858706	32	4
Mu1_vs_Mu2	Tryptophan metabolism	ko00380	0.012577873	0.005746905	79	8
	Starch and sucrose metabolism	ko00500	1.81577E-12	0.039731574	201	4
Mu1_vs_Mu3	Cyanoamino acid metabolism	ko00460	0.045165556	0.043430103	54	5
	Tropane, piperidine and pyridine alkaloid biosynthesis	ko00960	0.018237689	0.017365249	19	6
	Biosynthesis of secondary metabolites	ko01110	0	0.011639658	875	45
	Biosynthesis of amino acids	ko01230	0.012701418	0.008826043	113	18
mu1_vs_mu3	Tryptophan metabolism	ko00380	0.012577873	0.018888298	79	6

the three lines increased under both moderate and severe drought stresses (Supplementary Figure S1), which is consistent with Abid et al. (2018) and Cao et al. (2021). In accordance with the metabolomic results, the gene encoding P5CS, a key enzyme for proline, was up-regulated in all the three lines during drought stresses. Interestingly, *mu* accumulated more proline during severe drought stresses than the others, and the proline contents in *mu* and CK decreased after rehydration but sustained high in *Mu*, which is not in agreement with previous reports where drought-tolerant cultivars had higher proline content (Abid et al., 2018). This indicates that although proline is an indicator for drought stress but is not a biomarker for drought tolerance, which is in contrast to the conclusion of Dien et al. (2019). We suggest that the linear regulation of proline may be a more reliable indicator when evaluating drought tolerance. Similarly, soluble sugar and protein respond to drought rapidly, but their dynamic changes vary among cultivars according to previous studies (Dien et al., 2019; Du et al., 2020; Islam et al., 2020). In the present study, total soluble sugar and oligoses were significantly decreased under drought stresses and did not recover after rehydration (Figure 1; Supplementary Figure S2). This may be due to the consumption of energy for coping with stresses and the weakened photosynthesis.

Water deficiency damages the balance between reactive oxygen species (ROS) generation and scavenging, eliciting oxidative stress, and up-regulation of ROS production (Cruz De Carvalho, 2008). Plants have developed a series of precise regulatory strategies to cope with the toxic effect of ROS during their long-period evolution, mainly involving enzymic and non-enzymic detoxification systems (Asensi-Fabado and Munné-Bosch, 2010). In the present study, SOD and POD activity in both CK and *Mu* were significantly increased under drought stresses and recovered to pre-treatment levels, which is in accordance with a previous study (Abid et al., 2018). However, unlike previous reported researches (Farooq et al., 2021), it seemed that CAT failed to play a role in coping with ROS, since only the CAT activity in CK3 significantly decreased (Figure 1). It was reported that exogenous application of some phenolic acid would result in decrease in CAT activity, while other phenolic acids increased antioxidase activities including CAT and SOD (Bhardwaj et al., 2017). Since some phenolic acids were significantly accumulated in *Mu* during drought stress (Figure 1C), we speculate that the decreased CAT activity was specifically inhibited by the highly accumulated phenolic acids. Among the non-enzymic substances, flavonoids have been recognized to have excellent ROS scavenging competent and respond to biotic and abiotic stress situations in *Scutellaria baicalensis Georgi* (Yuan et al., 2012), rice (Ithal and Reddy, 2004) and maize (Christie et al., 1994). It was found in the present study that flavonoids and phenolic acids were highly accumulated and responded quickly to drought stress (Figure 2C), so were the flavonoids synthetic genes, such as *CHS*, *CHI*, *DFR* and *FLS* (Figure 6). The results are in agreement with those of Ma et al. (2014) and Liu et al. (2013). Although there were more kinds of flavonoids and derivatives thereof differentially accumulated in *mu* (Figure 2B), they seemed to make little contribution to ROS scavenging. Anthocyanins such as petunidin-3-O-glucoside, cyanidin-3-O-(6″-p-Coumaroylglucoside), and petunidin-3-(6″-p-Coumaroylglucoside), and flavonoids such as apigenin-3-O-rhamnoside, and Chrysoeriol-O-malonylhexoside contributed more to the non-enzymic antioxidation.

Abscisic acid functions as a major hormone for regulating plant stress response and adaptation for drought. The ABA signaling is conserved across plants (Chen et al., 2021). However,

as demonstrated by the present and other studies (An et al., 2019), the accumulation patterns of ABA and genes involved in this signaling vary according to the varieties and strength of drought stress. It is proposed that mitogen-activated protein kinase *TaMPK3* suppresses ABA response by destabilizing *TaPYL4* receptor in wheat (Liu et al., 2022). In the present study, the expression patterns of *MPK3* and *PYL4* showed opposite trend (Figure 7), providing evidences for such conclusion at transcriptional level. ABA and the genes *MPK3*, *snRK2*, *PYL4*, and *ABF* in *Mu* slightly responded to moderate drought stress and strongly to severe drought stress, while those in CK responded differently. We believe that proper responses of ABA and genes involved in ABA signaling may bring about drought tolerance, which is owed to increased antioxidant competence and decreased ROS accumulation, as demonstrated by the antioxidase activities and MDA content. That is, genes participating ABA signaling in drought-tolerant cultivars are more prone to show linear regulation thanks to the homeostasis mechanisms, which may separate plants with different drought tolerance (Rossdeutsch et al., 2016).

Stomata closure under drought leads to disruption of the supply of parenchyma cells with carbon dioxide, and consequently impacts the efficiency of photosynthesis by inhibiting carbon assimilation and light reactions (Razi and Muneer, 2021). Besides degradation of photosynthetic pigments, drought negatively affects the whole photosynthetic apparatus (López-Jurado et al., 2016). Concurrent with this, in the present study, a variety of genes participating PSI, PSII, cytochrome b6/f complex, photosynthetic electron transport, F-type ATPase, and light harvesting chlorophyll II protein complex were found to be down-regulated (Supplementary Figure S4). In addition, GO enrichment showed that almost all the top 10 most enriched terms were photosynthesis related (Figure 9B), suggesting that photosynthesis was greatly affected by drought. It is deemed that rehydration would not render great difference between CK and *Mu*, since the strategies for coping with drought seemed to be similar in the two lines. To our surprise, however, the photosynthesis in *Mu*4 recovered more thoroughly than that in CK4, since less DEGs were identified in *Mu* (Figure 8). Besides photosynthesis, ribosomal related biological processes were significantly enriched in *Mu* during rehydration as compared to *Mu*1. Only biosynthesis of secondary metabolites pathway was enriched in CK during recovery. We suggest that the difference may be attributed to the fact that severe drought caused irreversible damage to CK, but not to *Mu*, such that *Mu* could take advantage of the previously decomposed amino acids to recover growth after rehydration. However, this needs to be further validated through detecting growth indicators.

Correlation analysis between the metabolome and transcriptome is an effective method for identifying genes involved in drought response (Li et al., 2019). The correlation results between the metabolome and transcriptome revealed that the biosynthesis of amino acids and its downstream pathways, and biosynthesis of secondary metabolites were the co-regulated pathways during drought stresses and rehydration (Table 1). Further, the network constructed based on the pathways showed that shikimic acid, L-phenylalanine and N-Acetyl-L-glutamic acid were positively correlated with genes encoding FBA, P5CS, and CS. These genes were reported to regulate the tricarboxylic acid cycle or respond to drought stresses (Xie et al., 2019). Therefore, the up- or down-regulation of amino acids directly or indirectly provided substrates or energy for biosynthesis of drought response substances to alleviate the energy deficiency caused by decreased photosynthesis and ROS damage.

Collectively, *Mu* showed greater drought tolerance and recovery capability. We propose that increased amino acids biosynthetic capability and ROS scavenging ability resulted from higher antioxidase activities and increased flavonoids and phenolic acid may be the mechanisms underlying the drought tolerance characteristic of *Mu*. The above mechanisms further change the regulatory profile of drought response genes and metabolites (Figure 11). In addition, recovery from reversible ROS damage and rapid amino acid biosynthesis may contribute to the rapid recovery of *Mu*.

Data availability statement

The data presented in the study are deposited in the SRA repository, with the accession number PRJNA801431 and PRJNA800168.

Author contributions

AZ: conceived the project and set the scientific objectives. LL, XC, HL, and JH: contributed to the preparation of equipment and acquisition of data. LL: wrote the manuscript. YL and AZ: reviewed and edited the manuscript. All authors contributed to the article and approved the submitted version.

Funding

This research was supported by the Natural Science Foundation of Hebei Province (C2020301004), HAAFS Science and Technology Innovation Special Project (2022KJCXZX-LYS-2), Earmarked Fund for Hebei Wheat Innovation Team of Modern Agro-industry Technology Research System (21326318D), and Key R&D project of Hebei Province (20326313D).

Acknowledgments

We thank the staff of Wuhan Metware Biotechnology Co., Ltd. (Wuhan, China) for their support during the metabolite data analysis.

Conflict of interest

The authors declare that the research was conducted in the absence of any commercial or financial relationships that could be construed as a potential conflict of interest.

Publisher's note

All claims expressed in this article are solely those of the authors and do not necessarily represent those of their affiliated organizations, or those of the publisher, the editors and the reviewers. Any product that may be evaluated in this article, or claim that may be made by its manufacturer, is not guaranteed or endorsed by the publisher.

Supplementary material

The Supplementary material for this article can be found online at: https://www.frontiersin.org/articles/10.3389/fpls.2022.1008624/full#supplementary-material

References

Abebe, T., Guenzi, A. C., Martin, B., and Cushman, J. C. (2003). Tolerance of mannitol-accumulating transgenic wheat to water stress and salinity. *Plant Physiol.* 131, 1748–1755. doi: 10.1104/pp.102.003616

Abid, M., Ali, S., Qi, L. K., Zahoor, R., Tian, Z., Jiang, D., et al. (2018). Physiological and biochemical changes during drought and recovery periods at tillering and jointing stages in wheat (*Triticum aestivum* L.). *Sci. Rep.* 8:4615. doi: 10.1038/s41598-018-21441-7

An, J., Li, Q., Yang, J., Zhang, G., Zhao, Z., Wu, Y., et al. (2019). Wheat F-box protein TaFBA1 positively regulates plant drought tolerance but negatively regulates stomatal closure. *Front. Plant Sci.* 10:1242. doi: 10.3389/fpls.2019.01242

Asensi-Fabado, M. A., and Munné-Bosch, S. (2010). Vitamins in plants: occurrence, biosynthesis and antioxidant function. *Trends Plant Sci.* 15, 582–592. doi: 10.1016/j.tplants.2010.07.003

Basu, S., Ramegowda, V., Kumar, A., and Pereira, A. (2016). Plant adaptation to drought stress. *F1000Res* 5:F1000 Faculty Rev-1554. doi: 10.12688/f1000research.7678.1

Bhardwaj, R. D., Kaur, L., and Srivastava, P. (2017). Comparative evaluation of different phenolic acids as priming agents for mitigating drought stress in wheat seedlings. *Proc. Natl. Acad. Sci. India Sect. B-Biol. Sci.* 87, 1133–1142. doi: 10.1007/s40011-015-0690-y

Budak, H., Hussain, B., Khan, Z., Ozturk, N. Z., and Ullah, N. (2015). From genetics to functional genomics: improvement in drought signaling and tolerance in wheat. *Front. Plant Sci.* 6, 1–13. doi: 10.3389/fpls.2015.01012

Cao, L., Lu, X., Wang, G., Zhang, P., Fu, J., Wang, Z., et al. (2021). Transcriptional regulatory networks in response to drought stress and rewatering in maize (*Zea mays* L.). *Mol. Gen. Genomics.* 296, 1203–1219. doi: 10.1007/s00438-021-01820-y

Chance, B., and Maehly, A. C. (1955). Assay of catalases and peroxidases. *Methods Enzymol.* 2, 764–7775. doi: 10.1016/S0076-6879(55)02300-8

Chen, X., Ding, Y., Yang, Y., Song, C., Wang, B., Yang, S., et al. (2021). Protein kinases in plant responses to drought, salt, and cold stress. *J. Integr. Plant Biol.* 63, 53–78. doi: 10.1111/jipb.13061

Christie, P. J., Alfenito, M. R., and Walbot, V. (1994). Impact of low-temperature stress on general phenylpropanoid and anthocyanin pathways: enhancement of transcript abundance and anthocyanin pigmentation in maize seedlings. *Planta* 194, 541–549. doi: 10.1007/BF00714468

Cruz De Carvalho, M. H. (2008). Drought stress and reactive oxygen species: production, scavenging and signaling. *Plant Signal. Behav.* 3, 156–165. doi: 10.4161/psb.3.3.5536

Dien, D. C., Mochizuki, T., and Yamakawa, T. (2019). Effect of various drought stresses and subsequent recovery on proline, total soluble sugar and starch metabolisms in Rice (*Oryza sativa* L.) varieties. *Plant Prod. Sci.* 22, 530–545. doi: 10.1080/1343943X.2019.1647787

Du, H., Huang, F., Wu, N., Li, X., Hu, H., and Xiong, L. (2018). Integrative regulation of drought escape through ABA-dependent and-independent pathways in rice. *Mol. Plant* 11, 584–597. doi: 10.1016/j.molp.2018.01.004

Du, Y., Zhao, Q., Chen, L., Yao, X., Zhang, W., Zhang, B., et al. (2020). Effect of drought stress on sugar metabolism in leaves and roots of soybean seedlings. *Plant Physiol. Biochem.* 146, 1–12. doi: 10.1016/j.plaphy.2019.11.003

Farooq, M., Ahmad, R., Shahzad, M., Sajjad, Y., Hassan, A., Shah, M. M., et al. (2021). Differential variations in total flavonoid content and antioxidant enzymes activities in pea under different salt and drought stresses. *Sci. Hortic.* (Amsterdam) 287:110258. doi: 10.1016/j.scienta.2021.110258

Francki, M., and Appels, R. (2002). Wheat functional genomics and engineering crop improvement. *Genome Biol.* 3, 1013–1101. doi: 10.1186/gb-2002-3-5-reviews1013

Gao, H., Wang, Y., Xu, P., and Zhang, Z. (2018). Overexpression of a WRKY transcription factor TaWRKY2 enhances drought stress tolerance in transgenic wheat. *Front. Plant Sci.* 9:997. doi: 10.3389/fpls.2018.00997

Giannopolitis, C. N., and Ries, S. K. (1977). Superoxide dismutases: I Occurrence in higher plants. *Plant Physiol.* 59, 309–314. doi: 10.1104/pp.59.2.309

Gurrieri, L., Merico, M., Trost, P., Forlani, G., and Sparla, F. (2020). Impact of drought on soluble sugars and free proline content in selected *Arabidopsis* mutants. *Biology (Basel)* 9:367. doi: 10.3390/biology9110367

Islam, M. J., Kim, J. W., Begum, M. K., Sohel, M. A. T., and Lim, Y. S. (2020). Physiological and biochemical changes in sugar beet seedlings to confer stress adaptability under drought condition. *Plan. Theory* 9:1511. doi: 10.3390/plants9111511

Ithal, N., and Reddy, A. R. (2004). Rice flavonoid pathway genes, OsDfr and OsAns, are induced by dehydration, high salt and ABA, and contain stress responsive promoter elements that interact with the transcription activator, OsC1-MYB. *Plant Sci.* 166, 1505–1513. doi: 10.1016/j.plantsci.2004.02.002

Krasensky, J., and Jonak, C. (2012). Drought, salt, and temperature stress-induced metabolic rearrangements and regulatory networks. *J. Exp. Bot.* 63, 1593–1608. doi: 10.1093/jxb/err460

Li, Z., Lian, Y., Gong, P., Song, L., Hu, J., Pang, H., et al. (2022). Network of transcriptome and metabolomics reveals a novel regulation of drought resistance during germination in wheat. *Ann. Bot.* mcac102. doi: 10.1093/aob/mcac102

Li, H., Lv, Q., Ma, C., Qu, J., Cai, F., Deng, J., et al. (2019). Metabolite profiling and transcriptome analyses provide insights into the flavonoid biosynthesis in the developing seed of tartary buckwheat (*Fagopyrum tataricum*). *J. Agric. Food Chem.* 67, 11262–11276. doi: 10.1021/acs.jafc.9b03135

Li, P., Ma, B., Palta, J. A., Ding, T., Cheng, Z., Lv, G., et al. (2021). Wheat breeding highlights drought tolerance while ignores the advantages of drought avoidance: a meta-analysis. *Eur. J. Agron.* 122:126196. doi: 10.1016/j.eja.2020.126196

Liu, M., Li, X., Liu, Y., and Cao, B. (2013). Regulation of flavanone 3-hydroxylase gene involved in the flavonoid biosynthesis pathway in response to UV-B radiation and drought stress in the desert plant, *Reaumuria soongorica*. *Plant Physiol. Biochem.* 73, 161–167. doi: 10.1016/j.plaphy.2013.09.016

Liu, Y., Yu, T., Li, Y., Zheng, L., Lu, Z., Zhou, Y., et al. (2022). Mitogen-activated protein kinase TaMPK3 suppresses ABA response by destabilizing TaPYL4 receptor in wheat. *New Phytol.* doi: 10.1111/nph.18326

Livak, K. J., and Schmittgen, T. D. (2001). Analysis of relative gene expression data using real-time quantitative PCR and the $2^{-\Delta\Delta CT}$ method. *Methods* 25, 402–408. doi: 10.1006/meth.2001.1262

López-Jurado, J., Balao, F., and Mateos-Naranjo, E. (2016). Deciphering the ecophysiological traits involved during water stress acclimation and recovery of the threatened wild carnation, *Dianthus inoxianus*. *Plant Physiol. Biochem.* 109, 397–405. doi: 10.1016/j.plaphy.2016.10.023

Love, M. I., Huber, W., and Anders, S. (2014). Moderated estimation of fold change and dispersion for RNA-seq data with DESeq2. *Genome Biol.* 15, 550–521. doi: 10.1186/s13059-014-0550-8

Lv, L., Chen, X., Zhang, W., Zhao, A., Sun, L., Zhang, Y., et al. (2020). Selection and identification of the EMS-induced drought-resistant wheat mutants from Jimai 4. *Acta Agric. Boreali-sinca* 35, 47–55. doi: 10.7668/hbnxb.20190802

Ma, D., Sun, D., Wang, C., Li, Y., and Guo, T. (2014). Expression of flavonoid biosynthesis genes and accumulation of flavonoid in wheat leaves in response to drought stress. *Plant Physiol. Biochem.* 80, 60–66. doi: 10.1016/j.plaphy.2014.03.024

Ma, X., Xia, H., Liu, Y., Wei, H., Zheng, X., Song, C., et al. (2016). Transcriptomic and metabolomic studies disclose key metabolism pathways contributing to well-maintained photosynthesis under the drought and the consequent drought-tolerance in rice. *Front. Plant Sci.* 7:1886. doi: 10.3389/fpls.2016.01886

Ma, J., Zhang, Y., Wang, H., Zhen, W., Zhang, Y., Duan, H., et al. (2019). Differentially expressed genes and enriched pathways during drought-sensitive period under field conditions in bread wheat. *Plant Mol. Biol. Report.* 37, 389–400. doi: 10.1007/s11105-019-01163-4

Morran, S., Eini, O., Pyvovarenko, T., Parent, B., Singh, R., Ismagul, A., et al. (2011). Improvement of stress tolerance of wheat and barley by modulation of expression of DREB/CBF factors. *Plant Biotechnol. J.* 9, 230–249. doi: 10.1111/j.1467-7652.2010.00547.x

Muthusamy, M., Uma, S., Backiyarani, S., Saraswathi, M. S., and Chandrasekar, A. (2016). Transcriptomic changes of drought-tolerant and sensitive banana cultivars exposed to drought stress. *Front. Plant Sci.* 7:1609. doi: 10.3389/fpls.2016.01609

Osmolovskaya, N., Shumilina, J., Kim, A., Didio, A., Grishina, T., Bilova, T., et al. (2018). Methodology of drought stress research: experimental setup and physiological characterization. *Int. J. Mol. Sci.* 19:4089. doi: 10.3390/ijms 19124089

Paudel, G., Bilova, T., Schmidt, R., Greifenhagen, U., Berger, R., Tarakhovskaya, E., et al. (2016). Osmotic stress is accompanied by protein glycation in *Arabidopsis thaliana*. *J. Exp. Bot.* 67, 6283–6295. doi: 10.1093/jxb/erw395

Pierce, J., and Suelter, C. H. (1977). An evaluation of the Coomassie brilliant blue G-250 dye-binding method for quantitative protein determination. *Anal. Biochem.* 81, 478–480. doi: 10.1016/0003-2697(77)90723-0

Razi, K., and Muneer, S. (2021). Drought stress-induced physiological mechanisms, signaling pathways and molecular response of chloroplasts in common vegetable crops. *Crit. Rev. Biotechnol.* 41, 669–691. doi: 10.1080/07388551. 2021.1874280

Reddy, S. K., Liu, S., Rudd, J. C., Xue, Q., Payton, P., Finlayson, S. A., et al. (2014). Physiology and transcriptomics of water-deficit stress responses in wheat cultivars TAM 111 and TAM 112. *J. Plant Physiol.* 171, 1289–1298. doi: 10.1016/j. jplph.2014.05.005

Rossdeutsch, L., Edwards, E., Cookson, S. J., Barrieu, F., Gambetta, G. A., Delrot, S., et al. (2016). ABA-mediated responses to water deficit separate grapevine genotypes by their genetic background. *BMC Plant Biol.* 16:91. doi: 10.1186/ s12870-016-0778-4

Sivamani, E., Bahieldin, A., Wraith, J. M., Al-Niemi, T., Dyer, W. E., Ho, T. H. D., et al. (2000). Improved biomass productivity and water use efficiency under water deficit conditions in transgenic wheat constitutively expressing the barley *HVA1* gene. *Plant Sci.* 155, 1–9. doi: 10.1016/S0168-9452(99)00247-2

Svoboda, P., Janská, A., Spiwok, V., Prášil, I. T., Kosová, K., Vítámvás, P., et al. (2016). Global scale transcriptional profiling of two contrasting barley genotypes exposed to moderate drought conditions: contribution of leaves and crowns to water shortage coping strategies. *Front. Plant Sci.* 7:1958. doi: 10.3389/ fpls.2016.01958

Tatar, O., Cakalogullari, U., Aykut Tonk, F., Istipliler, D., and Karakoc, R. (2020). Effect of drought stress on yield and quality traits of common wheat during grain filling stage. *Turkish J. F. Crop.* 25, 236–244. doi: 10.17557/tjfc.834392

Tschaplinski, T. J., Abraham, P. E., Jawdy, S. S., Gunter, L. E., Martin, M. Z., Engle, N. L., et al. (2019). The nature of the progression of drought stress drives differential metabolomic responses in *Populus deltoides*. *Ann. Bot.* 124, 617–626. doi: 10.1093/aob/mcz002

Varet, H., Brillet-Guéguen, L., Coppée, J. Y., and Dillies, M. A. (2016). SARTools: a DESeq2-and edgeR-based R pipeline for comprehensive differential analysis of RNA-Seq data. *PLoS One* 11:e0157022. doi: 10.1371/journal.pone.0157022

Vendruscolo, E. C. G., Schuster, I., Pileggi, M., Scapim, C. A., Molinari, H. B. C., Marur, C. J., et al. (2007). Stress-induced synthesis of proline confers tolerance to water deficit in transgenic wheat. *J. Plant Physiol.* 164, 1367–1376. doi: 10.1016/j. jplph.2007.05.001

Wilkins, O., Bräutigam, K., and Campbell, M. M. (2010). Time of day shapes Arabidopsis drought transcriptomes. *Plant J.* 63, 715–727. doi: 10.1111/j. 1365-313X.2010.04274.x

Wood, E. J. (2002). Principles and techniques of practical biochemistry. *Biochem. Mol. Biol. Educ.* 30, 214–215. doi: 10.1002/bmb.2002.494030030062

Xiao, Y., Savchenko, T., Baidoo, E. E. K., Chehab, W. E., Hayden, D. M., Tolstikov, V., et al. (2012). Retrograde signaling by the plastidial metabolite MEcPP regulates expression of nuclear stress-response genes. *Cells* 149, 1525–1535. doi: 10.1016/j.cell.2012.04.038

Xie, C., Mao, X., Huang, J., Ding, Y., Wu, J., Dong, S., et al. (2011). KOBAS 2.0: a web server for annotation and identification of enriched pathways and diseases. *Nucleic Acids Res.* 39, W316–W322. doi: 10.1093/nar/gkr483

Xie, H., Wang, Y., Ding, Y., Qiu, C., Sun, L., Gai, Z., et al. (2019). Global ubiquitome profiling revealed the roles of ubiquitinated proteins in metabolic pathways of tea leaves in responding to drought stress. *Sci. Rep.* 9, 1–12. doi: 10.1038/s41598-019-41041-3

Xu, L., Hu, Y., Jin, G., Lei, P., Sang, L., Luo, Q., et al. (2021). Physiological and proteomic responses to drought in leaves of *Amygdalus mira* (*Koehne*) Yü et Lu. *Front. Plant Sci.* 12:620499. doi: 10.3389/fpls.2021.620499

Xue, G. P., Way, H. M., Richardson, T., Drenth, J., Joyce, P. A., and McIntyre, C. L. (2011). Overexpression of TaNAC69 leads to enhanced transcript levels of stress up-regulated genes and dehydration tolerance in bread wheat. *Mol. Plant* 4, 697–712. doi: 10.1093/mp/ssr013

Yang, P., Zhang, S., Xia, J., Zhan, C., Cai, W., Wang, W., et al. (2022). Analysis of drought and flood alternation and its driving factors in the Yangtze River basin under climate change. *Atmos. Res.* 270:106087. doi: 10.1016/j.atmosres.2022.106087

You, J., Zhang, Y., Liu, A., Li, D., Wang, X., Dossa, K., et al. (2019). Transcriptomic and metabolomic profiling of drought-tolerant and susceptible sesame genotypes in response to drought stress. *BMC Plant Biol.* 19, 267–216. doi: 10.1186/ s12870-019-1880-1

Yuan, Y., Liu, Y., Wu, C., Chen, S., Wang, Z., Yang, Z., et al. (2012). Water deficit affected flavonoid accumulation by regulating hormone metabolism in *Scutellaria baicalensis Georgi* roots. *PLoS One* 7, 1–9. doi: 10.1371/journal.pone.0042946

Zang, X., Geng, X., Wang, F., Liu, Z., Zhang, L., Zhao, Y., et al. (2017). Overexpression of wheat ferritin gene TaFER-5B enhances tolerance to heat stress and other abiotic stresses associated with the ROS scavenging. *BMC Plant Biol.* 17:14. doi: 10.1186/s12870-016-0958-2

Zhan, X., Zhang, Y. H., Chen, D. F., and Simonsen, H. T. (2014). Metabolic engineering of the moss physcomitrella patens to produce the sesquiterpenoids patchoulol and α/β-santalene. *Front. Plant Sci.* 5:636. doi: 10.3389/fpls.2014.00636

Zhang, Q. (2007). Strategies for developing green super Rice. *Proc. Natl. Acad. Sci. U. S. A.* 104, 16402–16409. doi: 10.1073/pnas.0708013104

Zhang, X., Lu, G., Long, W., Zou, X., Li, F., and Nishio, T. (2014). Recent progress in drought and salt tolerance studies in brassica crops. *Breed. Sci.* 64, 60–73. doi: 10.1270/jsbbs.64.60

Zhu, M., Li, N., Zhao, M., Yu, W., and Wu, J. L. (2017). Metabolomic profiling delineate taste qualities of tea leaf pubescence. *Food Res. Int.* 94, 36–44. doi: 10.1016/j.foodres.2017.01.026

frontiers | Frontiers in Plant Science

TYPE Original Research
PUBLISHED 26 October 2022
DOI 10.3389/fpls.2022.1022819

OPEN ACCESS

EDITED BY
Cheng Liu,
Shandong Academy of Agricultural Sciences, China

REVIEWED BY
Yunsheng Wang,
Hunan Agricultural University, China
Yanping Tian,
Shandong Agricultural University, China

*CORRESPONDENCE
Vijai Bhadauria
vijai.bhadauria@cau.edu.cn

SPECIALTY SECTION
This article was submitted to Plant Pathogen Interactions, a section of the journal Frontiers in Plant Science

RECEIVED 19 August 2022
ACCEPTED 30 September 2022
PUBLISHED 26 October 2022

CITATION
Ma W, Yang J, Ding J, Zhao W, Peng Y-L and Bhadauria V (2022) Gapless reference genome assembly of *Didymella glomerata*, a new fungal pathogen of maize causing Didymella leaf blight. *Front. Plant Sci.* 13:1022819. doi: 10.3389/fpls.2022.1022819

Gapless reference genome assembly of *Didymella glomerata*, a new fungal pathogen of maize causing Didymella leaf blight

Wendi Ma[1], Jun Yang[1,2], Junqiang Ding[3], Wensheng Zhao[1,2], You-Liang Peng[1,2] and Vijai Bhadauria[1,2]*

[1]Department of Plant Pathology, College of Plant Protection, China Agricultural University, Beijing, China, [2]Ministry of Agriculture and Rural Affairs, Key Laboratory for Crop Pest Monitoring and Green Control, China Agricultural University, Beijing, China, [3]College of Agronomy, Henan Agricultural University, Zhengzhou, China

Didymella leaf blight (DLB) caused by *Didymella glomerata* is a new fungal disease of maize (*Zea mays*), first detected in 2021 in Panjin, Liaoning province of China. Here we report the reference genome assembly of *D. glomerata* to unravel how the fungal pathogen controls its virulence on maize at the molecular level. A maize-infecting strain Pj-2 of the pathogen was sequenced on the Illumina NovaSeq 6000 and PacBio Sequel II platforms at a 575-fold genomic coverage. The 33.17 Mb gapless genome assembly comprises 32 scaffolds with L/N_{50} of 11/1.36 Mb, four of which represent full-length chromosomes. The Pj-2 genome is predicted to contain 10,334 protein-coding genes, of which 211, 12 and 134 encode effector candidates, secondary metabolite backbone-forming enzymes and CAZymes, respectively. Some of these genes are potentially implicated in niche adaptation and expansion, such as colonizing new hosts like maize. Phylogenomic analysis of eight strains of six *Didymella* spp., including three sequenced strains of *D. glomerata*, reveals that the maize (Pj-2)- and *Chrysanthemum* (CBS 528.66)-infecting strains of *D. glomerata* are genetically similar (sharing 92.37% genome with 98.89% identity), whereas Pj-2 shows truncated collinearity with extensive chromosomal rearrangements with the *Malus*-infecting strain M27-16 of *D. glomerata* (sharing only 55.01% genome with 88.20% identity). Pj-2 and CBS 528.66 carry four major reciprocal translocations in their genomes, which may enable them to colonize the different hosts. Furthermore, germplasm screening against Pj-2 led to the identification of three sources of DLB resistance in maize, including a tropical inbred line CML496. DLB resistance in the line is attributed to the accumulation of ROS H_2O_2 in the apoplastic space of the infected cells, which likely restricts the fungal growth and proliferation.

KEYWORDS

emerging maize diseases, fungal genomes, effectors, CAZymes, secondary, metabolism genes, genetic source of Didymella leaf blight resistance

Introduction

Didymella (syn. *Peyronellaea* or *Phoma*) *glomerata* (Corda) Q. Chen & L. Cai is an ascomycete fungal pathogen, which causes Didymella leaf blight (DLB). The pathogen has a broad host range and is known to infect both monocots and dicots, including although not limited to flax (*Linum usitatissimum*) (Reeder and Vanterpool, 1953), oilseed rape (*Brassica napus*) (Taber and Vanterpool, 1963), bread wheat (*Triticum aestivum*), durum wheat (*Triticum turgidum*) and triticale (*Triticale hexaploide*) (Hosford, 1975), pea (*Pisum sativum*) (Tran et al., 2014), sunflower (*Helianthus annuus*) (Roustaee et al., 2000), grapevine (*Vitis vinifera*) (Khani, 2014), peach (*Prunus persica*) (Thomidis et al., 2011), kiwi (*Actinidia chinensis*) (Pan et al., 2018), pistachio (*Pistacia vera*) (Moral et al., 2018), Chinese cornel dogwood (*Cornus officinalis*) (Huang et al., 2018) and apple (*Malus* spp.).

During a disease survey in the 2021 growing season, we observed gray leaf blight symptoms on maize in Panjin, Liaoning, a northeastern province of China. The symptoms differed from those caused by *D. zeae-maydis*, the only *Didymella* species infectious on maize and the causal agent of yellow leaf blight. Culture characteristics and molecular phylogeny based on multi-locus DNA barcodes (ITS, *Actin* and *β-tubulin*) showed that the single spore culture isolate Pj-2 retrieved from the infected leaf tissues was morphologically and genetically identical with the *D. glomerata* isolate D/034 from soybean (*Glycine max*) (Irinyi et al., 2009). This was the first report of *D. glomerata* causing DLB on maize (Ma et al., 2022).

D. glomerata is likely a heterothallic fungal pathogen as it harbors the mating-type gene *scaffold1.t522* (*MAT1-2*), whose protein product contains the characteristic high mobility group box domain. The pathogen likely deploys a subcuticular intramural necrotrophic infection strategy, whereby the pathogen colonizes maize leaves, resulting in DLB. The infection cycle starts when fungal spores (conidia) land on the leaf surface and germinate to form a germ tube. However, unlike hemibiotrophic fungal pathogens, the germ tube does not differentiate into appressoria (specialized structures dedicated to mechanized penetration of the host surface) but instead directly perforates the host cuticle, presumably *via* an infection peg. The pathogen can also gain access to host tissues through natural openings, such as stomata. Following successful penetration, the invasive hyphae emanating from the infection pegs rapidly colonize the host parietal layers and eventually kill and macerate the host cells. Black lesions appear on the maize leaves five to seven days after infection. Single-celled ellipsoidal conidia are produced in glabrous pycnidia developing in these lesions and are dispersed by splashing raindrops and wind to infect healthy neighboring plants.

Thus far, studies have revealed that *D. glomerata* produces phytotoxins zinniol (Sugawara and Strobel, 1986) and 5-dihydroxymethylfuran (Cimmino et al., 2021), which contribute to the virulence of the pathogen on sunflowers and grapevine, respectively. However, molecular and genetic factors regulating the *D. glomerata* virulence on various hosts, let alone maize, are still lacking. Only seven species in the genus *Didymella* have been sequenced, and the genomes thereof are available in the public domain. Of the sequenced *Didymella* species, two are pathogenic to humans (*D. keratinophila* [the causal agent finger-hand lesions in humans; GenBank accession GCA_011058865.1] and *D. heteroderae* [GenBank accession GCA_011058895.1]), whereas five are pathogenic to plants (*D. pinodes* [the causal agent of Ascochyta blight of pea; GenBank GCA_004151525.1], *D. lethalis* [pea root rot pathogen; GenBank accession GCA_004335245.1], *D. arachidicola* [the causal agent of web blotch of peanut; GenBank accession GCA_016630955.1], *D. exigua* [the causal agent of Didymella wilt and necrosis of yellow starthistle; GenBank accession GCA_010094145.1] and *D. rabiei* [the causal agent of Ascochyta blight of chickpea; GenBank accession: GCA_004011695.1]). More recently, fragmented genome assemblies of two *D. glomerata* strains CBS 528.66 (accession GCA_022559905.1; host: *Chrysanthemum* spp.) and M27-16 (accession GCA_022225945.1; host: *Malus* spp.) were deposited to GenBank.

In this study, we sequenced, assembled and annotated the genome of *D. glomerata* strain Pj-2, which infects maize and causes DLB. Therefore, the high-quality gapless assembly reported in the study represents the first sequenced genome of the maize-infecting *D. glomerata* strain. Furthermore, we also identified three genetic sources of DLB resistance in maize germplasm, including an elite tropical inbred line CML496, for potential introgression of resistance alleles into elite cultivars lacking resistance through intraspecific hybridization.

Results and discussion

High-quality gapless genome assembly of maize-infecting *D. glomerata*

We sequenced the *D. glomerata* strain Pj-2 genome on the second-generation (Illumina NovaSeq 6000) and third-generation (PacBio Sequel II) sequencing platforms, which yielded a *de novo* reference genome assembly of 33.17 Mb with a 575-fold genomic coverage (Table 1). Thirty-two contiguous super-sequences (called supercontigs or scaffolds) were assembled from 2,054,785 clean SMRT reads (average read length = 8,300 bp; summed read length = 17,055,541,969 bp) originating from the sequencing of a long DNA fragment (insert size = 10 Kb) library on PacBio Sequel II. The scaffolds were

TABLE 1 The *Didymella glomerata* Pj-2 genome assembly features.

Genome features	Statistics
Assembly size	33,173,266 bp
Scaffolds	32
Scaffold N/L50	11/1,359,674 bp
Gap	100 bp
Protein-coding gene models	10,334
GC content	53.44%
tRNA	145
rRNA	43
ncRNA	31
Repeat elements	1.93%
Gene model coverage[a]	
Complete BUSCOs	6,480 (97.6%)
Fragmented BUSCOs	12 (0.2%)
Missing BUSCOs	149 (2.2%)

[a]The completeness of genome assembly was evaluated using a set of 6,641 pleosporales BUSCOs (benchmarking universal single-copy orthologs).

confirmed and corrected by 250-bp 11,853,984 high-quality paired-end reads (summed length = 2,876,946,471 bp; average phred quality score on a sliding window of four nucleotides ≥30) generated from the sequencing of a short paired-end library (insert size = 500 bp) on NovaSeq 6000. As a result, a virtually gapless high-quality genome assembly was generated and consisted of 32 scaffolds with only a single gap of 100 bp in scaffold14 (coordinate: 515,915–516,014 bp). The analysis of *K*-mer frequency at the optimal length of 17 bp within 250-bp 11,853,984 paired-end reads revealed that the genome of Pj-2 is estimated to be 34.90 Mb in size. The genome size is comparable to the recently sequenced genome assemblies of the Chrysanthemum-infecting strain CBS 528.66 (33.98 Mb) and the apple-infecting strain M27-16 (35.52 Mb) of *D. glomerata*.

The scaffold N/L_{50} of the *D. glomerata* Pj-2 genome is 11/1,359,674 bp, which is far superior than the other two genome assemblies of *D. glomerata* strains CBS 528.66 (177 scaffolds; N/L_{50} = 7/635,919 bp) and M27-16 (946 scaffolds; N/L_{50} = 26/469,072 bp). In addition, the Pj-2 genome assembly is either comparable or better than that of other sequenced *Didymella* species: *D. keratinophila* 9M1 (577 scaffolds; N/L_{50} = 76/141,571 bp), *D. heteroderae* 28M1 (620 scaffolds; N/L_{50} = 38/283,873 bp), *D. pinodes* WTN-11-157 (1,593 scaffolds; N/L_{50} = 91/106,671 bp), *D. lethalis* GRM-16-623 (512 scaffolds; N/L50 = 50/196,696), *D. arachidicola* YY187 (25 scaffolds; N/L_{50} = 8/2,070,310 bp) (Li et al., 2021); *D. exigua* CBS 183.55 (176 scaffolds; N/L_{50} = 64/145,421 bp), *D. rabiei* ArMe14 (34 scaffolds; N/L_{50} = 9/1,812,190) (Shah et al., 2020) and *D. segeticola* GZSQ-4 (23 scaffolds; N/L_{50} = 6/2,254,797) (Ren et al., 2019).

Tandem telomeric repeats $(CCCTAA)_n$ or $(TTAGGG)_n$ were present in at least one end of the 23 scaffolds of the *D. glomerata* Pj-2 genome assembly. Of these 23 scaffolds, four (scaffold1 [1.90 Mb], scaffold14 [1.09 Mb], scaffold18 [1.05 Mb] and scaffold19 [1.03 Mb]) contain the telomeric repeats at both ends and hence represent full-length chromosomes. Transposable elements (TEs) comprise only 1.93% of the *D. glomerata* genome assembly (0.99% [328,869 bp] of retroelements, 0.90% [297,166 bp] of DNA transposons and 0.02% [7,437 bp] of unclassified TEs) and are scattered in the low GC content regions of the genome (Table S1). The GC content in the Pj-2 genome is 53.44%, which is similar to the CBS 528.66 (53.10%) and M27-16 (53.30%) genomes and other sequenced *Didymella* spp. A total of 6,480 (97.6%) out of 6,641 pleosporales (the order within Dothidiomycetes) single-copy genes were mapped on the *D. glomerata* Pj-2 genome, suggesting a near-complete genome assembly with regard to the genic content thereof. Overall, the assembled PacBio reads corrected by the Illumina reads produced a high-quality (32 scaffolds with 575-fold genome coverage), nearly gapless (single gap of 100 bp) genome assembly of the maize-infecting strain Pj-2 of *D. glomerata*.

Gene families implicated in the virulence/pathogenicity of *D. glomerata* on maize

The *D. glomerata* Pj-2 genome is predicted to contain 10,334 protein-coding genes, whose number is markedly lower than that of the *Chrysanthemum*-infecting strain CBS 528.66 (11,200) and the *Malus*-infecting strain M27-16 (11,650). Similarly, the predicted gene content of Pj-2 encodes is markedly lower than that of other *Didymella* spp., e.g., *D. keratinophila* 9M1 (11,880), *D. heteroderae* 28M1 (11,640), *D. exigua* CBS 183.55 (12,356) and *D. rabiei* ArMe14 (11,257), except *D. pinodes* WTN-11-157 (10,505). The clustering of 90,823 proteins coded by the eight strains based on their sequence similarity (≥90% over 50 aligned aa) showed that the strains carry 1,027 core orthologous proteins. Pj-2 shares 2,734 more orthologous proteins with CBS 528.66 (7,660) than M27-16 (4,927), suggesting that the maize-infecting *D. glomerata* strains are phylogenetically closely related to the *Chrysanthemum*-infecting *D. glomerata* strain. Pj-2 shares 5,444 orthologous proteins with 9M1, 4,771 with 28M1, 3,847 with CBS 183.55 and 1,958 with ArMe14 (Table S2).

Only a subset of genes in the genomes encodes virulence/pathogenicity-related factors, including although not limited to effectors, carbohydrate-active enzymes (CAZymes) and secondary metabolism enzymes. Effectors are the pathogen-secreted small proteins and are an example of the extended phenotype as they function in hosts instead of pathogens, whose genomes carry the effector-coding genes. Pathogens deliver effectors into plants to subdue the innate immune system of plants, thereby enabling colonization and proliferation (Stergiopoulos and De Wit, 2009). Only 1.88% of the Pj-2 genes encode effector candidates (211), whose number is

higher than that of the *Chrysanthemum*-infecting strain CBS 528.66 (176) and the *Malus*-infecting strain M27-16 (196) even though the latter two strains of *D. glomerata* have a larger gene content than the former (Tables S3-S5). Similarly, the pea-infecting *D. pinodes* WTN-11-157 genome carried a reduced number of effector candidate genes (180; Table S6). However, effector content in other four strains were slightly larger than that in Pj-2, e.g., 9M1 (231; Table S7), 28M1 (240; Table S8), CBS 183.55 (240; Table S9) and ArMe14 (223; Table S10). The majority of these effectors lack any known functional domain, e.g., 195 Pj-2 effectors show homology to hypothetical and uncharacterized proteins. Some of these effectors function in the host cell apoplast, which is replete with cysteine proteases, whereas some effectors are translocated into host cells wherein they subvert host cell immunity, viz., effector-triggered immunity (ETI). EffectorP (Sperschneider and Dodds, 2022) predicted that 111 encoded by the Pj-2 genome are likely translocated into the host cell apoplast. Seventy-four of the 111 apoplastic effector candidates possess ≥2% cysteine residues; cysteine residues in some of these effectors form disulfide bonds, which may provide stability to them in the hostile protease-rich milieu in the host cell apoplast (Figure 1A). The distribution of apoplastic effector candidates in the eight strains followed a similar pattern as effector candidates, i.e., Pj-2 carries a larger repertoire of apoplastic effector candidates than that in CBS 528.66 (71), M27-16 (97) and WTN-11-157 (88). A total of 58 effector candidates are likely transported into the host cell cytoplasm; notably, the number of these cytoplasmic effector candidates is lower than that in CBS 528.66 (64), M27-16 (60) and WTN-11-157 (59) (Figure 1A). Effectors in some plant pathogens, such as *Leptosphaeria maculans* (the causal agent of blackleg disease of oilseed crop), *Fusarium* spp., *Magnaporthe oryzae* (the causal agent of rice blast disease) and *Ustilago maydis* (the causal agent of corn smut), are localized in chromosomal regions enriched with transposable elements, including telomeres, or clustered in AT-rich blocks of the genomes (Kämper et al., 2006; Farman, 2007; Ma et al., 2010; Rouxel et al., 2011). Such a genomic environment drives rapid diversification of genes, including those coding for effectors, thereby enabling pathogens to evade the innate immune system of host cultivars. However, the effector candidates in Pj-2 are randomly distributed across the genome, with no evidence for enrichment of particular scaffolds, including full-length chromosomes (scaffold1, scaffold14, scaffold18 and scaffold19), or clustering in the proximity of genomic regions replete with repetitive elements, e.g., telomeres. The relatively larger effector repertoire of Pj-2, especially cytoplasmic effectors, may be an adaptation of *D. glomerata* to colonize new host maize under field conditions, which we reported recently (Ma et al., 2022).

Pj-2 is equipped with 134 carbohydrate-active enzymes (CAZymes; Figure 1B and Table S11) that likely degrade the host cell wall, composed mainly of cellulose, hemicellulose and pectin, to colonize the host tissues and drive nutrition from the macerated tissues (van den Brink and de Vries, 2011). The other two *D. glomerata* strains possess a slightly lower number of CAZymes, i.e., CBS 528.66 (132; Figure 1B and Table S12) and M27-16 (130; Figure 1B and Table S13). The number of CAZymes in other *Didymella* spp. (Figure 1B and Tables S1-S17) except CBS 183.55 (128; Figure 1B and Table S18) is higher than that in Pj-2. Notably, the number of hemicellulases (55) is higher than cellulases (31) and pectinases (48) in Pj-2, which is presumably associated with a higher amount of hemicellulose in the maize cell wall.

In fungal pathogens, secondary metabolism genes are generally localized in biosynthetic gene clusters (BGCs), and each BGC contains a backbone gene and a few decorating genes,

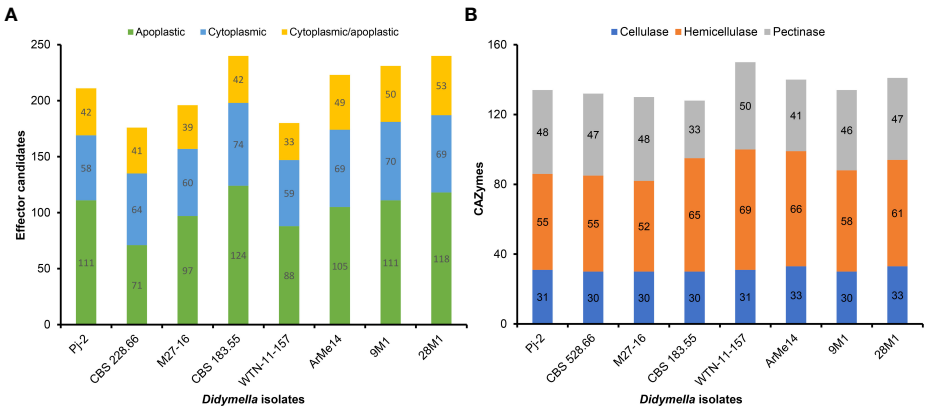

FIGURE 1
Distribution of effector candidates **(A)** and carbohydrate-active enzymes (CAZymes; **B**) in eight strains representing six *Didymella* spp. (*Didymella glomerata* Pj-2, CBS 528.66 and M27-16, *D. pinodes* WTN-11-157, *D. keratinophila* 9M11, *D. heteroderae* 28M1, *D. exigua* CBS 183.55 and *Ascochyta* [*Didymella*] rabiei ArMe14).

and encodes a specific secondary metabolite (Collemare et al., 2008). Secondary metabolites are indispensable for fungal virulence on hosts (Soanes et al., 2012). The Pj-2 genome contains 12 BGCs, similar to CBS 528.66 (12) but lower than M27-16 (16) (Tables 2, S19-S26). Likewise, the number of backbone genes encoding polyketide synthase (PKS) and nonribosomal peptide synthase (NRPS) is slightly higher in M27-16 (6 PKS and 7 NRPS-like) than Pj-2 (4 PKS and 4 NRPS-like) and CBS 528.66 (5 PKS and 4 NRPS-like) (Tables 2, S19-S26). Therefore, the *Malus*-infecting *D. glomerata* strain M27-16 may have more capacity to produce secondary metabolites than that of the maize- and *Chrysanthemum*-infecting *D. glomerata* strains.

Phylogenomics reveals intra- and inter-specific genetic diversity among *Didymella* spp.

The *D. glomerata* strain Pj-2 genome (33.17 Mb) is similar in size to the Chrysanthemum-infecting strain CBS 528.66 (33.98 Mb), apple-infecting strain M27-16 (35.52 Mb), as well as other *Didymella* spp., e.g., *D. pinodes* WTN-11-157 (33.77 Mb), and *D. exigua* CBS 183.55 (34.39 Mb). However, the other four sequenced *Didymella* spp. have slightly larger genomes, e.g., *D. rabiei* ArMe14 (40.92 Mb), *D. keratinophila* 9M1 (36.22 Mb) and *D. heteroderae* 28M1 (37.07 Mb).

To gauge genetic diversity among *Didymella* spp., we performed genome similarity and synteny analyses among eight strains, representing six species. An eight-strain whole-genome alignment was contrived using the following parameters: 50-bp seeds and extension thereof with HOXD scoring matrix (Chiaromonte et al., 2002) and ≥100-bp alignment block. Pairwise distance matrices between the genomes were calculated from the alignment blocks of size ≥100 bp and were expressed as alignment percentage (AP) and average nucleotide identity (ANI) (Figure 2B). The *D. glomerata* strain Pj-2 shares 92.37% (i.e., AP) of its genome with CBS 528.66, followed by 57.71% with 9M1, 55.01% with M27-16, 45.04% with WTN-11-157, 43.14% with 28M1, 23.31% with CBS 183.55 and 5.19% with ArMe14. The shared genomic regions showed ≥85% ANI; Pj-2 displayed 98.89% nucleotide similarity with CBS 528.66, followed by 88.79% with 9M1, 88.20% with M27-16, 87.01% with 28M1, 86.99% with WTN-11-1, 85.11% with CBS 183.55 and 84.56% with ArMe14. A neighbor-joining tree constructed from the pairwise distance matrices revealed that a clade comprising the three *D. glomerata* strains Pj-2, CBS 528.66 and M27-16, and *D. keratinophila* 9M1. These strains share 55.01% to 92.37% genomes (AP), with ANI values ranging from 88.20% to 98.89%. Within this clade, Pj-2 and CBS 528.66 formed a subclade, which is in agreement with high AP (92.37%) and ANI (98.89%) between their genomes (Figure 2B). Synteny analysis showed that the two *D. glomerata* strains possess a similar genomic architecture. However, a few structural variations (chromosomal rearrangements) exist between their genomes (Figure 2B). To further investigate these genomic rearrangements, whole-genome collinearity analysis was performed between the Pj-2 and the genomes of seven strains (CBS 528.66, M27-16, WTN-11-15, CBS 183.55, ArMe14, 9M1 and 28M1) (Figure 2). The Pj-2 genome is collinear with the CBS 528.66 genome, whereas it shows fragmented collinearity with the other genomes (due to low and extensive structural variations), including M27-16, which precluded further investigation (Figures 2, S1).

Although the dot plot shows a high degree of collinearity between the two *D. glomerata* strains Pj-2 and CBS 528.6;

TABLE 2 Biosynthetic gene clusters (BGCs) and secondary metabolite backbone-forming enzymes within BCGs in *Didymella* spp.

	Pj-2[3]	CBS 528.66[3]	M27-16[3]	CBS 183.55[4]	WTN-11-157[5]	ArMe14[6]	9M1[7]	28M1[8]
BGCs[1]	12	12	16	12	15	22	10	13
Genes in BGCs								
PKS	4	5	6	8	8	12	4	7
PKS-like	1	1	1	2	1	1	2	1
NRPS	2	2	2	3	2	2	2	2
NRPS-like	4	4	7	3	5	6	4	4
PKS-NRPS	0	0	0	0	0	1	0	0
DMAT	1	1	1	1	1	1	0	1
Total[2]	12	13	17	17	17	23	12	15

[1]BGCs, Biosynthetic gene clusters.
[2]Total number of secondary metabolite backbone-forming enzymes.
[3]Didymella glomerata isolates Pj-2 (sequenced in this study), CBS 528.66 and M27-16.
[4]Didymella exigua isolate CBS 183.55.
[5]Didymella pinnodes isolate WTN-11-157.
[6]Ascochyta (Didymella) rabiei isolate ArMe14.
[7]Didymella keratinophila isolate 9M1.
[8]Didymella heteroderae isolate 28M1.

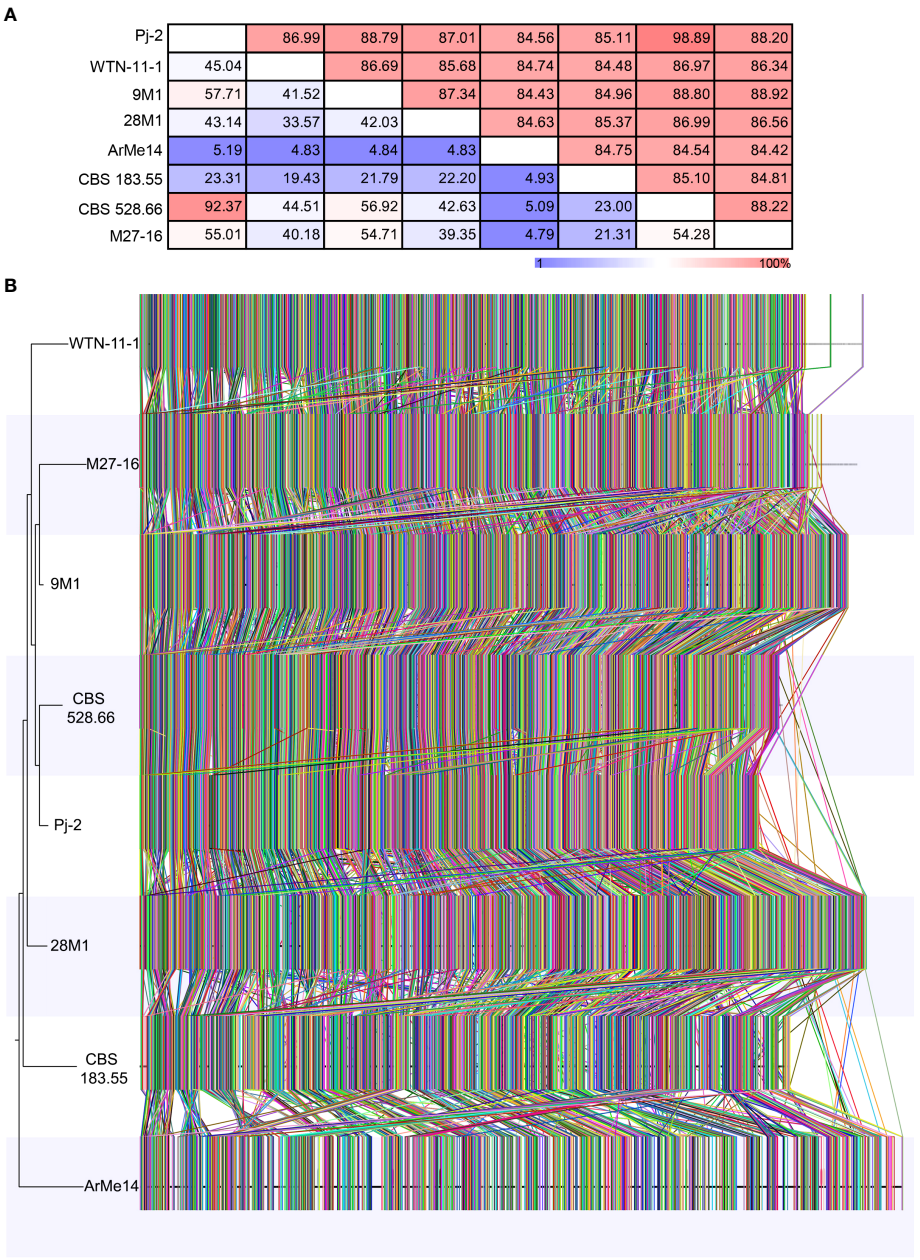

FIGURE 2
Phylogenomics of *Didymella* spp. The whole genomes of eight *Didymella* spp. strains are aligned using CLC Genomic Workbench with 50 bp seeds: *D. glomerata* Pj-2 (33.17 Mb; 32 scaffolds), CBS 528.66 (33.98 Mb; 177 scaffolds) and M27-16 (35.52 Mb; 946 scaffolds), *D. keratinophila* 9M1 (36.22 Mb; 577 scaffolds), *D. heteroderae* 28M1 (37.07 Mb; 620 scaffolds), *D. pinodes* WTN-11-157 (33.77 Mb; 1,593 scaffolds), *D. exigua* CBS 183.55 (34.39 Mb; 176 scaffolds) and *D. rabiei* ArMe14 (40.92 Mb; 34 scaffolds). The seeds were extended using a HOXD scoring matrix until the local alignment score dropped. Pairwise distance matrices between the aligned genomes are calculated from the alignment blocks of size ≥100 bp and are expressed as alignment percentage (AP; upper) and average nucleotide identity (ANI; lower) **(A)**. Genome-wide synteny analysis among the eight strains **(B)**. Each colored link represents a syntenic block (≥1,000 bp) that is shared among genomes. A neighbor-joining tree is also shown to the left of the whole-genome alignment.

however, there exist four major reciprocal translocations, viz. Pj-2 scaffold14/CBS 528.66 scaffold12 and Pj-2 scaffold18 (274 kb), Pj-2 scaffold22/CBS 528.66 scaffold6 and Pj-2 scaffold3 (166 kb), Pj-2 scaffold26/CBS 528.66 scaffold17 and Pj-2 scaffold13 (131 kb translocation), and Pj-2 scaffold26/CBS 528.66 scaffold17 and Pj-2 scaffold8 (217 kb translocation) (Figure 3A).

Pj-2 scaffold14 (size = 1094.13 kb; full-length chromosome) and CBS 528.66 scaffold12 (size = 763.58 kb) are collinear with a high degree of similarity in the genomic region located between 282 kb and 764 kb, whereas a 274-kb genomic region of CBS 528.66 scaffold12 (8 to 282 kb) shows alignment with a high degree of homology with a similar size genomic region located at the 5'-end of Pj-2 scaffold18 (size = 1051.93 kb; full-length chromosome). This is called the reciprocal translocation between Pj-2 scaffold14/CBS 528.66 scaffold12 and Pj-2 scaffold18. The 274 kb translocation region contains 92 genes in Pj-2 and 100 genes in CBS 528.66, 78 of which are homologous. This translocation encodes three apoplastic effector candidates with unknown functions. The Pj-2 effector candidates scaffold18.g41 (141 aa) and scaffold18.g46 (238 aa) are 100% identical to CBS 528.66 scaffold12.g4610 and scaffold12.g4605, respectively. The third effector candidate scaffold18.g5 (269 aa) is aligned with 100% identity from 6 aa to 265 aa of the 526 aa CBS 528.66 protein scaffold12.g4649 (526 aa); likewise, the third CBS 528.66 effector scaffold12.g4639 (186 aa) is matched with 97% identity from 1 aa to 184 aa of the 675 aa Pj-2 protein scaffold18.g16. Therefore, these proteins represent the truncated version of larger proteins and thus are unlikely effector candidates. In addition to effector candidates, the translocation codes for three CAZymes. The Pj-2 cellulase scaffold18.g13 (394 aa) and the CBS 528.66 protein scaffold12.g4641 (439 aa) are homologous proteins, showing 98% identity over the first 327 aligned aa, whereas the C-termini thereof are highly variable and former lacks 45 aa in this region. The Pj-2 hemicellulase scaffold18.g6 (837 aa) is homologous to the CBS 528.66 hemicellulase scaffold12.g4648 (837 aa), exhibiting 99% identity over the entire length of proteins. The Pj-2 pectinase scaffold18.g16 (675 aa) and the CBS 528.66 scaffold12.g4639 (186 aa) are homologous proteins with 99% identity over the first 184 aligned aa; however, scaffold12.g4639 was predicted as an effector candidate due to its length ≤300. Therefore, scaffold12.g4639 is a truncated pectinase rather than an effector candidate. The translocation does not carry any secondary metabolite backbone enzyme.

Pj-2 scaffold22 (size = 915.48 kb) and CBS 528.66 scaffold6 (size = 1123.25 kb) are collinear with a high degree of similarity in the genomic region located between the 7–911 kb (Pj-2 scaffold22) and 174–911 Kb (CBS 528.66 scaffold6); however, a 166-kb genomic region of CBS 528.66 scaffold12 (8–174 kb), which Pj-2 scaffold22 lacks, aligns with a high degree of homology with a similar size to the genomic region (25–191 kb) located at the 5'-end of Pj-2 scaffold3 (size = 1813.70 kb). This is the reciprocal translocation between Pj-2 scaffold22/CBS 528.66 scaffold6 and Pj-2 scaffold3. The 166 kb translocation contains 54 genes in Pj-2 and 60 genes in CBS 528.66, 53 of which are homologous. This translocation encodes two apoplastic and/or cytoplasmic effector candidates with unknown functional domains and one CAZyme hemicellulase; however, it does not code for any secondary metabolite backbone enzyme. The Pj-2 effector candidates scaffold3.g27 (226 aa; apoplastic/cytoplasmic localization) and scaffold3.g51 (300 aa; apoplastic localization) are 100% identical to the CBS 528.66 effector candidates sacffold6.g2757 and scaffold6.g2777, respectively. The Pj-2

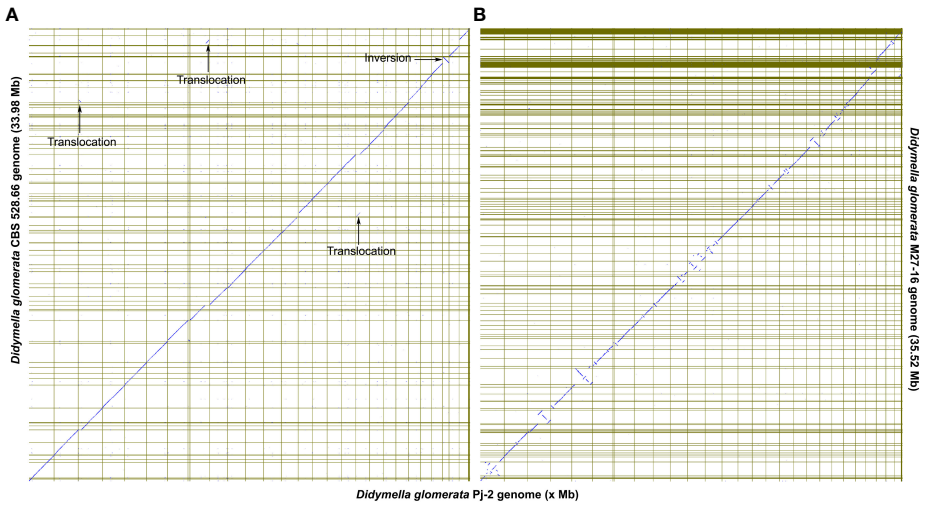

FIGURE 3
The dot plots show the collinearity of the *D. glomerata* Pj-2 genome (X-axis) with that of CBS 528.66 (Y-axis; **A**) and M27-16 (Y-axis; **B**). Four translocations are conspicuously present between Pj-2 and CBS 528.66.

hemicellulase scaffold3.g49 (338 aa) is homologous to the CBS 528.66 hemicellulase scaffold6.g2776 (1120 aa), displaying 99% over the 334-aligned aa, whereas the former lacks the remaining aa. Therefore, scaffold3.g49 is a truncated protein.

Pj-2 scaffold26 (size = 703.34 kb) and CBS 528.66 scaffold17 (size = 703.44 kb) are collinear with a high degree of similarity in the genomic region located between 1–277 kb (Pj-2 scaffold22) and 434–703 Kb (CBS 528.66 scaffold6). The remaining genomic region of Pj-2 scaffold26, spanning from 277 kb to 703 kb, is collinear with CBS 528.66 scaffold29 (size = 481.49 kb). However, a majority of the 430-kb genomic region located at the 5'-end of CBS 528.66 scaffold17 (15–430 kb), which Pj-2 scaffold26 lacks, matches with a high degree of homology with two genomic regions located at distinct Pj-2 scaffolds, i.e., scaffold13 (1,133–1,264 kb) and scaffold8 (1,222–1,439 kb). Therefore, there are two reciprocal translocations: Pj-2 scaffold26/CBS 528.66 scaffold17 and Pj-2 scaffold13 (131 kb translocation) and Pj-2 scaffold26/CBS 528.66 scaffold17 and Pj-2 scaffold8 (217–250 kb translocation). The 131-kb translocation contains 46 genes in Pj-2 and 55 genes in CBS 528.66, 45 of which are homologous genes. The translocation codes for one apoplastic and/or cytoplasmic effector candidate with an unknown functional domain; however, it does not encode

CAZymes and secondary metabolite backbone enzymes. The Pj-2 effector candidate scaffold13.g401(239 aa) is homologous to CBS 528.66 Scaffold17.g5676, showing 100% identity. The 217–250 kb translocation contains 77 genes in Pj-2 and 89 genes in CBS 528.66 (146-396 kb; scaffold17 of CBS 528.66), 77 of which are homologous genes. The translocation codes for two apoplastic and/or cytoplasmic effector candidates with an unknown function; however, it does not encode CAZymes and secondary metabolite backbone enzymes. The 136 aa effector candidates scaffold8.g410 (Pj-2) and scaffold17.g5766 (CBS 528.66) are homologous proteins, exhibiting 95% identity over their entire length; seven aa differ between the two effector candidates. Both are predicted to be localized in the apoplast and/or cytoplasm. However, the second effector candidate (294 aa; scaffold8.g423 in Pj-2 and scaffold17.g5781 in CBS 528.66) does not show any polymorphism between the two strains and is likely localized in the cytoplasm.

A spurious inversion is evident in the collinearity plot between Pj-2 and CBS 528.66. Pj-2 scaffold27 is flipped with respect to the 3'-end of CBS 528.66 scaffold4; the 3'-end of CBS 528.66 scaffold4 is aligned with Pj-2 scaffold 24. Therefore, we conclude that Pj-2 scaffold24 and scaffold27 are part of the same contiguous sequence.

The structural variations in the genomes are the major drivers of genetic diversity within and between species of the same genus, which enable the species or strains within the same species to colonize distinct ecological niches. For example, the maize- and Chrysanthemum-infecting strains of *D. glomerata* are genetically similar, sharing 92.37% genome with 98.89% sequence similarity. However, the *Malus*-infecting strain of *D. glomerata* M27-16 is highly diverse from the other two strains, Pj-2 (sharing only 55.01% genome with 88.20% sequence similarity) and CBS 528.66 (sharing 54.28% genome with 88.22% sequence similarity) (Figures 2A, 3B). The four translocations between Pj-2 and CBS 528.66 may be responsible for the two strains colonizing different hosts, *Z. mays* and *Chrysanthemum* spp. However, it is unlikely that CAZymes and secondary metabolism genes located the translocations. We found only one effector candidate showing polymorphism between the two strains, Pj-2 (scaffold8.g410) and CBS 528 (scaffold17.g5766). It would be interesting to investigate whether the targeted deletion of these two effectors in their respective strains contributes to virulence on their hosts.

Germplasm screening to identify the genetic sources of DLB resistance in maize

Deployment of resistant cultivars in the field offers an environmentally friendly way to control crop diseases and thus reduces the overreliance on pesticides, thereby increasing farm crop cash receipts. However, developing a resistant cultivar requires an intraspecific hybridization through the wide/top cross between a susceptible cultivar (elite cultivar) and a donor parent (inbred line, landrace or wild relative) that carries alleles conferring genetic resistance to the disease of interest. Identifying such genetic sources of disease resistance is the first key step in cultivar development. With the above objective and given that DLB is a new disease of maize, we conducted germplasm screening to identify the genetic source of DLB resistance in maize. Thirty maize lines representing inbred lines, cultivars and landraces were screened for reactions to the *D. glomerata* isolate Pj-2 in a growth chamber through spray-inoculation following an augmented randomized block design (Table S27). Three of these lines expressed complete resistance (immune; no lesion) to *D. glomerata*, followed by respectively sixteen and eleven lines exhibiting moderate resistance (few confined scattered lesions) and susceptible (coalesced lesions) reactions (Figure 4 and Table S27). The resistant lines were CML496, Jitiaojiao and Denglonghong; CML496 is an elite tropical inbred line, developed by CIMMYT, whereas the other two are local cultivars. CML496 is highly resistant to *Puccinia polysora*, the causal agent of southern corn rust (SCR) and carries a major QTL *RppCML496* for resistance to SCR (Lv et al., 2021). Among the moderately resistant lines were elite inbred lines, such as Ye478 (lesion area/2500 mm^2: 12.7 ± 19.2 mm^2), Zheng58 (16.7 mm^2), Chang7-2 (39.7 mm^2), CML470 (51.0 mm^2), PH4CV (32.6 mm^2), PH6WC (6.5 mm^2) and B73 (66.6 mm^2) (Figure S2 and Table S27). Ye478, Zheng58 and Chang7-2 are elite lines, heavily used as parental lines in hybrid breeding programs in China because of their high general combining ability and superior agronomic performance

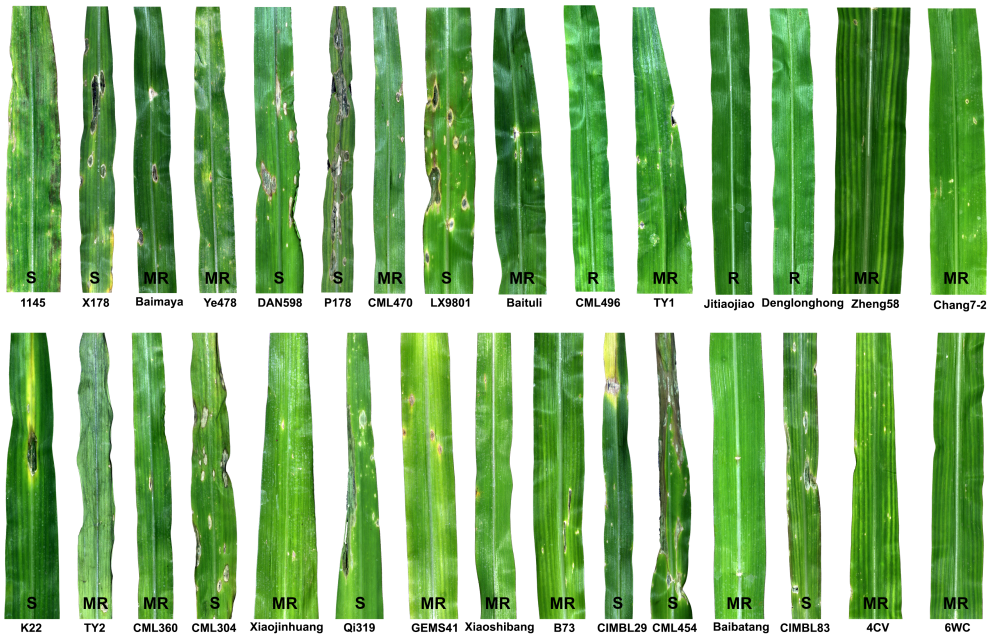

FIGURE 4
Maize germplasm screening to identify the genetic sources of resistance to *Didymella* leaf blight caused by *Didymella glomerata*. Fourth leaves of thirty lines (cultivars, inbred lines and landraces) at the V3 stage were spray-inoculated with conidial suspension (1 x 10^7 conidia/ml in 0.025%) until runoff. Three of the lines expressed complete resistance (R; no lesion) to *D. glomerata*, followed by respectively sixteen and twelve lines exhibiting moderate resistance (MR; few confined scattered lesions) and susceptible (S; coalesced lesions) reactions. An augmented randomized complete block design was used to evaluate the maize germplasm for DLB resistance. The leaves were photographed five days post-inoculation.

(Zheng et al., 2009). All three lines display moderate resistance to *Bipolaris maydis* (the causal agent of southern corn leaf blight) and *Puccinia sorghi* (common rust pathogen), whereas they are susceptible to *Curvularia lunata* (the causal agent of Curvularia leaf spot) and *P. polysora*. In addition, Zheng58 and Chang7-2 are moderately resistant to *Exserohilum turcicum* (northern corn leaf blight pathogen), and the latter line also manifests a similar resistance response to *Cercospora zeae-maydis* (gray leaf spot pathogen) (Wang et al., 2014). CML470, a CIMMYT inbred line, carries a dominant gene *RppC*, which controls resistance to *P. polysora* (Sun et al., 2020). PH4CV and PH6WC are the elite inbred lines developed by Pioneer HiBred International; however, their reactions to fungal pathogens are largely unexplored. B73 is susceptible to *B. maydis*, *C. lunata*, *C. zeae-maydis* and *P. polysora*, whereas the line shows moderate resistance to *E. turcicum* and complete resistance to *P. sorghi*.

Furthermore, we selected the most susceptible inbred line (P178) and the most resistant inbred line (CML496) for histochemical analysis. P178 is an inbred line, which is resistant to *P. polysora* SCR (six QTL for SCR resistance) (Tian et al., 2018) and *Exserohilum turcicum* (Wang et al., 2019). However, P178 exhibited extensive leaf blight following the inoculation with the *D. glomerata* strain Pj-2; over 50% of the inoculated leaf area showed blight (lesion area/2500 mm^2: 1278.6 ± 38.5 mm^2) while the CML496 leaves remained healthy (Figures 4, S2 and Table S27). DAB-staining of the *D. glomerata*-infected leaf tissues revealed the accumulation of H_2O_2, a reactive oxygen species, in the apoplastic space of the infected issues of CML496, not in P718 (Figure 5). The rapid and transient burst of ROS (called oxidative burst) at the infection site is the hallmark of the pathogen-associated molecular pattern (PAMP)-triggered immunity (PTI) and ETI, and is ensued upon successful recognition of pathogens by host cells (Torres, 2010). The CML496 infected cells likely successfully perceived *D. glomerata*, which in turn activated defense responses, such as oxidative burst that arrested fungal growth and proliferation (Figures 5A, C). The pathogen apparently requires successful penetration of the host epidermal cell cuticle, which may trigger its perception in the CML496 epidermal cells, leading to DLB resistance (Figure 5C). However, *D. glomerata* likely dodges surveillance (PTI and ETI) in the P178 epidermal cells, facilitating fungal growth and proliferation (Figures 5B, D). Altogether, the DLB of maize is likely a gene-for-gene disease in which the resistant maize genotypes (e.g., CML496, Jitiaojiao and Denglonghong) and *C. graminicola*

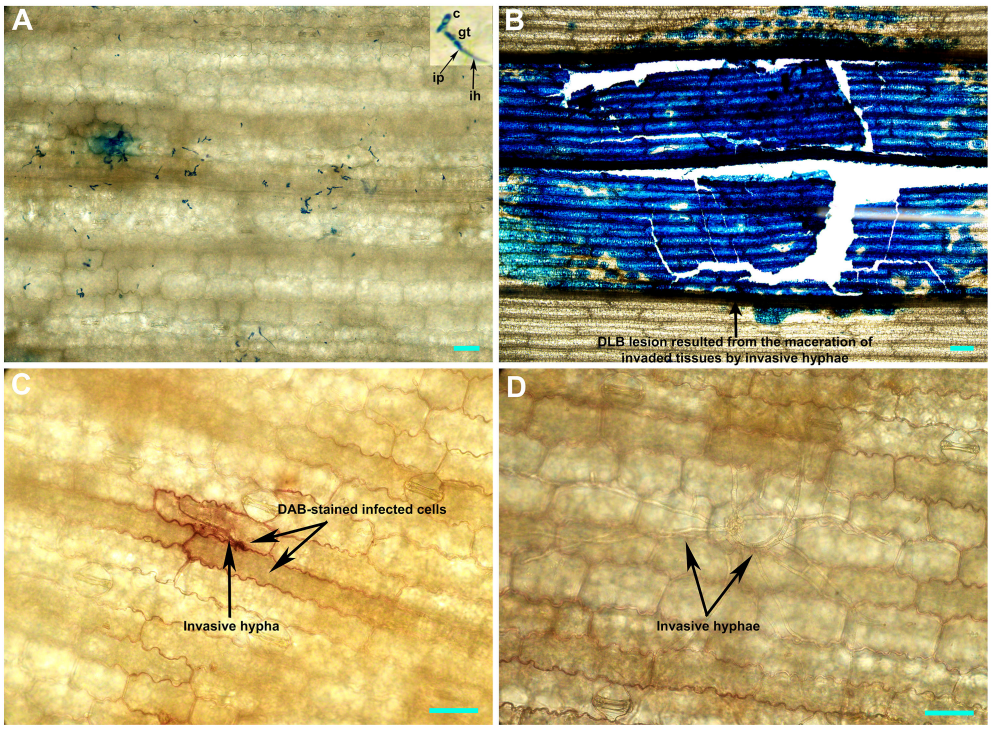

FIGURE 5
Histochemical staining of the *Didymella glomerata* strain Pj-2-infected tissues of susceptible (P178) and resistant (CML496) inbred lines of maize. The top image panel shows the acidic aniline blue-stained CML496 **(A)** and P718 **(B)** leaf tissues, and the bottom image panel illustrates the DAB-stained CML496 **(C)** and P178 **(D)** leaf tissues five days post-inoculation. The *D. glomerata* conidia germinate to form germ tubes, which directly breach the host cell cuticle, presumably *via* infection pegs. This invasion is restricted to the first infected epidermal cells **(A)** and leads to the accumulation of H_2O_2 (a reactive oxygen species; c) in CML496, whereas the invasion in P178 leads to the maceration of infected tissues **(B)** by invasive hyphae **(D)**. c, conidia; gt, germ tube; ip, infection peg; ih, invasive hypha; Bars = 20 μm.

recognize each other by corresponding pairs of the nucleotide-binding leucine-rich repeat receptors and effectors.

Concluding remarks

DLB is a new disease of maize, which we recently identified in Panjin, Liaoning, a northeastern province of China (Ma et al., 2022). In this study, we presented a nearly gapless genome assembly of the *D. glomerata* strain Pj-2, which comprises 32 scaffolds, including four full-length scaffolds (representing chromosomes) carrying telomeres at both ends. Phylogenomic analysis shows that the maize- and *Chrysanthemum*-infecting strains of *D. glomerata* are genetically similar and share 93.37% genome with 98.89% sequence similarity. However, they carry four major reciprocal translocation regions in their genomes, which may allow their adaptation to different hosts. Furthermore, germplasm screening against DLB identified three maize inbred lines (e.g., CML496, Jitiaojiao and Denglonghong) expressing complete resistance to the *D. glomerata* strain Pj-2. Therefore, these lines can be used as a donor parent to transfer genetic resistance into other elite cultivars lacking DLB resistance through intraspecific hybridization introgression. Further research, however, is required to identify genes in CML496 conferring resistance to DLB. In addition, field research should be undertaken to assess the economic impact of this new maize disease, both in terms of yield loss and down-gradation of grain quality.

Methods

Fungal and plant material

The *D. glomerata* strain Pj-2 was routinely maintained on PDA plates under a 12 h photoperiod at 25°C. Maize germplasm involving 30 lines representing cultivars, inbred lines and landraces (Table S27) was evaluated for reactions to Pj-2.

Genome sequencing, size, assembly and completeness

Conidia (ca. 10^7) were collected by swamping the five-day-old six-cm PDA culture plates of Pj-2 with five ml of distilled deionized H_2O. One ml of conidial suspension was incubated in a one-liter flask containing 200 ml of complete medium for four days in an orbital shaker set at 25°C and 120 rpm. Mycelia balls were collected by filtering the liquid culture through a one-layered Miracloth. The ENZA Fungal DNA kit (Omega Bio-Tek, Norcross, USA) was used to isolate genomic DNA (gDNA) from the mycelia.

Covaris E220 (Covaris, Brighton, UK) was used to fragment one µg of high-quality gDNA, and end-repaired fragments were used to construct a short insert (500 bp) paired-end library using TruSeq DNA LT Kit (Illumina, San Diego, USA). The library was assessed for the insert size and quality using BioAnalyzer 2100 using Agilent 1000 DNA Chip (Agilent Technologies, Palo Alto, USA) and sequenced on NovaSeq 6000 (Illumina, San Diego, USA), generating 2 x 250 bp reads. AdapterRemoval v2 (Schubert et al., 2016) was used to clip adapters and low-quality bases from the paired-end reads. SOAPec v2.0 (Luo et al., 2012) was used to correct sequencing errors based on the *K*-mer (17) frequency in the paired-end reads. Finally, Jellyfish v2.0 (Marçais and Kingsford, 2011) was used to count *K*-mer (17) within the high-quality paired-end reads to estimate the *D. glomerata* Pj-2 genome size.

g-TUBE (Covaris, Brighton, UK) was used to shear five µg of high-quality gDNA, and BluePippin (Sage Science, Beverly, USA) was utilized to size-select ~10 kb gDNA fragments. Finally, the end-repaired large fragments were used to construct a long insert (10 kb) library using SMRTbell Express Template Prep Kit 2.0 (Pacific Biosciences, Menlo Park, USA). The resulting library was assessed for insert size and quality on BioAnalyzer 2100 and sequenced on PacBio Sequel II (Pacific Biosciences, Menlo Park, USA) using Continuous Long Read mode. The polymerase reads generated on PacBio Sequel II were checked for adapter contamination, quality and size using SMRT analysis v2.3.0; the subreads (quality >0.8 and size >1,000 bp) were extracted from the adapter-free polymerase reads. Unicycler (Wick et al., 2017) was employed to contrive a hybrid genome assembly using high-quality 250-bp paired-end reads (NovaSeq 6000) and 1,000–10,000 bp subreads (PacBio Sequel II).

Phylogenomics

The whole genomes of eight strains of six *Didymella* spp. (*D. glomerata* Pj-2, CBS 528.66 and M27-16, *D. keratinophila* 9M1, *D. heteroderae* 28M1, *D. pinodes* WTN-11-157, *D. exigua* CBS 183.55 and *D. rabiei* ArMe14) were aligned using the Whole Genome Alignment tool plugged in CLC Genomics Workbench (Qiagen, Aarhus, Denmark) with the following parameters: 50-bp seed and minimum alignment block size ≥100 bp. AP and ANI were calculated from the whole-genome alignment using pairwise distance matrices.

Genome annotation

The following genomes were masked for repetitive DNA elements using RepeatMasker v4.0.6 (Smit et al., 1996) and RepeatModeler v2.1 (Smit and Hubley, 2015): the three *D. glomerata* strains (Pj-2, CBS 528.66 and M27-16), *D. exigua* CBS 183.55, *D. pinodes* WTN-11-157, *D. rabiei* ArMe14, *D. keratinophila* 9M1 and *D. heteroderae* 28M1. The masked genome of Pj-2 was assessed for its completeness using BUSCO v5.1.3 (Simão et al., 2015) with a set of 6,641 benchmarking universal single-copy orthologs (BUSCOs) in Pleosporales.

Augustus v3.03 (Stanke and Morgenstern, 2005), glimmerHMM v3.0.1 (Majoros et al., 2004) and GeneMark-ES v4.35 (Ter-Hovhannisyan et al., 2008) were used to predict gene models *ab initio* in the masked genomes. Protein models from the closely related *Didymella* species (*D. keratinophila*, *D. heteroderae*, *D. exigua* and *D. rabiei*) were mapped onto the *D. glomerata* genome using Exonerate v2.2.0 (http://www.ebi.ac.uk). The *ab initio* predictions and the Exonerate alignments were combined using EVidenceModeler v.r2012-06-25 (Haas et al., 2008) to obtain final gene models. CAZymes and secondary metabolism genes were predicted as described previously (Bhadauria et al., 2019). Genes that encode protein equal to or less than 300 aa in length, carrying N-terminal signal peptide (predicted using SignalP v5.0), lacking transmembrane domain (TMHMM v2.0) and GPI anchor addition site (PredGPI) were considered as effector candidate genes. In addition, EffectorP v3.0 was employed to discern their potential localization in the host cells, i.e., apoplast, cytoplasm and apoplast/cytoplasm. We also screened the effector candidates for possible N- and O-glycosylation sites using NetNGlyc v1.0 and NetOGlyc v4.0, respectively, as such sites allow their tethering to plasma membrane.

Germplasm screening and statistical analysis

Thirty maize lines were individually grown in pots (6 x 10 cm) containing peat moss (soilless medium) and perlite in a 2:1 ratio in a growth chamber following an augmented randomized block design. Plants were spray-inoculated at the V3 growth stage with the Pj-2 conidia (1 x 10^7 conidia/ml) following the method described previously (Vargas et al., 2012). The fourth leaves of the inoculated plants were photographed six days post-inoculation (dpi), and the lesion area (mm^2) was measured using ImageJ (https://imagej.net/). A linear mixed-effects model

using the R lm() function was used to calculate least-squares (LS) means of lesion areas on the maize lines (a fixed effect) while considering blocks (biological replications) as a random effect.

Histochemical analysis of the Pj-2 infected maize tissues

Acidic aniline blue and 3, 3-diaminobenzidine (DAB) staining of Pj-2 infected leaf tissues of the inbred lines P178 and CML496 were performed by methods described by Bhadauria et al. (2010) and Thordal-Christensen et al. (1997), respectively.

Data availability statement

The *D. glomerata* Pj-2 (BioSample: SAMN23554018) genome (32 scaffolds) has been deposited to GenBank/ENA/DDBJ under the accession number JAJOHN000000000 (BioProject: PRJNA785361).

Author contributions

VB conceived and performed research. Y-LP, VB, JD, WZ, JY and WM analyzed data. JD provided maize germplasm and VB, Y-LP, JD, WZ and JY wrote the paper. All authors contributed to the article and approved the submitted version.

Acknowledgments

The research was supported by grants from the National Natural Science Foundation of China (Grant No. 32172363) and the Chinese Universities Scientific Fund (Grant No. 10092004). Technical support for the incumbent study was provided by Hongjie Yuan at the Communication University of China, Beijing, China.

Conflict of interest

The authors declare that the research was conducted in the absence of any commercial or financial relationships that could be construed as a potential conflict of interest.

Publisher's note

All claims expressed in this article are solely those of the authors and do not necessarily represent those of their affiliated organizations, or those of the publisher, the editors and the reviewers. Any product that may be evaluated in this article, or claim that may be made by its manufacturer, is not guaranteed or endorsed by the publisher.

Supplementary material

The Supplementary Material for this article can be found online at: https://www.frontiersin.org/articles/10.3389/fpls.2022.1022819/full#supplementary-material

SUPPLEMENTARY FIGURE 1
Genome collinearity of D. glomerata Pj-2 with Didymella keratinophila 9M1, Didymella heteroderae, Didymella pinnodes WTN-11-157, Didymella exigua CBS 183.55 and the Didymella (Ascochyta) rabiei ArMe14.

SUPPLEMENTARY FIGURE 2
Reactions of the *Didymella glomerata* strain Pj-2 on 30 maize lines representing cultivars, inbred lines and landraces five days post-inoculation. Lesion areas were measured using ImageJ (https://imagej.net/).

References

Bhadauria, V., MacLachlan, R., Pozniak, C., Cohen-Skalie, A., Li, L., Halliday, J., et al. (2019). Genetic map-guided genome assembly reveals a virulence-governing minichromosome in the lentil anthracnose pathogen *Colletotrichum lentis*. *New Phytol.* 221 (1), 431–445. doi: 10.1111/nph.15369

Bhadauria, V., Miraz, P., Kennedy, R., Banniza, S., and Wei, Y. (2010). Dual trypan-aniline blue fluorescence staining methods to study fungal-plant interactions. *Biotech Histochem.* 85 (2), 99–105. doi: 10.3109/10520290903132196

Chiaromonte, F., Yap, V. B., and Miller, W. (2002). Scoring pairwise genomic sequence alignments. *PSB.* 7, 115–126. doi: 10.1142/9789812799623_0012

Cimmino, A., Bahmani, Z., Masi, M., Abdollahzadeh, J., Amini, J., Tuzi, A., et al. (2021). Phytotoxins produced by *Didymella glomerata* and truncatella angustata, associated with grapevine trunk diseases (GTDs) in Iran. *Nat. Prod. Res.* 36 (17), 1478–6419. doi: 10.1080/14786419.2021.1979544

Collemare, J., Pianfetti, M., Houlle, A. E., Morin, D., Camborde, L., Gagey, M. J., et al. (2008). *Magnaporthe grisea* avirulence gene ACE1 belongs to an infection-specific gene cluster involved in secondary metabolism. *New Phytol.* 179, 196–208. doi: 10.1111/j.1469-8137.2008.02459.x

Farman, M. L. (2007). Telomeres in the rice blast fungus *Magnaporthe oryzae*: the world of the end as we know it. *FEMS Microbiol.* 273, 125–132. doi: 10.1111/j.1574-6968.2007.00812.x

Haas, B. J., Salzberg, S. L., Zhu, W., Pertea, M., Allen, J. E., Orvis, J., et al. (2008). Automated eukaryotic gene structure annotation using EVidenceModeler and the program to assemble spliced alignments. *Genome Biol.* 9 (1), R7. doi: 10.1186/gb-2008-9-1-r7

Hosford, R. (1975). *Phoma glomerata*, a new pathogen of wheat and triticales. *Phytopathology* 65, 1236–1239. doi: 10.1094/Phyto-65-1236

Huang, S. L., Wang, L., Wang, T., Jiao, Z. J., Pang, F. H., Tao, A. L., et al. (2018). First report of didymella leaf blight on cornus officinalis caused by *Didymella glomerata* in China. *Plant Dis.* 102 (5), 1031. doi: 10.1094/PDIS-07-17-0933-PDN

Irinyi, L., Kövics, G. J., and Sándor, E. (2009). Taxonomical re-evaluation of phoma-like soybean pathogenic fungi. *Mycol. Res.* 113, 249–260. doi: 10.1016/j.mycres.2008.11.003

Kämper, J., Kahmann, R., Bölker, M., Ma, L., Brefort, T., Saville, B. J., et al. (2006). Insights from the genome of the biotrophic fungal plant pathogen *Ustilago maydis*. *Nature* 444 (7115), 97–101. doi: 10.1038/nature05248

Khani, M. (2014). *Aspects of epidemiology of phoma koolunga (Ascochyta blight of field pea)* (Adelaide: University of Adelaide).

Li, S., Xue, X., Gao, M., Wang, N., Cui, X., Sang, S., et al. (2021). Genome resource for peanut web blotch causal agent *Peyronellaea arachidicola* strain YY187. *Plant Dis.* 105 (4), 1177–1178. doi: 10.1094/PDIS-04-20-0898-A

Luo, R., Liu, B., Xie, Y., Li, Z., Huang, W., Yuan, J., et al. (2012). SOAPdenovo2: an empirically improved memory-efficient short-read *de novo* assembler. *GigaScience* 1 (1), 18. doi: 10.1186/2047-217X-1-18

Lv, M., Deng, C., Li, X., Zhao, X., Li, H., Li, Z., et al. (2021). Identification and fine-mapping of RppCML496, a major QTL for resistance to *Puccinia polysora* in maize. *Plant Genome* 14, e20062. doi: 10.1002/tpg2.20062

Ma, W., Yang, J., Gao, X., Han, T., Liu, J., Ding, J., et al. (2022). First report of didymella glomerata causing didymella leaf blight on maize in China. *Plant Dis.* 106 (9), 2522. doi: 10.1094/PDIS-02-22-0282-PDN

Ma, L. J., et al. (2010). Comparative genomics reveals mobile pathogenicity chromosomes in. *Fusarium Nat.* 464 (7287), 367–373. doi: 10.1038/nature08850

Majoros, W. H., Pertea, M., and Salzberg, S. L. (2004). TigrScan and GlimmerHMM: Two open source ab initio eukaryotic gene-finders. *Bioinformatics* 20 (16), 2878–2879. doi: 10.1093/bioinformatics/bth315

Marçais, G., and Kingsford, C. (2011). A fast, lock-free approach for efficient parallel counting of occurrences of k-mers. *Bioinformatics* 27 (6), 764–770. doi: 10.1093/bioinformatics/btr011

Moral, J., Lichtemberg, P. S. F., Papagelis, A., Sherman, J., and Michailides, T. J. (2018). *Didymella glomerata* causing leaf blight on pistachio. *Eur. J. Plant Pathol.* 151, 1095–1099. doi: 10.1007/s10658-018-1422-y

Pan, H., Chen, M. Y., Deng, L., Wang, Z. P., Li, L., and Zhong, C. H. (2018). First report of *Didymella glomerata* causing black spot disease of kiwifruit in China. *Plant Dis.* 102 (12), 2654. doi: 10.1094/PDIS-04-18-0583-PDN

Reeder, E. T., and Vanterpool, T. C. (1953). *Phoma* spp. on flax in Saskatchewan. *Proc. Can. Phytopathol. Soc* 21, 16.

Ren, Y., Li, D., Zhao, X., Wang, Y., Bao, X., Wang, X., et al. (2019). Whole genome sequences of the tea leaf spot pathogen *Didymella segeticola*. *Phytopathology* 109, 1676–1678. doi: 10.1094/PHYTO-02-19-0050-A

Roustaee, A., Costes, S., Dechamp-Guillaume, G., and Barrault, G. (2000). Phenotypic variability of *Leptosphaeria lindquistii* (anamorph: *Phoma macdonaldii*), a fungal pathogen of sunflower. *Plant Pathol.* 49, 227–234. doi: 10.1046/j.1365-3059.2000.00451.x

Rouxel, T., Grandaubert, J., Hane, J., Hoede, C., van de Wouw, A. P., Couloux, A., et al. (2011). Effector diversification within compartments of the leptosphaeria maculans genome affected by repeat-induced point mutations. *Nat. Commun.* 2, 202. doi: 10.1038/ncomms1189

Shah, R. M., Williams, A. H., Hane, J. K., Lawrence, J. A., Farfan-Caceres, L. M., Debler, J. W., et al. (2020). Reference genome assembly for Australian *Ascochyta rabiei* isolate ArME14. *G3 (Bethesda Md.)* 10 (7), 2131–2140. doi: 10.1534/g3.120.401265

Simão, D., Pinto, C., Piersanti, S., Weston, A., Peddie, C. J., Bastos, A. E., et al. (2015). Modeling human neural functionality *in vitro*: three-dimensional culture for dopaminergic differentiation. *Tissue Eng Part A* 21 (3-4), 654–668. doi: 10.1089/ten.tea.2014.0079

Smit, A., and Hubley, R. (2015) *Repeat modeler open-1.0*. Available at: http://repeatmasker.org.

Smit, B., McNabb, D., and Smithers, J. (1996). Agricultural adaptation to climatic variation. *Clim. Change* 33, 7–29. doi: 10.1007/BF00140511

Soanes, D. M., Chakrabarti, A., Paszkiewicz, K. H., Dawe, A. L., and Talbot, N. J. (2012). Genome-wide transcriptional profiling of appressorium development by the rice blast fungus *Magnaporthe oryzae*. *PloS Pathog.* 8, e1002514. doi: 10.1371/journal.ppat.1002514

Sperschneider, J., and Dodds, P. N. (2022). EffectorP 3.0: Prediction of apoplastic and cytoplasmic effectors in fungi and oomycetes. *Mol. Plant Microbe Interact.* 35 (2), 146–156. doi: 10.1094/MPMI-08-21-0201-R

Stanke, M., and Morgenstern, B. (2005). AUGUSTUS: a web server for gene prediction in eukaryotes that allows user-defined constraints. *Nucleic Acids Res.* 33 (W), W465–W467. doi: 10.1093/nar/gki458

Stergiopoulos, I., and De Wit, P. J. G. M. (2009). Fungal effector proteins. *Annu. Rev. Phytopathol.* 47, 233–263. doi: 10.1146/annurev.phyto.112408.132637

Sugawara, F., and Strobel, G. (1986). Zinniol, a phytotoxin, is produced by *Phoma macdonaldii*. *Plant Sci.* 43 (1), 19–23. doi: 10.1016/0168-9452(86)90102-0

Sun, Q., Yu, S., and Guo, Z. (2020). *Calmodulin-like (CML)* gene family in *Medicago truncatula*: Genome-wide identification, characterization and expression analysis. *Int. J. Mol. Sci.* 21 (19), 7142. doi: 10.3390/ijms21197142

Taber, R. A., and Vanterpool, T. C. (1963). Alternaria species on rape in Western Canada. *Proc. Can. Phytopathol.l Soc* 30, 10–21.

Ter-Hovhannisyan, V., Lomsadze, A., Chernoff, Y. O., and Borodovsky, M. (2008). Gene prediction in novel fungal genomes using an ab initio algorithm with unsupervised training. *Genome Res.* 18 (12), 1979–1990. doi: 10.1101/gr.081612.108

Thomidis, T., Michailides, T. J., and Exadaktylou, E. (2011). *Phoma glomerata* (Corda) wollenw. & hochapfel a new threat causing cankers on shoots of peach trees in Greece. *Eur. J. Plant Pathol.* 131, 171–178. doi: 10.1007/s10658-011-9796-0

Thordal-Christensen, H., Zhang, Z., Wei, Y., and Collinge, D. B. (1997). Subcellular localization of H2O2 in plants. H2O2 accumulation in papillae and hypersensitive response during the barley–powdery mildew interaction. *Plant J.* 11 (6), 1187–1194. doi: 10.1046/j.1365-313X.1997.11061187.x

Tian, Z., Ai, T., Deng, C., You, S., Shi, Q., Ma, Y., et al. (2018). QTL mapping of resistance to northern corn leaf blight in maize inbred line P178 and effect analysis. *J. Henan Agric. Sci.* 47 (2), 73–76.

Torres, M. A. (2010). ROS in biotic interactions. *Physiol. Plant* 138 (4), 414–429. doi: 10.1111/j.1399-3054.2009.01326.x

Tran, H. S., You, M. P., Lanoiselet, V., Khan, T. N., and Barbetti, M. J. (2014). First report of *Phoma glomerata* associated with the ascochyta blight complex on field pea (*Pisum sativum*) in Australia. *Plant Dis.* 98, 427. doi: 10.1094/PDIS-08-13-0809-PDN

van den Brink, J., and de Vries, R. P. (2011). Fungal enzyme sets for plant polysaccharide degradation. *Appl. Microbiol. Biotechnol.* 91, 1477–1492. doi: 10.1007/s00253-011-3473-2

Vargas, W. A., Sanz Martín, J. M., Rech, G. E., Rivera, L. P., Benito, E. P., Díaz-Mínguez, J. M., et al. (2012). Plant defense mechanisms are activated during biotrophic and necrotrophic development of *Colletotrichum graminicola* in maize. *Plant Physiol.* 158 (3), 1342–1358. doi: 10.1104/pp.111.190397

Wang, X., Zhang, Y., Xu, X., Li, H., Wu, X., Zhang, S., et al. (2014). Evaluation of maize inbred lines currently used in Chinese breeding programs for resistance to six foliar diseases. *Crop J.* 2 (4), 213–222. doi: 10.1016/j.cj.2014.04.004

Wang, S., Chen, Z., Tian, L., Ding, Y., Zhang, J., Zhou, J., et al. (2019). Comparative proteomics combined with analyses of transgenic plants reveal ZmREM1.3 mediates maize resistance to southern corn rust. *Plant Biotechnol. J.* 17 (11), 2153–2168. doi: 10.1111/pbi.13129

Wick, R. R., Judd, L. M., Gorrie, C. L., and Holt, K. E. (2017). Unicycler: Resolving bacterial genome assemblies from short and long sequencing reads. *PloS Comput. Biol.* 13 (6), e1005595. doi: 10.1371/journal.pcbi.1005595

Zheng, Y. J., Zhang, F. H., Meng, C. M., Hou, D. Y., and Sun, Z. (2009). Studies on characteristic differentiation of corn inbred line Ye478 and its related lines. *Seed* 28, 74–75.

Advantages of publishing in Frontiers

OPEN ACCESS
Articles are free to read for greatest visibility and readership

FAST PUBLICATION
Around 90 days from submission to decision

HIGH QUALITY PEER-REVIEW
Rigorous, collaborative, and constructive peer-review

TRANSPARENT PEER-REVIEW
Editors and reviewers acknowledged by name on published articles

Frontiers
Avenue du Tribunal-Fédéral 34
1005 Lausanne | Switzerland

Visit us: www.frontiersin.org
Contact us: frontiersin.org/about/contact

REPRODUCIBILITY OF RESEARCH
Support open data and methods to enhance research reproducibility

DIGITAL PUBLISHING
Articles designed for optimal readership across devices

FOLLOW US
@frontiersin

IMPACT METRICS
Advanced article metrics track visibility across digital media

EXTENSIVE PROMOTION
Marketing and promotion of impactful research

LOOP RESEARCH NETWORK
Our network increases your article's readership